Investigating Catalyst Performance

in Batch Reactive Distillation

Heather Elizabeth Todd

School of Chemical Engineering and Advanced Materials

Newcastle University

A thesis submitted to the Faculty of Science, Agriculture and Engineering at Newcastle University in partial fulfilment of the requirements for the degree of Doctor of Philosophy

December 2010

Abstract

Reactive distillation (RD) combines chemical synthesis with separation by distillation, but this leads to a non-trivial system: the hardware selection, the system components, the mode of operation and the operating conditions all affect the performance of the RD process. A key process development issue is the identification of suitable catalysts that perform well under reactive distillation conditions, as catalysts are crucial for increasing reaction rate when the operating temperature range is limited by evaporation.

The main goal of this research is to develop a method, utilizing high throughput technology, which can be used to assess many candidate catalysts for batch RD systems. The identification of potentially suitable catalysts should be made as early as possible, but before experimental work begins the only information available is the catalyst composition and structure. The approach taken in this research is to correlate catalyst properties to the performance in RD tests and the outputs from dynamic simulations. The case study used is a batch reactive distillation for the esterification of a long-chain fatty acid. Potential catalysts are studied at small scale in a high throughput platform, and further investigation is performed in an experimental batch RD unit.

The most active of the screened catalysts, sulfuric acid and MSA, also have the highest initial activity under RD. Heteropoly acids appear to have a good activity level, while ferric sulfate gives intermediate but apparently increasing activity. Some outcomes of the RD experiments were unexpected: the strong homogeneous acid catalysts entail low distillate water yield, and some metal acetates had higher activity than anticipated in the RD tests. This demonstrates that pilot scale experiments currently remain necessary for the evaluation of catalyst performance for RD processes.

The insights gained from this study lead to key recommendations for future studies: an increased scope of study with a larger number of candidates which preferably have similar structure; evaluation of additional catalyst performance indicators, performed over the full operating temperature range; use of the smallest suitable experimental column; and more focus on physical factors such as solubility. Use of a simulator with an established physical property calculation tool is essential for successful simulations of batch RD.

Acknowledgements

I would like to thank my supervisors, Professor Allen Wright and Dr Mark Willis for their ideas, support, advice and guidance. Also great thanks to Dr Katarina Novakovic for training in laboratory work and provision of values for heat of reaction, and to Mrs Julie Parker for her guidance in the use of laboratory equipment such as the ChemSpeed machine and advice regarding analytical procedures.

Many thanks to the technical staff at the School of Chemical Engineering and Advanced Materials, particularly Mr Rob Dixon, Mr Paul Sterling, Mr Stewart Latimer and Mr Simon Daley, who assisted with equipment set-up and troubleshooting. I would also like to thank Mr Vincent Scott and Mr Daniel Padgett for assistance with IT requirements throughout this project.

I am grateful to Dr Chris O'Malley for his help and advice, particularly regarding multivariate statistical tools. Thanks also go to Professor David Leahy, Dr Dominic Searson, Dr Vladimir Sykora and Dr Hugo Hiden for informative discussions about QSAR and the application of molcular modelling tools. Thanks also to Dr Christophe Grosjean of LyraChem Ltd and to Dr Kamelia Boodhoo for permitting use of apparatus and materials, and Cresset BioMolecular Discovery Ltd for use of free software evaluation packages.

Finally I would like to send a special thanks to all other CEAM staff, and my colleagues, family and friends for their continued advice, encouragement and patience.

Contents

Nomenclature

a	Interfacial area per unit volume (m^2/m^3)
A	Arrhenius constant: pre-exponential factor (m^3/mol s)
a_{CS}	ChemSpeed Glass Reactor
A_F	Pre-exponential factor of the forward reaction (m^3/mol s)
a_L	Heidolph MR Hei-Tec Magnetic Stirrer and Heater
AN	Acid number (mgKOH / g)
A_o	Initial concentration of component A (mol/100g)
a_o	Initial concentration of component A (mol/L)
A_R	Pre-exponential factor of the reverse reaction (m^3/mol s)
a_{RD}	RD Unit Glass Condenser
A_t	Concentration of component A at time 't' (mol/100g)
AV	Subscript for average
B	Matrix of PLS regression coefficients
b	Subscript for bottom product
B/A	Molar ratio of alcohol to acid
b_{CS}	ChemSpeed Reactor Oil Jacket
b_L	EKT Hei-Con Temperature Controller
b_o	Initial concentration of component B (mol/L)
b_{RD}	RD Unit Cooling Water Inlet & Outlet
C	PLS output loadings
c_{CS}	ChemSpeed Reactor Jacket Oil Inlet
CD	Catalytic Distillation
c_L	EKT Hei-Con Temperature Sensor
c_{RD}	RD Unit Connection to Vacuum Pump
CSTR	Continuous Stirred Tank Reactor
cX(i)	Concentration of component I (mol/L)
D	Dimensionless performance measure, D = Da / (1+ Da)
d	Subscript for distillate product
Da	Damköhler Number
D_A	Diffusivity of component A (m^2/s)
d_{CS}	ChemSpeed Reactor Jacket Oil Outlet
DIPE	Di-isopropyl ether

d_L	LyraChem Kit glass round-bottomed flask and stopper
d_{RD}	Column top PT100 temperature sensor
E	Arrhenius constant: activation energy (J/mol)
EB	Ethyl benzene
e_{CS}	ChemSpeed Condenser
E_F	Activation energy of the forward reaction (J/mol)
e_L	Lab Thermometer (76mm mercury filled)
E_R	Activation energy of the reverse reaction (J/mol)
e_{RD}	Distillate Collection Device
ETBE	Ethyl *tert*-butyl ether
f_{CS}	ChemSpeed Condenser Cooling Fluid Inlet
f_L	Lyrachem Kit Oil Bath
f_{RD}	Magnetic switch
GCMS	Gas chromatography mass spectrometry
g_{CS}	ChemSpeed Condenser Cooling Fluid Outlet
g_{RD}	Glass distillate collection arm
Ha	Hatta Number
Ho	Initial liquid hold-up (moles)
h_{RD}	Distillate collection vessel (100ml measuring cylinder)
H_{vap}	Heat of vaporisation (kJ/kg)
i	Number of descriptors
I.D.	Inner Diameter (mm)
i_{RD}	Lab jack
j_{RD}	Glass distillation column (packed, vacuum jacketed)
k_1	Isothermal rate constant (forward reaction)
k_1’	Pseudo 1st order rate constant (1/s)
k_2	Isothermal rate constant (reverse reaction)
K_{eq}	Equilibrium constant
$K_{forward}$	Forward isothermal rate constant
k_L	Liquid phase mass transfer coefficient (m/s)
k_{RD}	Column PT100 temperature sensor (T4)
$K_{reverse}$	Reverse isothermal rate constant
l_{RD}	Column PT100 temperature sensor (T3)
LV	Latent variable
MESH	Mass, Equilibrium, Summation and Heat

Mr	Molecular weight (kg/kmol)
m_{RD}	Column PT100 temperature sensor (T2)
Mr_{KHP}	Molar mass of KHP (204.2 g/mol)
Mr_{KOH}	Molar mass of KOH (56.1 g/mol)
Mr_{Non}	Molar mass of nonanoic acid (158.24g/mol)
MTBE	Methyl *tert*-butyl ether
n	Number of theoretical plates
nc	Non-complete run
n_{RD}	Column PT100 temperature sensor (T1)
o_{RD}	RD Unit Stirrer Motor
p	PCA loadings
P	Matrix of PCA loadings
p_A	Vapour pressure of component A (kPa)
p_A*	Vapour pressure of component A at relevant temperature (kPa)
PCA	Principal Components Analysis
PLS	Partial Least Squares
p_{RD}	RD Unit reactor/reboiler temperature probe
Q	PLS input loadings
q_{RD}	RD Unit Glass Reactor/Reboiler
R	Universal gas constant 8.314 (kJ/kmolK)
R1	ChemSpeed Reactor 1
R2	ChemSpeed Reactor 2
R3	ChemSpeed Reactor 3
R4	ChemSpeed Reactor 4
RD	Reactive Distillation
r_{RD}	RD Unit Reactor/Reboiler Oil Jacket
RRF	Relative Response Factor
rX(i)	Rate of change of component i (mol/L s)
S	PLS input scores
s_{RD}	RD Unit Stirrer rod (PTFE)
T	Matrix of PCA input scores
t	PCA input scores
T	Temperature (°C)
t	Time (s)
TAME	*Tert*-amyl methyl ether

t_{RD}	RD Unit Connections to recirculating oil bath
u_{RD}	RD Unit Reactor base outlet
V_{KOH}	Volume of KOH used in titration (ml)
VLE	Vapour-liquid equilibrium
Vo	Initial vapour rate (mol s^{-1})
VP	Vapour pressure (kPa)
v_{RD}	U-tube liquid lock chamber
W_{KHP}	Weight KHP used in standardisation (mg)
W_s	Weight of sample (g)
X	Conversion (%)
X	Matrix of inputs (descriptors)
x	Amount of product formed per unit volume (mol/L)
x_i	Mole fraction of most volatile component in liquid
x_j	Mole fraction of least volatile component in liquid
Y	Matrix of outputs
y_i	Mole fraction of most volatile component in vapour
y_j	Mole fraction of least volatile component in vapour
α_{ij}	Relative volatility
ΔH_R	Standard enthalpy change of reaction (kJ/mol)
ΔT	Oil – pot temperature difference (°C)
Є and **Ƒ**	PLS residual errors
ξ	PCA residual errors
ρ	Liquid density in (kg/m^3)
ρ_v	Vapour density (kg/m^3)
χ	Variable value
χ'	Normalised variable value
χ_{min}	Lowest variable value
χ_{max}	Highest variable value

List of Figures

List of Charts

List of Tables

List of Software Used

- ASTM CHETAH 8.0
- BatchCAD 7
- Cresset FieldTemplater 2.2.0
- DaqLAB™ Analysis Software, Fourier Systems Ltd
- Matlab 6.5
- Matlab 7
- Microsoft Office 2003
- Minitab15
- MultiDAT version 3.0 Beta (for Matlab 6.5)
- PreScreen version 2.1 (for Matlab 6.5)
- SigmaPlot11
- Varian MS Workstation

Chapter 1: Introduction

1.1 Overview

The aim of this thesis is the development of an improved procedure for assessing the performance and suitability of catalyst candidates for esterification of long chain fatty acids by reactive distillation. Previous studies described in available literature include those where many catalyst candidates have been screened for activity in a particular reaction, or where a small number of catalysts have been tested in reactive distillation units, but no studies have been found where a large number of catalysts have been tested under reactive distillation.

The objectives of the work are as follows:

- To perform screening tests on a range of candidate catalysts, utilising the high throughput technology facilities available in the School of Chemical Engineering and Advanced Materials.
- To test a number of catalysts under reactive distillation conditions in a newly-built batch reactive distillation unit.
- To develop a dynamic model of the unit to enhance understanding of the reactive distillation process.
- To combine the results of the screening and reactive distillation experiments with the outcomes of dynamic simulations, and implement multivariate statistical tools to investigate relationships between catalyst properties and performance.

1.2 Introduction to Reactive Distillation

1.2.1 Background

Reactive distillation (RD) is the combination of reaction and separation into one single step. For example, Spatschek (1995) states that reactive distillation is 'the combining of chemical reactions with vapour-liquid equilibrium (VLE) separation, simultaneously in one process unit'. Catalytic distillation (or CD) is a name often used to describe reactive distillation processes that involve a homogeneous or heterogeneous catalyst (Taylor and Krishna, 2000). There are many hardware configurations possible, and although reactive distillation is sometimes described as 'the simultaneous

implementation of reaction and distillation within a counter-current column' (Stichlmair and Frey, 1999), it is not always the case that a counter-current column is used (Sharma and Mahajani, 2003).

An illustrative schematic of a reactive distillation unit is shown in Figure 1.1, which has been adapted from the BatchCAD manual (Aspen Technology Inc., 2005). Other possible configurations include continuous columns with pre-reactors (Daniel and Jobson, 2007) or side reactor arrangements (Kaymak and Luyben, 2007).

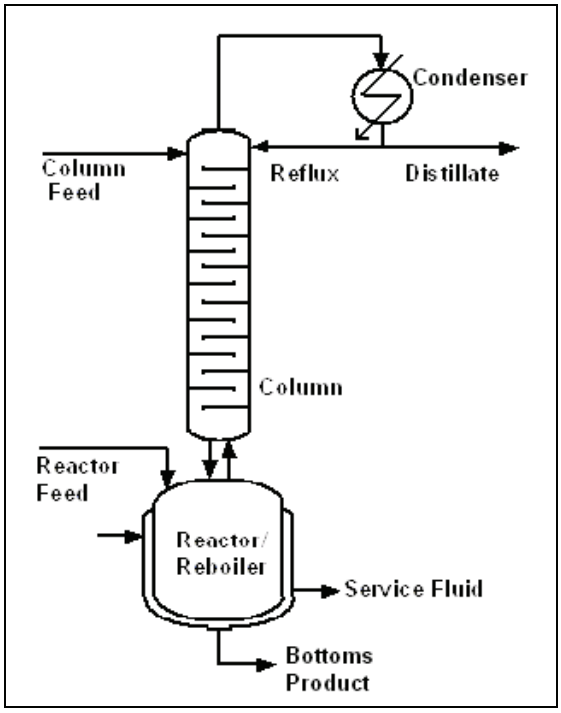

Figure 1.1: Illustration of a Reactive Distillation Unit (adapted from the BatchCAD manual, Aspen Technology Inc., 2005).

1.2.2 Advantages of Reactive Distillation

Reactions occurring during distillation operations were viewed as undesirable before the potential benefits were recognised in 1920s. Following a review by Doherty and Buzad (1992), there was a surge of interest in reactive distillation. The main reasons for this level of interest are the economic advantages that can be gained using reactive distillation. These benefits were summarised by Taylor and Krishna (2000):

- Simplification of processes
- Improved conversion
- Improved selectivity

- Reduced catalyst requirement for same conversion
- Avoiding azeotropes
- Reduced by-products
- Heat integration (the heat of reaction can be utilised)
- Hot spots and runaway problems are reduced

Malone and Doherty (2000) describe how the process advantages of reactive distillation can be divided into two categories: (1) using reaction to improve separation by removing azeotropes and contaminants, or (2) using separation to improve reaction, which overcomes limitations such as: reaction equilibrium, selectivity, and catalyst poisons. In reactive distillation involving reversible reactions, removing one product by distillation pushes the equilibrium further towards products. This allows increased conversion to be achieved, which can lead to reduced costs. Reactive distillation can also make it possible to use stoichiometric feed ratios instead of a large excess of one reactant (Doherty and Buzad, 1992). For a mixture that is difficult to separate conventionally because the components have very close boiling points, improvement can be implemented by use of a reactive entrainer, chosen to react with one of the components.

1.2.3 Applications of Reactive Distillation

Reactive distillation has been described as 'the most widely applied process intensification technique' (Harmsen, 2007). Sharma and Mahajani (2003) have identified around 70 reaction systems which have been performed as reactive distillation processes. Applications of reactive distillation that have been established on an industrial scale are: esterification, etherification and alkylation (Tuchlenski et al., 2001). Many of these applications clearly demonstrate the key advantages over conventional processes provided by the implementation of reactive distillation.

Esterification

Esterification is one of the main applications of reactive distillation in industry (Hiwale et al., 2004). The general form of an esterification reaction is:

Acid + Alcohol ⇔ Ester + Water

Esterification is described in greater detail in Chapter 2. The implementation of reactive distillation greatly simplified the process for the production of methyl acetate. The

conventional system had 2 reactors and 8 distillation columns, and this was replaced with only 1 reactive distillation column and 3 separating columns (Agreda et al., 1990).

Etherification

Demand for ethers rose with the introduction of legislation to reduce car emissions and remove lead from petrol. Ethers are used as octane enhancers to improve fuel quality because they are clean burning and less toxic than lead (Doherty and Buzad, 1992). Some important ethers are highlighted by Sharma and Mahajani, (2003). Reactive distillation allows inerts to be efficiently removed and avoids limitations due to azeotropes, such as those between MTBE and methanol and between isobutene and methanol (Doherty and Buzad, 1992). High purity reactants are not necessary, and this can give a significant competitive advantage (Towler and Frey, 2000).

Alkylation

The products of alkylation have varied applications:

- Ethyl benzene (EB) from benzene and ethylene: EB is an important intermediate for manufacturing styrene. The EB produced is more reactive with ethylene than benzene, so using reactive distillation to remove it prevents further reaction and reduces the need for a large excess of benzene (Qi and Zhang, 2004).
- *Iso*-octane *from iso*-butene and *n*-butene: *Iso*-octane can be used as an octane enhancer as an alternative to MTBE (Talwalkar et al., 2006). Again, removal of products prevents further reaction (Doherty and Buzad, 1992).
- Cumene from benzene and propylene: cumene is commercially important for the production of phenol and acetone. The use of reactive distillation with solid catalytic packing allows the separation of unreacted benzene (Buelna and Nenoff, 2005).

In industry, many fine chemicals and flavour and fragrance compounds are also made using reactive distillation, often in batch reactor/rectifier units (Wright, 2006).

1.2.4 Identification of Catalysts for Reactive Distillation

Many reactions performed in reactive distillation units require addition of a catalyst to speed up the reaction and to make the process more economically feasible. However, a suitable catalyst may not be easy to find. Some unit operations such as reactors are

easily miniaturised and incorporated into high throughput robotic platforms, and in the pharmaceutical industry developments in automated systems have led to the use of high throughput technology for screening large numbers of candidate compounds for characteristics of interest. This means that there is an increase in the number of candidates that can be rapidly tested for suitability, without investing much research effort on each one individually. The process development effort is then able to focus on the candidates which appear most promising.

Development of a new reactive distillation process may not advance far if a suitable catalyst is not identified early in the development phase, and if the uncatalysed reaction rate at the boiling temperature of the mixture is unsatisfactory. To find promising candidates quickly a high throughput screening method would be most useful, but the high throughput units used in the pharmaceutical industry employ closed batch conditions, and can not replicate reactive distillation. If catalyst screening is limited to this type of unit some potential candidates could be overlooked if their performance is different under reactive distillation conditions.

High throughput units able to replicate realistic reactive distillation conditions at small scale are not currently available, and may not be possible. Attempts to create and attach miniature distillation columns to miniature batch reactor pots (which can have a capacity of less than 20ml) would be likely to suffer from issues related to mass transfer and 'wall effects' which are significant at such small scales. The approach taken in this work is to perform experimental catalyst screening in small-scale batch reactors, followed by testing under reactive distillation conditions. The information gained is then evaluated and combined with simulation and statistical tools with the aim of developing an improved methodology for the assessment of catalysts for reactive distillation processes.

1.3 Organisation of the Thesis

Chapter 2 presents a survey of the available literature on reactive distillation and gives some background to the topic and the context of the work presented in this thesis. The current methods for the development of reactive distillation are discussed, with emphasis on studies involving the esterification of long chain fatty acids. This leads on

to further discussion of the motivation behind this work and how it will contribute to the existing research.

The next four chapters of this thesis are concerned with describing the development of experimental methodologies for assessing catalyst performance and the reporting of the results. Chapter 3 focuses on the development of the methods used for small-scale catalyst screening, and the trial runs used to establish key parameters and limitations. The equipment for catalyst tests is described, before the selection of reaction system is explained. The candidate catalysts to be tested for this reaction system are presented and finally a summary of the experimental procedures is given.

Chapter 4 reports the results from the catalyst screening work, which begins with the identification of the equilibrium point for the esterification reaction. The results of the screening for catalyst activity are presented, including the half life of the reaction with each catalyst candidate. Strong homogeneous acids are the most active in these tests, followed by the heteropoly acids, while ferric sulfate also shows some activity. The profiles of the catalyst activity during the runs reveal that the strong homogeneous acids deactivate during the run while the activity of the heteropoly acids stays approximately constant. This chapter concludes with the results of testing the performance of a selection of catalyst candidates at different temperatures, information that is used in Chapter 7 for building reactive distillation simulations.

Chapters 5 and 6 are concerned with the reactive distillation experimental work. Chapter 5 begins with a description of the batch reactive distillation unit and the characterisation of the unit through vapour rate tests and separation performance tests. It is confirmed the column, which contains Sulzer structured packing, has 20 theoretical separation stages. Column start-up is also explored through butanol boil-up tests and trial runs using the reaction mixture. Operating parameters and steps in the experimental procedure for the catalyst performance tests in the unit were based upon observations made during this preliminary work and are summarised at the end of this Chapter.

Chapter 6 reports the results of the catalyst performance tests in the batch reactive distillation unit using the nonanoic acid esterification system, and also four comparison runs using an alternative esterification system. Data from the runs included temperature profiles from the pot and the column, in which interesting trends were observed and the

different catalyst types can be seen to have made the system behave very differently. The strong acids have the highest initial activity, but this does not translate to the best performance in terms of distillate yield, which is low for these runs. The metal acetates appear to have improved activity under the reactive distillation conditions. Numerical outputs are identified that describe the behaviour of the unit, and which are taken forward for statistical analysis.

In Chapter 7 a dynamic simulation model of the reactive distillation unit is built in BatchCAD, with the aims of matching the observations from the experimental work and enabling improved understanding of the observed behaviour. The warm-up of the reaction pot and the separation performance of the column are matched well, however the time-varying temperatures in the column are not well matched, limiting the usefulness of these simulations. A simplified model was then built in Excel, which was based on observations made during the experiments. The simulated values of the numerical outputs of the reactive distillation experiments were reported and incorporated into the multivariate statistical work in Chapter 8.

The use of multivariate tools to explore for relationships between catalyst properties and catalyst performance is described in Chapter 8. The half life values from the screening tests are well predicted by a statistical model based on catalyst descriptors, and the descriptors which were key to explaining the observed activities are revealed. An attempt is then made to incorporate the results from screening and simulations into statistical models describing performance in the reactive distillation unit.

The main conclusions from the different parts of this thesis are summarised in Chapter 9, which also presents recommendations for future work.

Chapter 2: Literature Review

2.1 Overview

This chapter begins with a description of the constraints and research opportunities involved in the area of reactive distillation and the reasons for the importance of research to the development of new processes. The features and types of reactive distillation systems discussed in literature are considered, including the various operation modes that can be employed. A brief discussion is then given of the studies involving the techniques used to model reactive distillation systems.

Esterification is one of the most successful applications of reactive distillation; therefore there is a section of this review which gives some background information on this type of reaction system. The esterification of long chain fatty acids is discussed, and examples are given of processes for esterification of long chain fatty acids by reactive distillation. A review of the catalysts that have been described in literature sources for use with esterification systems, and some different approaches taken for the development of these processes, are presented. Some statistical tools that may be useful in taking forward the development process are also introduced in this review. In the context of the literature review, the motivation behind the current study is explained and the approach taken for this investigation is outlined.

2.2 Constraints and Research Opportunities

Reactive distillation is not suitable for all processes: it may offer no additional benefit, or it may not be feasible at all (Malone and Doherty, 2000). For application on an industrial scale, Tuchlenski et al. (2001) have described some important constraints, including the key prerequisite that the temperatures of reaction and separation by distillation must overlap. Some room for manoeuvre can be gained by changing the operating pressure, but it has been noted by Kaymak and Luyben (2007) that, when occurring in the same vessel, the reaction and separation processes must be feasible at the same pressure.

Many reactive distillation processes involve the use of a catalyst, which increases the rate of reaction but also introduces some constraints. The thermal stability of the catalyst may limit the maximum operating temperature at which the reaction can occur,

and when a solid catalyst is used, for the reaction to take place in the liquid phase, there must be good contact between the reactants and the catalyst. A fixed catalyst (e.g. catalytic packing used in a continuous column) must have a long lifetime. It is impractical to regularly have to disassemble the unit to remove and replace or reactivate the catalyst, so poisoning and deactivation of the catalyst must be avoided.

Malone and Doherty (2000) give a comprehensive summary of the challenges and opportunities for research presented by reactive distillation. Some of these are described below:

- New, highly effective catalysts are required that are suitable for the multiphase conditions found in reactive distillation.
- Experiments are required to evaluate the effects of fluid hydrodynamics on reaction rate, as modelling by itself cannot predict these effects and the complex interactions involved. Research is needed into how to decide on a suitable scale for pilot plant tests and how the results can be scaled up in a useful and reliable way.
- Computer simulation and design of experiments are currently used to cut down the number of pilot plant experiments required when reactive distillation processes are developed. Simple and reliable validation methods would enable this to be carried further.
- Side reactions can have a significant adverse effect on selectivity and therefore on the yield of product. Systematic methods are needed for studying how reactive distillation can influence which possible side reactions are promoted or restricted.
- Novel technology such as catalytic packing and internals are available, but with limited guidance about selection and application. Without further information, implementation in industry could be slowed.
- Self-catalysed reactions present a unique problem because the reaction occurs spontaneously, so it is currently difficult to measure the individual binary pair interactions for VLE calculations.
- Other possible research areas described by Malone and Doherty are the generation of conceptual design alternatives and energy management studies to achieve the maximum benefit from heat integration in reactive distillation columns.

As mentioned above, pilot scale experimentation is currently an essential phase in the development of reactive distillation processes. Different systems of components and reactants will behave differently, and a unit designed and optimised for one system will be specific to that system (Spatschek, 1995). The behaviour of reactive distillation processes is complex and occasionally counter-intuitive. In the MTBE process, for example, the product could be collected either as distillate or as bottoms product (Malone and Doherty, 2000). This unpredictability affects reactive distillation more than traditional processes, so there is a greater dependence on experimental studies to obtain reliable and relevant data for design and optimisation (Spatschek, 1995). However, pilot plant studies are expensive and time-consuming and in industry it is desirable to reduce the number of experiments required as much as possible.

Some attempts have been made to address the challenges described by Malone and Doherty (2000). Schoenmakers and Bessling (2003) describe two major European projects that have investigated reactive distillation. The first, known as the Brite-Euram project, ran from 1996 to 1999. The aim was to develop methods and tools for process synthesis and design. Some new computational tools resulted but they were not rapidly commercialised. The second project followed on from this and focused on the development of 'intelligent internals' specifically for reactive distillation. The 'INTINT' project involved collaboration between industry and academics to design, build and test new column internals that would reduce the need for expensive hydraulic experiments (Górak et al., 2005). Simulation tools were developed to allow pre-selection of available internal types, for the study of hydraulics of the column internals and to investigate reactive systems. This work continued in the European 'INSERT' Research Project, and utilised in a recent pilot plant study of a process to make n-propyl propionate, where good agreement was obtained between experimental and simulation profiles for the column temperatures and compositions (Altman et al., 2010).

2.3 Reactive Distillation Configuration and Operation

2.3.1 Batch, Semi-batch, Continuous

The decision as to which mode of operation should be used depends on the reactive system in question and where the catalyst is located. Continuous processes allow large amounts of commodity products to be made quickly and at low cost (Cuille and Reklaitis, 1986). However, non-continuous processes can be more flexible and

adaptable (Fernholz et al., 2000) which is useful if there are large variations in demand or feed composition (Sørensen and Skogestad, 1994). Batch processes are often used when small amounts of high added-value products are required, or to allow sufficient residence time if a reaction is very slow (Wajge and Reklaitis, 1999).

There are several examples where semi-batch reactive distillation has been found to be advantageous. Egly et al. (1979) obtained their best results when the reflux ratio was varied during the run and one reactant was added (semi-batch wise) during operation. Semi-batch mode was also found to be preferable for the set-up studied by Fernholz et al. (2000), where the reaction occurred in the column with catalytic packing. There was a great difference in volatility between the reactants acetic acid and methanol, so acetic acid is fed into the top of the column. Bollyn and Wright (1998) found that the use of semi-batch reactive distillation was preferable to the equivalent total batch option for their study of the production of the ethyl ester of pentanoic acid. Kinetic studies revealed that high selectivity for the desired product required high temperature operation. This was achieved through semi-batch operation by slowly adding the allyl alcohol reactant to the higher-boiling triethyl orthoacetate and removing the ethanol formed by distillation. A very high selectivity was achieved of> 98%, and the semi-batch process also allowed the whole volume of the reactor to be used at all times.

2.3.2 Performance

The performance of reactive distillation is often discussed in terms of conversion, yield, and selectivity (Gadewar et al., 2000). Wajge and Reklaitis (1999) used simulations to explore how the operating conditions influence the performance of reactive distillation, which they found to be more sensitive to changes than normal distillation. If the reflux ratio was too low then more distillate was collected but reactants were removed as well as products, leading to poor conversion. However, if the reflux ratio was too high the higher residence time promoted side reactions. Fernholz et al. (2000) also encountered this trade-off between conversion and productivity.

The Damköhler number (Da) is a measure of performance for continuous reactive distillation units, where the reaction occurs on the plates and is potentially limited by the residence time in the column. It is the ratio of the characteristic residence time to the characteristic reaction time (Venimadhavan et al., 1994 and Towler and Frey, 2000):

$$Da = Ho\ k_1' / Vo \qquad (2.1)$$

Where:

Ho = initial liquid hold-up (moles)

Vo = initial vapour rate (mol/s)

k_1' = a pseudo 1st order rate constant (1/s)

Venimadhavan et al. (1994) define k_1' as 'the forward rate of reaction at the lowest temperature on the boiling surface, the lowest boiling azeotrope/pure component'. The value is assumed to be constant. In order for the units of k_1' to be of the type time^{-1}, the rate expression should be in terms of mole fractions (Doherty and Buzad, 1994). If the value of the Damköhler number is between 0 and 1, the residence time is less than the time required by the reaction, but if Da is greater than 1, then the residence time is greater than the reaction time. As Da approaches infinity then the reaction is approaching equilibrium. The use of the Damköhler number when applied to design strategies for reactive distillation is described by Huss et al. (1999). Further development by Venimadhavan et al. (1999a) led to the following expression:

$$D = Da / (1+ Da) \qquad (2.2)$$

If the dimensionless measure 'D' is 0, there is no reaction (same as Da). If D lies between 0 and 0.5 then the residence time is less than the reaction time (this corresponds to when Da is between 0 and 1). The main difference is when the residence time is greater than the reaction time: D is between 0.5 and 1. At D =1 the reaction is at equilibrium, whereas Da approaches infinity and has no cut-off point. D is therefore considered by the authors to be more linear and more easily interpreted. Another performance measure is the Hatta number, which is described by Towler and Frey (2000). The equation for the Hatta number is:

$$Ha = \frac{\sqrt{D_A k_1'}}{k_L} \qquad (2.3)$$

Where : D_A = diffusivity of component A (m^2/s)

k_1' = pseudo 1st order rate constant (1/s)

k_L = liquid phase mass transfer coefficient (m/s)

The Hatta number helps determine which rate processes govern the overall reaction rate and therefore performance of a reactive distillation process. According to Towler and Frey (2000), the values of the Hatta number fall into categories that correspond to performance 'regimes':

- If Ha > 3, the reaction is very fast. This regime is unlikely to be encountered in reactive distillation: RD may offer no improvement.
- If Ha^2 <<1 this indicates one of the slow regimes.
    - If k_1'<<ak_L (where a = interfacial area per unit volume) this suggests the kinetics are slow and the process is reaction rate limited. Sufficient residence time is needed (i.e. liquid hold-up) in the column, but there is potential to improve the performance with a better catalyst.
    - If k_1'>>ak_L this suggests the process is mass transfer limited and increasing the kinetics with a better catalyst will not improve the performance but alternative packings could be tested.
    - k_1' ~ ak_L then a model for this slow mixed regime must consider both mass transfer and kinetics as neither dominates. It is possible that the performance could be improved by a catalyst.

To evaluate the Hatta number, the relevant mass transfer coefficients and diffusivities must be available, and this is not always the case.

2.3.3 Catalytic Column Packing

Many applications of reactive distillation involve heterogeneous catalytic packing, designed specifically for reactive distillation applications. The main manufacturers of these types of specialised packing are:

- Sulzer Chemtech, who produce 'Katapak™-SP'
- J. Montz Company, who produce 'Multipak'
- Koch-Glitsch, who produce 'Katamax ®′ packing

A heterogeneous catalyst such as Amberlyst-15, an ion exchange resin made of small gel beads with large macropores, is generally installed in the packing sections. Details such as the chemical composition of ion exchange resins suitable for reactive distillation involve commercially sensitive proprietary information, and the design and operation of many industrial reactive distillation units are not openly discussed (Harmsen, 2007). This highlights the difficulty of identifying the current state of the art, and some constraints as to which catalysts can be closely studied. A review of the different types of catalytic packing commercially available and various methods of loading it into the column are given by Towler and Frey (2000). Sundmacher and Qi (2003) also discuss the requirements of successful catalytic packings. These are divided into the requirements for the reaction and requirements for good separation:

For reaction:

- High activity and high activity to volume ratio
- High selectivity
- Accessible active sites
- Chemical and mechanical stability

For separation:

- High surface area for mass transfer
- Low pressure drop
- Fully wetted surface
- Good mechanical strength

It is not usually possible to meet all of these requirements simultaneously, so the solutions reached are often compromises. Non-reactive sections are often included above and/or below the catalytic packing. Advantages of using catalytic packing for sections of reactive distillation columns are that their size and location can be chosen (Steinigeweg and Gmehling, 2003). However, it must be taken into account that the activity of the packed catalyst is lower than if the same catalyst were fully immersed in reaction mixture (Kunz and Hoffman 2003). Also, using a catalyst fixed in the column in this way means that catalyst deactivation presents an issue because it is difficult and expensive to replace.

2.4 Reactive Distillation Models

Reactive distillation simulations are gradually replacing real experiments in the early development of new columns (Tuchlenski et al., 2001). However, these models must be accurate if they are to be confidently used for the design and optimisation of new units (Spatschek, 1995). In a typical RD simulation the state of the feeds, the equipment configuration, and values for independent design variables are known. The simulator is used to calculate the remaining variables including the composition and state of the product streams (Doherty and Buzad, 1992). When desired products have been specified, simulations can also be used to assess the ability of a range of column designs to deliver the required product streams (Groemping et al., 2004).

Taylor and Krishna (2000) have given a detailed review of the many papers that have been written regarding the modelling of reactive distillation, although only a small section of this review described batch reactive distillation. Many models in the literature are based on hypothetical systems, or look at only well-known systems such as the methyl acetate process. Few are then validated with real experimental data, so their accuracy and general applicability cannot be evaluated.

2.4.1 Reactive Distillation Model Types

The complexity of reactive distillation models varies greatly, as different assumptions are made depending upon the purpose of the model. Reactive distillation models can be divided into two main groups, which have been developed from the field of conventional distillation: equilibrium stage models and non-equilibrium stage models.

Equilibrium stage models:

When the vapour and liquid streams leaving a stage in the column are assumed to be in phase equilibrium with each other, the model is said to be an equilibrium stage model (Taylor and Krishna, 2000). The behaviour of a real column can be approximated using 'tray efficiencies' as a measure of its approach to phase equilibrium (Tuchlenski et al., 2001). Equilibrium models are built upon MESH equations and these are described by Taylor and Krishna (2000):

- M = material balances
- E = phase equilibrium
- S = summation equations
- H = enthalpy (heat) balances

Other equations that are sometimes added to equilibrium stage models are: the pressure drop along the column and controller equations (Taylor and Krishna, 2000). Equilibrium stage models can be very useful for initial feasibility studies because they allow quick solutions to be found with a moderate level of accuracy.

Non equilibrium stage models:

Non equilibrium stage models are necessary when the rates of reaction and mass transport processes occur on similar timescales. Non-equilibrium stage models are more complex, as they perform calculations for the vapour and liquid phases in the unit

separately (Tuchlenski et al., 2001). Using a method developed for non reactive distillation, the rate of mass and energy transfers between the liquid and vapour phases are calculated. Mass transfer coefficients, Maxwell-Stefan diffusivities and interfacial areas are required in order to perform these calculations (Taylor and Krishna, 2000). Information about the equipment used must also be included, for example: volumes and surface areas for evaluation of the driving forces influencing the mass transfer and reaction kinetics. Thermodynamic properties are required, so it is desirable that these models are designed to interface with commercial thermodynamic packages. Further details of non-equilibrium models are provided by Taylor and Krishna (2000).

2.4.2 Model Complexity and Assumptions

Selection of the correct level of complexity is an important consideration when modelling reactive distillation – enough detail should be included so that the model is accurate enough for its purpose. Rigorous simulations can be used to assess the design and control strategy of a novel or unfamiliar technology, which may encourage its acceptance by cautious industrialists (Jobson, 2005). However, it is sometimes found that increasing the level of detail leads to minor improvements but major increases in the computing demand so a balance must be achieved (Tuchlenski et al., 2001).

In the simplest models, both chemical equilibrium and phase equilibrium are assumed to be achieved on each stage of the reactive distillation unit. This kind of simulation can be valuable, for example in the production of preliminary designs before data for reaction kinetics have been obtained (Daniel and Jobson, 2007). Complexity is increased by the inclusion of calculations for the mass transfer between phases or chemical reaction kinetics, or both. The simplest models are often used in the simulation of continuous columns at steady state, for example Grosser et al. (1987) assume that both chemical and phase equilibrium are reached in their model of a column for the production of Nylon 6,6. This is in contrast with the work by Kreul et al. (1998), who described a complex non-equilibrium model for packed columns with a porous heterogeneous catalyst. Their model includes consideration of the mass transfer of material to the catalyst surface and within the pores.

A team at Dortmund University presented a detailed and flexible non-equilibrium simulator called DESIGNER, which was developed as a reactive distillation design tool

during the European Brite-Euram research project (Kenig et al., 2004 and Górak et al., 2005). The rates of interphase mass transport, heat transfer and reaction kinetics are included in the simulator, and catalyst efficiency terms are included for mass transfer inside a heterogeneous catalyst. Different hydrodynamic modelling options are available, giving DESIGNER the flexibility to be adapted to fit the user's needs. However, it was found that the long computational times involved limited the applications of DESIGNER to final design checks and accuracy checks of simpler models (Kenig et al., 2004).

Many dynamic equilibrium models of reactive distillation use a compromise, where phase equilibrium on the stages is assumed but reaction kinetics are calculated. The dynamic model described by Reuter et al. (1989) falls into this category, as it takes into account the kinetics of reactions occurring in the liquid phase, but assumes perfect mixing on the individual stages so rates of mass transfer between phases are not evaluated. This model is, however, more detailed than many equilibrium models in that the vapour phase hold-up is included and column pressure drop is calculated.

2.4.3 Dynamic Models

Dynamic models are required for batch and semi-batch reactive distillation units because the majority of their operation is performed under non-steady state conditions. Spatschek (1995) produced a PhD thesis on the modelling of reactive distillation. It was found that accurate data for the reaction kinetics was required, over the whole range of component concentrations and operating temperatures, in order to fully model the dynamics of reactive distillation. Various systems and column configurations were investigated and it was concluded that the best configuration to use with any particular system can only be discovered by study of that particular system.

Cuille and Reklaitis (1986) investigated numerical solution techniques for a dynamic model for multicomponent batch reactive distillation. Their model is an equilibrium model, with reaction occurring in the liquid phase in the reboiler, in the condenser and on the plates. The vapour phase hold-up is assumed to be negligible, with constant volumetric hold-up on the stages, and the pressure drops and Murphree tray efficiencies are also taken to be constant. The authors state that the hydrodynamics on the trays do not vary greatly but that equations can be added to model their effects if needed. The

model described by Cuille and Reklaitis was applied by Wajge and Reklaitis (1999) in their optimisation module RBDOPT (reactive batch distillation optimisation). Written in C++, it is able to communicate with other scientific programs written in FORTRAN. This is extremely useful as it allows interaction with existing physical property databases, increasing the applicability of RBDOPT to a wide range of reaction systems and enabling the potential to extend the model and include new features in the future.

Reuter et al. (1989) also describe multicomponent batch reactive distillation, but this model is more thorough than that of Cuille and Reklaitis (1986), as it does not ignore the vapour hold up and control equations are included. This model does assume that reactions occur only in the liquid phase in the reboiler only, and that the liquid hold-up in the column is constant. Hydrodynamics on the trays are again not considered: the liquid on the trays is assumed to be perfectly mixed. The vapour and liquid phases are assumed to be in equilibrium and a tray efficiency term is included. The vapour liquid equilibrium relationship used is selected by the user and could be, for example: Raoult's law for ideal systems, the Wilson equation or UNIFAC. Reuter et al. (1989) compared the results of their simulations with experimental plant data, and found good agreement.

The dynamic model described by Sørensen and Skogestad (1994) is similar in some ways to that of Cuille and Reklaitis (1986): the vapour phase hold-up is assumed to be negligible and the liquid and vapour phases are assumed to be perfectly mixed and at equilibrium. The pressures and the tray efficiencies are assumed to be constant, but the reactions are assumed to occur only in the reboiler and enthalpy changes of the liquid are ignored. The model is used by the authors to explore various control strategies.

The aim of Ruiz et al. (1997) was to develop a general dynamic model that could be applied to both batch and continuous reactive distillation. The model they used was applied in a computer package known as READYS (reactive distillation dynamic simulator). The vapour hold-up is again assumed negligible and the chemical reactions occur only in the liquid phase in the reboiler, condenser and column stages, which significantly shortens the calculation time required. The liquid and vapour phases are assumed to be well mixed and in thermal equilibrium on each tray, and a tray efficiency factor is included in the model. Each stage is taken to be equivalent to a CSTR and the authors stated that PID controller equations can be included in the model. Some hydraulic effects are included: entrainment, weeping and flooding are considered, taking

into account the geometry of the column plates, the liquid hold-up and the pressure drop across each stage. However, the authors stated that the READYS model is not suitable for use with heterogeneous catalytic packing, as it was developed on the basis that the column internals are trays. This is a serious limitation on the applicability of this model, as catalytic packings are increasingly widely used.

Mujtaba and Macchietto (1997) looked at the problem of the computational time required to optimise a batch reactive distillation. Each solution of an RD model is slow, and optimisation tools need to run many repeats of the solution. They developed a new approach whereby the behaviour of the column was approximated by polynomials, which could be solved much more quickly. This approach requires much preliminary work to develop accurate polynomials. Venimadhavan et al. (1999b) used a short cut method with their batch reactive distillation model to investigate a distillate policy which involved keeping the instantaneous Damköhler number constant by varying the reflux ratio. This model was based on the simplifying assumptions that the column and condenser hold-ups are negligible compared to that in the reboiler, that the column is in a quasi-steady state, and that approximately total reflux ratio is used. Gadewar et al. (2000) simplify their batch model even further: they do not use VLE equations to calculate equilibrium compositions on each stage, and instead they simply assume that the required separation is attainable. The only aim in this case was to estimate the yield and selectivity that could be obtained.

Guo et al. (2003) investigated the feasible products that could be obtained from hypothetical ternary systems using residue curve maps. The focus of the work is on azeotropic systems. The model they use is highly simplified, with an infinite reflux ratio assumed, and the kinetics of the reactions assumed to be temperature independent, and there is no comparison with real data. J. Chin et al. (2006) followed up this work with a study of feasible products in complex batch reactive distillation. Residue curve maps were used and feasibility studies were performed on model systems but there is no comparison with real data. A single, very fast rate constant is assumed for all their simulations, independent of temperature, so effectively the reaction was assumed to instantly reach equilibrium.

Models devoted specifically to semi-batch reactive distillation are more difficult to find. Egly et al. (1979) began with a model for the optimisation of a batch reactive distillation

column, but found that semi-batch gave the best performance when combined with a controlled reflux ratio. The reaction is assumed to occur in the liquid phase, in the stages of the column as well as in the reboiler. Phase equilibrium is assumed to exist in the column, but the model did account for the non ideal behaviour and the reaction kinetics in the reboiler mixture. Bollyn and Wright (1998) used BatchCAD software to model the production of pentanoic acid ethyl ester by semi-batch reactive distillation. First the reaction kinetics were investigated experimentally through use of the BatchCAD kinetic fitting tool, before simulations of the semi-batch process were performed using the capability of BatchCAD to perform rigorous stage-wise calculations. The model was refined and validated with data from pilot plant experiments

Li et al. (1998) describe a model for the optimisation of a semi-batch reactive distillation, in terms of reflux ratio and feed flow rate profile. A detailed dynamic model was developed, which was validated using experimental data for a transesterification reaction, and a brief outline of unit start-up was given. The assumptions are as follows: constant molar hold-up in stages and condenser, constant tray pressure, constant tray efficiency, total condenser with no sub-cooling, ideal vapour phase, negligible vapour phase hold-up, ideal heat transfer and reaction occurring only in the reboiler. Fernholz et al. (2000) also describe the optimisation of a semi-batch reactive distillation column. In this study, the reactions occur in the reboiler and also in the condenser and the column stages, and thermodynamic equilibrium is assumed between the liquid and vapour phases. Structured catalytic packing is used in the column, so a quasi-homogeneous correlation is used for the calculation of reaction kinetics. As in the model used by Li and co-workers, Fernholz and co-workers assume the vapour phase behaviour is ideal and the vapour hold-up is assumed to be negligible. The molar hold-up of liquid in the packing is calculated and that of the condenser is assumed to be constant. The model is fairly detailed: the pressure drop in the packed column is calculated, and dynamics of the tray liquid hydraulics and enthalpy are taken into account.

Validated models for start-up and shutdown procedures are not widely available (Fernholz et al., 2000). This is because in most cases the target of the design process was a continuous production unit so the start-up and shut down phases of the unit were not considered to be of great importance at the early stages of development. Start-up

and shut down of the unit are ignored by Cuille and Reklaitis (1986), while Scenna and et al. (1998) considered the simulation of start-up procedures in RD columns but there was no comparison with experimental data.

2.5 Esterification

Reactive distillation was first described as a method for the continuous production of esters (Backhaus, 1921) and esterification has continued to be one of the main applications of reactive distillation in industry (Hiwale et al., 2004). The most well known study of successful application of reactive distillation is the Eastman Chemical Company process to make methyl acetate by esterification of methanol and acetic acid (Agreda et al., 1990).

2.5.1 Esterification: Background

A general, reversible esterification reaction between an acid and an alcohol is represented by the following simple expression:

$$\text{Acid} + \text{Alcohol} \Leftrightarrow \text{Ester} + \text{Water}$$

$$\text{RCOOH} + \text{HOR'} \Leftrightarrow \text{RCOOR'} + \text{HOH} \qquad (2.4)$$

Where R and R' are different alkyl groups. Leyes and Othmer (1945a) and Markley (1961) give descriptions of catalysed esterification reactions, in which the free hydrogen ion of an acid acts as a catalyst by combining with the alcoholic hydroxyl to form a complex:

$$\text{RCOOH} + \text{R'OH}_2^+ = \text{RCOOR'} + \text{H}_2\text{O}^+ \qquad (2.5)$$

Rate of formation of ester can therefore be described by:

$$d[\text{RCOOR'}]/dt = k_1\,[\text{RCOOH}][\text{R'OH}_2^+] \qquad (2.6)$$

Where R'OH_2^+ is the activated alcohol complex and k_1 is a rate constant (with units of $\text{Lmol}^{-1}\ \text{min}^{-1}$) and the performance of a catalyst depends upon its ability to cause the formation of the alcohol complex (Leyes and Othmer, 1945a). However, Liu et al. (2006) describe the process as the protonation of the carbonyl oxygen of the carboxylic acid group by the acid catalyst, which enables nucleophilic attack by the alcohol. Both sources agree that the rate-limiting step occurs more slowly if there are fewer activated species available. Water has an inhibiting effect on the reaction, as it reduces the availability of free hydrogen ions (Markley, 1961 and Liu et al. 2006). This reduces the rate of the forward reaction and an equilibrium balance exists, believed by Markley to be between the alcohol and water complexes, with an equilibrium constant given by:

$$K = [H_3O^+][ROH] / [ROH_2^+][H_2O] \quad (2.7)$$

Water is so effective at inhibiting the reaction because as a polar molecule it is able to orientate itself to oppose the electronic field caused by a cation, so the protons become engulfed in a self-arranging network of water molecules (Liu et al. 2006). The use of reactive distillation to remove water produced during the esterification reaction may potentially reduce this inhibition.

2.5.2 Long Chain Fatty Acids

Hiwale et al. (2004) give an overview of industrially important esterification reactions for reactive distillation. There have been many developments and studies investigating the esterification of short-chain carboxylic acids, but very little information is available in open literature for the esterification of long chain fatty acids (Tesser et al., 2005). The esters of long chain fatty acids have many different applications, from fragrances and flavours to fuel additives. They are also important as chemical intermediates (Steinigeweg and Gmehling, 2003). Direct esterification is preferred to trans-esterification as a route to the production of specific, desired esters (Gervajio, 2005). An example on an important long chain ester is n-butyl oleate, which can be used as a biodiesel additive to prevent clogging problems encountered at low temperature due to the high cloud point of biodiesel (Salis et al., 2005). Other uses of butyl oleate include: a PVC plasticizer, a water-resisting agent and as a component in hydraulic fluids (Ghamgui et al., 2004).

Othmer and Rao (1950) published a study of the kinetics of the production of n-butyl oleate via esterification of oleic acid and n-butanol, using sulfuric acid as the catalyst. The effects studied were: the molar ratio of n-butanol to oleic acid (B/A), the catalyst concentration (0 to 2.85% H_2SO_4), and the reaction temperature (80 to 100˚C). One parameter was varied at a time while the other parameters were kept constant: a total of 18 experiments were performed, and the raw data is supplied. The variation of density with temperature was also studied for n-butyl oleate and oleic acid, as this was not previously available in literature. The performance of the system was reported in terms of the conversions achieved and also the reaction rate constants for each set of conditions. This paper also discussed the side reaction between sulfuric acid and butanol, in which butyl sulfuric acid is formed. This reaction had been observed in an

earlier study by the same research group (Leyes and Othmer, 1945a). The rate of this reaction depends upon the temperature: at 100˚C it is very fast, so above this temperature the catalyst was considered to be a mixture of sulfuric acid and butyl sulfuric acid.

Ling and Geankoplis (1958) studied of the esterification of oleic acid with isobutyl alcohol focussing on the effect of the same variables: the molar ratio of alcohol to oleic acid, catalyst concentration and reaction temperature. Comparison with the results of Othmer and Rao showed that, without catalyst, steric hindrance due to the isobutanol slowed the reaction compared to the normal alcohol. However, when sulfuric acid catalyst was used, the reaction with isobutanol was slightly faster. Both groups developed an empirical equation for estimating the rate constants within the range of conditions studied.

2.5.3 Connection to Biodiesel Production

Much recent work has been linked to the recent research drive to enable the conversion of materials such waste vegetable oil into biodiesel, which is generally produced by transesterification of triglycerides into fatty acid methyl esters (FAME). The triglycerides can be found from many sources such as vegetable or palm oil but unless high purity oil is used, additional pre-treatments stages are required (Tesser et al., 2005). Poor quality vegetable oil contains higher levels of free fatty acids (Sendzikiene et al., 2004) which are usually esterified before the transesterification process is undertaken. Reducing the cost or eliminating this stage of the process would make biodiesel a more realistic option for the replacement of fossil fuels, so much research has been conducted in this area.

For example, Sendzikiene et al. (2004) studied the kinetics of the esterification of free fatty acids with methanol and aimed to increase the competitiveness of the biodiesel process by focussing on achieving the highest possible reaction rate. The use of alkaline catalysts (potassium and sodium hydroxides) had shown some promise as a good option for fast reaction, but the performance of these alkaline catalysts is affected by any moisture or free acidity. This is because water and free fatty acids react with the catalysts, allowing undesirable long-chain soaps to form (Tesser et al. 2005). Sulfuric and hydrochloric acids are the most well-studied liquid acid catalysts for the single step

acid-catalysed transesterification reaction (Lam et al. 2010). Detailed reviews on this subject are available: Melero et al. (2009) provide a review of solid acid catalysts suitable for biodiesel production, while Lam et al. (2010) focus on the development of the process to utilise waste cooking oil.

2.6 Catalysts for Esterification

Catalysts have been found to be essential for many esterification systems in reactive distillation. Since the Eastman methyl acetate process was developed (Agreda et al., 1990), reactive distillation processes have often employed a catalyst, such as solid catalytic packing (Towler and Frey, 2000). In the following section, literature relating to catalysts used for the esterification of long chain aliphatic fatty acids has been considered.

2.6.1 Strong Homogeneous Acids

Strong homogeneous acids, particularly sulfuric acid, are the most frequently used catalysts but downstream separation is required to get good purity of product and recover the catalyst (Peters et al. 2006). Sulfuric acid is used as the benchmark to which any new catalysts are compared (Harmer et al. 1998 and Kiss et al. 2006b). Markley (1961) discussed the catalysts used for the esterification of long chain fatty acids, stating that hydrochloric acid is occasionally used in laboratory studies, but it is considered too corrosive for industrial equipment. A further disadvantage to the use of hydrochloric acid is that it can lead to undesirable alkyl chloride side products forming if the esterification is slow. Side reactions can also occur when sulfuric acid is used, for example Markley (1961) identifies that tertiary and secondary alcohols can be dehydrated to form olefins or could even form polymers.

Other acid catalysts suggested as alternatives to sulfuric acid are phosphoric and sulfonic acids (Sendzikiene et al., 2004), and Markley (1961) additionally suggested use of aromatic sulfonic acids, e.g. benzene-sulfonic and p-toluenesulfonic acid (PTSA) for catalysis of esterification. Peters et al. (2006) considered PTSA as a catalyst for their reaction system, but also identified that the problems related to sulfuric acid (corrosion, side reactions, difficult separation) also apply to PTSA.

2.6.2 Heteropoly Acids

The heteropoly compounds phosphotungstic acid and phosphomolybdic acid are described by Lam et al. (2010) as "strong, water tolerant Brønsted acid" catalysts that are highly active and available from commercial suppliers. They are also soluble in the organic reaction mixtures encountered in processes for the production of biodiesel. Phosphomolybdic acid was included in the study by Peters et al. (2006) for comparison to commercially available solid acid catalysts, for esterification of acetic acid and butanol, and appeared to give fairly good activity. Kiss et al. (2008a and 2008b) found that phosphomolybdic acid also had high activity for the esterification of dodecanoic acid with methanol, but was too soluble in water (200g/100g). The authors also prepared and tested the caesium salt of phosphomolybdic acid, which was insoluble in water but much less active.

Juan et al. (2007) reported high catalytic activity with a supported phosphotungstic acid (also called 12-Tungstophosphoric acid) for the esterification of lauric acid (a long chain fatty acid). The support used is known as MCM-41 and has a high surface area, high thermal stability and large pores, which are desirable for reactions involving large molecules. Kulkarni et al. (2006) tested 12-Tungstophosphoric acid on four different support materials for catalytic activity in the production of biodiesel from oil high in free fatty acids. Hydrous zirconia was the support in the case which gave the best yield of ester, compared to the others which used silica, alumina and activated carbon. Tests were also performed to find the optimum operating conditions for the catalyst and assess its reusability.

2.6.3 Superacids

Candidate catalysts with 'superacid' properties are those that are claimed to be able to achieve acid strength equivalent to that of sulfuric acid (Harmer et al. 1998). However, acid strength is not the only property of importance to catalyst activity; the type of acid activity required for the particular application should also be considered. Solid superacids may have a combination of Lewis and Brønsted acid sites upon the surface, and a solid catalyst that is not a strong acid may be powerful enough to activate a key step in a reaction mechanism. Fărcaşiu et al. (1996) discussed some of the controversies regarding classification and comparison of different acid types.

Sulfated Zirconium Hydroxide

Sulfated zirconium hydroxide was considered as a candidate catalyst for esterification by Peters et al. (2006) and the researchers at the University of Amsterdam (Omota et al. 2003b, Kiss et al. 2006, 2008a and 2008b). The performance of sulfated zirconium hydroxide was good compared to the other solid acid catalysts considered, and it exhibited good thermal stability. It also has the advantage that it is commercially available and therefore the cost is reasonable compared to more obscure candidates that would have to be custom-made. There was no loss of activity due to sulfate groups escaping from the catalyst, but the presence of water caused loss of activity (Omota et al. 2003b).

Peters et al. (2006) studied the effect of the calcination temperature on the number and type of acid sites on the surface available for catalytic activity. The properties of the catalyst were very strongly dependent upon the preparation conditions, and an optimum calcination temperature to achieve catalytic activity was found at 525°C. The activity of the catalyst was noticed to decrease as the reaction progressed, the authors suggested that this could be due to deactivation by water or loss of sulfur groups, however the catalyst was able to be recovered and re-used with a similar activity to the initial run. Furuta et al. (2004) reported that sulfated zirconia had a high acid strength, but low activity below 120°C for the esterification of n-octanoic acid and methanol.

It is not universally accepted that sulfated zirconia compounds should be described as ‘superacids’ (Omota et al. 2003b). For example, Fărcaşiu et al. (1996) reported that for reactions with hydrocarbons, sulfated zirconia acts as an oxidation reagent, rather than as an acid catalyst as expected, because no covalent bond is formed during the interaction.

Niobium oxide

Niobium oxide has received some attention as it can be a highly active catalyst. Peters et al. (2006) described niobium oxide as the most promising superacid, but their study found that the catalytic activity for the reaction of acetic acid and butanol was quite low. The authors suggested that this may be due to the relatively high abundances of Lewis acid sites compared to Brønsted acid sites on the surface. Kiss et al. (2008b) tested niobium oxide for the esterification of dodecanoic acid and 2-ethyl hexanol, and found

that the performance was quite similar to that observed with sulfated zirconium hydroxide.

Other Sulfated Metal Oxides

In addition to sulfated zirconia, the other sulfated metal oxides investigated by Kiss et al. (2006b) were sulfated titania and sulfated tin oxide. They were found to have good activity and pores that were sufficiently large for mass transfer of long chain molecules. Of the metal oxides included in this study, sulfated zirconia had the lowest cost, while Furuta et al. (2004) found that sulfated tin oxide was more active than sulfated zirconia but would be more expensive to use on an industrial scale. Tests indicated that sulfated tin oxide had a higher acid strength than sulfated zirconia and a narrower range of acid strengths at the active sites.

2.6.4 Zeolites

Zeolites are solid acid catalysts with a porous structure, very high surface area and many active sites. They are generally composed of oxides of the metals Al, Si, and Ti (Rothenberg, 2008a), and many of their properties (catalytic activity, surface hydrophobicity) are related to their composition, in particular to the ratio of Si to Al (Kiss et al. 2006b and 2006c). The properties of zeolites are also strongly affected by the preparation conditions used, and this can enable some control over their character (Zielinska-Nadolska et al., 2006).

Hydrophobic high silica zeolites are good catalysts for esterification of short chain acids and short chain alcohols such as ethanol, but their small pore size limits their use even with acetic acid and isobutanol (Okuhara, 2002). They are therefore unsuitable for use with long-chain molecules, as was confirmed by Kiss et al. (2006b and 2006c) when they included three types of zeolites (Y, H-ZSM-5, and Beta) in a study of the esterification of dodecanoic acid.

2.6.5 Metal Acetates and Stearates

A range of metal acetates and stearates were tested at 200°C by Di Serio et al. (2005) as catalysts for the production of biodiesel from methanol and soybean oil, with 0.2wt% free fatty acids content. The most active metal acetates and stearates were found to be those with the following metal centres: Cd, Pb, Zn and Mn. The stearates were found to

be more active than the acetates, and the authors suggested that this was due to better solubility of stearates in the oily mixture. The authors stated that every pair of reactants would be likely to have one specific metal centre that would give optimum performance. Previous work by these authors included testing acetates of the metals Zn, Cd, Co, Mg, and Mn as catalysts for the transesterification of dimethylterephtalate (DMT). In that study, Mn appeared to give the highest activity (Di Serio et al. 1998), while a mixture of Mg, Mn and Zn acetates had previously shown higher activity than the individual components (Di Serio et al. 1996).

S. Y. Chin et al. (2006) tested supported zinc acetate complexes as catalysts for the esterification of long-chain palmitic acid with isopropanol. The catalysts were shown to be thermally stable and they were also active and had large enough pores and surface area to give good performance. Bhatia et al. (2006a) continued this work and successfully tested zinc acetate supported on silica gel as a solid catalyst for the same reaction in a continuous reactive distillation pilot unit. Zinc acetate is a divalent metal ion, and is thought to act as a Lewis acid catalyst by causing co-ordination of the palmitic acid carbonyl group with the positively charged metal ion (Zn^{2+}). The shift in electron density from the carbonyl group to the metal ion allows the carbonyl to interact with the nucleophilic oxygen atom of the isopropanol, triggering the first step in the esterification reaction (S. Y. Chin et al. 2006).

The high temperatures generally required when using metal salts could be an issue. Wang et al. (2007) described the findings from an earlier study in a Chinese-language journal where carboxylic salts were tested for the esterification of free fatty acids and it was found that high temperatures were needed (around 200°C) to give 90% conversion. Parshall and Ittel (1992) noted that metal salts that are successful as catalysts for transesterification tend not to be as effective for direct esterification. These authors also give information relating to the order of activity of metal salts for two cases where 'extensive screening' was performed. For the first case, the esterification of ethylene glycol and benzoic acid, the order of activity of metal centres is:

$$Ti^{4+} > Sn^{2+} > Sn^{4+} > Bi^{3+} > Zn^{2+} > Pb^{2+}, Sb^{3+} > Al^{3+}, Mn^{2+} > Co^{2+} > Cd^{2+} > Mg^{2+}$$

The second case was the esterification of ethylene glycol and terephthalic acid, in which case the order of activities became:

$$Sn^{2+} > Ti^{4+} >> Zn^{2+} > Pb^{2+}, Co^{2+}, Cd^{2+}$$

This difference in the order of activities is in line with the theory of Di Serio et al. (2005) that each reaction system catalysed by a metal salt would have one 'optimum' candidate.

2.6.6 Metal Sulfates

Wang et al. (2007) describe a two-step process for the manufacture of biodiesel, the first step of which is the esterification of methanol and free fatty acids from waste cooking oil. The catalyst used for this first step was ferric sulphate, which was found to show high catalytic activity, and was easily recovered as it is insoluble in the oil. A conversion of 97% was achieved under the optimum conditions. The catalyst could be recovered by centrifuge and re-used. Extensive preliminary work on the development of the experimental procedure was performed (Wang et al., 2006). Further previous work by this group is in Chinese-language journals, but the catalysis of the esterification of aromatic carboxylic acids by ferric sulfate hydrates was described earlier by Zhang (1999).

2.6.7 Ion Exchange Resins

The two commercially available ion exchange resins were studied by Kiss et al. (2006b): Amberlyst-15 and Nafion-NR50. They were found to have good catalytic activity for the esterification of dodecanoic acid with a variety of alcohols, but poor thermal stability at higher temperatures (up to 160°C). Tesser et al. (2005) used a heterogeneous ion exchange polymeric resin known as Relite CFS as a catalyst for the esterification of oleic acid and methanol. The catalyst is produced by Resindon, and it is a cation exchange resin with sulfonic active groups and a Styrene-DVB porous copolymer matrix. The catalyst itself is produced as stable, insoluble, spherical beads (S.R.L. Resindon, 2006). The main advantage of using a heterogeneous (solid) catalyst is that no further separation is required to recover the catalyst from the reaction mixture.

Marchetti et al. (2007) used a mixture of oleic acid and soybean oil to simulate waste cooking oil. They tested two catalyst resins for the esterification step for the production of biodiesel: Dowex monosphere 550A and Dowex Upcore Mono A-625. The conversion achieved using Dowex monosphere 550A was around 80% in 3 hours, which was considerably higher than the A-625. However, poor re-usability was reported: when the catalyst was re-used the conversion achieved dropped to around 25%

in 3 hours. Pasias et al. (2006) used a real feedstock of waste oil rather than a 'model mixture' and a PUROLITE polystyrensulfonic acid catalyst, manufactured by Purolite International Limited. It is insoluble in oil and water and therefore easy to separate from the reaction mixture. The performance was relatively low, with a conversion using fresh catalyst of around 70% after 12 hours at 110˚C.

2.6.8 Mixed Catalysts

Twitchell's reagent, which is 'a sulfonated mixture of oleic or other fatty acid and naphthalene' (Gervajio, 2005), was reviewed as a catalyst for the esterification of fatty acids by Markley (1961). Its main industrial use was for fat splitting but this has declined, superseded by more efficient processes. Twitchell's reagent was found to be effective for esterification of a variety of fatty acids with low molecular weight alcohols but not effective for longer chain fatty acids. A mixed catalyst of ferric sulfate and sulfuric acid was tested by Xu et al. (2001) for the esterification of aromatic acids with short chain alcohols. They reported that the mixed catalyst gave better performance than either catalyst alone.

2.6.9 Lipases

Lipases have been found to catalyse some esterification reactions and there is an increasing amount of literature available on this topic. As biological agents, they are able to function under mild conditions, which could present an advantage in terms of heating requirements and therefore costs. Lipases are also able to display high selectivity, for example between the cis and trans isomers of 9-octadecanoic acid, oleic and elaidic acid (Borgdorf and Warwel, 1999).

Salis et al. (2005) tested the performance of four immobilised lipases for the reaction of triolein (triglyceride formed from oleic acid) with short chain alcohols to produce butyl oleate. *Pseudomonas cepacia* lipase was found to show excellent performance: 100% conversion was reported after 6hr. Linko et al. (1998) screened 25 commercially available lipases for the direct esterification of butanol and oleic acid at 37˚C, and found that, even without additional water, *Chromobacterium viscosum* lipase yielded 98% n-butyl oleate in 12hr with 1 butanol excess. *Candida rugosa* lipase gave both high yield and good cost/benefit ratio.

The conversion of vegetable oil triglycerides into biodiesel took 34 hours to reach 97.3% conversion when lipases were used (Wang et al. 2007). The rates of reaction with lipases are generally slow compared to more conventional catalytic systems, and lipases can be sensitive to alcohol. Use of biocatalysts can be more expensive than traditional catalysts, so the lipases must be recycled to prevent excessive costs. This would probably not be possible if lipases were tested under reactive distillation conditions, as the high temperatures required to achieve boiling point would cause degradation.

2.6.10 Other Esterification Catalysts

Other, more unusual catalysts described for esterification reactions include the use of surfactant-combined catalysts dodecylbenzene sulfonic acid (DBSA) and copper dodecylbenzene sulfonate (CDBS). These candidates are able to self-assemble into reverse micelles in an organic reaction mixture, with the hydrophobic, organic phase on the outside and a hydrophilic region on the inside (Gang et al. 2007). In addition to the large surface area available for acid-catalysed reactions, an extra benefit of this is that any water formed is taken into the centre of the micelles, and so the equilibrium reaction is shifted towards increased formation of products. Esterification of carboxylic acids at room temperature was most successful when the reactants or the ester were insoluble in water.

Diarylammonium salts were considered for the catalysis of oleic acid and methanol (Zafiropoulos et al. 2007). These candidates gave very high conversion, even comparable to sulfuric acid, and the authors also found that the immobilised version gave good performance, with easier recovery and reactivation. Tang et al. (1999) described the use of rare earth sulfates for the esterification of phthalic anhydride and butanol, producing a large ester molecule. The sulfates of: Y, La, Ce, Pr, Nd, Sm, Dy, Eu, and Tb were tested and gave quite good performance, with Ce sulfate appearing to be the best. Like some of the candidates discussed previously, these are affected by the temperature of any pre-treatment and also by the presence of water of hydration.

Another class of catalysts that is likely to see further development in the future is that of metal nanoparticles, which it is hoped will enable researchers to close the gap between homogeneous and heterogeneous catalysis (Rothenberg, 2010). Metal nanoparticles of 1

to 5nm were found to be very active as catalysts and able to be removed from the reaction mixture by filtration (Witham et al., 2010)

2.7 Process Development for Esterification of Long Chain Fatty Acids by Reactive Distillation

2.7.1 Esterification of Long Chain Fatty Acids by RD

In many esterification reactions currently performed by reactive distillation, such as the methyl acetate process, the ester product is the most volatile component in the mixture, allowing it to move up the column and be removed as distillate (Spatschek, 1995). However, the esters of long chain fatty acids have high molecular weights and therefore high boiling points, so they are more likely to be recovered as bottoms products. The high temperatures that would be required for boiling long chain fatty acids would require huge amounts of energy and may have adverse effects, for example on catalyst activity. The focus of an important area of research has been to find efficient entrainers for these systems (Hiwale et al., 2004; Dimian et al. 2004). Examples of esterification of long chain fatty acids by reactive distillation are not widespread in literature (Steinigeweg and Gmehling, 2003), but their numbers are increasing as the advantage of removing water to shift the equilibrium towards higher formation of ester products is realised (Bhatia et al. 2006).

Brock et al. (1997) discuss simulations of the esterification of myristic acid with isopropanol. A continuous counter-current reactive distillation column is utilized, where isopropyl myristate is recovered as bottoms product. The column temperature ranged from around 130˚C to 155˚C. No discussion of any catalyst is given within this paper: the system is described as sluggish, but the conversion (99%) and purity of the products were reported to be very high. No reflux was used, as it was felt that this would cause the temperature in the column to fall.

Steinigeweg and Gmehling (2003) studied the esterification of decanoic acid with methanol in a pilot-scale counter-current column where the ester methyl decanoate was the bottoms product and water was removed as distillate. Two types of column packing manufactured by Sulzer Chemtech were tested for performance with Amberlyst-15 installed in the packing sections. The operating conditions of the column were also investigated: reflux ratio and reactant ratio were varied, but temperature

studies were limited due to safety requirements. Reaction kinetics were first studied in a lab scale (500ml) batch glass reactor, and a detailed pseudohomogeneous kinetic model using the Langmuir-Hinshelwool-Hougen-Watson method was developed, which accounted for water sorbtion on the catalyst surface. Experimental data validated the simulation and indicated that for this system Katapak S showed greatest performance. A small reflux ratio of 0.01 was used to give high conversion, and a feed ratio of decanoic acid to methanol of 1:2 was used.

Kumar and Mahajani (2007) investigated the esterification of dilute lactic acid with butanol with heterogeneous catalyst (Amberlyst-15). They began by defining an 'ideal' kinetic model and establishing kinetic parameters through tests in the lab, before using these parameters to simulate reactive distillation using Aspen software. The results of the simulations were compared with experimental data from both a batch reactive distillation unit and a continuous unit, making this a very unusual study. The single stage distillation for the batch experiments was composed of a condenser and a Dean-Stark separation, rather than a distillation column. The pot temperature during the batch reactive distillation was 90 to 130°C, which is a significant mismatch with the kinetic experiments, which were performed at 45 to 96°C. However, the authors found that the models built on the kinetic parameters obtained matched the data from the continuous RD unit quite well, and high conversions were achieved.

Yang et al. (2007) focussed on batch reactive distillation, this time for the esterification of acrylic acid and 1,4-butanediol, catalysed by Amberlyst-15. The reaction kinetics were studied at 100°C and atmospheric pressure (760mmHg), before the reactive distillation process was investigated using the same molar ratios of reactants, catalyst loading, and temperature. The separation column used in these studies had a 1 inch diameter and was 150cm tall, packed with glass beads. The column was placed above the 1L pot, where the reactions took place. Temperature increases were observed in the pot when long-chain, high-boiling point polymers began to form. To prevent thermal damage to the desired product, the reactive distillation was performed under vacuum (600mmHg). The authors had difficulty achieving their target of complete reaction of butanediol due to the sequential polymerisation reactions.

In the study by Schmitt et al. (2008), hexyl acetate was produced by the esterification of hexanol and acetic acid in reactive distillation. Two continuous counterflow columns

were used: a lab scale column with a column of 55mm inner diameter and a larger pilot scale unit of 162mm diameter column, both with the catalytic packing Amberlyst CSP2. This allowed observation of scale up effects, and it was found that the kinetic parameters determined through bench-top experiments were not sufficient to accurately simulate the behaviour under reactive distillation, even for the smaller lab scale column. A significant 'mass transfer factor' was required to account for the behaviour of the liquid as it passed over the packing. The same mass transfer factor was used for the pilot scale simulations, which matched the experimental data reasonably well, but the authors were not able to demonstrate from the experimental data that this was an optimal value on the larger scale.

2.7.2 Process Development Approaches

Steinigeweg and Gmehling (2003) gave a description of steps recommended for the development of a reactive distillation system. Reaction feasibility is evaluated through thermodynamic analysis, before reaction kinetics are investigated in bench-top experiments under suitable conditions. This information is then used in simulations to determine the factors which are expected to have the greatest effect on the performance of the column. Experimental data is required to validate the simulations, but the model can then be used to target and reduce the experimental work required.

There is a lack of open literature studies where a range of catalysts have been studied under reactive distillation conditions and compared in terms of behaviour and performance. Studies involving reactive distillation and catalysts have tended to select one catalyst, from a range screened at bench scale, and then develop a reactive distillation process from this point. The following section describes the work of two groups of researchers who have taken this type of approach to develop reactive distillation processes for the continuous esterification of long chain fatty acids, and highlights the different approaches that can be taken towards the development of new reactive distillation processes.

One of these research groups is located at the University of Amsterdam in the Netherlands. This series of papers begins with a conceptual design for a reactive distillation system for general esterification of long chain fatty acids (Omota et al. 2003a). The initial feasibility of the system was investigated using an equilibrium based

model where the reaction was assumed to be fast, implying that reaction equilibrium was assumed to be achieved on each stage. This study was used to set the targets for further development and experimental work. A follow up study (Omota et al. 2003b) described the development of a kinetics-based model where the rates of reaction of dodecanoic acid and 2-ethylhexanol with a sulfated zirconia catalyst were included and Arrhenius constants were calculated to represent the variation of reaction rate with temperature. The rate based model had to be adjusted with the inclusion of an equilibrium constant based on liquid activity coefficients, in order to take into account that the reaction mixture was highly non-ideal, with possible liquid-liquid phase separation.

The team gave a proposed outline procedure for the development of reactive distillation processes where the development of a new suitable catalyst is necessary (Kiss et al. 2006a). It was noted that both experiments and simulations are required during the development scheme, but the conditions that the new catalysts are tested under are generally not the same as the operating conditions of the eventual production unit. To mitigate this, a plan was developed to link the information from both experiments and simulations in an iterative workflow. In the proposed scheme the catalyst performance requirements (in terms of the achieved rate of reaction) are determined by simulations and economic analysis of the conceptual process design. Catalyst synthesis and characterisation are time-consuming and non-trivial tasks, so fast catalyst screening experiments are performed to identify a shortlist of promising candidates for further development. The design is gradually updated as new information becomes available.

The focus of the work by this research group shifted to processes for the production of biodiesel, with the aim of developing a solid acid catalyst that would enable the process to be performed by reactive distillation. This would achieve an intensified process that would remove the water product from the reaction mixture, shifting the equilibrium in favour of more ester, and avoiding additional neutralisation and separation steps needed with homogeneous catalyst (Kiss et al. 2006b). Candidate catalysts were synthesized, characterised and tested at bench scale for activity in esterification of dodecanioc acid + methanol, propanol and 2ethyl hexanol. The variety of alcohols used allowed determination of whether the candidate catalysts would be suitable for a range of esterification reactions, and a set of beneficial properties were identified for suitable solid acid catalysts. The range of catalysts tested was later widened (Kiss et al. 2006c:

Kiss et al. 2008b) with a number of metal oxide compounds considered. The chosen catalyst was sulfated zirconia, which was favoured as a compromise between giving high activity with practical issues such as availability and cost. The team also looked at factors that affect the activity of solid acid catalysts, including the intraparticle pore size, surface hydrophobicity, and calcination temperature used in the production process. The bench-top unit used to perform these experiments was a STEM Omni Reacto Station with six parallel 100ml reactors.

The aim of the studies remained the same, seeking to find a solid acid catalyst that would reduce the costs involved in an overall design for a continuous production process. The process was optimised using Aspen Plus simulations to refine the design and implement heat recovery (Kiss et al. 2008a). Comparisons with this refined model were made against the original 'base case' revealed that the addition of heat recovery made the process more economically viable. The design proposed at the end of this was a multifunctional plant with high productivity and low equipment and operating costs compared to a conventional batch esterification process.

During this series of papers, there were no pilot scale experiments described, so the catalysts were tested only at the bench scale and there were no comparisons of the catalysts under reactive distillation conditions. For the final design produced, there was a high reliance upon the outcomes of the simulations and upon the assumption that the kinetic data obtained at bench scale could be applied to the reactive distillation unit. However, the team have connections with a private company, who are unlikely to publish commercially useful information, so it may not be possible to know whether a pilot plant based upon this work was ever built through study of the available literature. More recent work has involved simulating and developing control strategies for novel reactive distillation configurations, such as dual reactive distillation (Dimian et al. 2009), and integrating bioethanol and biodiesel production (Kiss et al. 2010).

A group at the Universiti Sains Malaysia also considered the development of reactive distillation processes for esterification. Their aim was the development of a heterogeneous catalyst for reactive distillation production of isopropyl palmitate, an ester that is used in personal care products and fine chemicals, and represents a value-added product that can be made from the country's plentiful palm oil supplies (S. Y. Chin et al. 2006). The focus of this research was to improve the efficiency of the ester

production process and to avoid high temperatures which can degrade the valuable product.

The team also began with lab scale catalyst tests, although a small number of catalysts from a narrow range of types were tested. Aafaqi et al. (2004) describe the study of heterogeneous zinc ethanoate coated on silica gel, which was compared against the homogeneous acid catalyst PTSA. The two candidates were tested across a wide range of conditions and different kinetic models were developed for them. The parameters for the homogeneous and heterogeneous kinetic models were mathematically obtained and the models gave a good fit against the experimental data. S. Y. Chin et al. (2006) gave a literature review of the similar catalysts already described in previous studies. They continued the focus on zinc-based catalysts, comparing the data from the previous work with silica-gel zinc catalyst with a new hybrid silica gel-succinic acid zinc acetate catalyst. The results were also compared with those in the literature review, and it was found that the new hybrid offered 'high activity' and had similar characteristics to those previously described. Again, a wide range of conditions were tested and parameters for a detailed kinetic model were fitted.

The work by this group that has been described so far was conducted in a 500ml batch reactor, but the team also moved on to perform experimental studies in a pilot scale reactive distillation unit (Bhatia et al. 2006a). This was a continuous, counterflow unit where the reactants were passed over catalyst held in the reactive zone of the column in Sulzer Katapak-SP packing. The catalytic packing was filled with the zinc acetate silica gel catalyst, which was the only catalyst tested in this column. There were also non-reactive sections of an alternative Sulzer packing above and below the catalyst. The experimental runs in the RD unit were long, 'nearly 15 hours', so any start-up and shut down phases were likely to be insignificant compared to the operation phase at steady state.

The authors noted that when the composition of the more volatile components was lower, the temperature in the reactive zone of the column increased. The performance of the unit was investigated and also how the performance was affected by factors such as the feed flow rate, the reboiler duty, feed composition, and the reflux ratio. The design was optimised for the one reaction system with one catalyst. Simulations with different model complexity revealed that a detailed rate-based model was required for

accurate representation of the unit. This was confirmed in a later paper which described much more simulation work in which the unit design and configuration was optimised. The unit was further improved through identification of suitable values for the operating parameters of the unit, including the column pressure, the distillate to feed ratio, the feed location, the catalyst loading in the column, and the height of the reactive zone.

Comparing the outline workflows for the development of RD processes from the two groups of authors, it can be seen that there are considerable differences. The Malaysian group put a much greater emphasis on pilot plant experiments to provide information and validation for their models aiming to design a full scale unit, while the Amsterdam group focus more upon simulation studies in their papers. However, both research teams quickly focus on one catalyst, chosen based upon the results of lab bench-scale studies, and this decision is carried forward in the subsequent development of the reactive distillation unit. Both groups used the Aspen Plus reactive distillation simulation tools as part of their process development, but neither group tested a wide range of catalysts under reactive distillation conditions.

The Amsterdam group see the main challenge in the development process as identifying a suitable active catalyst for the reaction (Kiss et al. 2006a), while the Malaysian group focus more on understanding the process through pilot scale tests. The proposed development workflow by the Amsterdam group was more complex, with feedback loops involving the catalyst composition development, performance screening and bench tests, and simulation studies. The link from the bench experiments to the final design does not appear to include pilot plant experimentation (Kiss et al. 2006a).

2.7.3 Screening Catalysts for Reactive Distillation

It is very rare to find published studies for the screening of new catalysts for use in reactive distillation systems, and none were found that involved the use of high throughput technology.

Several heterogeneous metallic catalysts for the dehydration of glycerol to acetol under reactive distillation conditions were studied by Chiu et al. (2006). Glycerol is a by-product of the process to manufacture biodiesel, the market value of which is decreasing due to the increasing number of biodiesel production plants starting up. By converting

glycerol into acetol, an intermediate for the production of propylene glycol, the authors' intention was to make the low-value waste product into a more useful substance that could be sold. The acetol has a lower boiling point than the glycerol, so it can be removed as distillate. In addition to shifting the equilibrium towards the formation of products, reactive distillation purifies the acetol and limits the reactor temperature, avoiding thermal degradation.

The reactive distillation experiments were performed at 240°C and 98kPa using a single stage unit, with the catalyst pre-loaded into the reactor, and the glycerol fed in during the run. The catalysts tested were commercially available, heterogeneous metals and mixed metal catalysts, and were used as supplied. The catalysts considered were: Mg/Alumina, Mg/Chromium, 5% Ru/C, 5% Ru/Alumina, 5% Pd/C, 5% Pt/C, 10% Pd/C, 20% Pd/C, alumina, copper, copper-chromite, Raney nickel, Ni/C, Ni/Silica-Alumina. The catalyst that gave 'outstanding' performance was a copper chromite mixed catalyst giving high selectivity of 86.6%. The chromite catalyst was also found to have good reusability: the conversion achieved after 5 runs was still around 85%. The performance was due to the mixed nature of the catalyst: the copper provided catalytic activity while the chromite stabilised the catalyst against sintering. This study had a number of limitations, such as the small reactor capacity of only 125ml, the lack of scale-up in the experimental work, and the lack of simulation work to build a model based upon the experimental results.

2.8 QSAR Tools

Studies involving many catalysts would be most useful if the activity and performance of the catalysts could be related to characteristics such as their composition. This would allow researchers to gain insight into what the most desirable characteristics are for effective catalysts. A tool that may be useful to achieve this understanding is the use of quantitative-structure-activity relationships (QSAR), which are used to correlate experimentally determined properties or attributes of compounds to representations of their molecular composition. Application of QSAR techniques is most widely found in the pharmaceutical industry, where companies apply them to quickly identify new candidates for development towards new drug products (Agrafiotis et al., 2007). QSAR models based on established experimental data can be used to build a model of a large variable space e.g. a wide range of candidates for a suitable catalyst ligand, allowing

researchers to identify regions that appear promising. The follow-up experimental screening work can then be much more focussed and efficient (Burello et al., 2005). A quick initial screen is often used to provide a qualitative guide to the relative performance of a set of candidate compounds, followed by more in depth, time-consuming quantitative analysis of a smaller range (Burello and Rothenberg, 2006).

QSAR techniques have been investigated by Avantium Technologies, who develop methodologies and workflows for molecular design, and have published a series of papers on this topic (Van der Linden et al., 2005). They describe some examples of successful application of QSAR, such as a study to predict the behaviour of substrates involved in hydrogenation of benzophenone systems with asymmetric catalysts under controlled conditions. Molecular descriptors for the substrates were related to their enantiomeric excess values, which are a measure of the asymmetry of the systems. The model was built using a training set of 13 benzophenones and a validation set of 69, and for each compound a variety of descriptor types (composition, geometrical and topological) were generated using DRAGON software. The results were consistent with the trends that were expected through knowledge of the chemistry of these systems, and the predictions obtained from the model were described as realistic.

A descriptor can be any quantitative numerical value derived from knowledge of a chemical structure (Katritzky and Fara, 2005). DRAGON software is a popular descriptor generation tool available from Talete srl, a company who specialise in QSAR and chemometrics (Tetko et al., 2005). E-Dragon is a version of DRAGON that is available on-line as the result of collaboration between several research groups, and is part of a set of on-line tools on the VCCLAB webpage (2005). E-Dragon can process up to 150 molecules per task (commercial versions of DRAGON for windows can run 50,000) and both versions of the software are able to generate thousands of descriptors: E-Dragon can produce more than 1600 (commercial versions more than 3000). Generally, however, it is not useful to include too many descriptors in a model; if there are more descriptor variables than experimental data points the model is described as over-defined. A minimum level of experimental data of 5 to 15% of the possible variable space was recommended by Maldonado and Rothenberg (2009).

Other tools available online include open source software produced by teams of researchers who aim to develop ‘web services’ for chemoinformatics (Guha et al. 2006),

which will open the field up to users who are not computer programmers or experts in the details of how the computational systems work. The Chemistry Development Kit (CDK) includes many tools which are useful throughout the application of chemoinformatics, from creation of molecule representations (SMILES), through to interaction with other Java based applications (Steinbeck et al., 2003).

Development of molecular descriptor generators and high throughput technology for rapid experimental screening have enabled QSAR techniques to be applied to an increasing range of fields. Process development, however, has been slow to benefit from these capabilities despite the demonstrated benefit from drug companies that development times can be shortened (Verspui et al. 2004). In addition to the pharmaceutical industry, other fields of application includes fuel properties science and screening of materials for sensor technologies. Katritzky and Fara (2005) describe studies where properties of interest to fuels science are related to the molecular structure. The prediction of boiling points is discussed, as well as the prediction of other properties including melting points and viscosity. Some properties relating to mixed substances were also included, such as flash point and solvent effects. Potyrailo and Mirsky (2008) reviewed the screening of materials for chemical and biological sensors, as parallel screening, robotics and high throughput technologies could drastically cut the time required to indentify suitable materials for a new application. The wide range of skills required to fully utilise these tools, and the type of potential applications, increase the importance of multidisciplinary teams and could potentially change the way much research in this field will be done in the future.

With increasing legislation relating to the safe handling and use of chemicals, such as REACH in Europe, understanding the effects of compounds on biological systems is increasingly important. Several studies which aimed to relate toxicity to chemical structure have been published (McKinney et al. 2000; Wolterbeek and Verburg, 2001; Martin et al. 2008). McKinney (2000) highlighted the usefulness of quantitative and qualitative structure-activity relationships in initial assessments of biological toxicity. Screening for toxicity now involves huge numbers of chemicals that must be tested in different mixtures and for different toxicity factors, based on minimal experimental data. Computer based models aim to understand how a chemical structure will interact with biological systems, revealing trends across groups of compounds which are more informative than looking at each in isolation. One limitation outlined by the authors of

this paper is that there is much less detailed knowledge about how compounds containing metals interact with biological systems, compared to organic compounds. Martin et al. (2008) included a small number of metals in their consideration of toxicity. They implemented a hierarchical clustering followed by QSAR within the clusters, with good prediction ability. This approach requires a very large data set with sufficient data points in each cluster to create a statistically valid QSAR model.

Wolterbeek and Verburg (2001) aimed to develop a way of using a fixed set of parameters to develop a relationship between metal properties and their toxicity. They also classified metals into groups (based upon their configuration, their interaction with certain ligands, their electronegativity and tendency to become polarised or form covalent bonds) but obtained poor results. The benefit of classification is that the resulting multi-level model can be more reliable than a single model which has been fitted over totally dissimilar compounds, but a disadvantage is that this model cannot be applied to any compounds that do not fall into one of the categories.

A second approach in this paper involved the building of generalisations across the widest range possible, to enable interpolation for unknown compounds. 'Ordering indices' were developed to give an idea of where a new compound is likely to fall in the order of toxicity. Metal oxidation state and solubility were found to have a significant impact on the results of toxicity tests, but it is very difficult to control these effectively during experimental work. Occhipinti et al. (2006) use non-trivial density functional theory derived molecular descriptors to predict the order of activity for organo-metallic ruthenium - based compounds as metathesis catalysts. However, transition metal compounds pose a particular problem as geometric and coordination number changes with temperature can alter the behaviour of transition metal compounds (Guidoni et al., 2002).

Rothenberg (2008b) described the generation and utilisation of 2D and 3D descriptors for homogeneous catalysts, and found that 2D descriptors are quicker and cheaper to generate, and in many cases an adequate model can be built from these, but 3D descriptors are needed when information about shape is crucial to capturing the behaviour of the molecule e.g. protein folding. In this paper Rothenberg also explained that there are currently no suitable descriptors for screening solid catalysts, although development work is continuing in this area. Activity on a surface does not depend only

on composition, but also on the types of active sites present (surface defects/metastable phases), and significant changes may occur with variations in temperature, pressure, or composition of the reaction mixture. Fărcaşiu et al. (2006) attempted to correlate catalytic activity of heterogeneous catalysts with their acidity, reported as the Hammett number. This approach was unsuccessful, even when the different surface areas of the catalysts were taken into account.

A very different approach to molecular modelling is taken by Cresset BioMolecular Discovery Limited, who have developed software which generates a representation of the fields around a molecule, rather than focussing on the atomic composition (Vinter and Rose, 2007). This is because the behaviour of many compounds of interest is due to the way in which they interact with other molecules. This is particularly true for biological systems, where there is strong focus on understanding the nature of the interaction step e.g. for pharmaceutical development. The basis for using the field model is that molecules with similar electronic fields will 'appear' similar to another interacting molecule, and so activity may be more successfully predicted by a representation of fields rather than atomic structure. Currently the main output from the software is a visual 3D template of the fields around a molecule, rather than numerical descriptors, however the software tools are being developed continuously and this may become an interesting new way of investigating new catalysts, particularly for homogeneous systems.

2.9 Summary and Motivation

The focus of the present investigation is a key challenge described by Malone and Doherty: the identification of effective catalysts. Esterification of long chain fatty acids by reactive distillation has been the subject of an increasing level of published research, including much work related to biodiesel production, but so far this has not included the screening of a range of catalysts for esterification to observe their behaviour under reactive distillation conditions.

The approach taken for this investigation is to bring together the facilities available in the School of Chemical Engineering and Advanced Materials at Newcastle University to investigate catalysts for the esterification of long chain fatty acids in reactive distillation. Experimental data will be obtained via parallel screening and tests

performed in a reactive distillation unit in order to develop tools and procedures. The experiments testing the catalysts for esterification of long chain fatty acids will be performed in a batch reactive distillation unit, where the reaction and the catalyst will be confined to the reboiler. Catalytic column packing is therefore not the focus of this study, but the identification of catalysts that can give good performance under the conditions of reactive distillation.

The dynamic simulation capabilities available at Newcastle will be utilised with a model of the unit built using BatchCAD^{TM} software. It has been shown in this review that reactive distillation models can range from highly complex, (which could be used to produce a general tool for utilisation in many systems) to very simplified (usually focussed on one particular application). The simulations used in this investigation are specifically directed towards understanding the observed behaviour, rather than the creation of a general, all-purpose model.

The behaviour of the catalysts during the experiments will be studied, with an attempt to use QSAR-type correlations to relate the observations to the catalyst composition. As indicated in this review, the descriptor generating tools that are currently available are not suitable for a study involving some types of molecules. This includes several types of catalysts that are used for esterification and that have been selected as candidates for testing in this work: heterogeneous catalysts, molecules that dissociate in solution and those that include unusual atoms such as niobium all cannot be processed by the available on line tools such as E-Dragon.

This review has identified that QSAR models which aim to simply classify catalysts into groups representing good and poor performance were relatively more successful. The current investigation will therefore focus on establishing a relative order of activity, and comparing performance relative to the case with no catalyst and to the most well established catalyst (H_2SO_4). Differences in behaviour between the different types of catalyst will also be a key factor.

Chapter 3: Development of Experimental Methods and Analysis for Catalyst Screening

3.1 Overview

This chapter describes the development of the method to perform screening experiments to gain insight on the effectiveness of a range of candidates to act as catalysts in a chosen esterification system. An overview of the equipment used is given, and the reasoning behind the choice of reaction system is explained. Preliminary experiments have been performed to establish suitable conditions, taking leads from studies described in the published literature. The equipment and materials used to perform this work are described, including the selected catalyst candidates. Consideration is given to the heat of reaction and to the development of the analysis methods used to follow the reaction progress. A summary of the catalyst screening experimental procedure and the automated ChemSpeed protocol are presented.

3.2 Introduction

Before a set of catalyst candidates can be compared for performance, a reaction system must be chosen and an experimental procedure must be developed. The facilities available for catalyst testing in the School of Chemical Engineering and Advanced Materials include a ChemSpeed SLT106 Synthesizer, bench-top apparatus and analytical facilities such as GCMS. The ChemSpeed machine is a complex piece of experimental apparatus, and determining how the experiments should be performed required some trial and error development, for example to establish the timings to be used in the protocol and in the settings used such as agitation rate. A suitable agitation rate is necessary to avoid the influence of mass transfer effects on the outcomes of the catalyst screening.

As discussed in the literature review in Chapter 2, there are many different types of catalyst that can be used to enhance esterification systems. A range of 20 diverse candidates have been selected and screened for activity in the chosen reaction system. It was essential that the analysis method used was be able to evaluate the performance of the catalysts over the full range of potential outcomes, from very poor conversion resulting in very little change in composition, to very high conversion, where almost all of the reactant may have been consumed. The esterification reaction used is an

equilibrium reaction, so the equilibrium point of the reaction is must be determined. The heat released by reaction is also evaluated through use of an established software tool, and if it is significantly high then this may impact upon the experimental procedure.

3.3 Equipment

3.3.1 ChemSpeed SLT 106 Synthesizer

The ChemSpeed SLT 106 Synthesizer is an automated robotic platform which is capable of performing multiple reactions in parallel. Controlled agitation and heating can be applied to sets of scaled-down batch reactors, which are fitted with condensers. The automated system follows a protocol entered by the user in a method file, performing tasks such as controlled dosing and sampling at prescribed times.

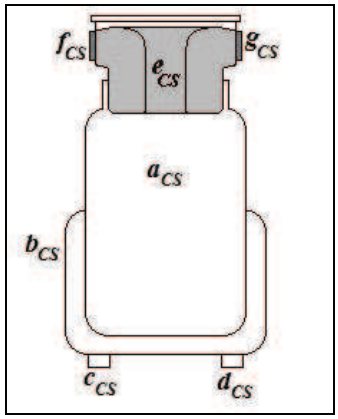

Figure 3.1: Individual ChemSpeed Reactor

Main features of the individual ChemSpeed Reactor illustrated in Figure 3.1:

a_{CS}	Glass Reactor (100ml)
b_{CS}	Oil Jacket
c_{CS}	Oil Inlet
d_{CS}	Oil Outlet
e_{CS}	Condenser
f_{CS}	Cooling Fluid Inlet
g_{CS}	Cooling Fluid Outlet

Samples are taken via a sampling needle on a robot arm, and which are then stored in vials in a sample rack. Above the condenser, a flexible connection attaches the reactor

to the control block, which holds the reactors in place and controls the mechanism for permitting the sampling needle to reach the reactors.

The reactors are loaded into the ChemSpeed Synthesizer in sets of four, sitting in a base which provides oscillatory agitation. This is illustrated in Figure 3.2, which is a photograph of a set of four reactors in place.

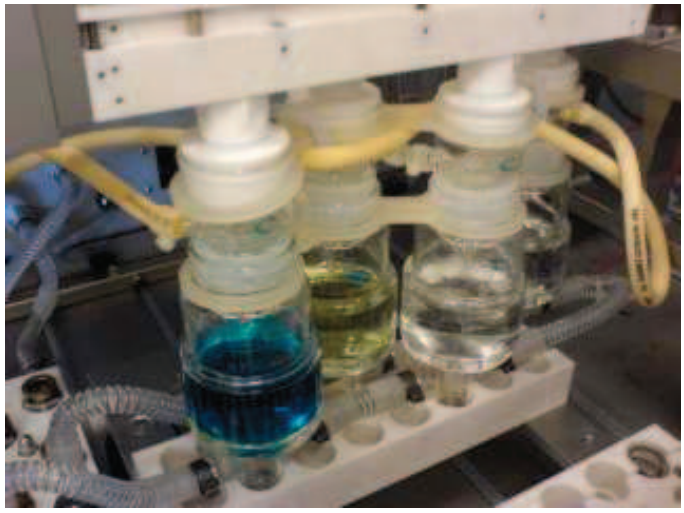

Figure 3.2: Set of four ChemSpeed Reactors Loaded into the ChemSpeed Synthesizer.

3.3.2 LyraChem Bench-Top Apparatus

A bench-top set up was used, with the kind permission of LyraChem Limited, for the study of equilibrium point. A small, round bottomed flask acts as the reaction vessel and a stopper prevents vapours from escaping from the closed system. The maximum recommended volume charge to the small reaction vessel is only 15 ml (Grosjean 2008), so it is not possible to take a large number of samples.

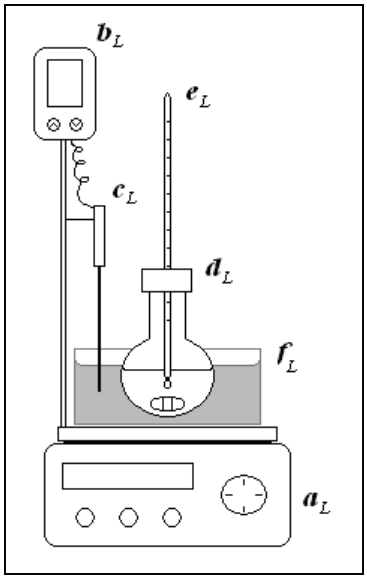

Figure 3.3: Bench-Top Apparatus for Study of Equilibrium Point

List of main features of the bench-top apparatus illustrated in Figure 3.3:

a_L	Heidolph MR Hei-Tec Magnetic Stirrer and Heater
b_L	EKT Hei-Con Temperature Controller
c_L	EKT Hei-Con Temperature Sensor
d_L	Glass round-bottomed flask and stopper
e_L	Lab Thermometer (76mm mercury filled)
f_L	Oil Bath

3.4 Chosen reaction system

3.4.1 Reaction Selection

The system chosen to be the case study used for this investigation is an esterification of a long chain saturated fatty acid. Fatty acid esters are important in the flavour and fragrance industry and in cosmetics. The general formula is as follows:

Acid + Alcohol ⇔ Ester + Water

Compared to unsaturated fatty acids, the range of molecules which are liquids at room temperature is small, due to low solidification temperatures. Table 3.1 shows the melting point data for a range of saturated fatty acids, taken from Sigma-Aldrich on-line MSDS sheets (2010). It can be observed that, from this series of molecules, the molecule with the longest carbon chain that would be in the liquid phase at room temperature is nonanoic acid. This is an important consideration when using the

ChemSpeed Synthesizer, as solidification of material in the narrow sampling tubes is undesirable.

Carboxylic Acid Name	**Formula**	**Molecular Weight**	**Melting Point °C**
Propanoic (Propionic) acid	$C_3H_6O_2$	74.08	- 24.0 to -23.0
Butanoic (Butyric) acid	$C_4H_8O_2$	88.11	-7 to -5
Pentanoic (Valeric) acid	$C_5H_{10}O_2$	102.13	-20 to -18
Hexanoic (Caproic) acid	$C_6H_{12}O_2$	116.16	-4
Heptanoic (Enanthic) acid	$C_7H_{14}O_2$	130.18	-10.5
Octanoic (Caprylic) acid	$C_8H_{16}O_2$	144.21	15 to 17
Nonanoic (Pelargic) acid	**$C_9H_{18}O_2$**	**158.24**	**9**
Decanoic (Capric) acid	$C_{10}H_{20}O_2$	172.26	27 to 32
Dodecanoic (Lauric) acid	$C_{12}H_{24}O_2$	200.32	44 to 46
Tetradecanoic (Myristic) acid	$C_{14}H_{28}O_2$	228.37	52 to 54
Hexadecanoic (Palmitic) acid	$C_{16}H_{32}O_2$	256.42	61 to 62.5
Octadecanoic (Stearic) acid	$C_{18}H_{36}O_2$	284.48	67 to 72

Table 3.1 Melting point data for a range of saturated fatty acids

The chosen reaction is:

Nonanoic Acid + n-Butanol ⇔ n-Butyl Nonanoate + Water

3.4.2 Preliminary ChemSpeed run with Nonanoic Acid

A 24 hour run was performed with the nonanoic acid-butanol reaction system in two of the ChemSpeed reactors (R1 and R3), with no added catalyst. The results are shown in Chart 3.1, where it can be observed that the reaction without catalyst is very slow, and did not reach completion. The data from there tests are shown in Appendix A, and information about the materials used can be found in Appendix B.

These runs were completed successfully, and the ChemSpeed was able to take samples at the pre-determined times without the tubes becoming blocked, confirming the suitability of nonanoic acid for use in the ChemSpeed machine. The similarity of the two concentration profiles indicates that the comparability between the reactors is good and the relatively slow pace of the uncatalysed reaction is useful, as it will be possible to distinguish between the effects of highly active catalysts.

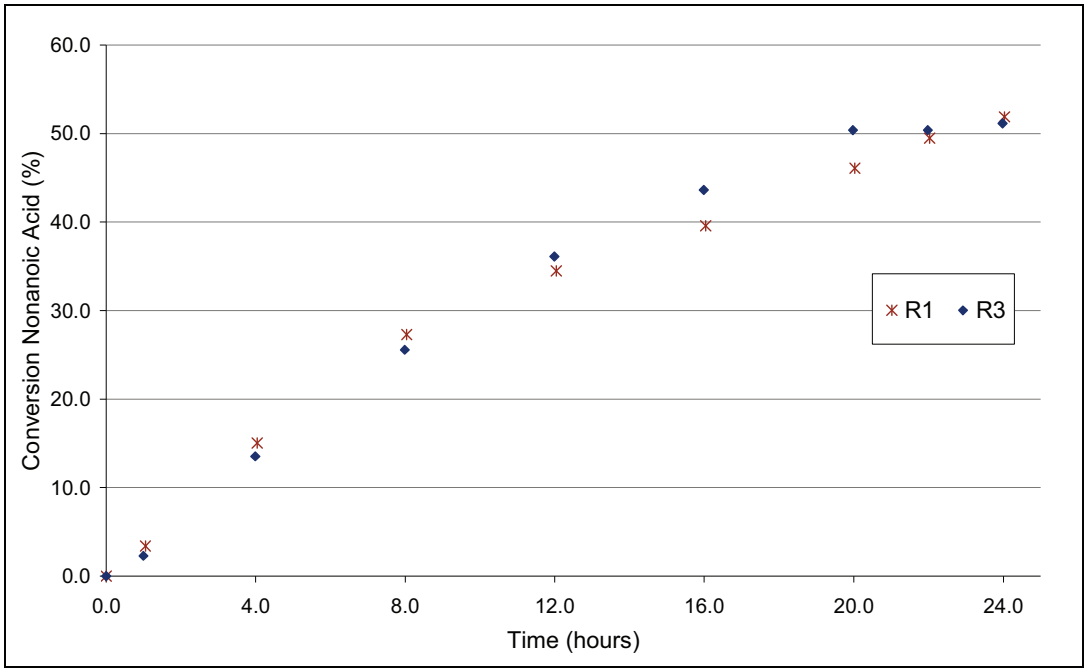

Chart 3.1: Trial nonanoic acid - butanol esterification in ChemSpeed Synthesizer.
(Temperature 100°C, 2:1 butanol molar excess, no catalyst, 700rpm agitation speed.)

3.4.3 Heat of Reaction

The theoretical standard enthalpy change of reaction was calculated for the esterification of nonanoic acid with butanol to form butyl nonanoate and water. The calculation was based on standard heats of formation taken from the BatchCAD database. The value obtained was:

$$\Delta H_R = -17.7 \text{ kJ/mol} = -4.2 \text{ kcal/mol}$$

This low exothermic heat of reaction was compared with values supplied by Novakovic (2007), which were computed using the ASTM CHETAH 8.0 software:

$$\Delta H_R = -4.77 \text{ kcal/mol at } 25°C \text{ and } -4.87 \text{ kcal/mol at } 100°C.$$

The value obtained by CHETAH for 25°C is quite close to that obtained by theoretical calculations, and the similar value for 100°C indicates that the heat of reaction for this system does not vary greatly with an increase in temperature.

A literature survey reveals three papers which report the heat of reaction of esterification of long chain fatty acids with an alcohol. Othmer and Rao (1950) studied the reaction between oleic acid and butanol, and reported a weight-based heat of reaction of -27 cal/kg, which is equivalent to the value of -0.02 kJ/mol (based on the weight of 1 mole of 50:50 reactant mixture), while Aafaqi et al. (2004) studied the esterification of palmitic acid and isopropanol, and reported an endothermic heat of

reaction of 7.98 kJ/mol (1.91 kcal/mol). Tesser et al. (2005) studied the reaction between oleic acid and methanol, and reported an experimental endothermic heat of reaction of 2.68 kcal/mol (11.21 kJ/mol), which was quite different to their theoretical calculation value of -0.67 kcal/mol (-2.80 kJ/mol).

The examples from literature above demonstrate that there can be some variability between experimental and theoretical values for the heat of reaction for an esterification. The values from the examples are all small in magnitude, indicating that the heat of reaction for this type of system is very mild. For comparison, the heat of reaction of potassium reacting with water is 198 kJ/mol (Ketchen and Wallace, 1951). The esterification of nonanoic acid appears to be more exothermic than the examples from literature, but still unlikely to affect the reaction or to require special consideration in terms of safety.

3.5 Candidate Catalysts

The starting point for the selection of catalyst candidates was a survey of the available literature regarding esterification studies involving catalysts. A similar approach was used by Kiss et al. (2008a), who based their catalyst choice on literature surveys and in-house tests conducted previously. In this paper, the team also describe an ideal catalyst as one that would be commercially available in large quantities at low cost. Peters et al. (2006) also focussed on commercially available catalysts.

Twenty catalyst candidates were identified for screening, and they are listed in Table 3.2, together with shortened ‘tag’ labels used throughout this study. Some candidates were chosen with the expectation of potential to act as catalysts for this system, based on the literature reports. These are indicated in Table 3.2 by the references to literature sources. Then, where potential candidates were readily available, the range of candidates was widened. Some of the additional candidates, such as the metal acetates, enable comparisons to be made within this group of candidates. The candidate catalysts were used in the form ‘as supplied’ by commercial vendors. Details of the commercial vendor, the grade and PubChem ID for each candidate catalyst included in this study are provided in Appendix B.

Candidate Catalyst	Name Tag	References
Bismuth (III) acetate	Bi Ac	
Copper (II) acetate monohydrate	Cu Ac	
Copper chromite	Cu chromite	Chiu et al. (2006)
Ferric sulfate hydrate (iron III)	FeSulf	Wang et al. (2006; 2007)
Hydrochloric acid	HCl	Markley (1961) ; Liu et al. (2006); Lam et al. (2010)
Hypophosphorous acid	HPA	
Lead (II) acetate trihydrate	Pb Ac	Di Serio et al. (2005)
Methane sulfonic acid	MSA	
Nickel (II) acetate tetrahydrate	Ni Ac	Di Serio et al. (2005)
Niobium (V) oxide	Nb oxide	Peters et al. (2006); Kiss et al. (2008b)
Phosphomolybdic acid hydrate	PhosMo	Peters et al. (2006); Lam et al. (2010)
Phosphotungstic acid hydrate	PhosW	Kiss et al. (2006b; 2008a)
Potassium acetate	K Ac	
PTSA monohydrate	PTSA	Markley (1961); Peters et al. (2006)
Sodium acetate trihydrate	Na Ac	
Sulfuric acid	H_2SO_4	Liu et al. (2006); Peters et al. (2006); Kiss et al. (2006b; 2008a) ; Lam et al. (2010)
Tin (II) acetate	Tin II Ac	
Tin (IV) acetate	Tin IV Ac	
Zinc acetate dihydrate	Zn Ac	Di Serio et al. (1996); S. Y. Chin et al. (2006); Bhatia et al. (2006a)
Zirconium (IV) hydroxide, sulfated	ZHS	Omota et al. (2003b); Furuta et al. (2004); Peters et al. (2006); Kiss et al. (2006b)

Table 3.2: Candidate catalyst names, shortened labels and references

The candidate catalysts fall in to several categories: homogeneous acids, heteropoly acids, metal acetates and 'others'. The homogeneous acids are the H_2SO_4, HCl, PTSA, MSA and HPA. Phosphomolybdic acid hydrate (PhosMo) and phosphotungstic acid hydrate (PhosW) are heteropoly acids, which have been identified as active for esterification, while ferric sulphate, niobium oxide, sulfated zirconium hydroxide and copper chromite are all described as heterogeneous catalysts in the literature studies.

Bismuth, lead, zinc, tin (II) and tin (IV) acetates are available commercially, and contain the metal centres indicated by Parshall and Ittel (1992) to have some activity for esterification. Other metal acetates (of Cu, K and Na) have been included for

comparison as they were readily available within the School of Chemical Engineering and Advanced Materials.

3.6 Analysis Methods

The behaviour of the different catalyst candidates was studied by sampling during the run and observing changing concentration profiles with time. The methods available to analyse composition were titration for nonanoic acid or GC analysis to evaluate the ester composition.

3.6.1 Titrations of Nonanoic Acid

The methodology for performing titrations to determine the nonanoic acid composition has three parts:

1) Standardisation of KOH solution.
Approximately 350mg of potassium hydrogen phthalate (KHP) was weighed out, to the nearest mg, into a 500ml conical flask. Then100ml of demineralised water was added, and the flask was stirred until the KHP was dissolved. Five drops of phenolphthalein (PP) indicator were then added before the mixture was titrated with a solution of solution potassium hydroxide (KOH) in methanol, to a permanent faint pink end point.

The normality (N_{KOH}, in mol/L) of the KOH solution is calculated by:

- $N_{KOH} = W_{KHP} / Mr_{KHP} \times V_{KOH}$ (3.1)

Where:

W_{KHP} = actual weight KHP, mg
V_{KOH} = volume of KOH used in the titration, ml
Mr_{KHP} = the molar mass of KHP (204.2 g/mol)

2) Acid number of nonanoic acid.
Acid number is the number of milligrams of potassium hydroxide needed to neutralise the acid in one gram of sample. Approximately 200mg (again weighed to the nearest mg) of nonanoic acid was transferred to a 100ml conical flask. Next 40ml isopropanol was added the mixture and swirled so that the mixture was well mixed. Four drops of

PP indicator were then added and the mixture titrated with the standardised KOH solution, to a permanent faint pink end point.

The acid number (AN) is calculated by:

- $AN = (V_{KOH} \times N_{KOH} \times Mr_{KOH}) / W_S$ (3.2)

Where:

W_s = weight of sample, in grams

Mr_{KOH} = the molar mass of KOH (56.1 g/mol)

3) Nonanoic acid composition of the reaction samples.

Approximately 800microlitres (also weighed to the nearest mg) was taken from the pre-diluted sample vial and transferred to a 100ml conical flask. Then 40ml isopropanol was added, the mixture was swirled and then four drops of PP indicator was added. This was titrated with the standardised KOH solution, to a permanent faint pink end point.

The weight of nonanoic acid in the sample is calculated by:

- $W_{Non} = (V_{KOH} \times N_{KOH} \times Mr_{KOH}) / AN_{Non}$ (3.3)

And the concentration of acid (mol/L) in the sample is calculated by:

- $C_{Non} = 1000 \times W_{Non}/Mr_{Non})/$Volume of sample (0.8ml) (3.4)

Where

Mr_{Non} = the molar mass of nonanoic acid, 158.24g/mol

An example calculation using this procedure in given in Appendix C. When following the acid concentration in a set of samples from a run, it was found that there were problems of repeatability, in that the end point detection at low acid concentrations was difficult, as the colour change was extremely faint even when only a small quantity of isopropanol was used.

3.6.2 GCMS Analysis of Ester

The gas chromatography-mass spectrometry method for following ester formation is detailed in Appendix D. The typical approximate retention times for the components which appear on the chromatographs are shown in the Table 3.3.

Compound Name	Retention Time (Minutes)
Nonanoic Acid	6.1
Butyl Nonanoate	8.7
Butyl Laurate (IS)	12.1

Table 3.3: Typical GC retention times, nonanoic acid reaction system

The following figures show screen shots of example chromatographs for samples which have been run using the developed method on the Varian GCMS.

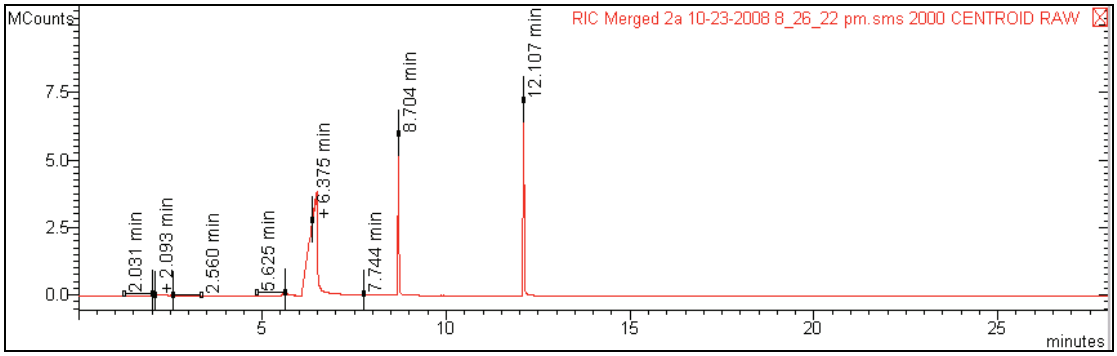

Figure 3.4: Example Chromatograph 1 (RD Run, No catalyst, Sample 2, 1st Dilution)

The peak for the nonanoic acid is the short, wide, asymmetrical peak visible just after the 6 minute mark. The peak shape reflects the way in which this compound interacts with the column stationary phase, and is an indication that accurate quantification may be unfeasible. Acid determination by GCMS was found to be unable to pick up low acid concentrations, so calibration for nonanoic acid proved unreliable and this approach was discontinued after the preliminary testing phase.

Focus was shifted to the determination of ester concentration by GCMS. Ester is visible as a sharp, well-defined peak at 8.7 minutes in Figure 3.4, even though the concentration at this stage is very low. When conversion is high, the ester concentration is high and the column can become overloaded. Performing a second dilution of the

samples allows the concentration of ester to be determined accurately. The following 2 figures show the GC chromatographs for the same sample at two different dilutions.

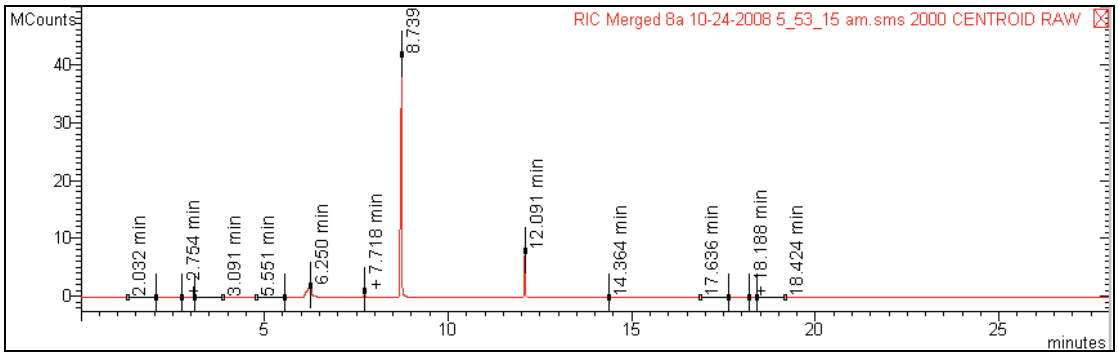

Figure 3.5: Example Chromatograph 2 (RD Run, No catalyst, Final Sample, 1st Dilution)

Figure 3.5 demonstrates that the column can become overloaded by the more concentrated sample towards the end of the reaction. The peak response area for the ester has gone outside of the range for which the machine has been calibrated, and some material may remain in the system and require flushing out. As demonstrated in Figure 3.6, a second dilution brings the response back within a more reasonable range (the ester peak has a comparable height to the internal standard peak).

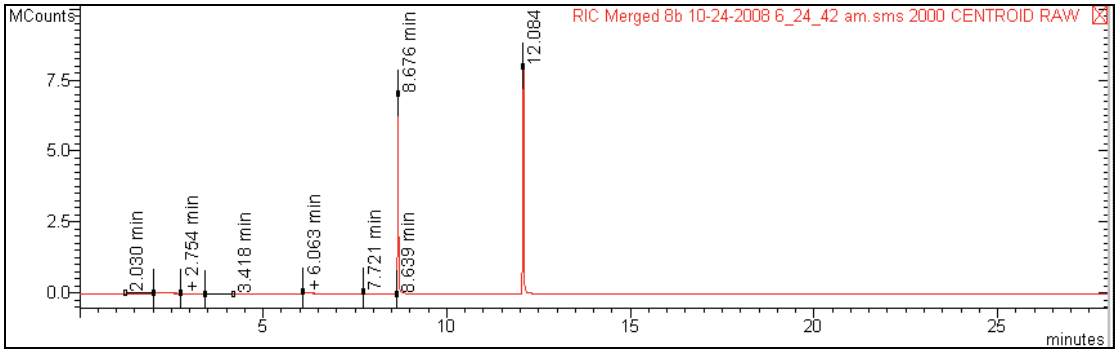

Figure 3.6: Example Chromatograph 3 (RD Run, No catalyst, Final Sample, 2nd Dilution)

3.6.3 GCMS Concentration Calculation

Each reaction sample was run in the GC twice, so the data output from the GC analysis is the average peak response area. The further processing of this data required 3 steps:

1) Calculate RRF from standards

To enable the Relative Response Factor (RRF) to be calculated a set of standards were run each time a set of samples were analysed.

- Internal Standard Response Factor = $\frac{\text{Internal Standard Response Area}}{\text{Internal Standard Concentration}}$ (3.5)

- Ester Response Factor = $\frac{\text{Ester Response Area}}{\text{Ester Concentration}}$ (3.6)

- RRF = $\frac{\text{Internal Standard Response Factor}}{\text{Ester Response Factor}}$ (3.7)

2) Calculate Ester Concentration in the sample

- Ester Concentration = $\frac{\text{Ester Response Area}}{\text{RRF x Internal Standard Response Factor}}$ (3.8)

This is the concentration in the GC vial, to find the concentration in the reactor the dilutions made during sample make – up must be reversed.

3) Reverse sample make-up dilutions:

- Concentration in ChemSpeed sample vial
  = Dilution Factor x Concentration in GC vial (3.9)

Two dilutions with isopropanol were performed on each sample from the ChemSpeed, so two GC vials were run for each sample. The first dilution allowed the early formation of small amounts of ester to be detected accurately, and the second dilution was required when the concentration of ester had increased so that the response went outside of the range for which this method was valid (the range of the concentrations in the standard vials, as illustrated by figure 3.5). The dilution factor for samples of the first dilution is 11.11, and when the second dilution is required, the dilution factor is 100. Each ChemSpeed vial in the sample rack already contained a known amount (1.5ml) of isopropanol before the sample from the reactor was added, so this dilution must also be reversed. A modified version of equation 3.9 is applied where the dilution factor in this case was 7. An example calculation using the procedure described here is presented in Appendix E.

3.6.4. Preferred Method

Following the method development and analysis of samples from preliminary work, the GCMS method of following ester formation was chosen as the preferred analytical method, and the performance of titrations was discontinued. Crucially, the GCMS method is able to detect very low concentrations of ester, and performing two dilutions enables the reaction progress to be followed even at high conversion, as the sensitivity to small further increases in ester remains very good. When both methods have been applied it was observed that, even when titrations indicate there appears to be no more carboxylic acid remaining, GC analysis can reveal that the concentration of ester is still increasing slightly. GCMS quantification of the ester is also not affected by presence of acid catalyst, which may affect titrations. An additional benefit is that any unexpected peaks will give an indication if something unexpected is present in the reaction mixture, for example due to the formation of a dimer.

The GCMS method is less manually intensive, requires significantly lower quantities of solvent, and once the diluted samples have been prepared they can be run on the GC automatically. Tiny amounts of sample from the ChemSpeed vials (100 microlitres) are required for the GCMS sample preparation, and the remainder is stored in a refrigerator, which provides the option for any erroneous-looking samples to be re-prepared and re-analysed. For example, errors such as mistakes in the dilution of the samples can be easily visually highlighted by the GC chromatographs, and the samples re-prepared.

3.7 Catalyst Screening Methodology Development

To reduce the amount of preliminary work needed, some decisions were made following a survey of the conditions used in esterification studies described in the published literature. These studies are summarised in Appendix F. The studies are listed in this table with the most relevant papers describing esterification of long chain fatty acids with a range of catalysts nearest to the top, followed by those that look at similar fatty acids with just one catalyst.

3.7.1 Temperature

From the summary in Appendix F, it can be seen that the University of Amsterdam team used a wide range of 60 to 180°C in one study (Omota, et al. 2003b), but in later papers

focussed on the range 120 to 180°C and recommend use of high temperatures (100°C+) to avoid phase separation (Kiss et al. 2006b and 2008b). Other studies, including some that focus on faster catalysts such as H_2SO_4 and PTSA, also often use 100°C (Othmer and Rao, 1950 and Aafaqi et al. 2004).

A temperature of 100°C would be a reasonable choice for use in the ChemSpeed screening tests, as it is not advantageous go higher. Water produced in the esterification reaction would boil, and a significant vapour production would enable some to escape from the system as the condensers are not sealed and may become overwhelmed.

3.7.2 Molar excess of alcohol

Three of the studies of various catalysts by Kiss et al. at the University of Amsterdam use a molar ratio of 2 to 1 alcohol to fatty acid when comparing the different catalysts (2006b, 2008a and 2008b). A 2:1 molar excess of alcohol is typical of this type of study and also provides a reasonable quantity for the nonanoic system, where the volumetric amounts of nonanoic acid (23ml) and butanol (24.5ml) are almost the same.

3.7.3 Catalyst Loading

The University of Amsterdam team generally used 2wt% of catalyst (based on the mass of the mixture) when performing studies of various catalysts (Kiss et al. 2006b, 2008a and 2008b). Other researchers using fast catalysts such as H_2SO_4 tended to use a lower range of catalyst loadings of 0.25 to 0.9 wt% (Othmer and Rao, 1950 and Ling and Geankoplis, 1958). Wang et al. (2007) investigated the use of ferric sulfate catalyst and found that a catalyst loading of 1wt% based on the amount of oil already gave 90% conversion and that there was not much benefit to increasing loading past this point. Tang and co-workers (1999) found a similar pattern, with little increase in benefit over 0.4 wt% catalyst.

The catalyst loading chosen for this study falls towards the lower end of the scale described in literature: 1wt% based on the mass of nonanoic acid charged to the reactor (or 0.52 wt % based on total mixture in the pot). A balance was required between the speed at which the reaction would progress with strong or weak catalysts, and practical concerns. It is desirable for it to be possible to quantify differences in behaviour between different catalysts, but it is important that the catalyst does not work its way

into the narrow ChemSpeed tubes and cause blockages. In the preliminary tests, it was found that the bulk of catalysts varied greatly, for example zinc acetate is supplied as small beads which dissolve in the reaction mixture, while ferric sulfate is a fluffy, yellow powder which occupies a much larger volume, and can form lumps when first added to the reaction mixture.

3.7.4 Preliminary Tests: ChemSpeed Agitation Rate

The ChemSpeed Synthesizer applies agitation to the reactors by shaking the reactor block, in an oscillatory manner, at a frequency set by the user. The effectiveness of the applied agitation rate is specific to the particular equipment set-up used. Agitation rate tests were performed to determine a suitable rate of oscillation for this system, using a readily soluble catalyst candidate (Zn Ac) and an insoluble catalyst (Ferric Sulfate). The conditions were as follows: 2:1 molar excess of alcohol, 100°C, 1wt% of catalyst based on the mass of nonanoic acid charged to the reactor. The results of these runs are shown in Charts 3.2 and 3.3, where it appears that there is no improvement in the rate of reaction above 700rpm.

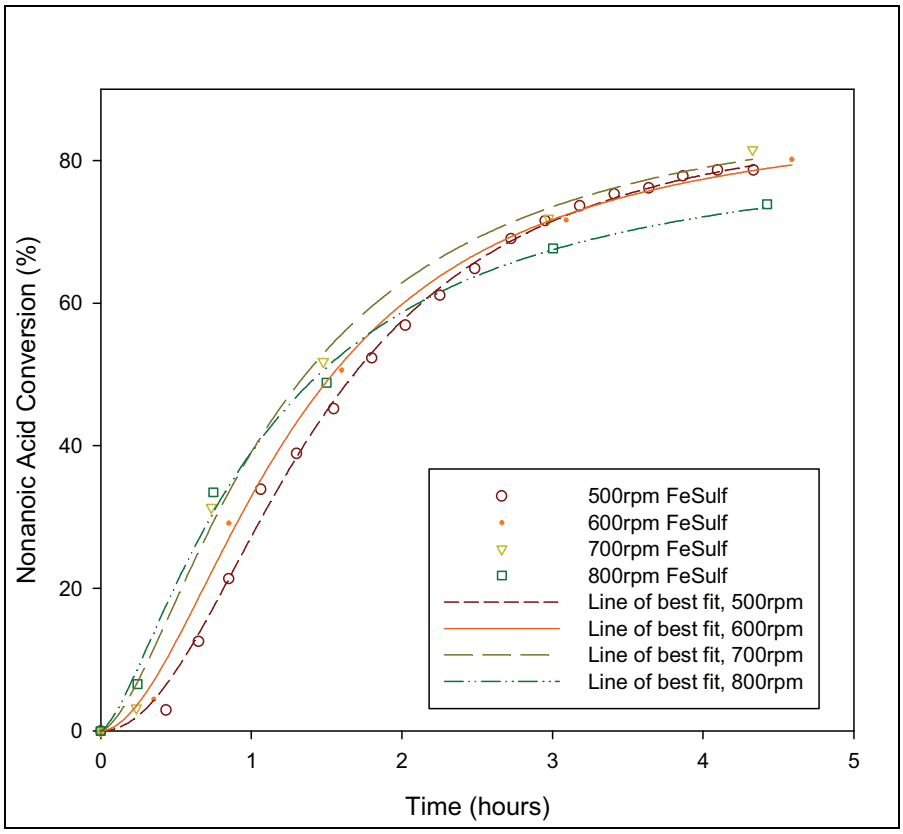

Chart 3.2: Varying ChemSpeed Agitation Rate, Ferric Sulfate Catalyst

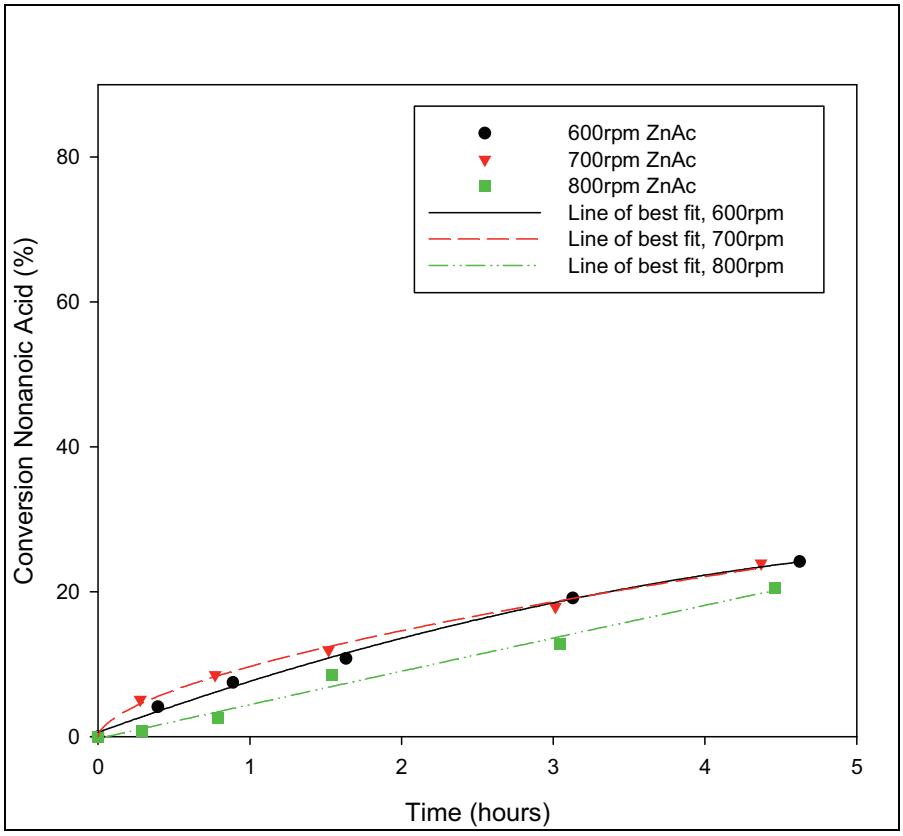

Chart 3.3: Varying ChemSpeed Agitation Rate, Zinc Acetate Catalyst

3.7.5 ChemSpeed Reaction Procedure

Nonanoic acid (23ml) and catalyst (209mg) are charged to the reactors, and butanol (24.5ml) is held in a storage flask at the rear of the ChemSpeed machine. The ChemSpeed follows a pre-programmed protocol, shown in the Table 3.4. The sampling intervals and the order of the steps are partly determined by the speed that the robot arm is able to perform the steps in the procedure: only one sample or dose can be performed at a time as there is only one robot arm.

After the initial heating interval, during which the nonanoic acid and catalyst are heated to the reaction temperature, the butanol is charged to the first reactor using the robot arm. Butanol addition takes approximately 1 minute and heating and agitation are applied during the dosing. Samples are taken before and after each butanol addition, in order to establish the starting composition. The 0.25ml samples taken by the needle head are injected into vials containing 1.5 ml isopropanol solvent at room temperature, which cools and dilutes the sample to quench the reaction. These steps are similar to those taken in experimental procedures described in literature (Peters et al. 2006; S. Y. Chin et al. 2006; Liu et al. 2006). The agitation rate is reduced slightly as the first

sample is taken from each reactor, to avoid the possibility of small air bubbles being drawn into the tubes, as the liquid level in the reactor is fairly low before the butanol is dosed. In these cases the agitation rate is returned to normal before the needle is rinsed.

3.7.6 Automated ChemSpeed Protocol

The ChemSpeed method program details are shown in the following table (all times are approximate, as the duration of the various tasks performed by the robot arm varied a little each time).

		Time	Vial	Reactor Run Time (min)			
Step	ChemSpeed Task	(min)	No.	R1	R2	R3	R4
1	Reflux ON						
2	Reaction block closed						
3	Agitation 700rpm						
4	Thermo ON 100°C at 10°C/min						
5	Wait 30min						
6	Agitation DOWN 450rpm						
7	Sample R1 before BuOH, no rinse	2.4	1	Pre-Start			
8	Agitation UP 700rpm						
9	Rinse needle 1						
10	Dose BuOH to R1 from back	7.4		0.0			
11	Sample R1 after BuOH with rinse	8.8	2	1.5			
12	Wait 3 mins						
13	Agitation DOWN 450rpm						
14	Sample R2 before BuOH, no rinse	16.0	3	8.6	Pre-Start		
15	Agitation UP 700rpm						
16	Rinse needle 1						
17	Dose BuOH to R2 from back	21.0			0.0		
18	Sample R2 after BuOH with rinse	22.5	4		1.5		
19	Sample R1 with rinse ~ 20 min	26.6	5	19.3	5.6		
20	Agitation DOWN 450rpm						
21	Sample R3 before BuOH, no rinse	30.8	6	23.4	9.8	Pre-Start	
22	Agitation UP 700rpm						
23	Rinse needle 1						
24	Dose BuOH to R3 from back	35.8				0.0	
25	Sample R3 after BuOH with rinse	37.3	7	29.9	16.3	1.5	
26	Sample R2 with rinse ~ 20min	41.5	8	34.1	20.4	5.6	
27	Agitation DOWN 450rpm						

28	Sample R4 before BuOH, no rinse	45.6	9	38.2	24.6	9.7	Pre-Start
29	Agitation UP 700rpm						
30	Rinse needle 1						
31	Dose BuOH to R4 from back	50.6					0.0
32	Sample R4 after BuOH with rinse	52.1	10	44.7	31.0	16.2	1.5
33	Sample R3 with rinse ~ 20 min	56.2	11	48.8	35.2	20.3	5.6
34	Sample R1 with rinse ~ 55min	60.3	12	53.0	39.3	24.5	9.8
35	Wait 6 mins						
36	Sample R4 with rinse ~ 20 min	70.5	13	63.1	49.5	34.6	19.9
37	Sample R2 with rinse ~ 55min	74.7	14	67.3	53.6	38.8	24.1
38	Wait 10 mins						
39	Sample R3 with rinse ~ 55min	89.5	15	82.1	68.4	53.6	38.9
40	Wait 10 mins						
41	Sample R4 with rinse ~ 55min	104.2	16	96.9	83.2	68.4	53.6

Table 3.4: Automated ChemSpeed Method Protocol

3.8 Equilibrium Point of Reaction

For a reaction of the type,

$$A + B \Leftrightarrow C + D$$

The equilibrium constant is often calculated using the concentrations of the species:

$$K_{eq} = \left\{\frac{[C][D]}{[A][B]}\right\}_{eq} = \frac{k_{forward}}{k_{reverse}} \qquad (3.10)$$

To confirm the end point of the esterification reaction between nonanoic acid, data was brought together from the early ChemSpeed runs and from using the LyraChem bench-top kit (illustrated in Figure 3.3). The ChemSpeed runs were performed according to a similar procedure to that described above, extended for a longer time period. The LyraChem equipment procedure was as follows:

Nonanoic acid (6.7 g, 7420microL) and 1-butanol (2 molar equivalents: 6.1 g, 7550microL) were added to a 50 ml round-bottom flask. The mixture was heated by an oil bath using a temperature controller, and once the internal temperature reached the set point, 67mg catalyst (1 wt % based on the mass of nonanoic acid) was added. After approximately 5 hours, a sample was withdrawn from the reaction vessel and added to a pre-weighed conical flask. The sample mass was calculated before 20 ml isopropanol

and 2 drops of phenolphthalein indicator were added. The flask contents were titrated against a 0.1 M aqueous solution of sodium hydroxide to a permanent faint pink end-point to determine the amount of nonanoic acid remaining. The equilibrium point was determined by calculating the composition of the reaction mixture.

3.9 Summary

This chapter presents the development of the experimental procedures for the testing of candidate catalysts at small scale, to screen for activity in the chosen reaction system. The reasoning for the selection of the esterification of nonanoic acid with butanol to act as a case study for this work has been outlined. Candidates of different types have been identified and sourced, and this range includes homogeneous acids, heteropoly acids, metal acetates, and a number of others including heterogeneous catalysts described in literature studies.

Discussion of the development of suitable analytical methods has been given, including an account of the decision to use GC analysis (rather than titrations) for quantification of ester composition as the primary method of following the reaction progress. The ChemSpeed Synthesizer and has been trialled and shown to be suitable for the screening tests, and preliminary tests have enabled determination of a suitable agitation rate. A summary of the experimental procedure used to perform the catalyst screening has been given, including the automated protocol followed by the ChemSpeed.

These procedures have been implemented in the testing of the 20 catalyst candidates for activity in the esterification of nonanoic acid with butanol, and the results of this work is presented in Chapter 4.

Chapter 4: Catalyst Performance in Batch Screening Tests

4.1 Overview

This chapter describes the results from the experimental work investigating the nature and performance of the 20 catalyst candidates with the nonanoic acid esterification system. The methods used for this work are described in previous Chapter 3. The equilibrium point of the esterification is determined to be 4.58, which indicates the reaction equilibrium lies further towards products compared to examples from literature studies. The half life of the esterification of nonanoic acid with the various catalyst candidates is reported and it is seen that the strong homogeneous acids are the most active, with the shortest half lives, followed by the heteropoly acids and ferric sulfate. It is also observed that the strong acids appear to deactivate during the experimental runs, while the activity of the heteropoly acids remains steady. Five catalyst candidates were also tested over a range of temperatures, in order to provide data which is used to build dynamic simulations in Chapter 7.

4.2 Introduction

There are 3 sections to this chapter: the determination of the equilibrium point of the esterification of nonanoic acid and butanol, comparison of candidate catalyst activity in screening tests at 100°C, and determination of parameters for use in dynamic simulations through tests performed at different temperatures.

The equilibrium point is determined to evaluate how far towards products the esterification reaction will go under closed conditions. This is also used later for fitting forward rate constants in BatchCAD, and to confirm the half life of the nonanoic acid esterification even in cases when the catalysed reaction was very slow.

All 20 catalyst candidates are then ranked in order of activity through the performance of screening tests at a constant temperature (100°C) and determination of the half life of the nonanoic acid esterification. The most active candidates are those that cause the concentration of the nonanoic acid to fall by half in the shortest time. The half life result provides a single quantitative output from the screening study, and enables the screening to be performed quickly with each catalyst tested only once.

For the development of dynamic simulations, BatchCAD requires the specification of Arrhenius parameters to describe the variation of reaction rate with temperature in order to build a model that matches the observed changes in composition. The final part of this chapter describes a set of tests at a range of temperatures, with a selection of five catalysts and with no catalyst, which are used to fit the necessary parameters. These Arrhenius parameters are not used as part of the catalyst activity testing, because the parameters cannot be directly compared for systems with different catalysts.

4.3 Equilibrium Point Determination

Appendix G contains the raw data from the runs which were allowed time to reach equilibrium point. Once the equilibrium point has been reached, leaving the reaction to continue past this point serves no purpose, and may in some cases lead to product degrading if the temperatures are high. The amount of catalyst used in each of these runs was 1wt% based on the mass of nonanoic acid. The volume in the reactor was taken to be constant, so knowledge of one component enables calculation of the extent of reaction.

Once the composition at equilibrium has been determined, the equilibrium point is calculated using equation (3.10). Table 4.1 shows data from four runs at different temperatures which were allowed to run to equilibrium. The temperatures were chosen to represent a range up to the boiling point of water, which was not exceeded during the screening tests in order to avoid losing vapours from the ChemSpeed reactor pots.

Temperature (°C)	Equipment	Catalyst	Concentrations at Equilibrium (mol/L)				Equilibrium Constant
			Nonanoic	Butanol	Ester	Water	
73	LyraChem	H_2SO_4	0.46	2.97	2.49	2.49	4.54
80	LyraChem	PTSA	0.38	3.14	2.33	2.33	4.57
90	LyraChem	PTSA	0.38	3.15	2.32	2.32	4.45
100	ChemSpeed	H_2SO_4	0.30	3.42	2.21	2.21	4.76

Table 4.1: Data for the Determination of Equilibrium Point.

The average equilibrium constant was 4.58. Plotting the equilibrium constants against the temperatures of each of the runs above reveals that the equilibrium point seems almost constant with temperature (the average equilibrium point of 4.58 is illustrated by the dotted line on Chart 4.1). This is not contrary to expectation since only one case of

temperature-dependent equilibrium point for esterification was found in literature; Tesser et al. (2005) reported that the esterification oleic acid and methanol was found to have an equilibrium point that increased very slightly with temperature.

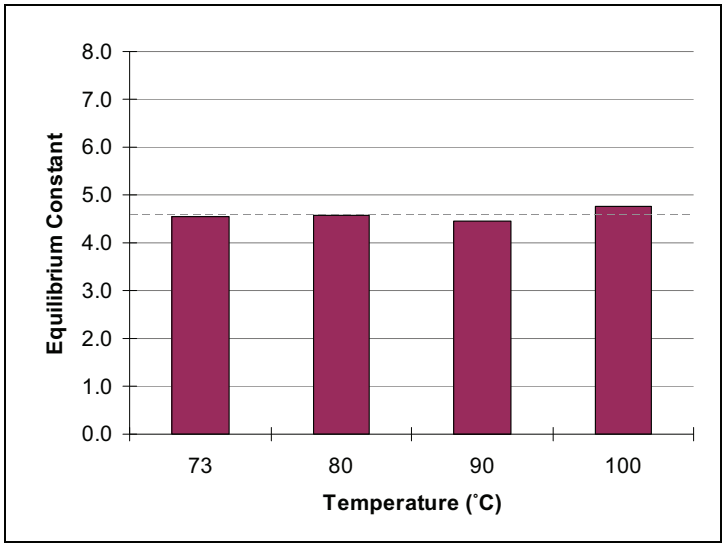

Chart 4.1: Plot of Equilibrium Point against Temperature.

It also appears that performing the tests on different apparatus and with different catalysts has not affected the result. A literature search has revealed that there are a small number of studies available in open literature where the equilibrium points for esterification of long or medium chain fatty acids have been reported. This information is summarised in Table 4.2, and more detail is available in Appendix F.

Carbon Chain	**Reference**	**Temp**	**Alcohol : Acid Ratio**	**K_{eq}**
Short, saturated	Leyes & Othmer (1945a)	100	3:1	2.25
	Lee & Lin (1999)	100	1:1	2.03 (av.)
Long, unsaturated	Othmer & Rao (1950)	100	2:1	0.48
	Tesser et al. (2005)	50 - 100	8.7 (av.) :1	>1
Long, saturated	Yalçinyuva et al. (2008)	80	2:1	1.49
Meduim di-carboxylic	Kolah et al. (2008)	78-120	10:1	5.3

Table: 4.2 Equilibrium Data from Literature Sources

It can be seen that the values for the equilibrium constants in Table 4.2 are generally "relatively close to unity", as would be expected (Perry & Green, 1997). An equilibrium point of 1 would indicate that at equilibrium the concentrations of reactants and products are equal. The studies involving esterification of long-chain oleic acid with butanol (Othmer & Rao, 1950) and methanol (Tesser et al., 2005) resulted in lower equilibrium constants than the studies involving esterification of the shorter-chain acetic acid with butanol (Leyes & Othmer, 1945a) and isoamyl alcohol (Lee & Lin, 1999).

Yalçinyuva et al. (2008) studied the esterification of myristic acid, which has a chain of 14 carbon atoms and is the most similar to nonanoic acid out of the molecules considered in the studies in Table 4.2. However, the equilibrium point of the esterification with isopropanol is low, at only 1.49. The literature source which gave the closest value for equilibrium point to that obtained in this study involved the esterification of the medium-length, saturated di-carboxylic acid succinic acid with ethanol (Kolah et al., 2008). However, the molar ratio of alcohol to acid was 10:1, much higher than the 2:1 used with the nonanoic acid system in the present study. The equilibrium point of 4.58 therefore seems to indicate that this reaction progresses quite far towards products compared to similar studies.

4.4 Compare Catalysts: Screening at 100˚C

4.4.1 Results and Discussion

Twenty candidates were screened for catalytic performance in the nonanoic acid-butanol esterification reaction. The screening experiments were performed in the ChemSpeed Synthesizer at 100˚C for just under 1 hour, using the method program "4Reactors16vials.app" (described in Chapter 3). The formation of ester was followed during this time, and the tables of data from the screening experiments are shown in Appendix H. Chart 4.2 presents the results from these experiments as increasing yield with time, where the yield is calculated against the maximum theoretical ester production based on the exact amount of nonanoic acid charged to the reactor. The data sets for the less active candidates seem to overlap with the case for where no catalyst was used; the line of best fit for the uncatalysed case is the black line.

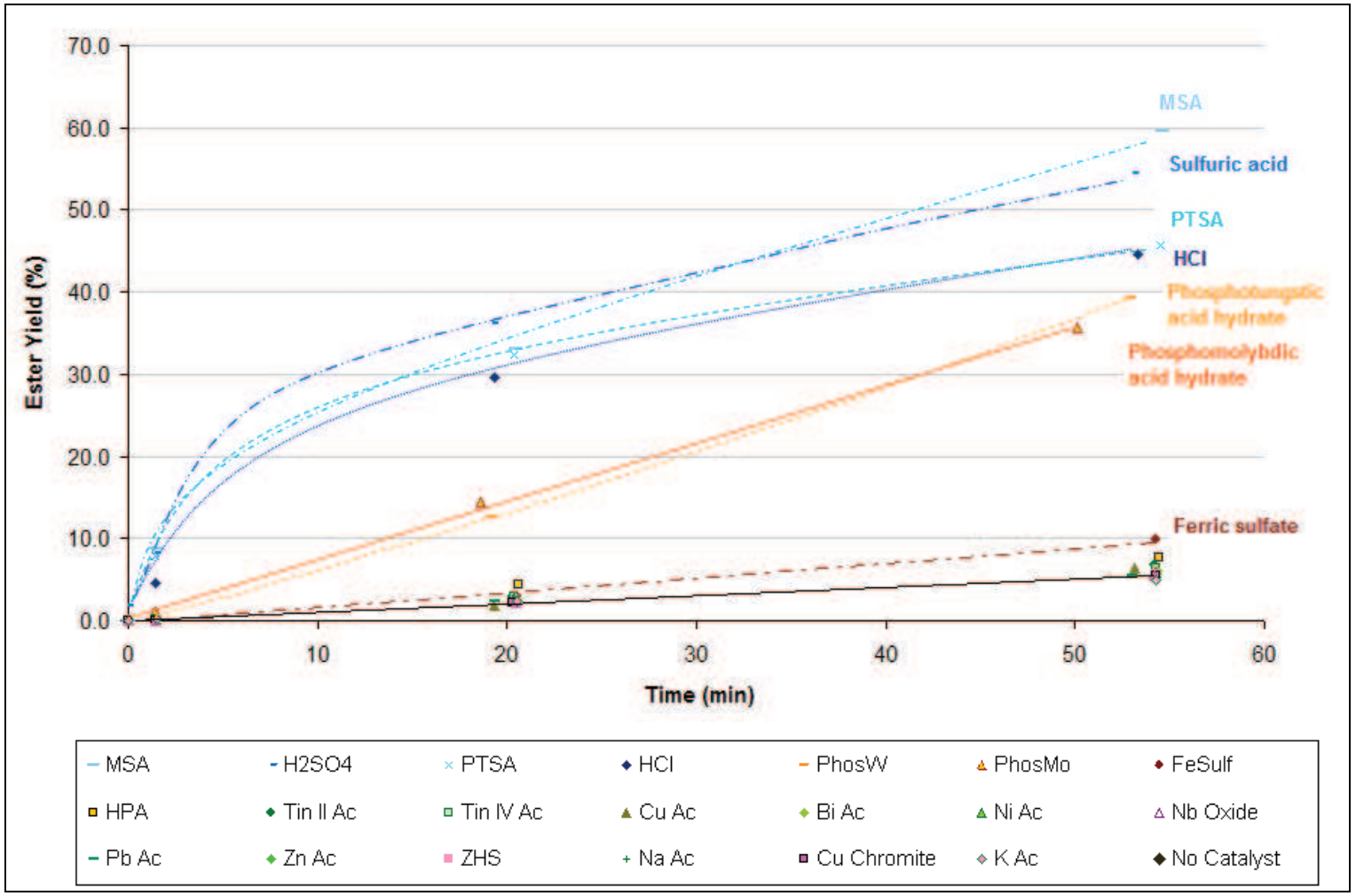

Chart 4.2: Ester Yield (in percent) vs. Time for all Candidates Screened

Initially it appears that the most effective catalysts are the strong homogeneous acids: methane sulfonic acid, sulfuric acid, PTSA and hydrochloric acid. These catalysts give a rapid production of ester and highest yield. The performance of PTSA was very similar to that of hydrochloric acid, the heteropoly acids appear to give intermediate performance, while ferric sulfate and hypophosphorous acid give a slight improvement over the case with no catalyst.

Sulfuric acid is a very good catalyst for this esterification, although the performance here is not as high as that reported by Zafiropoulos et al. (2007), who attained approximately 80% conversion in the esterification of oleic acid and methanol in 50 minutes at 95°C (0.5mol% catalyst, 2 equivalents of methanol). In the results for sulfuric acid shown in Chart 4.2, after 53 minutes the ester yield was just over 54%. Peters et al. (2006) reported that for the esterification of acetic acid and butanol in an equimolar mixture at 75°C, sulfuric acid was the most effective of the catalysts they studied, and PTSA gave a similar high rate of observed reaction. Phosphomolybdic acid had a lower weight-based activity but still gave fast observed rates. The relative performances for these catalysts in Chart 4.2 give some agreement with this description, although the profile for PTSA lags behind that for sulfuric acid significantly.

The poor performance of sulfated zirconia is disappointing in comparison to the performance described by Kiss et al. (2006b and 2008b) for the esterification of decanoic acid and 2ethylhexanol at 120°C (alcohol: acid molar ratio 2:1 and 2wt% catalyst). Sulfuric acid, phosphotungstic acid and sulfated zirconia were among the most promising catalysts discussed by these authors. Reading from the graphs presented in their work, the approximate conversions attained after 1 hour were:

- Sulfuric acid 95%
- Phosphotungstic acid 92%
- Sulfated zirconia 75%
- No catalyst 30%

Again, the performance described by the literature studies is higher than that observed in the experimental results in Chart 4.2. However, the order of the catalysts' effectiveness agrees in that sulfuric acid outperforms phosphotungstic acid, which in turn outperforms sulfated zirconia, and the difference between phosphotungstic acid and sulfated zirconia is greater than that between the sulfuric acid and phosphotungstic acid.

Phosphotungstic acid was extremely active in the literature study, however it was noted that this candidate is soluble in water and so not of interest to the search for a heterogeneous catalyst, and when immobilised as a salt it was insoluble but displayed lower catalytic activity and acidity.

Kiss et al. (2008b) found that sulfated zirconia gave very good performance: it was the most promising of the metal oxides in terms of activity and selectivity (none of the others achieved over 60% conversion in 1 hour), and it was also stable under the conditions of the study. In contrast, Furuta et al. (2004) obtained low performance in the esterification of n-octadecanoic acid and methanol with 4g of sulfated zirconia catalyst fixed in a flow reactor (methanol: acid molar ratio 4.5). When using reaction temperatures below 120°C, the yield obtained was no higher than 20% after 20 hours of reaction time, which is much closer to the performance level observed in Chart 4.2. However, with temperatures over 150°C, Furuta et al. (2004) obtained very high activities, with over 90% yield ester. This suggests that the temperature may be very important for sulfated zirconia catalyst, and there may be a minimum temperature required for high activity.

Peters et al. (2006) found that the weight-based activity of sulfated zirconia and niobium oxide was relatively low for the system studied, giving around 60% conversion for sulfated zirconia and about 10% conversion for niobium oxide after 200 minutes at 75°C (equimolar acetic acid and butanol reactants, 5.7wt% catalyst). The low temperature may have inhibited the sulfated zirconia, and the authors suggested that the very low activity of niobium oxide was possibly explained by a finding that there were fewer Brønsted acid sites on the surface than observed in a previous study. If a high level of Brønsted acid sites, rather than Lewis acid sites, is necessary for the catalysis of esterification, then the niobium oxide performance would be highly dependent on catalyst preparation and calcination temperature. Calcination steps are described for niobium oxide by Peters et al. (2006) but not by Kiss et al. (2006b).

Of the other solid catalysts tested, Chart 4.2 indicates that the ferric sulfate offers some activity as an esterification catalyst for this reaction system, although the activity again seems low when compared with the literature. In the esterification of free fatty acids in waste cooking oil, Wang et al. (2007) report achieving 90% conversion of free fatty acids in 1 hour at 95°C (2.5 wt% ferric sulfate, 10:1 methanol excess). Chiu et al.

(2006) report that when the dehydration of glycerol was allowed to run to completion under reactive distillation conditions with a copper chromite catalyst, the reaction reached over 86% conversion at 240°C even with the lowest catalyst loading (0.83wt%). The results from the screening experiment shown in Chart 4.2 indicate that this candidate is not active as a catalyst for the esterification reaction.

The metal acetates do not appear to enhance the reaction rate significantly above that observed in the case with no catalyst, achieving ester yields of only 4.9 to 6.8%. Di Serio et al. (2005) investigated the use of metal acetates for the esterification of fatty acids in soybean oil with methanol, and found very good conversions of glyceride groups with lead acetate (81%) and zinc acetate (67%), at 200°C, but at 150°C the conversions were much lower (approximately 45% and 30% respectively). Nickel acetate did not show catalytic activity at either temperature.

To summarise, if the catalysts are ranked in order of performance then the order matches that expected from the literature studies, however the reaction rates observed in the screening experiments were generally slow compared to literature studies. This can be partly explained by the fact that nonanoic acid is a fairly long molecule and most of the esterification studies described in literature were performed with shorter acids and with methanol rather than butanol, therefore steric hindrance could be a factor. For example, Lotero et al. (2005) reported that the esterification of palmitic acid with ethanol was 'less efficient' than the same reaction with methanol.

4.4.2 Half Life Comparisons

Catalysed reactions happen by a different mechanism to uncatalysed reactions, so it is not appropriate to directly compare the values of kinetic parameters to assess the catalyst performance (Rothenberg, 2008a). The chosen useful quantitative output in this case is the half life, taken as the time required for the concentration of the nonanoic acid to fall to half the initial value. The half life provides a 'snapshot' measure of the performance of the candidates at the start of the reaction, which can easily be ranked and compared. However it should be noted that the half life does not take into account other important considerations, such as the longer-term performance over the entire life cycle of the catalyst candidates. Further discussion of these issues is given in Chapter 9.

The BatchCAD software in Simulation Mode allows the half life to be found from the concentration vs. time profiles from the screening experiments, even where the fixed-time run in the ChemSpeed did not allow the reaction to proceed far enough. This was necessary for analysis of the slower catalysts as the reaction would require a long time (more than 12 hours) to approach equilibrium. A model of a ChemSpeed reaction vessel was built in BatchCAD, setting the dimensions and characteristics of the vessel to correspond to the real case, and entering the stoichiometry of the reversible esterification reaction. The BatchCAD model for the ChemSpeed reactor pot is described in Appendix I, and further discussion of how BatchCAD performs the kinetic fitting is given later, in section 4.5.2.

The equilibrium point information and the raw experimental data (n-butyl nonanoate ester concentration vs. time) from the catalyst screening was loaded into the BatchCAD data manager and a simulation of the reaction was allowed to run for a suitable amount of time so that the reaction exceeded half conversion and the concentration profiles of the other components were generated. A typical concentration profile (for the data from the screening experiment using methane sulfonic acid as the catalyst) is shown below in Chart 4.3. It can be seen that BatchCAD has replicated the concentration profile from the experimental data, and simulated the continuation of the reaction.

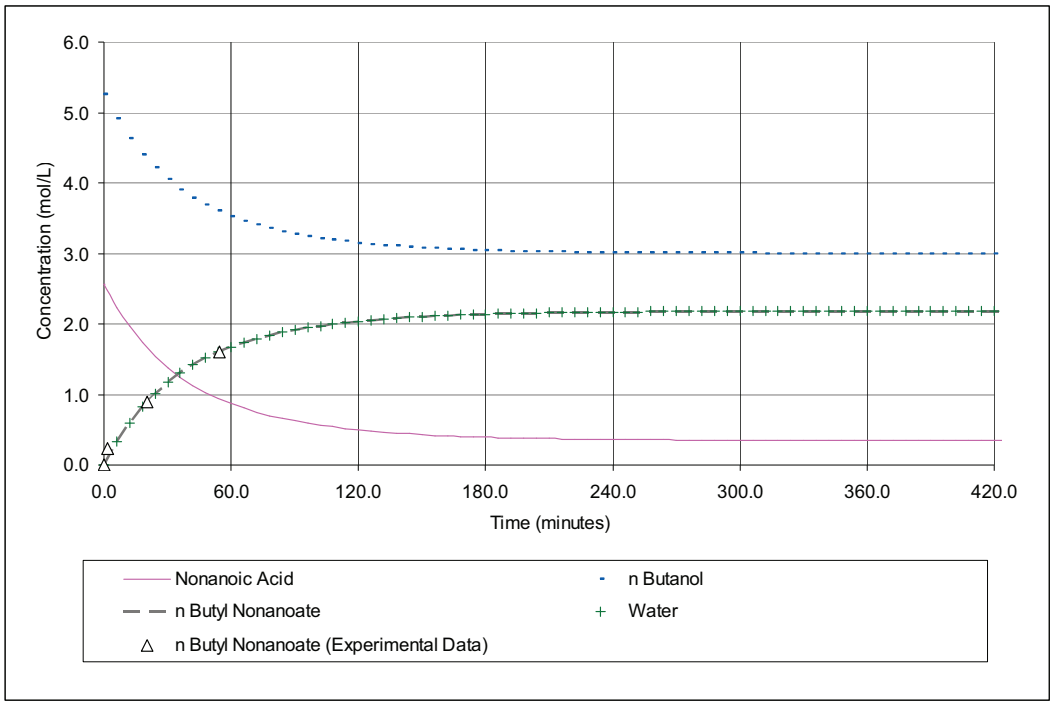

Chart 4.3: Example BatchCAD Screening Simulation Output for MSA

The BatchCAD simulation output of nonanoic acid concentration vs. time is a good match to the experimental data, and allows the half life to be calculated as the time taken for the nonanoic acid concentration to fall to half its initial value. This procedure was applied to each of the data sets from the screening experiments, and the results are shown in Table 4.2. The catalysts are listed in order of increasing half life.

Candidate Catalyst	**BatchCAD Generated Half Life**		**Improvement vs. No Catalyst**
	Min	**hour**	**%**
Methane sulfonic acid	34.6	0.58	95.4
Sulfuric acid	38.0	0.63	94.9
PTSA monohydrate	48.6	0.81	93.5
Hydrochloric acid	49.9	0.83	93.3
Phosphotungstic acid hydrate	78.1	1.30	89.5
Phosphomolybdic acid hydrate	81.5	1.36	89.1
Ferric sulfate hydrate (iron III)	411	6.85	44.8
Hypophosphorous acid	481	8.01	35.4
Tin (II) acetate	569	9.48	23.6
Tin (IV) acetate	600	10.0	19.3
Copper (II) acetate monohydrate	626	10.4	15.8
Bismuth (III) acetate	643	10.7	13.6
Nickel (II) acetate tetrahydrate	662	11.0	11.1
Niobium (V) oxide	679	11.3	8.7
Lead (II) acetate trihydrate	686	11.4	7.8
Zinc acetate dihydrate	697	11.6	6.3
Zirconium (IV) hydroxide, sulfated	701	11.7	5.7
Sodium acetate trihydrate	719	12.0	3.4
Copper chromite	720	12.0	3.2
No catalyst	744	12.4	n/a
Potassium acetate	777	13.0	-4.5

Table 4.3: Nonanoic Acid Esterification Half Life with the Screened Candidate Catalysts

All of these half life values are well over ‘several minutes’ so the reaction with any of these catalysts would be classified as ‘slow’ by Bamford & Tipper (1969). To visually illustrate the range of half life values obtained, Chart 4.4 presents a bar chart displaying the percent improvement over the case with no catalyst.

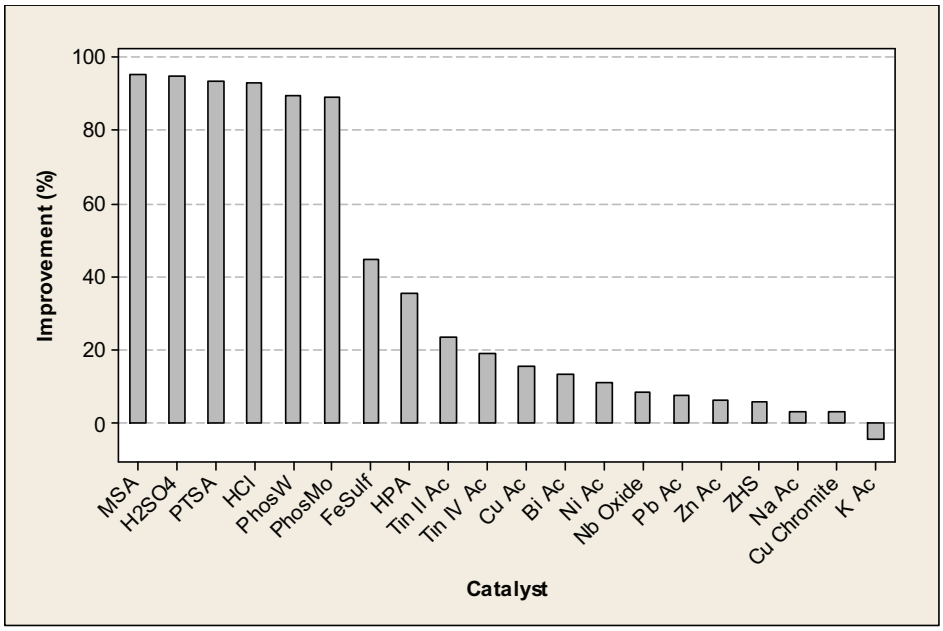

Chart 4.4: Bar Chart of Percent Improvement in Half Life

As previously seen in Chart 4.2, it is observed that the strong homogeneous acids (methane sulfonic acid, sulfuric acid, PTSA and hydrochloric acid) appear to be the most effective catalysts, causing the reaction to proceed with half life values below one hour. These are followed by the heteropoly acids, giving half life values below one and a half hours. Apart from ferric sulfate hydrate and hypophosphorous acid, which speed up the reaction to some degree, the other catalysts seem to offer little improvement over the case with no catalyst, and potassium acetate even appears to inhibit the reaction slightly.

4.4.3 Activity vs. Catalyst Concentration Trends Observed

The amounts of catalyst used in each of the screening experiments were calculated based on 1 weight percent for the nonanoic acid charged; therefore the same weight was used in each. However, it is possible that these screening results could appear different if it could be taken into account that the molar quantities of the catalyst candidates were different. In order to gain an indication of how the catalyst activity varies during the runs and the effect of the different molar concentrations of catalyst used, the curve fitting tool of Matlab was applied to each set of experimental data (n-butyl nonanoate yield in percent vs. time in minutes) from the catalyst screening experiments to generate the gradients of the curves as 1st differential values.

The gradients describe the rate of ester production, and dividing their values by the catalyst concentration in moles per litre translates this information into an indicator of the rate of ester production per mole of catalyst. These 'activity scores' (shown on the following charts as {*d* yield/ *d* t} / [cat]) were plotted on a log scale against time in order to observe the different behaviour of the catalysts. The heights of the catalyst activity profiles along the y-axis allow comparison of the molar activities, and the shapes of the profiles give an indication of any loss of initial activity during the runs. There is a wide range in the behaviour of the catalysts during the screening experiments, so in order to view the detail of the different behaviour types, the catalysts are plotted in separate groups.

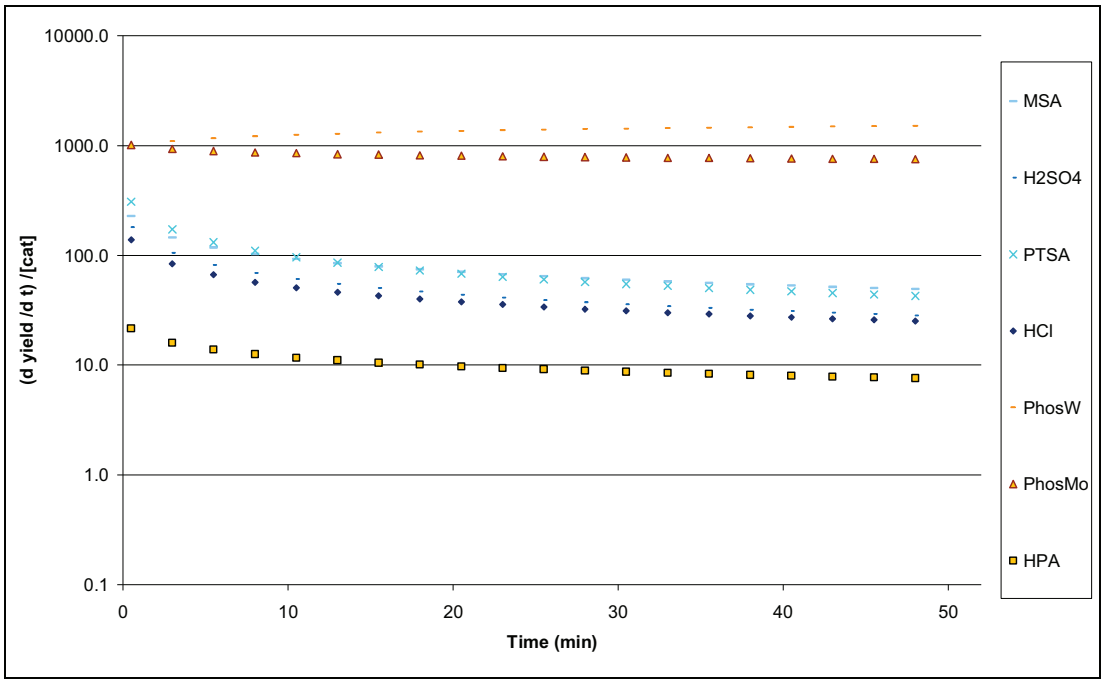

Chart 4.5: Activity Scores vs. Time for Acids

Chart 4.5 shows the molar activities for the non-heteropoly, homogeneous acids start relatively high but then a rapid fall in activity per mole occurs in the first 20 minutes, followed by a more gradual decrease in activity. Heteropoly acids appear to have a very high activity per mole, due to their very high molecular weight compared to the other acids, and this high activity is maintained throughout the run. In contrast to the other acids, hypophosphorous acid appears to have low performance compared to the other acids but still follows the general profile shape for acid behaviour.

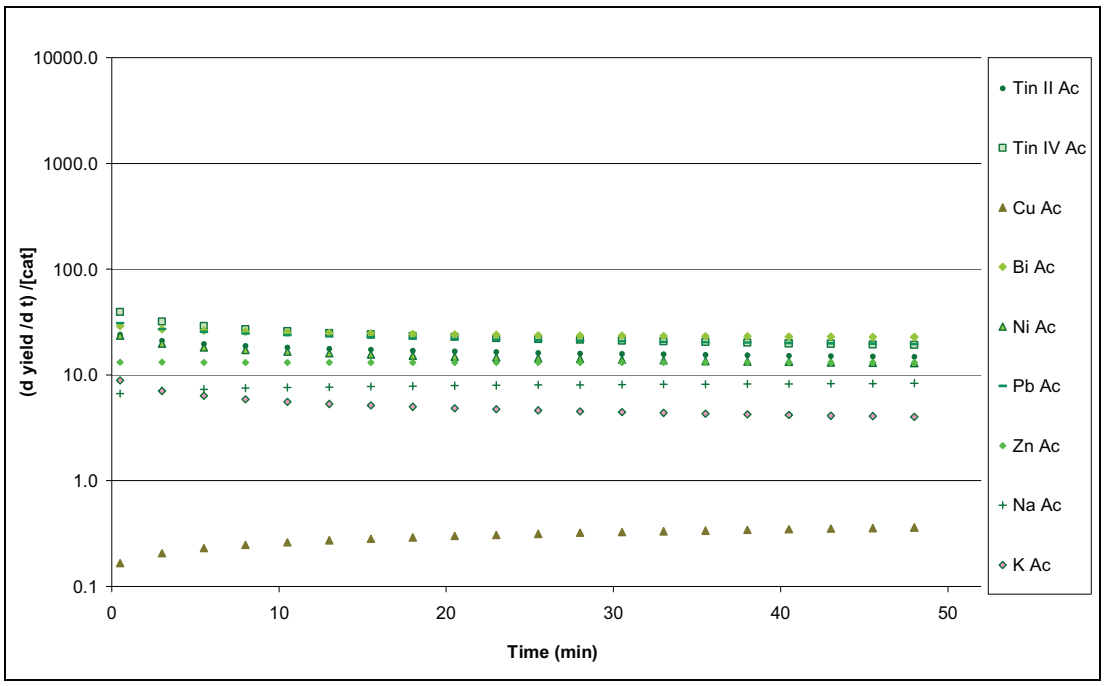

Chart 4.6: Activity Scores vs. Time for Metal Acetates

Chart 4.6 shows the variation in the activity scores with time for the metal acetate candidates. Generally the metal acetates start with a low activity and follow a characteristic profile shape of gradually reducing activity per mole of catalyst, which then levels off. The profiles for zinc acetate dihydrate and sodium acetate trihydrate are almost flat, while the anomalous profile for copper acetate monohydrate gradually increases with time.

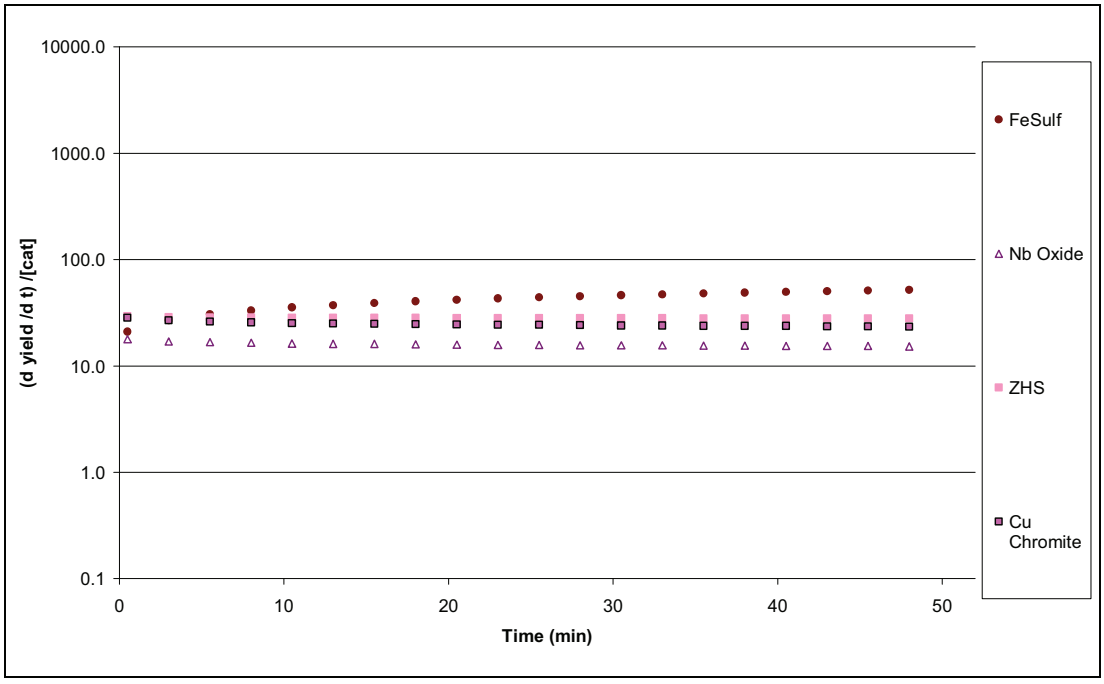

Chart 4.7: Activity Scores vs. Time for Other Candidates

Chart 4.7 shows that niobium oxide, sulfated zirconium hydroxide and copper chromite, which all demonstrate poor performance in the screening tests, also follow fairly flat-shaped activity scores vs. time profiles. This suggests that they behave similarly to zinc acetate dihydrate and sodium acetate trihydrate under the reaction conditions, resulting in similar poor performance. Ferric sulfate appears better than the ineffective catalysts in Chart 4.7, but it also does not fit the 'acid catalyst' behaviour profile shape seen in Chart 4.5. The activity per mole increases slowly and after about 15 minutes, the performance of ferric sulfate is comparable to the acid catalysts in the same time frame. This seems to suggest that the relative performance of the ferric sulfate as a catalyst improves during the reaction.

In the next part of this chapter, the results of tests performed with a selection of the candidate catalysts at varying temperatures are presented.

4.5 Experiments at Varying Temperatures

In order to perform dynamic reactive distillation simulations in BatchCAD, it is necessary to enter some information into the model describing how the rate of reaction changes with temperature. Experiments at various temperatures were therefore performed, simply to obtain parameters which will enable the model to fit experimental observations, even though it is not technically correct to fit kinetics where different catalysts have been used (Rothenberg, 2008a).

ChemSpeed runs of the esterification of nonanoic acid and butanol were performed at three different temperatures: 60, 80 and 100°C. Experiments were performed without catalyst, and also with five catalysts which were selected to represent the different categories present in the range candidates which have been screened. The BatchCAD model of a ChemSpeed reaction vessel was then used to fit Arrhenius kinetic parameters from the results of these experiments.

4.5.1 Charts of Experimental Results

The following set of graphs show the results from experiments using five different catalysts, and the uncatalysted reaction, over a range of temperatures. It can be seen that in every case, the rate of reaction is increased with increasing temperature.

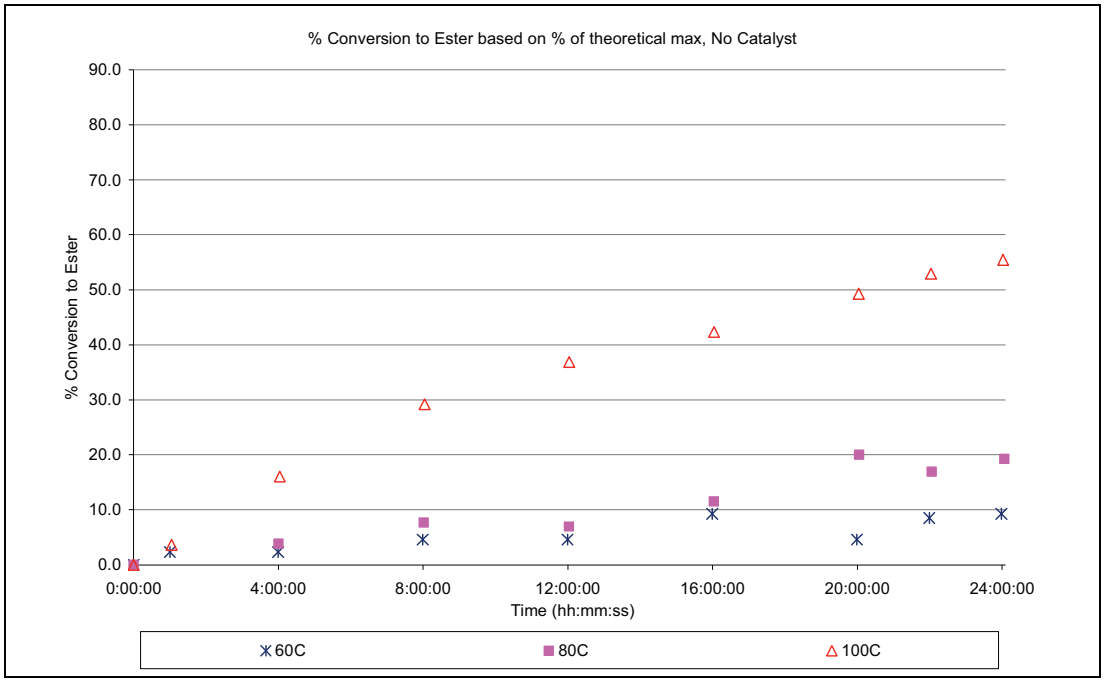

Chart 4.8: No Catalyst (24 Hour Runs) at 60, 80 and 100°C

The apparent divergence at the 20 hour mark in the data for 80°C and 60°C in Chart 4.8 may have been due to a ChemSpeed sampling issue, for example a stuck sampling needle or a mistake in the method protocol. Very long runs in the ChemSpeed Synthesizer allowed slight changes in rates for the slowest reactions to be seen more distinctly, but were generally avoided because it is undesirable to leave the machine running unattended. Shorter runs were performed where possible, and for this reason the x-axes of the following graphs are not of equal length.

Chart 4.9 shows the results for the runs in which the candidate used was zinc acetate dihydrate. The profiles seen are similar to those in Chart 4.8 (for the case with no catalyst), where the yield of ester is less than 30% after 8 hours at 100°C.

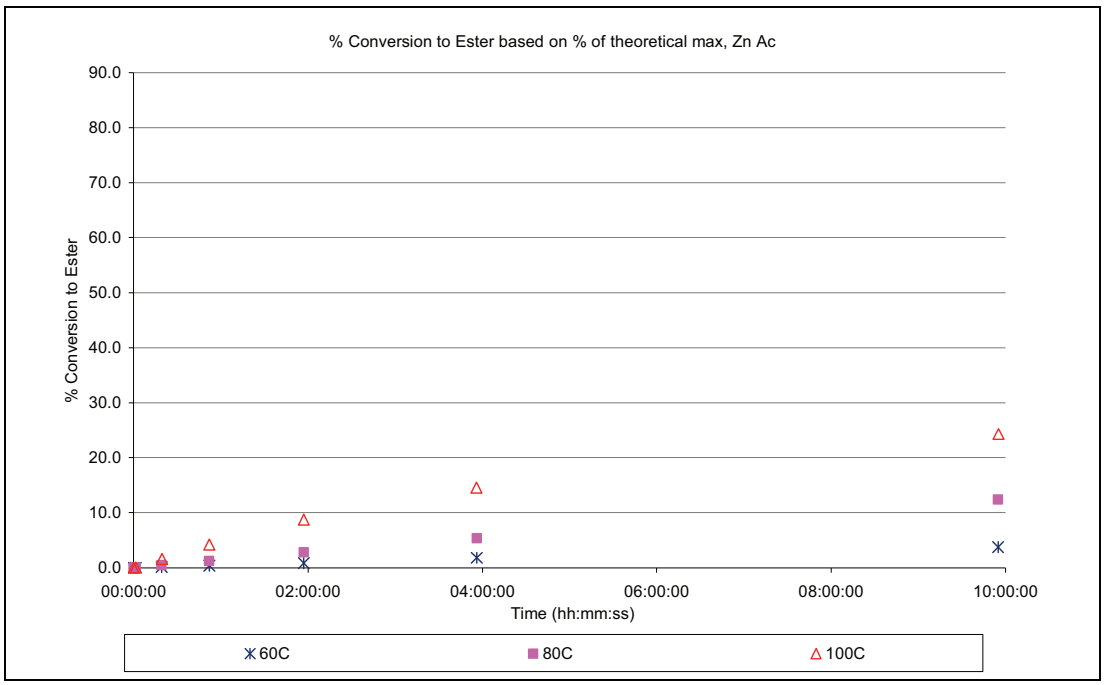

Chart 4.9: Zinc Acetate Dihydrate at 60, 80 and 100°C

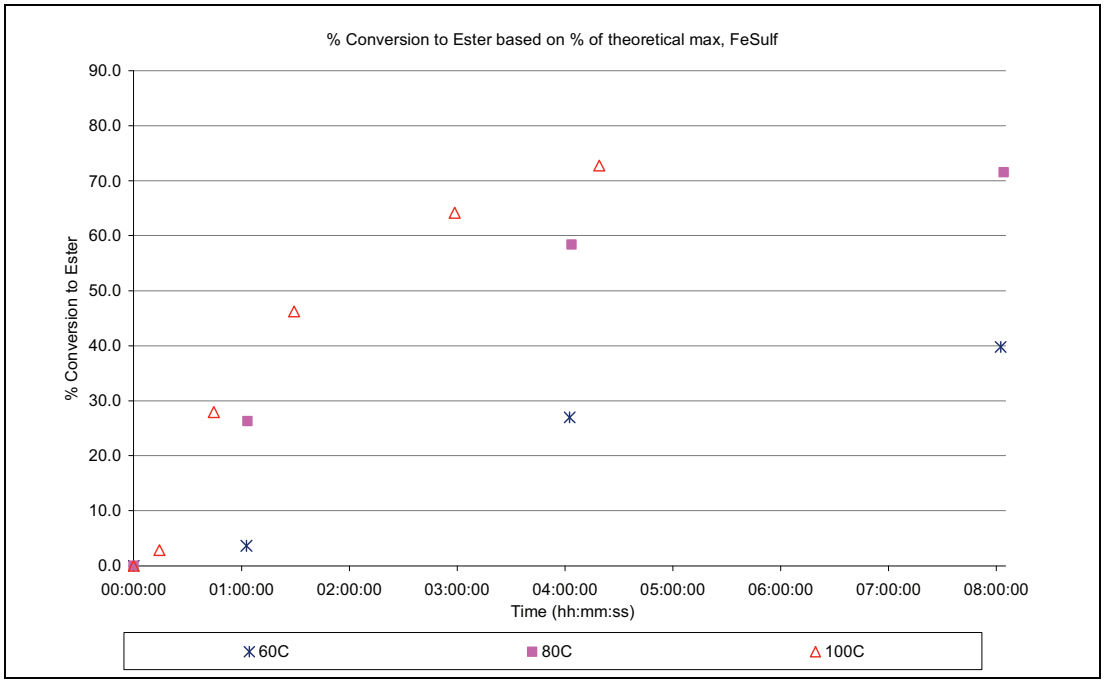

Chart 4.10: Ferric Sulfate at 60, 80 and 100°C

In Chart 4.10 it is seen that the reaction progresses more quickly, with over 70% yield of ester after 4 hours at 100°C. Charts 4.11 to 4.13 show the temperature-dependence test results for the acid catalysts, which had a higher activity than the other candidates and so the duration of these runs was shortened.

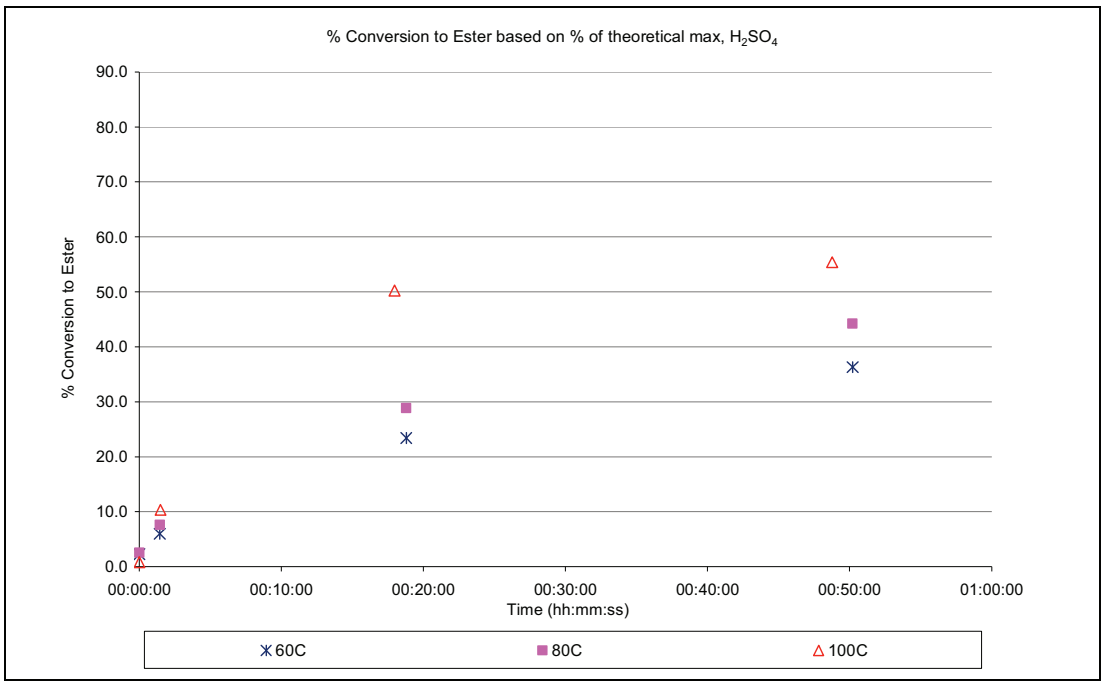

Chart 4.11: Sulfuric Acid at 60, 80 and 100°C

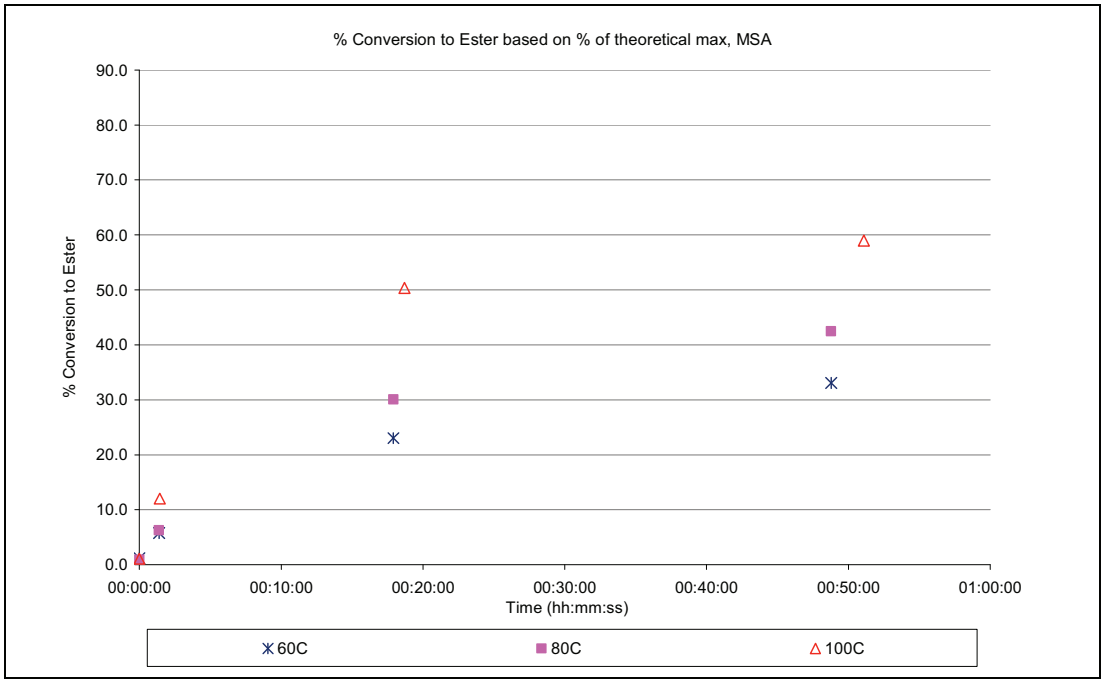

Chart 4.12: Methane Sulfonic Acid at 60, 80 and 100°C

The sets of concentration profiles for the runs using sulfuric acid (Chart 4.11) and MSA (Chart 4.12) are very similar, with well over 50% yield of ester achieved in only 50 minutes. This confirms the result observed in Chart 4.2, that these two candidates have very similarly high initial activity as catalysts for this esterification reaction. Chart 4.13 confirms that phosphomolybdic acid hydrate is less active than these two acids, with less than 40% yield of ester in 50 minutes.

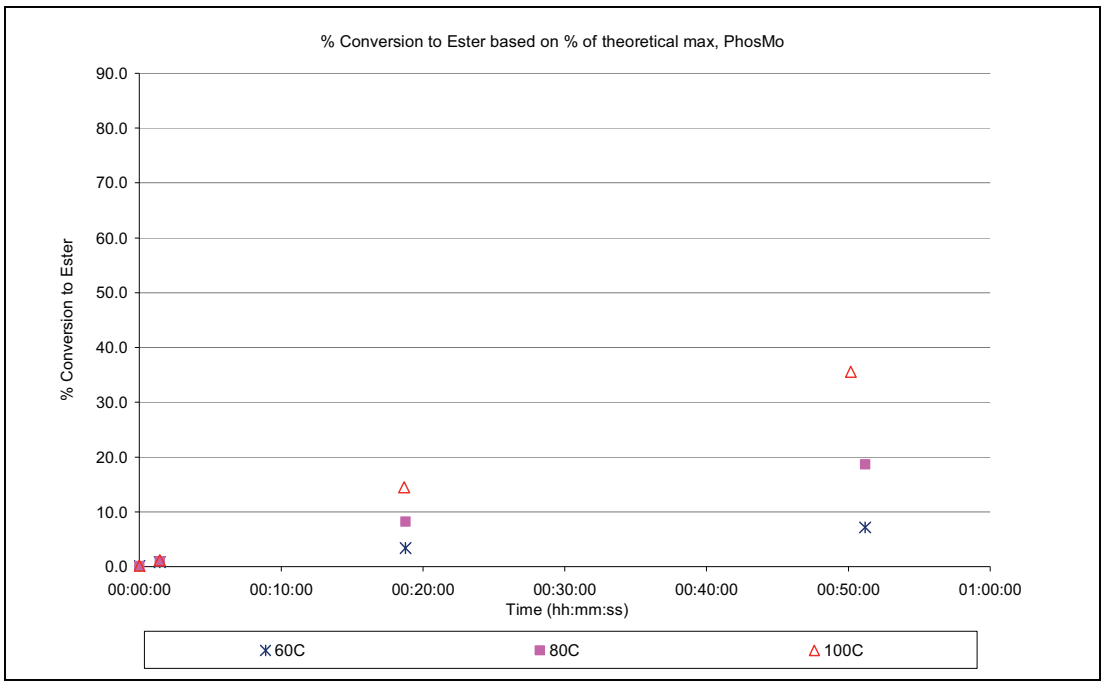

Chart 4.13: Phosphomolybdic Acid Hydrate at 60, 80 and 100°C

4.5.2 Arrhenius Parameters for BatchCAD Model

In all of the above cases, the rate of reaction increases with increasing temperature. The experimental data (n-butyl nonanoate ester concentration vs. time) was loaded into the BatchCAD data manager with the reaction temperature and equilibrium constant, and the Kinetic Fitting tool was utilised to perform fitting of isothermal rate constants.

From the reactor set-up and reaction information, BatchCAD generates a set of mass balance equations which include the forward and reverse isothermal rate constants, values for which must be determined during the kinetic fitting process. As BatchCAD performs the first step of this process, a 'first guess' of 10^{-4} is made for these values, the mass balance calculations are performed, and the results are evaluated against the experimental data. Each time a new 'guess' is made, the error is re-evaluated and a direction for the next guess is determined using an advanced simplex method. Through successive simulations, values for the isothermal rate constants are found which enable BatchCAD to generate concentration profiles that match the experimental data.

When forward and reverse isothermal rate constants have been obtained for the reaction at 3 different temperatures, they are entered into the BatchCAD Arrhenius Constant Calculation tool. These results are shown in Table 4.4.

Catalyst	A_F m3 mol^{-1} s^{-1}	E_F $Jmole^{-1}$	A_R m3 mol^{-1} s^{-1}	E_R $Jmole^{-1}$
None	1.03	62,100	$2.25x10^{-1}$	62,100
H_2SO_4	$1.29x10^{-3}$	29,400	$2.81x10^{-4}$	29,400
FeSulf	3.63	57,600	$7.92\ x10^{-1}$	57,600
MSA	$6.62\ x10^{-3}$	34,200	$1.45x10^{-3}$	34,200
PhosMo	$4.88\ x10^{-1}$	51,400	$1.07x10^{-1}$	51,400
Zn Ac	$2.22x10^{-1}$	57,600	$4.85x10^{-2}$	57,600

Table 4.4: Arrhenius Parameters for BatchCAD models (SI units)

Smith and Reichardt (1941) studied the esterification of methanol and various acids with carbon chains of one to eleven atoms and reported that the average activation energy is around 10,000 cal/mol (41,840 J/mol). The order of magnitude of this value agrees fairly well with the values for activation energy in Table 4.4 above.

4.6 Summary

Screening experiments have been performed on twenty candidate catalysts. The half life values for the nonanoic acid esterification range from 35 minutes to over 12 hours. The most effective catalysts based on half life are:

Catalyst	BatchCAD Predicted Half Life	
	min	hour
Methane sulfonic acid	34.6	0.58
Sulfuric acid	38.0	0.63
PTSA monohydrate	48.6	0.81
Hydrochloric acid	49.9	0.83
Phosphotungstic acid hydrate	78.1	1.30
Phosphomolybdic acid hydrate	81.5	1.36

Table 4.5: Summary of Half Life Values for the Most Active Screened Catalysts

The strong acids have good catalytic activity for the esterification, with short half life values and relatively high activity throughout the course of the reaction. The heteropoly acids also appear to have good performance, giving quite short half lives and consistently high activity during the reaction. Ferric sulfate appears to be an interesting case, with a longer half life but improving activity during the reaction. The Sigma-

Aldrich MSDS information indicates that ferric sulfate is soluble in water, while Wang et al. (2007) report that it is insoluble in their organic-rich reaction mixture of methanol and waste cooking oil. Some of the apparent improvement in the performance of ferric sulfate may therefore be due to increasing solubility in the reaction mixture as the water level increases.

The metal acetates and sulfated zirconia had poor performance in the catalyst screening experiments but literature studies suggest that their performance may be better at higher temperatures. Niobium oxide appears not to be an effective catalyst without the correct preparation and calcination conditions. Hypophosphorous acid does not appear to be effective compared to the other homogeneous acids, giving a slow rate of reaction, a long half life and low activity, while copper chromite shows no activity as a catalyst for this esterification.

The behaviour of the candidates during the reaction, taking into account their molar concentrations, is seen to fall into categories which follow characteristic activity profiles. There is some overlap between these categories, for example the behaviour of the metal acetates zinc acetate dihydrate and sodium acetate trihydrate is similar to that of the ineffective heterogeneous candidates. Ferric sulfate does not fit into any of the categories as it has a very distinct profile in which its activity appears to improve during the reaction, possibly due to changing solubility in the reaction mixture as water forms.

The discussion in the paper by Peters et al. (2006) suggests that for esterification, Brønsted acid availability may be important. A Brønsted acid is one which always transfers a H+ cation. Lotero et al (2005) suggested that the key step in the reaction was the protonation of the carboxylic group in the fatty acid. It may be that this is more effectively achieved with a strong Brønsted acid.

The numerical half life values are taken forward to be used in correlations to attempt to relate the performance of the catalyst candidates to their molecular properties in Chapter 8. The equilibrium point and Arrhenius parameters are used in Chapter 7 during the development of dynamic reactive distillation simulations. The next section of this thesis moves on to discussion of the reactive distillation experimental work.

Chapter 5: Characterisation of the Batch Reactive Distillation Unit

5.1 Overview

This chapter describes the apparatus used for the reactive distillation experimental work and the preliminary work to investigate and characterise the performance of the unit. The capability of the unit is investigated using vapour rate tests, and the number of theoretical stages is confirmed by separation tests with an alcohol binary mixture. Column start-up using the components of the esterification reaction system is also considered in boil-up tests of n-butanol and trial runs using the reaction mixture. Finally, the experimental procedure to be used for the reactive distillation catalyst experimental work is developed.

5.2 Introduction

The batch reactor – rectifier type reactive distillation unit was newly built in the Pilot Plant Lab of the School of Chemical Engineering and Advanced Materials at Newcastle University. Prior to the start of this test work the unit was unused, and parameters such as the separation capability had not been characterised. The unit was intended to be a flexible, general-purpose unit, and was not specifically designed for the work in this project. However, a batch reactor-rectifier type of distillation unit is suitable for the testing of catalysts, because the catalysts can be conveniently charged to the reactor-reboiler pot, which can then be emptied and cleaned after each run. Experimental work was required to establish the capability of the unit, and a suitable experimental start up procedure and operating policy.

The performance of the reactive distillation unit must be established in terms of: boil-up rate, separation capability, investigation of the function of reflux controller and the responsiveness to attempts to control the unit by altering the oil temperature. The boil-up rate must be high enough so that material boiling up from the reactor-reboiler pot reaches the condenser and the distillate collection system and so that a controllable distillate collection rate can be observed during experimental work. The separation ability of the packed column must be high enough to obtain the best separation possible between components as they move up the column. A suitable driving force is applied by selection of an appropriate temperature difference between the oil and the pot contents, which are held at the boiling pot of the mixture, which changes with time. The changing

temperature will influence the rate at which reaction occurs in the pot, so the oil temperature must be able to be adjusted promptly in order to avoid long phases where it is higher or lower than intended.

5.3 Batch Reactive Distillation Unit

The batch reactive distillation unit is illustrated in Figure 5.1, which has been adapted from a technical diagram by HWS Labortechnik of Germany. The main glassware items of the unit were manufactured by HWS Labortechnik and supplied by Ken Kimble in the UK.

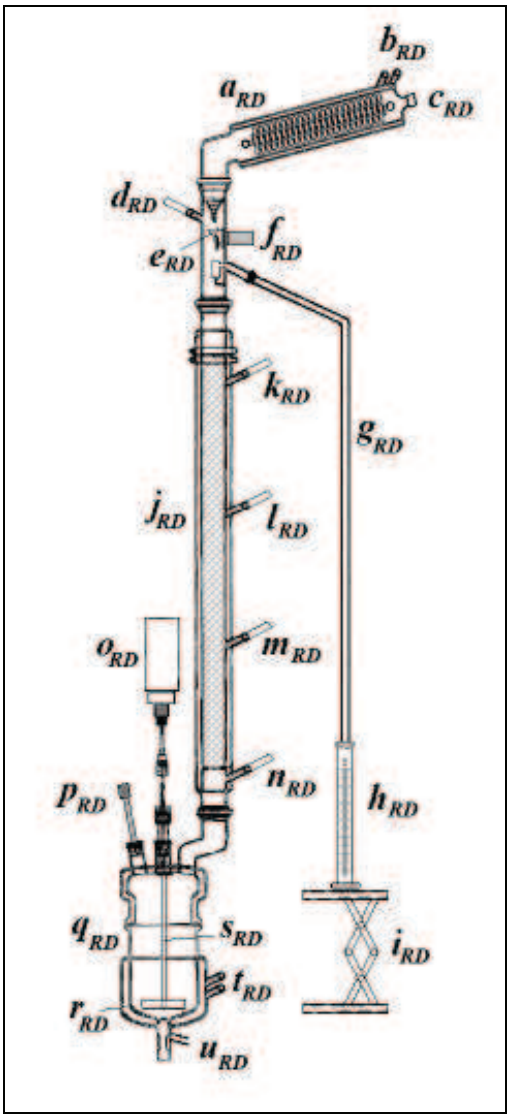

Figure 5.1: Diagram of Reactive Distillation Unit Main Items adapted from HWS Technical Diagram

a_{RD} Glass Condenser

b_{RD} Cooling water inlet & outlet

c_{RD} Connection to vacuum pump

d_{RD} Column top PT100 temperature sensor

e_{RD} Distillate collection device

f_{RD} Magnetic switch

g_{RD} Glass distillate collection arm

h_{RD} Distillate collection vessel (100ml measuring cylinder)

i_{RD} Lab jack

j_{RD} Glass distillation column (packed, vacuum jacketed)

k_{RD} Column PT100 temperature sensor (T4)

l_{RD} Column PT100 temperature sensor (T3)

m_{RD} Column PT100 temperature sensor (T2)

n_{RD} Column PT100 temperature sensor (T1)

o_{RD} Stirrer Motor

p_{RD} Reactor/reboiler temperature probe

q_{RD} Glass reactor/reboiler (2L)

r_{RD} Oil jacket

s_{RD} Stirrer rod (PTFE)

t_{RD} Connections to recirculating oil bath

u_{RD} Reactor base outlet

The distillation column has an internal diameter of 50mm and is packed with Sulzer DX-type hastelloy structured column packing, to a height of 1m. The column is silvered and insulated by a vacuum jacket to prevent heat loss. There are four entries for temperature probes along the column and one at the top by the reflux divider device. The probes used are all PT100 type, and numbered from the column base upwards. Beneath the column is the reactor-reboiler which has a volume of 2 litres and has temperature control provided by oil circulating around the jacket. The reactor lid is vacuum-jacketed and has entries for sampling/dosing, temperature probes and the connection to the electrically-powered overhead stirrer.

The condenser is a water-cooled double-spiral type which also has a cooling jacket. A funnel directs returning condensate towards a glass ‘swinging bucket’ collecting/refluxing device (with a metallic actuator arm) inside the column (illustrated in Figure 5.2). An electromagnetic switch positioned on the outside of the column moves this device to the ‘collect’ position when the magnet is activated, and when the

magnet is switched off the device returns to the ‘reflux’ position. The electromagnet can be set to operate automatically on a time-interval basis. The digital reflux controller is a HWS RS04 unit and is connected to the PT100 temperature sensor at the top of the column.

Initially liquid distillate collects in the U-tube chamber. When this is almost full, liquid starts overflowing down the collection arm to the collection vessel. The liquid lock which forms here provides a barrier to prevent vapour flowing straight down the collection arm.

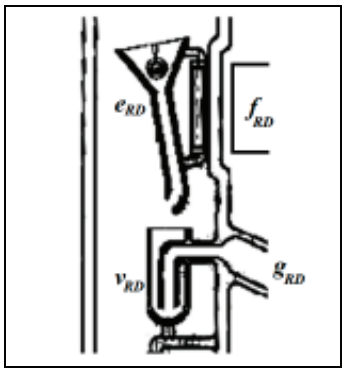

Figure 5.2: Detail of Reflux Divider Device adapted from HWS Technical Diagram

e_{RD}	Distillate collection device
f_{RD}	Magnetic switch
g_{RD}	Glass distillate collection arm
v_{RD}	U-tube liquid lock chamber

The distillate collection vessel was usually a measuring cylinder, as this allowed the observation of the rate of distillate collection. It could also be replaced with one or a pair of round-bottom flasks, suitable for use under vacuum operation. A single round bottom flask can be seen in the photo in Figure 5.3, where the data collection PC and digital reflux controller can also be seen upon a table, and beneath this table is the vacuum pump and digital pressure gauge, which are linked to the top of the column by NALGENE vacuum tubing. The Julabo recirculating oil bath is situated behind this table, and is connected to the reactor/reboiler by red tubes. Non-vacuum jacketed sections of the column are covered by silver-backed insulation material. The unit is supported within a metal structure.

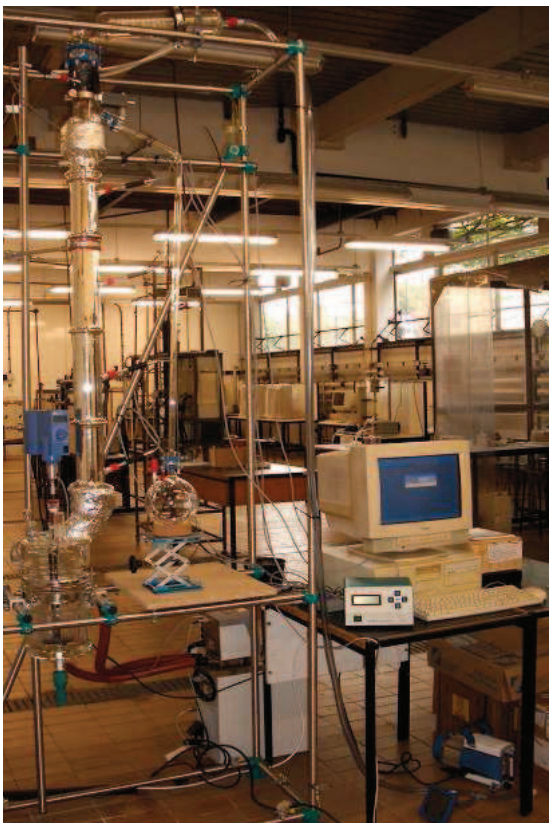

Figure 5.3: Photo of Reactive Distillation Unit

Data is automatically recorded from these probes as they are connected to a DaqPro data logger and a PC. The Julabo oil bath and the reflux controller however, were not supplied with PC connections and so temperature readings from these devices were recorded manually.

A series of tests were performed with the column in order to investigate the capability of the unit and to develop the operating procedures. These tests are described in the following sections of this chapter.

5.4 Vapour Rate Tests

5.4.1 Aims

The aims of these tests were to: investigate the capability of the RD unit, determine the boil-up rate achievable by the column and to observe how boil-up rate and power consumption vary with oil-reboiler pot temperature difference. These tests were performed using 1L of water at atmospheric pressure, and with oil set temperatures of 125, 135 and 145°C.

5.4.2 Method

The reboiler was charged with 1L water, the condenser cooling water flow was started and the Julabo oil bath was set to give the specified oil temperature. A pre-weighed round-bottomed flask was used as the distillate collection vessel.

The reboiler pot temperature reached 100°C as the water was heated to its boiling point, and the temperatures along the column rose as water vapour formed and started to move up the column. When the column had been observed at steady state for a short while, the reflux controller was switched to 'total collect' and the distillate collected for a measured time. The weight of the collection flask containing water was then taken.

The condensate collection rate was determined, and this was then used to calculate the f-factor, vapour velocity and the heat supplied to vaporise the water. For these calculations it was assumed that at steady state the collection rate is equal to the boil-up rate, and that all the vapour reached the condenser, where it condensed and flowed back down the column. These calculations also assumed that when the refluxer was in total collect mode, all of the condensate was collected as distillate and did not flow back down the column.

5.4.3 Results of Vapour Rate Tests

Table 5.1 shows the results of the vapour rate tests. It can be seen that, as the oil temperature and the oil-pot temperature difference increased, the collected mass of distillate and the distillate collection rate increased. This is further visually illustrated in Chart 5.1.

Test	**1**	**2**	**3**
Oil Temperature (°C)	125	135	145
Oil – Pot ΔT (°C)	24.5	34.3	43.8
Mass Collected (g)	34.3	292.1	466.7
Collection Time (min)	111	205	170
Mass Collection Rate (g/min)	0.31	1.42	2.75
Mass Collection Rate (kg/hr)	0.02	0.09	0.16

Table 5.1: Results of Vapour Rate Tests

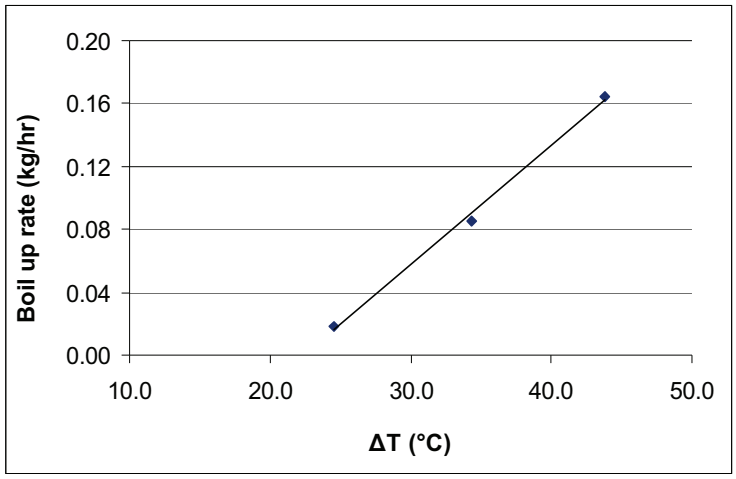

Chart 5.1: Boil-up Rate vs. Oil-Pot Temperature Difference

The equations used to calculate further derived results from the data in Table 5.1 are as follows. The vapour density is calculated by equation 5.1:

$$\text{Vapour density (kg/m}^3\text{)} = \rho_v = Mr \times \left[\frac{\text{Pressure (kPa)}}{R \times \text{Temperature (K)}} \right] \quad (5.1)$$

Where:

- Mr = the molecular weight (18.02 kg/kmol for water)
- R = universal gas constant 8.314 J/kmolK
- The pressure is 101 kPa (atmospheric)
- The pot temperature remained at the boiling point of water, 100°C (373K)
- Property information for water is taken from Perry & Green (1997)

Assuming that the boil-up rate is equal to the mass collection rate, the vapour velocity is given by equation 5.2:

$$\text{Vapour velocity (m/s)} = \frac{\text{Mass collection rate (kg/s)}}{\rho_v \ / \ \text{Column XS Area (m}^2\text{)}} \quad (5.2)$$

The column cross sectional area is given by equation 5.3:

$$\text{Column XS Area (m}^2\text{)} = \pi \times 0.025^2 \quad (5.3)$$

Where 0.025 is the inside radius of the column, in metres. The F-factor is a measure of vapour loading of the column, and is calculated by equation 5.4:

$$\text{F Factor} = \text{Vapour velocity (m/s)} \times \sqrt{\rho_v} \quad (5.4)$$

The heating that must be supplied to the column in order to achieve the boil up rate is given by equation 5.5:

$$\text{Heating} = H_{vap} \times \text{Mass collection rate (kg/s)} \quad (5.5)$$

Where:

- H_{vap} = heat of vaporisation (2259 kJ/kg for water)

The derived results are summarised in Table 5.2 below.

Test	**1**	**2**	**3**
Oil – Pot ΔT (°C)	24.5	34.3	43.8
Vapour Density (kg/m^3)	0.58	0.58	0.58
Vapour Velocity (m/s)	0.005	0.022	0.038
F factor (Pa$^{0.5}$)	0.004	0.016	0.029
Heating (W)	12.6	56.5	100.4
Heating per degree C ΔT (W/°C)	0.51	1.65	2.30

Table 5.2: Derived Results of Vapour Rate Tests

In Chart 5.2 the vapour velocity is plotted against the oil-pot temperature difference. It is observed that the vapour velocity increased as the oil-pot temperature difference, which provides the driving force for boil-up, was increased.

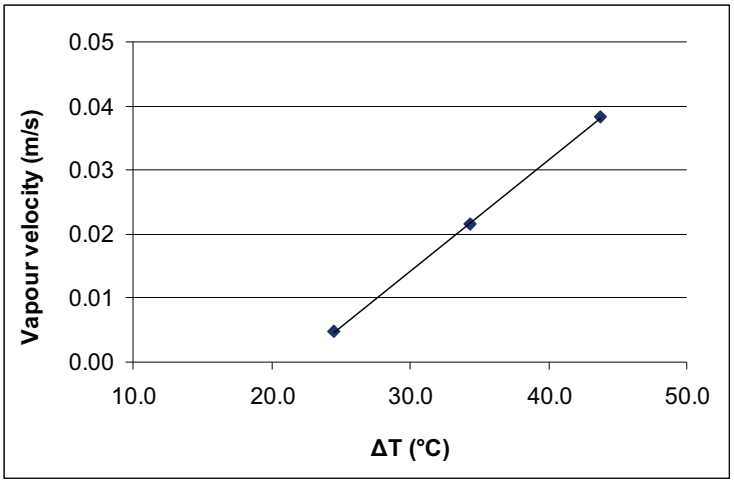

Chart 5.2: Vapour Velocity vs. Oil-Pot Temperature Difference

The F-Factor also increased with the oil-pot temperature difference, but the F-factor range of 0.004 to 0.03 seems low compared to the range discussed by Tuchlenski et al. (2001) of 1 to 2.5. Additionally it was revealed that more heat must be applied per °C of

the desired temperature difference between the oil and the pot, as the magnitude of the temperature difference increases. This is demonstrated in Chart 5.3.

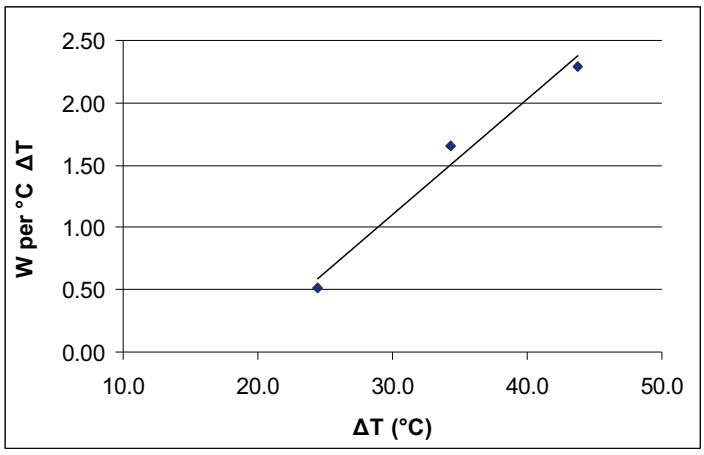

Chart 5.3: Heating per °C ΔT vs. Oil-Pot Temperature Difference

5.4.4 Summary of Vapour Rate Tests

The vapour velocity, F-factor and heating all increased with a higher oil temperature and higher ΔT between the oil and the water. However, their actual values were lower than expected. It is possible that the reboiler heat transfer coefficient is poor, or that the assumptions that the collection rate was equal to the boil-up rate were invalid, e.g. because not all the water was collected as it flowed down from the condenser.

It was observed during the tests that, at the higher oil temperature of 145°C, the liquid-lock-overflow collection device on the column was occasionally overwhelmed and not able to collect all of the condensate. Also there were some parts of the system, for example in the condenser and in the liquid lock, where some 'dead volumes' of liquid collected. It was assumed that once these had been filled during the warm-up phase of a run, they no longer had an impact on the collection rate.

From these vapour rate tests it was concluded that:

- It is necessary to allow sufficient time for the system to settle to steady temperatures and hold-up when operating
- The driving force for boil-up, the oil-pot temperature difference, needs to be high enough to achieve good collection rates but not so high that the collection system is overwhelmed.

5.5 Separation Power Tests

5.5.1 Aim

The aim of performing separation power tests is to confirm the theoretical number of stages in the column packing.

5.5.2 Method

The reboiler was charged with 1100ml of a 50/50 mixture of 1-propanol and 2-butanol. (The actual composition was checked before each run by sampling and analysis on GC). These two alcohols were chosen due to their close boiling points, which are shown in Table 5.3.

Compound information	**1-Propanol**	**2-Butanol**
Boiling point	97.1°C	99°C
Supplier	Sigma-Aldrich	Sigma-Aldrich
Catalogue Number	34871	B85919
Grade	99.9%	99%

Table 5.3: Separation Mixture Information

The column took approximately 1 hour and ten minutes to heat up, and then was held under the full reflux setting for a further hour and twenty minutes to get as near to steady state as possible. A small sample was then taken by switching the reflux controller to total collect for a short time (less than 1 minute) to collect a sample for analysis by GC.

The temperature setting for the oil (135˚C) was chosen as it is high enough to get a good boil-up rate so that the material reaches the condenser at the top of the column, but was also a compromise. Increasing the oil-pot temperature difference by increasing the oil temperature revealed a problem whereby the alcohol vapour passes straight through the collection line, and condenses as it passes through towards the collection vessel. This means that there is a distillate collection even when the reflux controller is not set to collect and therefore the column was not completely at steady state. This problem did not occur when water was used in the previous vapour-rate tests but was difficult to

avoid with the alcohol mixture: even when the temperature was reduced slightly, a small amount of material escaped through to the distillate collection.

Observation of the operation of the reflux collection system during the preliminary tests revealed that a small plug of liquid would collect and sit in the liquid-lock U-tube section (illustrated in Figure 5.2), but would be quickly pushed through to the collection line. A possible explanation for this issue is that the alcohol has a different surface tension to water, and there was very little 'grip' between the liquid and the glass surface to keep the liquid in place.

Compound Name	**Surface Tension 20°C (dyn/cm)**	**Surface Tension 100°C (dyn/cm)**	**Source**
Water	72.74	58.92	Perry & Green (1997)
1 Propanol	25.38	15.60	Yaws (2003)
2 Butanol	24.96	15.32	Yaws (2003)
1 Butanol	26.26	17.08	Yaws (2003)

Table 5.4: Water and alcohol surface tensions

5.5.3 Sample Analysis

The results were analysed using a calibration curve that was prepared from GC analysis of standards of known concentrations of 1-propanol and 2-butanol. Calculations were then performed to determine the compositions of the samples taken from the column.

GC System

Varian CP3800 GC with Saturn 2200 GCMS

Detector: FID

Carrier gas: Mixture (Nitrogen, Helium, Air)

GC Column: CP Porabond Q

GC Analysis Method File Settings

- MS Scan From 0.1 minutes to 10 minutes
- (Low mass 40 m/z, high mass 500 m/z)
- Column flow 1ml/min
- Front injector Temperature 150˚C
- Split ratio 40

Oven temperature

- Start: 40˚C, hold for 1 minute.
- Ramp temperature to 60˚C by 4˚C per minute, then hold for 4 minutes.
- Total time: 10 minutes.

Typical retention times

Compound Name	Retention Time (Minutes)
1 Propanol	4.9
2 Butanol	7.5

Table 5.5: GC retention times for separation alcohols

Calibration curves

Sample vials containing a small amount of original sample, diluted with methanol, are run in the GC in duplicate and average areas of the alcohol peaks are determined. The concentrations of 1-propanol and 2-butanol are evaluated separately, because the optimal data processing settings for the two peaks were different. Calibration standards were prepared for a range of concentrations of each alcohol to produce calibration curves, which were used to determine the composition of the samples. These are shown in Charts 5.4 and 5.5.

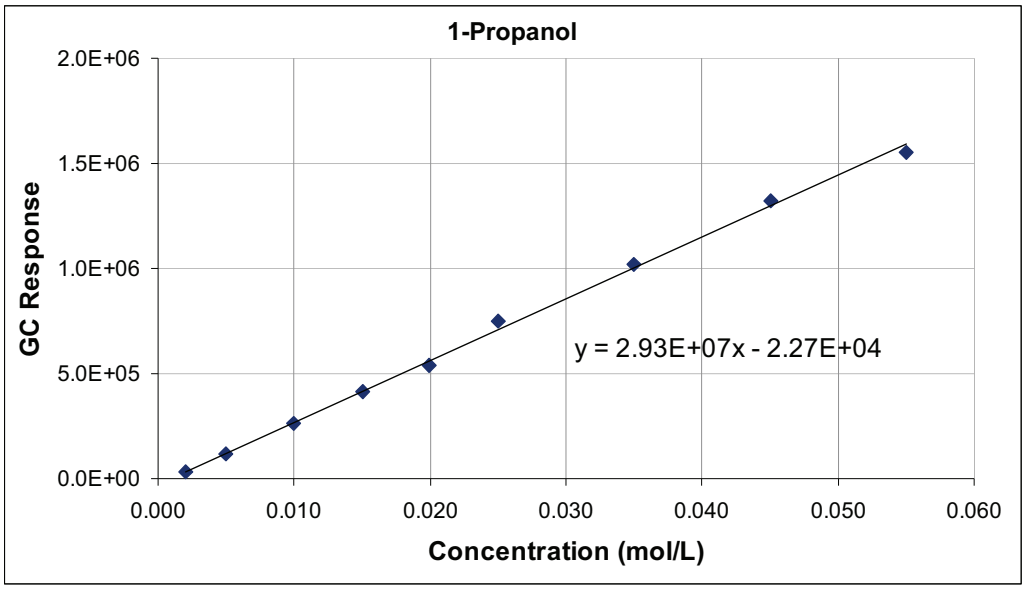

Chart 5.4: 1-Propanol GC calibration curve

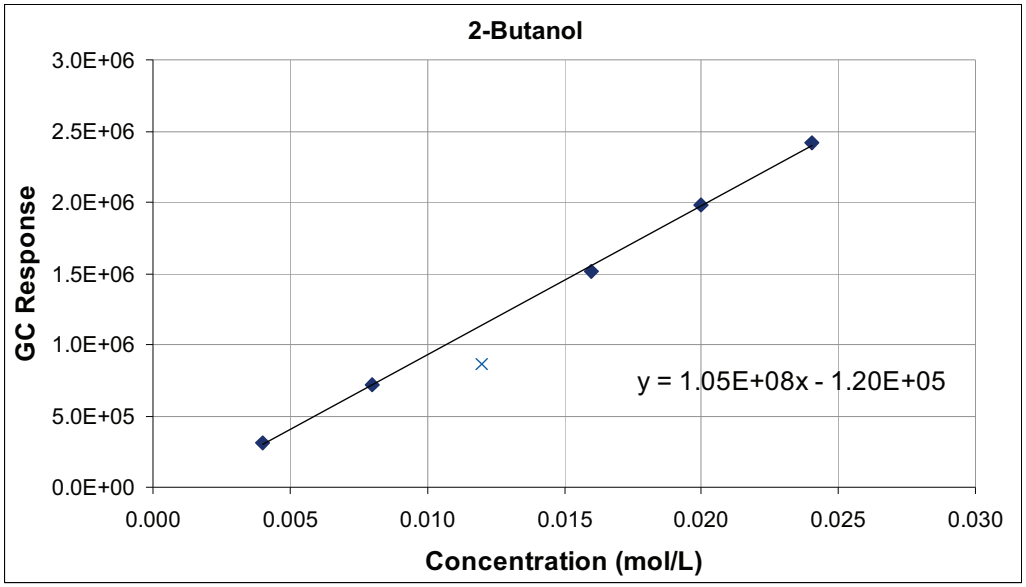

Chart 5.5: 2-Butanol GC calibration curve

An anomalous point seen in the calibration curve for 2-butanol (shown as a cross on Chart 5.5) was not used for the calculation of concentration. This anomalous point could have been due to an incorrect dilution during sample make-up, or an incorrect injection by the automated GC sample handling system.

The values for the mole fractions of the two alcohols in the pot at the start, in the pot at the end and in the distillate are then used to determine the theoretical number of stages in the column.

5.5.4 Calculation of Theoretical Stages

The Fenske Equation for the calculation of the number of theoretical plates for a given separation (at total reflux), as described by Richardson et al. (2002), has been used.

$$n+1=\frac{\log\left[\left(\frac{x_i}{x_j}\right)_d\left(\frac{x_j}{x_i}\right)_b\right]}{\log\left(\alpha_{ij}\right)_{AV}} \tag{5.6}$$

Where:

- n = number of theoretical plates
- x_i = mole fraction most volatile component in liquid product
- x_j = mole fraction of least volatile component in liquid product

Subscripts *d* and *b* indicate the distillate and bottom products, respectively. The boiling point of 1-propanol is 97°C, lower than that for 2-butanol at 100°C, making 1-propanol the more volatile component.

Average relative volatility is calculated as:

$$\left(\alpha_{ij}\right)_{AV} = \left[\left(\alpha_{ij}\right)_d \left(\alpha_{ij}\right)_b\right]^{1/2} \tag{5.7}$$

Relative volatility is given by:

$$\alpha_{ij} = \frac{\left(y_i / x_i\right)}{\left(y_j / x_j\right)} \tag{5.8}$$

Where:

- x_i = mole fraction 1-propanol in liquid
- x_j = mole fraction 2-butanol in liquid
- y_i = mole fraction 1-propanol in vapour
- y_j = mole fraction 2-butanol in vapour

5.5.5 Results: Separation Test 1

Feed composition:

$x_i = 0.56$

$x_j = 0.44$

Distillate composition:

$x_i = 0.86$

$x_j = 0.14$

$y_i = 0.87$

$y_j = 0.13$

Therefore, from Equation 5.8:

$$\left(\alpha_{ij}\right)_d = \frac{0.87/0.86}{0.13/0.14} = 1.09$$

Bottom product composition:

$x_i = 0.54$

$x_j = 0.46$

$y_i = 0.56$

$y_j = 0.44$

Therefore, from equation 5.8:

$$\left(\alpha_{ij}\right)_b = \frac{0.56/0.54}{0.44/0.46} = 1.08$$

Therefore, from equation 5.7, the average relative volatility is:

$$\left(\alpha_{ij}\right)_{AV} = \left[1.09 \times 1.08\right]^{1/2} = 1.087$$

The number of theoretical plates is given by equation 5.6:

$$n+1 = \frac{\log\left[\left(\frac{0.86}{0.14}\right)_d \left(\frac{0.46}{0.54}\right)_b\right]}{\log(1.087)}$$

$n + 1 = 19.8$ stages (including the reboiler)

$n = 18.8$ theoretical plates.

5.5.6 Results: Separation Test 2

Feed composition:

$x_i = 0.45$

$x_j = 0.55$

Distillate composition:

$x_i = 0.78$

$x_j = 0.22$

$y_i = 0.79$

$y_j = 0.21$

Therefore, from equation 5.8:

$$\left(\alpha_{ij}\right)_d = \frac{0.79/0.78}{0.21/0.22} = 1.06$$

Bottom product composition:

$x_i = 0.42$

$x_j = 0.58$

$y_i = 0.44$

$y_j = 0.56$

Therefore, from equation 5.8:

$$\left(\alpha_{ij}\right)_b = \frac{0.44/0.42}{0.56/0.58} = 1.09$$

Therefore, from equation 5.7, the average relative volatility is:

$$\left(\alpha_{ij}\right)_{AV} = \left[1.06 \times 1.09\right]^{1/2} = 1.073$$

The number of theoretical plates is given by equation 5.6:

$$n+1 = \frac{\log\left[\left(\frac{0.78}{0.22}\right)_d \left(\frac{0.58}{0.42}\right)_b\right]}{\log(1.073)}$$

$n + 1 = 22.5$ stages (including the reboiler)

$n = 21.5$ theoretical plates.

The average result for the number of theoretical plates is 20.2.

5.5.7 McCabe-Thiele Diagrams

Visual confirmation of the number of theoretical stages was given by McCabe-Thiele diagrams based upon the starting and end compositions from the experiments. These were drawn up based on the guidelines from Richardson et al. (2002) and are shown in Figures 5.4 and 5.5. The equilibrium curve for the 1-propanol, 2-butanol mixture at atmospheric pressure was obtained from BatchCAD and the steps between the operating line and the equilibrium curve were drawn manually.

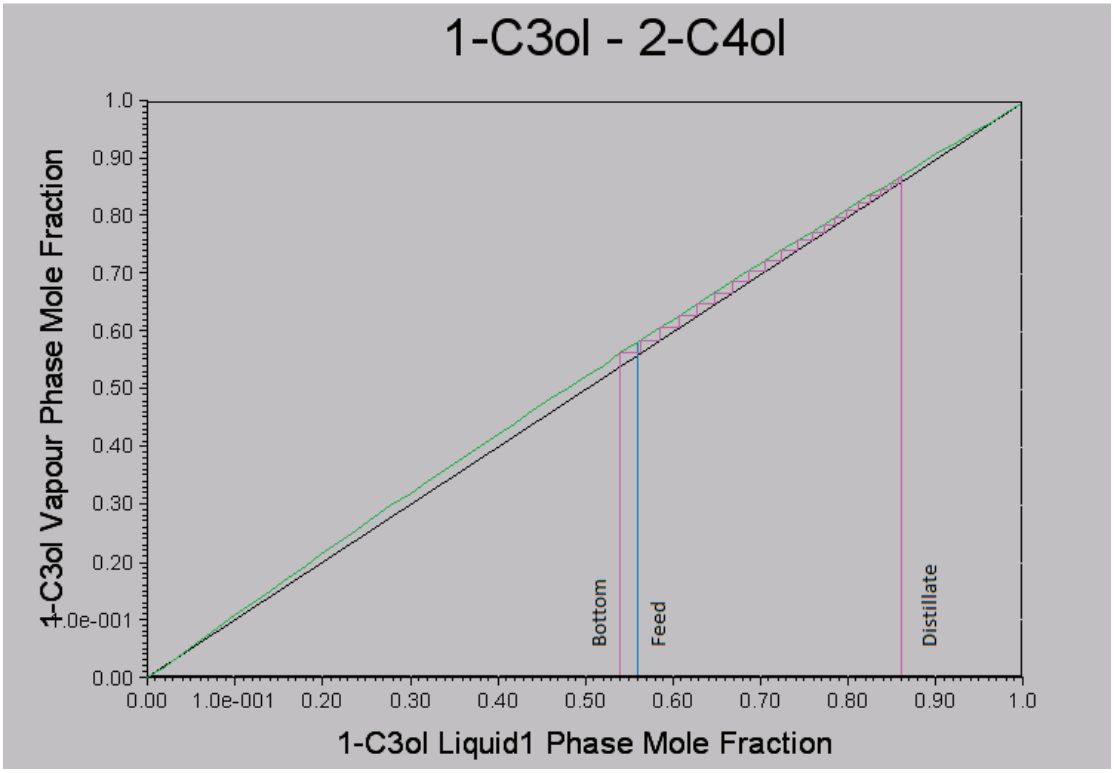

Figure 5.4: McCabe-Thiele diagram: Separation Test 1

The McCabe-Thiele diagram based upon the first separation test (Figure 5.4) suggests that the column has 20 theoretical stages (19 theoretical plates + reboiler).

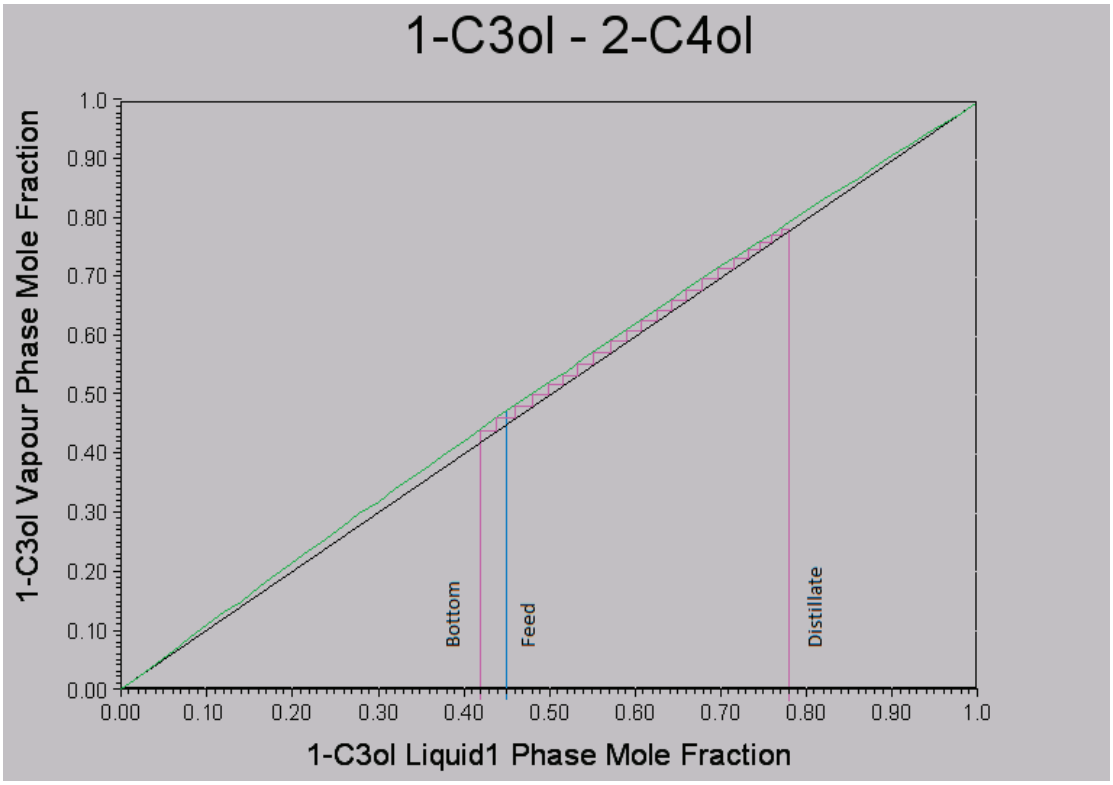

Figure 5.5: McCabe-Thiele diagram: Separation Test 2

The McCabe-Thiele diagram based upon the second separation test (Figure 5.5) suggests that the column has 21 theoretical stages (20 theoretical plates + reboiler).. The average result from both McCabe-Thiele diagrams is 19.5 theoretical plates.

5.5.8 Summary of Separation Power Tests

The averaged result from Fenske calculations to determine the number of theoretical plates in the column was 20.2 plates, while the averaged result from McCabe-Thiele diagrams was 19.5 plates. These tests have confirmed that the column is able to deliver the separation performance described by the supplier of around 20 theoretical stages.

5.6 Butanol Boil-up Test

5.6.1 Aim

The appropriate operation strategy of the reactive distillation unit will depend upon the materials charged to the reactor/reboiler pot. A boil-up test was performed in order to observe how the alcohol to be used in the reactive runs, n-butanol, behaves in the column. Observations were made as to whether the carry-over issues that were observed in the previous separation tests also happen when n-butanol is used.

5.6.2 Method

The reactor-reboiler pot was charged with 750 ml 1-butanol, and the oil temperature was set to 125°C. The pot temperature increases until it becomes steady at 118.5 °C (close to the literature boiling point of 117.7°C). The pot temperature was then increased and observations made as to the effects on the column temperatures, the boil-up rate, and the distillate collection.

5.6.3 Results of Butanol Boil-up Test

After the pot temperature had been held at 118.5°C for 30 minutes, the column temperatures had not started to increase, so a higher oil temperature was applied (set to 155°C, giving a temperature difference of 38.4°C). After 15 minutes the temperature detected by the Pt100 at position 1 (T1) started to rise. However the oil temperature had to be increased to 160°C in order for the temperatures along the whole length of the column to increase.

As seen in Chart 5.6, a long heat-up time was required for the column temperatures to rise, with long intervals between the temperatures at each Pt100 position rising. The final top temperature took longer than the others, and did not reach the temperature seen at the lower positions.

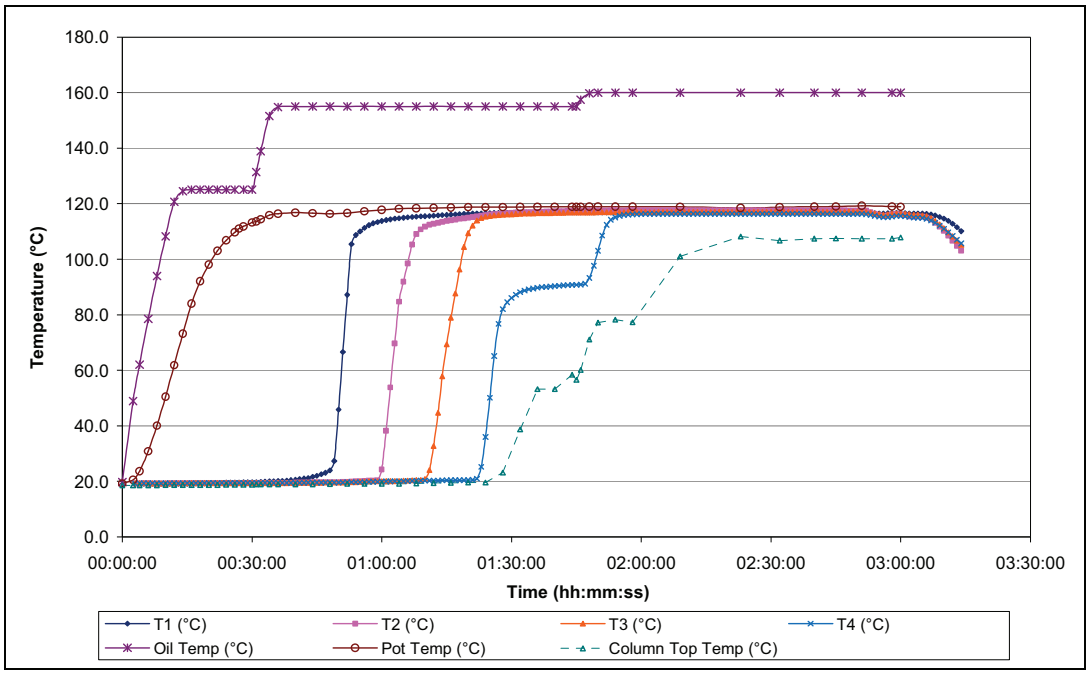

Chart 5.6: Temperature Profiles from Butanol Warm up Test

The following interpretation of these column warm up observations is based on Richardson et al. (2002). At the start of the run, the walls and packing of the column are dry and at room temperature. When vapour begins to form and rise from the pot, it moves up the column but soon meets a cold surface and condenses. As time goes on, the amount of vapour and its velocity increase, and the column and packing gradually start to warm as the vapour is able to travel further up the column. This is the cause of the long delay before the temperature at T1 increases, and the reason for the long pauses before T2, T3, T4 and the top temperature start to rise.

At first, the flow of vapour up the column is not significantly affected by liquid flow back down the column, but as the flow of returning liquid increases, the level of interaction increases. The liquid hold-up takes up some of the free space between the packing material and causes increased resistance to the flow of vapour travelling upwards. The readings from the top temperature probe are affected by the flow of cold liquid from the condenser.

5.6.4 Summary of Butanol Boil-up Test

Good operation of a distillation column requires reasonable hold-up, to provide enough contact for efficient vapour-liquid mass transfer. In this batch distillation column, it takes a while for a reasonable hold-up to be established and for the temperature of the column walls and packing to stabilise. A weaker vapour flow will mean that more time is required for stable conditions to be achieved.

5.7 RD Trial Experiments

5.7.1 Aim

The aim of the following tests was to investigate the behaviour of the nonanoic acid esterification mixture in the reactive distillation unit, identify suitable operating parameters, and develop the procedure to be used when comparing catalyst candidates. In particular, the selection of an appropriate temperature difference between the oil and the pot contents must be made.

5.7.2 Summary of Trial Runs and Outcomes

The parameters that were varied in the method development tests were: the catalyst, the reactant total volume and the temperature control settings used. The butanol to nonanoic acid (NA) molar ratio of the feed charged to the reboiler was kept constant, as was the amount of catalyst (where used).

Trial Run	Catalyst	Volume NA ml	Volume BuOH ml	B/A Molar Ratio
1	None	400	407	2
2	H2SO4	400	407	2
3	PTSA	500	509	2

Table 5.6: Trial Run Conditions and Materials

Trial Run 1: Low oil-pot temperature difference, no catalyst.

- Reactants charged to pot
- Initial oil temperature fixed at 137°C
- Observed pot temperature increasing
- Tested control by changing oil temperature
- Increased oil temperature until some collection occurred (ΔT 26°C)

From this test, it appeared that the minimum ΔT required to give a sufficient boil-up rate from the reaction mixture is 26 °C.

Trial Run 2: Maintain oil-pot temperature difference, H_2SO_4 catalyst

- Trial of keeping ΔT within the range 26°C to 28°C
- A drop in pot temperature occurred when the catalyst was added due to the rapid formation of water
- To maintain ΔT a quick adjustment of oil temperature was needed

A total of only 18ml of distillate was collected, suggesting a ΔT of 26°C would be too low and 28 to 30°C would be more suitable. It was also noted that the catalyst was not charged completely, with some material remaining in the sample vial.

Trial Run 3: Higher charge volume and oil-pot temperature difference, PTSA catalyst

- Target ΔT at 32°C, reduced to 30°C due to a large amount of alcohol passing through to the collection vessel
- Much more distillate collected (38.5ml, of which 11.5ml was aqueous phase)
- PTSA catalyst was much easier to charge due to its solid state.

At 30°C ΔT, the carry-over while the unit was set to reflux was reduced compared to that at 32°C, but still significant, so a temperature difference of 30°C still appears too high.

General Observations

The boil up rate that would be expected for an oil-pot temperature difference of 28°C, based on information from the previous vapour rate tests with water would be 43.5 g/hr. With a reflux ratio of 1 the collection rate would be half this value, approximately 20 g/hr. In the last two hours of the final test run, approximately 17.5 ml of distillate was collected, giving a collection rate of 8.75ml/hr.Taking into account the densities of water and butanol, this is less than 9g/hr, and significantly less than the collection rate expected. However, the operation conditions of the reaction mixture trial runs and the water vapour rate test runs were different. To prevent excessive loss of butanol, the temperature difference (and therefore the driving force for boil-up) was kept much lower in the trial reactive runs.

Distinct phase separation was observed between the aqueous and alcohol phases of the distillate liquid once enough had been collected. The collected material is an azeotrope between water and n-butanol, which will only form once there is some water present in the pot. If the reaction is slow, the slow formation of water will limit the water-butanol azeotrope boil up rate and therefore the collection will be lower. The water-butanol azeotrope has a boiling point of 91.45°C, which is lower than the boiling point of butanol alone, so as long as some water is present the azeotrope would appear first.

5.7.3 Selected Operating Parameters and Techniques

Reactor Warm-up Phase

It was decided to allow an interval of 40 minutes at the start of each experiment so that the reactor contents reached the same temperature each time (the boiling point of the mixture at this temperature and composition was 129°C). This was taken as the starting point for each run, so a sample of the pot contents was taken for analysis to confirm the composition at this point, immediately before the catalyst (if used) was charged. The samples taken from the pot were all small, (a couple of millilitres) so that they cooled quickly to room temperature and were not thought to risk disturbing the column.

Charging of Catalysts

Catalyst candidate compounds were weighed out into a glass vial which was sealed until the catalyst was charged to the reactor. The vial used was weighed before and after the addition in order to record exactly how much was charged. The liquid acids were pre-mixed with a small, known amount of the reaction mixture at room temperature in the lab before charging to the pot.

Oil Temperature at Catalyst Addition

The oil in the Julabo unit is able to heat up much more quickly than it is able to cool down, so the starting temperature of the oil when the catalyst is added requires careful selection. If a very active catalyst is added, then the rapid rate of the drop in pot temperature cannot be matched by cooling of the oil, and if the oil temperature had been initially set to give the desired operating oil-pot ΔT, there will be a considerable phase where the ΔT is too high.

Use of a lower starting oil temperature would shorten the cooling time if a rapid step down is required, however it is not known beforehand how much or how quickly the temperature will change upon catalyst addition. When no catalyst is added, or the catalyst is not as active, then there is no large change in the pot temperature, and the oil temperature must be increased to achieve the specified ΔT. Temperature increases can be achieved in a relatively short time.

- 145°C was taken as 'starting' oil temperature.

Oil-Pot Temp Difference

During the trial runs, the problem of carry over to the collection system when the reflux divider device was set to total reflux (not collecting) was observed. A compromise must be made between adequate driving force and preventing butanol loss.

- 28°C was taken as oil-pot temperature difference.

Reflux Operation

A reflux ratio of 1 is implemented using the reflux controller as a timing device, with the flow directed one way for 10 seconds and then the other for 10 seconds. This allows a good rate of distillate collection without disrupting the flow down the column for too long at any one time and potentially destabilising the column temperatures.

5.8 RD Experimental Procedure

5.8.1 Procedure: Nonanoic Acid Esterification in RD Unit

Initial Charge

- Measure out nonanoic acid, taking temperature
- Measure out n-butanol, taking temperature
- Measure out Catalyst in 8ml glass vial (taking vial weight beforehand)
- Seal vial for transport to pilot plant RD unit
- Charge nonanoic acid and butanol to the pot, mix and take small sample.

RD Unit Start-up

- Reflux controller on and set to full reflux
- Stirrer on and set to 180rpm

- Set oil temperature to 145°C
- Start column temperature data logger and timer
- Record manually: pot temperature, oil temperature, top Pt100 temperature

After Warm-Up Interval

- Sample when pot reaches constant T (129˚C/~40 mins)
- Record manually: pot temperature, oil temperature, top Pt100 temperature
- Add catalyst
- Take sample to fridge, weigh empty catalyst container
- Sample every hour
- Continue recording temperatures frequently

Switch Reflux Operation

- At 1 hour 40 min, switch reflux controller to timed collection.
- Record the volume of any collected distillate
- Continue recording temperatures frequently

End of Run (4 hours 40 minutes)

- Oil temperature switched to cool
- Record distillate volume
- When at room temperature, measure pot content volume and take final sample
- The unit is cleaned with acetone at the end of each run and allowed to dry

A Timeline drawing summarising this procedure is shown in Figure 5.6.

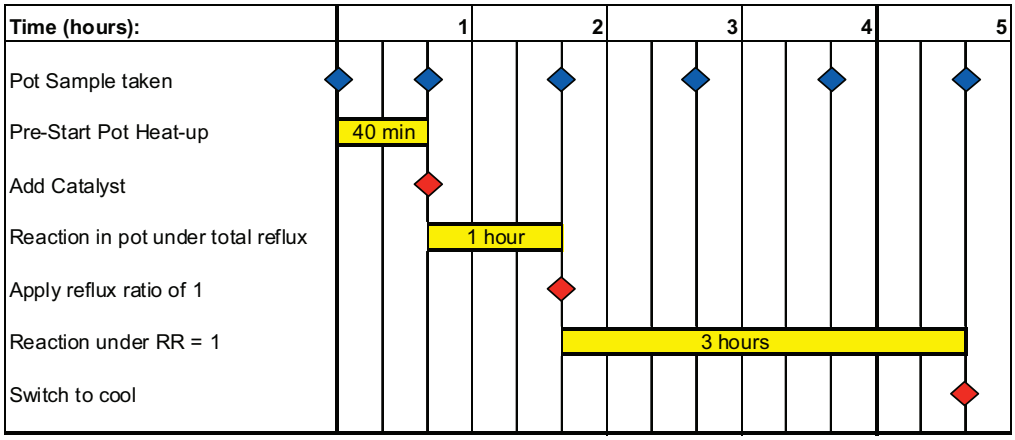

Figure 5.6.: Experimental Protocol Timeline

It was noted from the trial runs that that the distillate collection started at different times in each case, because collection cannot start until water is present in the pot and vapour flows to the top of the column have become established. Therefore, even when reflux ratio is switched to collect at a certain time in the experimental protocol, for a while there may be no collection in some cases such as when there is no catalyst and the reaction is slow. For each experimental run, the actual time that distillate starts collecting is noted. The phase of total reflux operation at the start is to allow some water to form and to prevent high removal of butanol while there is no water present.

The time required for the column to stabilise seems very long, and is a limitation due to the equipment available. The experimental procedure can be compared with that described by Leyes & Othmer (1945b) and shown in Figure 5.7, which involved the complex start up of a continuous unit with feed and sampling from the stages. These authors also found that establishing steady state can take a considerable time: 5 hours had passed before steady state operation began.

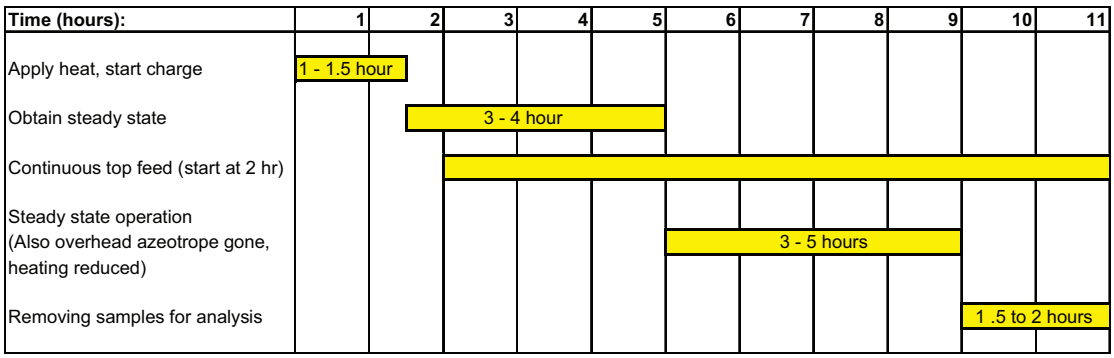

Figure 5.7.: Leyes & Othmer (1945b) Experimental Protocol Timeline

To stop the reaction, the samples were initially stored in a cold water bath in a refrigerator, and later diluted (at room temperature). 250 microL of sample was charged into 1.5ml isopropanol. The further dilutions were then performed in the same way as previously described in Chapter 3, before the analysis was performed by GC.

Distillate composition was recorded as visual observations of the volumes of the aqueous and alcohol phases. The actual composition was then calculated based on interpolation of data for the binary vapour-liquid-liquid equilibrium between butanol and water described by Lee et al. (2004) for atmospheric pressure (101kPa). The values used are shown in Table 5.7.

Temperature (°C)	Alcohol phase mole fraction		Aqueous phase mole fraction	
	Butanol	Water	Butanol	Water
92.27	0.355	0.645	0.021	0.979

Table 5.7: Water - butanol vapour-liquid-liquid equilibrium data (interpolated from Lee et al., 2004)

When the distillate first starts collecting, it is not possible to see two distinct phases. During this time the composition has been estimated using an overall water composition of 74 mol% water in the liquid (Wiley 2007). GC tests of the butanol phase (it was not possible to run the water phase in the GC) indicated that there was no ester in the distillate. The column temperatures and pot boiling temperature confirm this: at 268°C, the boiling point of ester is significantly higher than water-butanol azeotrope.

The example chromatograph shown in Figure 5.8 is an example chromatograph of a sample from the reactor/reboiler pot from a nonanoic acid esterification RD run. The peaks that can be seen are: nonanoic acid at 6.3 minutes, the ester peak at 8.6 minutes, and the butyl laurate internal standard peak at around 12 minutes. Figures 5.9 and 5.10 are from a sample of the butanol phase the end of the same run, when the temperature in the pot was high. Figure 5.10 is the same chromatograph as that in Figure 5.9, but showing a close-up of the baseline, where it can be confirmed that no ester is present.

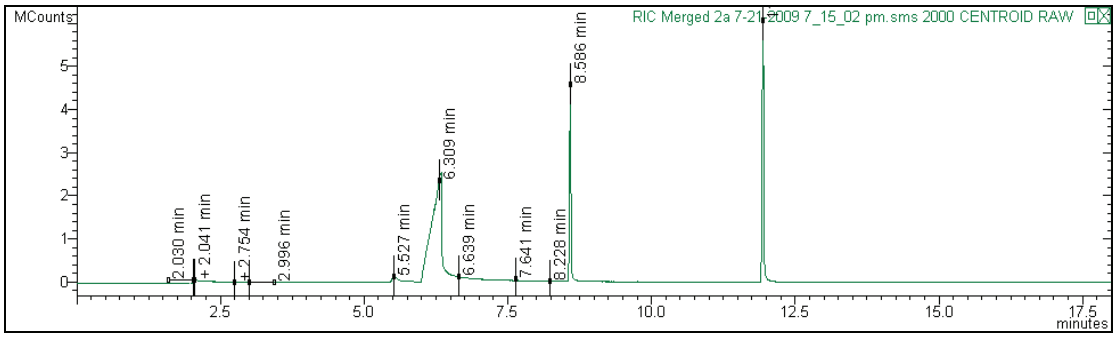

Figure 5.8 Example Sample from Reactor Pot during Esterification RD Run

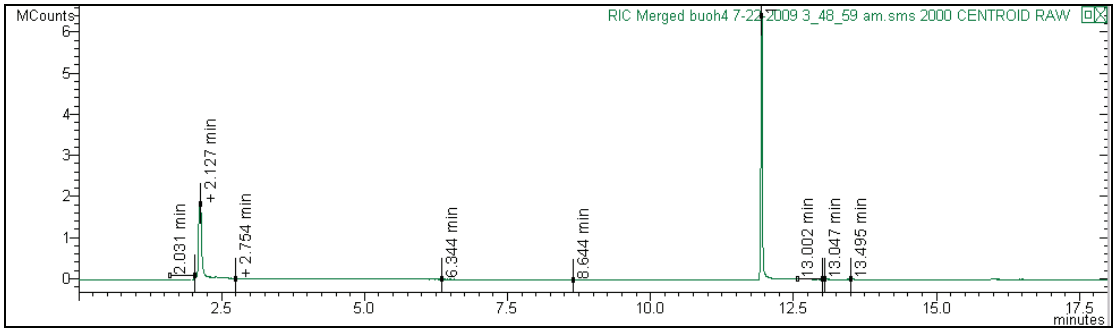

Figure 5.9 Example of GC analysis of Butanol Phase from Esterification RD Run

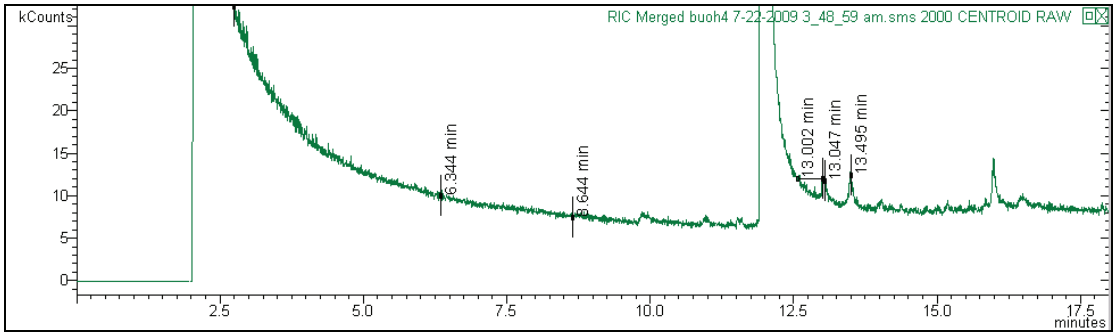

Figure 5.10 Confirmation of Absence of Ester in Butanol Phase by GC Analysis

A small butyl acetate peak is seen at 2.1 minutes in Figure 5.9, this is due to the use of potassium acetate as a candidate catalyst in this run. When the metal acetate has dissociated in the reaction mixture, some acetate groups have formed an ester with the butanol. The amount of this ester was quantified with the GC method developed for propionic acid runs (described in the following section), and it was found that only 21% of the possible acetate groups available from the potassium acetate charged had formed butyl acetate and been collected in distillate.

5.8.2 Propionic Acid Runs

A small number of reactive distillation runs were performed where the reaction system was the esterification of propionic acid with n-butanol. Propionic acid is a shorter carboxylic acid, and the aim of these runs was to compare the results with those from the runs with nonanoic acid. Of particular interest was whether or not the trends and behaviours observed with the catalysts in the nonanoic system are likely to apply to other systems.

In order for the runs to be as comparable as possible, minimal changes were made to the experimental procedure. The runs were shorter, and a different GC method was developed to give analysis of the shorter ester. The same oil-pot temperature difference was maintained, the same molar ratio of reactants was charged to the pot, and the amount of candidate catalyst charged was calculated in the same way (1wt% of the mass of acid charged).

5.8.3 Propionic Acid System GC Method

A GCMS method was developed for following the formation of the shorter-chain ester, butyl propionate.

GC System

Varian CP3800 GC with Saturn 2200 GCMS
Detector: GC Mass Spectrometer with ion trap
Carrier gas: Helium
GC Column: VF-5ms

GC Analysis Method File Settings

MS Scan From 0.5 minutes to 12.5 minutes
(Low mass 40 m/z, high mass 500 m/z)
Column flow 1ml/min
Front injector Temperature 250˚C

Oven temperature:

- Start: 60˚C, hold for 2 minutes.
- Ramp temperature to 250˚C by 25˚C per minute, then hold for 2.9 minutes.
- Total time: 12.5 minutes.

Propionic Acid

Supplier:	Sigma-Aldrich
Catalogue Number:	P1386
Grade:	99%

Butyl Laurate Internal Standard

Supplier: Sigma-Aldrich

Catalogue Number: 435589

Grade: 98%

Butyl Propionate Calibration Standard

Supplier: Sigma-Aldrich

Catalogue Number: 307378

Grade: 99%

Typical retention times

Compound Name	Retention Time (Minutes)
Propionic Acid	2.6
Propionic Ester	4.2
Butyl Laurate	9.4

Table 5.8: Typical GC Retention Times for Propionic Acid System

A seen in Figure 5.9, occasionally butyl acetate is formed when a metal acetate candidate catalyst is used. When these samples are analysed with this GC method, the butyl acetate peak is observed after 3.4minutes (rather than 2.1minutes as seen in Figure 5.9 when the nonanoic acid system GC method was used). Figures 5.11 and 5.12 show typical chromatograms obtained from analysis of samples from the propionic acid esterification system.

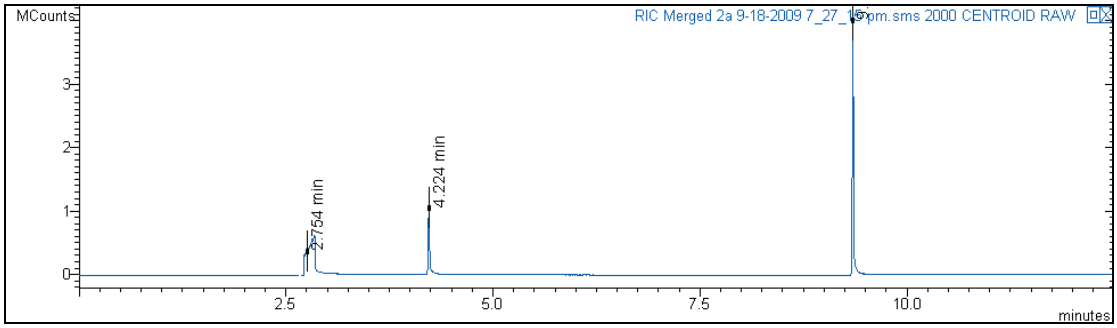

Figure 5.11 Typical chromatogram for the Propionic Acid esterification system: 1st Dilution

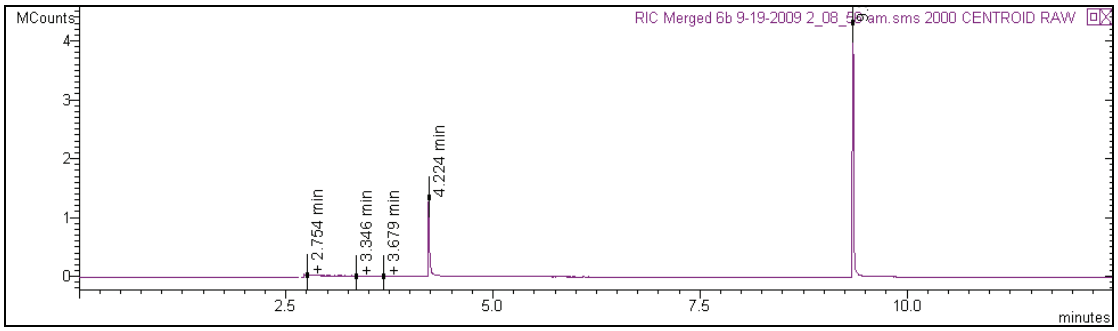

Figure 5.12 Typical chromatogram for the Propionic Acid esterification system: 2nd Dilution

Again, as described previously in Chapter 3, two stages of dilution are used to ensure that the analysis can be performed accurately at both low and high concentrations of ester.

5.9 Summary

This chapter describes the apparatus used for the reactive distillation experimental work and the preliminary work to investigate and characterise the performance of the unit.

The reactive distillation unit in the School of Chemical Engineering and Advanced materials is capable of achieving a strong boil-up rate, but is however limited by the capability of the distillate collection and reflux control system. With high liquid return rates, the collection device is overwhelmed and unable to collect the specified proportion of the flow, and when alcohols are used there is a carry-over through the liquid-lock tube. The boil-up rate is low compared to a literature description, and the values for the F-Factor and vapour velocity were lower than expected.

The separation efficiency was confirmed to match that described by the supplier as 20 theoretical stages. The butanol boil up tests and the trial runs with the reaction mixture revealed that the problem with carry-over also occurs with butanol and the butanol-water azeotrope. To prevent excessive loss of distillate, the temperature difference used, and therefore the driving force available for boil-up from the reaction system, is limited to 28°C.

The experimental methodology has been developed for batch reactive distillation runs to test a range of catalysts with the nonanoic acid esterification system, and this has been extended to be applied to the propionic acid esterification system. The results from the testing of catalysts for performance under batch reactive distillation conditions are presented in Chapter 6.

Chapter 6: Catalyst Performance in Batch Reactive Distillation

6.1 Overview

This chapter reports the results of experiments in which the performance of a selection of candidate catalysts was tested under reactive distillation conditions. The number of catalysts tested was limited by the available time and resources, so 12 candidates were tested and compared against each other and the case with no catalyst for activity in the nonanoic acid esterification system. One run with this system was also performed with a mixture of two of the catalysts charged, and four runs were performed using a different esterification system: the esterification of propionic acid with butanol.

The data presented in this chapter includes temperature profiles from the reactor reboiler pot and the column, distillate collection trends and ester composition charts. The sources of error in the experiments are considered, before a summary is presented of the numerical results which are taken forward for further analysis. Interesting trends were observed during the runs as the system responded to the addition of the catalyst candidates and to the change in reflux ratio policy. It is revealed that the half life of the nonanoic acid esterification obtained from the screening tests is strongly related to the initial behaviour of the reactive distillation system when the catalyst is added.

6.2 Introduction

Data were obtained from 12 experimental runs involving the batch esterification of nonanoic acid and butanol in the reactive distillation unit using various catalyst candidates, in addition to one run where no catalyst was added and one run where a mixed catalyst was used. The time and resources available for these experiments was limited, and each run was time consuming, so all 20 catalysts tested in the screening stage were not tested in the batch reactive distillation unit.

The catalysts which were chosen were prioritised, so that the reactive distillation tests included the most active candidates from the screening tests: the strong acids, the heteropoly acids and ferric sulfate. A number of metal acetates were also included in order to enable the observation of any trends in the order of activity for this group. Some of these metal acetates had not appeared active in the screening tests, but it was anticipated that, along with sulfated zirconium hydroxide, there may have been some

improvement at the higher temperatures used in reactive distillation compared to the ChemSpeed screening. A run with no catalyst charged provided a baseline against which to judge the performance of the catalysts. Four runs were also performed where an alternative reaction system was used: the esterification of propionic acid with butanol. The purpose of performing these tests was to explore whether the trends seen with the nonanoic acid system were unique to that system, or whether similar trends could be expected with similar reaction systems. One run with no catalyst again provided a baseline, while 3 catalysts were chosen to represent different types of catalyst: one strong homogeneous acid (PTSA), one intermediate strength catalyst (phosphotungstic acid) and one metal acetate compound (zinc acetate).

The experimental methodology used is described in Chapter 5, and involves several key points during the experimental runs:

- 40 minutes after start-up, catalyst was added to the pot.
- 1 hour 40 minutes after start-up a change occurred from operating under total reflux to a set reflux ratio of 1 (by selection of time intervals)
- Reactor samples were taken hourly from the 40 minute mark onwards.

During each run, various temperatures were recorded, notes were made of the amount of distillate collected and samples were taken from the reactor/reboiler pot for GC analysis for ester content.

6.3 Experimental Data from Reactive Distillation Runs

In the following section, the results from the experimental RD runs with different catalyst candidates are examined and compared to observe the effect that the addition of the different candidates has on the system. The case with no catalyst is also shown for comparison.

6.3.1 Temperature Profiles: Nonanoic Acid System

Charts 6.1 to 6.3 show comparison charts of the temperature profiles for the reactive distillation runs using the nonanoic acid system, arranged so that the different cases are overlaid. The data from the individual runs with this chemical reaction system are presented in Appendix J. The reactor/reboiler pot temperature profiles are shown in Chart 6.1, while Chart 6.2 shows the temperatures at position T1, just above the pot at

the column base. The temperature at the top of the column near the refluxer device is shown in Chart 6.3.

The x-axis of these charts begins at the 40 minute mark, which is when the catalyst was added (if used). The temperature in the pot depends upon the composition of the liquid, which is affected simultaneously by the reaction and the removal of material by distillation. During the run more ester is formed and levels of the lighter-boiling components water and butanol fall, so the boiling point of the reactor contents increases. In order to maintain the driving force for boil up, which is a result of the oil-pot temperature difference, it was necessary to adjust the oil temperature on a continual basis.

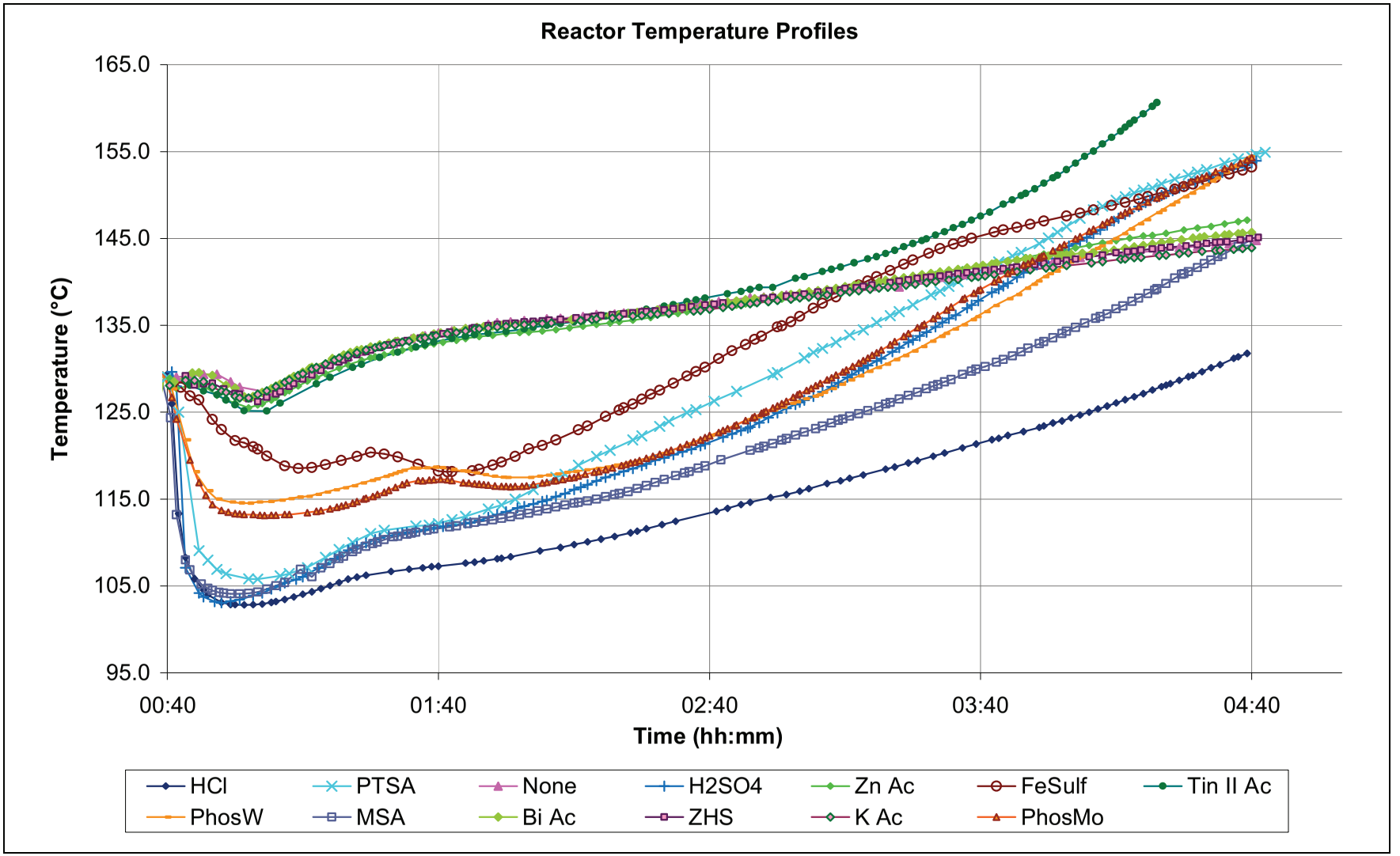

Chart 6.1: Reactor/Reboiler Pot Temperature Profile for Nonanoic Acid Esterification

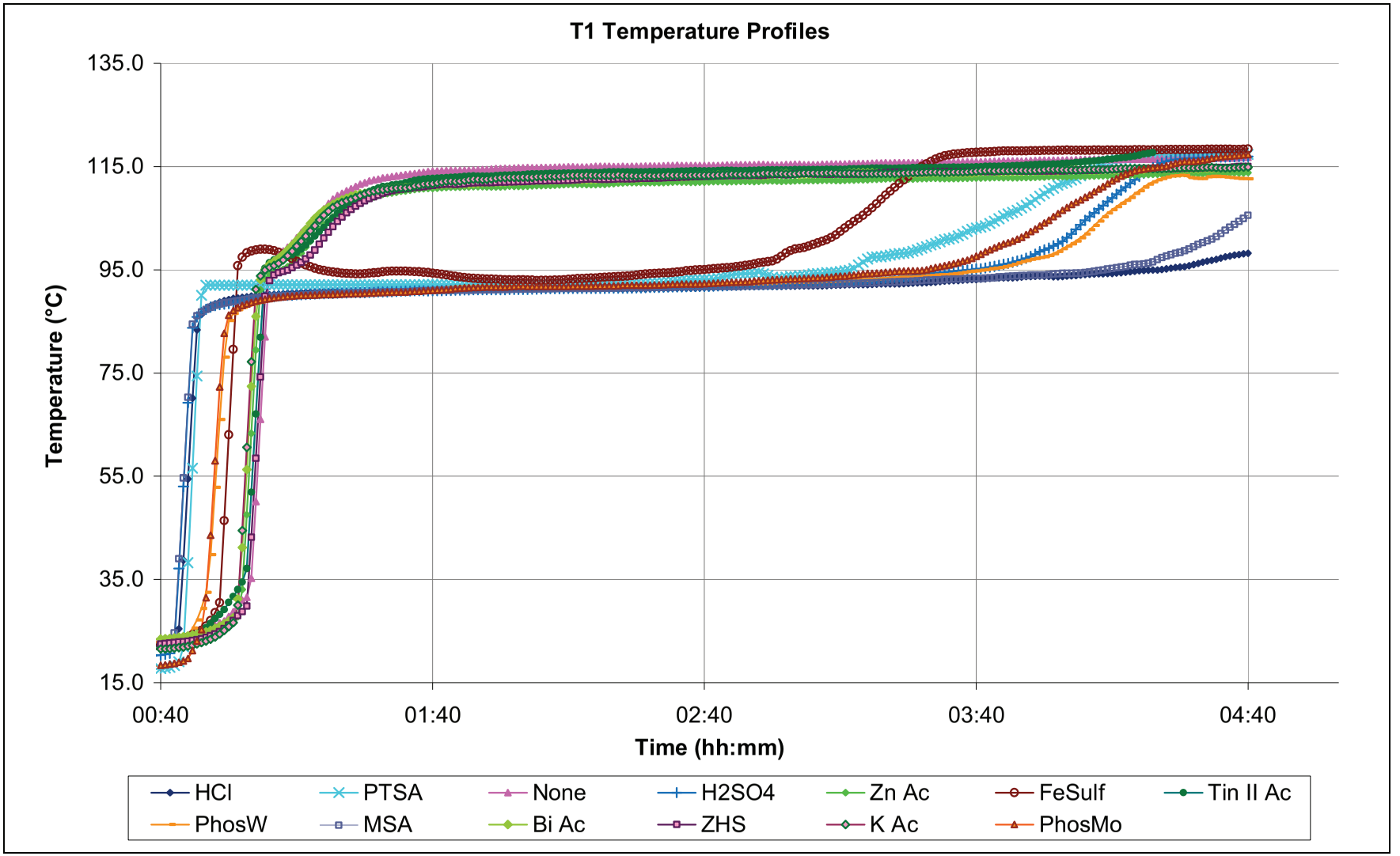

Chart 6.2: Temperature Profile at the T1 Position in the Column: Nonanoic Acid Esterification

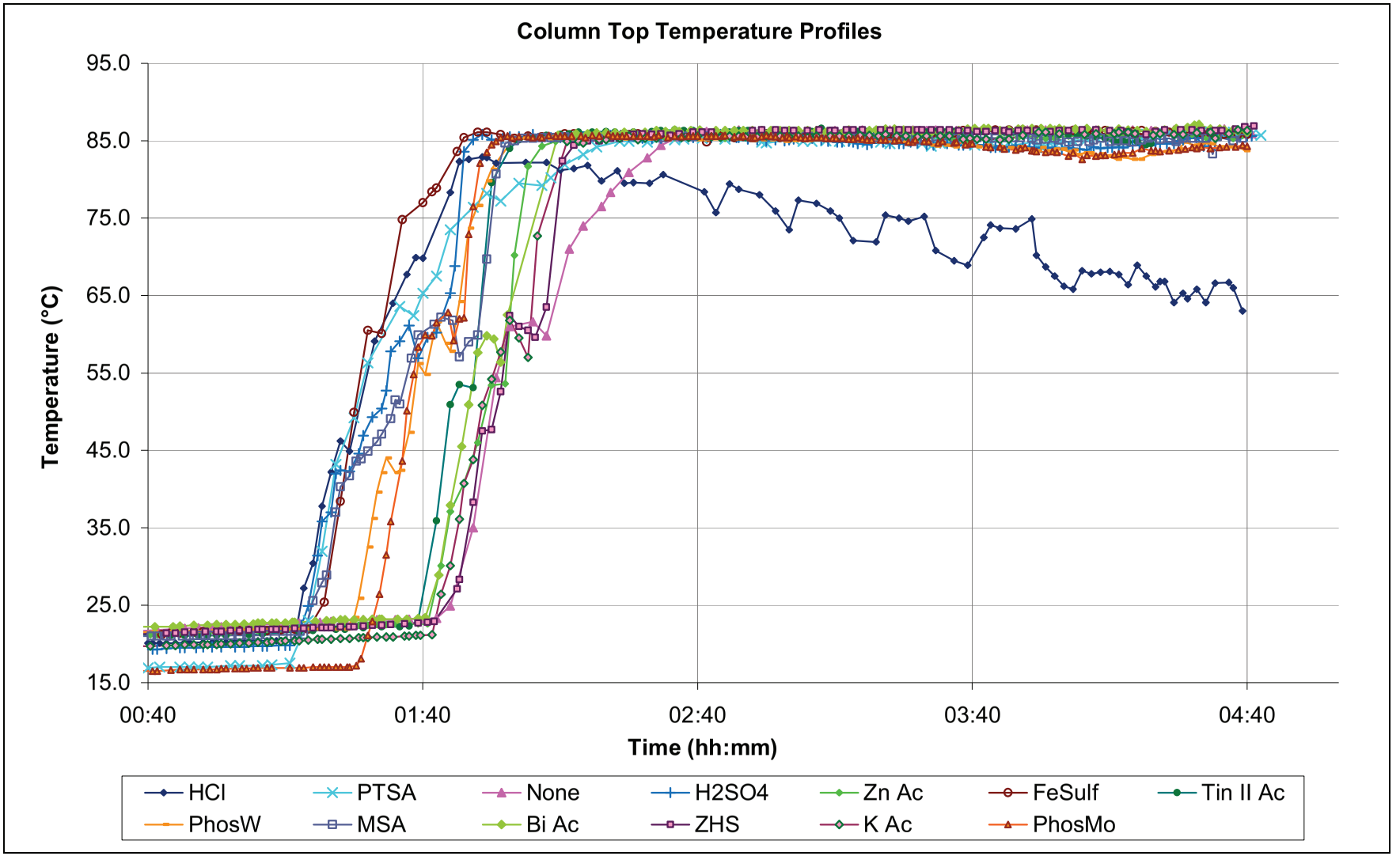

Chart 6.3: Temperature Profile at the Top of the Column: Nonanoic Acid Esterification

From Chart 6.1 it can be seen that the different catalyst candidates cause the system to behave in different ways. The addition of strong acids causes a large amount of water to form suddenly, which boils in an azeotrope with butanol and causes the temperature in the pot to fall rapidly, and the temperatures in the column to rise rapidly (see Charts 6.2 and 6.3). The temperature is then much lower than before, so the reaction proceeds less quickly and the temperature in the pot recovers only very gradually due to slow production of ester. The system is under total reflux, so there is no distillate collection yet and the liquid hold-up capacity of the column packing is occupied by butanol-water mixture. The change in reflux ratio policy from full reflux to a ratio of 1, which allows more water to be removed from the reaction mixture, does not have a dramatic effect on the pot temperature profiles in Chart 6.1 for the cases with strong acids. The rate of temperature increase levels off slightly before this change occurs, and very gradually picks up some time afterwards. It appears that at the time the change occurs, there is not much water present in the pot mixture, available to cause a quick boil-up.

The pot temperature profiles in Chart 6.1 for the cases with no catalyst, sulfated zirconium hydroxide and potassium acetate are almost identical to each other, and in the first half of the chart the metal acetates also appear to follow the same pattern. For a short time after the 40 minute mark, the temperature in the pot slowly decreases. This occurs even in the case with no catalyst candidate. The reaction proceeds at a slow pace and a small amount of water is formed, which lowers the boiling point of the mixture. At first, the amount of butanol-water vapour produced is too low to quickly heat the column walls and packing, so it travels only a short distance up the column before condensing and returning to the reaction mixture (internal refluxing). For a significant time the column liquid hold-up is therefore very low. The pot temperature is observed to increase once the temperatures in the column have started to increase (see Charts 6.1 and 6.2). When the vapour can travel further up the column the liquid hold up is higher and more low-boiling material is removed from the mixture.

From the temperature profiles from position T1 at the bottom of the column, shown in Chart 6.2, it can be seen that the column warm-up begins in these 3 slow-reacting cases much later than in the cases where strong acids are used. When a strong acid is added to the reaction mixture, lots of water is formed quickly and the strong flow of hot vapour ensures that the column walls and packing heat up quickly. In cases where the initial vapour flow is much weaker, there is much more of a delay before the vapour is able to

move a significant distance up the column, become held up on the packing and become effectively removed from the reaction mixture. Comparison of Charts 6.2 and 6.3 demonstrates that it then takes quite some time for the temperatures at the top of the column to rise.

The pot temperature profiles in Chart 6.1 for cases using metal acetates start very similar to the case with no catalyst. The pot temperature profiles for runs with zinc and bismuth acetates rise slightly above that for the case with no catalyst towards the end of the run, however those for cases with potassium acetate and sulfated zirconium hydroxide do not. The pot temperature profile of the tin (II) acetate run appears highly anomalous, as the pot temperature increased rapidly in the second half of the run, such that this run had to be ended earlier than intended as the high temperature cut-out of the oil bath was reached. In Chart 6.2 it is seen that the temperatures at the base of the column start to rise at approximately the same time for all cases where metal acetates are used and the case with no catalyst. However, Chart 6.3 indicates that the top temperatures for the cases with the acetates of tin, zinc and bismuth rise slightly before those for the cases involving no catalyst, potassium acetate and sulfated zirconium hydroxide.

The runs with heteropoly acids and ferric sulfate display more complex behaviour. Chart 6.1 shows that these candidates also cause a drop in the pot temperature when added to the reaction mixture, but the effect is not as pronounced as that seen with strong acids. Charts 6.2 and 6.3 show the column temperatures with these candidates start to rise slower than the cases with strong acids but quicker than the other remaining cases, indicating a fairly strong vapour flow. Under full reflux, the liquid hold-up capacity in the column is limited, so some condensed material is continually returned down the column to the reactor.

An interesting, second fall in pot temperature is seen in the profiles for the cases with these intermediate-activity candidates, around the time when the reflux policy is changed at 1 hour 40 minutes. With the heteropoly acids, the pot temperature levels off and then falls very slightly. In the case with ferric sulfate this fall is more pronounced, and starts slightly before the reflux policy change. The collection of distillate is also seen earlier than in the other cases, due to the occurrence of some carry-over, indicating a very strong vapour rate at this time. Once the reflux ratio was implemented more

water could leave the reaction mixture in vapour and not return, so after a quick boil-up of the accumulation (reducing the temperature slightly) the reaction mixture starts to increase in ester level and therefore boiling point. The ferric sulfate run pot temperature profile changes direction quite rapidly once the second boil-up phase occurs after the reflux policy change, more so than seen with the heteropoly acids, which could be due to the higher pot temperature.

In Chart 6.2 it can be seen that the profile plots for the temperatures just above the pot split into two distinct groups. For slower runs (no catalyst, ineffective candidates and metal acetates) not enough water is available for the butanol-water azeotrope to occupy the whole column, and butanol also boils up to some extent. By the 1 hour 40 minutes mark the temperatures in Chart 6.2 have moved up towards the boiling point of butanol. For the more active catalysts (the strong acids, ferric sulfate and the heteropoly acids) the temperature generally remains steady below 95°C in the early part of the run, and this temperature is not far from the literature value of 91.5 °C for the boiling point of the butanol-water azeotrope (Luyben, 2008). Later there is less water available, so some butanol moves up the column and the temperatures are observed to rise towards the boiling point of butanol.

Despite the higher temperatures at position T1 (Chart 6.2) throughout most of the run duration in the cases of no catalyst and the slow catalysts, the temperatures at the top of the column (Chart 6.3) approach a steady temperature and do not rise above around 86°C. The 'stepped' rise seen in Chart 6.3 is probably due to cold material starting to return down the column from the condenser. The top temperature profile for the run using HCl catalyst is highly anomalous, as the temperature seems to fall in an irregular manner. It is possible that this was caused by the formation of an azeotrope between HCl and water, which could have moved up to the top of the column. However, this run was not repeated, because HCl is not compatible with the hastelloy packing, and it was decided not to risk damage to the packing, so further investigation of this anomaly was not possible.

By the 2 hours 40 minutes mark on Chart 6.1 the pot temperatures are rising quite quickly. The reaction rates with the intermediate catalysts are high, even though they are not the most active catalysts, probably because the pot temperatures have remained fairly high for the duration of the run, in comparison to the strong acids where the

temperatures remained low for a long time. The runs with intermediate catalysts, sulfuric acid and PTSA reach a higher final pot temperature than the case with no catalyst by the end of the 4hr 40 minute run, indicating that a higher-boiling mixture is present in the pot, and potentially a high composition of ester.

6.3.2 Temperature Profiles: Propionic Acid System

Representatives from each category of catalyst run with the nonanoic acid esterification system were also tested with the propionic acid system, in order to compare the trends seen. Data for the four individual runs using the propionic acid system are presented in Appendix K. Only a small number of runs were performed due to time and resource constraints, and it was not possible to test the whole range of candidates again. Shorter runs were also used for the propionic acid experiments, compared to the nonanoic acid tests, as this was more manageable, and less information was required from these runs as they are only to be used for comparison.

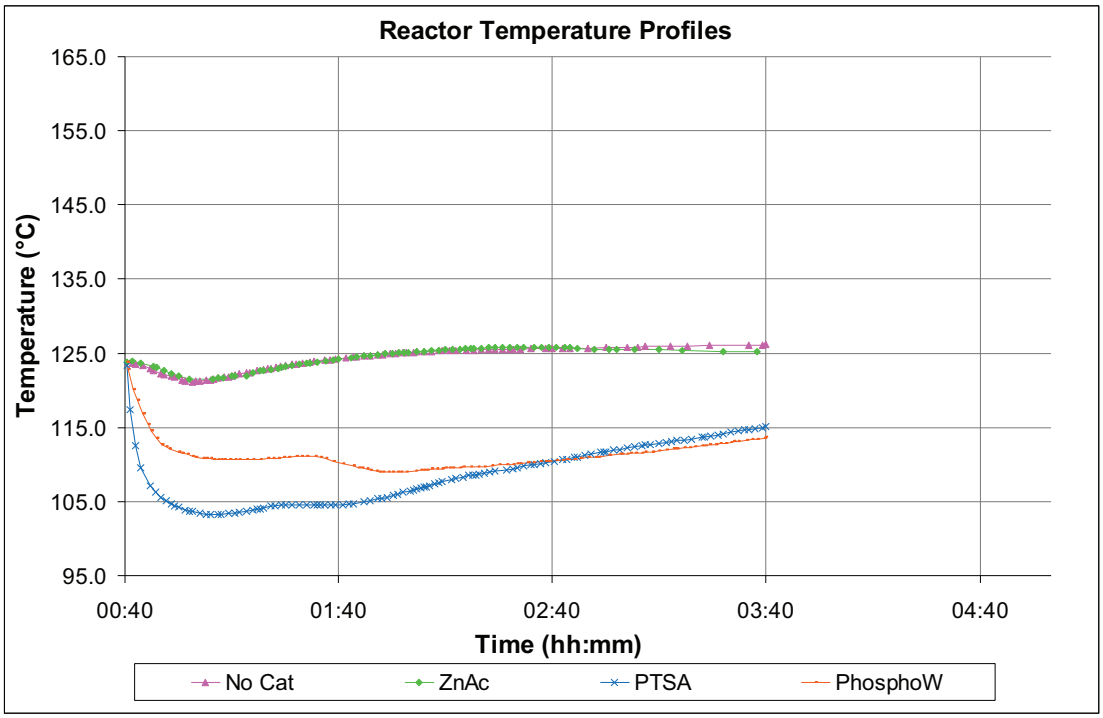

Chart 6.4: Reactor/Reboiler Pot Temperature Profile for Propionic Acid Esterification

Chart 6.4 shows the pot temperature profiles for the four propionic acid RD experimental runs. The initial boiling point of the reaction mixture at the point when the catalyst is added is 124°C, slightly lower than that seen with the nonanoic system which was at 129°C. Some trends are repeated from the nonanoic acid system:

- The case with zinc acetate appears very similar to the case with no catalyst, in which pot temperature falls slightly at the start of the run, then rises very gradually.
- The intermediate strength catalyst candidate (PhosW) causes an intial drop in the pot temperature, followed by a slight second fall when the reflux ratio policy is changed. The temperature then gradually rises from this point.
- The strong acid PTSA causes the biggest drop in pot temperature, which does not seem to be greatly affected by the change in reflux ratio policy, and gradually rises in the later stages of the run.

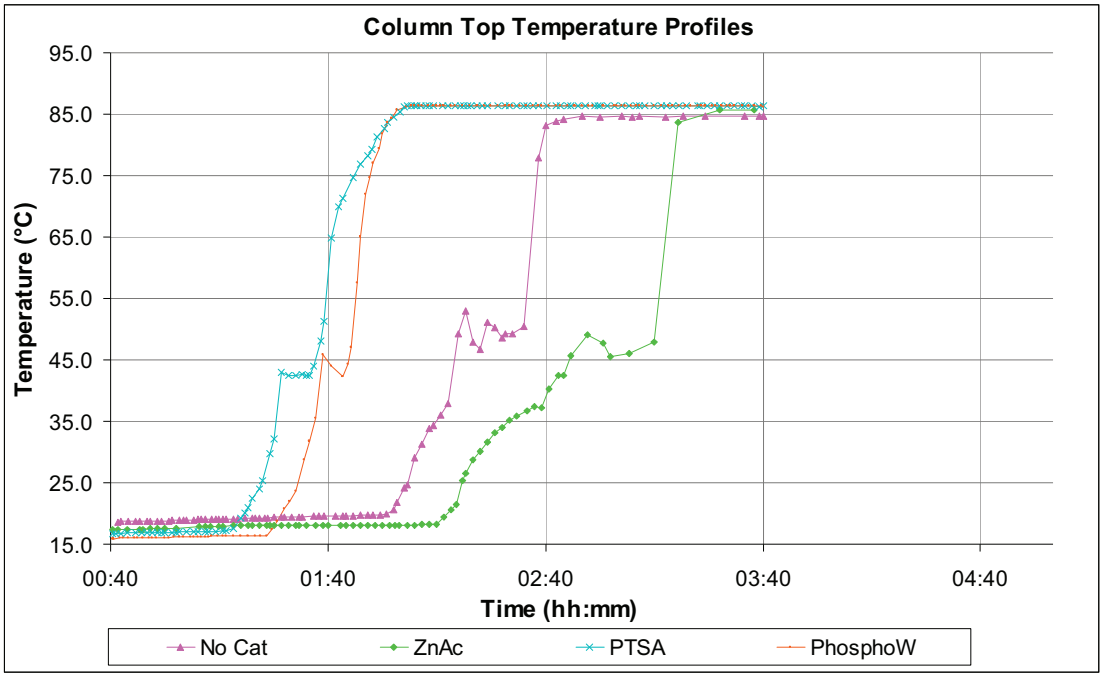

Chart 6.5: Temperature Profile at the Top of the Column: Propionic Acid Esterification

Chart 6.5 shows the temperature profiles from the top of the column. The temperatures reach a steady level of approximately 85°C, as would be expected as the same butanol-water azeotrope is present in the column. The stepped rise is again seen, as cold material returning from the column appears to have a significant effect, particularly where the vapour rate is lower in the cases with no catalyst or a very weak one. The order of column warm up is the same as that seen with the nonanoic acid system: cases with strong acids, followed by intermediate-activity catalysts, followed by weak or no catalyst.

The column heat up is very slow in the cases for no catalyst candidate and zinc acetate. The pot temperature stayed relatively flat at around 125°C after 1 hr 40 minutes during

these runs, rather than increasing as the reaction progresses, as was seen with the nonanoic acid system. The boiling point of the butyl propionate ester is 145°C (Sigma, 2010), which is much lower than butyl nonanoate which boils at 230°C at atmospheric pressure. Therefore, the boiling point of the propionic acid reaction mixture does not change much during the run as ester is formed. The lower reaction temperatures may have caused the slow warm-up rate and distillate collection, if the driving force for boil-up was insufficient.

6.3.3 Distillate Collection

The chart comparing the distillate volume collected with time for each of the cases reveals that almost nothing is collected before the reflux ratio policy switch at 1 hour 40 minutes. This indicates that the problems of unwanted carry-over of distillate material to the collection system has generally been avoided, with only a small occurrence observed during the case with ferric sulfate. In Chart 6.6 it is seen that, despite the high activity of the strong acids, the cases in which the most distillate was collected were those involving the metal acetates and ferric sulfate.

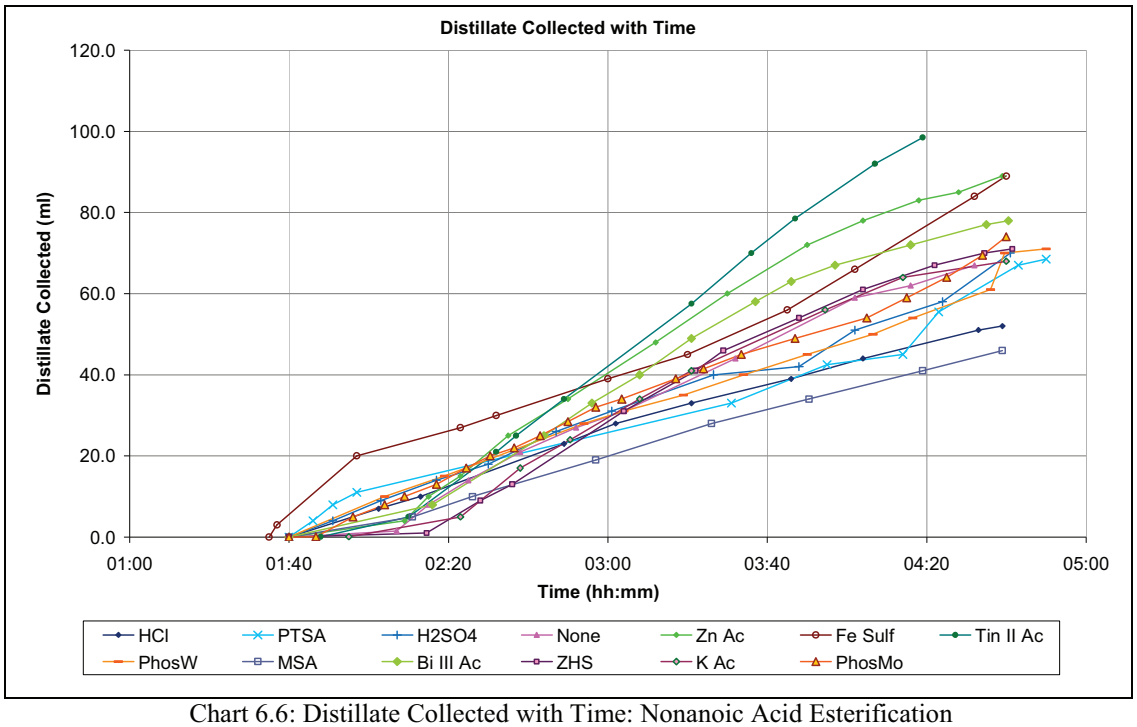

Chart 6.6: Distillate Collected with Time: Nonanoic Acid Esterification

The profiles seen in Chart 6.6 are quite difficult to interpret clearly so the data sets are split into sub categories by the type of catalyst in Charts 6.7 and 6.8.

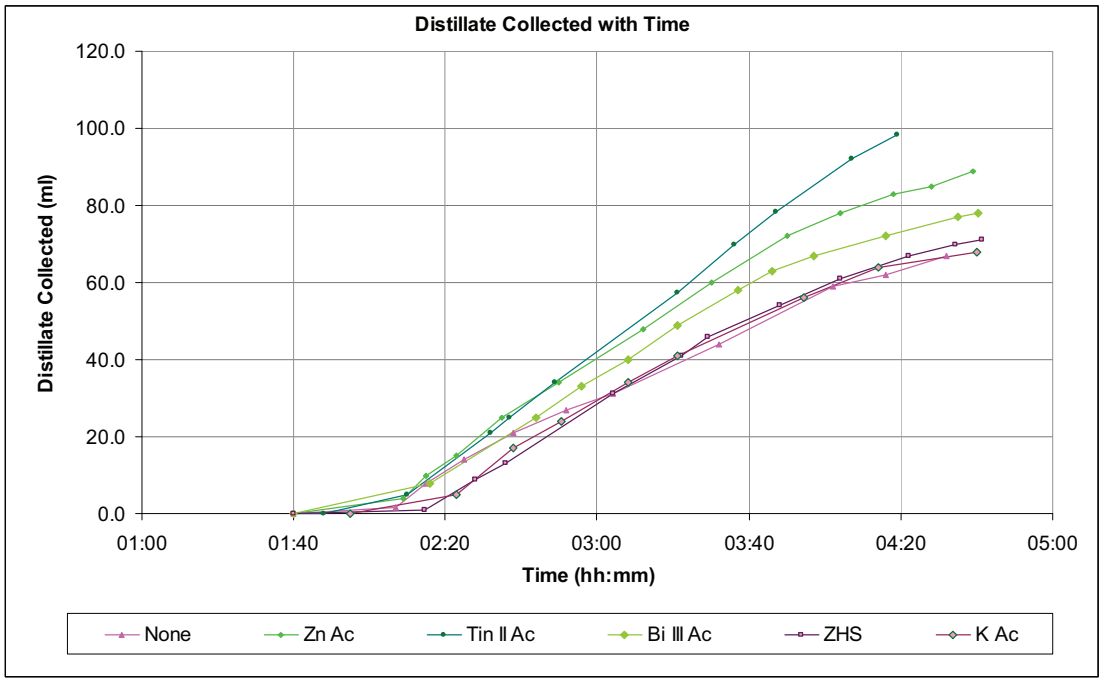

Chart 6.7: Distillate Collected with No/Poor Candidates: Nonanoic Acid Esterification

In Chart 6.7 it can be seen that the cases which use no catalyst, ZHS and K Ac give very similar distillate collection profiles. An order of increasing distillate collection is observed between the metal acetates, which becomes more apparent after the 3 hour mark. Ranking the metal acetate candidates in order from highest to lowest distillate collection, the order of activity based on this chart is:

Tin (II) Acetate > Zinc Acetate > Bismuth (III) Acetate > Potassium acetate

A general trend is observed in Chart 6.8, in which the runs with the candidates which were more active in the screening tests, tend to have an earlier onset of distillate collection. The collection rate continues at a fairly steady pace; slower than that seen in Chart 6.7 for the weaker catalysts where collection starts later. This slow rate is most likely due to the lower temperatures which persist in the cases where the addition of a highly active catalyst such as a strong acid causes the temperature in the pot to fall as water is formed rapidly.

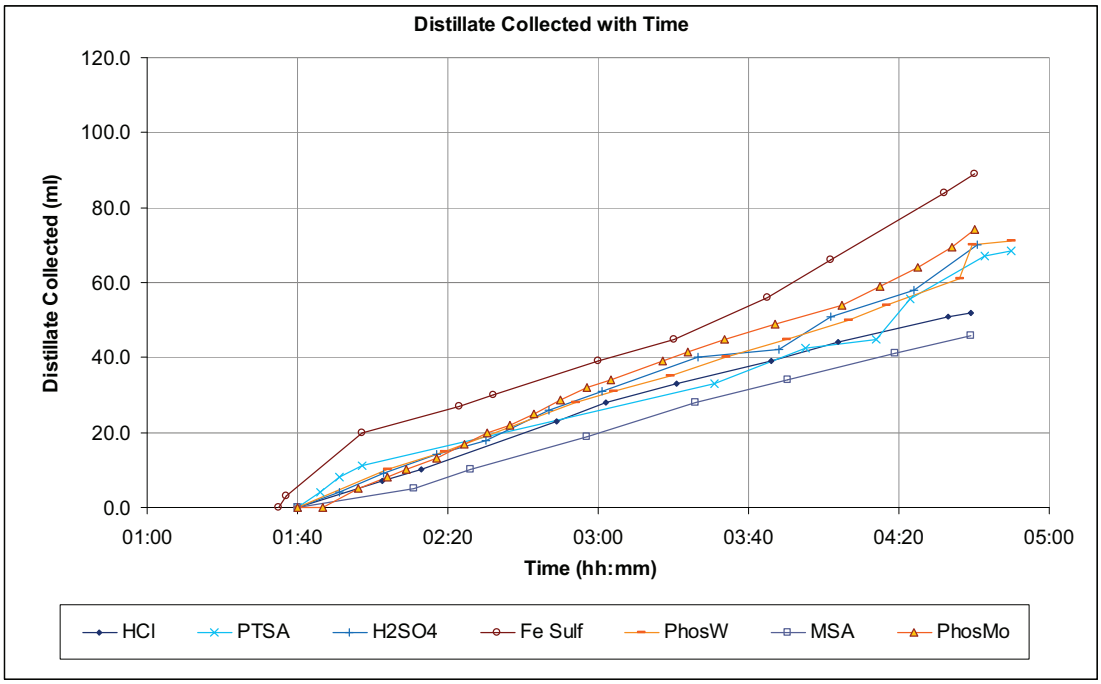

Chart 6.8: Distillate Collected with Acids and More Active Candidates: Nonanoic Acid Esterification

Chart 6.9 shows that the total distillate collected with the nonanoic acid system is highest in the cases where ferric sulfate and the metal acetates of tin, zinc and bismuth have been used. There is large group of the other candidates in the middle, with very little difference in total distillate collection between them. There is even very little difference between the cases with no catalyst, and with one of the more active catalysts from ChemSpeed screening, PTSA.

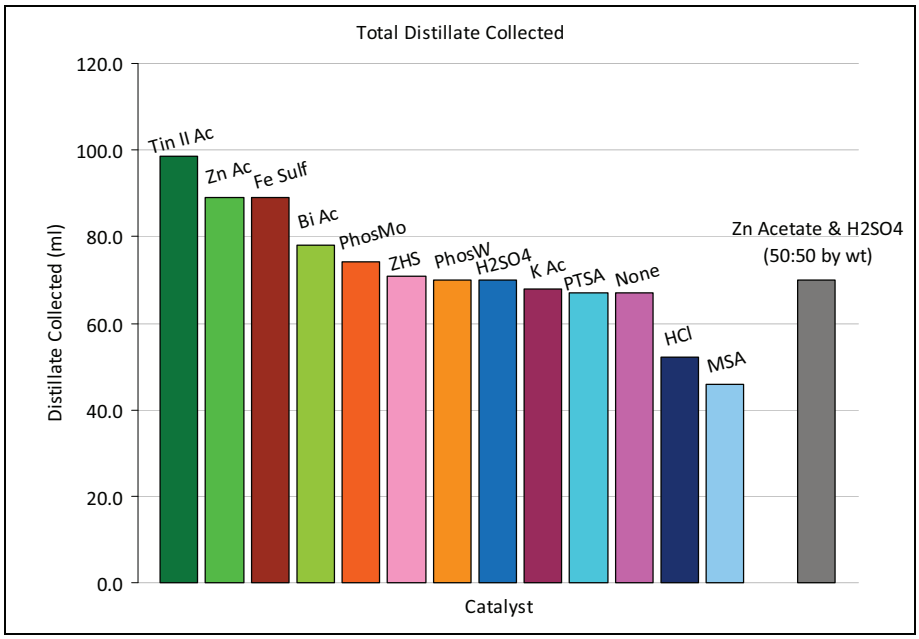

Chart 6.9: Total Distillate Collected with All Candidates: Nonanoic Acid System

Chart 6.10 shows the yield of water collected, which is calculated based on the number of moles of carboxylic acid charged to the pot and upon the assumption that the liquid collected is at the azeotropic composition. The methodology for the calculation of the yield of water collected in the distillate has been discussed in Chapter 5. The water yield chart shows that the cases where ferric sulfate and the metal acetates of tin, zinc and bismuth have been used have the highest yields, as seen with the total distillate collected. Hydrochloric acid and methanesulfonic acid have very disappointing yields. Use of a combination of zinc acetate and sulfuric acid does not give an intermediate yield, but a low yield.

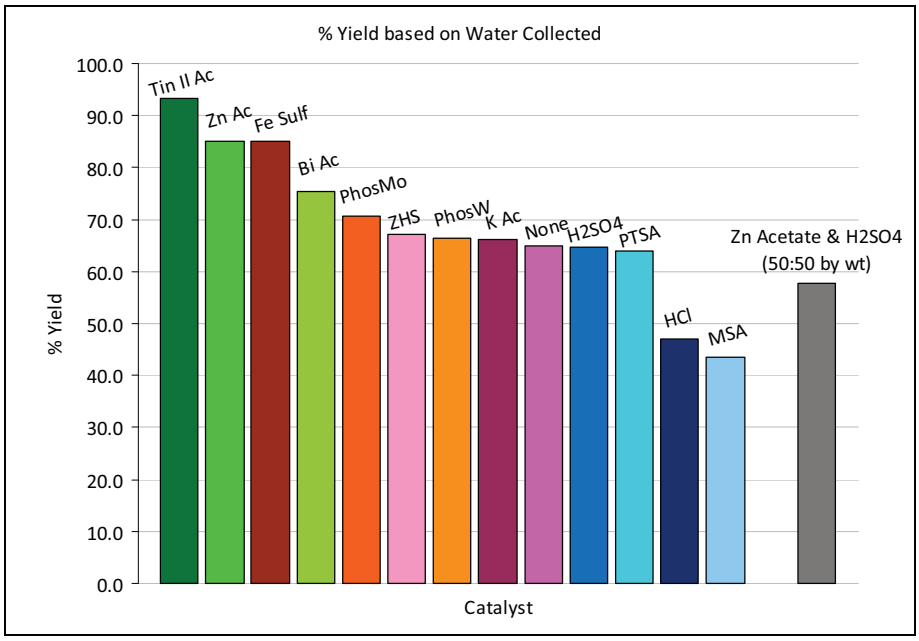

Chart 6.10: Yield based on Water Collected: Nonanoic Acid System

Chart 6.11 shows the water yield with time for the different cases for the nonanoic acid system. A clearer distinction between the different categories of catalyst are seen in Chart 6.12 where the yield of water is plotted against the corresponding temperature in the reactor/reboiler pot.

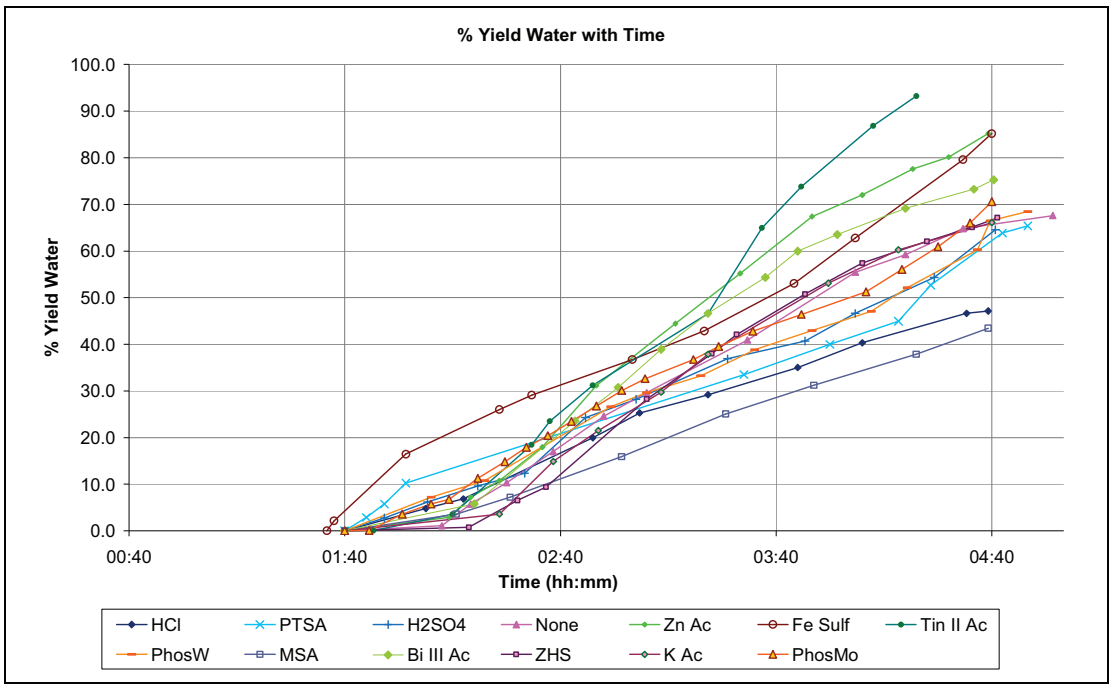

Chart 6.11 Water Yield (%) vs. Time: Nonanoic Acid System

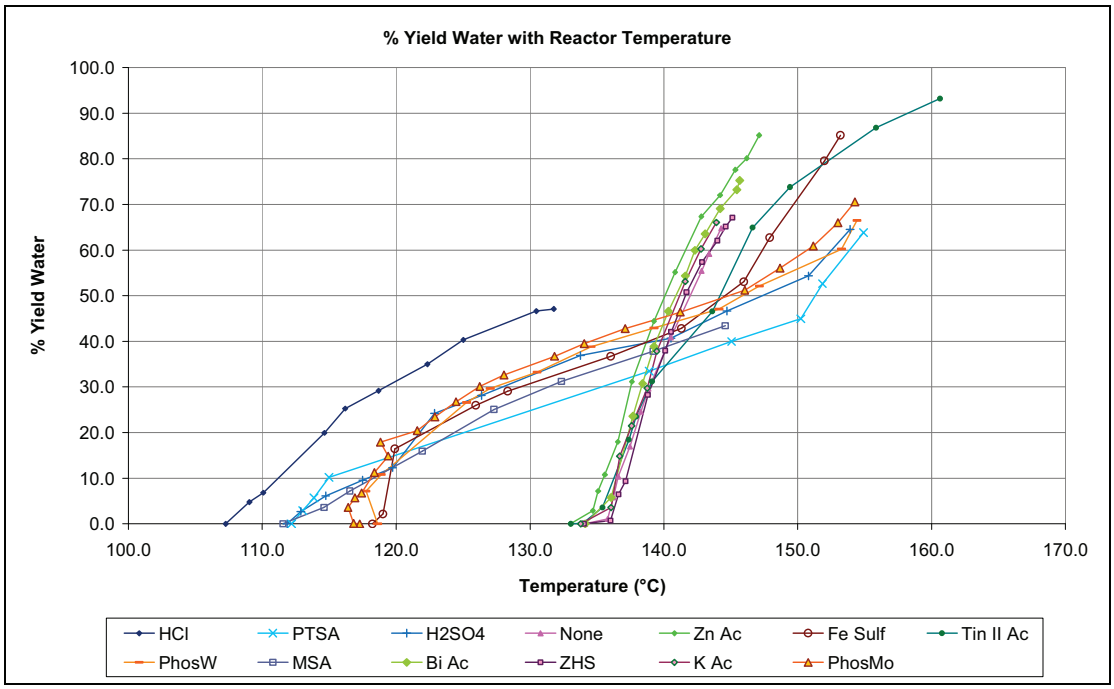

Chart 6.12 Water Yield (%) vs. Pot Temperature: Nonanoic Acid System

The more active catalysts all group together on the left hand side of Chart 6.12, while the less active candidates all group together along with the case of no catalyst on the right hand side. The case with ferric sulfate is grouped with the more active catalysts to start with, as some water is collected at lower temperatures. Then, towards the end of the run, the yield rises quickly with a small increase in temperature above 145°C, rising with a similar gradient to that seen in the profiles with less active candidates. The case with tin (II) acetate on the other hand begins in the group with the slower candidates but

then branches off and starts to rise more slowly. The case with HCl is anomalous and falls far over to the left hand side of the chart.

It was observed that there is a relationship between the water to butanol ratios in the distillate collected and the reactor/reboiler pot temperature. Chart 6.13 shows this for the cases using the more active candidates: MSA, PTSA, H_2SO_4, ferric sulfate, phosphotungstic acid and phosphomolybdic acid. Chart 14 shows the same information for the cases with no catalyst, metal acetates, and sulfated zirconium hydroxide.

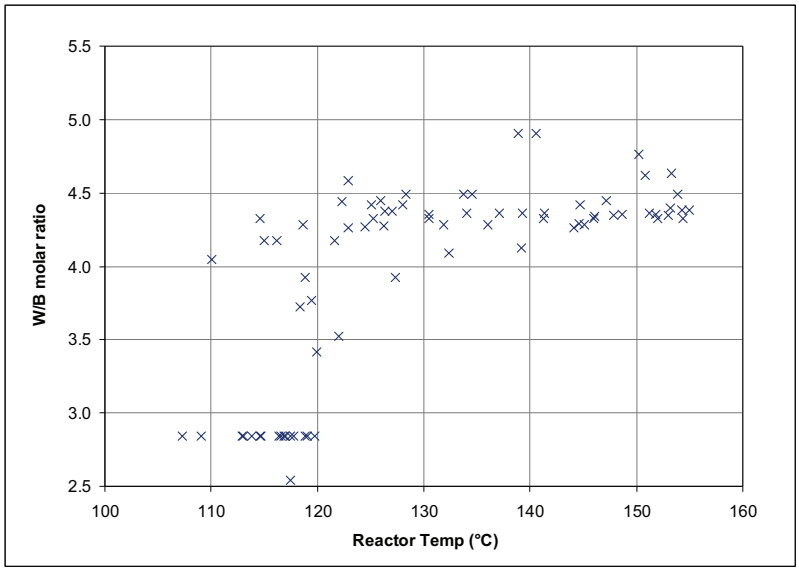

Chart 6.13 W to B Molar Ratio for Nonanoic Acid Cases with Highly Active Catalysts

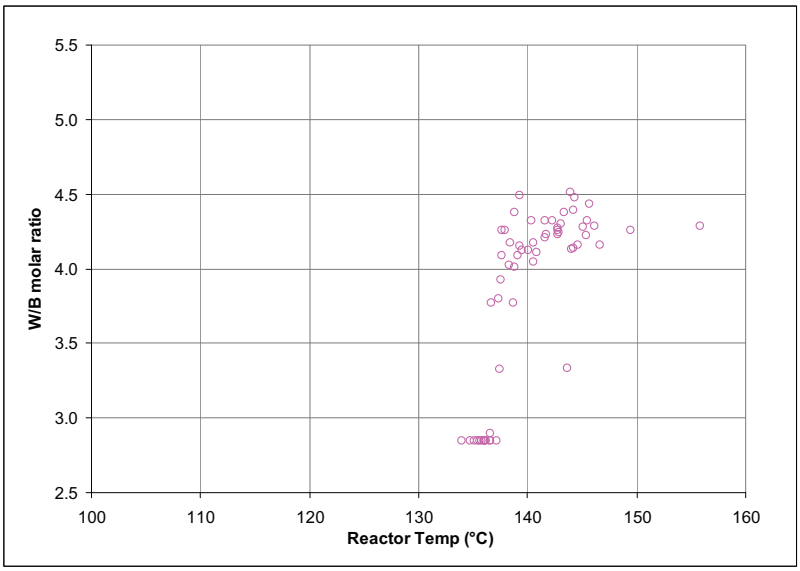

Chart 6.14 W to B Molar Ratio for Nonanoic Acid Cases with No/Less Active Catalysts

Comparison of Charts 6.13 and 6.14 shows that the step change from a low water to butanol (W/B) molar ratio of around 2.8 (only seen at the very start of distillate

collection, before two phases are identifiable) to around 4.3 occurs much sooner in the cases with the more active catalysts than with the less active catalysts. This reflects the stronger boil up rate and higher availability of water in the column at the point when the reflux ratio change was applied.

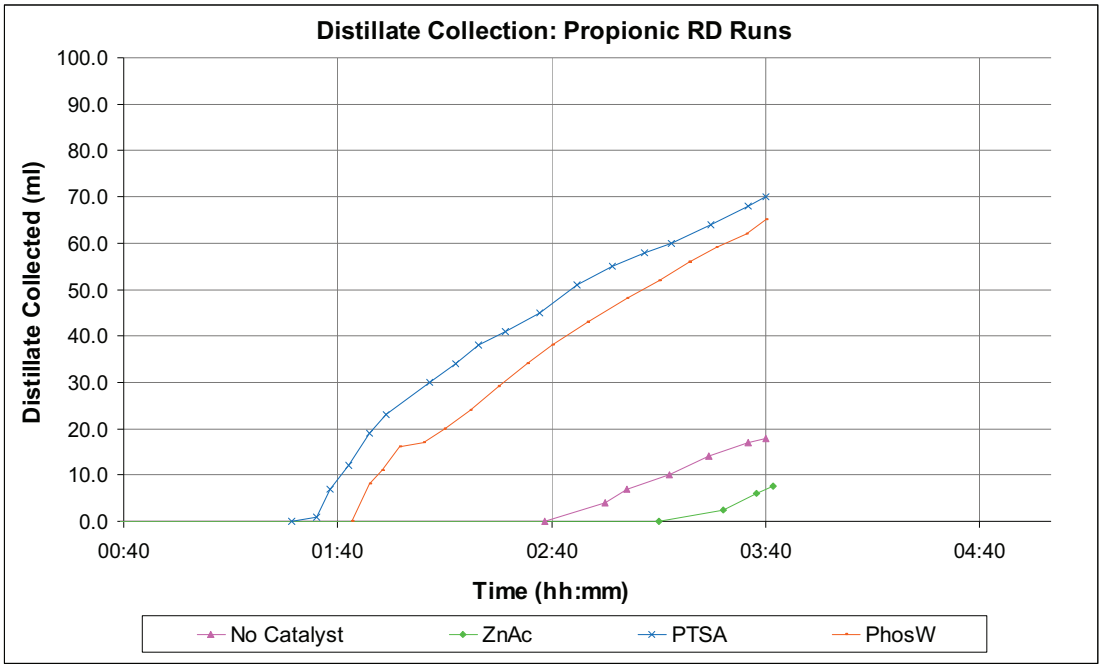

Chart 6.15: Distillate Collected with Time: Propionic Acid Esterification

The distillate collection with the propionic acid esterification system is shown in Chart 6.15. The cases with the highest distillate collection are those in which PTSA and phosphomolybdic acid have been used, while the cases involving zinc acetate and no catalyst candidate have much lower collection. This is a noticeable change from the results obtained using the nonanoic acid system, in which the metal acetates gave high distillate collection and there was not much difference between the cases with no catalyst, PTSA and phosphomolybdic acid. The lower pot temperatures and the very slow column heat-up observed during the runs using this reaction system have had a significant effect on the volume of distillate collected.

6.3.4 Ester Concentration

The results of the GC analysis of samples taken from the pot during the nonanoic acid runs are shown in Chart 6.16. The composition of ester was determined using the methodology described in Chapter 5.

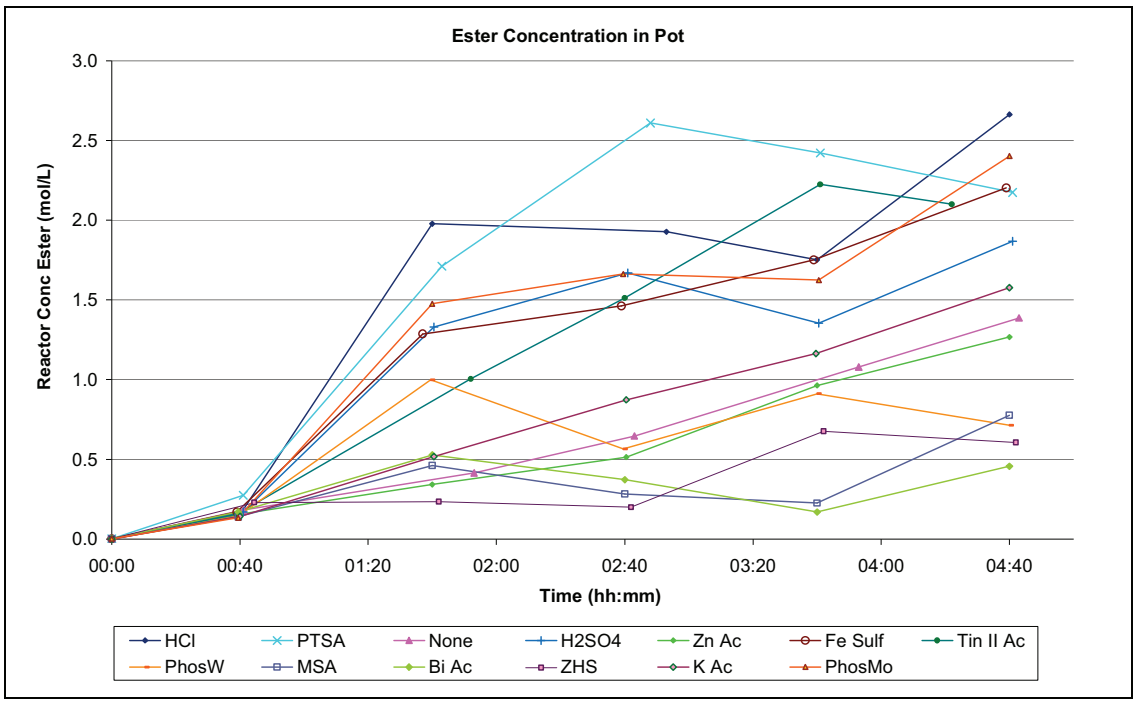

Chart 6.16: Ester Concentration in the Reactor-Reboiler Pot: Nonanoic Acid System

The data for the ester concentration in the reactor-reboiler pot, which could not be interpreted clearly in Chart 6.16, has been split by candidate type into Charts 6.17 and 6.18. However, comparison of these charts does not reveal consistent trends or groups of similar behaviour.

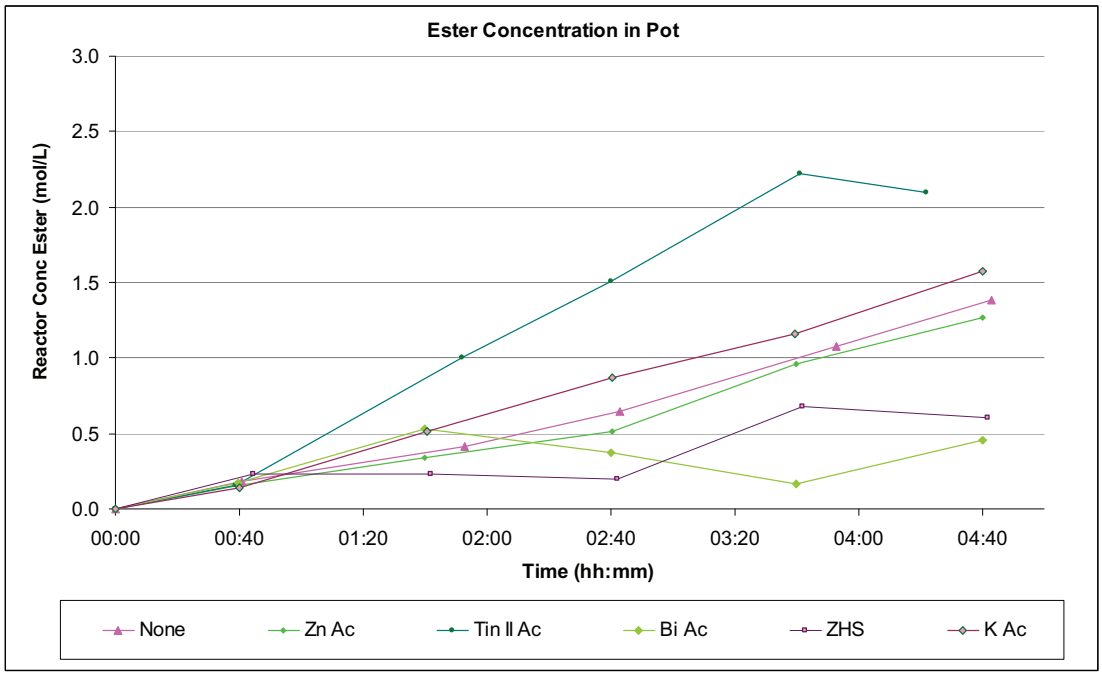

Chart 6.17: Pot Ester Composition with No / Poor Catalyst Candidates: Nonanoic Acid System

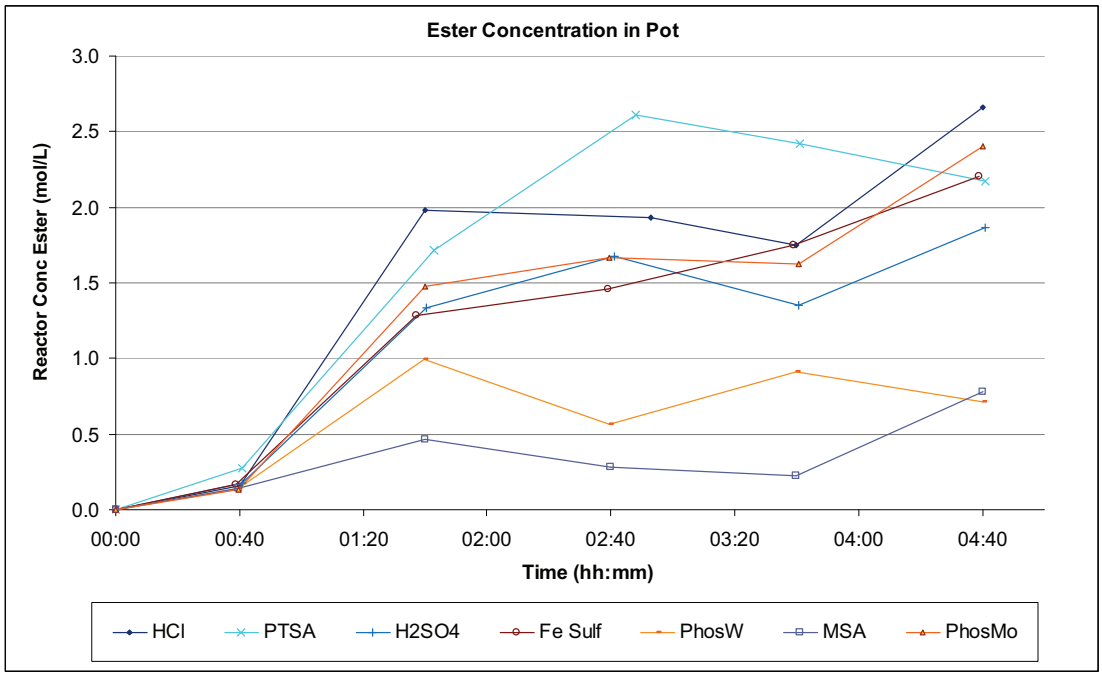

Chart 6.18: Pot Ester Composition with Acids and More Active Candidates: Nonanoic Acid System

The final yields of ester in the pot at the end of each of the runs with nonanoic acid are shown in Chart 6.19. The final samples shown here were taken some time after the end of the experiments, when the pot contents had cooled and material held up in the column had returned to the pot.

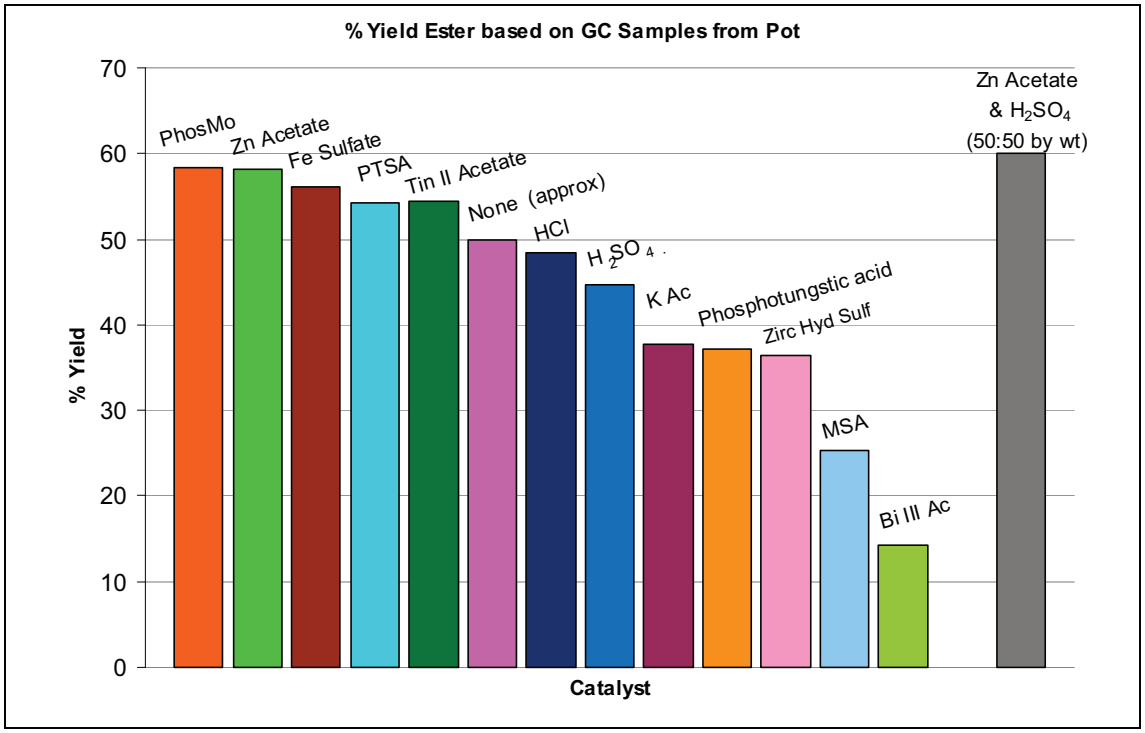

Chart 6.19: Ester Yield with All Candidates: Nonanoic Acid System

It can be seen that both the ester composition with time and the final ester yield data is very inconsistent. It may be that the sampling methodology was flawed, for example it could be that taking samples from the bottom of the reactor pot may not have given representative samples, even with the mixture at boiling point and the stirrer running. Chart 6.20 shows the ester composition with time data for the four runs performed with the propionic acid system.

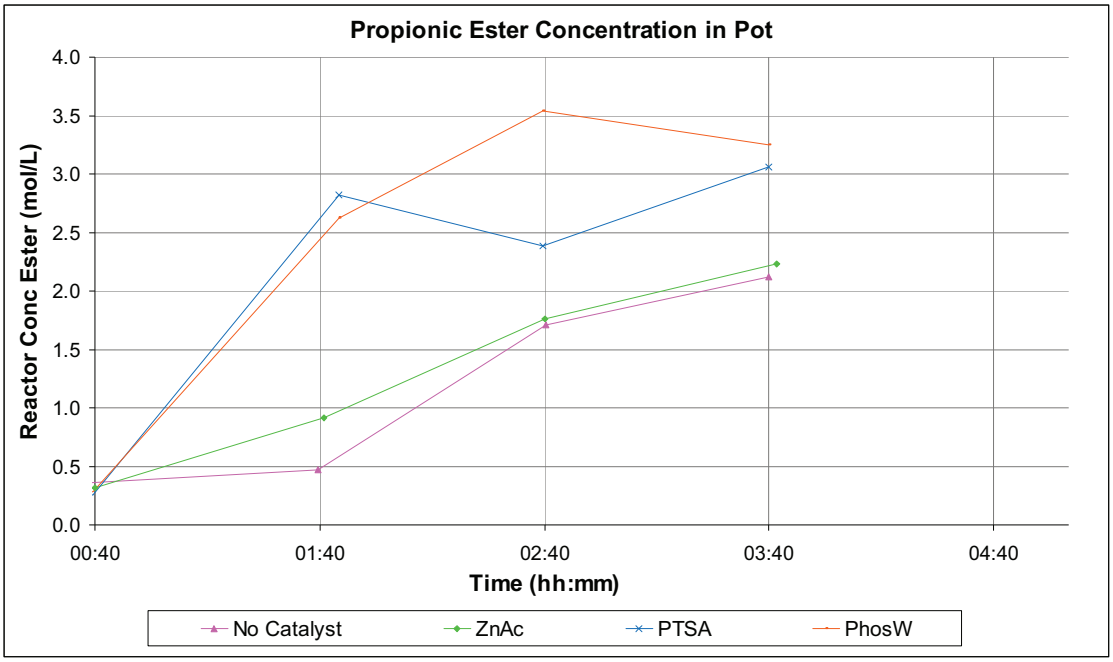

Chart 6.20: Ester Concentration in the Reactor-Reboiler Pot: Propionic Acid System

It is difficult to draw conclusions based on Chart 6.20 of ester composition because so few runs with the propionic acid esterification system were performed. At first glance it seems that the more active catalysts (PTSA and PhosW) cause more ester to be formed than the cases with no catalyst and zinc acetate. Further tests would be required to confirm whether or not this pattern continued to emerge with a larger range of candidates tested.

6.4 Discussion of Errors in Raw Data

The time and resources available for performing the reactive distillation experimental runs was constrained, and there were also difficulties experienced with the experimental equipment, overall this meant that the number of experiments that could be performed with the reactive distillation unit were limited. Unfortunately no direct repeats of individual runs were performed.

It was noted previously that in Charts 6.1, 6.2 and 6.7 of the nonanoic acid results that the cases of no catalyst, sulfated zirconium hydroxide and potassium acetate are almost the same. The addition of sulfated zirconium hydroxide and potassium acetate appears to have had very little effect on the behaviour of the system when compared to the case with no catalyst. In the following section, these three runs have been considered as repeats of the same conditions

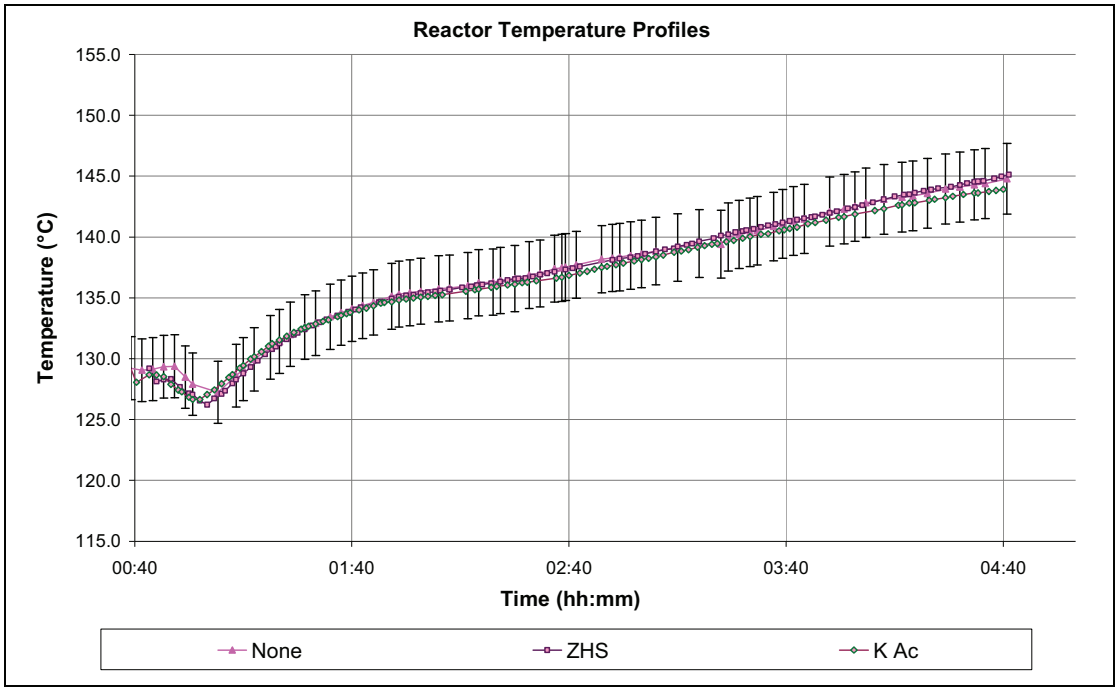

Chart 6.21: Pot Temperatures for Three Similar Nonanoic Cases with 2% Y-Error Bars

Chart 6.21 shows the reactor/reboiler pot temperatures with small (2%) Y-error bars applied to the profile line for the case with no catalyst, and demonstrates that there is very little difference between the pot temperature profiles during these three runs. Chart 6.22 shows the temperature profiles at the T1 position for the same three cases. When the T1 temperatures are all steady above 95°C, the profiles for the cases with sulfated zirconium hydroxide and potassium acetate almost overlap with the profile line for the case with no catalyst.

Some variability between the cases is seen during the heat-up phase: in the case with potassium acetate, the temperature at T1 starts to rise slightly earlier. This variability is small, and can be captured by a 5% envelope applied to the profile line for the case with no catalyst, which has been included in Chart 6.22.

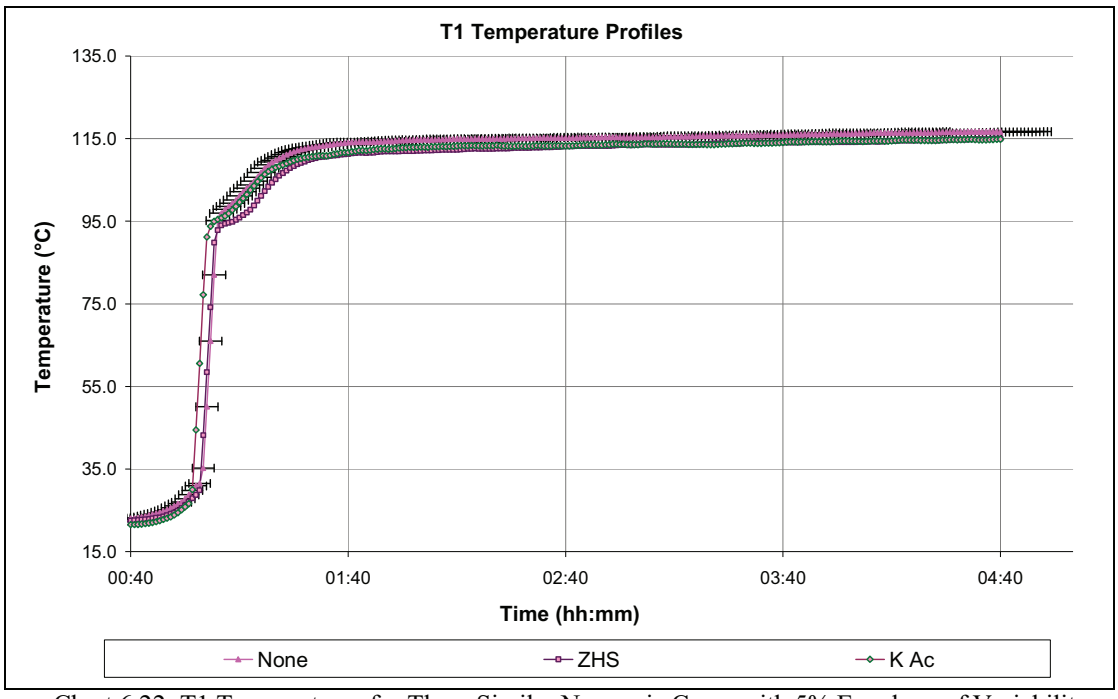

Chart 6.22: T1 Temperatures for Three Similar Nonanoic Cases with 5% Envelope of Variability

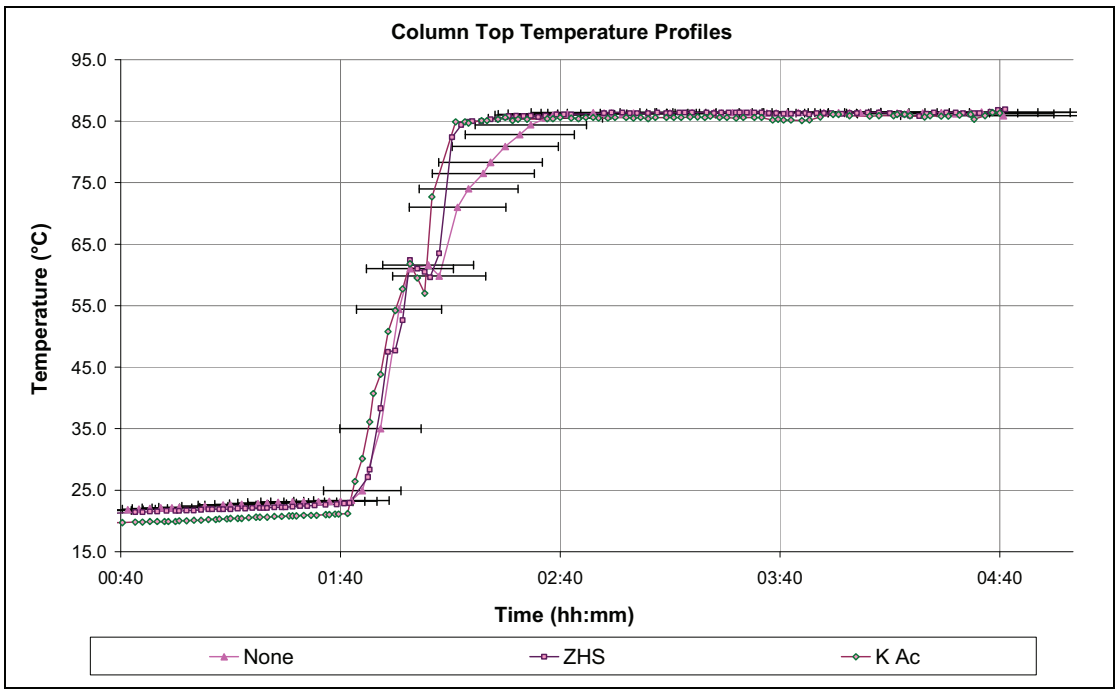

Chart 6.23: T1 Temperatures for Three Similar Nonanoic Cases with 10% Envelope of Variability

Chart 6.23 shows the profiles of the temperature at the top of the column for the cases with no catalyst, ZHS and potassium acetate. When the temperature profiles are all steady, all 3 data sets again almost overlap with the profile line for the case with no catalyst. During the warm up phase the rate of temperature increase varies between the cases, as the temperatures at the top of the column were strongly affected by cold material returning from the condenser. The variability between the profiles is almost completely captured by a 10% envelope.

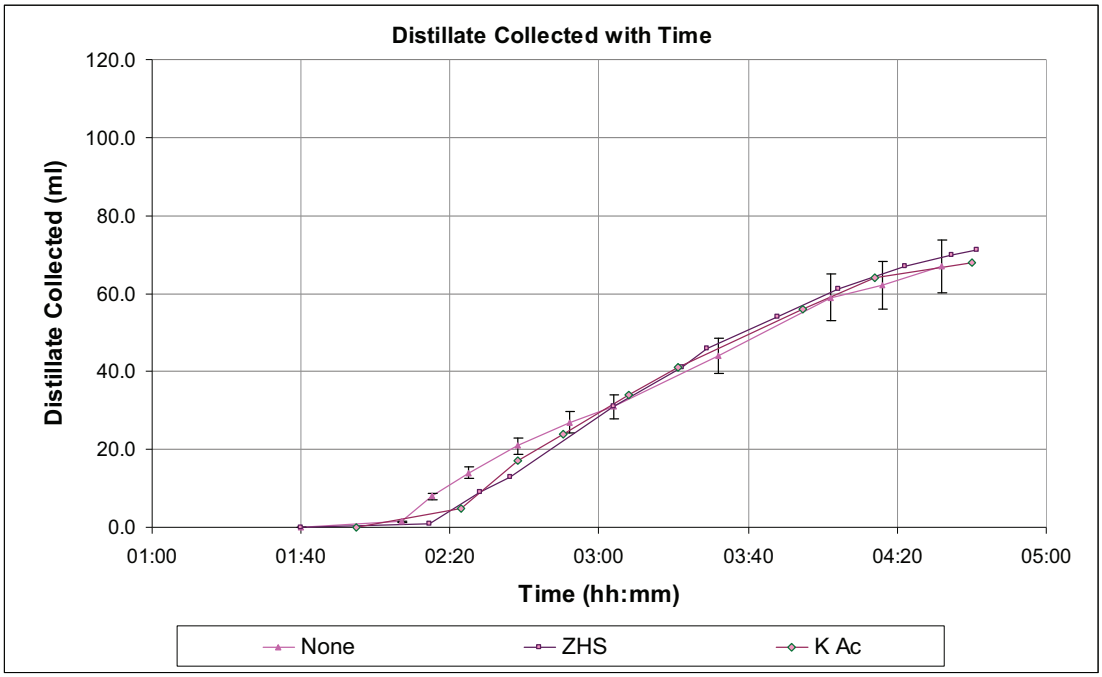

Chart 6.24: Distillate Collection for Three Similar Nonanoic Cases with 10% Y-Error Bars

Chart 6.24 shows the profiles for the distillate volume collected with time for the cases with no catalyst, ZHS and potassium acetate. It can be seen that in the early part of the chart, there is some difference seen in that the profile for the case with no catalyst indicates that more distillate was collected than in the other cases, however after the 3 hour mark this is no longer the case. With 10% Y-error bars applied to the profile line for the case with no catalyst, the early data falls outside this envelope, which is very narrow at this point due to the small numbers involved. In the later stages of the chart all the data falls well within 10%. The variation in the early part of the chart seems quite high when it is considered that the errors in the reading of the distillate volume would be expected to be accurate to within +/- 0.5 ml, as this was the smallest interval on the measuring cylinder used. However, there will be more variation introduced due to slight random variations in the way the vapour travels up through the packing, and in the way in which the liquid distillate is handled by the reflux collection system.

Chart 6.25 shows the ester concentration in the pot for the three cases of interest, with 10% Y-error bars applied to the profile line for the case with no catalyst. It can be seen that the data for the other cases falls far outside the error bars, as there is very large variation in the ester concentrations.

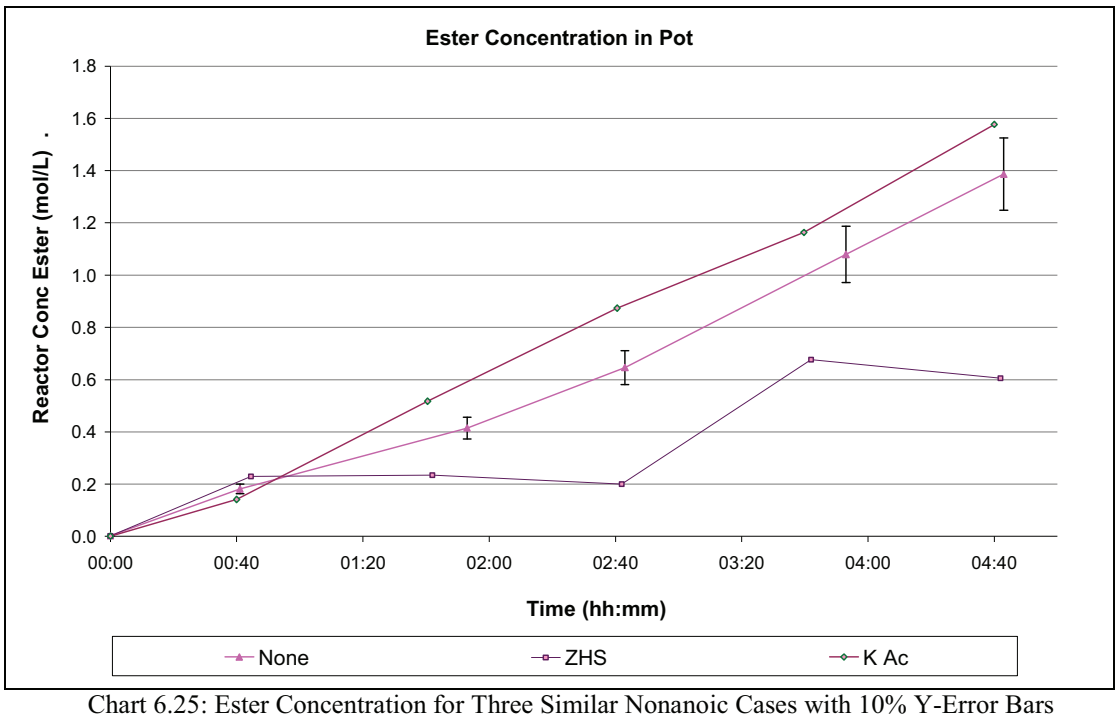

Chart 6.25: Ester Concentration for Three Similar Nonanoic Cases with 10% Y-Error Bars

For the three cases shown in Figure 6.25 (no catalyst, sulfated zirconium hydroxide and potassium acetate) the reactor temperatures, the column temperatures and the final distillate collection were fairly repeatable, generally within 10%. However the ester composition appears very inconsistent, despite the very similar reaction conditions. To attempt to investigate the source of this variation, the ester compositions of 'Sample 2, 1st dilution' for each of the RD runs with nonanoic acid were compared. This sample was taken at 40 minute mark in each run, just before the catalyst is added and before any boil-up occurs, and so the composition of the reaction mixture in the pot should be very similar each time. Any variation in this data will come from:

- Measurement of initial reactant volumes
- Slight differences in the rate of reaction as the pot warms up
- Removal of samples from the pot and performance of dilutions
- Performance of GC analysis and data processing

The ester concentrations are summarised in Table 6.1. The average reactor ester concentration at the 40 minute mark was: 0.17 mol/L, and the standard deviation was 0.04 mol/L. Chart 6.26 shows the pattern of how the individual data points deviate around the mean.

Run	Reactor Ester Concentration mol/L
Run1	0.27
Run2	0.16
Run3	0.18
Run4	0.17
Run5	0.17
Run6	0.15
Run7	0.16
Run8	0.18
Run9	0.14
Run10	0.14
Run11	0.17
Run12	0.23
Run13	0.14
Run14	0.13

Table 6.1: Ester Concentration in Sample 2 From Each Run with Nonanoic Acid

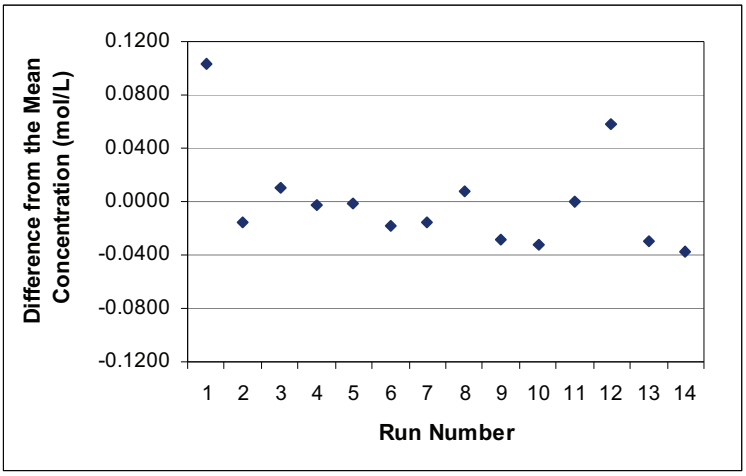

Chart 6.26: Variation of Ester Concentration: Sample 2 from Each Nonanoic Acid Run

From Chart 6.26 it can be seen that there are two probable outliers. The value from Run 1 appears to be an outlier, and this could be attributed to this run being the first successful run of the experimental unit. The sample from Run 12 was taken approximately 4 minutes late compared to the others, which could explain why this value is also slightly different. The new average calculated without Runs 1 and 12 is: 0.16 mol/L, with a standard deviation of: 0.02 mol/L. The data values now all fall within approx +/- 15% of the average value. Chart 6.27 shows the ester concentration in the pot for the three cases of interest, with 15% Y-error bars applied to the profile line for the case with no catalyst.

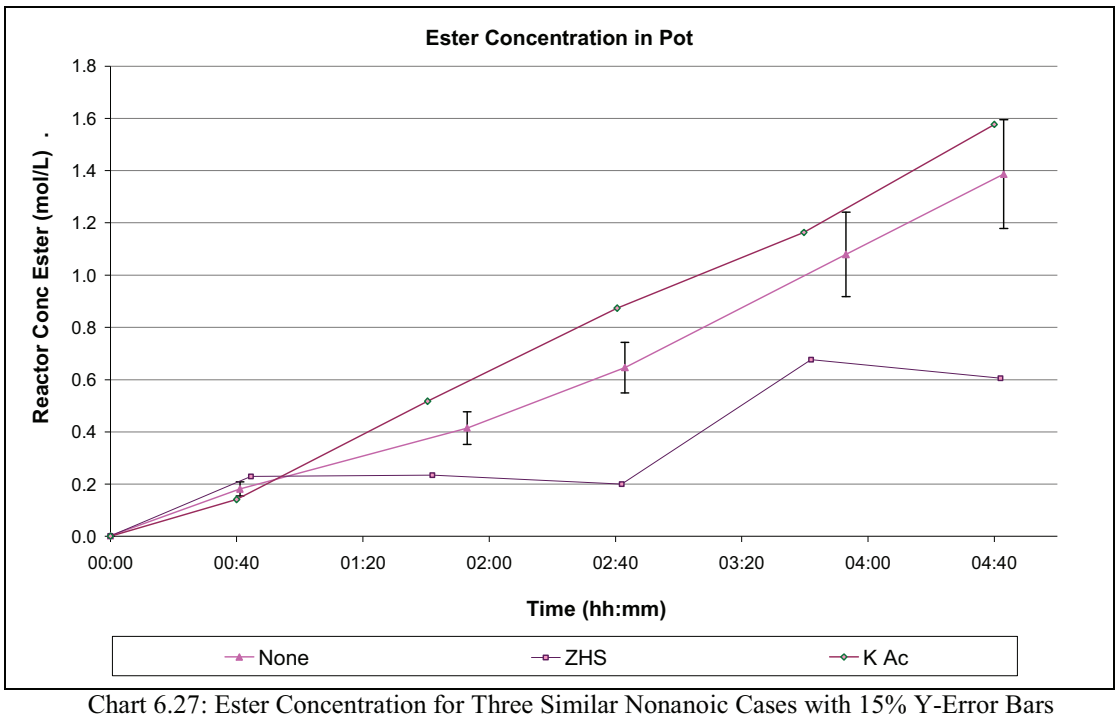

Chart 6.27: Ester Concentration for Three Similar Nonanoic Cases with 15% Y-Error Bars

It is clear from Chart 6.27 that the errors due to sampling, sample make up and GC analysis and processing do not account for the variation in the GC profiles, therefore further variation must be coming from somewhere else. The samples used to assess these errors are all from the 40 minute mark, before the addition of catalyst, which can be seen in Chart 6.16 to be a relatively repeatable data point. The ester concentration profiles become very inconsistent after the catalyst has been added, and it can be deduced that there must have been other factors which further affected the ester production. For example, some catalysts became stuck to the inside of the reactor, and may have clogged in the valve at the base which was used to take samples. Also, because the sampling point was the valve at the base of the reactor, any phase separation or sinking of solid particles will have affected the results. The temperatures observed in the column do not go higher than the boiling point of butanol, there is no evidence that any ester is boiling up and moving up the column, so this can not be used to explain the ester composition charts.

6.5 Nonanoic RD Outputs Taken Forward for Further Analysis

The results from the nonanoic acid system runs are presented in Table 6.2. This is a summary table of the important data from each of the runs, and includes numerical representations of many of the features of these results that have been described qualitatively in the previous sections of this chapter.

Catalyst	End Yield Ester (%) $ ¥	End Yield Water (%) $ ¥	Initial Rate Pot T Fall (˚C/min)	Lowest Pot T (˚C)	Time to Lowest Pot T (min)	Time Col TopT Starts Rising (min)	Time Top T Stabilised (min)	Rate Pot T Rise 2hr40m (˚C/min)	Pot T at End (4hr40¥)
Methanesulfonic acid	25.3	43.4	4.35	104	13.3	35.3	42.0	0.18	145
Sulphuric Acid	44.7	64.6	7.94	103	11.0	32.5	37.5	0.19	154
PTSA monohydrate	54.3	63.8	2.94	106	20.0	35.0	39.0	0.23	154
Hydrochloric Acid	48.4	47.1	5.65	103	17.0	34.0	34.0	0.13	132
Phosphotungstic acid hydrate	37.2	66.5	1.63	115	19.0	46.0	35.0	0.20	154
Phosphomolybdic Acid Hydrate	58.5	70.6	1.71	113	20.5	45.5	28.5	0.21	154
Iron (III) Sulphate Hydrate	56.2	85.2	0.39	119	30.0	39.5	30.5	0.28	153
Tin (II) Acetate	54.4	93.2	0.18	125	24.0	65.0	18.0	0.10	161
Bismuth (III) Acetate	14.3	75.3	0.12	127	17.5	64.0	26.0	0.06	146
Zinc Acetate Dihydrate	58.3	85.2	0.17	126	17.5	63.5	25.0	0.07	147
Zirconium (IV) hydroxide, sulfated	36.4	67.1	0.17	126	16.0	63.5	25.5	0.06	145
Potassium Acetate	37.7	66.1	0.10	127	15.5	63.5	27.5	0.06	144
None	50.0	64.8	0.01	127	24.0	67.0	53	0.06	145

Table 6.2: Results from Nonanoic Acid System RD Runs taken forward for Further Analysis

$ No catalyst run was longer, 50% value interpolated

¥ Tin II Acetate run ended at 4h19min

6.6 Correlations of RD Outputs vs. Screening Half Life

In order to evaluate how strongly the activity of the catalyst candidates seen from the results of the screening experiments in the ChemSpeed machine influences the reactive distillation system, the nonanoic acid system RD outputs from Table 6.2 have been plotted against the half life results from Chapter 4. The aim of this is to evaluate how much of the variation in the results from the RD experiments can be explained by the half life for the esterification of nonanoic acid determined in the screening tests.

In the following charts, a short screening half life close to zero indicates an active catalyst which causes the reactants to be consumed quickly. The R-squared values are shown on these plots in order to give an indication of the strength of any correlations observed. (An R-squared value close to 1 indicates a very strong correlation, while a low value closer to 0 indicates a weak correlation.) Chart 6.28 demonstrates that the magnitude of the initial drop in pot temperature when the catalyst is added to the reaction mixture is very strongly correlated to the activity of the catalyst (as described by the half life from the screening experiments). As the activity of the candidate increases, the magnitude of the fall in the pot temperature increases.

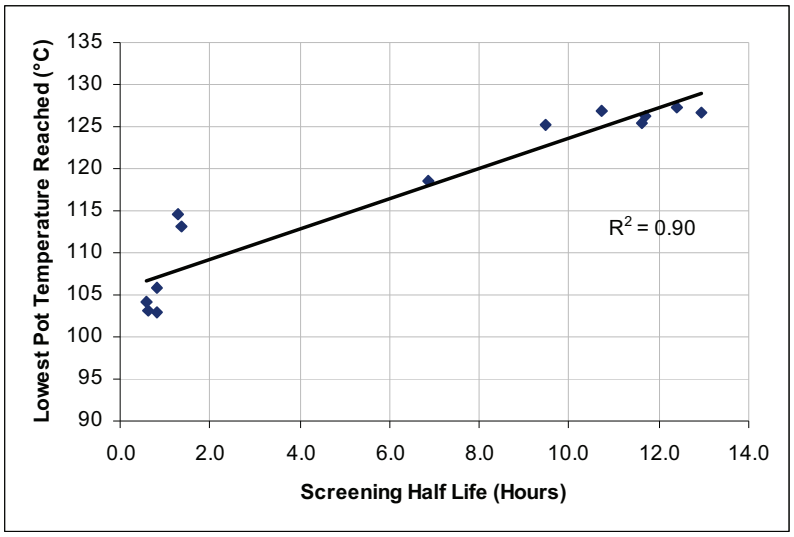

Chart 6.28: Lowest Pot Temperature in Nonanoic RD vs. Screening Half Life

An interesting, very strong relationship is observed in Chart 6.29 between the half life and the initial rate of temperature fall when the catalyst is added. Here it can be seen that as the activity of the catalyst decreases, the initial rate of temperature fall in the pot when the catalyst is added decreases rapidly.

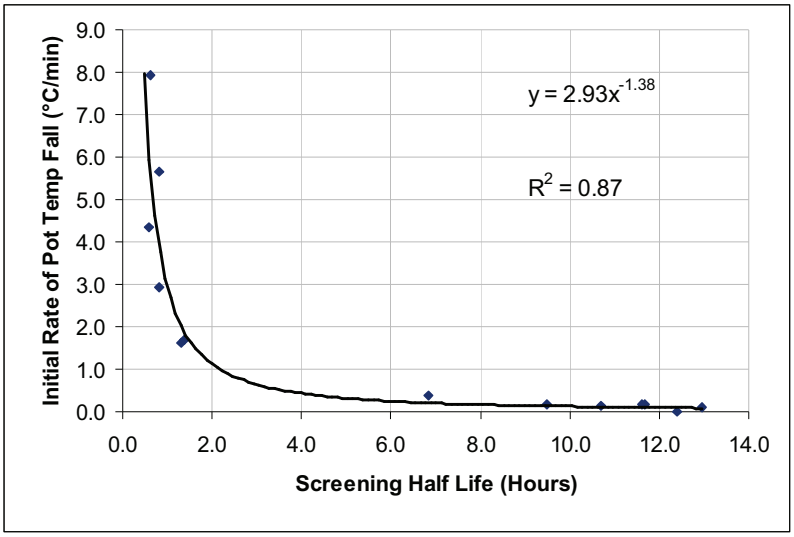

Chart 6.29: Rate of Pot Temperature Fall in Nonanoic RD vs. Screening Half Life

There is also a strong correlation between the catalyst activity and the time at which the temperature at the top of the column starts to rise. This reflects the rate at which water is produced and moves up the column: more active catalysts cause the highest initial vapour rates and shortest times for the column temperature to begin to rise.

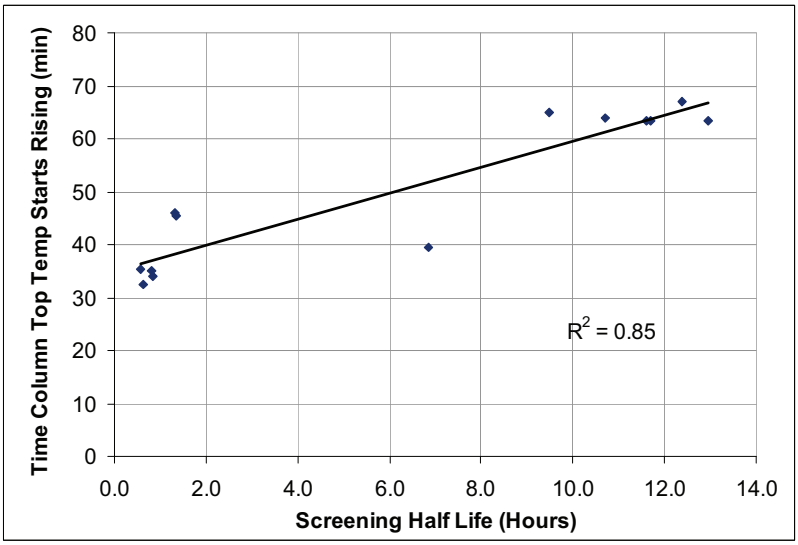

Chart 6.30: Start Time of Pot Temperature Recovery in Nonanoic RD vs. Screening Half Life

The pot temperature generally recovers during the run, after the initial fall when catalyst is added. The rate of pot temperature rise during this phase of each run (at 2hr 40min) is plotted against half life in Chart 6.31. It is noted that data clusters appear in this chart: the strong acids and heteropoly acids that gave short half lives all group together on the left hand side of the chart and have a pot temperature rise of around 0.2 °C/min. The pot temperature is rising relatively quickly, but from a lower base due to the more significant fall in temperature when the catalyst is added.

On the right hand side of Chart 6.31 the metal acetates, the ZHS and the case with no catalyst have a slower rate of increasing pot temperature at just over 0.05°C/min. The ferric sulfate is anomalous, as it has the highest rate of increase in pot temperature but gave only an intermediate half life during the screening tests.

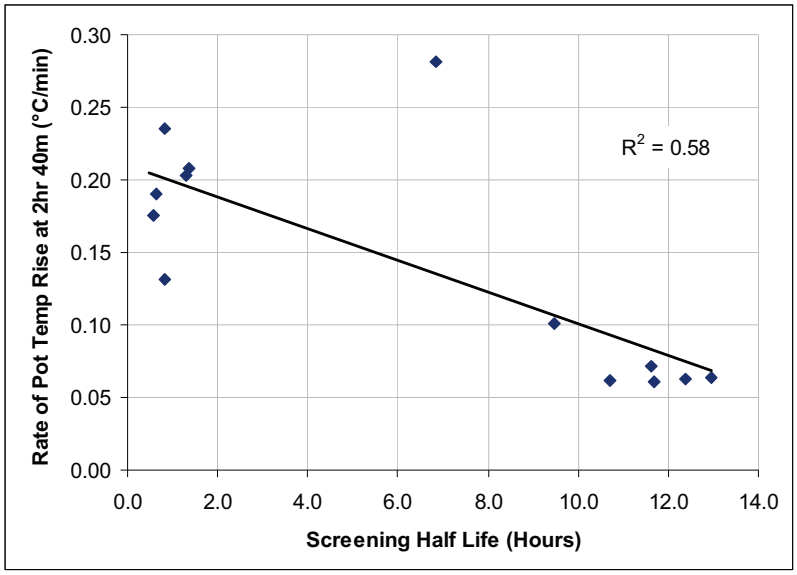

Chart 6.31: Rate of Pot Temperature Rise at 2h40m in Nonanoic RD vs. Screening Half Life

The R-squared value on Chart 6.31 is below 0.6, so it is a much weaker correlation than those seen in previous charts. A very weak correlation is seen when the final distillate water yield is plotted against the screening half life obtained with the catalysts in Chart 6.32, and it is observed that the clustering in this case is also much less strongly defined.

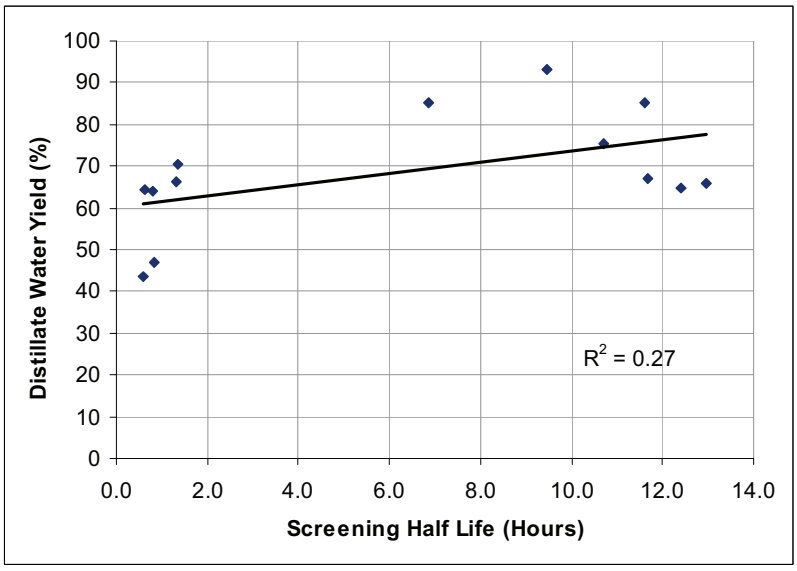

Chart 6.32 Final Distillate Water Yield in Nonanoic RD vs. Screening Half Life

The R-squared value in Chart 6.33 is very close to zero, which indicates that the end ester yield in the pot of the RD unit and the screening half life values obtained with the candidates are uncorrelated.

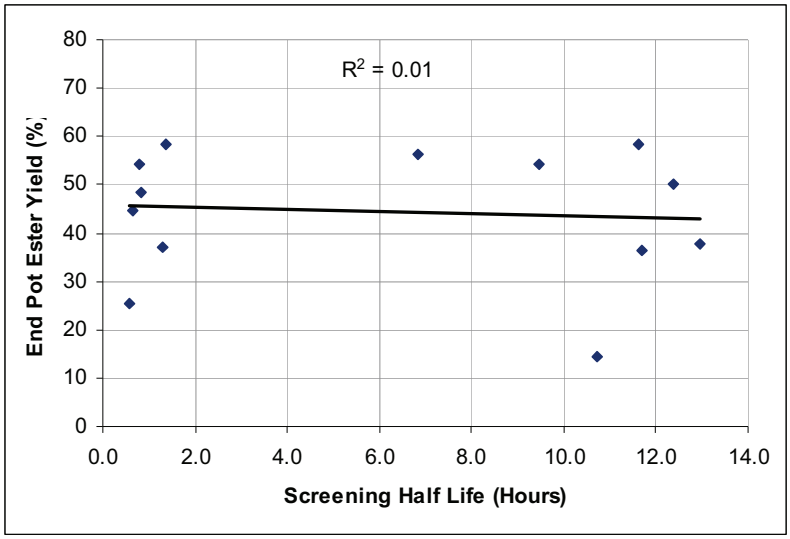

Chart 6.33: Final Pot Ester Yield in Nonanoic RD vs. Screening Half Life

Using simple correlations, the last 3 charts have strongly indicated that information about the screening half life alone is not enough to explain all of the results from the RD experiments. In particular, it appears unlikely that the final yields of the products could be predicted using this type of simple correlation. Further variables need to be taken into account if the outputs which are not well correlated with the screening half life are to be explained, and the behaviour of the catalyst candidates under reactive distillation conditions is to be understood.

More complex statistical tools than the simple correlations used in Charts 6.28 to 6.33 will be required in order to incorporate further parameters, and to investigate further for the existence and strength of relationships between these parameters and the outputs of the RD experiments. For this reason, the outputs shown in Table 6.2 are taken forward for further examination using multivariate analysis in Chapter 8.

6.7 Summary

The temperature profiles observed during the reactive distillation experiments reveal how the nonanoic acid esterification system behaved with 12 different catalyst candidates. Groups of distinctive behaviour patterns are seen in the strong acids, the intermediate-strength catalysts, the metal acetates of tin, zinc and bismuth, and the other, ineffective candidates. Some interesting relationships have been observed between the half life of the nonanoic acid esterification observed during the screening experiments, and the outcomes of the reactive distillation runs. However, the half life alone is not able to explain all of the trends seen.

The metal acetates appear to have been more active under the higher temperature conditions seen in the RD runs, compared to the results from the ChemSpeed screening. The metal acetates of tin, bismuth and zinc gave the highest yields of water distillate, which would not have been expected from the screening result alone. Based on the distillate collection, the order of activity for the metal acetates is:

Tin (II) Acetate > Zinc Acetate > Bismuth (III) Acetate > Potassium acetate

The order of activity of the metal acetates is different to that described in literature for esterification of a different system (Parshall and Ittel, 1992), but as explained by Di Serio et al. (2005), each system that is catalysed by metal acetates will have a corresponding metal centre with an ‘optimum’ Lewis acid strength. The rapidly increasing pot temperature profile seen in the run with tin (II) acetate appears highly anomalous. The pot temperatures from this run do not go outside the range that would be possible, since they do not go above the boiling point of the butyl nonanoate of around 230°C. The water collection was high and corresponding GC traces of the samples from the pot indicated that the amount of ester increased towards the end of the run, and it was also noted that there was no indication of the presence of any longer chain molecules such as dimers on the chromatographs.

The strong acids cause the fastest initial fall in the pot temperature, and also the fastest warm-up of the column. However, this has not translated into high distillate yields. An interesting, strong relationship has been observed between the pot temperature and the distillate collection rate. The pot temperature also depends directly on the composition in the pot, which changes due to the reaction, and for very active catalysts which have a large effect on the composition it can be seen that the distillate collection profile is very

different to that for the other candidates. Higher temperatures drive a higher boil-up, and conversely the dramatic reduction in temperature when the strong acids were added led to slow reaction rates for the rest of the run and ultimately to low distillate yields. Ferric sulfate behaves anomalously compared to the others, and seems a promising candidate with intermediate activity and giving good yields of water. There was very little difference between the runs with no catalyst, with potassium acetate and sulfated zirconium hydroxide.

The temperature profiles along the length of the column allow observation of the gradual heating of the column due to vapour boil-up from the pot. The temperature at the top of the column does not go above around 86°C, suggesting that there is always butanol-water azeotrope present here, but the temperatures lower down in the column show that butanol increasingly dominates the composition in the column as the rate of water formation slows. The data from the PT100 temperature probes seems to have relatively small errors associated with it, and revealed a large amount of information about the process.

The data for the ester composition in the pot seems to be very unreliable, with high variation in the data. Approximately +/- 15% errors are introduced during sample acquisition, sample make-up, and GC analysis. There may also have been problems, for example with the sampling methodology when taking samples from the base of the pot, so it is not possible to base any real conclusions on this data.

Further discussion of these results will focus on the groups of candidates which display similar performance, and on the trends seen during the runs. In Chapter 7 dynamic reactive distillation simulations are built for the nonanoic acid reaction system, with the aim of matching the observations from the experiments. It has been shown that the half life from the screening experiments does not provide enough information to fully explain the results from the RD experiments. In Chapter 8 multivariate statistical tools are used to continue the search for relationships between the numerical outputs in Table 6.2, the half life from the screening experiments, and catalyst molecular descriptors.

Chapter 7: Reactive Distillation Simulations

7.1 Overview

This chapter begins with an introduction to the BatchCAD dynamic simulation tool, and describes how it has previously been used for the simulation of reactive distillation. The development stages of a BatchCAD model are described, in which the parameters and operation mode are set to give the best match possible to the observed patterns. BatchCAD and Excel-based simulations are performed for six reactive distillation runs: the case for no catalyst, along with the five catalysts for which kinetic parameters were obtained through ChemSpeed runs at different temperatures. The results of the simulations using the two different modelling approaches are presented and their strengths and weaknesses are discussed.

7.2 Introduction

As shown in Chapter 2, the range of models that can be applied to reactive distillation systems can range from very detailed, complex simulations which take many factors into account to very simplified models. Simulations have a great importance in the study of reactive distillation, as it allows savings to be made in terms of the time and experimental work which is required. Successful accurate models of continuous RD have been demonstrated in the available literature, and it has been documented that dynamic simulation of batch RD systems is also possible.

The output of simulations produced in this chapter will be used in the investigation of links between the catalyst descriptors and performance in RD. This contributes to the overall aim of this work by investigating the possibility of the use of simulations in the development of a tool that can help determine the suitability of a catalyst for RD. The commercial software tool used in this study is BatchCAD, which is a dynamic simulator suitable for batch processes.

7.2.1 BatchCAD Background

BatchCAD is quite different to many of the reactive distillation modelling techniques described in literature due to the reasons behind the development of the software and the difficulties it was designed to overcome. BatchCAD was the first commercial package

for the simulation of reaction with non-equilibrium batch, semi-batch or continuous distillation, meeting the demand for a tool capable of performing dynamic simulations of systems with varying time, temperatures, pressures and compositions (Wright, 2010). The simulator was able to cope with significant discontinuities such as the start or end of a feed stream addition into a semi-batch reactor, or extreme limiting conditions, for example thermal runaway. Evaporation in a closed vessel causes the pressure to increase until a pressure relief device is activated, in which case the simulator must cope with the sudden pressure release and evaporation in an open system. The ability of BatchCAD to calculate the vapour release rate and composition and to simulate the change in pressure with time in this kind of process means that it can be a useful guide for engineers and provide basic information for calculations to indicate suitable safety devices.

The kinetic fitting tool in BatchCAD has been identified by Avantium Technologies as a facility that could help process the vast amounts of experimental data that result from high-throughput catalyst screening (Maxwell et al., 2003). It is also recognised that BatchCAD can assist in scale-up work as it incorporates a database containing data for a wide range of reactor vessels for which it is possible to accurately predict the thermal behaviour with time, and the user can select or enter custom values for parameters such as heat transfer coefficients and heat transfer area (van Aken, 2003). BatchCAD includes a physical property database which covers not only the most common compounds, but also many that are important to the flavour and fragrance industry, an area which regularly employs the type of batch and semi-batch processes BatchCAD was designed for.

7.2.2 Reactive Distillation in BatchCAD

BatchCAD has been used previously for RD simulation, as the simulator has the option of the addition of a basic distillation column above a reaction vessel to simulate a batch reactor-rectifier type RD unit. Temperature-dependant properties such as the vapour pressure of the reaction mixture are calculated by BatchCAD and used during the simulation, during which reaction and vapour-liquid equilibrium calculations are performed simultaneously.

Bollyn and Wright (1998) describe the application of BatchCAD to develop a semi-batch reactive distillation process where a complex reaction occurs in the reactor-reboiler vessel and separation is performed in an attached distillation column. In this paper a model is developed which accurately represents the kinetic scheme and allows the interdependence of the reaction kinetics and the reactor temperature to be explored. The changes in composition due to distillation are represented in the BatchCAD model as removal of volatile compounds from the reaction mixture. The column used in experimental work had only around 6 theoretical plates and scale up was based on the assumption that the use of the same type of Sulzer packing would mean consistent column performance. Chemical conversion and the composition of the distillate were found to be well predicted by the model.

Some explanation of the calculations used by BatchCAD is given by Bollyn and Wright (1998) but the actual equations themselves are commercially sensitive information and are not published. Most comparable examples in literature describe models in which the equations are based on the assumption of reaction equilibrium; however BatchCAD has the capability to simulate a process with non equilibrium chemistry occurring in all stages of an RD unit. Fully dynamic simulations are possible which involve the reaction kinetics, non equilibrium vapour and liquid balance, and variable volume on the trays of the column, in the reactor and distillate collection. BatchCAD is also able to simulate continuous processes, as constant addition and withdrawal rates can be specified. For batch and semi-batch systems, the sequence of events is defined by the user in the operations list feature.

To simulate reactive distillation, BatchCAD performs a mass and energy balance for every component in every phase on all stages (pot, trays, and condenser). The same equations are used for every stage, with some constraints applied: for example in the reboiler there is no vapour flow in, and if the condenser is a total condenser, all vapour components are condensed down to the user-specified temperature (Wright, 2010). The liquid and vapour flow rates are calculated individually and may often converge, so it may appear that the values are the same, but there is no assumption of constant overflow in the BatchCAD equations. There is an assumption of uniform pressure drop across the stages, and this is most significant in simulations of vacuum distillation processes where the drop in pressure across a stage can be of the same magnitude as the working pressure of the unit.

7.3 BatchCAD Model: Reactor Thermal Characteristics

The heat transfer characteristics of the reactor/reboiler in a BatchCAD model can be matched to a real case through selection and inputting of suitable parameters by the user. In this case, temperature profile data is available for the warming of butanol in the reactor/reboiler pot at the start of the butanol boil-up characterisation test (described in Chapter 5). A simple model of the glass reactor vessel of the reactive distillation unit was built in BatchCAD:

- Jacketed glass vessel with impeller
- Dimensions as measured from the reactor
- Properties of glass taken from literature.
- Initial charge: 750ml 1-Butanol at room temperature

Further details such as the dimensions of the pot are given in Appendix M. The performance of the heating/cooling system was matched to the real temperature profile by adjusting the characteristics of a heating fluid flow control valve in the BatchCAD simulation by trial and error until the heat-up profile matched the observed data. A pressure drop across the control valve from 200 to 100 kPa was applied and then the valve flow coefficient (CV) was adjusted to obtain sufficient flow of heating fluid (supply temperature 102˚C) to deliver the required heat input to the reactor. The initial guess at a suitable flow rate is based on the rule of thumb that the flow should be approximately ten times the volume in the reactor per hour. The final settings which give suitable flows are:

- Heating fluid flow $0.108 m^3/hr$
- CV 1×10^{-4}
- Rangeability 10

BatchCAD calculates the U-value (overall heat transfer coefficient) of the reactor to be 92 W/m^2K, which is low, as would be expected for a pot constructed entirely out of glass. A glass lined carbon steel pot using heat transfer oil to heat up an organic reaction mixture would have a higher U value of 140 to 370 W/m^2K (Perry and Green, 1997).

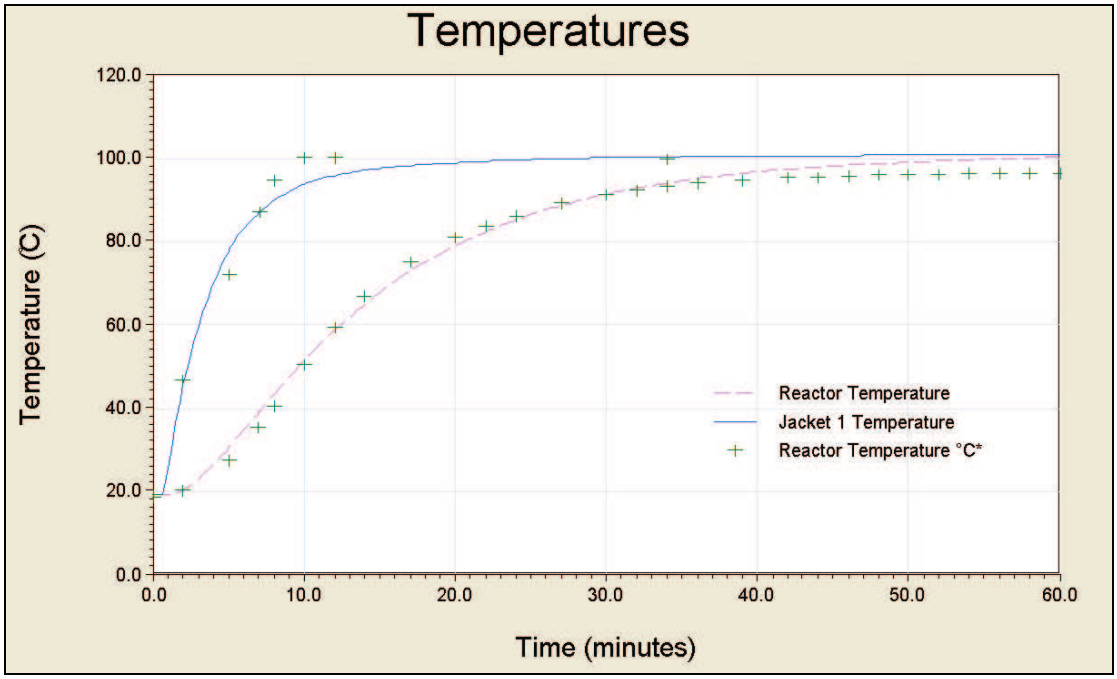

Figure 7.1: Real vs. BatchCAD-Simulated Temperature Profile of Butanol Warm-up

Figure 7.1 shows that the BatchCAD simulation is able to fairly closely match the experimental temperature profile for the warming of butanol using the thermal characteristics that have been selected for the reactor/reboiler.

7.4 BatchCAD Model: Separation

The model of the reactor/reboiler was then built upon to add the distillation facility which provides separation. The aim is to build a BatchCAD model of the RD unit which is able to replicate the separation performance observed in the separation tests performed to test the column, which are described in Chapter 5.

7.4.1 Separation Model Development

The equipment configuration can be changed easily through the BatchCAD user interface; in this case a condenser and distillation column were added. The parameters and dimensions for the condenser and the distillation column were selected to match the real unit as closely as possible and the values entered are described in Appendix M. The reactor/reboiler thermal characteristics were retained from the model of the heating of butanol, and the fluid package components were changed to match the mixture used in the separation tests: 1-Propanol and 2-Butanol.

The simulation operating steps are entered to match the procedure used in the experiments: the unit and feed start at room temperature; heating is applied to boil the mixture; the column is then held under total reflux for three hours and allowed to settle so that the temperatures and compositions are steady, before the reflux policy is switched to total collect for five minutes to represent a sample being taken. In BatchCAD, the distillation simulation cannot start with a stage hold up volume of zero as this would cause the calculations to fail, so when the simulation is initialised some feed is allocated to the column trays. As a result, the column tray compositions and temperatures match those of the feed at the start of the simulation.

7.4.2 Matching Separation Performance

The simulation requires values to be selected for the following parameters:

- Stage efficiency (realistic values would be 65 to 70%)
- Number of stages (always giving a total of 20 theoretical stages when efficiency is taken into account)
- Stage volumetric hold-up
- Tray spacing (set by total height/ no of trays).

The user can select the number of stages and the Murphree tray efficiency so that the number of theoretical stages comes to the desired value (in this case 20). The number of stages cannot be set without an efficiency factor, because BatchCAD performs mass transfer calculations by adjusting the value of the mass transfer coefficient on the trays to obtain the user-specified efficiency. It is not possible to have 100% efficiency as this would require BatchCAD to specify an infinite mass transfer coefficient.

The values of the parameters listed above were set through trial and error testing with repeated simulations in BatchCAD to match separation performance. Initially the more extreme values for the settings were used, in order to explore the full variable space and give direction which allowed the next run to move closer to a suitable result. The values which must be matched to the experimental data are:

- Condensate composition in mole fractions
- Reactor composition in mole fractions
- The range of temperatures in the column at steady state.

	Experiment	Simulation
Condensate Mole Fraction 1-Propanol	0.86	0.88
Condensate Mole Fraction 2-Butanol	0.14	0.12
Reactor Mole Fraction 1-Propanol	0.54	0.52
Reactor Mole Fraction 2-Butanol	0.46	0.48
Temperature at T1 (°C)	97.5	98.2
Temperature at T4 (°C)	95.7	97.5

Table 7.1: Experimental vs. BatchCAD-Simulated Separation Power (values displayed to 2 d.p.)

The closest match between the simulations and the experimental data is shown in Table 7.1 and was obtained with the following parameters:

- Number of stages: 27
- Stage efficiency: 74.07% (theoretical stages = 20)
- Tray spacing: 3.61 cm
- Maximum hold-up per stage: 6.85ml

Separation characteristics were matched on the final values for the target parameters, which Table 7.1 shows to be very close to those obtained in reality, but is was noted that the simulated tray temperature vs. time profiles do not match the experimental profiles during the heat-up phase. On Chart 7.1 it can be seen that the simulated profiles lie far to left hand side of the experimental data, indicating that BatchCAD predicts the column to heat up much faster than occurs in reality.

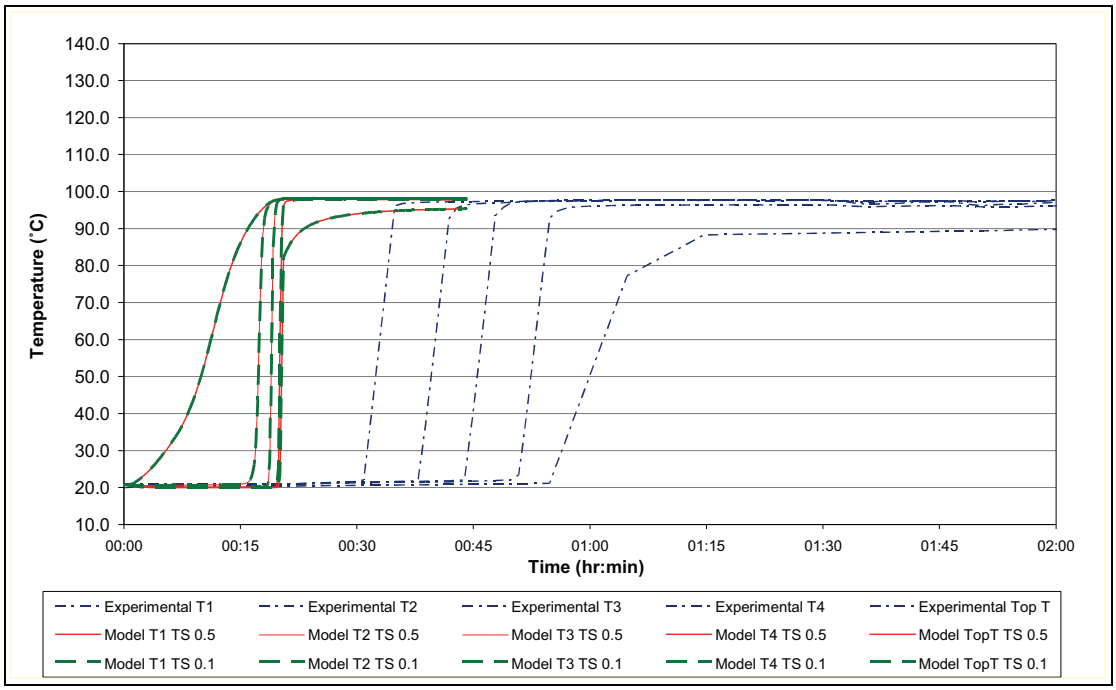

Chart 7.1: Real vs. BatchCAD-Simulated Column Temperature Profiles for the Separation Test

Unlike the reactor thermal characteristics, the column thermal characteristics cannot be specified by the user, and it is not possible to set a heat-up time for the column. Some attempts to reduce the mismatch were made but did not give significant improvement:

- Increased tray spacing distances of 0.5m and 0.1m were tested in the simulation but made no difference (the red and green lines overlaid in Chart 7.1).
- The addition of 200ml nitrogen vapour into the initial charge of the model delayed the heating of the column by a very small margin.
- The addition of a small amount of liquid at -20°C onto the trays in the column at the start of the simulation, also delayed warm up only very slightly.
- Increasing column liquid hold-ups did not slow the simulated heating of the column.

Further heat transfer adjustments could be made if BatchCAD included a range of heat transfer options for the distillation column, in a similar manner to that for the reactor. However, this is not currently possible.

7.5 BatchCAD Model: Esterification

Simulations have been performed in BatchCAD, which have been set up with the aim to give a representation of the RD esterification experiments. The purpose of this was to determine whether BatchCAD can help to interpret the experimental data and whether it could be able to predict how the process behaves. BatchCAD simulations were performed for six reactive distillation runs: the case for no catalyst, along with the five cases involving catalysts for which Arrhenius parameters were obtained in ChemSpeed runs at different temperatures. The simulations were performed with the simulated jacket oil temperature following the experimental jacket oil temperature profile in each case, which was loaded via the Data Editor feature in BatchCAD.

7.5.1 Esterification Model Development

Starting from the separation model, the thermal characteristics of the reactor, and the dimensions and other parameters for the column were retained. The BatchCAD model for the batch reactive distillation unit is illustrated in Figure 7.2.

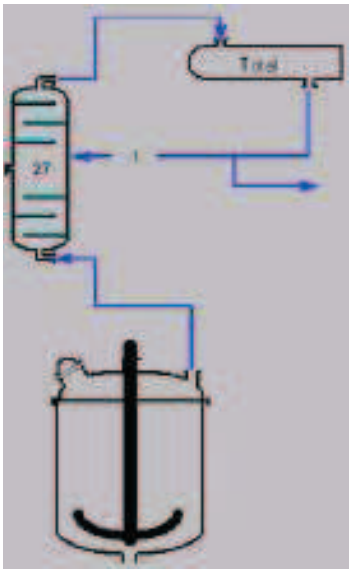

Figure 7.2: Illustration of the BatchCAD Model of the Batch Reactive Distillation Unit

The list of components to be used by BatchCAD for these simulations was changed to: n-nonanoic acid, n-butanol, n-butyl nonanoate (which was entered into BatchCAD based on a database component), and water. The BatchCAD-calculated properties of these components were cross referenced with those from literature: in particular, corrections were made to the estimated properties of the ester (density, melting point, and vapour pressure data). For each case involving the different catalyst systems, the relevant esterification kinetic parameters and the jacket oil temperature profile data were loaded into BatchCAD. The sequence of operating steps was entered to match those which occurred during the experiment, which have been described in Chapter 5. The reactor is heated during the first 40 minutes of each run, before the catalyst is added to the reaction mixture. One hour later, the reflux ratio policy is changed from total reflux to a reflux ratio of 1.

7.5.2 Run with No Catalyst Simulated in BatchCAD

A detailed description and comparison between the experimental data and the BatchCAD simulation outputs are given for the simulation of the experimental reactive distillation run with no catalyst. This is the simplest case considered, and gives the closest match between the simulation predictions and the experimental data. The purpose of this discussion is to demonstrate the performance of the simulations and highlight strengths and weaknesses of this modelling approach. The key charts of interest are Charts 7.2 and Chart 7.3, which show the comparison plots for the real and simulated data from the reactor-reboiler pot and the column, respectively. Description

and comparison of the simulations against the real experimental data is given as a commentary as the simulation progresses.

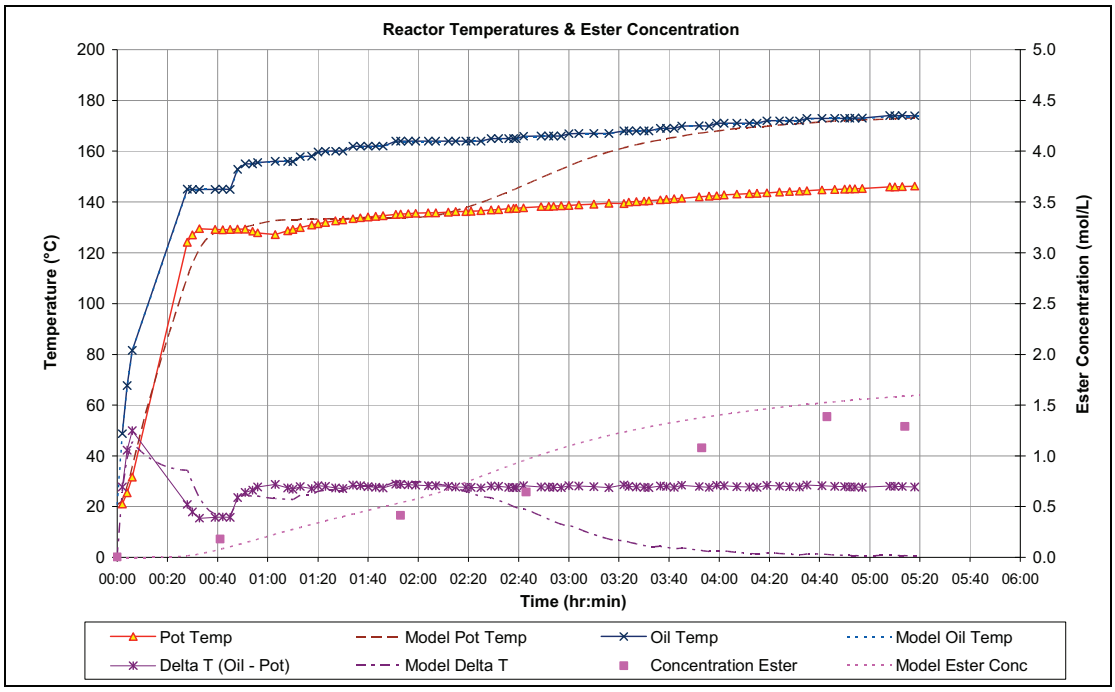

Chart 7.2: Real vs. BatchCAD-Simulated Reactor Profiles for the RD Esterification: No Catalyst

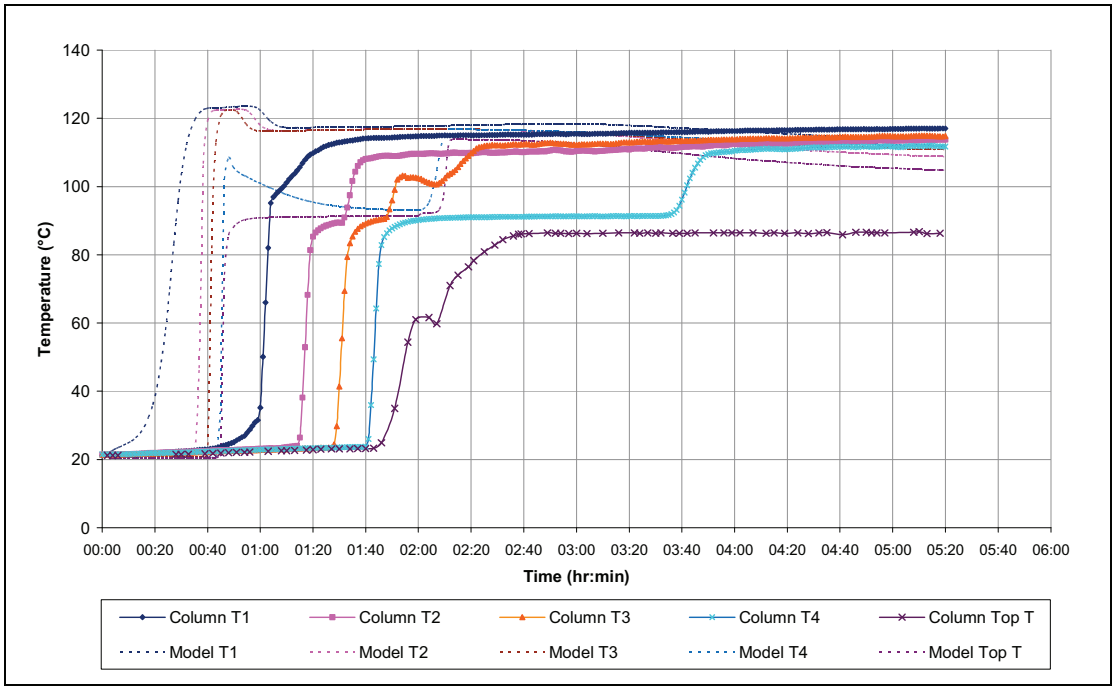

Chart 7.3: Real vs. BatchCAD-Simulated Column Temperatures for the RD Esterification: No Catalyst

Up to 40 minutes

In Chart 7.2 it can be seen that the oil and pot contents start at room temperature (approximately 20°C) and then, after the initial sample has been taken to confirm that no ester is already present in the mixture, these temperatures increase rapidly in

response to the heating by the oil bath on the unit. The oil temperature rises until it reaches the set point of 145°C, and the pot temperature rises until it reaches the boiling point of the mixture, approximately 129°C. The temperatures then remain relatively steady and at the 40 minute mark the second sample is taken. It is observed that at the 40 minute mark, after the warm-up phase, there is a good match between the real and simulated data in terms of pot temperature, jacket oil temperature and ester composition. The simulated composition in the pot at the 40 minute mark is shown in Table 7.2:

Component	Nonanoic Acid	Butanol	Ester	Water
Number of Moles	2.35×10^{-3}	4.27×10^{-3}	6.80×10^{-5}	3.95×10^{-5}

Table 7.2: BatchCAD-Simulated Pot Composition at 40 minutes for the RD Esterification: No Catalyst

Chart 7.3 shows that the real column temperatures start at room temperature, and remain at around 20°C during this phase of the process, but the BatchCAD simulated column temperatures start to rise far too early. Examination of how far ahead the simulations are compared to the real profiles reveals that BatchCAD predicts that the temperature at the bottom of the pot (T1) rises to 40°C in around a third of the time required in reality:

- Approximate time real T1 reaches 40°C: 1 hour and 20 seconds
- Approximate time simulated T1 reaches 40°C: 20 minutes 30 seconds

BatchCAD is unable to accurately replicate the temperature profiles in the column, as it significantly underestimates the time required for the temperature in each section of the column to start to rise and overestimates the rate of increase.

40 minutes to 1 hour

During the experimental runs, the temperature difference is maintained at 28°C during the run by continuous small adjustments in the oil temperature, responding to changes in the pot temperature. The simulated oil temperature in Chart 7.2 is programmed to replicate the real profile followed by the oil bath during each experiment. The real pot temperature falls slightly before the 1 hour mark; probably due to condensation returning from inside the column. At this point the BatchCAD simulated pot temperature is slightly mismatched as it does not predict this slight fall in temperature.

As the simulation progresses, the reaction causes ester and water to form. Chart 7.4 shows the pot compositions generated by the BatchCAD simulation, where it is observed that the number of moles of ester increases slowly as it is produced by the

esterification reaction and the number of moles of nonanoic acid reduces. Prior to the reflux ratio change at 2 hours, the number of moles of butanol falls steadily while the number of moles of water remains at trace levels, as it boils up rapidly as it is formed.

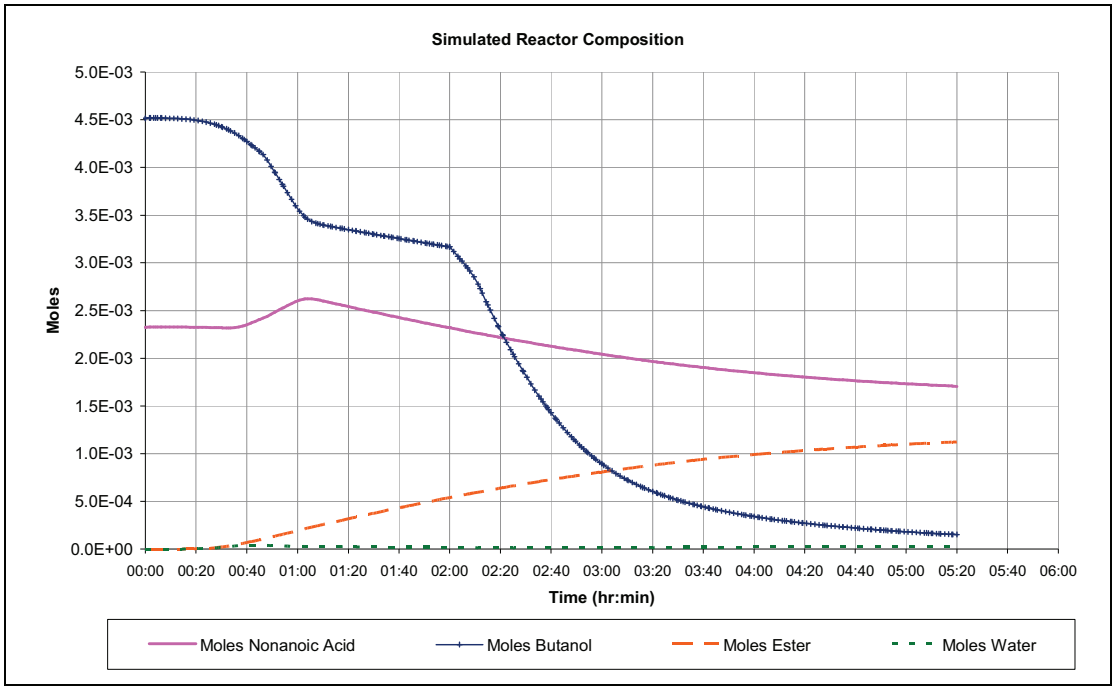

Chart 7.4: BatchCAD-Simulated Pot Compositions for the RD Esterification: No Catalyst

In the simulated reactor composition in Chart 7.4, BatchCAD appears to predict that the number of moles of nonanoic acid increases slightly after 40 minutes. This is not due to formation of nonanoic acid by reaction but is rather a feature of the way the BatchCAD simulation is initialised. BatchCAD is unable to begin the simulation with empty trays, so at initialisation the trays are 'filled' with some of the feed liquid. The composition of this liquid is the same as that of the initial charge to the reactor: a mixture of nonanoic acid and butanol. As the simulation progresses, nonanoic acid is displaced from the trays as water-butanol azeotropic mixture begins to boil and move up the column.

In the simulated composition profiles of the trays in Charts 7.5 and 7.6, the rapid displacement of nonanoic acid from the trays can be clearly seen after the 40 minute mark. At the start of the simulation the compositions on tray 1 (Chart 7.5) and the top tray (Chart 7.6) are the same, as they match the composition of the initial charge to the reactor. Water starts to appear on the top tray approximately 50 minutes into the simulation, and at the same time the nonanoic levels on this tray fall sharply. Shortly afterwards the nonanoic acid levels on tray 1 also fall and around the 1 hour mark the nonanoic acid rapidly disappears and is replaced by butanol. This nonanoic acid moves

down the column to the reactor/reboiler pot, where it combines with the reaction mixture as observed in the concentration profiles in Chart 7.4.

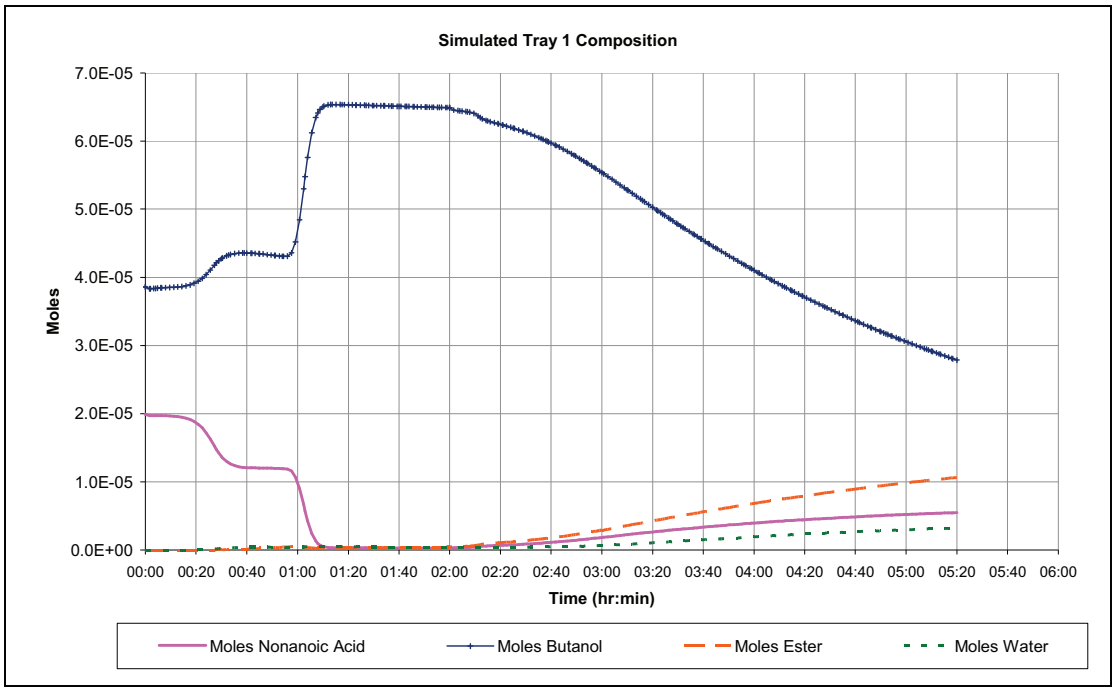

Chart 7.5: BatchCAD-Simulated Tray 1 Composition for the RD Esterification with No Catalyst

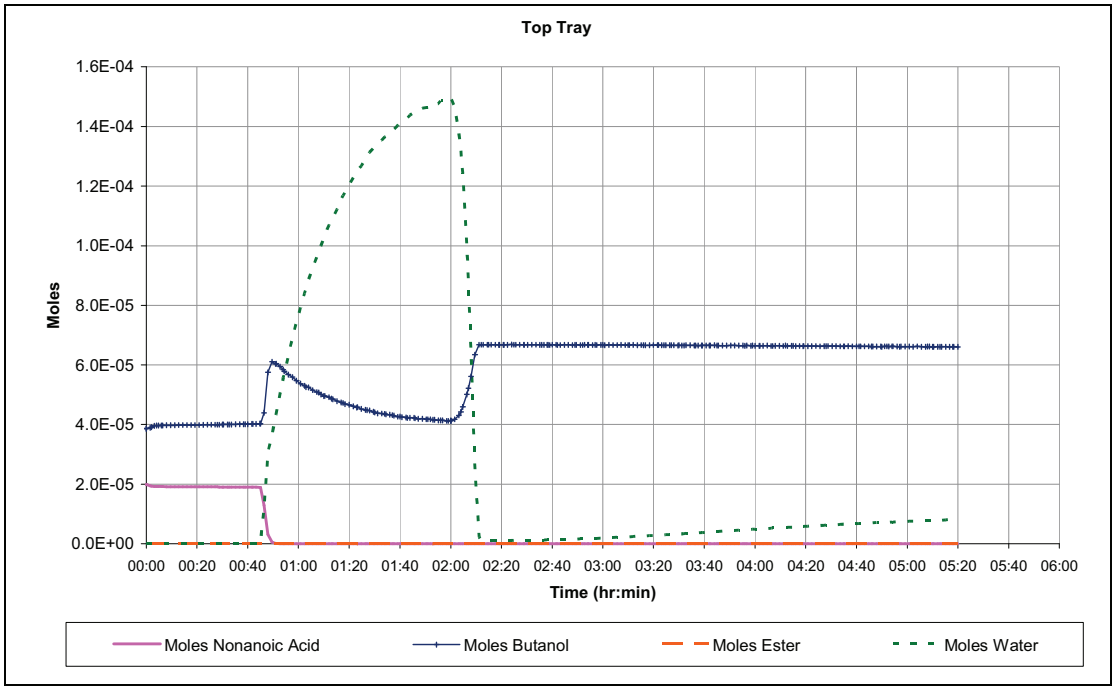

Chart 7.6: BatchCAD-Simulated Top Tray Composition for the RD Esterification with No Catalyst

In the simulations it is observed that the tray temperatures correspond to the changing tray compositions. In Chart 7.3 the BatchCAD simulated column temperatures 1 to 3 are steady at 118°C while T4 and the top temperature are at around 90°C at the 2 hour mark. In Chart 7.5 it is seen that at the 2 hour mark, while the temperature on tray 1 is

approximately 118°C, the simulated liquid on the tray is almost all butanol. At the same time point the top tray is simulated to be steady at around 90°C, and is revealed by BatchCAD to be dominated by water-butanol azeotrope. From Chart 7.2 it can be seen that, for this simulation, after 2 hours have passed there is still a good match between the real data and the simulations in terms of pot temperature, jacket oil temperature and ester composition.

Reflux ratio switch (2 hours)

In the run with no catalyst added, the reflux controller was switched from full reflux to a time-controlled reflux ratio of 1 at the 2 hour mark. No immediate changes in the pot temperature or oil temperature are observed in either the real or simulated data in Chart 7.2. After a slight delay, the BatchCAD simulated pot temperature increases gradually and starts to approach the oil temperature, causing a mismatch with the experimental data. The simulated ester compositions are slightly above those of the experimental data after the reflux ratio change. The BatchCAD pot compositions in Chart 7.4 show a gradual decrease in the number of moles of nonanoic acid, and an increase in the number of moles of ester. The water composition remains at trace level, but the butanol is falling rapidly, as it is removed from the pot both by reaction and by vaporisation.

In the experimental temperature profiles in Chart 7.3, a transition is observed at around 3 hours 40 minutes, when T4 increases from around 90°C to approximately 115°C. This suggests a change occurs in the composition of the liquid on the tray. The BatchCAD-generated profiles of the temperatures at the top of the column show a similar increase from around 90°C to 115°C following the reflux ratio change. The corresponding change in the simulated composition of the liquid on the top tray is shown in Chart 7.6: the number of moles of water falls suddenly and butanol dominates the new composition of the liquid on the tray.

In the BatchCAD simulation, the collection of distillate begins as soon as the reflux ratio change is applied, while in the real experimental data the collection of distillate begins after a short delay of 7 minutes (as seen in Chart 7.7). The simulated distillate collection rate is significantly higher than the real distillate rate, and this will in turn affect the prediction of the composition of the mixture in the pot.

- Real distillate collection start: 2 hour 07 minutes.
- BatchCAD simulated collection start: 2 hours (reflux ratio change point).

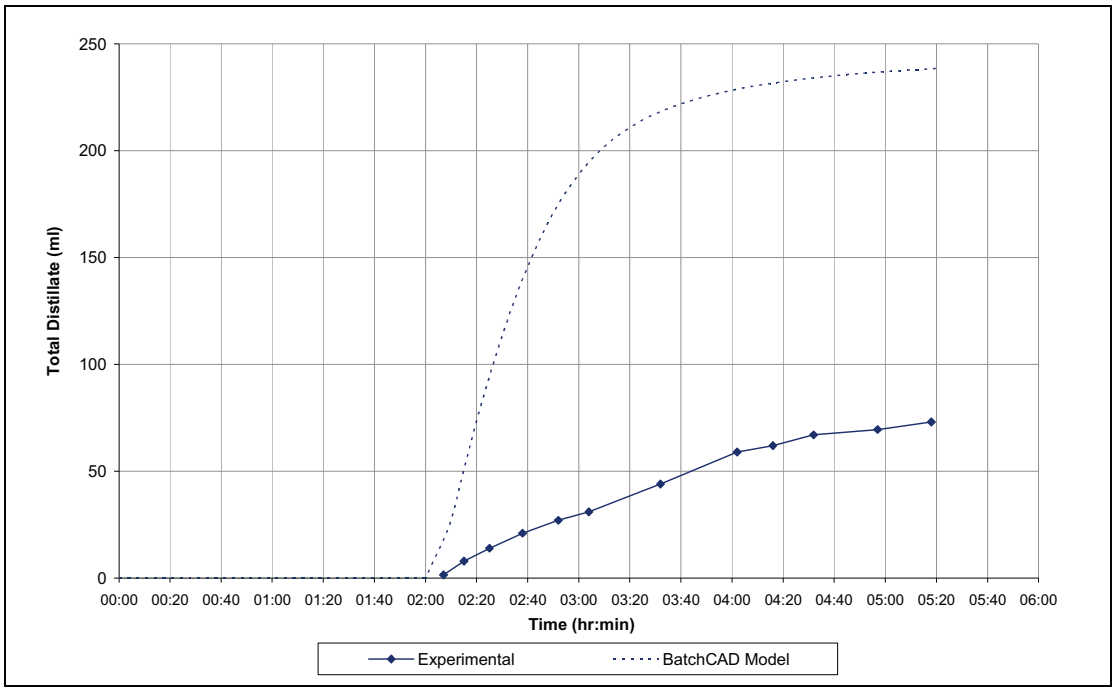

Chart 7.7: Real vs. BatchCAD-Simulated Distillate Collection for the RD Esterification: No Catalyst

From 3 hours 40 minutes onwards

The driving force for boil-up is the temperature difference between the oil and the pot, which diminishes in the simulations (and approaches zero) as the pot temperature approaches the oil temperature. This indicates that the BatchCAD-predicted pot temperature, which is at the mixture boiling point, increases above that observed during the experiments. The rate of distillate collection slows (as seen in Chart 7.7), and the rate of ester production also slows (Chart 7.4) despite the presence of remaining nonanoic acid.

The simulated reaction is not being inhibited by the presence of water, as examination of the pot compositions reveals that water is still at negligible levels in the pot. However, the number of moles of butanol has fallen significantly, and the lack of butanol causes the reaction to stall and the boil-up rate, and therefore the distillate rate, to decrease. The simulated ester composition in the pot does not go significantly over that observed during the real experiment; this is because in the simulation the butanol level in the pot is so low.

7.5.3 Summary of the BatchCAD Simulation Performance

The outcomes of BatchCAD simulations of the nonanoic acid system under reactive distillation with five catalysts are presented in Appendix N. The profiles of the simulated and experimental data show that all the cases have very similar start-up phases, and a good match between the experimental and simulated pot and oil temperatures at the 'pre-catalyst addition' point. Table 7.3 presents the predicted pot compositions at this point in each of the cases. The consistency of the values for the compositions and the temperatures at this point of the simulations, and the similarity with experimental data, indicate that BatchCAD is capable of accurately predicting the extent of reaction, the composition and boiling point of the reaction mixture.

Catalyst	**Time (min)**	**Oil Temp (˚C)**	**Pot Temp (˚C)**	**Reactor Moles**			
				N Acid	**Butanol**	**Ester**	**Water**
No Cat	40	145	129.2	2.4×10^{-3}	4.3×10^{-3}	6.8×10^{-5}	3.9×10^{-5}
ZnAc	40.5	145	128.9	2.4×10^{-3}	4.2×10^{-3}	8.9×10^{-5}	4.0×10^{-5}
MSA	40	145	129.4	2.4×10^{-3}	4.2×10^{-3}	8.5×10^{-5}	4.0×10^{-5}
H_2SO_4	41	145	129.6	2.3×10^{-3}	4.3×10^{-3}	7.2×10^{-5}	4.1×10^{-5}
PhosMo	39.5	145	129.6	2.4×10^{-3}	4.2×10^{-3}	8.7×10^{-5}	4.0×10^{-5}
FeSulf	39	145	129.4	2.3×10^{-3}	4.3×10^{-3}	6.3×10^{-5}	3.9×10^{-5}
Average	**40**	**145**	**129.4**	$\mathbf{2.4 \times 10^{-3}}$	$\mathbf{4.2 \times 10^{-3}}$	$\mathbf{7.7 \times 10^{-5}}$	$\mathbf{4.0 \times 10^{-5}}$

Table 7.3: BatchCAD-Simulated Temperatures and Compositions in the Pot at 40 minutes

Further valuable information is provided by the BatchCAD simulations about the compositions of the material in the column. When the column temperatures are around 90°C, the BatchCAD simulations indicate that the liquid contains a significant amount of water, corresponding to the water-butanol azeotrope. When the column temperatures are higher, in the range 110 to 118°C, the liquid compositions are dominated by butanol. This gives some insight as to what is occurring in the experimental column when a step change in the column temperature is observed, information that is not available otherwise as there is no capability to take samples from the column itself.

In Appendix N it is shown that the column heat-up time is highly mismatched in all of the BatchCAD simulations, as the column temperatures start to rise earlier then the real temperatures. The rate of reaction was overestimated in most simulations, and the distillate collection rate was predicted to be higher than reality in every case. The effects of the overestimated column-heat up rates and reaction kinetics are as follows:

- In the simulation, water forms too fast, so the boil up rate is predicted to be higher than in reality.
- Material is predicted to move extremely quickly up the column without any internal reflux hindrance (which appears to have had a major effect in the experimental runs).
- The composition in the pot is therefore highly mismatched with reality, making it impossible to recreate the experimental observations with the simulations.
- When the simulations are started from the point where the catalyst is added, i.e. the 'reactor heat-up' phase is skipped; this does not fix the mismatch between the simulations and the real data.

The BatchCAD simulations have been able to provide some information about the process, and it is believed that if the column temperature mismatch could be corrected, the accuracy of the simulations as a whole would be improved. However it is not currently possible to adapt BatchCAD to include a specified warm-up time, heat loss from the column or boil up limitation term.

Table 7.4 summarises the outcomes of the simulations of the batch reactive distillation runs in BatchCAD. These results are taken forward for further analysis in Chapter 8, to investigate whether their inclusion as variables in a multivariate model assists in the prediction of the performance of these catalysts under reactive distillation conditions.

	MSA	**H_2SO_4**	**FeSulf**	**PhosMo**	**No Cat**	**Zn Ac**
End Yield Water Distillate (%)	81.8	90.0	94.7	92.6	32.9	27.6
End Yield Ester in Pot (%)	96.7	95.2	96.9	94.3	38.6	33.1
Initial Rate of T Fall (°C/min)	-44.4	-34.2	-18.5	-24.4	3.4	3.5
Lowest Pot Temp (°C)	119	119	123	124	128	129
Time to Lowest Pot Temp (hh:mm:ss)	00:52:30	00:53:37	00:45:02	00:49:07	00:40:00	00:40:00
Rate of Pot Temp Rise at 2h40min (°C/min)	4.3	4.9	7.6	5.1	10.1	8.8
Pot Temp At End (°C)	166	172	174	173	171	173

Table 7.4 BatchCAD Model Outputs Taken Forward

7.6 Simplified Excel-Based Model for Esterification

Experimental information from the RD unit shows that it does not behave in ways such as an ideal model would predict due to internal heat transfer issues, slow warm-up, internal refluxing, and the limited collection system capability (described in Chapter 5). Accurate dynamic simulations of the column which give accurate column temperature profiles and compositions on the trays are not feasible using BatchCAD. Therefore a simplified model is proposed based on the observations of the experimental results described in Chapter 6, where the boil up rate was shown to be strongly related to the reboiler pot temperature. Changes in composition in the pot are due to both reaction and removal of distillate, which can be described by equations fitted onto experimental data.

7.6.1 Setting up the New Model

A key difficulty when modelling distillation processes is that it is very difficult to predict the boil up rate of material from the reboiler. Luyben (1990) described a mass transfer coefficient parameter (K_{MT}) that is often applied in order to approximate the boil up rate in steady state simulations. Selection of the correct value for this parameter is not a trivial task. For a preliminary model, a K_{MT} value was found that appeared to enable the simulation to run, but this model was not robust. When a parameter such as the reflux ratio set point was changed the simulation became unstable, taking a very long time to complete or crashing. Finding a value for K_{MT} by trial and error that worked for all cases was not possible.

Polynomial equations have therefore been developed to allow the calculation of the rate of water removal in the distillate (in mol/s) with reactor temperature. There is also a strong correlation between the reboiler pot temperature and the water to butanol molar ratio in the distillate, which provides further information about the composition of the material removed from the pot. One set of equations were developed for the strong acids and other active candidates, and a second set was used to model the slower cases, as the results in Chapter 6 indicate that the behaviour of the two groups is very different. If this technique were to be extended to include further candidates, the category that a candidate falls into would be determined at the ChemSpeed screening stage. The kinetic parameters established through testing candidates over a range of temperatures, and presented in Chapter 4, were used to calculate the composition change due to reaction.

The sequence of the calculations, the equations and the macro used to calculate composition change in each time interval are given in Appendix O.

BatchCAD simulations have predicted the composition at the point where the catalyst is added quite well, so the average simulated composition at this time point (see Table 7.3) is taken as the starting input for a model built in Microsoft Excel which continues from the 40 minute mark. The simplified Excel model performs a calculation procedure for every 1 second interval for the time span from 40 minutes to 4hours 40 minutes, so that the outputs of the simulations can be compared with those of experiments. For each time interval, the model calculates:

- The change in the composition of the reaction mixture in the reactor/reboiler.
- The boiling point of the mixture, which is also the temperature of the pot.
- The amount of water and butanol removed in the distillate.

This is a fully predictive model, in contrast to the BatchCAD simulations for which the experimental oil temperature profiles were loaded for the simulation to follow. The boiling point of the reaction mixture is calculated via component vapour pressures, which are based on literature values rather than experimental data so there is expected to be some slight mismatch. Also it should be noted that this pragmatic model has been built on specific experimental observations, and is not applicable to any other column, or reaction system. An illustration of the simplified model basis is shown in Figure 7.3, where it is seen that there is no description of the separation column included.

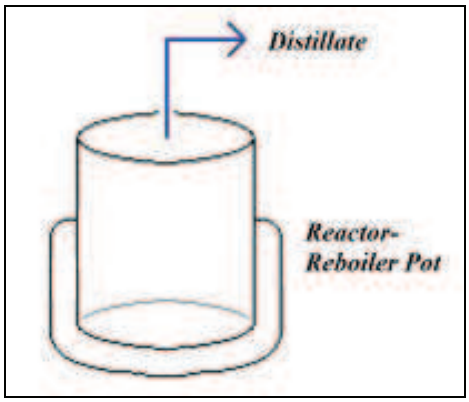

Figure 7.3: Illustration of the Excel Model of the Batch Reactive Distillation Unit

7.6.2 Run with No Catalyst Simulated in Excel Model

A comparison between the experimental data and the Excel model simulation outputs are given for the simulation of the experimental reactive distillation run with no catalyst.

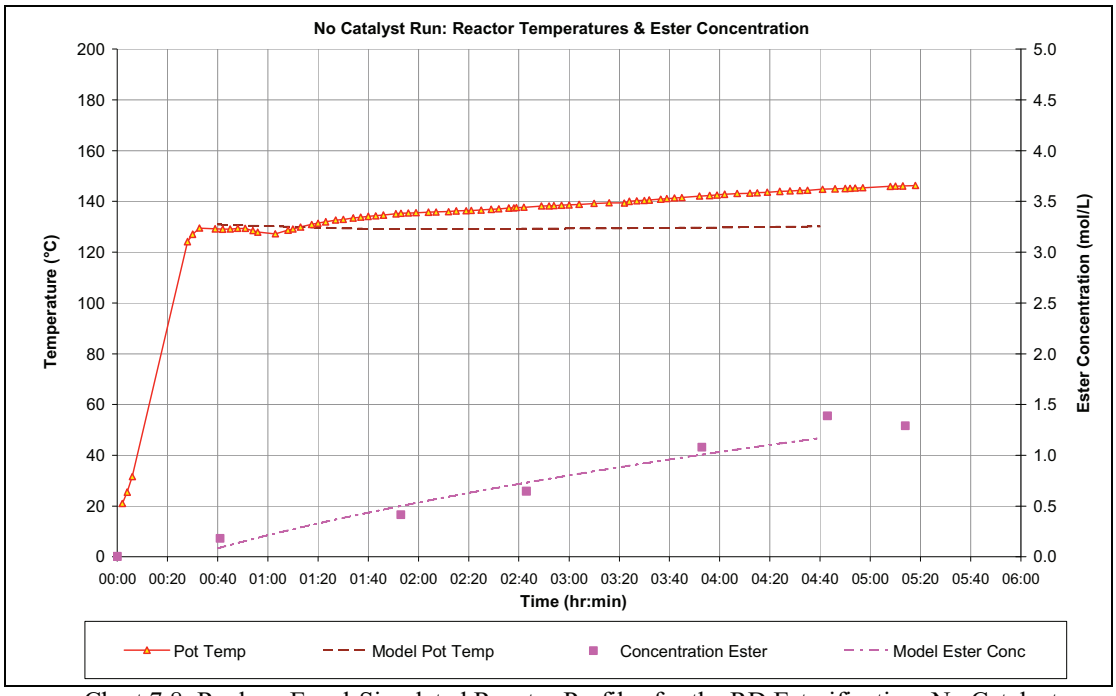

Chart 7.8: Real vs. Excel-Simulated Reactor Profiles for the RD Esterification: No Catalyst

In Chart 7.8 it is seen that, although the ester composition profile is well matched with the experimental data, the simulated temperature in the pot did not increase with time as levels of high-boiling ester increased, as was seen in the experimental runs. It may be that this model is not correctly calculating the boiling point of the reaction mixture as the composition changes. The calculation of boiling point for these simulations is an estimate based on information available from open literature, rather than experimental data or an established physical property databank such as that used in BatchCAD. This is a likely cause of the mismatch seen in Chart 7.8, and is one of the limitations of creating a simplified model. BatchCAD has been found to give predictions of the boiling point of the mixture which did match the experimental observations.

Chart 7.9 shows that the distillate rate is poorly predicted by the Excel model, with the simulation predicting almost no distillate collection during the run. This could be a knock-on effect of the inability to match the changing boiling point, and therefore temperature, of the reaction mixture. In this case, the simulated temperature in the pot does not reach the conditions under which a higher collection rate would be seen, which

were set based upon observations of the runs described in Chapter 6. It is a weakness of this type of pragmatic model based on experimental data that the simulations cannot deal with cases which do not fall within the boundaries of the experimental conditions that they have been built upon.

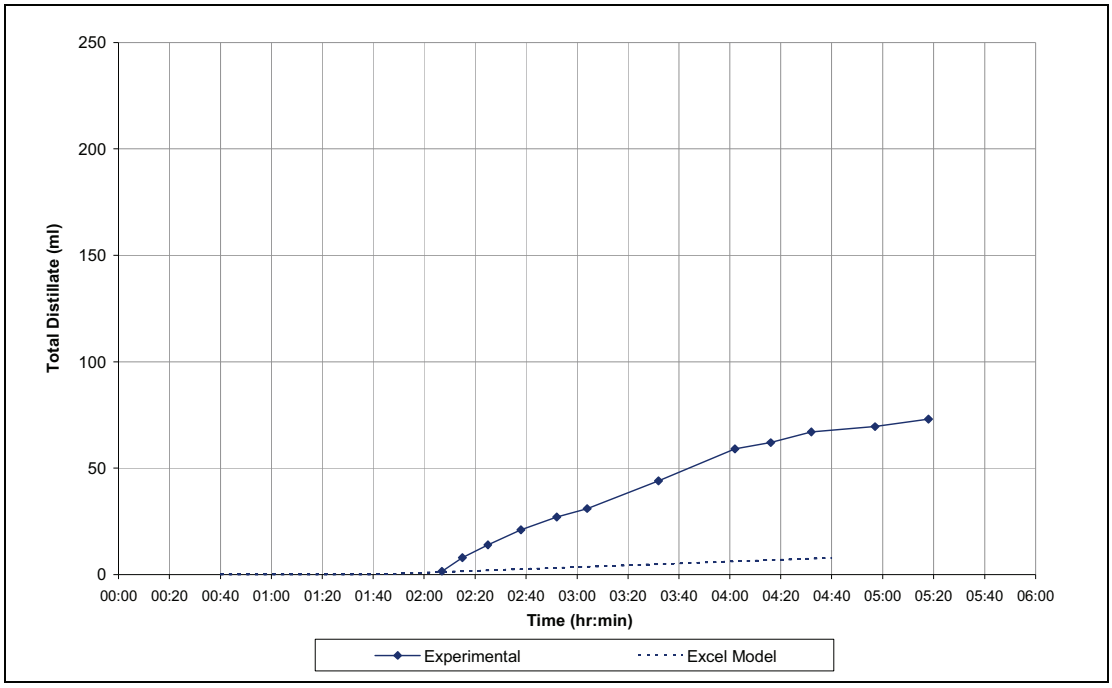

Chart 7.9: Real vs. Excel-Simulated Distillate Collection for the RD Esterification: No Catalyst

7.6.3 Summary of Simulation Performance

Excel simulations were performed for six RD runs: the case for no catalyst, along with the five catalysts for which kinetic parameters were obtained through ChemSpeed runs at different temperatures. The results of the simulations for the cases involving catalysts are presented and compared with the experimental data in Appendix P.

For the cases with no catalyst and zinc acetate (the slow cases) the ester composition is well predicted, but the real and simulated pot temperatures profiles diverge as the simulation fails to predict the temperature rise, and the distillate collection rate is underestimated. For the cases with the strong acids (H_2SO_4 and MSA) the ester concentration is overestimated, and the pot temperature in the simulations does not fall as rapidly as in reality, although the distillate collection is matched fairly well. The cases with medium activity candidates (the heteropoly acid PhosMo and ferric sulfate) give overestimated ester concentrations in the simulations, but the pot temperatures are more closely matched and the distillate collection is predicted well.

Generally, in the cases where a temperature drop occurs after the catalyst has been added, the simulations are able to capture that the pot temperature falls and then rises again, but the simulated temperature does not fall as low as in the experimental profiles. The distillate sometimes matches very closely, for example for the acids and ferric sulfate, but not in all cases. The ester compositions match quite well for the slowest reacting systems, no catalyst and zinc acetate, however there is greater mismatch for the acids, especially MSA.

	MSA	**H2SO4**	**FeSulf**	**PhosMo**	**No Cat**	**Zn Ac**
End Yield Water Distillate (%)	74.9	74.7	73.7	73.3	18.2	18.2
End Yield Ester in Pot (%)	84.4	84.6	84.5	84.4	43.0	38.6
Initial Rate of T Fall (°C/min)	-16.7	-14.8	-8.9	-8.2	-0.8	-0.7
Lowest Pot Temp (°C)	122	122	123	123	129	129
Time to Lowest Pot Temp (hh:mm:ss)	01:00:00	01:00:00	01:00:00	01:00:00	01:19:00	01:00:00
Rate of Pot Temp Rise at 2h40min (°C/min)	3.5	3.4	3.3	3.2	0.2	0.2
Pot Temp At End (°C)	175	174	170	169	130	131

Table 7.5 Excel Model Outputs Taken Forward

Table 7.5 summarises the outcomes of the simulations of the batch reactive distillation runs in Excel. These results are also taken forward for further analysis in Chapter 8, to investigate whether their inclusion as variables in a multivariate model assists in the prediction of the performance of these catalysts under reactive distillation conditions.

7.7 Summary

In this chapter it has been shown that BatchCAD, which uses an established physical property calculation engine, is able to accurately predict the reaction extent, the pot composition and temperatures in the early phase of the experimental RD runs (prior to catalyst addition). A simplified model that uses less sophisticated techniques to estimate physical properties is unable to do this and is therefore not suitable for simulation of reactive distillation processes. Study of the BatchCAD simulation outcomes has also provided insight into changes in the composition of material in the column that lead to the temperature profiles observed in the data from the experiments.

Each of the experimental batch RD runs performed effectively has a very long column warm-up phase: the vapour rises up the column, and the temperature of the cold surfaces of the column walls and structured packing must rise and the large surface area of the packing must become wetted. In this study the experimental runs lasted 4 hr 40 minutes, but the distillate collection did not start until after 1 hr 40 minutes (and in some cases even later) which represents a very significant part of the process time.

BatchCAD was not able to simulate the column warm-up phase of the process accurately, as there is no facility in BatchCAD to represent this slow process. The Literature Review of Chapter 2 found that simulations of start-up, validated against real data and taking into account column size, are rarely reported. The creation of accurate simulations of batch RD processes will be particularly difficult where the warm-up time for the column is large, relative to the complete run itself. Models available at the time of the development of BatchCAD usually made many assumptions such as the assumption of reaction equilibrium, constant molar overflow and steady process conditions. More recent advances in commercial software have led to rapid progression and development of more intricate tools, but not yet any which are able to capture the effects of slow heat-up time, wall surface wetting and internal refluxing, which have a very significant effect in small, pilot-scale equipment.

The outputs from the simulations summarised in Tables 7.4 and 7.5 are taken forward to Chapter 8, in which multivariate statistical tools are used to investigate whether the inclusion of these simulation outputs can improve the prediction of how the different catalysts behave under batch reactive distillation conditions.

Chapter 8: Relating Catalyst Performance and Properties

8.1 Overview

In Chapter 6 it was shown that not all of the outputs from the reactive distillation experiments with different catalyst candidates are strongly correlated to the half life of the esterification of nonanoic acid observed in the screening stage. The half life is a poor indicator of the final distillate collection, which is one of the key outputs from an RD process. This chapter describes the implementation of multivariate statistical tools and QSAR (quantitative-structure-activity relationship) analysis, which may enable the outputs of the RD experiments to be more fully understood.

An introduction to QSAR techniques is given in section 2.8 of Chapter 2. The principle behind the use of QSAR is to relate experimentally determined attributes of a candidate to numerical descriptors of its composition and structural features. Multivariate statistical tools are used to look for connections between the molecular information and the performance of the candidate as a catalyst, and to quickly give an indication as to which catalyst features may determine the observed behaviour. Interpretation of the descriptors that have the strongest influence also has the potential to give insight into the chemical and physical reasons behind the experimental observations.

The application of QSAR techniques in this study will enable the investigation of whether this use of multivariate statistical tools could reveal key descriptors or underlying trends that may explain the observed outputs. The first statistical models relate the experimental ChemSpeed screening half life values to molecular descriptors, including the consideration of all 20 candidates, and then a subcategory within the catalyst types. This reveals a set of descriptors that could be useful for explaining the observed screening activities, and the model is able to pick up on distinctions between the categories of candidates. To investigate any relationships between the experimental batch reactive distillation results and the candidate molecular descriptors, a statistical analysis is performed on all the experimental outputs grouped together, before the individual outputs are considered separately.

The effect of the inclusion of an alternative type of descriptor upon the correlations is also assessed. Finally the effect of inclusion of simulation outputs as descriptors is evaluated, in order to investigate whether information from dynamic batch reactive

distillation models could help improve the prediction of the behaviour of the reaction system when different catalysts are present. Not enough experimental data is available to build robust predictive models and to perform validation procedures, but an attempt is made to look for indications as to whether or not use of multivariate models could be a useful approach, in order to provide guidelines and direction for future work.

8.2 Introduction

From the work described in previous chapters, three sets of information are available: the results of the screening experiments, the results of the reactive distillation experiments, and the simulation outputs. Multivariate statistical analysis is performed to look for trends in the available data and to investigate whether there is a set of descriptors that can explain the different catalyst behaviour observed experimentally. Specifically, it is desirable to identify the features of the most successful catalysts that enable them to display high catalytic activity, and to attempt to explain the performance of the candidates under reactive distillation conditions.

Descriptors can be any information about a catalyst that takes a numerical value, for example molecular weight, number of oxygen atoms, refractive index, etc. The descriptors can be from physical attributes or more abstract parameters such as shape indices. Potential sources of descriptors include:

- Supplier information
- Databases e.g. PubChem (online)
- Literature e.g. CRC Handbook, Merck Index
- Molecular modelling \ descriptor-generating software e.g. E-Dragon

Composition information from the molecular formula, supplier information and PubChem database entries were available for all twenty candidates. The literature sources available did not contain information for all twenty of the candidates, however it was noted that the coverage is increasing. There was no information for seven of the candidates in the 77th Edition of the CRC Handbook of Chemistry and Physics, but this reduced to only four not covered in the 90th Edition (Lide, 1996 and 2009). Very few of the catalyst structures were able to be run in E-Dragon, as this software is not able to cope with dissociated molecules such as the metal acetates, or with atoms that are not currently included in its database, such as niobium.

It was also the case that not all the catalyst candidates were able to be run in the Cresset FieldTemplater molecular modelling tool, for example niobium was again not recognised, although all of the metal acetates were able to be processed and visually represented by this software. The software was able to generate three numerical descriptors based on scores of the similarity of each candidate against a 'target' molecule, which is a useful capability for applications such as pharmaceutical screening. In this case the target molecule to which all the others were compared was sulfuric acid, the most widely utilised catalyst for esterification.

The following variables are given by the PubChem Online Database for each catalyst *PubChem* (2010):

- Molecular Weight [g/mol]
- Number of H-Bond Donors
- Number of H-Bond Acceptors
- Heavy (Non-H) Atom Count
- Topological Polar Surface Area
- Complexity
- Covalently-Bonded Unit Count

From the chemical formula for the catalyst, the following information can be deduced:

- Number of water of hydration groups
- Number of acetate groups
- Carbon Atom Count
- Hydrogen Atom Count
- Metal Atom Count
- Phosphorus, Sulfur or Chlorine Atom Count

From these variables, others can be derived which could be useful for the comparison of the catalysts. For example:

- H-Bond Donor per Unit of MW
- Metal Percent by Mass
- MW per Covalently-Bonded Unit

A total of 44 possible catalyst descriptor variables were defined, this number was reduced to 38 (listed in Appendix Q) as some were revealed to be duplicates through processing with a Rank correlation matrix.

8.3 Statistical Tools and Data Processing

A method of sifting through the descriptor data is required that will identify those descriptors that are most useful for understanding how the descriptors relate to catalyst performance. Brief descriptions of some widely used multivariate statistical tools are given in the following sections.

8.3.1 Multiple Linear Regression (MLR)

MLR is the simplest, most easy-to-apply multivariate regression analysis. With this technique, a regression coefficient is fitted to each descriptor, and a large regression coefficient indicates that the associated descriptor is of high importance. However, MLR is not suitable if there are more descriptors than catalyst candidates, or if the descriptors are correlated (Rothenberg, 2008b and Albert et al., 2001).

8.3.2 Principal Component Analysis (PCA)

A PCA analysis generates a set of principal components (linear relationships between the descriptors) that explains the variability within the descriptors as well as possible, and then correlates this with the output data. PCA does not use the output data to produce the principal components. A simple PCA model can be described by the following matrix notation (Rothenberg, 2008b):

$$\mathbf{X} = \mathbf{T}\mathbf{P}^{T} + \xi \tag{8.1}$$

So:

$$\mathbf{X} = \mathbf{t}_1\mathbf{p}_1^{T} + \mathbf{t}_2\mathbf{p}_2^{T} + \ldots + \mathbf{t}_i\mathbf{p}_i^{T} + \xi \tag{8.2}$$

Where:

X= matrix of inputs (descriptors)

T = matrix of input scores

P = matrix of loadings

ξ = residual errors

t = input scores (representing the spread of the catalyst descriptor values in the variable space)

p = loadings

i = number of descriptors (= total number of PCs possible)

A high loading value would indicate that the associated descriptor has a high importance in explaining the variance in the input data. The first principal component is always the one that explains the greatest amount of variance in the data, and the others follow sequentially e.g. principal component 2 is the next most important and so on. A PCA plot, of the first two principal components plotted against each other, is useful for getting an overall 'feel' for the data. These plots can highlight any clusters or multivariate outliers in the data.

A PCA model would often not use all the available principal components generated, but only include those that can add 'information' to the model. Leaving out the lowest-ranked principal components, which tend to have little information value, can remove noise from the model. For a good model, examination of the residuals should reveal them to be randomly distributed, with no structure. If there is a structured pattern to the residuals then this would indicate that there are factors which have not been accounted for in the model (Rothenberg, 2008b).

8.3.3 Projection to Latent Structures (Partial Least Squares)

In a PLS analysis, latent variables are created for the descriptors matrix and for the outputs matrix, and then a correlation is performed between these to build a model that explains the output variables as well as possible. PLS is the most frequently used method for this type of multivariate analysis. A PLS model can be described by the following matrix notation (Brown et al., 2006):

$$\mathbf{X} = \mathbf{S}\mathbf{Q}^{T} + \mathbf{\epsilon} \quad (8.3)$$

$$\mathbf{Y} = \mathbf{S}\mathbf{C}^{T} + \mathbf{f} \quad (8.4)$$

And:

$$\mathbf{Y} = \mathbf{B}\mathbf{X} + \mathbf{f} \quad (8.5)$$

Where:

X = descriptors (input) matrix

S = Input scores

Q = Input loadings

Y = output matrix

C = Output loadings

B = matrix of regression coefficients

Є and **Ƒ** = residual errors

The values of the regression coefficients (matrix **B**) reveal which are the most important latent variables, as it is not always the case that LV1 is the most heavily weighted. The Matlab MultiDAT toolbox (developed within CPACT at the School of Chemical Engineering and Advanced Materials at Newcastle University) offers a convenient facility to examine these regression coefficients and descriptor loadings within the latent variables, which allows investigation of whether there is a set of descriptors that are important in explaining the output variables. The NIPALS algorithm is the most widely used method for the calculation of the necessary coefficients (Albert et al., 2001).

Like a principal components model, a PLS model can contain fewer latent variables than original input variables. The number of latent variables retained in the model is determined in the MultiDAT toolbox by cross validation and by looking at the cumulative explained variances. PLS has been chosen as the most suitable tool for detailed multivariate analysis because it is recommended for situations where there are highly correlated variables or there are more variables than samples (Albert et al., 2001). Other advantages PLS offers over other methods are that the model created is focussed on explaining the outputs rather than the variance in the descriptor set, and PLS can handle datasets with many outputs, such as the results from the reactive distillation catalyst tests.

8.3.4 Normalisation

To attempt to reduce distortion due to the wide range of values taken by the descriptor variables, the data values were normalised to lie between 0 and 1 using Equation 8.6:

$$\chi' = \frac{\chi - \chi_{min}}{\chi_{max} - \chi_{min}} \tag{8.6}$$

Where:

χ = variable value

χ' = normalised variable value

χ_{min} = lowest variable value

χ_{max} = highest variable value

Normalisation was chosen, rather than the alternative of transformation to mean of 0 and unit variance, because the variables are not normally distributed, as demonstrated by a histogram of the values for molecular weight for the catalyst candidates. The histogram of a normally distributed variable would take a symmetrical, bell-shaped plot.

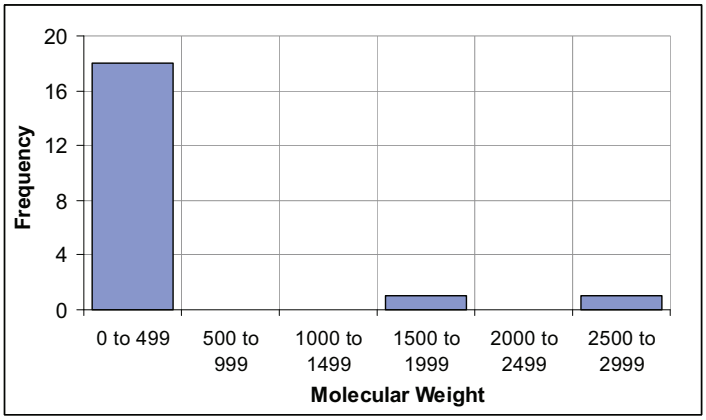

Chart 8.1: Histogram of Molecular Weight of the Catalyst Candidates

An illustrative PCA plot of the first 2 principal components, created using these normalised descriptor variables, shows that the heteropoly acids lie far from the other candidates, in the bottom left-hand corner of Figure 8.1. The confidence bounds illustrated on this figure are 95% and 99%.

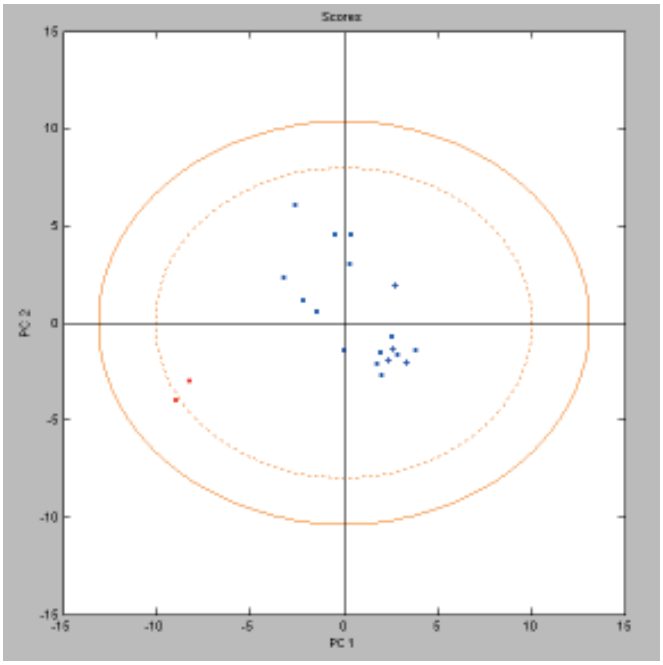

Figure 8.1: PCA Plot of the Twenty Screened Candidates

This indicates that, although normalisation has been applied to attempt to reduce the effects of distortion due to large-value variables, and all the candidates fall within the

outer confidence interval, the two high molecular weight heteropoly acids still appear different to the other candidates.

8.3.5 Randomisation

To check the validity of a fitted PLS model, three further PLS models were generated for each case using the same procedure, but with the outputs for each candidate shuffled randomly, and the average percentage variance explained then calculated. Models built on this basis, with randomised outputs, should give a low percentage of variance explained in comparison to the 'real' model. If this is not the case then this is a strong indication that the model is poor (Rothenberg, 2008b).

In this work, the final data sets are quite small, particularly for the reactive distillation studies, and in cases focussed on subsets of catalyst types. The analysis is still performed, however the results of the randomisation tests are taken into consideration and the outcomes of the models indicated to be poor are treated as indicators only.

8.3.6 Rank Correlation Matrix

The rank correlation matrix is a visual tool, available in the Matlab Pre-Screen Toolbox, which can be used to identify duplicate variables for removal from a data set. Two variables with a correlation of '1' may not have exactly the same definition, but for the data set in question it is not useful to include both. Figure 8.2 shows a rank correlation matrix, generated using the Pre-Screen toolbox, for the half life and the 38 catalyst descriptor variables remaining after removal of duplicates.

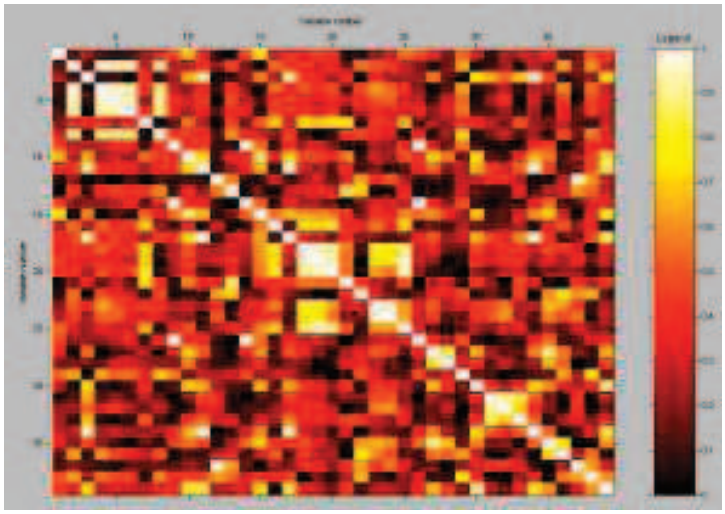

Figure 8.2: Rank Correlation Matrix

The areas of light colours in the figure indicate that many of the variables are strongly correlated. This screening technique was applied for every data set prior to the application of multivariate statistical tools.

8.4 ChemSpeed Half Life vs. Properties

8.4.1 All 20 Candidates screened in the ChemSpeed

The aim of performing this analysis is to explore any relationships between the catalyst properties and the numerical output from the experimental catalyst screening in the ChemSpeed machine. The full sequence of steps is shown only for this first case, for other cases the full details can be found in Appendix R. A summary of this single-output model is as follows:

- Catalyst candidates: all 20
- Inputs (X-block): 38 catalyst descriptors (PubChem & derived)
- Output (Y-block): half life

Cross validation indicates an optimum number of latent variables to be four, as shown by Figure 8.3.

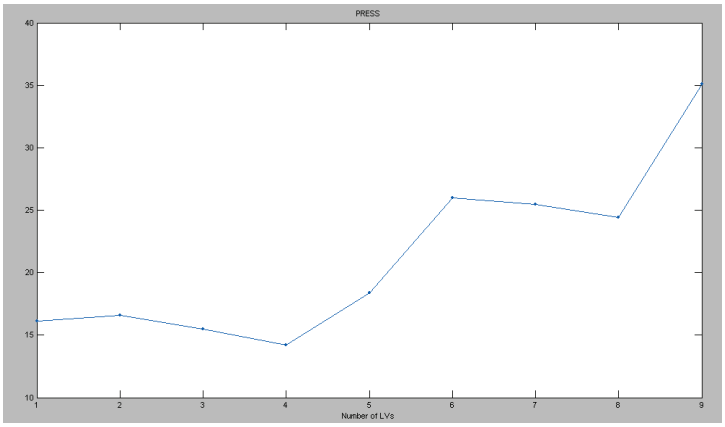

Figure 8.3: Cross Validation Plot for PLS Model of Screening Results

Looking at the proportions of the variances explained by four latent variables in Table 8.1, it can be confirmed that four latent variables covers a large proportion of the variance in the outputs, and the benefit gained in going over four would be very small. Comparing the cumulative explained variance (in Table 8.1) with the average given by 3 runs based randomised outputs and the same number of latent variables (Table 8.2)

reveals that the PLS model built on the real data set explains 30.2% more of the variance in the half life (88.0% compared to 57.8%).

Latent Variable	% Cumulative Variance in Descriptors	% Cumulative Variance in Output
1	28.4	61.8
2	46.9	78.4
3	61.9	83.3
4	**71.5**	**88.0**
5	79.8	92.5
6	86.6	94.6

Table 8.1: Cumulative Explained Outputs for PLS Model of Screening Results

Randomised Run	% Cumulative Variance in Descriptors	% Cumulative Variance in Output
1	68.7	63.3
2	64.9	53.3
3	74.6	56.7
Average	**69.4**	**57.8**

Table 8.2: Explained Outputs for Three PLS Models of Randomised Screening Results

The substantial margin over the randomised models indicates that the PLS model has captured information that has enabled it to account for the variation in the half life. Looking at the regression coefficients and the weighting on the individual descriptors will give an indication of what is the important information that the model is using. Examining the regression coefficients for the PLS model built on the real data (illustrated in Chart 8.2) shows that the heaviest weighting is applied to the first two of the four latent variables, and LV1 has the strongest weighting.

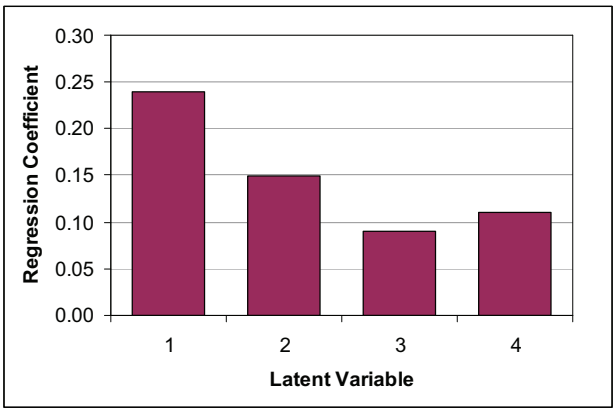

Chart 8.2: Regression Coefficients for PLS Model of Screening Results

Examination of Figure 8.4, which shows the input loadings for the first two latent variables, reveals the key molecular descriptors that the model is using to explain the variance between the half life values for the different candidates.

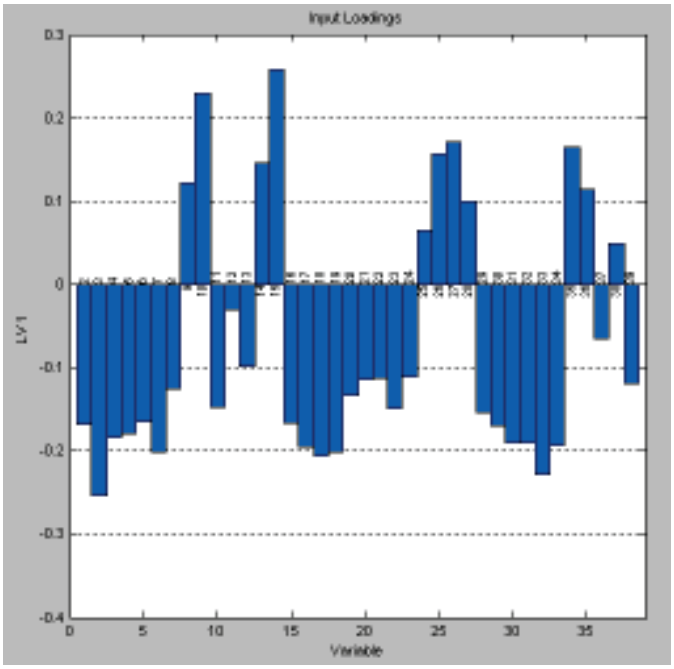

Figure 8.4: Input Loadings Plot of LV1 for PLS Model of Screening Results

The LV1 descriptors with the highest input loadings are listed in order of weighting are as follows:

- Acetate groups per Unit of MW (15)
- Number of H Bond Donors (3)
- Number of acetate groups (10)
- Complexity per H atom (33)

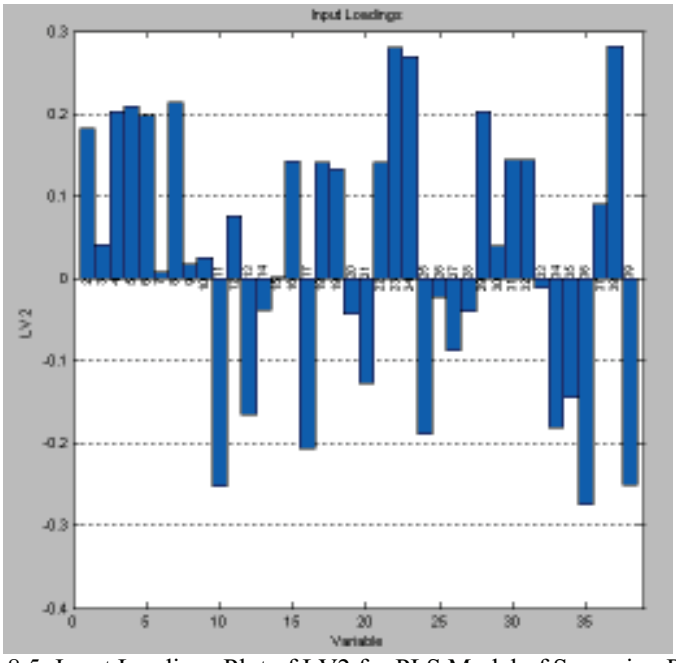

Figure 8.5: Input Loadings Plot of LV2 for PLS Model of Screening Results

LV2 descriptors with highest input loadings, greatest first:

- Metal Percent by Mass (38)
- H Bond Acceptors per heavy (Non-H) atom (23)
- Hydrogen Percent by Mass (38)
- Topological Polar Surface Area per heavy (Non-H) atom (24)
- H Bond Donors per Unit of MW (11)
- Phosphorus, Sulfur or Chlorine Percent by Mass (39)

The first latent variable looks for the presence and proportional composition of acetate groups, and for the presence of a H bond donor. The complexity of the catalyst in relation to the number of H atoms available is also considered. The second latent variable gives weight to variables describing the availability of H atoms, and also to size and composition.

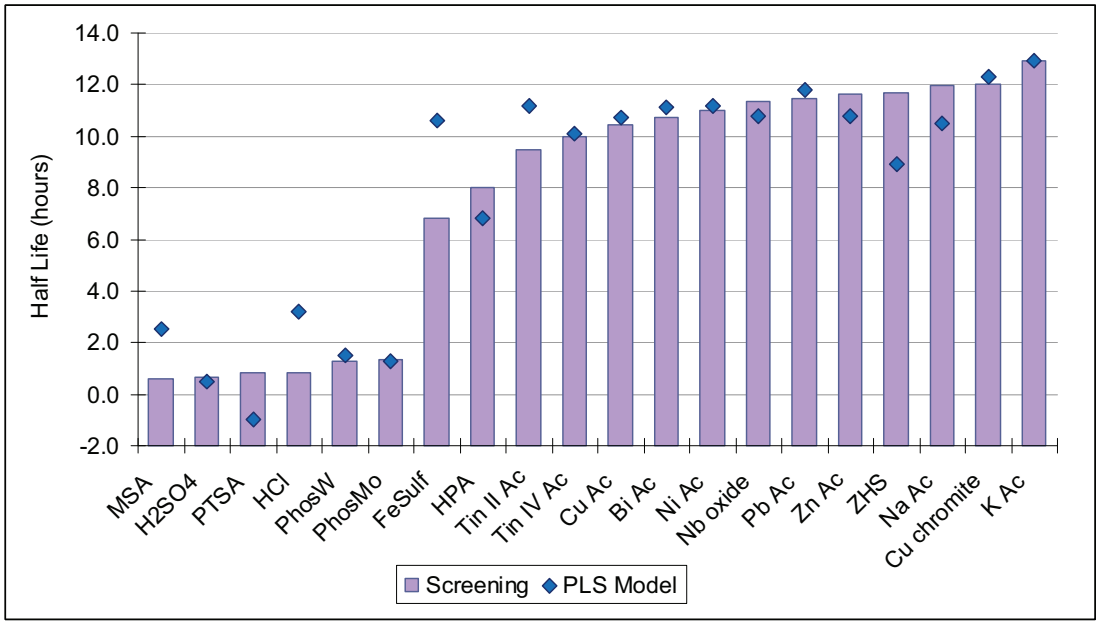

Chart 8.3: Plot of Predicted vs. Real Half Life from the Screening Results

Many of the half life values are predicted fairly well. Overall, nearly half (9 out of 20) are predicted to within +/- 5% of the experimental value. Six out of 9 of these more accurately predicted candidates are metal acetates; two thirds out of the metal acetates are predicted to within +/- 5% of the experimental value. Most of the strong acids, however, are poorly predicted, with only sulfuric acid predicted well. Sulfuric acid is one of the six catalyst candidates which the PLS model predicts within 0.25 hours of the actual half life value. It is interesting to note that both of the heteropoly acids are predicted well despite their large molecular weight and complicated composition

affecting their numerical molecular descriptors and causing them to appear anomalous in the data set.

8.4.2 Metal Acetates Only

To see if a better model could be obtained if only candidates from within one type or category were considered, analysis of the data for the nine metal acetates has been performed. The presence of fewer candidates leads to many variables becoming redundant, and there is a higher probability that the variables all take the same value for every sample. After processing with a rank correlation matrix, the data set contained seven catalyst descriptor variables.

- Catalyst candidates: 9
- Inputs (X-block): 7 catalyst descriptors
- Output (Y-block): half life

Model	Latent Variables	% Explained Variance in Output
PLS Model	4	67.4
Randomised Model	4	49.7

Table 8.3: PLS Model of Screening Results for Metal Acetates vs. Randomised Output Runs

Table 8.3 shows that the PLS model for this case (detailed in Appendix R Section 1) explains 67.4% of the cumulative variance in the outputs, 17.7% more than the models based on randomised outputs, which explains 49.7%. The explained variance is not as high as in the previous model where all the candidates were included (in the previous case the 'real' PLS model explained 30.2% more variance than the randomised model), indicating that this PLS model for the metal acetates alone less was sound.

The regression coefficients for this PLS model apply the heaviest weighting to LV3, and examination of the input loadings for LV3 reveals the key variables that the model uses to explain the variance between the half life values obtained with the different candidates. The variables with greatest input loadings are as follows, with the most significant listed first:

- Topological Polar Surface Area per H atom
- Number of water of hydration groups
- Complexity per H atom

The descriptors relating to the presence of acetate groups are now less important, as all of the candidates considered in this case are metal acetates. In attempting to distinguish between the metal acetates the model appears to be picking up on the size and complexity of the molecule, and the presence of water of hydration. The acetates of copper, lead, nickel, sodium and zinc were supplied as hydrates, and from Chart 8.4 it can be seen that they display a range of half life values, however the two most active catalysts in this category, the acetates of tin, were not hydrates.

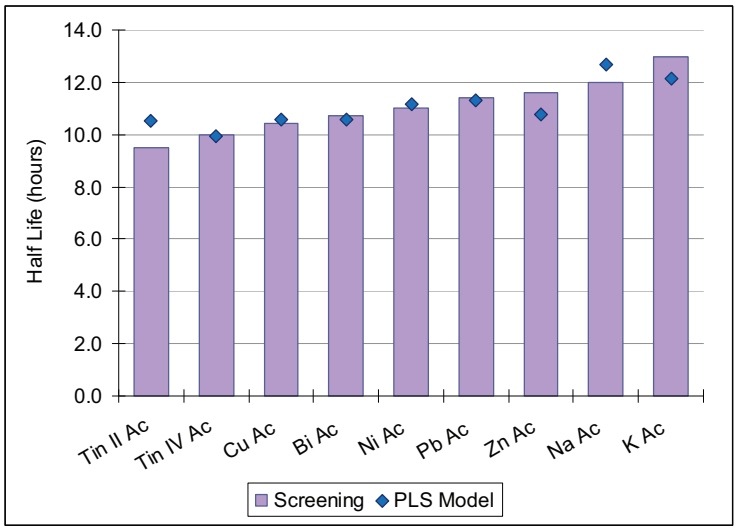

Chart 8.4: Plot of Predicted vs. Real Half Life for Metal Acetates

From studying the explained variances in Table 8.3, it is seen that this model based on only the nine metal acetates does not appear to offer an improvement over the previous model which included all 20 candidates. This time, 5 out of 9 half lives obtained with metal acetates are predicted to within +/- 5%, while the previous model was able to achieve this for 6 metal acetates.

8.5 Reactive Distillation Outputs

8.5.1 All 12 RD Candidates, All 9 Outputs from RD Experiments

There are many different outputs with which to measure the behaviour of the RD unit. Nine outputs have been identified and used as 'process quality' output variables for the following multi-output PLS analysis.

1 Distillate Water Yield (%)

2 End Pot Ester Yield (%)

3 Rate of Pot Temperature Increase at the 2hr 40min mark (°C/min)
4 Lowest Pot Temperature (°C)
5 Initial Rate of Pot Temperature Fall (°C/min)
6 Time to Lowest Pot Temperature (min)
7 Time Temperature at Top of Column Starts Rising (min)
8 Time for Top Temperature to Stabilise (min)
9 Pot Temperature at End 4hr40 (°C)

After processing with a Rank correlation matrix, the data set contained 37 input variables, including the half life values from the screening experiments, which have been included as an input. This will allow evaluation of the strength of the connection between the catalyst activity in the screening tests and the performance under reactive distillation conditions.

- Catalyst candidates: 12
- Inputs (X-block): 37 catalyst descriptors
- Output (Y-block): 9 outputs

Model	Latent Variables	% Explained Variance in Output
PLS Model	5	73.7
Randomised Model	5	58.3

Table 8.4: Comparison of PLS Model for All RD Outputs with Randomised Output Runs

Table 8.4 shows that the PLS model for this case (detailed in Appendix R.2) explains 73.7% of the cumulative variance in the outputs, while the average of three models based on randomised outputs explain 58.3%. The difference in the explained variance in the outputs between the 'real' PLS model and the average of those based on randomised data is only 15.4%, indicating that this model does not have strong prediction ability. In this PLS model, LV1 is the most heavily weighted, and the outputs with the greatest loadings for LV1 are:

- Lowest Pot Temperature
- Time Column Top Temperature Starts Rising
- Initial Rate of Pot Temperature Fall
- Time for Top Temperature to Stabilise

Out of these, only the last (Time for Top Temperature to Stabilise) is NOT strongly correlated to the half life from the ChemSpeed screening experiments (as seen in the simple correlations in Chapter 6), so the three most strongly 'explained' variables have a strong correlation to the half life and it is expected that this variable will appear in the LV1 input loadings, which is confirmed as the half life is one of four variables with a strong loading of around +/- 0.3:

- H bond donor per covalently-bonded unit
- Acetate groups per unit MW
- Number of acetate groups
- **Half Life**

The variables with strong loadings mostly describe the presence of and abundance of acetate groups, and the presence of H atoms and their availability, relative to the catalyst size. This model may be able to separate the catalyst candidates into groups of metal acetates and strong acids.

There are strong relationships between the half life from the ChemSpeed screening experiments and several of the reactive distillation outputs. A model has been created that is based only upon the RD outputs that are not correlated to the half life:

1 Distillate Water Yield (%)
2 End Pot Ester Yield (%)
3 Time to Lowest Pot Temp (min)
4 Time for Top Temp to Stabilise (min)
5 Pot Temp at End 4hr40 (°C)

Model	Latent Variables	% Explained Variance in Output
PLS Model	4	59.6
Randomised Model	4	50.6

Table 8.5: PLS Model of RD Outputs not correlated to Half Life vs. Randomised Output Runs

The PLS model for this case (detailed in Appendix R.3) explains 59.6% of the cumulative variance in the outputs, while the models based on randomised outputs explain 50.6%. The difference in the explained variance in the outputs between the 'real' PLS model and those based on randomised outputs is now only 9%, indicating

that this is a poor model, which has not found any underlying trends that can explain these outputs.

8.5.2 Individual RD Outputs

Rather than trying to explain of all the outputs with one model, which had limited success, PLS models were built for each output individually, in the same way as described previously. The results from these PLS models are summarised in Table 8.6, where it can be seen that only 4 of the models gave a margin of over 15% between the real and the randomised models. The models for ester yield and the time that the temperature at the top of the column stabilises explain less of the variance than the randomised models, so it is not possible to build useful models for these.

	% Explained Variance in Output		
Output	**PLS Model**	**Randomised PLS Model**	**Difference**
Distillate Water Yield	77.3	70.2	7.1
Ester Yield	63.7	65.7	-2.0
Pot T Inc Rate at 2h40m	95.7	77.9	17.8
Lowest Pot T	97.6	87.6	10.0
Time Top T Rise	96.9	71.3	25.6
Time Top T Stable	83.3	85.3	-2.0
Pot Temp End of Run	71.0	63.3	7.7
Time Lowest T	83.5	64.7	18.8
Time Initial T Fall	98.4	83.3	15.1

Table 8.6: Results of PLS Models built on Individual RD Outputs

Charts 8.5 to 8.8 give a visual indication of how well the PLS models fit the experimental data for those models which gave a margin of at least 15% over the model based on randomised outputs. The charts illustrate that where the comparison with the randomised outputs indicates that the model is strong, the outputs and the predictions are close.

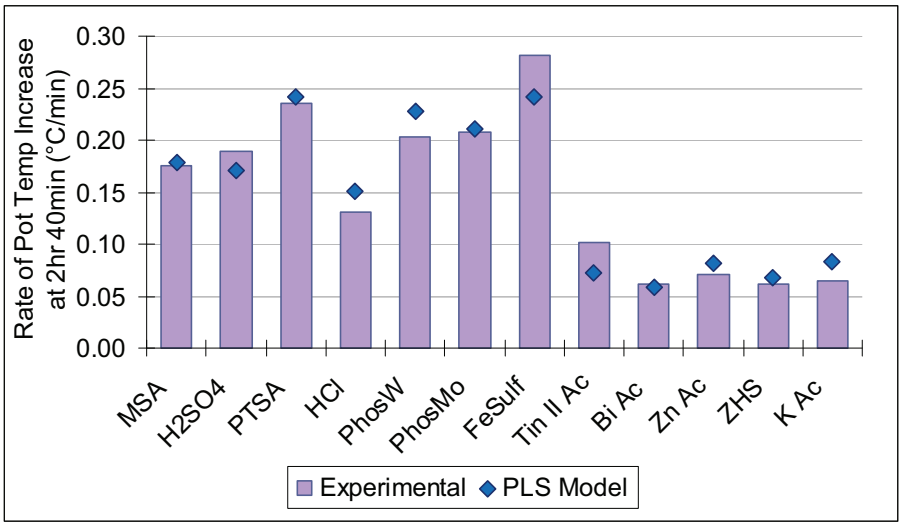

Chart 8.5: Experimental vs. Predicted Rate of Pot Temperature Increase at 2hr 40min

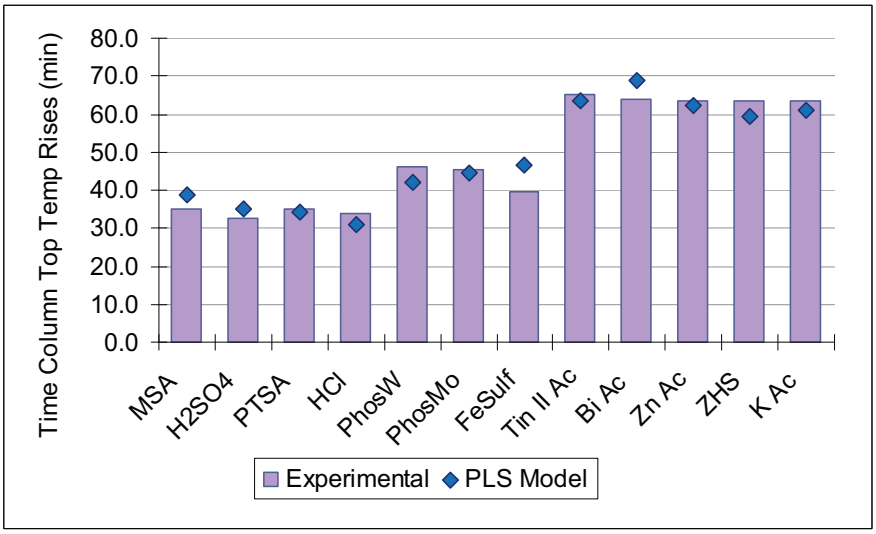

Chart 8.6: Experimental vs. Predicted Time Temperature at Top of Column Starts Rising

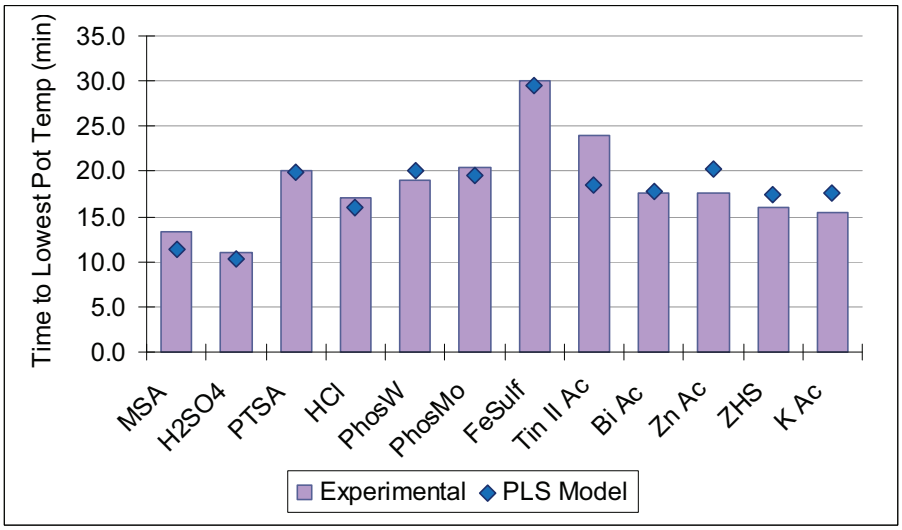

Chart 8.7: Experimental vs. Predicted Time to Lowest Pot Temperature

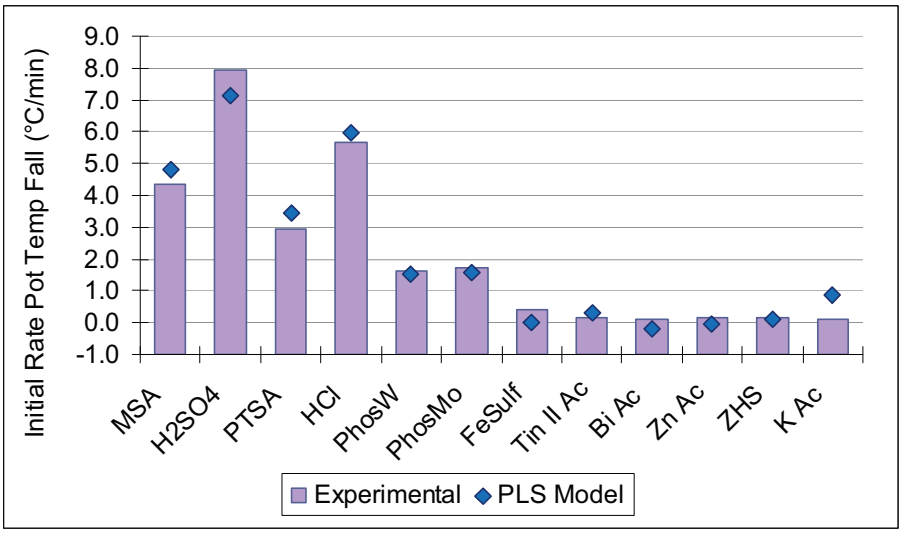

Chart 8.8: Experimental vs. Predicted Initial Rate of Pot Temperature Fall

The outputs of the reactive distillation experiments that are associated with a high margin between the randomised runs and the 'real' PLS model relating the molecular descriptors and the half life are observed to be all temperature readings. Three of these temperature outputs are concerned with the temperature of the reaction mixture in the pot, which is determined by the boiling point of the mixture, which in turn depends upon the composition in the pot. The connection between the reaction and separation occurring under the reactive distillation conditions has a great effect on the results.

8.6 Effect of Including FieldTemplater variables

It may be that considering descriptors of the molecular field surrounding a candidate catalyst molecule could yield more useful information than simply considering the molecular composition. Inclusion of structural details that are unhelpful or irrelevant may bring little benefit, while there may be features of the electronic fields around the 3D molecule which may play a key role in the behaviour of that molecule during important reaction steps. FieldTemplater software was developed by Cresset BioMolecular Discovery Limited, and generates a representation of the fields around a molecule, rather than focussing on the atomic composition (Vinter and Rose, 2007). Figure 8.6 shows the visual output of the software when four of the homogeneous acids (H_2SO_4, MSA, PTSA and Hypophosphorous acid) are overlaid, in which the similarity between the molecular structures can be seen.

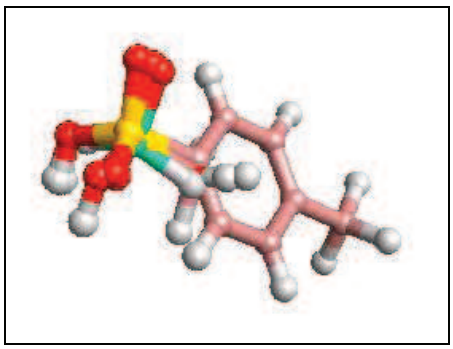

Figure 8.6: FieldTemplater Visual Output showing four Overlaid Homogeneous Acids

When the electronic fields are displayed on the image they are shown as spheres, the size of which is proportional to the field strength. The alignment of the positive (red) and negative (blue) fields around the overlaid homogeneous acid molecules is seen in Figure 8.7. The negative fields are seen to be bunched together on the top left hand side of the image, on the opposite side of the overlaid molecules to the positive fields.

Figure 8.7: FieldTemplater Visual Output for four Homogeneous Acids with Fields Applied

The molecular structures of the catalyst candidates were entered into the software as 'sdf' files, available from the PubChem on-line database. (The FieldTemplater software was unable to process five candidates: the two heteropoly acids, HCl, copper chromite and niobium oxide.) Three new descriptor variables were calculated for the candidate catalysts as FieldTemplater compared each to sulfuric acid: Shape Similarity, Field Similarity and Overall Similarity.

8.6.1 Effect on Prediction of Screening Half Life

The effect of including the FieldTemplater similarity scores on the prediction of the screening half life was investigated. After processing with a rank correlation matrix, the input data set contained 41 descriptor variables.

- Catalyst candidates: 15
- Inputs (X-block): 41 (38 PubChem descriptors, 3 FieldTemplater similarity scores)
- Output (Y-block): half life

Model	Latent Variables	% Explained Variance in Output
PLS Model	4	95.4
Randomised Model	4	60.6

Table 8.7: Screening PLS Model with FieldTemplater Similarity Scores vs. Randomised Runs

Table 8.7 shows that the PLS model for this case (detailed in Appendix R.4) explains 95.4% of the cumulative variance in the outputs, while the models based on randomised outputs explain 60.6%. The real PLS model explains much higher (34.8% more) variance than the result based on randomised outputs. Latent variable 1 is the most heavily weighted and examination of the input loadings for LV1 reveals the key variables that the model is using to explain the variance between the half life values obtained with the different catalyst candidates in the screening tests:

- H Bond donors per covalently-bonded unit
- H Bond acceptors per covalently-bonded unit
- H Bond donors per unit MW
- Metal percentage by mass

As seen previously, this set of latent variables should be able to distinguish well between strong acids (with H bond availability) and metal acetates (with metal atoms). The FieldTemplater similarity variables do not appear in the input loadings, and only appear as an input weight on LV4, the least strongly weighted latent variable. Inclusion of these variables does not appear to have had a significant effect on the resulting PLS model for the relationship between the catalyst properties and the half life. Compared to the previous model, this PLS model explains a slightly (approx 5%) higher proportion of the variance in the data and appears slightly stronger when the variances from models based on randomised data are compared. However, these differences are very small, and the 5 candidates removed included the most anomalous from the set: the heteropoly acids. Chart 8.9 shows a comparison of the experimental half life values and those predicted by the PLS model in this case.

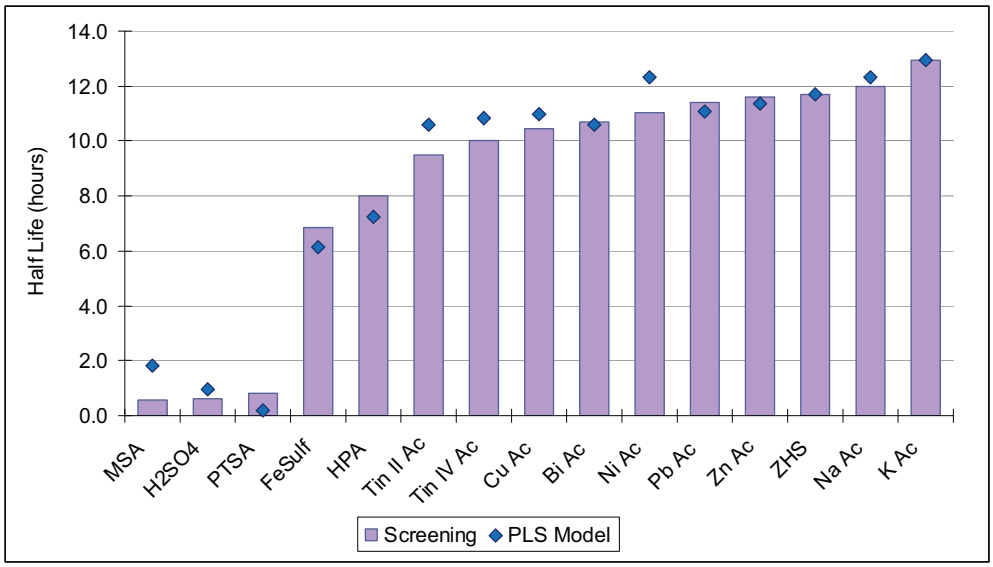

Chart 8.9: Experimental Half Live Values vs. Predicted Values using FieldTemplater Scores

The original model built on data for all 20 candidates was able to predict 9 of the half life values to within +/- 5%, including 6 out of 9 of the metal acetates. Now only 6 out of 15 predictions are this close. Even though all of the metal acetates were able to be run in FieldTemplater, only 5 out of 9 are within +/- 5%, compared to 6 in the original model.

A PLS model was also built using the same 15 candidates that could be run in FieldTemplater, but this time the similarity scores were not used as descriptor variables. This PLS model explains a high proportion of the output variance, (95.6%) while that for the randomised-outputs model is much lower (59.7%). Out of the 15 candidates, 6 are predicted to within 5% and only 2 are within 0.25 hours of the experimental half life value. This is almost the same as the model with the similarity scores included, confirming that in this case, the inclusion of the FieldTemplater information has not significantly changed the model. All 9 of the metal acetates were able to be processed by the FieldTemplater software, so a further PLS model was built to investigate whether or not the inclusion of the Cresset's FieldTemplater similarity scores improves the model including for metal acetates only.

Model	Latent Variables	% Explained Variance in Output
PLS Model	4	73.9
Randomised Model	4	61.6

Table 8.8: Screening Model for Metal Acetates & FieldTemplater Scores vs. Randomised Runs

Table 8.8 shows this PLS model (detailed in Appendix R.5) explains 73.9% of the cumulative variance in the outputs, while the models based on randomised outputs explain 61.6%, so the difference is now only 12.3%. This model is therefore weaker than those previously seen and there is also little improvement over previous model, without the FieldTemplater variables, which explained 67.4% of the variance in 4 latent variables. Out of 9 metal acetates in this model, the half lives of 6 cases are predicted to within +/-5% and only 4 are within 0.25hours.

Inclusion of the FieldTemplater variables does not seem to have improved the model in this case. With only 9 candidates included in this subset, it must be noted that there are too few samples to draw positive conclusions. The leverage due to each individual sample is very high and small changes, for example due to experimental error in the determination of half life could significantly change the outcomes.

8.6.2 Effect on Prediction of RD Outputs

To investigate whether including FieldTemplater variables in the data set could improve the prediction of the RD outputs, further models with and without these new descriptors were built. Three of the RD candidates could not be processed by FieldTemplater, so the data set is reduced from 12 to 9 candidates.

Model	Latent Variables	% Explained Variance in Output
PLS Model	3	67.0
Randomised Model	3	50.9

Table 8.9: PLS Model for RD Outputs on 9 candidates vs. Randomised Output Runs

The PLS model for this case (detailed in Appendix R.6) explains 67.0% of the cumulative variance in the outputs, while the models based on randomised outputs explain 50.9%, and the difference is 16.1%.

Model	Latent Variables	% Explained Variance in Output
PLS Model	3	68.4
Randomised Model	3	49.2

Table 8.10: PLS Model for RD Outputs & FieldTemplater Scores vs. Randomised Output Runs

The FieldTemplater similarity variables are then included, and Table 8.10 shows the PLS model for this case (detailed in Appendix R.7) explains 68.4% of the cumulative variance in the outputs, while the models based on randomised outputs explain 49.2% so the difference is 19.2%.

There is no sign of the FieldTemplater variables in the input loadings plots of the most important latent variables, and there is very little difference between the two models described by Tables 8.9 and 8.10, so there is no evidence of any benefit gained by including the FieldTemplater variables. The very small set of candidates that could be included in this assessment means that it is not possible to draw firm conclusions from these results.

8.7 Effect of Including RD Simulation Outputs in RD Output Predictions

Accurate dynamic reactive distillation simulations could potentially reduce the amount of experimental work that must be done to obtain a first indication of how well a candidate is likely to perform under reactive distillation conditions. The simulations described in Chapter 7 were not able to match the time-varying profiles of the experimental data from the reactive distillation runs, but the outputs from the simulations may still provide some information about the relative differences that could help explain the candidate behaviour.

8.7.1 BatchCAD Model Outputs Included

The first of these cases looks at how the PLS model describing the RD outputs changes if the BatchCAD simulation outputs are included as input variables.

- Catalyst candidates: 5
- Inputs (X-block): 44 including 7 simulation outputs, screening half life, and 36 catalyst descriptors
- Output (Y-block): 9 outputs

Model	Latent Variables	% Explained Variance in Output
PLS Model	3	88.9
Randomised Model	3	74.9

Table 8.11: PLS Model for RD Outputs & BatchCAD Outputs vs. Randomised Output Runs

Further details can be found in Appendix R.8.2. The difference between the 'real' PLS model and those based on randomised outputs is only 14.0%, which is small and indicates that this model has not found any underlying trends in the data.

8.7.2 Simplified Excel Model Outputs Included

Finally an assessment was made of how the PLS model describing the RD outputs changes if the simplified Excel model outputs are included as input variables.

- Catalyst candidates: 5
- Inputs (X-block): 43 including 6 simulation outputs, screening half life, and 36 catalyst descriptors
- Output (Y-block): 9 outputs

Model	Latent Variables	% Explained Variance in Output
PLS Model	3	87.8
Randomised Model	3	83.0

Table 8.12: PLS Model for RD Outputs & Excel Model Outputs vs. Randomised Output Runs

Further details can be found in Appendix R.8.3. The difference between the 'real' PLS model and the average of 3 based on randomised outputs is only 4.8%, which is very small, suggesting that this PLS model offers almost no improvement over one based on completely randomised outputs.

The inclusion of information from the BatchCAD simulations appears to give a slightly higher improvement over a randomised model compared to inclusion of the outputs from the simplified Excel model. However, there is almost no difference in the percentages of the variation explained by either of the PLS models which included the simulation outputs, and a run performed with the same five candidates and molecular descriptors only (no simulation information), which explained 87.1% (details in Appendix R.8.1). Therefore, the inclusion of the RD simulation data has not given any benefit in these cases.

8.8 Summary

8.8.1 ChemSpeed Half Life vs. Molecular Descriptors

The relationships between the half life values obtained with the candidate catalysts from the ChemSpeed screening experiments and the molecular descriptors have been studied using a series of single-output PLS correlations. The first PLS model included all 20 candidates, and it was found that 4 latent variables were able to explain 88.0% of the variance in the data. This was 30.2% more than the average of three models built on data sets with randomised outputs, indicating that this model has picked up on some useful underlying information. Overall, 9 out of 20 of the half life values were predicted to within +/-5%. These results are summarised in Table 8.10.

PLS Model	LVs	% Output Variance Explained		Predicted to Within +/- 5%	Predicted to Within 0.25hrs
		Actual Model	Average of Randomised		
All Catalysts (20)	4	88.0	57.8	Total: 9 /20 M Ac: 6 /9	Total: 6 /20 M Ac: 3 /9
Metal Acetates (9)	4	67.4	49.7	5 / 9	5 / 9

Table 8.13: Results from PLS Models for ChemSpeed Half Life

Variables found to be of importance from this model are: the number of acetate groups relative to the size of the catalyst, the number of H-bond donors, and the molecular complexity relative to the number of H atoms in the catalyst. The compositions of metal, H-bond acceptors (oxygen atoms) and hydrogen are also of some importance. The model could therefore be expected to distinguish well between strong acids (with good H atom availability) and metal acetates (with acetate groups and metal atoms).

A subdivision within the range of candidates was examined as a PLS model was built for only the 9 metal acetates. Narrowing the dataset down to metal acetates alone saw a drop in the proportion of variance explained to only 67.4%, and no improvement in the prediction of the half life values. This PLS model also only explained 17.7% more of the variance than the models based on randomised outputs, indicating that this is a poorer model. If a set of candidates to be investigated includes different sub-categories,

from this work it would be recommended that each sub category should be evenly represented in the overall data set, so a good number of each type of candidate should be included.

8.8.2 RD Outputs vs. Molecular Descriptors

The subsequent investigation of relationships between the reactive distillation results and the candidate molecular descriptors was less successful. An important factor in this is likely to be the small number of candidates for which full experimental results are available.

PLS Model	LVs	% Output Variance Explained		
		Actual Model	Average of Randomised	Difference
All RD Catalysts (12) All 9 Outputs	5	73.7	58.3	15.4
All RD Catalysts (12) 5 Outputs	4	59.6	50.6	9.0

Table 8.14: Results of PLS Models for all RD Outputs vs. those not Correlated with Half Life

The model produced using all of the reactive distillation outputs was fairly poor, with a difference in the explained variance in the outputs between the 'real' PLS model and the average of those based on randomised data of only 15.4%. The outputs that were most well predicted were generally strongly correlated to the screening half life. Focussing on the subset of those outputs that were not correlated with the screening half life values gave an even poorer model.

8.8.3 Individual RD Outputs

PLS models were built for each output individually, and it was shown that, where the comparison with the randomised outputs indicates that the model is strong, the outputs and the predictions are also close. All 4 of the reactive distillation outputs that can be explained relatively well by a PLS model built on the molecular descriptors and the half life are derived from temperature readings:

- Time Temperature at Top of Column Starts Rising

- Time to Lowest Pot Temperature
- Initial Rate of Pot Temperature Fall
- Rate of Pot Temperature Increase at 2hr 40min

The first three of these were shown in Chapter 6 to have a strong correlation with the half life seen in the screening experiments. The last three in the list come from the pot temperature profiles, underlining the importance of the pot temperature and the relationship between the boiling point of the reacting mixture and the behaviour under reactive distillation conditions.

8.8.4 Cresset FieldTemplater

The effect of including the FieldTemplater similarity scores on the prediction of the screening half life was investigated by building PLS models on the 15 catalysts that could be processed, both with and without these new variables included as descriptor variables. The sub-category of the metal acetates was also considered, as all of these were processed by the software. A summary of the results is shown in Table 8.15.

PLS Model	**LVs**	**% Output Variance Explained**		**Predicted to Within +/- 5%**	**Predicted to Within 0.25hrs**
		Actual Model	**Average of Randomised**		
15 Catalysts without scores	4	95.6	59.7	Total: 6 / 15 M Ac: 5 / 9	Total: 2 / 15 M Ac: 2 / 9
15 Catalysts with scores	4	95.4	60.6	Total: 6 / 15 M Ac: 5 / 9	Total: 3 / 15 M Ac: 2 / 9
Metal Acetates Only (9)	4	73.9	61.6	6 / 9	4 / 9

Table 8.15: Results from PLS Models for Screening Half Life & FieldTemplater Scores

For the cases with 15 candidates, the difference in the explained variance in the outputs between the 'real' PLS model and the average of those based on randomised data is high, however, the FieldTemplater similarity scores were found not to be weighted heavily by the model. Inclusion of the FieldTemplater similarity scores did not appear to have a strong influence on the model, and narrowing the dataset down to metal acetates alone saw a drop in the proportion of variance explained, with no improvement

in the prediction of the half life values. Comparisons were also made to determine whether including FieldTemplater variables in the data set could improve the prediction of the RD outputs. A summary of the results is shown in Table 8.16.

PLS Model	LVs	% Output Variance Explained		
		Actual Model	Average of Randomised	Difference
9 RD Catalysts All 9 Outputs Without Scores	3	67.0	50.9	16.1
9 RD Catalysts All 9 Outputs With Scores	3	68.4	49.2	19.2

Table 8.16: Results from PLS Models for RD Outputs & FieldTemplater Scores

There is almost no difference between the two cases shown in Table 8.16, confirming that there is no evidence of any benefit gained by including the FieldTemplater variables to these data sets. It is however noted that the number of samples in this subset of candidates which were tested in RD unit and able to be processed by FieldTemplater is small, and the results may be different if a larger data set is used.

8.8.5 Simulation Outputs

When PLS models were built including the outputs of the dynamic reactive distillation simulations, it was found that the models had poor prediction ability. Both cases offer almost no improvement over a model with randomised outputs.

PLS Model	LVs	% Output Variance Explained		
		Actual Model	Average of Randomised	Difference
Including BatchCAD Model Outputs	3	88.9	74.9	14.0
Including Excel Model Outputs	3	87.8	83.0	4.8

Table 8.17: Results from PLS Models for RD Outputs Including Simulation Results

This information indicates that inclusion of the outputs from the BatchCAD simulations is slightly preferable to inclusion of the outputs from the simplified Excel model, but the inclusion of the RD simulation data does not give any significant benefit in these cases.

8.8.6 General Comments

More reactive distillation data would improve the quality of the multivariate models, but studying a very large number of catalyst candidates would have been necessary in order to explore the full variable space, and there were limits on the resources and time available for this project. Around 60 catalyst candidates would be required in order to build a robust and reliable QSAR model (Leahy, 2007). When subsets of the catalyst candidates were considered, this quickly caused the number of examples available to become too small to draw real conclusions, and gave lower margins over randomised models. The uneven coverage of the variable space was due to the literature-driven choice of candidates for study, which led to small numbers of different types of candidates with completely different characteristics to be selected.

Figure 8.8 is a dendrogram, built using the cluster observation tool in Minitab. Using the matrix of descriptors for all 20 candidates, this visualisation tool arranges the candidates so that the most similar are close together.

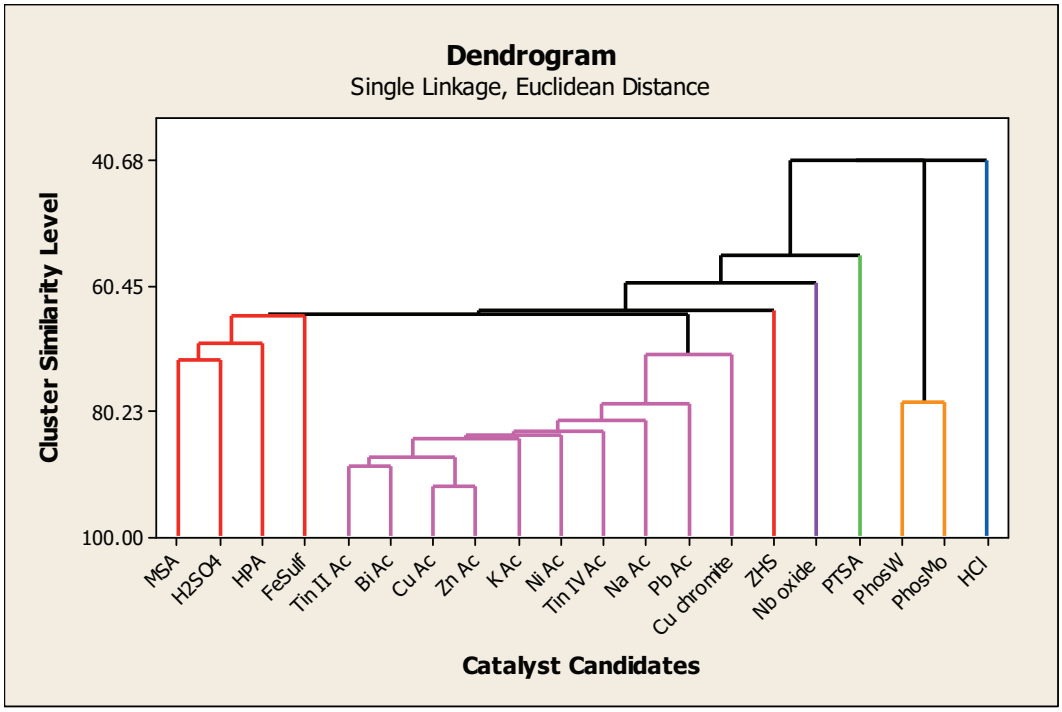

Figure 8.8: Illustration of the Uneven Cluster Sizes in the Catalyst Candidate Types

All of the candidates are linked, and the closer to the base line (x-axis) that the link between two candidates occurs, the more closely they are related. The tool keeps splitting the set into clusters until there are no dissimilar individuals left within an unsuitable cluster. Each 'fork' in the diagram represents the splitting of the set into clusters, and each of the clusters are shown with a different colour.

This image provides a visualisation of the degree of dissimilarity between the candidates and uneven coverage of the catalyst types, which are the underlying problems which come from the catalyst selection method. It was found that 7 clusters are required before all the metal acetates are grouped together in their own cluster (shown in pink). The five 'clusters' on the right of the figure contain only one or two entries, as the candidates within them are so different from the others that they are isolated. The heteropoly acids can be seen to have clustered together, and on the left hand side of the figure the homogeneous acids have clustered together.

There was some difficulty in obtaining full information for all of the candidates, and in some cases even supplier information was limited. In the future it is probable that the range of candidates included in literature sources, descriptor databases and computational tools will be extended. A large number of further descriptors could be available if more of the compounds were able to be processed by molecular modelling software such as E-Dragon, however, increasing the number of descriptors to several thousand would probably not improve the reliability of the present model. For catalytic studies it may be that a focus on the electronic fields, using an approach similar to that used by the FieldTemplater software, would be extremely useful. This is because the electrostatic fields surrounding the catalyst molecules are likely to play a highly significant role in the reaction mechanism between the polar molecules of carboxylic acid and alcohol.

Chapter 9: Concluding Comments and Recommendations for Future Work

9.1 Summary of the Work and Contributions

For the development of batch reactive distillation (RD) processes it would be highly desirable to establish an enhanced method for the early identification of candidates that are both highly active and suitable for use under reactive distillation conditions. Studies described in available literature include examples in which a number of catalyst candidates were assessed for activity in esterification through small-scale batch tests; however no studies were identified in which the wide range of the catalysts tested was then carried through to investigation of performance in reactive distillation. Studies involving catalyst testing under reactive distillation conditions generally involve only a small number of candidates (usually 1 or 2). In other studies many simulations have been performed, but these are usually restricted to continuous processes while descriptions of non continuous batch or semi-batch process simulations are more limited.

In this work, a novel approach has been taken to address this research challenge through the combination of a wide range of techniques. Small-scale batch pot tests have been performed to screen a number of candidates, and this has been followed up with: the testing of a selection of these candidates in novel batch reactive distillation experiments; the performance of dynamic simulations; and the application of multivariate analytical tools to investigate the behaviour of candidate catalysts in batch reactive distillation.

9.1.1 Catalyst Screening Experimental Work

The key experimental work began with screening of twenty catalyst candidates for activity with the nonanoic acid – n-butanol esterification system using the ChemSpeed SLT106 Synthesizer, a high throughput robotic platform. The results of these tests show that the strong homogeneous acids have good catalytic activity for the esterification, giving the shortest nonanoic acid half lives and the highest level of activity. The heteropoly acids also appear to have good performance, with quite short nonanoic acid half lives and consistently high activity. Ferric sulfate is an interesting case, giving a lower but apparently increasing activity during the reaction. The remaining candidates,

including the metal acetates, did not show a significant improvement over the case with no catalyst at this screening stage. Table 9.1 lists the six most effective catalysts, based on the corresponding half life values.

Catalyst	**BatchCAD Predicted Half Life**	
	min	**hour**
Methane sulfonic acid	34.6	0.58
Sulfuric acid	38.0	0.63
PTSA monohydrate	48.6	0.81
Hydrochloric acid	49.9	0.83
Phosphotungstic acid hydrate	78.1	1.30
Phosphomolybdic acid hydrate	81.5	1.36

Table 9.1: Summary of Half Life Values for the Most Active Screened Catalysts

9.1.2 Batch Reactive Distillation Experimental Work

Twelve of the twenty catalyst candidates were then tested with the same reaction system under batch reactive distillation conditions. Four groups of distinctive behaviour patterns are seen in the strong acids, the heteropoly acids, the metal acetates of tin, zinc and bismuth, and the ineffective candidates. It emerged that the strong homogeneous acids, which were the most active catalysts from the screening tests, were also initially the most active in the RD tests but this did not translate into high distillate yields. It was observed that some of the metal acetates were more active in the RD runs than would have been expected from the results of the ChemSpeed screening tests, and that this activity was most apparent towards the end of the runs when the reaction temperature was high. An order of catalytic activity of the metal acetates has been established for this reaction based on the final distillate collection from the batch RD runs, in which the metal acetates of tin, bismuth and zinc were the most active:

Tin (II) Acetate > Zinc Acetate > Bismuth (III) Acetate > Potassium acetate

The temperature profiles from the reactive distillation experiments give an illustration of the interaction between the reaction temperature and reaction rate in this batch RD system, and shed some light on the way the different catalysts affect the reactive process. The most active catalysts, the strong acids, cause a significant temperature decrease when they are added to the reaction mixture because they cause lots of water to be formed rapidly. However this drop then causes the reaction rate to fall, and it is

observed that the temperature does not recover for the remainder of the run, suppressing the rate of reaction and causing low distillate yields. These temperature patterns occur due to the novel way in which the reactions have been performed, with the catalyst added at a specific point when the reaction mixture had reached boiling point, so that the temperature and composition were comparable between runs. Heteropoly acids seem to offer a trade-off in this system as they give fairly high activity without incurring the large temperature drop. The higher, more consistent pot temperatures maintained the reaction rate during the run and enabled higher distillate water yields.

The screening tests were found to give useful early indications of the most active catalysts for RD, in that the catalysts that were found to be most active in screening were also initially the most active under reactive distillation conditions. However, the screening tests did not reveal that the metal acetates would also have some activity during the reactive distillation experiments, and would not have enabled prediction of the order of candidates that gave the highest distillate water yield. This provides a demonstration that pilot scale reactive distillation experiments are currently necessary as part of the development of these processes.

9.1.3 Dynamic Batch RD Simulations

The simulations performed using the tools available for this work were not able to give a good match in terms of the dynamic behaviour of the reactive distillation unit. BatchCAD was not able to simulate the column warm-up phase of the process accurately, as there is no facility in BatchCAD to represent the slow process of the heating of the cold, large surface area of the column walls and structured packing by the vapours rising from the reactor/reboiler pot.

However BatchCAD was able to accurately predict the reaction extent, the pot composition and temperatures in the early phase of the experimental RD runs (prior to boil-up and catalyst addition), while a simplified model was unable to do this. Through this the importance of the use of an established physical property calculation engine has been demonstrated for the simulation of reactive distillation processes. Study of the BatchCAD simulation outcomes has also provided valuable information about how changes in the composition of material in the column during the run are related to the

column temperatures, and this knowledge has contributed to the interpretation of the temperature profiles observed in the data from the experiments.

9.1.4 Application of Multivariate QSAR Analysis

The application of QSAR techniques began with exploration of relationships between the molecular descriptors and the half life values obtained with all 20 candidate catalysts from the ChemSpeed screening experiments. This model was able to explain a very high proportion (88%) of the variance in the data. Variables found to be of importance from this model are: the number of acetate groups relative to the size of the catalyst, the number of H-bond donors, and the molecular complexity relative to the number of H atoms in the catalyst. The compositions of metal, H-bond acceptors (oxygen atoms) and hydrogen are also of some importance. The model could therefore be expected to distinguish well between strong acids (with good H atom availability) and metal acetates (with acetate groups and metal atoms).

The investigation of relationships between the reactive distillation results and the candidate molecular descriptors was less successful. An important factor in this is likely to be the small number of candidates for which full experimental results are available. When PLS models were built for each output individually, 4 of the reactive distillation outputs could be explained relatively well by a PLS model built on the molecular descriptors and the half life, and all 4 of these are outputs derived from temperature readings. In this study, the application of QSAR did not enable the final distillate collection or ester yield to be modelled more accurately than by simple correlations. The results of the multivariate studies also did not indicate an improvement in the capability to predict the outcomes of the reactive distillation experiments when the simulation outputs were incorporated, or when descriptors of a new type, FieldTemplater similarity scores, were introduced.

Through the application of QSAR techniques, insight has been gained into the requirements and limitations of studies attempting to relate catalyst properties to the performance in reactive distillation. The number of candidates screened and then tested under reactive distillation conditions needs to be large, and any subtypes in the selected catalyst range rapidly increase the overall number of candidates required. Only when large enough numbers of catalysts are tested, will the results be representative and

applicable to others outside of the range initially studied when correlation studies are performed. The knowledge of the candidates used to build QSAR-type correlation studies needs to be detailed, as incomplete data matrices are of little use in developing statistical models. However it is very difficult to obtain the same level of detail for all, even through the use of descriptor generating software. These tools cannot currently process many of the types of molecules that are used as catalysts, although this has been an area of rapid recent development.

Based on the lessons learned from this work, a set of recommendations can be made for future work in this area.

9.2 Recommendations for Future Work

Many improvements over the study presented in this thesis could be made if sufficient time and resources were available. These can be classified as: improvements in scope of the study; evaluation of additional measures of catalyst performance; greater consideration of other factors such as physical effects; changes in the equipment; and potential for improved simulations.

9.2.1 Increase the Scope of the Study

Predictive multivariate models are usually built on a large 'training' data set of samples, and then the model is tested using a smaller 'validation' set. Ideally the training set should be based on a large set of similar molecules with only slight composition differences, and predictions would not be made on candidates which fall outside of the range used for training the model. These are known limitations to QSAR methodologies, and highlight the importance of a large dataset (Katritzky and Fara, 2005). The inclusion of a much larger number of catalyst candidates in the investigation, particularly in the reactive distillation experimental work, would greatly increase the possibility of gaining a better understanding of any relationships between the catalyst characteristics and their behaviour under reactive distillation conditions.

Further metal acetates, and additionally metal stearates, could be considered and compared as catalyst candidates. In the study described by Di Serio et al. (2005) the researchers synthesised 'in-house' a small range of metal stearate candidates which they tested for catalytic activity. However, only a very small range of metal stearates are

available commercially, and they have a relatively high cost per compound. Further study of metal sulfate hydrates was considered, but due to practical difficulties removing ferric sulfate from the equipment after the run, this range of potential candidates was not investigated further. Also, it has been noted that another of the heterogeneous candidates used in this study, sulfated zirconium hydroxide, has been withdrawn from the Sigma Aldrich product line.

There are some possible candidates for which it would be difficult to describe the composition and the character of active sites accurately. Mixtures such as Twitchell's reagent, which is 'a sulfonated mixture of oleic or other fatty acid and naphthalene' (Gervajio, 2005), would be difficult to characterise and there may be interactions between the components. The catalytic activity at the active sites on a solid surface depends on both the nature of the catalyst itself and also on the influence of the surrounding environment, to such an extent that Peters et al. (2006) found no clear relationship between the total number of available acid sites on the surface of their catalysts and the observed activity. A significant difficulty in a study of supported catalysts such as ion exchange resins would be that many are commercial products, making it difficult to obtain information about exact composition for a large number of candidates. Also, many require unique preparation and pre-treatment techniques in order to give optimum activity.

The catalysts have been used 'as supplied' rather than made and purified in-house, and have not been characterised in great detail (for example, mean particle size and surface area measurements have not been taken). A disadvantage of this approach is that it relies upon the supplier to provide reliable information about purity and composition, and some information which could be used as catalyst descriptors is omitted. Preparation of catalysts 'in house' would require significant time, facilities and expertise, but would provide more well-defined catalyst materials and more information that could be used for catalyst descriptors. This would also increase the number of possible variables that could be studied even further, due to complications of identifying the optimum preparation conditions.

Widening the range of reaction systems used in the investigation would involve repeating the investigation for different fatty acid-alcohol combinations. Taking this approach would allow a search for optimum combinations of reaction system and

catalyst. If future work is to be performed using the ChemSpeed machine (or similar automated equipment), the choice of carboxylic acids is restricted to those that are liquid over the whole range of temperatures the material may experience during the experimental procedure, including sample acquisition. Unsaturated fatty acids such as oleic acid have been preferred in studies described in literature as they generally have lower melting points than the corresponding saturated fatty acid, so they are less likely to freeze and handling and processing steps are more convenient.

9.2.2 Evaluation of Additional Catalyst Performance Measures

As briefly mentioned in Chapter 4, the half life (in this case the time taken for the concentration of nonanoic acid to fall to half its initial value) is a useful quantitative measure of the effectiveness of the candidate catalysts. This measure can be applied with the same units when any heterogeneous or homogeneous candidate has been tested, allowing the results to be ranked and compared (Rothenberg, 2008a). The half life observed for this esterification of nonanoic acid depends upon the initial concentration of the reactants (Atkins, 1988), so it was very important that the starting compositions of the mixtures were the same in all of the screening tests.

The use of half life as a catalyst performance measure has advantages, such as providing a quick measure of activity, but it also has limitations. The performance of the candidates is only studied at the start of the reaction, in a reactant-rich mixture which would not be present for the rest of the batch time. The half life at the start of the reaction is only a snapshot at one point in time and does not take into account that fact that the performance of the catalyst may change over the course of a whole batch run. Two other measures of catalyst efficiency are described by Rothenberg (2008a):

- Total turnover number: how much of a reactant can be converted to products by the catalyst over its active lifetime (moles of reactant per mole of active catalyst)
- Turnover frequency: the rate at which the catalyst can convert reactant into product (moles of reactant per moles of active catalyst per second).

Different meanings of these measures are used in different fields. For homogeneous catalysts, such as mineral acids, the amount of catalyst moles present in the reaction mixture is known from its concentration. However, when heterogeneous catalysts are used, the number and of active sites on the surface is much more difficult to determine,

and so the turnover number and frequency may be expressed per gram of catalyst (Rothenberg, 2008a).

Evaluation of additional measures that reflect the performance of the catalyst over time, such as the total turnover number, would give valuable extra information about the performance of the catalyst and may increase the industrial relevance of this type of study. However, the purpose of the use of half life in this work was merely to gain a quick indication of potential catalyst activity, while a decision about the choice of catalyst for an industrial process would not go ahead without significant tests of performance over longer timescales, and evaluation of catalyst selectivity and susceptibility to poisons.

9.2.3 Include More Study of Physical Factors

Study of the solubility of the catalyst candidates, which may change as the temperature and composition of the reaction mixture change, could be used as a 'pre-screening' stage to the investigation. This would help identify catalysts which may cause problems such as settling on surfaces in the reactor and would assist with interpretation of experimental observations. For less well known compounds, experiments may also be required to establish the VLE characteristics of the components and the reaction mixture, to give advance warning of any unexpected azeotropes or non-ideal behaviour that could occur. For example, not only does propionic acid form an azeotrope with water, but as a vapour it can also form dimers which could lead to non-ideal vapour phase behaviour (Banat et al., 2003).

The salt effect could also potentially be important in a batch reactive distillation unit when a catalyst is added to a boiling reaction mixture and the compound dissociates in the liquid. A small amount of a salt can have a strong effect, changing the boiling point of a mixture or even the relative volatilities of the components (Banat et al., 2003). The salt effect is a complex phenomenon which occurs due to interactions between the salt, solvent and any other components, and is not currently well understood.

The temperature profiles from the RD experiments for the cases with no catalyst and with potassium acetate and sulfated zirconium hydroxide are reported in Chapter 6. These cases reveal no clear evidence of the influence of the salt effect on these runs

because the results with and without catalyst material are so similar. This suggests that the salt effect does not have a strong impact on this system, and also highlights that it would be very difficult to isolate a salt effect for a compound which may also have a catalytic effect.

9.2.4 Improvements in Equipment used for Screening

The ChemSpeed Synthesizer used for the screening experiments in this work is a complex machine, and only a ChemSpeed technician is able to make hardware changes or repairs. There were some physical limitations due to the configuration of the ChemSpeed Synthesizer. A particular difficulty is that there is only one single robot arm for performing all the automated dosing and sampling tasks, and significant pauses are required in the protocol so that the needles can be rinsed between the sampling tasks. For example, running 8 reactors simultaneously rather than 4 was attempted but the screening tests themselves were relatively short (less than 1 hour), and the run in the first reactor dosed with butanol was over before the 8th and final reactor had been dosed.

Screening at a higher temperature may be necessary to pick up on candidates which are only active above 100°C, and more thorough testing of all the catalyst candidates over a wide range of temperatures would be needed to gain awareness of candidates whose activity varies significantly with temperature. Data collected over a suitable range of temperatures would also potentially be much more useful for building models to simulate reactive distillation performance. This time consuming process could be essential for simulations which must be valid over a range of temperatures.

The range of screening temperatures considered should cover the possible range of boiling points of the mixture, however the ChemSpeed reactor pots and their condensers do not provide a perfect seal, so a small amount of vapour may escape despite the presence of the condensers. The choice of temperature (100°C) used in the ChemSpeed screening experiments was based on practical limitations of the reaction system and aimed to avoid overloading the condensers and losing water-butanol vapours. Pressure reactors are available for the ChemSpeed which would be able to run at higher temperatures, however they are not as versatile and would not allow frequent sampling because they must remain sealed during the run. Further restrictions are introduced because the temperatures within the pots are not individually controlled, and ultimately

it may be that the ChemSpeed machine is not suitable for higher-temperature screening and alternative equipment would be required.

9.2.5 Improvements in Equipment used for Reactive Distillation

Better control of the reflux ratio on the reactive distillation column would require an improved reflux control system and a different design of collection system. For example, a reflux control system has recently been installed on reaction calorimeter apparatus in the School of Chemical Engineering and Advanced Materials. The controller completely closes off the flow to the collection system when total reflux is required, and is able to completely capture the flow when the mode is switched. If such a device could be supplied in a larger size for the reactive distillation unit this would be a great improvement upon the current configuration. The use of automatic rather than manual control of the temperature of the oil in the reactor jacket would also be a significant improvement.

The ability to measure the column liquid downflow returning back from the condenser as well as the distillate collection rate would enable determination of how well the unit was achieving the specified reflux ratio. For example, Steingeweg and Gmehling (2003) used a 'graduated device' installed inside the column itself to measure the column liquid load during experimental runs. When butanol is used for the esterification, an azeotrope with water is inevitable (Kiss et al. 2008b) but butanol loss could be avoided through use of a decanter to separate the phases of the distillate collected, or through use of an entrainer to enhance the separation between water and butanol.

More detailed information about changes that occur during the reactive distillation runs could be achieved through performing different types of analysis in addition to GC analysis for ester, as this could allow monitoring of the other reaction components. Taking samples along the length of the column could confirm the composition profile on the stages in the column, and an improved method of sampling from an intermediate depth in the reactor reboiler pot (rather than only at the very bottom) may retrieve more representative samples for analysis of ester yield. The benefit gained through greater sampling would have to be weighed against the disadvantage of the significant increase in the number of samples which must be processed and analysed, and a corresponding increase in the required sample processing time and use of analytical facilities.

The multipurpose reactive distillation unit used for the experiments reported in this thesis required a 40 minute reboiler heat-up phase (before catalyst addition) followed by a minimum of around 1 hour for the temperatures in the column to rise and begin to steady out. A smaller column, sized for the separation taking place and the expected distillate production, would warm up faster and reach equilibrium quicker. Two recent papers have included descriptions of the start-up phase of systems in which reaction and distillation have been combined and comparison of these demonstrates that the packed height of the distillation column can strongly affect the start up time of a unit.

De Lima Da Silva et al. (2010) describe experimental studies using a small, semi-continuous column with a height of only 43 cm, and an inner diameter of 4cm. This unit required a 20 minute column and reboiler warm up phase and 30 minutes under full reflux conditions to reach steady state operation, resulting in a very quick start-up time of less than 1 hour in total. Altman et al. (2010) describe a column with the same inner diameter (50mm) and reboiler capacity (2L) as the unit used in the work presented in this thesis, but with a much greater packed height of 5.5m (rather than 1m). The charts which report their 16 hour experimental runs display a very long start-up phase of over 4 hours before the temperatures reach a steady state. Although counter flow operation and the use of a 'natural circulation' reboiler rather than a stirred pot may also have contributed to the very slow initial warm-up, the much larger packed height of the distillation column has greatly increased the start-up time.

An important consideration for future studies using this kind of equipment configuration will therefore be the size of the column and the resulting warm-up/start-up time, which must be small compared to the entire run time in order not to have a strong effect on the results of the experiment. Higher columns with long start-up times are less suitable for batch processes with relatively short batch cycle times, so a smaller column with a shorter start-up time would be more suitable for this reaction system, as the amount of distillate produced is quite small. This could allow a smaller oil-pot temperature difference to be maintained, as less driving force for boil-up would be needed. The shorter warm-up time could also mean that any mismatch during the simulation of the start-up of the RD unit would have a less significant effect on the overall usefulness of the simulation predictions.

9.2.6 Simulations

Although there are examples of dynamic models in the literature, very few consider the start-up phase for a reactive distillation unit. Continuous columns with long experimental campaigns have been the focus of most reported simulation work, which did not require detailed consideration of start-up and shut down. The simulations performed using the facilities available for this work were not able to match the dynamic behaviour observed during the experiments, particularly during the column heat-up phase.

Use of a simulation package with more built in options for the description of the column thermal characteristics would allow more accurate models to be built, but unfortunately BatchCAD is not flexible enough to incorporate such developments. Pöpken et al. (2001) simulated the continuous reactive distillation process to produce methyl acetate using the Aspen Plus RadFrac tool, and found it was necessary to account for the heat loss from their mini plant column. The authors experimentally determined the heat loss from different sections of the unit and were able to include this information in their model using the options available in the software.

More flexible simulation tools in which code can be modified by the user according to the requirements of the particular application would enable simulation outputs that are more closely matched with the real case. The European INSERT research project developed correlations describing mass transfer coefficients, specific contact area, liquid hold-up and pressure drop for Sulzer Katapak packing, which were then used by researchers at Delft university to build a model of their column through incorporation of the correlations in Aspen Custom Modeller (Altman et al., 2010).

It should also be noted that much more research may have been performed by industrial researchers within private companies, who prefer not to publish commercially useful information, making it impossible to establish the state of the art of the application of reactive distillation in industry with certainty using only the material available in open literature (Harmsen, 2007).

9.3 Suggested Protocol for Catalyst Investigation for RD

A new protocol for the identification of catalysts for a reactive distillation process could include the following steps:

1. A catalyst candidate range is identified that includes a minimum of around 20 candidates, preferably many variations of a very similar structure.
2. Tests for solubility are conducted in solutions representing compositions possible during the reactive distillation experimental run. Those which are likely to cause severe fouling issues are rejected.
3. Screening tests are performed at more than one temperature: preferably the highest and lowest temperatures likely to occur in the process. Those which show no activity in any of these tests are unlikely to be suitable. The remaining candidates are then tested at a range of intermediate temperatures, in order to gain information about how the activity changes with temperature.
4. Batch reactive distillation tests are performed on these candidates, in a unit with the smallest suitable column so that a short warm up phase is encountered. Observations are made of any unexpected behaviour.

References

Aafaqi, R., A.R. Mohamed, and S. Bhatia, *Kinetics of esterification of palmitic acid with isopropanol using p-toluene sulfonic acid and zinc ethanoate supported over silica gel as catalysts.* J. Chem. Tech. Biotechnol. 2004. **79**(10): p. 1127-1134.

Agrafiotis, D.K., D. Bandyopadhyay, J.K. Wegner, and H. Van Vlijmen, *Recent advances in chemoinformatics.* J. Chem. Inf. Model., 2007. **47**(4): p. 1279-1293.

Agreda, V.H., L.R. Partin, and W.H. Heise, *High-purity methyl acetate via reactive distillation.* Chem. Eng. Progr., 1990. **86**(2): p. 40-46.

Albert, S.; Hiden, H.; Conlin, A.; Martin, E. B.; Montague, G. A.; Morris, A. J., *Inferential quality assessment in breakfast cereal production.* J. Food Eng., 2001. **50**(3): p. 157-166.

Altman, E., P. Kreis, T. van Gerven, G.D. Stefanidis, A. Stankiewicz, and A. Górak, *Pilot plant synthesis of n-propyl propionate via reactive distillation with decanter separator for reactant recovery. Experimental model validation & simulation studies.* Chem. Eng. Process. 2010. **49**(9): p.965-972.

Aspen Technology Inc., *BatchCAD Manual, Aspen BatchCAD Version Number: 2004.2*., 2005.

Atkins, P.W., *Physical Chemistry*. 3rd Edition 1988: Oxford University Press. ISBN: 0-19-855186-X

Backhaus, A.A., *Continuous Process for the Manufacture of Esters*, in *US Patent Number 1400849 Serial Number 248754*. 1921.

Bamford, C. H and Tipper, C. F. H. (eds.) *Comprehensive Chemical Kinetics Section 1: The Practice and Theory of Kinetics.* 1969, Amsterdam: Elsevier Publishing Company. SBN: 444-40673-5

Banat, F., S. Al-Asheh, and J. Simandl, *Vapor-liquid equilibria of propionic acid-water system in the presence of different types of inorganic salts: effect of temperature and salt concentration.* Chem. Eng. Process., 2003. **42**(11): p. 917-923.

Berman, S., A.A. Melnychuk, and D.F. Othmer, *Dibutyl Phthalate - Reaction Rate of Catalytic Esterification.* Ind. Eng. Chem., 1948. **40**(7): p. 1312-1319.

Bhatia, S., A.L. Ahmad, A.R. Mohamed, and S.Y. Chin, *Production of isopropyl palmitate in a catalytic distillation column: Experimental studies.* Chem. Eng. Sci., 2006. **61**(22): p. 7436-7447.

Bock, H., G. Wozny, and B. Gutsche, *Design and control of a reaction distillation column including the recovery system.* Chem. Eng. Process., 1997. **36**(2): p. 101-109.

Bollyn, M.P. and A.R. Wright, *Development of a process model for a batch reactive distillation -- A case study.* Comput. Chem. Eng. 1998. **22** ESCAPE-8(Supplement 1): p. S87-S94.

Borgdorf, R. and S. Warwel, *Substrate selectivity of various lipases in the esterification of cis- and trans-9-octadecenoic acid.* Appl. Microbiol. Biotechnol., 1999. **51**(4): p. 480-485.

Brown, N., B. McKay, and J. Gasteiger, *A novel workflow for the inverse QSPR problem using multiobjective optimization.* J. Comput. Aided Mol. Des., 2006. **20**(5): p. 333-341.

Buelna, G. and T.M. Nenoff, *A one-step catalytic separation process for the production of cumene.* Catal. Lett., 2005. **102**(3-4): p. 285-288.

Burello, E. and G. Rothenberg, *In silico design in homogeneous catalysis using descriptor modelling.* Int. J. Mol. Sci., 2006. **7**(9): p. 375-404.

Burello, E., P. Marion, J.-C. Galland, A. Chamard, and G. Rothenberg, *Ligand descriptor analysis in nickel-catalysed hydrocyanation: A combined experimental and theoretical study.* Adv. Synth. Catal., 2005. **347**(6): p. 803-810.

Chin, J., J.W. Lee, and J. Choe, *Feasible products in complex batch reactive distillation.* AlChE J., 2006. **52**(5): p. 1790-1805.

Chin, S.Y., A.L. Ahmad, A.R. Mohamed, and S. Bhatia, *Characterization and activity of zinc acetate complex supported over functionalized silica as a catalyst for the production of isopropyl palmitate*. Appl. Catal., A, 2006. **297**(1): p. 8-17.

Chiu, Chuang-Wei ; Dasari, Mohanprasad A. ; Suppes, Galen J. ; Sutterlin, Willam R, *Dehydration of glycerol to acetol via catalytic reactive distillation.* AIChE J., 2006. **52**(10): p. 3543-3548.

Cresset BioMolecular Discovery Ltd. (2009) *FieldTemplater Version 2.2.0 Manual*, Welwyn Garden City, UK

Cuille, P.E. and G.V. Reklaitis, *Dynamic simulation of multicomponent batch rectification with chemical reactions.* Comput. Chem. Eng. , 1986. **10**(4): p. 389-398.

Daniel, G. and M. Jobson, *Conceptual design of equilibrium reactor-reactive distillation flowsheets.* Industrial and Engineering Chemistry Research, 2007. **46**(2): p. 559-570.

De Lima Da Silva, N., C.M.G. Santander, C.B. Batistella, R.M. Filho, and M.R.W. Maclel, *Biodiesel production from integration between reaction and separation system: Reactive distillation process.* Applied Biochemistry and Biotechnology, 2010. **161**(1-8): p. 245-254.

Di Serio, M.; Apicella, B.; Grieco, G.; Iengo, P.; Fiocca, L.; Po, R.; Santacesaria, E., *Kinetic and catalytic aspects of dimethylterephtalate transesterification also through the use of model molecules.* J. Mol. Catal. A: Chem., 1998. **130**(3): p. 233-240.

Di Serio, M.; Tesser, R.; Dimiccoli,M.; Cammarota,F.; Nastasi,M.; Santacesaria,E., *Synthesis of biodiesel via homogeneous Lewis acid catalyst.* J. Mol. Catal. A: Chem, 2005. **239**(1-2): p.111-115.

Di Serio, M.; Tesser, R.; Trulli, F.; Santacesaria, E., *Kinetic and catalytic aspects in melt transesterification of dimethyl terephthalate with ethylene glycol in the presence of different catalytic systems.* J. Appl. Polym. Sci., 1996. **62**(2): p. 409-415.

Dimian, A.C. ; Bildea, C. S.; Omota, F.; Kiss, A. A., *Innovative process for fatty acid esters by dual reactive distillation.* Comput. Chem. Eng., 2009. **33**(3): p. 743-750.

Dimian, A.C., F. Omota, and A. Bliek, *Entrainer-enhanced reactive distillation.* Chem. Eng. Process., 2004. **43**(3): p. 411-420.

Doherty, M.F. and G. Buzad, *New tools for the design of kinetically controlled reactive distillation columns.* Comput. Chem. Eng. , 1994. **18**: p. S1-S13.

Doherty, M.F. and G. Buzad, *Reactive distillation by design.* Chem. Eng. Res. Des., 1992. **70**(A5): p. 448-458.

E-Dragon (2005) [Online] VCCLAB, Virtual Computational Chemistry Laboratory, Available at: http://www.vcclab.org, (Accessed: 13 May 2010)

Egly, H., V. Ruby, and B. Seid, *Optimum design and operation of batch rectification accompanied by chemical reaction.* Comput. Chem. Eng. , 1979. **3**(1-4): p. 169-174.

Fărcaşiu, D., A. Ghenciu, and J.Q. Li, *The Mechanism of Conversion of Saturated Hydrocarbons Catalyzed by Sulfated Metal Oxides: Reaction of Adamantane on Sulfated Zirconia.* J. Catal., 1996. **158**(1): p. 116-127.

Fernholz, G., Engell, S., Kreul, L.U., Górak, A., *Optimal operation of a semi-batch reactive distillation column.* Comput. Chem. Eng, 2000. **24**(2-7): p. 1569-1575.

Furuta, S., H. Matsuhashi, and K. Arata, *Catalytic action of sulfated tin oxide for etherification and esterification in comparison with sulfated zirconia.* Appl. Catal., A, 2004. **269**(1-2): p. 187-191.

Gadewar, S.B., M.F. Malone, and M.F. Doherty, *Selectivity targets for batch reactive distillation.* Ind. Eng. Chem. Res., 2000. **39**(6): p. 1565-1575.

Gang, L., L. Xinzong, and W. Eli, *Solvent-free esterification catalyzed by surfactant-combined catalysts at room temperature.* New Journal of Chemistry, 2007. **31**(3): p. 348-351.

Gervajio, G.C., *Fatty Acids and Derivatives from Coconut Oil*, in *Bailey's Industrial Oil and Fat Products*, F. Shahidi, Ed. 2005, John Wiley & Sons: Hoboken, N.J. ISBN: 978-0-471-38460-1

Ghamgui, H., M. Karra-Chaâbouni, and Y. Gargouri, *1-Butyl oleate synthesis by immobilized lipase from Rhizopus oryzae: A comparative study between n-hexane and solvent-free system.* Enzyme Microb. Technol., 2004. **35**(4): p. 355-363.

Górak, A., E. Kenig, and P. Moritz, *Intelligent Column Internals for Reactive Separations.* Chem. Eng. Process., 2005. **44**(6): p. 607-608.

Groemping, M., R.-M. Dragomir, and M. Jobson, *Conceptual design of reactive distillation columns using stage composition lines.* Chemical Engineering and Processing, 2004. **43**(3): p. 369-382.

Grosjean, C. (2008) *Personal Communication,* University of Newcastle upon Tyne

Grosser, J.H., M.F. Doherty, and M.F. Malone, *Modeling of Reactive Distillation Systems.* Ind. Eng. Chem. Res., 1987. **26**(5): p. 983-989.

Guha, R., M.T. Howard, G.R. Hutchison, P. Murray-Rust, H. Rzepa, C. Steinbeck, J. Wegner, and E.L. Willighagen, *The Blue Obelisk-Interoperability in Chemical Informatics.* J. Chem. Inf. Model., 2006. **46**(3): p. 991-998.

Guidoni, L., P. Maurer, S. Piana, and U. Rothlisberger, *Hybrid Car-Parrinello/Molecular Mechanics Modelling of Transition Metal Complexes: Structure, Dynamics and Reactivity.* Quantitative Structure-Activity Relationships, 2002. **21**(2): p. 119-127.

Guo, Z., M. Ghufran, and J.W. Lee, *Feasible Products in Batch Reactive Distillation.* AlChE J., 2003. **49**(12): p. 3161-3172.

Harmer, M.A., W.E. Farneth, and Q. Sun, *Towards the Sulfuric Acid of Solids.* Adv. Mater., 1998. **10**(15): p. 1255-1257.

Harmsen, G.J., *Reactive distillation: The front-runner of industrial process intensification: A full review of commercial applications, research, scale-up, design and operation.* Chem. Eng. Process., 2007. **46**(9): p. 774-780.

Hiwale, R. S., Bhate, N. V., Mahajan, Y. S., Mahajani, S. M., *Industrial Applications of Reactive Distillation: Recent Trends.* Int. J. Chem. Reactor Eng., 2004. **2**: R1.

Huss, R.S.; Chen, F.; Malone, M.F.; Doherty, M.F., *Computer-aided tools for the design of reactive distillation systems.* Comput. Chem. Eng. , 1999. **23** SUPPL: p. S955 - S962.

Jobson, M., *Dividing wall distillation comes of age.* Chemical Engineer, 2005(766): p. 30-31.

Jong-Wu, C. and C. Leo-Wang, *The glycolysis of poly(ethylene terephthalate).* J. Appl. Polym. Sci., 1999. **73**(1): p. 35-40.

Juan, J.C., J. Zhang, and M.A. Yarmo, *12-Tungstophosphoric acid supported on MCM-41 for esterification of fatty acid under solvent-free condition.* J. Mol. Catal. A: Chem., 2007. **267**(1-2): p. 265-271.

Katritzky, A.R. and D.G. Fara, *How chemical structure determines physical, chemical, and technological properties: An overview illustrating the potential of quantitative structure-property relationships for fuels science.* Energy & Fuels, 2005. **19**(3): p. 922-935.

Kaymak, D.B. and W.L. Luyben, *Optimum design of a column/side reactor process.* Ind. Eng. Chem. Res., 2007. **46**(15): p. 5175-5185.

Kenig, E.; Górak, A.; Pyhälahti, A.; Jakobsson, K.; Aittamaa, J.; Sundmacher, K., *Advanced Rate-Based Simulation Tool for Reactive Distillation.* AlChE J., 2004. **50**(2): p. 322-342.

Kenig, E.; Jakobsson, K.; Banik, P.; Aittamaa, J.; Górak, A.; Koskinen, M.; Wettmann, P.; *An integrated tool for synthesis and design of reactive distillation.* Chem. Eng. Sci. 1999. **54**(10): p.1347-1352.

Ketchen, E. E. and W. E. Wallace, *Thermal Properties of the Alkali Metals. I. The Heats of Reaction of Sodium and Potassium with Water at 25°.* J. Am. Chem. Soc., 1951. **73**(12): p. 5810-5812.

Kiss, A.A., *Separative reactors for integrated production of bioethanol and biodiesel.* Computers & Chemical Engineering, 2010. **34**(5): p. 812-820.

Kiss, A. A.; Dimian, A. C.; Rothenberg, G.; Marquardt, W.; Pantelides, C., et al., *Linking experiments to modeling in biodiesel production.* Computer Aided Chemical Engineering, 2006a. Volume **21,** Part 1: p. 731-736.

Kiss, A.A.; Omota, F.; Dimian, A.C.; Rothenberg, G., *The heterogeneous advantage: Biodiesel by catalytic reactive distillation.* Top. Catal., 2006b. **40**(1-4): p. 141-150.

Kiss, A A.; Dimian, A. C.; Rothenberg, G, *Solid Acid Catalysts for Biodiesel Production -Towards Sustainable Energy.* Adv. Synth. Catal., 2006c. **348**(1-2): p. 75-81.

Kiss, A A.; Dimian, A. C.; Rothenberg, G, *Biodiesel production by heat-integrated reactive distillation.* Computer Aided Chemical Engineering, 2008a. **25**: p. 775-780.

Kiss, A A.; Dimian, A. C.; Rothenberg, G, *Biodiesel by Catalytic Reactive Distillation Powered by Metal Oxides.* Energy Fuels, 2008b. **22**(1): p. 598-604.

Knovel (2003) *Knovel Critical Tables (2nd Edition)* [Online] Available at: www.knovel.com (Accessed: 30 July 2010)

Kolah, A. K.; Asthana, N. S.; Vu, D. T.; Lira, C. T.; Miller, D. J., *Reaction kinetics for the heterogeneously catalyzed esterification of succinic acid with ethanol.* Ind. Eng. Chem. Res., 2008. **47**(15): p. 5313-5317.

Kreul, L. U.; Górak, A.; Dittrich, C.; Barton, P. I., *Dynamic catalytic distillation: Advanced simulation and experimental validation.* Comput. Chem. Eng., 1998. **22** ESCAPE-8 (Supp.1): p.S371-S378.

Kumar, R. and S.M. Mahajani, *Esterification of lactic acid with n-butanol by reactive distillation.* Ind. Eng. Chem. Res., 2007. **46**(21): p. 6873-6882.

Kunz, U. and U. Hoffmann, *Development of Unstructured Catalytic Packing for Reactive Distillation Processes*, in *Reactive Distillation: Status and Future Directions*, K. Sundmacher and A. Kienle, Editors. 2003, Wiley-VCH: Weinheim.

Lam, M.K., K.T. Lee, and A.R. Mohamed, *Homogeneous, heterogeneous and enzymatic catalysis for transesterification of high free fatty acid oil (waste cooking oil) to biodiesel: A review.* Biotechnol. Adv., 2010. **28**(4): p. 500-518.

Leahy, D. (2007). *Personal Communication,* University of Newcastle upon Tyne

Lee, L.-s. and R.-g. Lin, *Reaction and phase equilibria of esterification of isoamyl alcohol and acetic acid at 760 mm Hg.* Fluid Phase Equil., 1999. **165**(2): p. 261-278.

Lee, M.-J., L.-H. Tsai, G.-B. Hong, and H.-M. Lin, *Multiphase equilibria for binary and ternary mixtures containing propionic acid, n-butanol, butyl propionate, and water.* Fluid Phase Equil., 2004. **216**(2): p. 219-228.

Leyes, C.E. and D.F. Othmer, *Esterification of Butanol and Acetic Acid.* Ind. Eng. Chem., 1945a. **37**(10): p. 968-977.

Leyes, C.E. and D.F. Othmer, *Continuous esterification of butanol and acetic acid, kinetic and distillation considerations.* Trans. Am. Inst. Chem. Eng., 1945b. **41**: p. 157–196.

Li, P.; Garcia, H.A.; Wozny, G.; Reuter, E., *Optimization of a Semibatch Distillation Process with Model Validation on the Industrial Site.* Ind. Eng. Chem. Res., 1998. **37**(4): p. 1341-1350.

Lide, D. R. (Ed.), *CRC Handbook of Chemistry and Physics*. 77th ed. 1996, Boca Raton: CRC Press. ISBN: 0-8493-0477-6

Lide, D. R. (Ed.), *CRC Handbook of Chemistry and Physics*. 90th ed. 2009, Boca Raton: CRC Press, Taylor & Francis Ltd. ISBN: 978-1420090840

Ling, W. and C. Geankoplis, *Liquid-Phase Esterification of Oleic Acid and Isobutyl Alcohol.* Ind. Eng. Chem., 1958. **50**(6): p. 939-942.

Linko, Y.-Y.; Lamsa, M.; Wu, X.; Uosukainen, E.; Seppala, J.; Linko, P., et al., *Biodegradable products by lipase biocatalysis.* J. Biotechnol., 1998. **66**(1): p. 41-50.

Liu, Y., E. Lotero, and J.G. Goodwin Jr, *Effect of water on sulfuric acid catalyzed esterification.* J. Mol. Catal. A: Chem., 2006. **245**(1-2): p. 132-140.

Lotero, E.; Liu, Y.; Lopez, D. E.; Suwannakarn, K.; Bruce, D. A.; Goodwin Jr, J. G., *Synthesis of biodiesel via acid catalysis.* Ind. Eng. Chem. Res., 2005. **44**(14): p. 5353-5363.

Luyben, M. *Process Modeling, Simulation and Control for Chemical Engineers*. 2nd ed, 1990, McGraw-Hill. ISBN: 978-0070391598

Luyben, W.L., *Control of the Heterogeneous Azeotropic n-Butanol/Water Distillation System.* Energy & Fuels, 2008. **22**(6): p. 4249-4258.

Maldonado, A.G. and G. Rothenberg, *Predictive Modeling in Catalysis - From Dream to Reality.* Chem. Eng. Progr., 2009. **105**(6): p. 26-32.

Malone, M.F. and M.F. Doherty, *Reactive Distillation.* Ind. Eng. Chem. Res., 2000. **39**(11): p.3953-3957.

Marchetti, J.M., V.U. Miguel, and A.F. Errazu, *Heterogeneous esterification of oil with high amount of free fatty acids.* Fuel, 2007. **86**(5-6): p. 906-910.

Markley, K.S., *Fatty Acids: Their Chemistry, Properties, Production, and Uses*. 2nd ed. Fats and Oils, ed. H.A. Boekenoogen, et al. 1961, New York: Interscience Publishers, Inc. ISBN 0-470-57024-5

Martin, T.M., P. Harten, R. Venkatapathy, S. Das, and D.M. Young, *A hierarchical clustering methodology for the estimation of toxicity.* Toxicol. Mech. Method., 2008. **18**(2-3): p. 251-266.

Maxwell, I.E., P. van den Brink, R.S. Downing, A.H. Sijpkes, S. Gomez and Th. Maschmeyer, *High-throughput technologies to enhance innovation in catalysis.* Top. Catal., 2003. **24**(1): p.125-135.

McKinney, J.D., A. Richard, C. Waller, M.C. Newman, and F. Gerberick, *The practice of structure activity relationships (SAR) in toxicology.* Toxicol. Sci., 2000. **56**(1): p. 8-17.

Melero, J.A., J. Iglesias, and G. Morales, *Heterogeneous acid catalysts for biodiesel production: current status and future challenges.* Green Chem., 2009. **11**(9): p. 1285-1308.

Mujtaba, I.M. and S. Macchietto, *Efficient optimization of batch distillation with chemical reaction using polynomial curve fitting techniques.* Ind. Eng. Chem. Res., 1997. **36**(6): p. 2287-2295.

Novakovic, K. (2007) *Personal Communication,* University of Newcastle upon Tyne

Occhipinti, G., H.R. Bjorsvik, and V.R. Jensen, *Quantitative Structure-Activity Relationships of Ruthenium Catalysts for Olefin Metathesis.* J. Am. Chem. Soc., 2006. **128**(21): p. 6952-6964.

Okuhara, T., *Water-tolerant solid acid catalysts.* Chem. Rev., 2002. **102**(10): p. 3641-3666.

Omota, F., A.C. Dimian, and A. Bliek, *Fatty acid esterification by reactive distillation. Part 1: equilibrium-based design.* Chem. Eng. Sci., 2003a. **58**(14): p. 3159-3174.

Omota, F., A.C. Dimian, and A. Bliek, *Fatty acid esterification by reactive distillation: Part 2--kinetics-based design for sulphated zirconia catalysts.* Chem. Eng. Sci., 2003b. **58**(14): p. 3175-3185.

O'Neil, M. J. (Ed.), *The Merck Index: an encyclopedia of chemicals, drugs, and biologicals*. 14th ed. 2006, Whitehouse Station, Merck & Co., Inc. ISBN: 978-0-91191000-1

Othmer, D.F. and S.A. Rao, *n-Butyl Oleate from n-Butyl Alcohol and Oleic Acid.* Ind. Eng. Chem., 1950. **42**(9): p. 1912-1919.

Parshall, G.W. and S.D. Ittel, *Homogeneous catalysis: the applications and chemistry of catalysis by soluble transition metal complexes* 2nd ed. 1992, New York: Wiley. ISBN:0-471-53829-9

Partington S. and Waldram S.P., *Runaway reaction during production of an azo dye intermediate.* Process Saf. Environ. Prot.: Trans IChemE, Part B, 2002. **80** (1), pp. 33-39

Pasias, S.; Barakos, N.; Alexopoulos, C.; Papayannakos, N., *Heterogeneously Catalyzed Esterification of FFAs in Vegetable Oils.* Chem. Eng. Technol., 2006. **29**(11): p. 1365-1371.

Perry, R.H. and D.W. Green, eds. *Perry's Chemical Engineers' Handbook* 7th ed. 1997, McGraw-Hill. ISBN: 0-07-049841-5

Peters, T. A.; Benes, N. E.; Holmen, A.; Keurentjes, J. T.F., *Comparison of commercial solid acid catalysts for the esterification of acetic acid with butanol.* Appl. Catal., A, 2006. **297**(2): p.182-188.

Pöpken, T., S. Steinigeweg, and J. Gmehling, *Synthesis and hydrolysis of methyl acetate by reactive distillation using structured catalytic packings: Experiments and simulation.* Industrial and Engineering Chemistry Research, 2001. **40**(6): p. 1566-1574.

Potyrailo, R.A. and V.M. Mirsky, *Combinatorial and high-throughput development of sensing materials: The first 10 years.* Chem. Rev., 2008. **108**(2): p. 770-813.

PubChem (2010) [Online] Available at: http://pubchem.ncbi.nlm.nih.gov (Accessed: 13 May 2010)

Qi, Z. and R. Zhang, *Alkylation of benzene with ethylene in a packed reactive distillation column.* Ind. Eng. Chem. Res., 2004. **43**(15): p. 4105-4111.

Reuter, E., G. Wozny, and L. Jeromin, *Modeling of multicomponent batch distillation processes with chemical reaction and their control systems.* Comput. Chem. Eng. , 1989. **13**(4-5): p. 499-510.

Richardson, J.F.; Harker, J.H.; Backhurst, J.R. (2002) *Coulson and Richardson's Chemical Engineering - Particle Technology and Separation Processes*, Vol 2, 5th Ed., Elsevier. ISBN: 978-0750644457

Rose, S. and A. Vinter, *Molecular Field Technology and its Applications in Drug Discovery.* Innovat. Pharmaceut. Tech., 2007. **23**: p. 14-18.

Rothenberg, G., *Catalysis: concepts and Green Applications*. 2008a, Weinheim: Wiley VCH. ISBN: 978-3-527-31824-7

Rothenberg, G., *Data mining in catalysis: Separating knowledge from garbage.* Catal. Today, 2008b. **137**(1): p. 2-10.

Rothenberg, G., *Catalysis: The best of both worlds.* Nat. Chem., 2010. **2**(1): p. 9-10.

Ruiz, C.A., M.S. Basualdo, and N.J. Scenna, *Reactive distillation dynamic simulation.* Chem. Eng. Res. Des., 1995. **73**(A4): p. 363-378.

S.R.L. Resindon. *Relite Ion Exchange and Adsorbent Resins*. [Website] 2006 [cited 21/05/07]; Available from: http://www.resindion.com/relite/relite.html. Accessed 16/10/10

Salis, A.; Pinna, M.; Monduzzi, M.; Solinas, V., *Biodiesel production from triolein and short chain alcohols through biocatalysis.* J. Biotechnol., 2005. **119**(3): p. 291-299.

Scenna, N.J., C.A. Ruiz, and S.J. Benz, *Dynamic simulation of start-up procedures of reactive distillation columns.* Comput. Chem. Eng. , 1998. **22** ESCAPE-8 (Supplement 1): p. S719-S722.

Schmitt, M., S. Blagov, and H. Hasse, *Mastering the Reaction Is the Key to Successful Design of Heterogeneously Catalyzed Reactive Distillation: A Comprehensive Case Study of Hexyl Acetate Synthesis.* Ind. Eng. Chem. Res., 2008. **47**(16): p. 6014-6024.

Schoenmakers, H.G. and B. Bessling, *Reactive Distilllation Process Development in the Chemical Process Industries*, in *Reactive Distillation: Status and Future Directions*, Eds. K. Sundmacher and A. Kienle. 2003, Wiley VCH: Weinheim. ISBN: 3-527-30579-3

Sendzikiene, E., V. Makareviciene, P. Janulis, and S. Kitrys, *Kinetics of free fatty acids esterification with methanol in the production of biodiesel fuel.* Eur. J. Lipid Sci. Technol., 2004. **106**(12): p. 831-836.

Sharma, M.M. and S.M. Mahajani, *Industrial Applications of Reactive Distillation*, in *Reactive Distillation: Status and Future Directions*, Eds. K. Sundmacher and A. Kienle, 2003, Wiley-VCH: Weinheim. p. 1-29. ISBN: 3-527-30579-3

Sigma Aldrich (2010) *MSDS Database* [Online] Available at: http://www.sigmaaldrich.com/safety-center.html (Accessed: 14 October 2010)

Smith, H.A. and C.H. Reichardt, *The acid catalyzed esterification of normal fatty acids.* J. Am. Chem. Soc., 1941. **63**(2): p. 605-608.

Sørensen, E. and S. Skogestad, *Control strategies for reactive batch distillation.* J. Process Control, 1994. **4**(4): p. 205-217.

Spatschek, R., *Investigations into Reactive Distillation Systems*, in *Department of Chemical and Process Engineering*. 1995, University of Newcastle upon Tyne: Newcastle upon Tyne.

Steinbeck, C., Y. Han, S. Kuhn, O. Horlacher, E. Luttmann, and E. Willighagen, *The Chemistry Development Kit (CDK): An open-source Java library for chemo- and bioinformatics.* J. Chem. Inf. Comput. Sci., 2003. **43**(2): p. 493-500.

Steinigeweg, S. and J. Gmehling, *n-Butyl Acetate Synthesis via Reactive Distillation: Thermodynamic Aspects, Reaction Kinetics, Pilot-Plant Experiments, and Simulation Studies.* Ind. Eng. Chem. Res., 2002. **41**(22): p. 5483-5490.

Steinigeweg, S. and J. Gmehling, *Esterification of a Fatty Acid by Reactive Distillation.* Ind. Eng. Chem. Res., 2003. **42**(15): p. 3612-3619.

Stichlmair, J. and T. Frey, *Reactive distillation processes.* Chem. Eng. Technol., 1999. **22**(2): p. 95-103.

Sundmacher, K. and Z. Qi, *Importance of reaction kinetics for catalytic distillation processes*, in *Reactive Distillation: Status and Future Directions*, Eds. K. Sundmacher and A. Kienle, 2003, Wiley-VCH: Weinheim. ISBN: 3-527-30579-3

TALETE srl., (2007) *Dragon User Manual,* [Online] Available at: http://www.talete.mi.it/help/dragon_help/index.html (Accessed: 13 May 2010)

Talwalkar, S.; Chauhan, M.; Aghalayam, P.; Qi, Z.; Sundmacher, K.; Mahajani, S., *Kinetic studies on the dimerization of isobutene with ion-exchange resin in the presence of water as a selectivity enhancer.* Ind. Eng. Chem. Res., 2006. **45**(4): p. 1312-1323.

Tang, D., Huang, J., Zhou, Y., Zhang, Y. and Chen, Q., *Preparation and activity of the catalysts for the synthesis of carboxylic ester with high boiling point.* J. Mol. Catal. A: Chem., 1999. **147**(1-2): p. 159-163.

Taylor, R. and R. Krishna, *Modelling reactive distillation.* Chem. Eng. Sci., 2000. **55**(22): p. 5183-5229.

Tesser, R.; DiSerio,M.; Guida,M.; Nastasi,M.; Santacesaria, E., *Kinetics of Oleic Acid Esterification with Methanol in the Presence of Triglycerides.* Ind. Eng. Chem. Res., 2005. **44**(21): p.7978-7982.

Tetko, I. V.; Gasteiger, J.; Todeschini, R.; Mauri, A.; Livingstone, D.; Ertl, P.; Palyulin, V. A.; Radchenko, E. V.; Zefirov, N. S.; Makarenko, A. S.; Tanchuk, V. Yu; Prokopenko, V. V., *Virtual computational chemistry laboratory - Design and description.* J. Comput. Aided. Mol. Des., 2005. **19**(6): p. 453-463.

The Dow Chemical Company (2003) *Syltherm XLT Product Information Datasheet* [Online] Available at: http://www.dow.com/heattrans/tech/data.htm (Accessed: 8th August 2010)

Towler, G.P. and S.J. Frey, *Reactive distillation*, in *Reactive separation processes*, S. Kulprathipanja, Editor. 2000, Taylor and Francis: Philadelphia. p. 18-50. ISBN: 1-56032-825-8

Tuchlenski, A.; Beckmann, A.; Reusch, D.; Düssel, R.; Weidlich, U.; Janowsky, R., *Reactive distillation -- industrial applications, process design & scale-up.* Chem. Eng. Sci., 2001. **56**(2): p. 387-394.

van Aken, T. *High-throughput Process Research and Development Solutions –Strategies for Accelerating and Intensifying Pharma Process R&D,* in Business Briefing: Pharmatech. 3rd ed., 2003: *Touch Briefings* p. 1-6

Van Der Linden, J.B., E.J. Ras, S.M. Hooijschuur, G.M. Klaus, N.T. Luchters, P. Dani, G. Verspui, A.A. Smith, E.W.P. Damen, B. McKay, and M. Hoogenraad, *Asymmetric catalytic ketone hydrogenation: Relating substrate structure and product enantiomeric excess using QSPR.* QSAR Comb. Sci., 2005. **24**(1): p. 94-98.

VCCLAB, Virtual Computational Chemistry Laboratory, http://www.vcclab.org, 2005

Venimadhavan, G.; Buzad, G.; Doherty, M. F.; Malone, M. F., *Effect of kinetics on residue curve maps for reactive distillation.* AlChE J., 1994. **40**(11): p. 1814-1824.

Venimadhavan, G., M.F. Malone, and M.F. Doherty, *Bifurcation study of kinetic effects in reactive distillation.* AlChE J., 1999a. **45**(3): p. 546-556.

Venimadhavan, G., M.F. Malone, and M.F. Doherty, *A novel distillate policy for batch reactive distillation with application to the production of butyl acetate.* Ind. Eng. Chem. Res., 1999b. **38**(3): p. 714-722.

Verspui, G., M. Hoogenraad, E. Damen, E.J. Ras, and N. Luchters, *Rational Screening: Parallel Experimentation and Predictive Modeling applied to Chemical Process R&D.* PharmaChem, 2004. **April**: p. 2-6.

Wajge, R.M. and G.V. Reklaitis, *RBDOPT: a general-purpose object-oriented module for distributed campaign optimization of reactive batch distillation.* Chem. Eng. J., 1999. **75**(1): p. 57-68.

Wang, Y., P. Liu, S. Ou, and Z. Zhang, *Preparation of biodiesel from waste cooking oil via two-step catalyzed process*. Energy Convers. Manage., 2007. **48**(1): p. 184-188.

Wang, Y., S. Ou, P. Liu, F. Xue, and S. Tang, *Comparison of two different processes to synthesize biodiesel by waste cooking oil.* J. Mol. Catal. A: Chem., 2006. **252**(1-2): p. 107-112.

Wiley Critical Content (2007) Petroleum Technology, Volume 1-2.. John Wiley & Sons. Knovel, . [Online] Available at: www.knovel.com (Accessed: 13 May 2010)

Witham, C.A.; Huang, W.; Tsung, C. K.; Kuhn, J. N.; Somorjai, G. A.; Toste, F. D., *Converting homogeneous to heterogeneous in electrophilic catalysis using monodisperse metal nanoparticles.* Nat. Chem., 2010. **2**(1): p. 36-41.

Wolterbeek, H.T. and T.G. Verburg, *Predicting metal toxicity revisited: general properties vs. specific effects.* Sci. Total Environ., 2001. **279**(1-3): p. 87-115.

Worth, R. (2008) *Personal Communication,* University of Newcastle upon Tyne

Wright, A. (2006) *Personal Communication,* University of Newcastle upon Tyne

Wright, A. (2010) *Personal Communication,* University of Newcastle upon Tyne

Yalçinyuva, T., Deligöz, H., Boz, İ. and Gürkaynak, M. A., *Kinetics and mechanism of myristic acid and isopropyl alcohol esterification reaction with homogeneous and heterogeneous catalysts.* Int. J. Chem. Kinet., 2008. **40**(3): p. 136-144.

Yang, J.I., S.H. Cho, J. Park, and K.Y. Lee, *Esterification of acrylic acid with 1,4-butanediol in a batch distillation column reactor over Amberlyst 15 catalyst.* Can. J. Chem. Eng., 2007. **85**(6): p.883-888.

Yaws, Carl L. (2003). *Yaws' Handbook of Thermodynamic and Physical Properties of Chemical Compounds*.. Knovel. [Online] Available at: http://knovel.com (Accessed: 12 October 2010) ISBN: 978-1-60119-797-9

Zafiropoulos, N.A., Ngo, H.L., Foglia, T.A., Samulski, E.T. and Lin., W, *Catalytic synthesis of biodiesel from high free fatty acid-containing feedstocks.* Chem. Commun., 2007(35): p.3670-3672.

Zhang, G.S., *$Fe_2(SO_4)_3 \cdot xH_2O$ in synthesis: A convenient and efficient catalyst for the esterification of aromatic carboxylic acids with alcohols.* Synthetic Communications, 1999. **29**(4): p. 607-611.

Zielinska-Nadolska, I., K. Warmuzinski, and J. Richter, *Zeolite and other heterogeneous catalysts for the transesterification reaction of dimethyl carbonate with ethanol.* Catal. Today, 2006. **114**(2-3): p. 226-230.

Appendix A: Data from 24 Hour ChemSpeed Runs with No Catalyst

Running Time (hours)	Conversion Nonanoic Acid (%)
0.00	0.00
1.05	3.41
4.04	15.02
8.04	27.30
12.04	34.47
16.04	39.59
20.03	46.08
22.03	49.49
24.03	51.88

Table A1: Data from 24hour run, No Catalyst, Reactor 1

Running Time (hours)	Conversion Nonanoic Acid (%)
0.00	0.00
1.00	2.28
3.99	13.53
7.99	25.57
11.99	36.11
15.99	43.63
19.98	50.39
21.98	50.39
23.98	51.14

Table A2: Data from 24hour run, No Catalyst, Reactor 3

Appendix B: Materials Used

In the following tables, the PubChem IDs refer to the 'as supplied' compounds.

Reactants

	Nonanoic Acid	**n-Butanol**
Supplier:	ACROS	Sigma-Aldrich
Catalogue No.:	35624-0010	34867-2.5L
Grade:	97%	Chromasolv Plus ≥99.7%

Table B1: Reactants for the Nonanoic Acid Esterification System

Homogeneous Acids

Candidate	**Supplier**	**Grade**	**Catalogue No.**	**PubChem ID**
Sulfuric acid (H_2SO_4)	Sigma-Aldrich	98%	435589	1118
Hydrochloric acid (HCl)	Sigma-Aldrich	37%	258148	313
PTSA	ACROS	99%	139025000	521998
Methane sulfonic acid	Sigma-Aldrich	≥99.5%	471356	6395
Hypophosphorous acid	ACROS	50% wt	20100-5000	6326996

Table B2: Supplier details for homogeneous acids

Hydrochloric acid (HCl) was supplied in its concentrated grade at 37% and hypophosphorous acid was available as a 50% wt in water, the form in which it is normally supplied.

Heteropoly Acids

Candidate	**Supplier**	**Grade**	**Catalogue No.**	**PubChem ID**
Phosphomolybdic acid hydrate	Sigma-Aldrich	99%	221856	11251951
Phosphotungstic acid hydrate	Sigma-Aldrich	90%	P4006	16212977

Table B3: Supplier details for heteropoly acids

The grades of the heteropoly acid catalysts have been estimated from the Certificates of Analysis provided by the supplier.

Metal Acetates

Candidate	Supplier	Grade	Catalogue No.	PubChem ID
Bismuth (III) acetate	Sigma-Aldrich	≥99.99%	401587	31132
Tin (II) acetate	Sigma-Aldrich	98%	345164	69488
Tin (IV) acetate	Sigma-Aldrich	99.5%	9863446	345172
Zinc acetate dihydrate	Sigma-Aldrich	99%	25056	2724192

Table B4: Supplier details for metal acetates

The grades of tin (II) acetate and tin (IV) acetate have been estimated from the Certificates of Analysis provided by the supplier.

Candidate	Grade	PubChem ID
Copper (II) acetate monohydrate	99%	165397
Lead (II) acetate trihydrate	99.5%	16693916
Nickel (II) acetate tetrahydrate	98%	62601
Potassium acetate	99%	517044
Sodium acetate trihydrate	99.5%	23665404

Table B5: Additional metal acetates available.

Other Heterogeneous Candidates

Candidate	Supplier	Grade	Catalogue No.	PubChem ID
Ferric sulfate hydrate	Sigma-Aldrich	97%	307718	167265
Niobium (V) oxide	Fisher	99.4%		123105
Zirconium (IV) hydroxide, sulfated	Sigma-Aldrich	99%	464341	3594980
Copper chromite	Sigma-Aldrich		209317	3084101

Table B6: Supplier details for other heterogeneous candidates

The grade of sulfated zirconium hydroxide has been estimated from the Certificate of Analysis provided by the supplier. The Certificate of Analysis for copper chromite does not give a quantitative analysis, but ‘confirms copper and chromium components’. An alternative was not available at the time of placing the order.

Appendix C: Worked Example of Titration Calculation

1) Standardisation of KOH solution

The normality (N_{KOH}, in mol/L) of the KOH solution is calculated by:

- $N_{KOH} = W_{KHP} / Mr_{KHP} \times V_{KOH}$

W_{KHP} = actual weight KHP, mg
V_{KOH} = volume of KOH used in the titration, ml
Mr_{KHP} = the molar mass of KHP (204.2 g/mol)

For this sample:
W_{KHP} = 351mg (+/- 0.5mg, relative error 0.14%)
Burette reading – start: 2.36 ml KOH (+/- 0.01ml, relative error 0.42%)
Burette reading – end: 5.76 ml KOH (+/- 0.01ml, relative error 0.17%)

KOH used: 3.40 ml (+/- 0.02ml, relative error 0.59%)

N_{KOH} = 351 / 204.2 x 3.40 = 0.506 mol/L

Relative error N_{KOH} = relative error W_{KHP} + relative error V_{KOH}
= 0.14 + 0.59
= 0.73%

Absolute error (+/-) = 0.506 x (0.73/100) = 0.004 mol/L

So N_{KOH} = 0.506 mol/L (+/- 0.004 mol/L)

An average value of 0.510mol/L was obtained, with a relative error of 1.27%.

2) Acid number of nonanoic acid

The acid number (AN) is calculated by:
$AN = (V_{KOH} \times N_{KOH} \times Mr_{KOH}) / W_S$

Where

W_s = weight of sample, in grams

Mr_{KOH} = the molar mass of KOH (56.1 g/mol)

For this sample:

W_S = 201 mg (+/- 0.5mg, relative error 0.25%)

Burette reading – start: 0.82 ml KOH (+/- 0.01ml, relative error 1.22%)

Burette reading – end: 3.38 ml KOH (+/- 0.01ml, relative error 0.30%)

KOH used: 2.56 ml (+/- 0.02ml, relative error 0.78%)

AN_{Non} = (2.56 x 0.510 x 56.1) / 0.201 = 364.4 mgKOH / g nonanoic acid

Relative error AN_{Non}

= relative error W_S + relative error V_{KOH} + relative error N_{KOH}

= 0.25+ 0.78 + 1.27

= 2.30%

Absolute error (+/-) = 364.4 x (2.30/100) = 8.38 mgKOH / g nonanoic acid

So AN_{Non} = 364.40 (+/- 8.38) mgKOH / g nonanoic acid

An average value of 365.49 mgKOH / g nonanoic acid was obtained, with a relative error of 2.29%. For further calculations, only 1 decimal place was deemed necessary, so the value used is 365.5 mgKOH / g nonanoic acid.

3) Nonanoic acid composition of the reaction samples.

The weight of nonanoic acid in the sample is calculated by:

- $W_{Non} = (V_{KOH} \text{ x } N_{KOH} \text{ x } Mr_{KOH}) / AN_{Non}$

And the concentration of acid (mol/L) in the sample is calculated by:

- C_{Non}= 1000 x W_{Non}/Mr_{Non})/Volume of sample in mls, 0.8

Where

Mr_{Non} = the molar mass of nonanoic acid, 158.24g/mol

For this example:

W_S = 644 mg (+/- 0.5mg, relative error 0.08%)

Burette reading – start: 1.90 ml KOH (+/- 0.01ml, relative error 0.53%)

Burette reading – end: 3.70 ml KOH (+/- 0.01ml, relative error 0.27%)

KOH used: 1.80 ml (+/- 0.02ml, relative error 1.11%)

W_{Non} = (1.80 x 0.51 x 56.1) / 365.5 = 0.141 g

Relative error W_{Non} = relative error V_{KOH} + relative error N_{KOH} + relative error AN_{Non}

= 1.11 + 1.27 + 2.29

= 4.67%

Absolute error (+/-) = 0.141 x (4.67/100) = 0.007 g

C_{Non} = 1000 x (W_{Non}/Mr_{Non})/Volume of sample in mls, 0.8

= 1000 x (0.141/ 158.24) / 0.8

= 1.11 mol/L

(IUPAC Mr values taken as exact numbers.)

Appendix D: Details of GCMS Method to Analyse Ester Composition

Nonanoic Acid Esterification System

GCMS Machine

- Varian CP3800 GC with Saturn 2200 GCMS
- Detector: GC Mass Spectrometer with ion trap
- Carrier gas: Helium
- GC Column: VF-5ms

GCMS Analysis Method File Settings

- MS Scan From 2 minutes to 28 minutes
- (Low mass 40 m/z, high mass 500 m/z)
- Column flow 1ml/min
- Front injector Temperature 250˚C

Oven temperature protocol:

- Start: 100˚C, hold for 1 minute.
- Ramp temperature to 250˚C by 10˚C per minute, then hold for 12 minutes.
- Total time: 28 minutes.

Butyl Laurate Internal Standard

Supplier:	Sigma-Aldrich
Catalogue Number:	435589
Grade:	98%

Butyl Nonanoate Calibration Standard

Supplier:	AccuStandard
Catalogue Number:	S-17068
Grade:	99%

Appendix E: Worked Example of GCMS Concentration Calculation

1) Calculate Relative Response Factor:
(Data from RD run with FeSulf as catalyst)

- Internal Standard Response Factor = $\frac{\text{Internal Standard Response Area}}{\text{Internal Standard Concentration}}$

- Ester Response Factor = $\frac{\text{Ester Response Area}}{\text{Ester Concentration}}$

- Relative Response Factor (RRF) = $\frac{\text{Internal Standard Response Factor}}{\text{Ester Response Factor}}$

This calculation is performed for each of a set of standards of known concentration:

Standard Number	Conc (mol/L)		Area Response		RF(IS)	RF(Ester)	RRF
	Ester	IS	Ester	IS	A(IS)/C(IS)	A(est)/C(est)	
1	0.0042	0.0025	$1.87x10^7$	$1.44x10^7$	$5.74x10^9$	$4.50x10^9$	0.783
2	0.0030	0.0025	$1.41x10^7$	$1.49x10^7$	$5.95x10^9$	$4.76x10^9$	0.800
3	0.0021	0.0025	$9.91x10^6$	$1.44x10^7$	$5.74x10^9$	$4.76x10^9$	0.829
4	0.0017	0.0025	$7.75x10^6$	$1.40x10^7$	$5.57x10^9$	$4.66x10^9$	0.836
5	0.0008	0.0025	$3.91x10^6$	$1.40x10^7$	$5.57x10^9$	$4.70x10^9$	0.843
6	0.0004	0.0025	$1.85x10^6$	$1.38x10^7$	$5.49x10^9$	$4.44x10^9$	0.810
7	0.0003	0.0025	$1.09x10^6$	$1.41x10^7$	$5.63x10^9$	$4.35x10^9$	0.773

Table E1: Standards data for calculation of RRF

Average RRF = 0.811

2) Calculate ester concentration in the sample
(Data from last sample, RD run with FeSulf as catalyst)

Example GCMS output of peak areas for ester and internal standard are shown in the following table. Each sample vial is run twice in the GC, and an average response used for the calculations that follow.

Compound Name	Area Response 1	Area Response 2	Average Area Response
Butyl Nonanoate	$1.26x10^7$	$1.22x10^7$	$1.24x10^7$
Butyl Laurate (IS)	$1.47x10^7$	$1.45x10^7$	$1.46x10^7$

Table E2: Example GCMS output of peak areas

The concentration of internal standard in the sample is known to be 0.0025mol/L.

- Ester Concentration = $\frac{\text{Ester Response Area}}{\text{RRF x Internal Standard Response Factor}}$

- Ester Concentration = $\frac{1.24x10^7}{0.811 \text{ x } (1.46x10^7 / 0.0025)}$

$= 0.0026\text{mol/L}$

This is the concentration in the GC vial, to find the concentration in the reactor the dilutions made during sample make – up must be reversed.

3) Reverse sample make-up dilutions:

- Concentration in ChemSpeed sample vial = 100 x Concentration in GC vial
  = 0.26mol/L

- Concentration in ChemSpeed reactor vial
  = Concentration in GC vial x 7
  = 1.84 mol/L

Appendix F: Conditions Used for Catalyst Studies in Literature

Reaction System	**Temperature °C**	**Reactant Molar Ratio** (Alcohol:Acid)	**Catalyst Loading**	**Catalyst**	**Reference**
Dodecanoic acid + Methanol	130	Test Catalysts 2:1 Range 1:1 and 2:1	Test Catalysts: 2wt% Range: 0.5 to 10wt%	Various	Kiss et al. 2008a
Dodecanoic acid + Methanol/Propanol/ 2ethylhexanol	Test Catalysts: 130 Range: 120 to 180	Test Catalysts 2:1 or 1:1 Range 1:1 to 5:1	Test Catalysts: 1 or 2 wt% Range 0 to 5wt% (basis acid + alcohol)	Various	Kiss et al. 2008b
Dodecanoic acid + Methanol/Propanol/ 2ethylhexanol	Test Catalysts: 130 Range: 120 to 180	Test Catalysts: 2:1 Range 1:1 to 5:1	Test Catalysts: 2 wt% Range: 0 to 10wt% (basis acid + alcohol)	Various	Kiss et al. 2006b
Dodecanoic acid + 2ethylhexanol	Range: 60 to 80	Range 1:9 to 25:1	Range: 0 to 3wt% (mixture basis)		Omota et al. 2003b
Oleic acid + Butanol	Test Catalysts: 100 Range: 80 to 100	Test Catalyst: 5:1 Range: 1 to 20	Test Catalysts: 0.9% Range: 0 to 2.85%	H2SO4	Othmer and Rao 1950
Oleic acid + Isobutanol	Test Catalysts: 100 Range: 80 to 150	Test Catalyst: 5:1 Range: 1:1 to 20:1	Test Catalysts: 0.25wt% Range: 0 to 1	H2SO4	Ling and Geankoplis 1958
Palmitic acid + Isopropanol	Range: 99.85 to 169.85	Range: 1:1 to 5:1	Range: 1 to 5 g cat /L	PTSA / Zn ethanoate	Aafaqi et al. 2004
Palmitic acid + Isopropanol	Test Catalysts: 139.85 Range: 99.85 to 139.85	Test Catalysts 5:1 Range 1:1 to 5:1	Test Catalysts: 3g (in 200ml) Range: 1 to 5g	ZnAc complex	S. Y. Chin et al. 2006
Myristic Acid + Isopropanol	Range: 60 to 80	Test Catalysts 2:1 Range 1:1 to 10:1	Range 0.2mol% to 2mol%	Various	Yalçinyuva et al. 2008

Table F1: Conditions Used for Catalyst Studies in Literature

Reaction System	**Temperature °C**	**Reactant Molar Ratio** (Alcohol:Acid)	**Catalyst Loading**	**Catalyst**	**Reference**
Oleic acid + Methanol	Range: 50 to 100	Range: 8.6 to 10.7	Range approx 1.3 wt% to 3.2wt%	Relite CFS het	Tesser et al. 2005
Waste oil (& FFA) + Methanol (esterification and transesterification)	95	MeOH excess used 10:1 (range 3:1 to 10:1) based on oil	Range: 0 to 4 wt% (oil basis)	FeSulf	Wang et al. 2007
Acetic acid + Isoamyl alcohol	100	1:1	1.5wt%	Zeolite	Lee and Lin, 1999
Acetic acid + Butanol	75	1:1	Different amounts results normalised for cat weight	Various	Peters et al. 2006
Acetic acid + Butanol	Test Catalysts: 100 Range: 100 to 120	B/A 5, range 3 to 20	Range up to 0.13 wt% (based on reactant mix)	H2SO4	Leyes and Othmer, 1945
Succinic acid + Ethanol	Test Catalysts: 78 & 90 Range: up to 120	Test Catalysts 10:1 Range up to 20:1	Test Catalyst: 2 solution wt% Range: 1 to 5	Amberlyst 15	Kolah et al. 2008
Refined oil & Oleic acid + Methanol	Range: 20 to 60	Not discussed	1% concentration basis Range: 0.1 to 5%	H_2SO_4	Sendzikiene et al. 2004
High FFA soybean oil + Methanol (transesterification)	Range: 150 to 200	2g Oil to 0.88g MeOH	0.06mmol Cat	M2+ metal ions	Di Serio et al. 2005
Oil-Methanol system	Range: 200 to 250		0.5 wt%	Ca Ac / Ba Ac	Di Serio et al. 2005
High FFA oil / Oleic acid + Methanol	95	2 equiv. meOH (range 2 to 20)	Tests 0.5mol% range 0.5 to 3mol%	Diaryl-ammonium	Zafiropoulos, et al. 2007

Table F1: Conditions Used for Catalyst Studies in Literature

Reaction System	**Temperature °C**	**Reactant Molar Ratio** (Alcohol:Acid)	**Catalyst Loading**	**Catalyst**	**Reference**
Phthalic anhydride + Butanol	Test Catalysts: 100 Range 80 to 150	Test Catalyst: 10 Range: 3 to 30	Test Catalyst: 1wt% Range: 0.77 to 3.6	H2SO4	Berman, Melnychuk, and Othmer 1948
Phthalic anhydride + Butanol	Not discussed	Test Catalyst 1 : 1.3	0.08 mol% based on acid	Rare earth sulfates	Tang, et al. 1999
Gylcolysis of PET	190	PET to EG 1:4	0.5 wt% PET basis	ZnAc	Jong-Wu and Leo-Wang, 1999

Table F1: Conditions Used for Catalyst Studies in Literature

Appendix G: Data Used for Equilibrium Determination

Temperature: 73°C

- B/FA = 2, Catalyst PTSA (0.91wt%)
- Analysed by titrations

Running time (hh:mm:ss)	Conc Nonanoic Acid (mol/L)
0:00:00	2.71
3:25:00	0.46
4:45:00	0.46

Table G1: Data for equilibrium run at 73°C

Temperature: 80°C

- B/FA = 2, Catalyst PTSA (0.93wt%)
- Analysed by GC

Running time (hh:mm:ss)	Conc Butyl Nonanoate (mol/L)
0:00:00	0
04:50:00	1.92
05:38:00	2.33

Table G2: Data for equilibrium run at 80°C

Temperature: 90°C

- B/FA = 2, Catalyst PTSA (0.91wt%)
- Analysed by GC

Running time (hh:mm:ss)	Conc Butyl Nonanoate (mol/L)
0:00:00	0
04:45:00	2.05
05:49:00	2.32

Table G3: Data for equilibrium run at 90°C

Temperature: 100°C

- B/FA = 2, Catalyst H_2SO_4 (4wt%), 500rpm
- ChemSpeed Run, Analysed by titrations

Running time (hh:mm:ss)	**Conc Nonanoic Acid (mol/L)**
0:00:00	2.51
0:16:00	0.59
0:28:00	0.36
0:53:00	0.32
1:05:40	0.30
1:20:30	0.30
1:34:59	0.27
2:03:42	0.30
2:31:05	0.30
2:59:27	0.30
3:26:55	0.27
3:54:16	0.27

Table G4: Data for equilibrium run at 100°C

Appendix H: Experimental Data from Screening Experiments

Ester (n-buyl nonanoate) concentration and percent yield with time is presented for each catalyst tested.

Bismuth (III) Acetate

Running Time (min)	Concentration Ester (mol/L)	% Yield based on maximum Ester
0.0	0.00	0.00
1.4	0.00	0.12
20.5	0.07	2.49
54.3	0.16	6.08

Table H1: Screening test results: Bismuth (III) Acetate

Copper (II) Acetate Monohydrate

Running Time (min)	Concentration Ester (mol/L)	% Yield based on maximum Ester
0.0	0.00	0.00
1.4	0.00	0.08
19.4	0.05	1.84
53.1	0.17	6.35

Table H2: Screening test results: Copper (II) Acetate Monohydrate

Copper Chromite

Running Time (min)	Concentration Ester (mol/L)	% Yield based on maximum Ester
0.0	0.00	0.00
1.4	0.00	0.07
20.3	0.06	2.19
54.3	0.15	5.45

Table H3: Screening test results: Copper Chromite

Ferric Sulfate Hydrate

Running Time (min)	Concentration Ester (mol/L)	% Yield based on maximum Ester
0.0	0.00	0.00
1.4	0.00	0.10
20.5	0.08	2.86
54.2	0.26	9.80

Table H4: Screening test results: Ferric Sulfate Hydrate

Hydrochloric Acid

Running Time (min)	Concentration Ester (mol/L)	% Yield based on maximum Ester
0.0	0.00	0.00
1.5	0.13	4.65
19.4	0.80	29.61
53.3	1.20	44.58

Table H5: Screening test results: Hydrochloric Acid

Hypophosphorous Acid

Running Time (min)	Concentration Ester (mol/L)	% Yield based on maximum Ester
0.0	0.00	0.00
1.5	0.00	0.00
20.6	0.12	4.35
54.5	0.21	7.74

Table H6: Screening test results: Hypophosphorous Acid

Lead (II) Acetate Trihydrate

Running Time (min)	Concentration Ester (mol/L)	% Yield based on maximum Ester
0.0	0.00	0.00
1.5	0.00	0.06
19.3	0.06	2.38
53.0	0.15	5.52

Table H7: Screening test results: Lead (II) Acetate Trihydrate

Methane Sulfonic Acid

Running Time (min)	Concentration Ester (mol/L)	% Yield based on maximum Ester
0.0	0.00	0.00
1.4	0.24	8.82
20.4	0.89	33.13
54.6	1.60	59.65

Table H8: Screening test results: Methane Sulfonic Acid

Nickel (II) Acetate Tetrahydrate

Running Time (min)	Concentration Ester (mol/L)	% Yield based on maximum Ester
0.0	0.00	0.00
1.4	0.00	0.12
20.4	0.07	2.66
54.3	0.16	5.81

Table H9: Screening test results: Nickel (II) Acetate Tetrahydrate

Niobium (V) Oxide

Running Time (min)	Concentration Ester (mol/L)	% Yield based on maximum Ester
0.0	0.00	0.00
1.4	0.00	0.03
20.4	0.06	2.31
54.2	0.16	5.77

Table H10: Screening test results: Niobium (V) Oxide

Phosphomolybdic Acid Hydrate

Running Time (min)	Concentration Ester (mol/L)	% Yield based on maximum Ester
0.0	0.00	0.00
1.4	0.03	1.17
18.7	0.38	14.50
50.2	0.94	35.58

Table H11: Screening test results: Phosphomolybdic Acid Hydrate

Phosphotungstic Acid Hydrate

Running Time (min)	Concentration Ester (mol/L)	% Yield based on maximum Ester
0.0	0.00	0.00
1.4	0.01	0.21
19.2	0.34	12.55
52.9	1.06	39.31

Table H12: Screening test results: Phosphotungstic Acid Hydrate

Potassium Acetate

Running Time (min)	Concentration Ester (mol/L)	% Yield based on maximum Ester
0.0	0.00	0.00
1.5	0.00	0.10
20.5	0.07	2.44
54.3	0.13	4.92

Table H13: Screening test results: Potassium Acetate

PTSA Monohydrate

Running Time (min)	Concentration Ester (mol/L)	% Yield based on maximum Ester
0.0	0.00	0.00
1.4	0.21	7.79
20.4	0.87	32.29
54.5	1.23	45.62

Table H14: Screening test results: PTSA Monohydrate

Sodium Acetate Trihydrate

Running Time (min)	Concentration Ester (mol/L)	% Yield based on maximum Ester
0.0	0.00	0.00
1.4	0.00	0.09
20.5	0.05	1.98
54.2	0.15	5.56

Table H15: Screening test results: Sodium Acetate Trihydrate

Sulfuric Acid

Running Time (min)	Concentration Ester (mol/L)	% Yield based on maximum Ester
0.0	0.05	1.88
1.4	0.17	8.17
19.3	0.92	36.15
53.1	1.41	54.46

Table H16: Screening test results: Sulfuric Acid

Tin (II) Acetate

Running Time (min)	Concentration Ester (mol/L)	% Yield based on maximum Ester
0.0	0.00	0.00
1.4	0.01	0.25
20.3	0.08	2.95
54.2	0.18	6.80

Table H17: Screening test results: Tin (II) Acetate

Tin (IV) Acetate

Running Time (min)	Concentration Ester (mol/L)	% Yield based on maximum Ester
0.0	0.00	0.00
1.4	0.00	0.18
20.4	0.08	3.01
54.3	0.17	6.36

Table H18: Screening test results: Tin (IV) Acetate

Zinc Acetate Dihydrate

Running Time (min)	Concentration Ester (mol/L)	% Yield based on maximum Ester
0.0	0.00	0.00
1.4	0.00	0.10
20.4	0.06	2.15
54.3	0.15	5.68

Table H19: Screening test results: Zinc Acetate Dihydrate

Zirconium (IV) Hydroxide, Sulfated

Running Time (min)	Concentration Ester (mol/L)	% Yield based on maximum Ester
0.0	0.00	0.00
1.4	0.00	0.06
20.6	0.06	2.19
54.3	0.15	5.63

Table H20: Screening test results: Zirconium (IV) Hydroxide, Sulfated

Appendix I: BatchCAD Model of a ChemSpeed Reactor

Building a BatchCAD model of a ChemSpeed reactor

1) Fluid Package Menu
   - Select components
   - Property package (NRTL Ideal-Estimate)
   - Estimate binary coefficients
   - Enter reaction stoichiometry and kinetics.

2) Phase Equilibrium Properties
   - Select pressures

3) Equipment
   - Reactor Heat Transfer parameters (select power input, heat loss, ambient temperature, scale resistance)
   - Jacket Heat Transfer parameters (liquid type, film coefficient)
   - Simulated impeller diameter 1 cm, speed 700 rpm

4) Reactor Dimensions

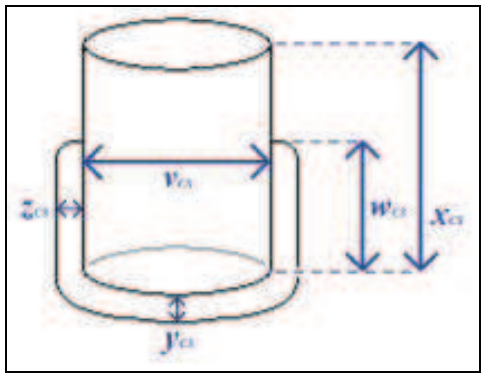

Figure I1: Sketch, not to scale.

Approximated to a flat bottomed cylinder, measured dimensions:

v_{CS}: 4.7 cm
w_{CS}: 3.3 cm
x_{CS}: 5.8 cm
y_{CS}: 0.4 cm
z_{CS}: 0.4 cm

Total (max) Volume $= \pi r^2$ x height

$= \pi$ x $(4.7/2)^2$ x 5.8

= 100.6 ml

Inner Volume within the jacket = πr^2 x height

$= \pi$ x $(4.7/2)^2$ x 3.3

= 57.3 ml

Heat transfer area depends upon volume:

A_{min} = Area if volume ~ 0 = Area of inner base

$= \pi (4.7/2)^2$

= 17.35 cm^2.

A_{max} = Area inner base + area of inner cylinder when volume is at maximum.

$= 17.35 + (\pi \text{ x } v_{CS} \text{ x } w_{CS})$

$= 17.35 + (\pi \text{ x } 4.7 \text{ x } 3.3)$

= 66.08 cm^2.

Volume of jacket

$V_{total} = V_{cylinder} + V_{base}$

$V_{cylinder} = V_{outer} - V_{inner}$

$= [\pi (5.5/2)^2 \text{ x } 3.3] - [\pi (4.7/2)^2 \text{ x } 3.3]$

= 21.15 cm^3

$V_{base} = [\pi (5.5/2)^2 \text{ x } 0.4]$

= 9.50 cm^2

$V_{total} = 21.15 + 9.50$

= 30.65 cm^2.

Glass properties

- Thickness approx 1mm.
- Density 2225 kg/m3 (Perry & Green, 2007)
- Specific heat 0.78 kJ/kgK (Perry & Green, 2007)
- Thermal conductivity 1.1 W/mK (Perry & Green, 2007)

Recirculation fluid properties

- Capacity heater recirculation loop 0.0005 m^3 (estimated)
- Dimethyl polysiloxane CAS 9016-00-6 (The Dow Chemical Company, 2003)
- Specific heat capacity Cp ~ 2 kJ/kg°C (The Dow Chemical Company, 2003)
- Density 0.9g/ml (The Dow Chemical Company, 2003)
- Heat transfer coefficient ~ 360 kJ/hm^2°C (The Dow Chemical Company, 2003)
- Thermal conductivity = 0.151 W/mK (Knovel, 2003)

Model Settings

Initial Charge				
Temperature	°C	100	80	60
Pressure	kPa	101	101	101
Moles	kgmole	0.00037	0.00038	0.00039
Mass	kg	0.037	0.038	0.039
Volume	m^3	$4.70x10^{-05}$	$4.70\ x10^{-05}$	$4.70\ x10^{-05}$
Feed Mole Fraction				
A		0.325	0.325	0.325
B		0.675	0.675	0.675
C		0	0	0
D		0	0	0

Table I.1: Operations List for BatchCAD model of ChemSpeed Reactor

Run Simulation For		24hr 2min
Stop Simulation at		24hr 2min
Current time		00:00:00
Integrator		Adaptive Euler
Step size	s	0.5
Max step size	s	unlimited
Tolerance		0.0001
Discontinuity monitoring		off
Plot frequency		auto
Number of points		200

Table I.2: Simulation Control for BatchCAD model of ChemSpeed Reactor

Fitting Options: Method	Simplex
Max resets	Infinite
Max iterations	100
Parameter	Isothermal rate constants

Table I.3: Fitting Control for BatchCAD model of ChemSpeed Reactor

Stop time		All data
Weight		1
Variance		y
1/n		n
Fractional Error		n
Integrator		Adaptive Euler
Step size	s	0.5
Max step size	s	unlimited
Tolerance		0.0001
Discontinuity monitoring		off
Plot frequency		auto
Number of points		200
Stop time		024:02:0.00

Table I.4: Objective Function for BatchCAD model of ChemSpeed Reactor

Appendix J: Nonanoic Acid System RD Graphs

The data from the individual runs from the reactive distillation runs with the nonanoic acid reaction system are presented in this section.

Final concentration of ester in the pot after the column has cooled and hold up from the column has returned. For demonstration purposes, this is displayed as a data point at the 6 hour mark, although this is not the time point when this occurred.

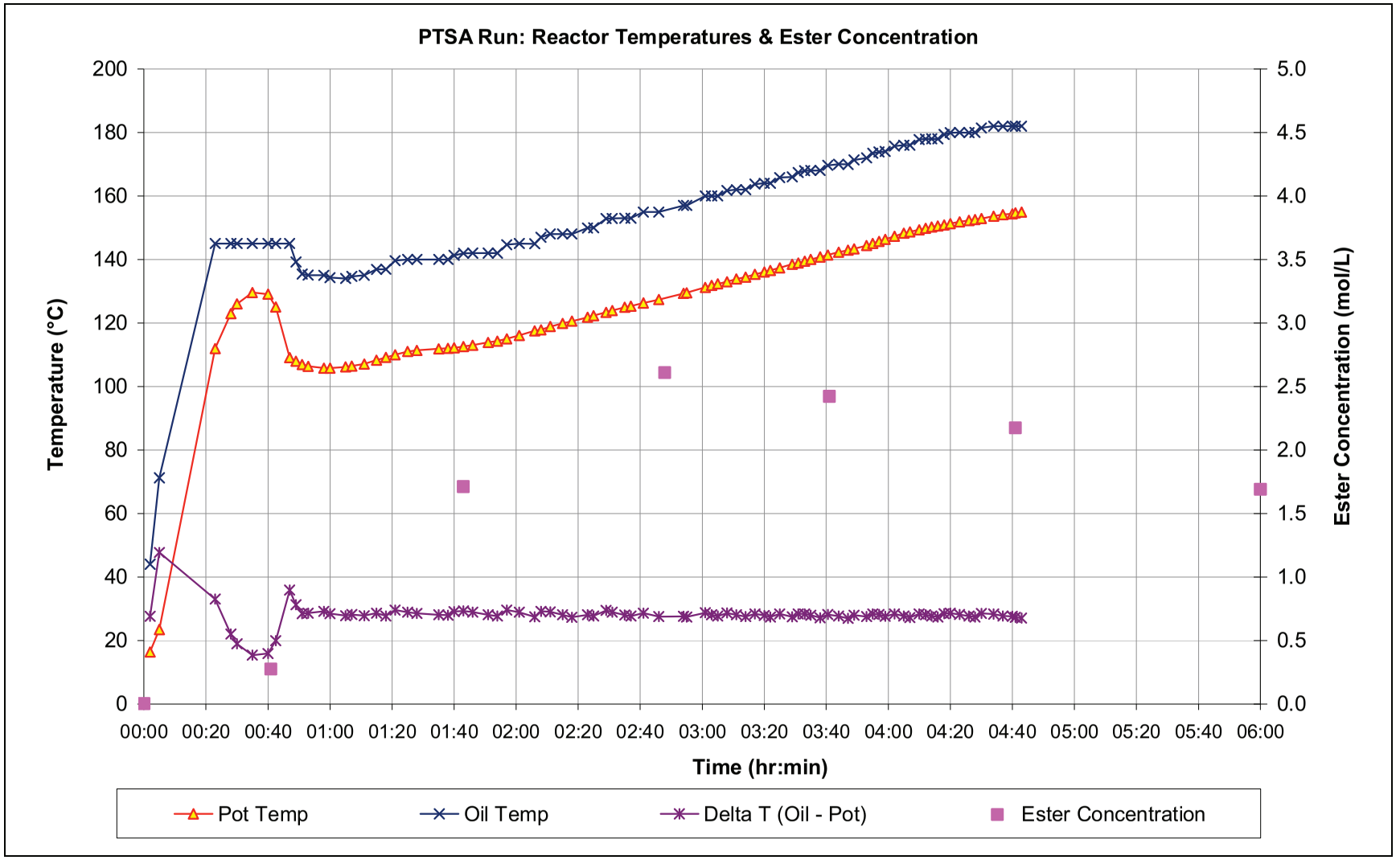

Chart J1: Nonanoic System RD Run 1 - PTSA Catalyst – Reactor Data

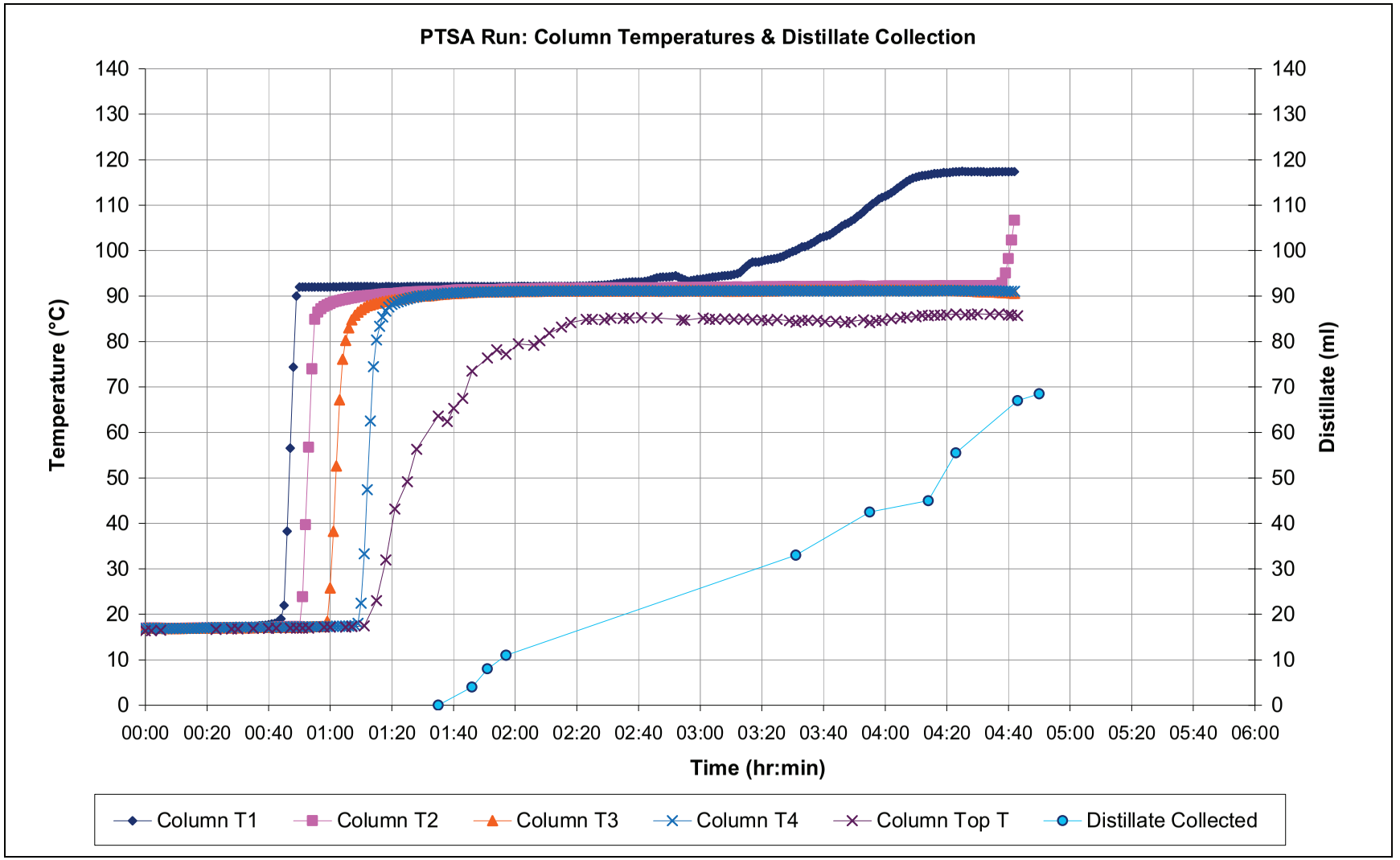

Chart J2: Nonanoic System RD Run 1 - PTSA Catalyst – Column Data

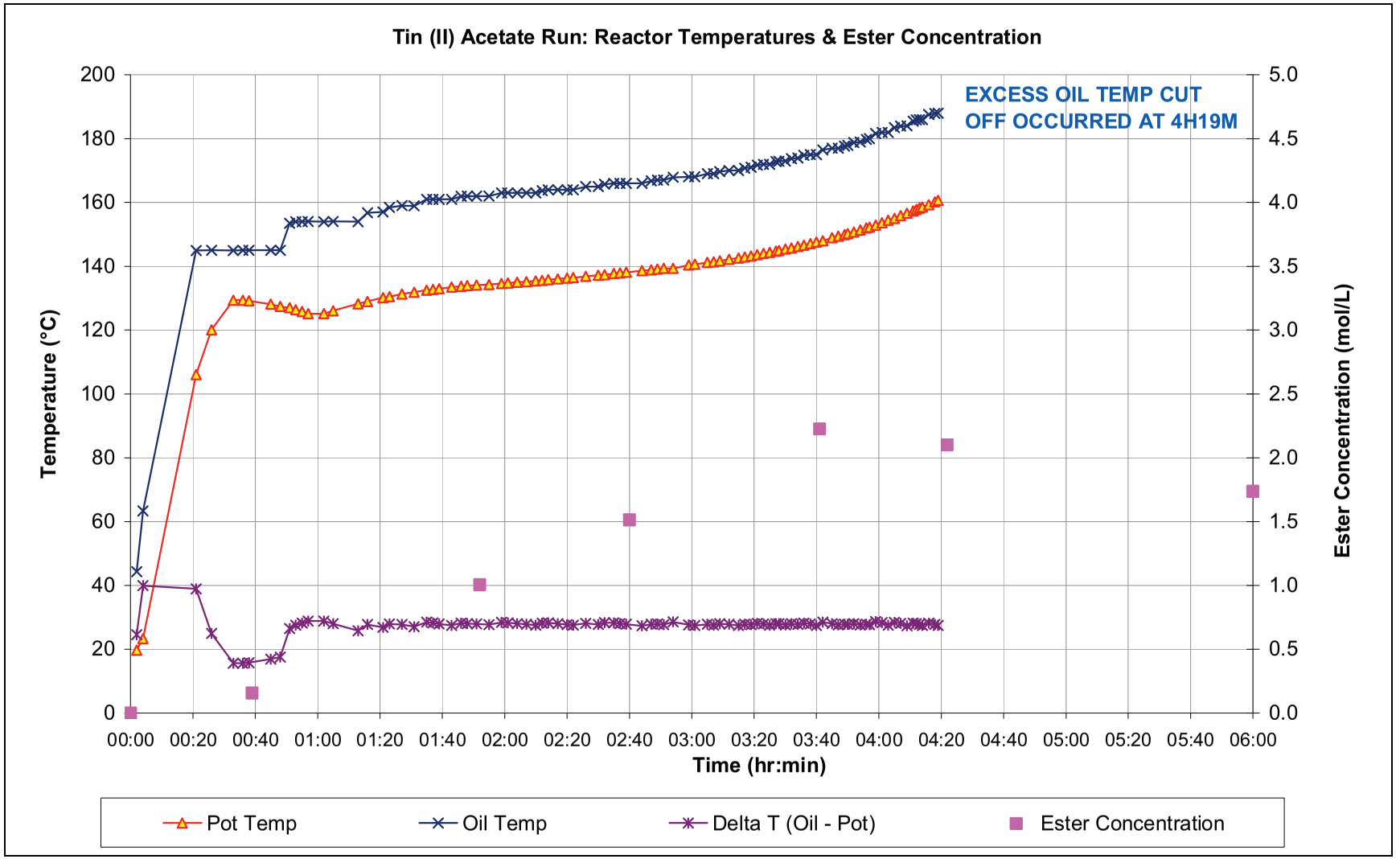

Chart J3: Nonanoic System RD Run 2 - Tin II Acetate Catalyst – Reactor Data

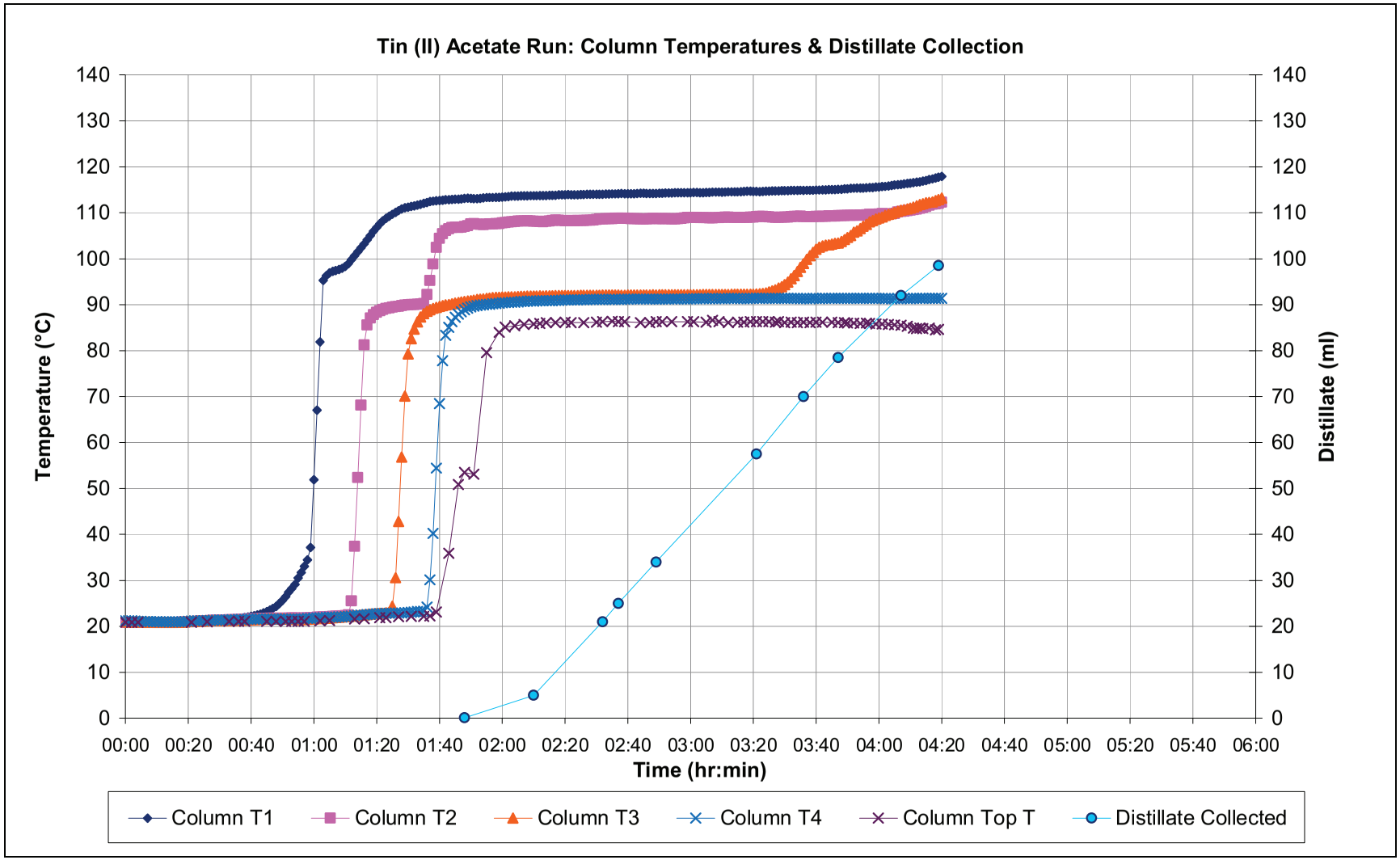

Chart J4: Nonanoic System RD Run 2 - Tin II Acetate Catalyst – Column Data

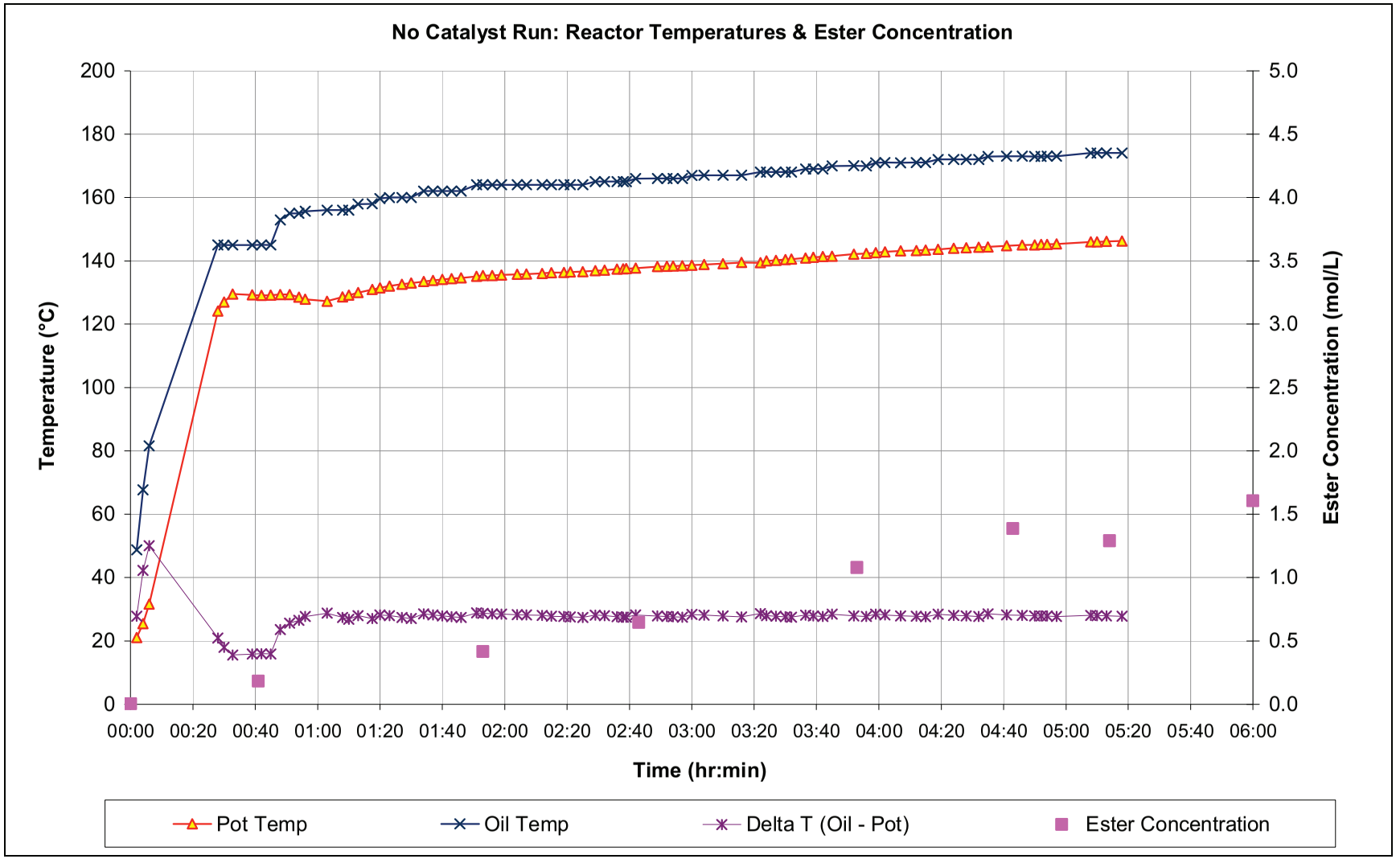

Chart J5: Nonanoic System RD Run 3 - No Catalyst – Reactor Data

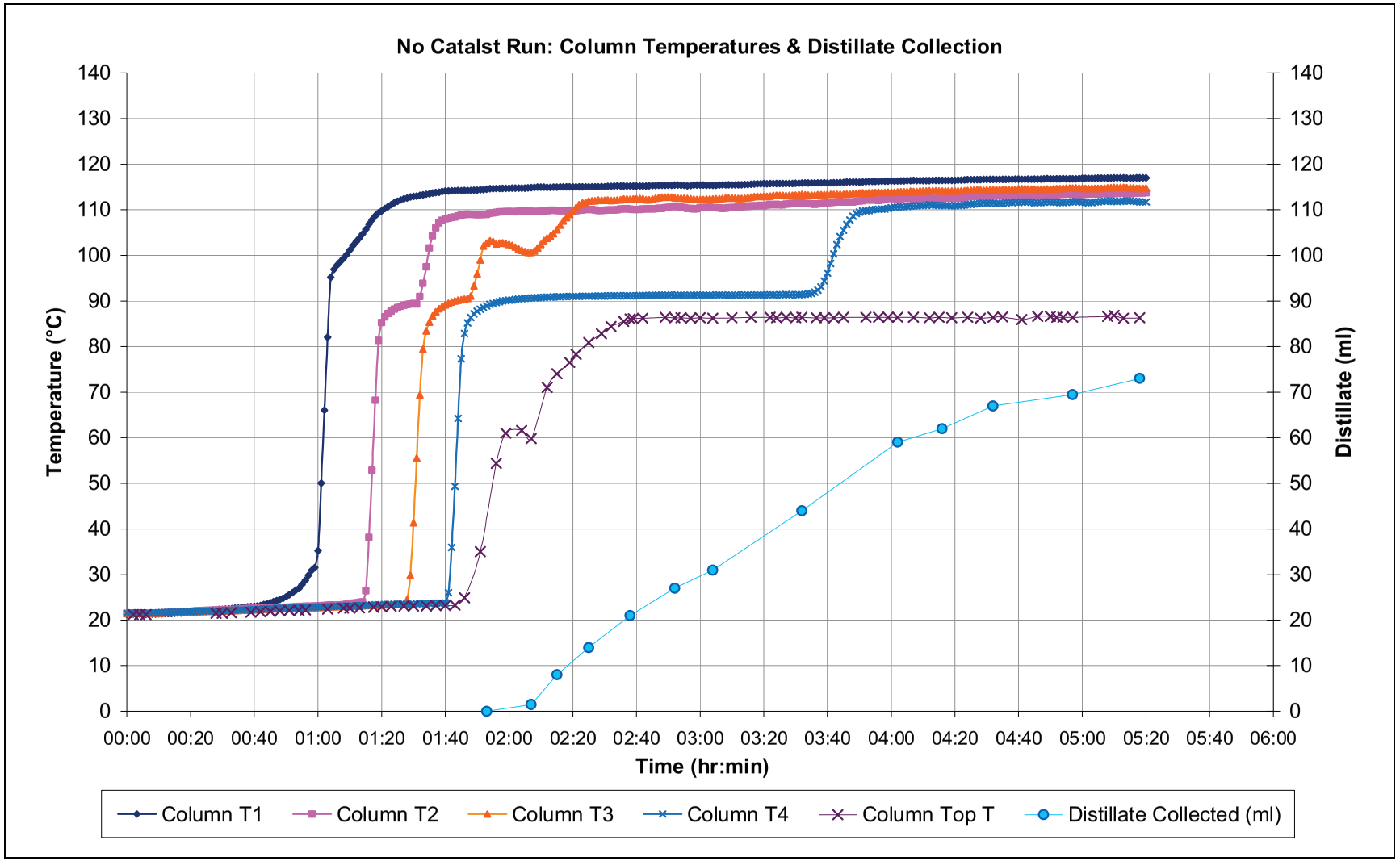

Chart J6: Nonanoic System RD Run 3 - No Catalyst – Column Data

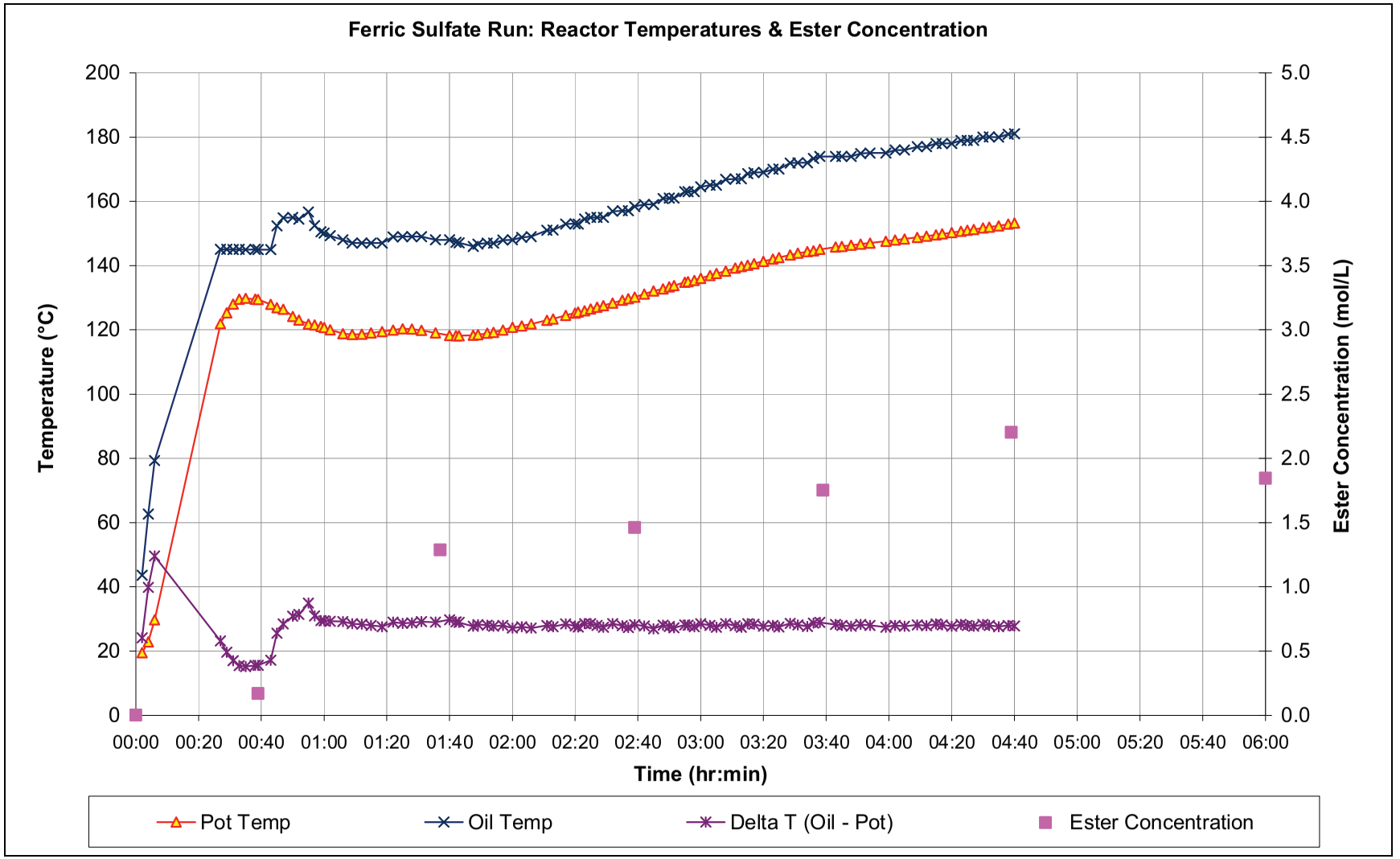

Chart J7: Nonanoic System RD Run 4 - Ferric Sulfate Catalyst – Reactor Data

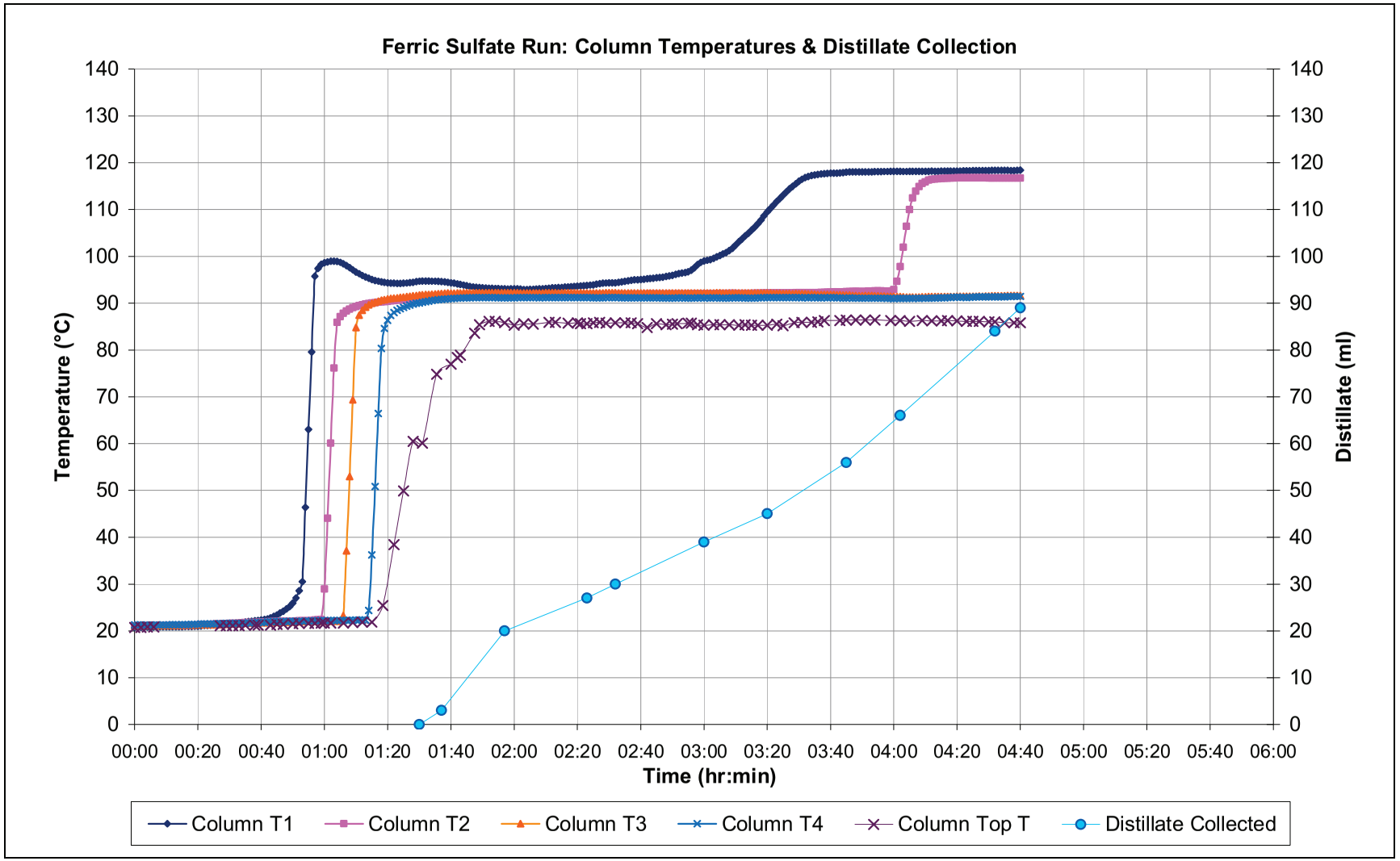

Chart J8: Nonanoic System RD Run 4 - Ferric Sulfate Catalyst – Column Data

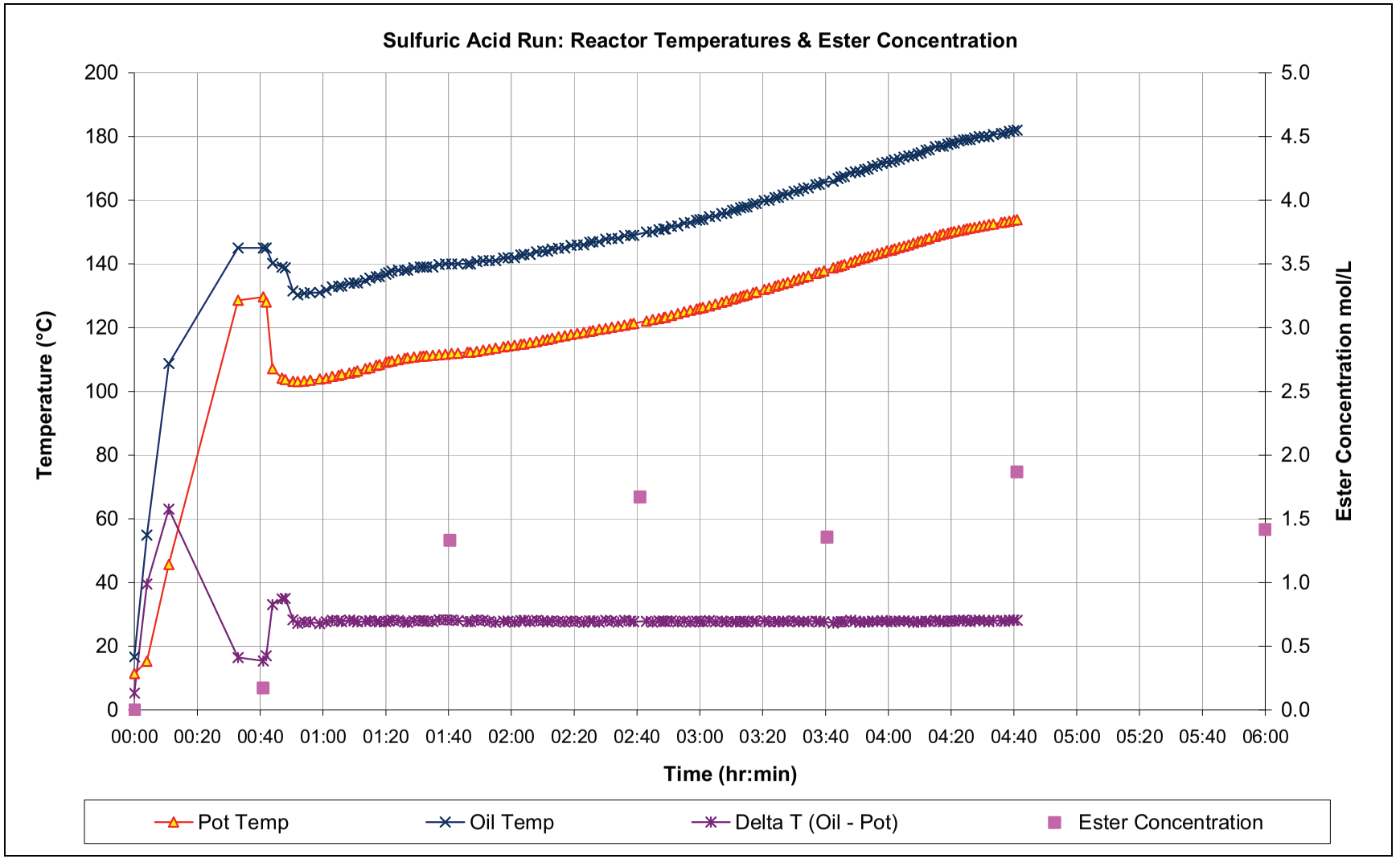

Chart J9: Nonanoic System RD Run 5 - Sulfuric Acid Catalyst – Reactor Data

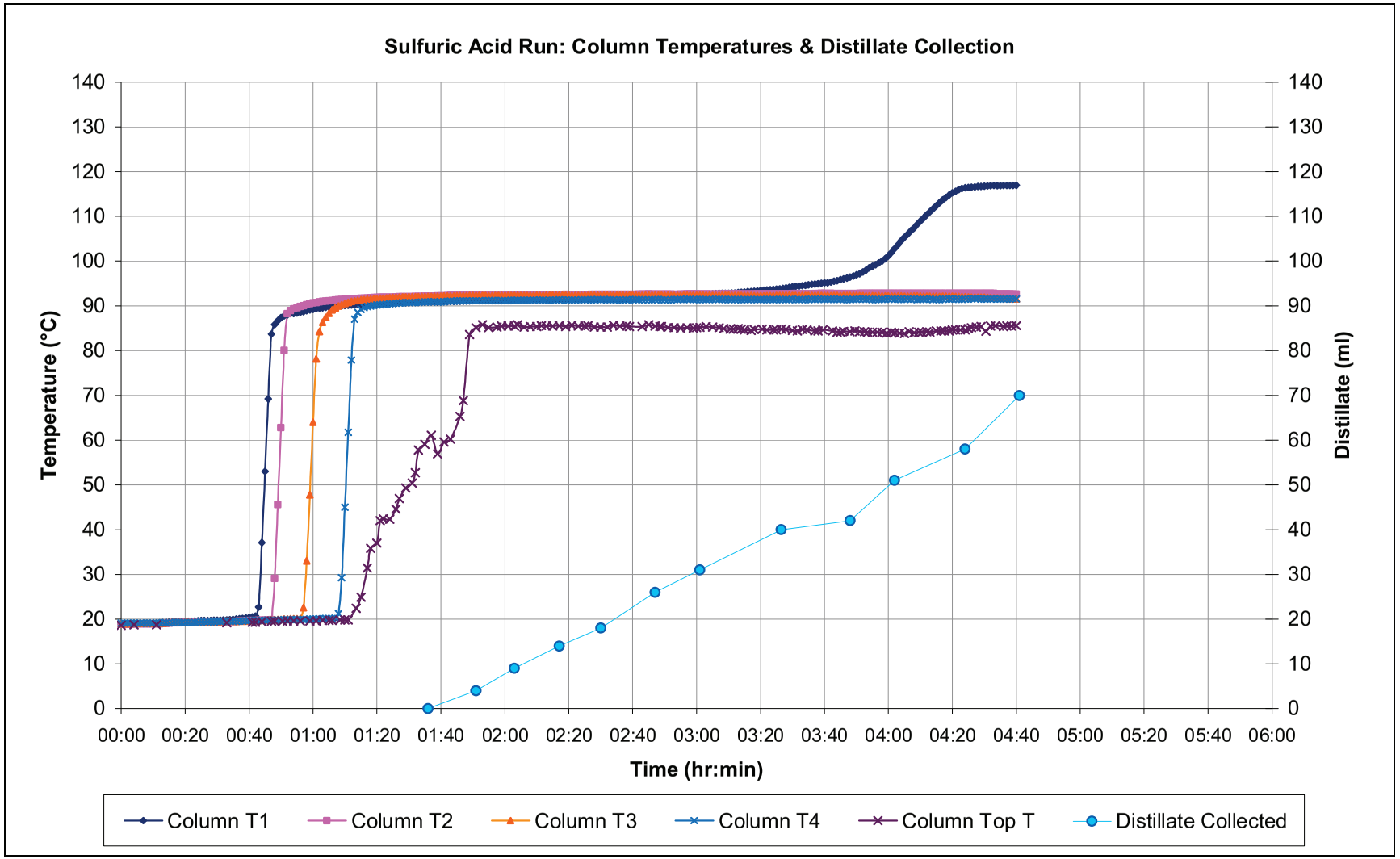

Chart J10: Nonanoic System RD Run 5 - Sulfuric Acid Catalyst – Column Data

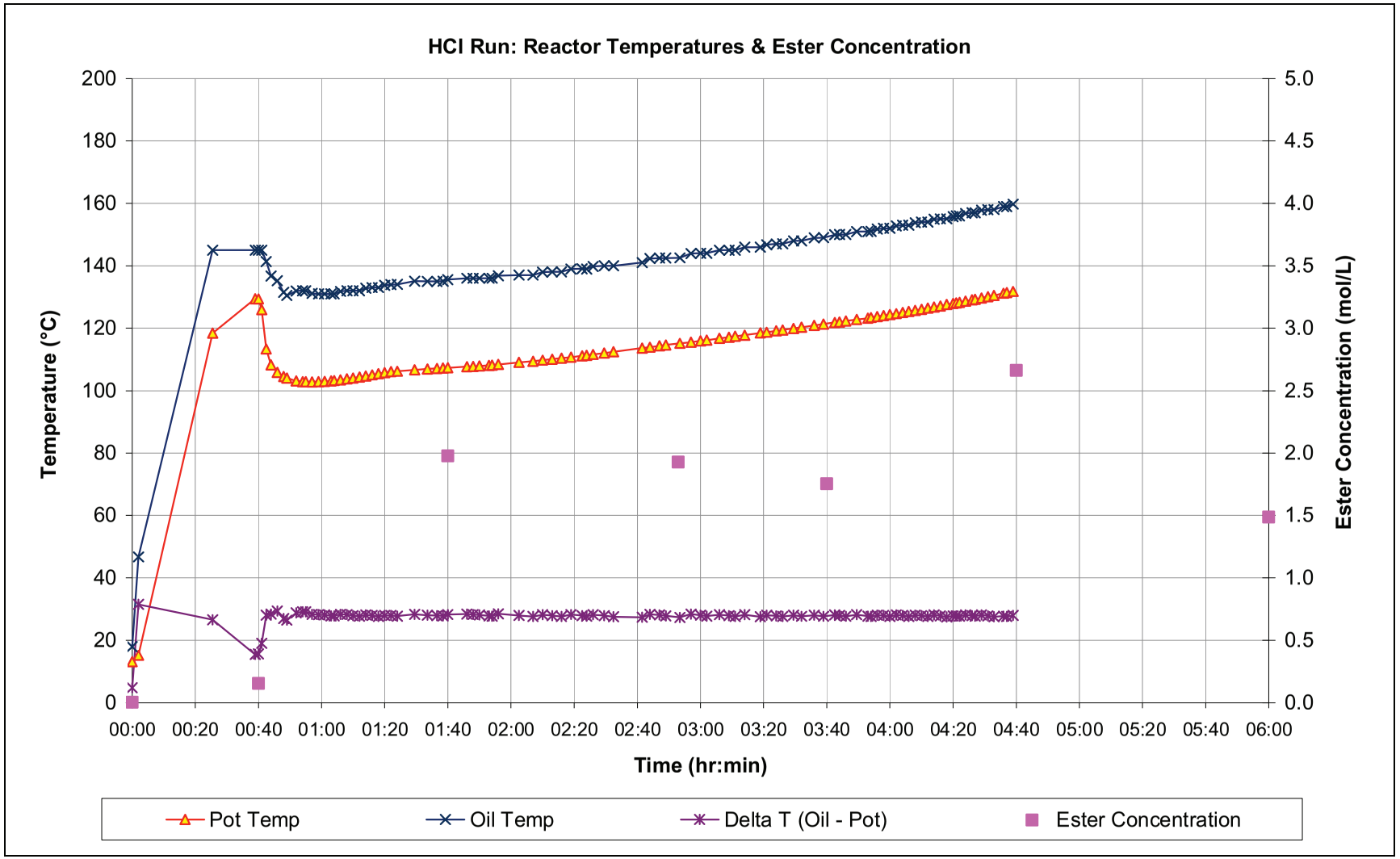

Chart J11: Nonanoic System RD Run 6 - Hydrochloric Acid Catalyst – Reactor Data

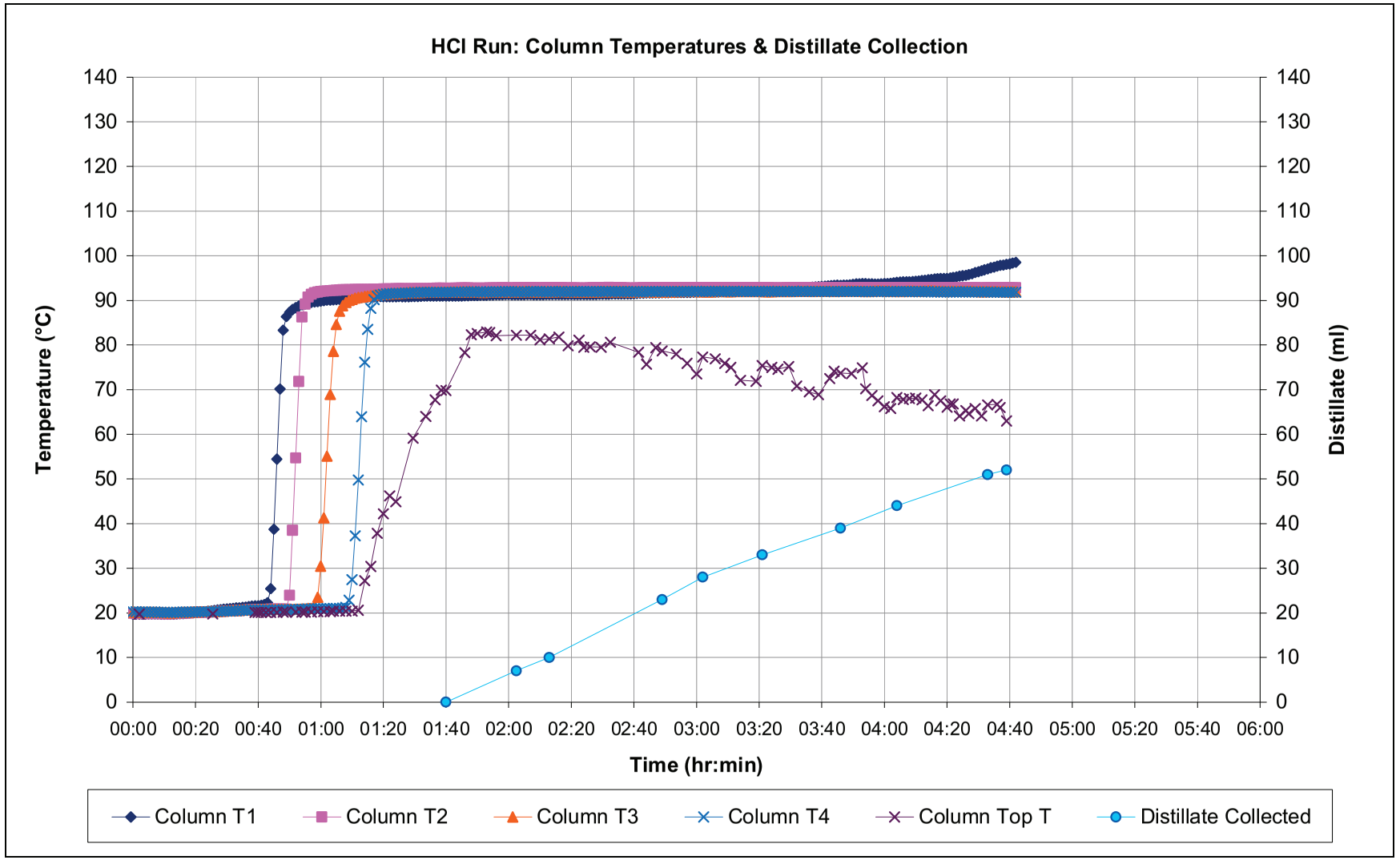

Chart J12: Nonanoic System RD Run 6 - Hydrochloric Acid Catalyst – Column Data

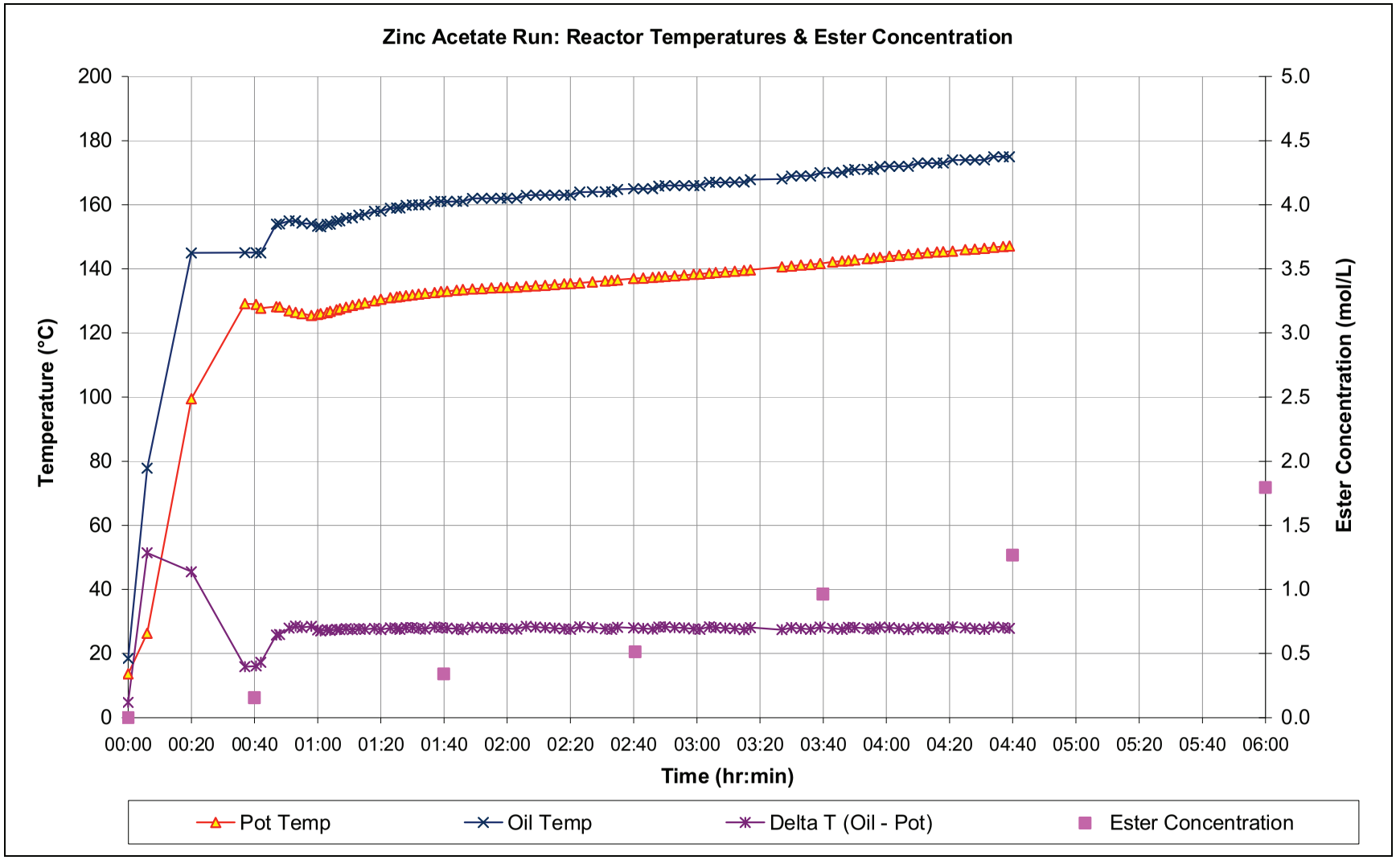

Chart J13: Nonanoic System RD Run 7 - Zinc Acetate Catalyst – Reactor Data

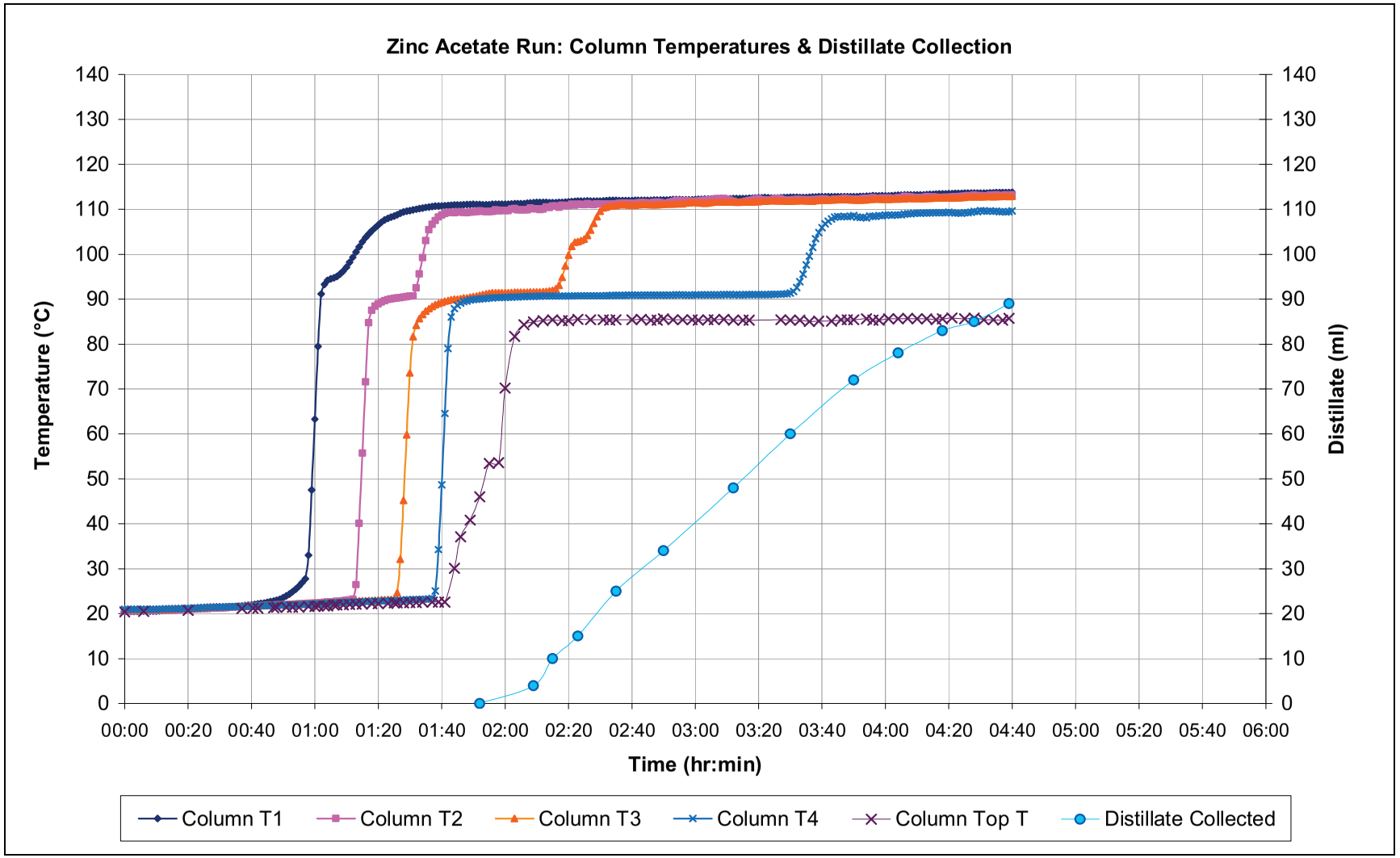

Chart J14: Nonanoic System RD Run 7 - Zinc Acetate Catalyst – Column Data

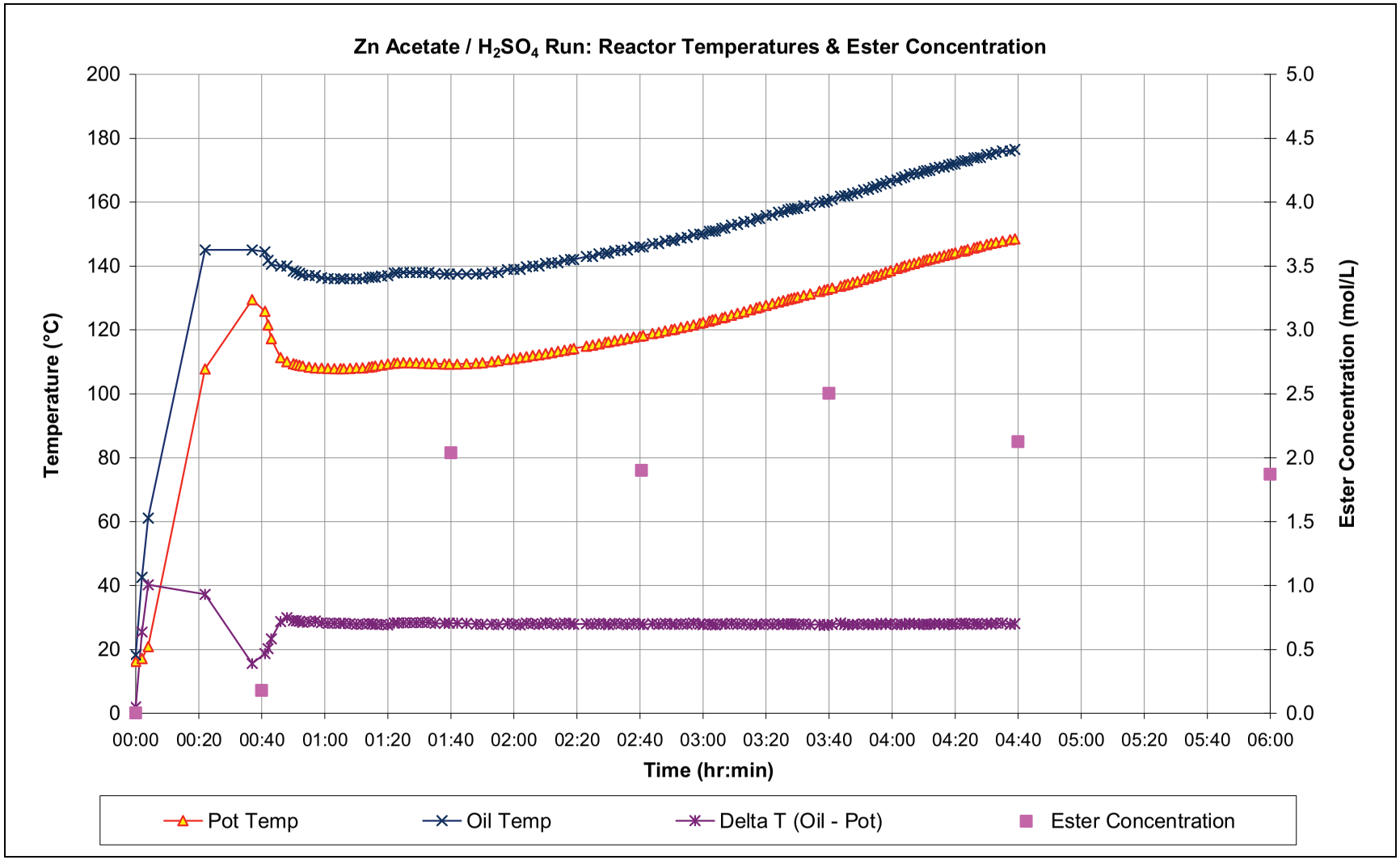

Chart J15: Nonanoic System RD Run 8 - Zinc Acetate / Sulfuric Acid Catalyst – Reactor Data

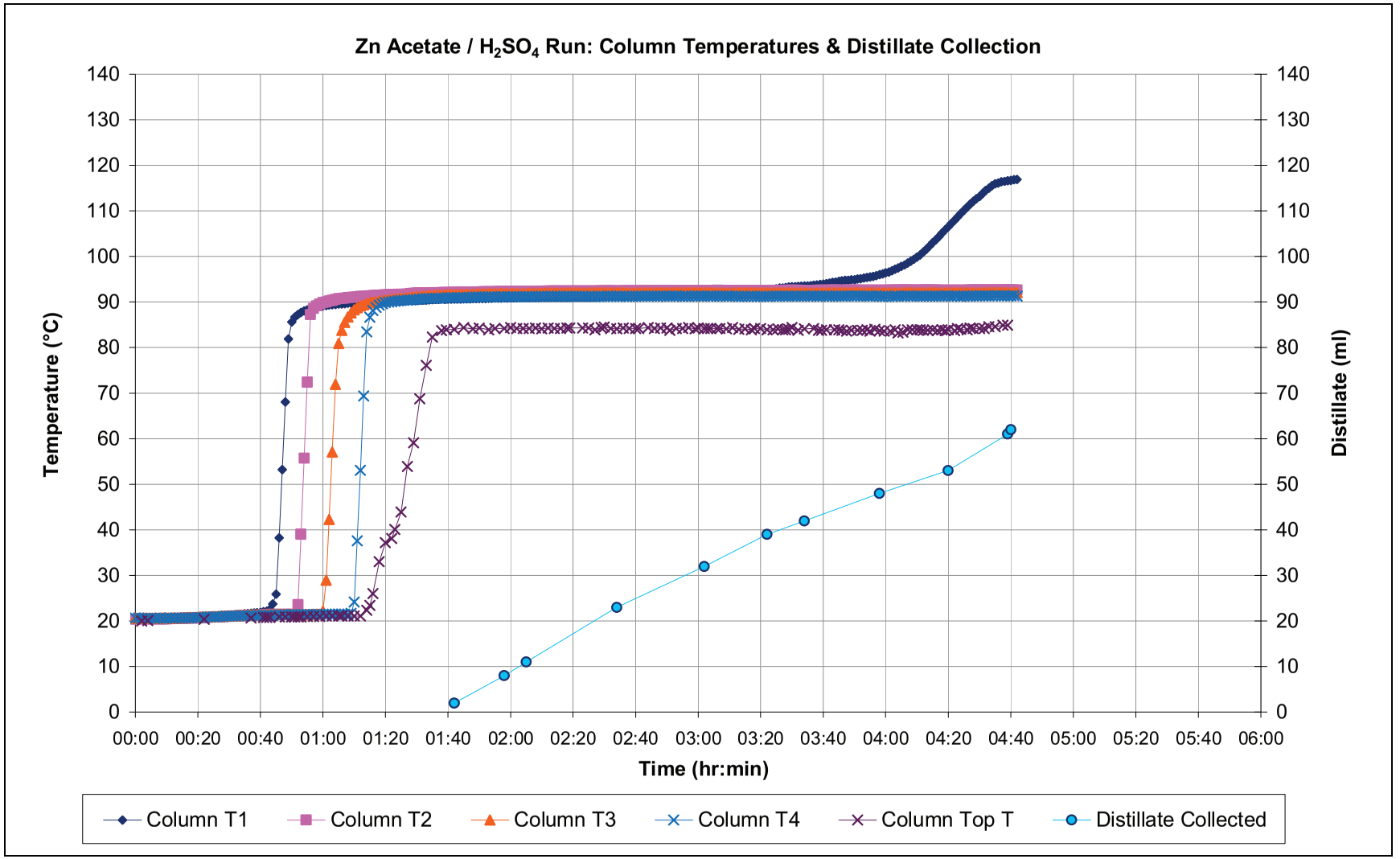

Chart J16: Nonanoic System RD Run 8 - Zinc Acetate / Sulfuric Acid Catalyst – Column Data

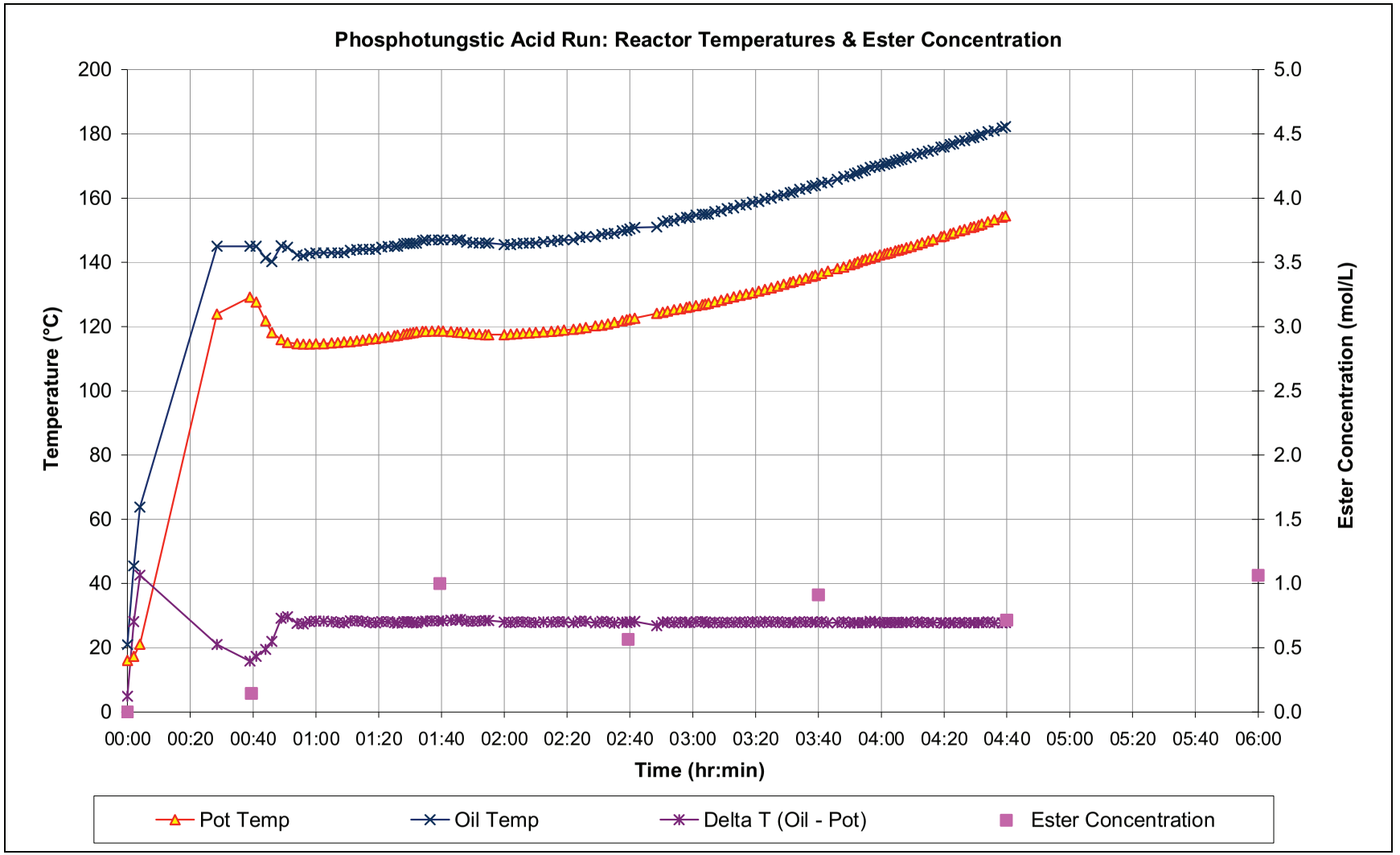

Chart J17: Nonanoic System RD Run 9 - Phosphotungstic Acid Catalyst – Reactor Data

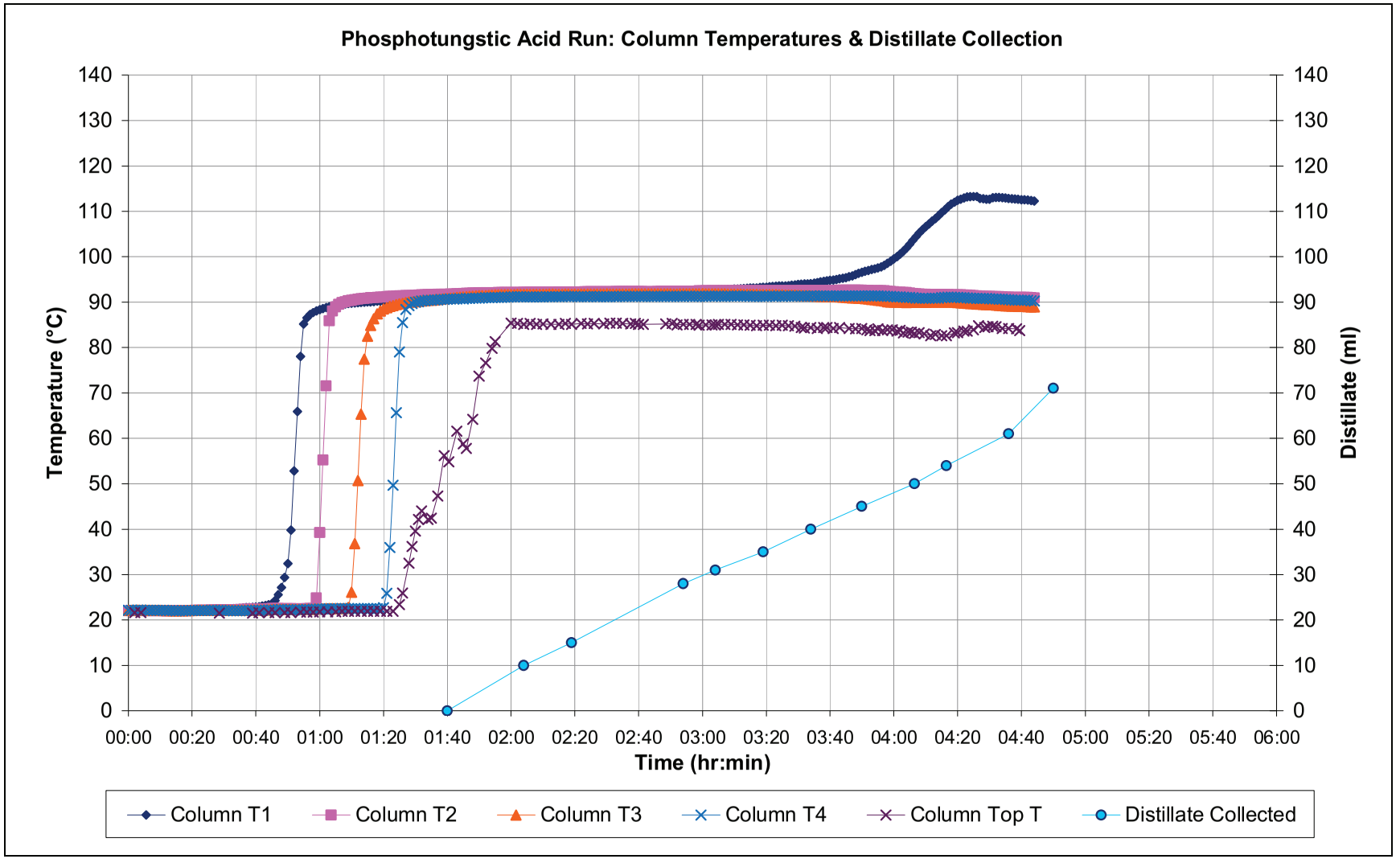

Chart J18: Nonanoic System RD Run 9 - Phosphotungstic Acid Catalyst – Column Data

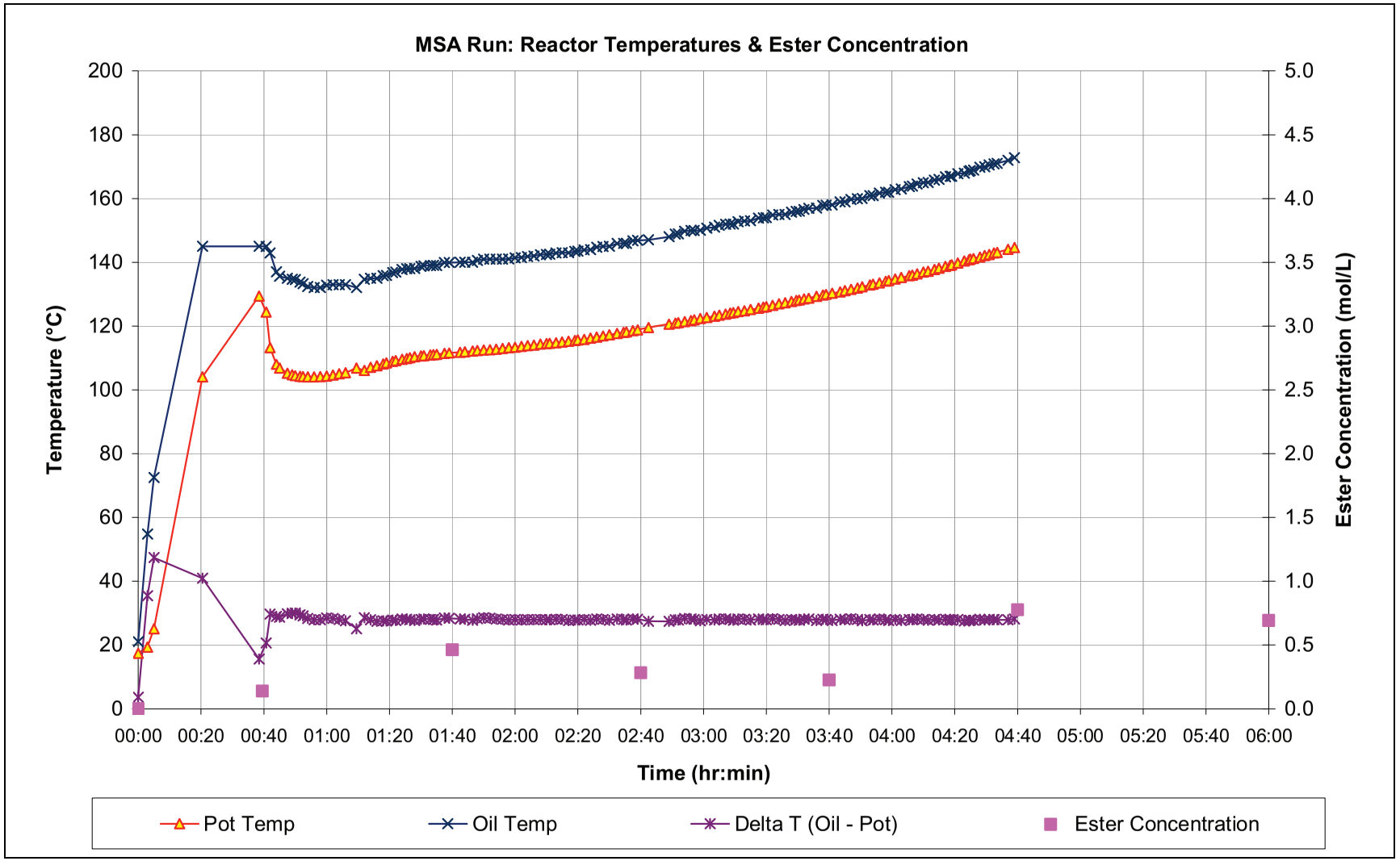

Chart J19: Nonanoic System RD Run 10 - MSA Catalyst – Reactor Data

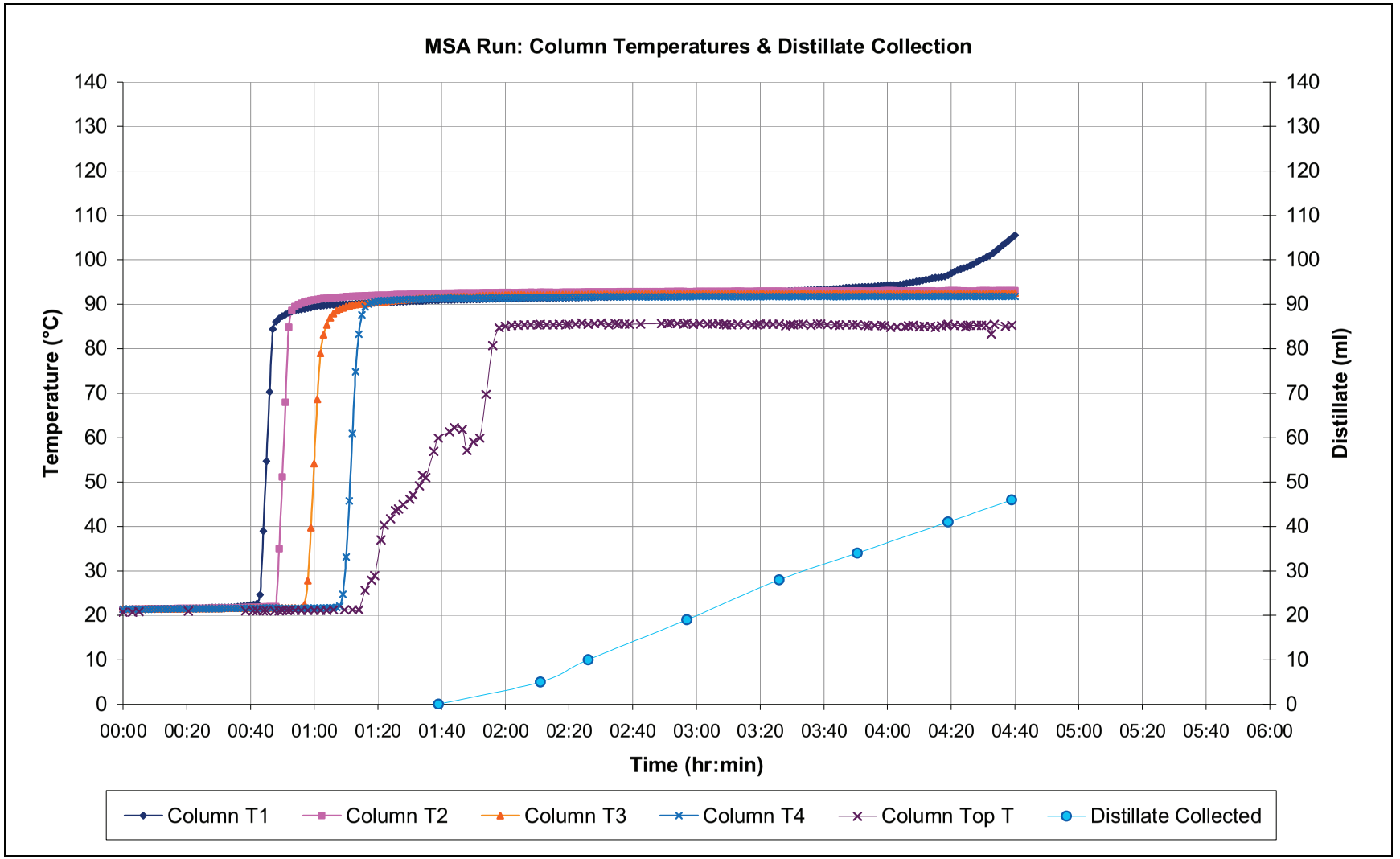

Chart J20: Nonanoic System RD Run 10 - MSA Catalyst – Column Data

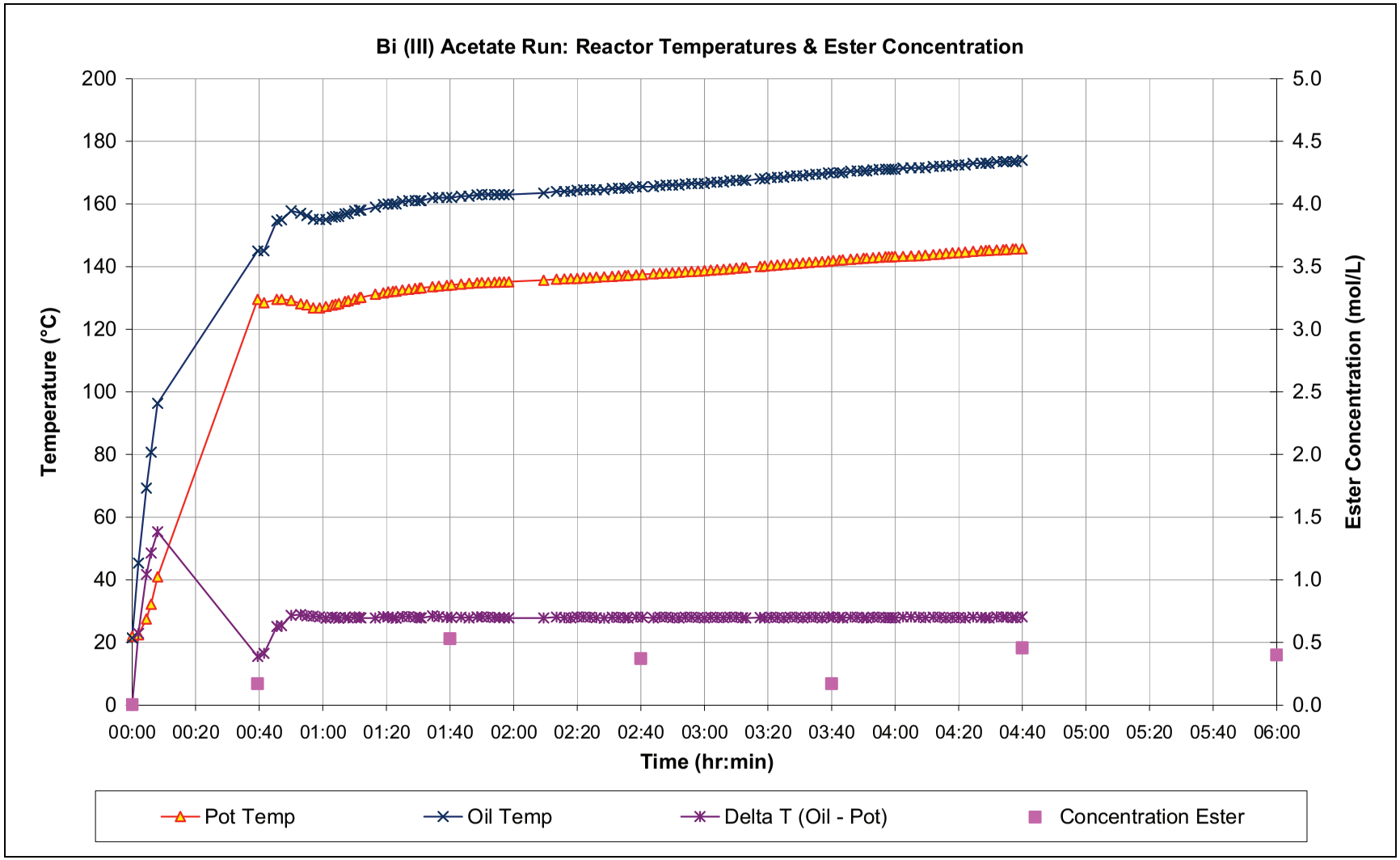

Chart J21: Nonanoic System RD Run 11 - Bismuth Acetate Catalyst – Reactor Data

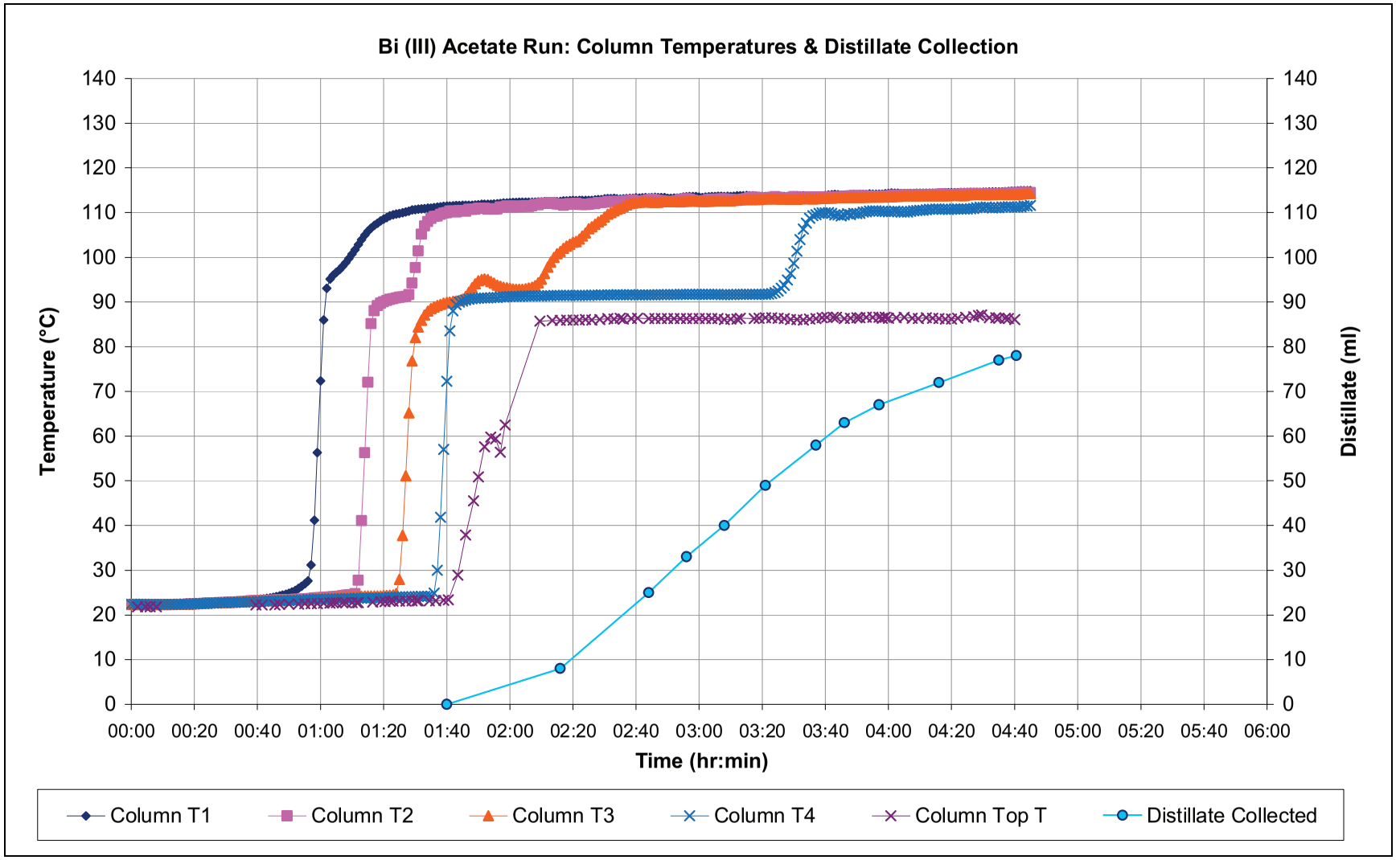

Chart J22: Nonanoic System RD Run 11 - Bismuth Acetate Catalyst – Column Data

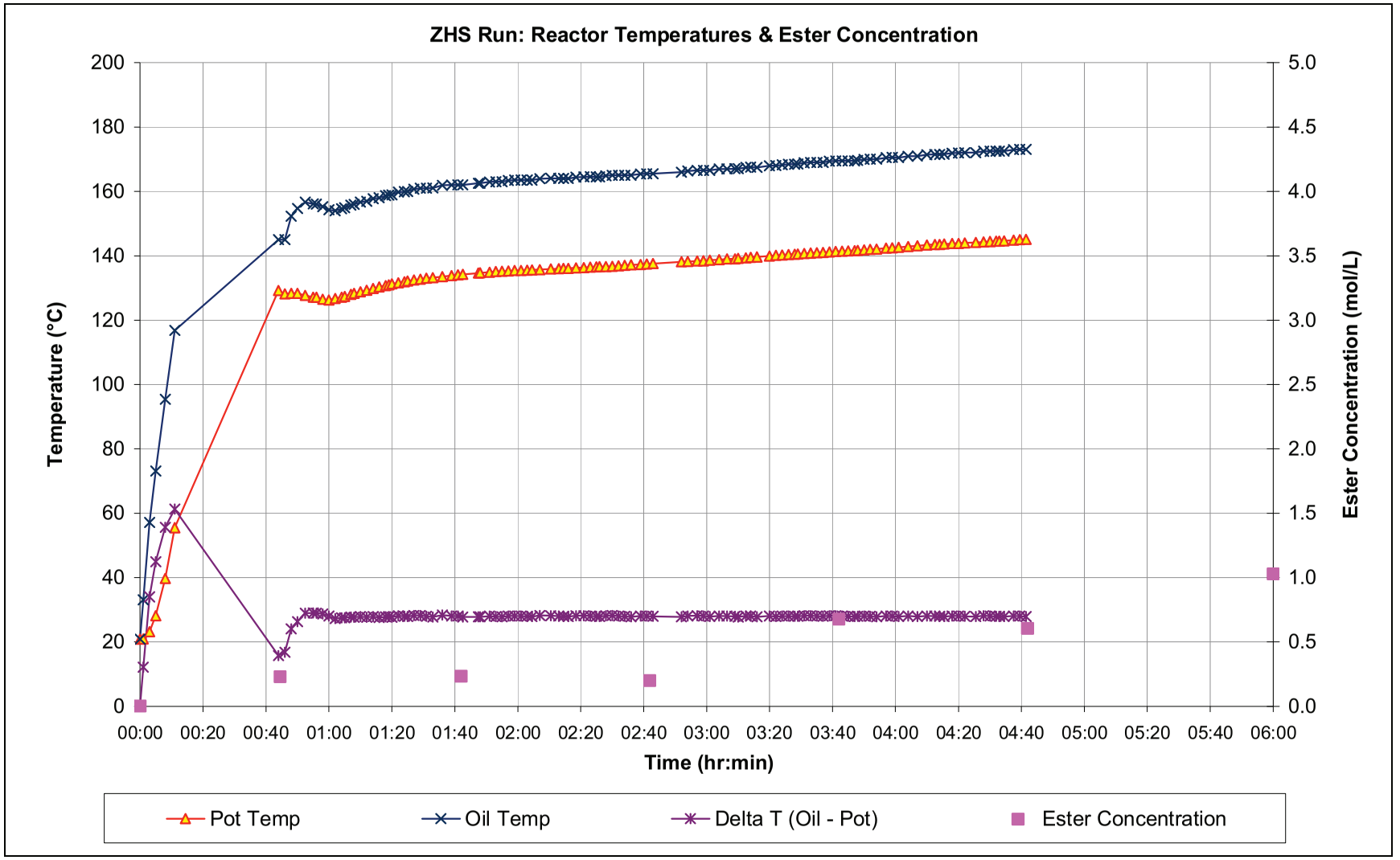

Chart J23: Nonanoic System RD Run 12 - Sulfated Zirconium Hydroxide Catalyst – Reactor Data

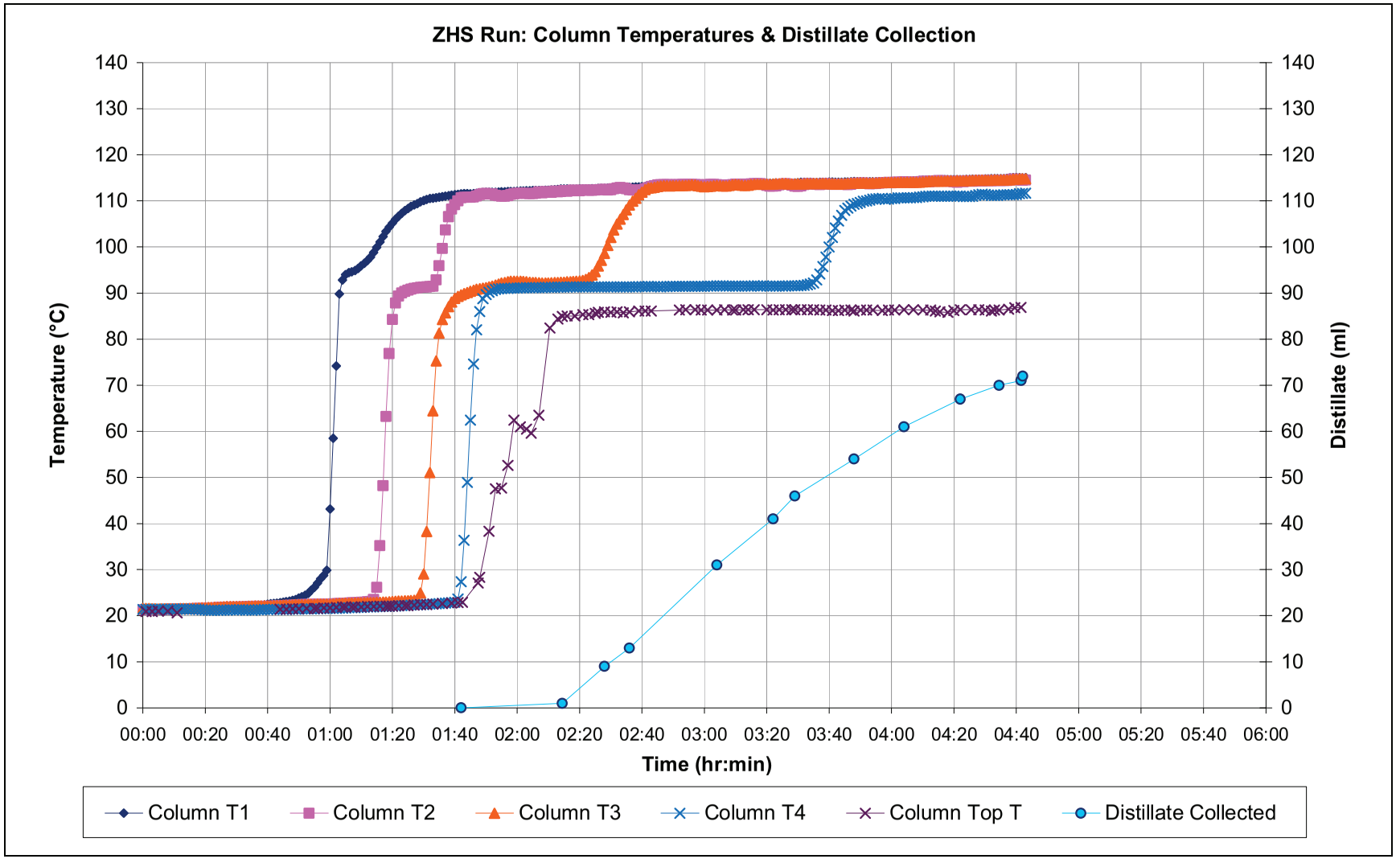

Chart J24: Nonanoic System RD Run 12 - Sulfated Zirconium Hydroxide Catalyst – Column Data

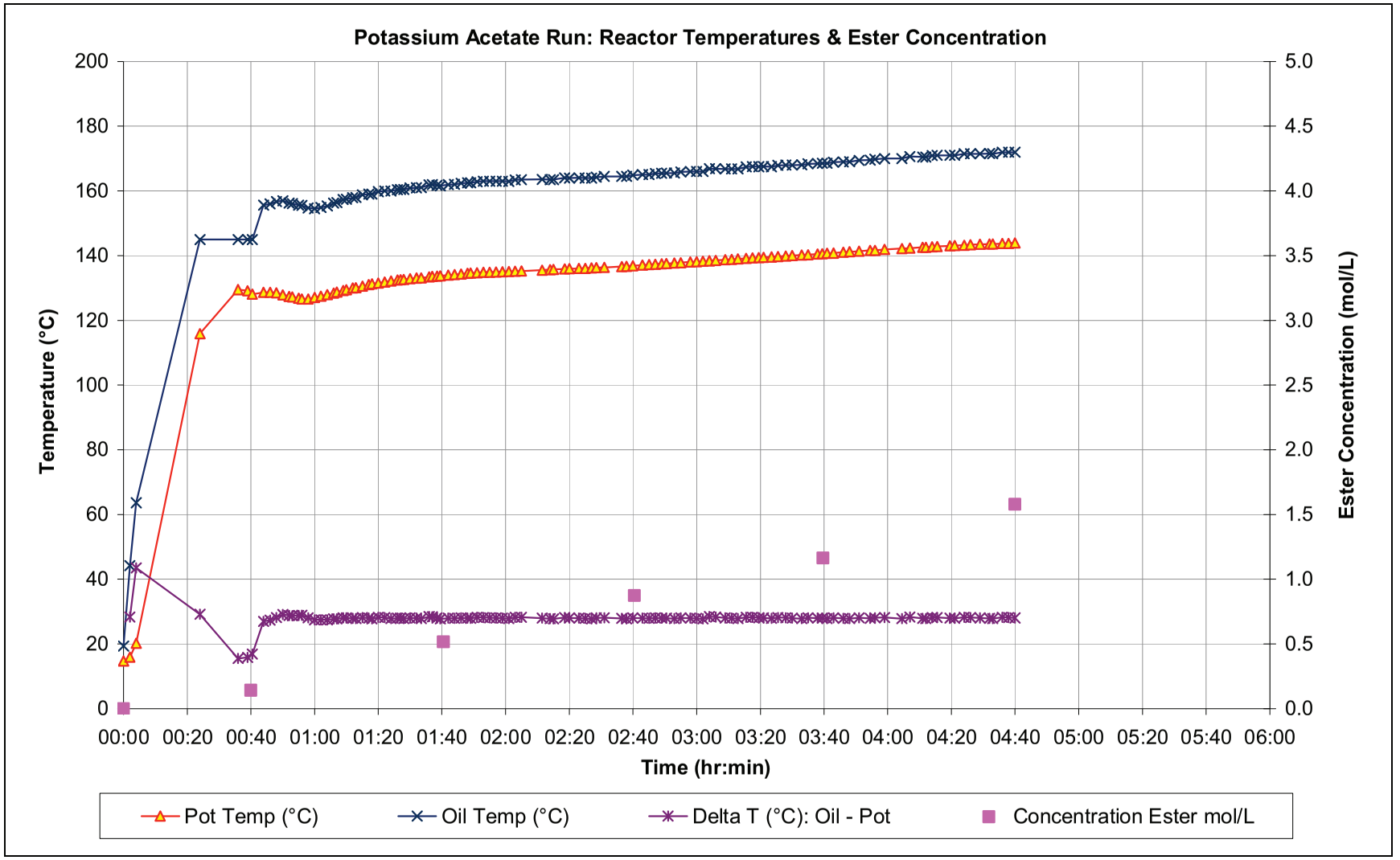

Chart J25: Nonanoic System RD Run 13 - Potassium Acetate Catalyst – Reactor Data

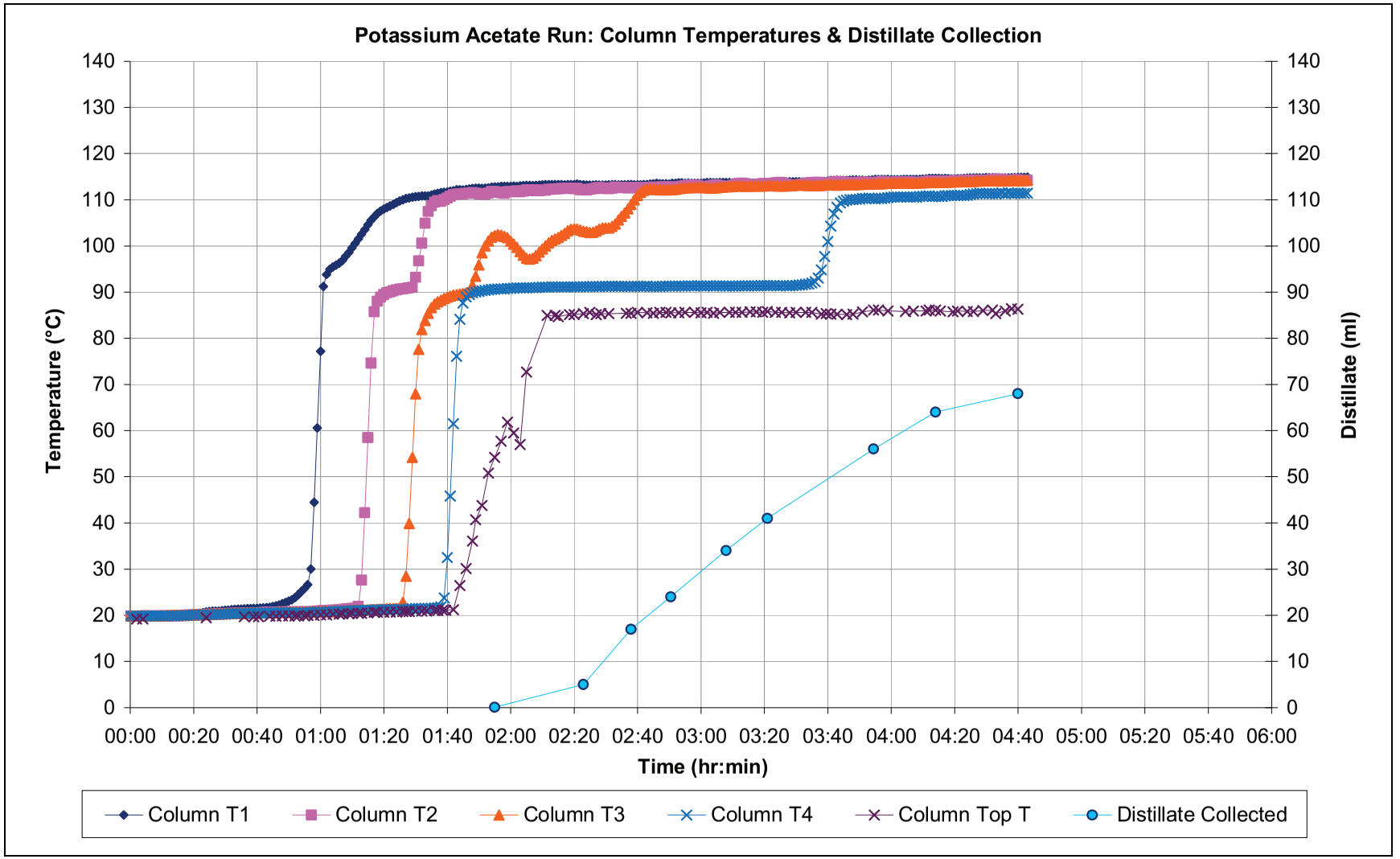

Chart J26: Nonanoic System RD Run 13 - Potassium Acetate Catalyst – Column Data

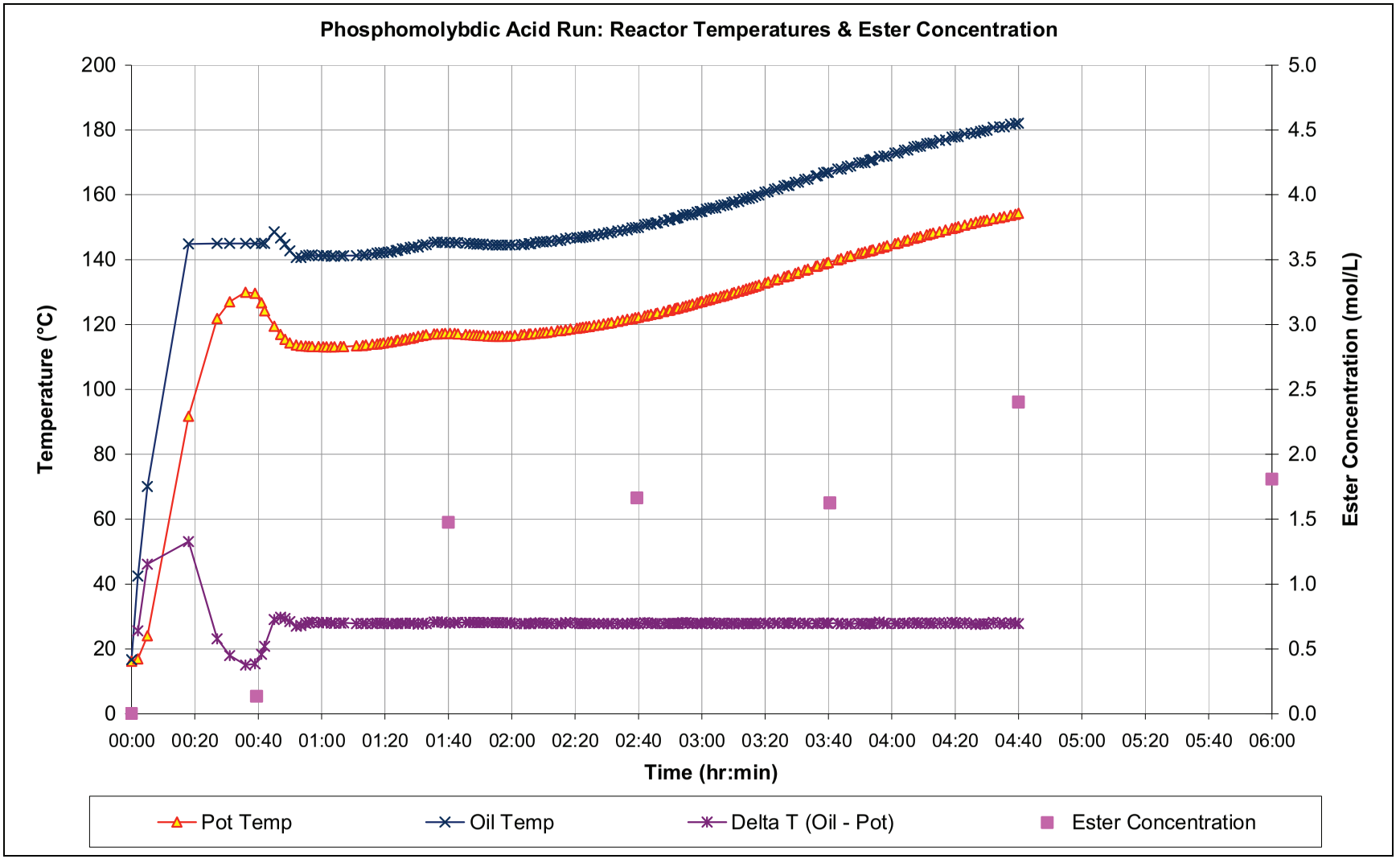

Chart J27: Nonanoic System RD Run 14 - Phosphomolybdic Acid Catalyst – Reactor Data

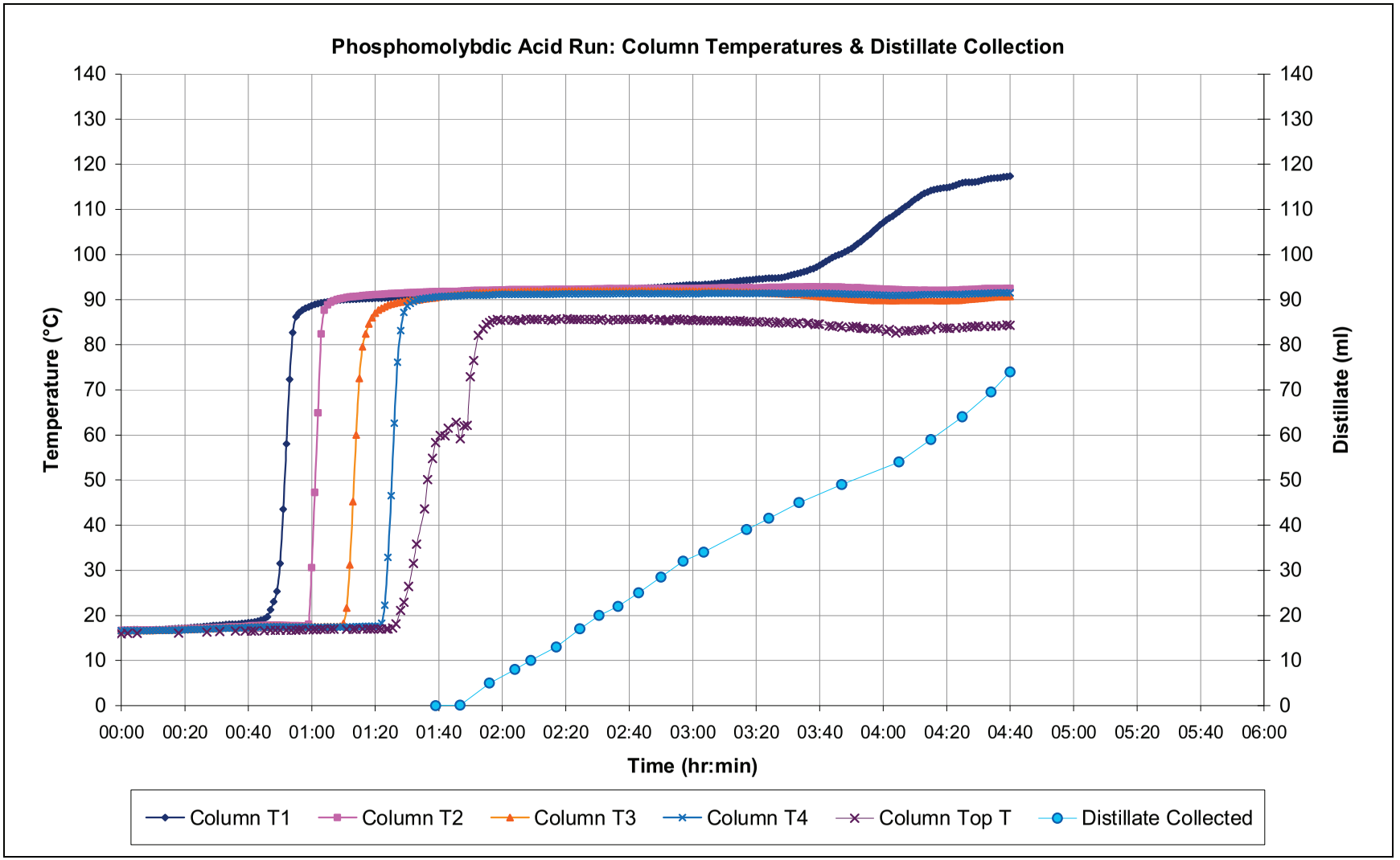

Chart J28: Nonanoic System RD Run 14 - Phosphomolybdic Acid Catalyst – Column Data

Appendix K: Propionic Acid System RD Graphs

The data from the individual runs from the reactive distillation runs with the nonanoic acid reaction system are presented in this section.

Final concentration of ester in the pot after the column has cooled and hold up from the column has returned. For demonstration purposes, this is displayed as a data point at the 6 hour mark, although this is not the time point when this occurred.

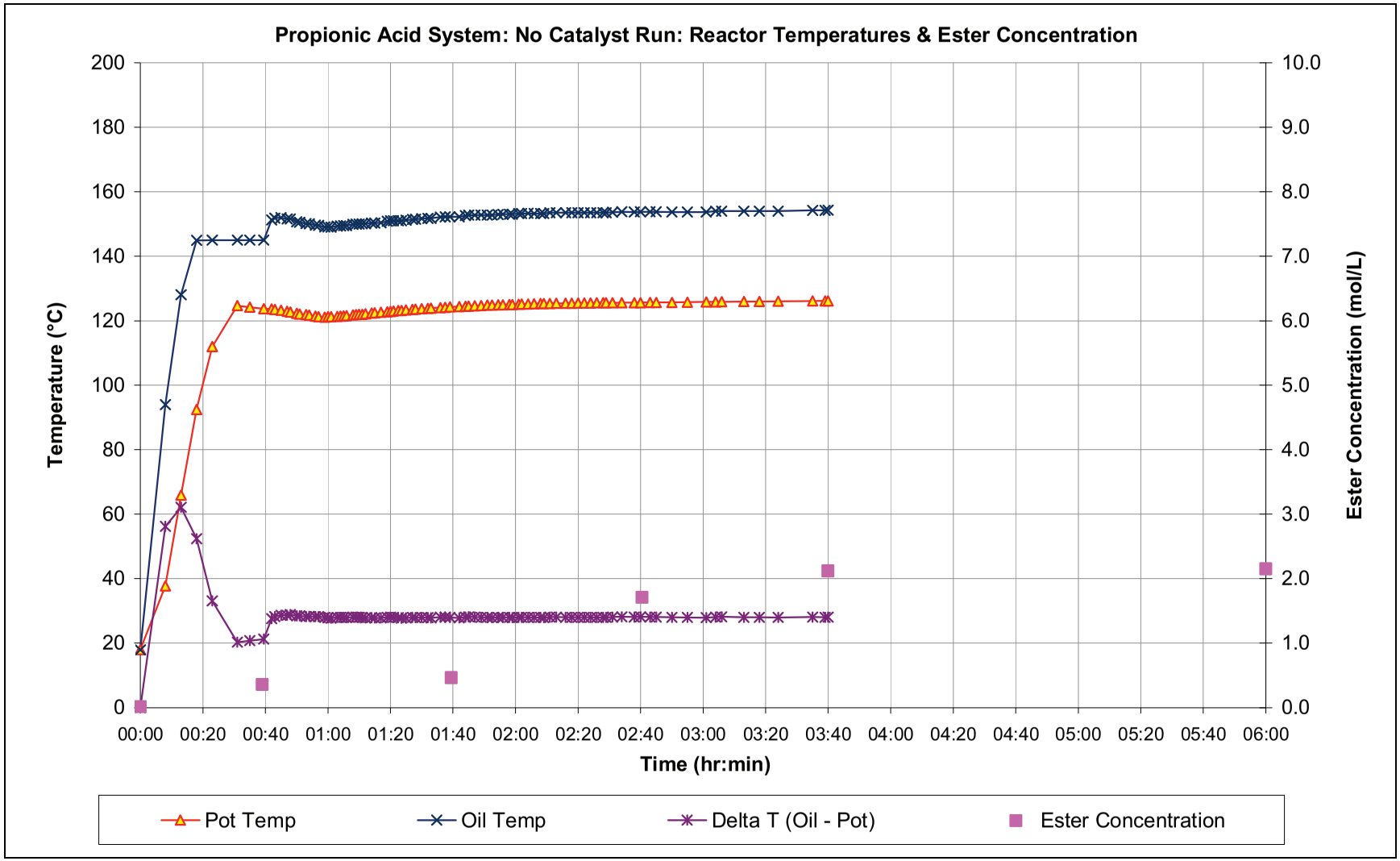

Chart K1: Propionic System RD Run No Catalyst – Reactor Data

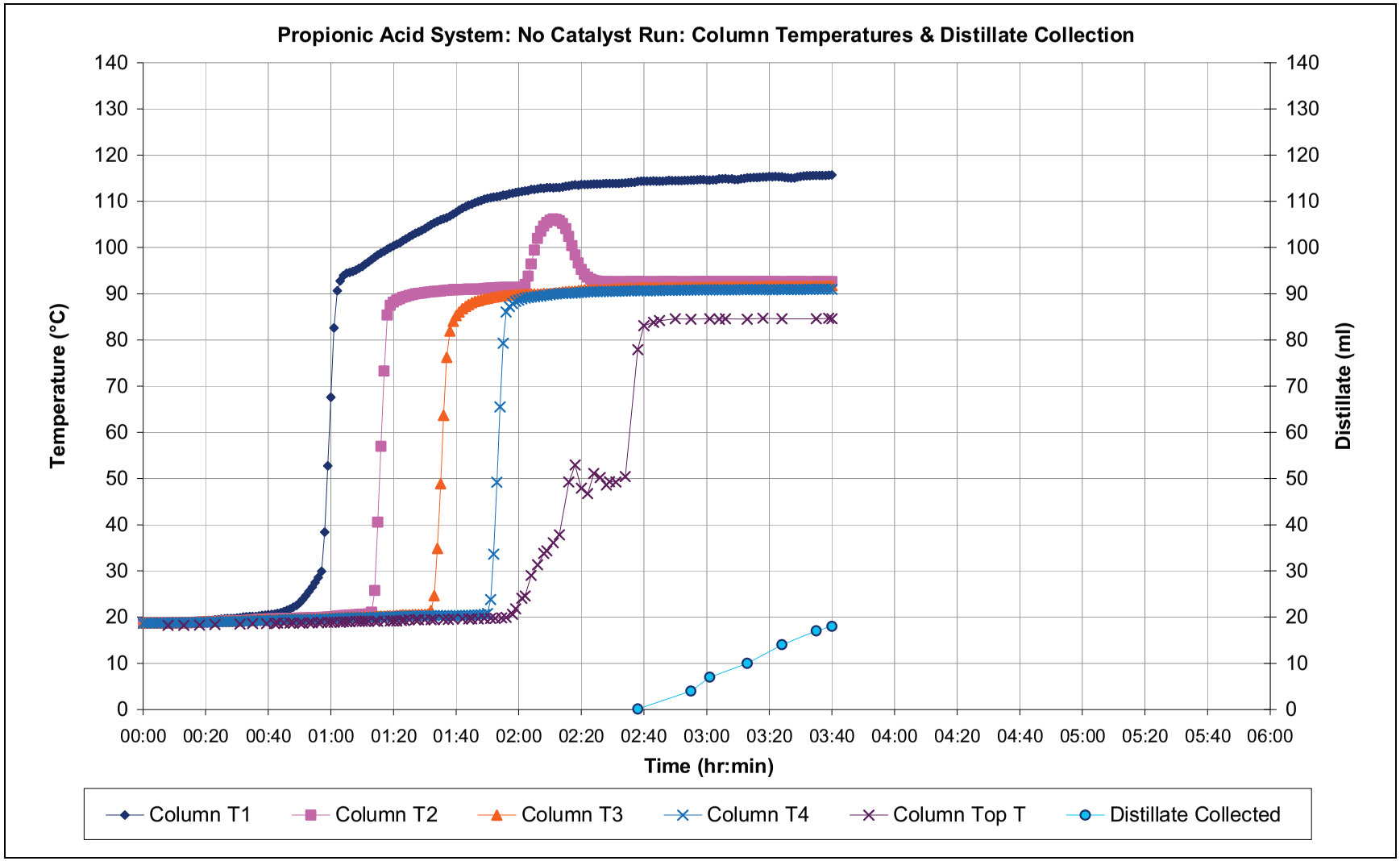

Chart K2: Propionic System RD Run No Catalyst – Column Data

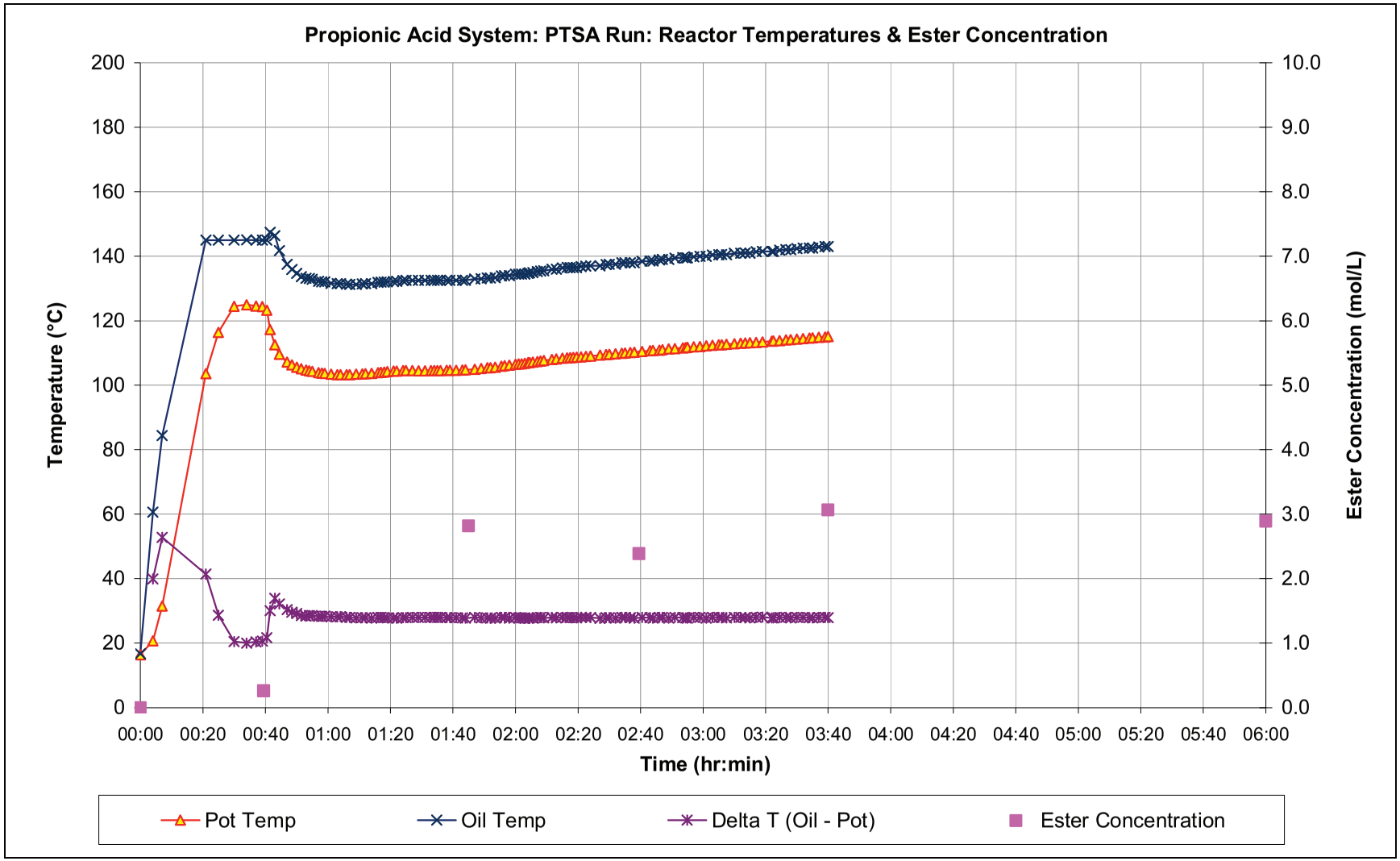

Chart K3: Propionic System RD Run PTSA Catalyst – Reactor Data

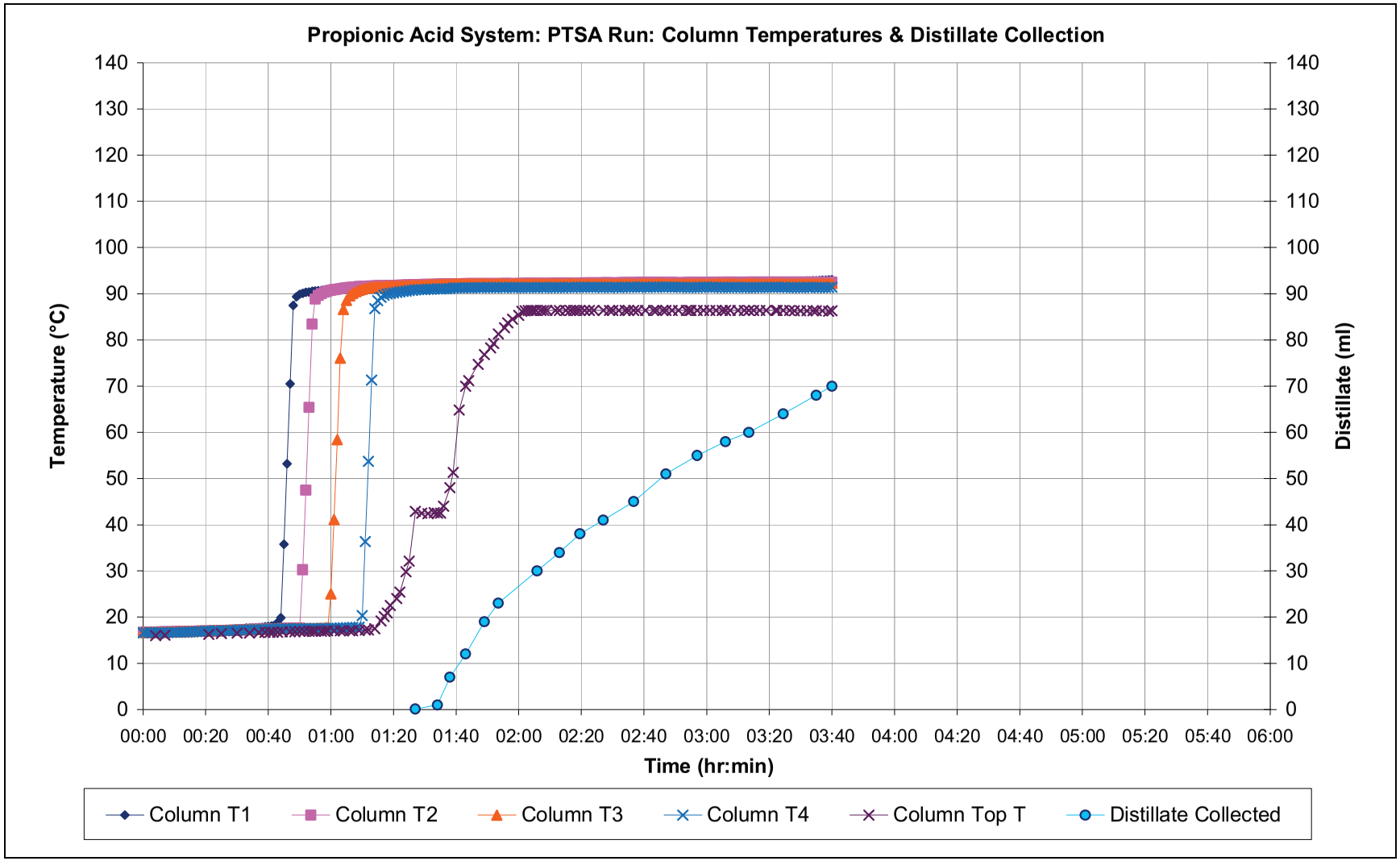

Chart K4: Propionic System RD Run PTSA Catalyst – Column Data

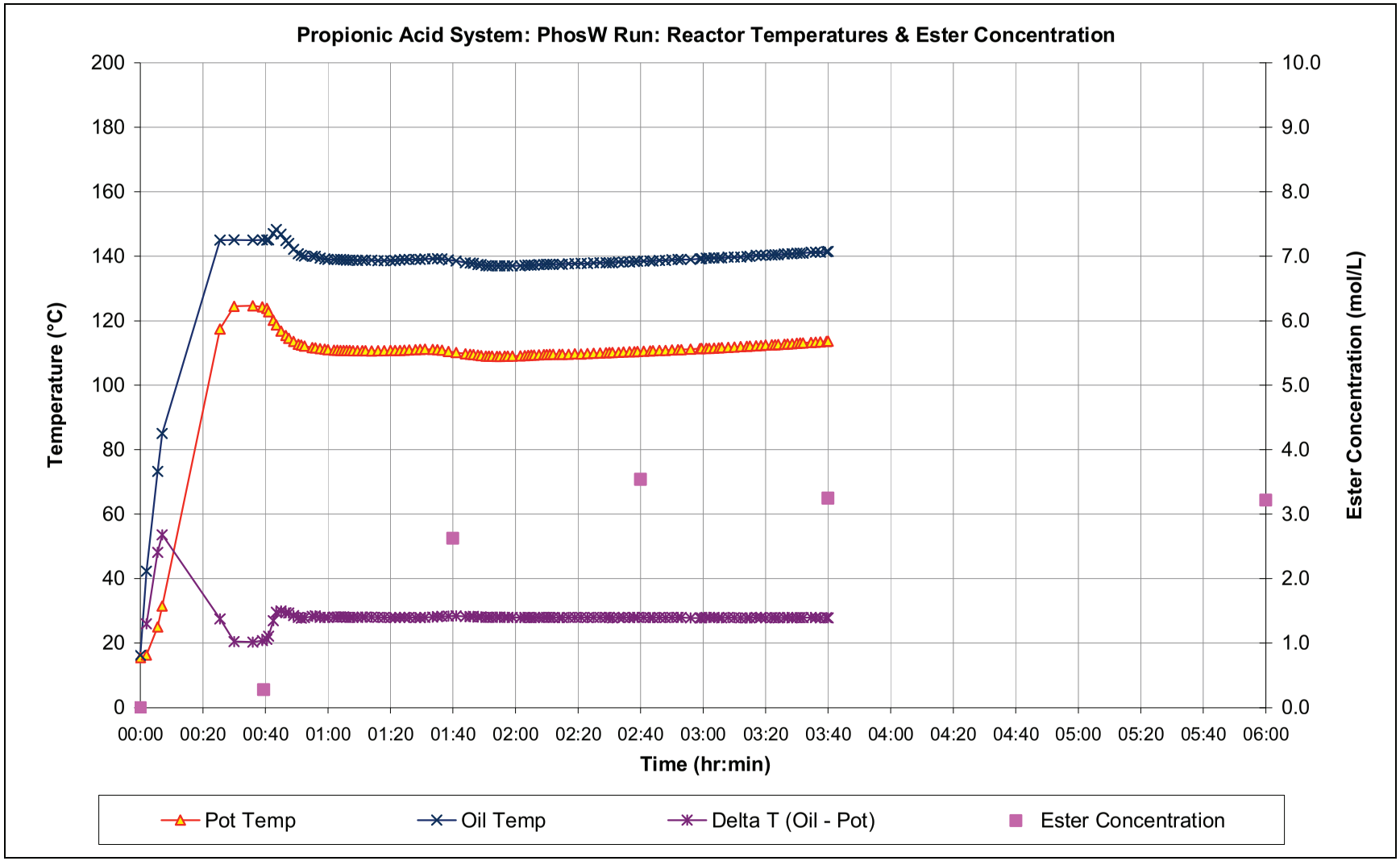

Chart K5: Propionic System RD Run PhosW Catalyst – Reactor Data

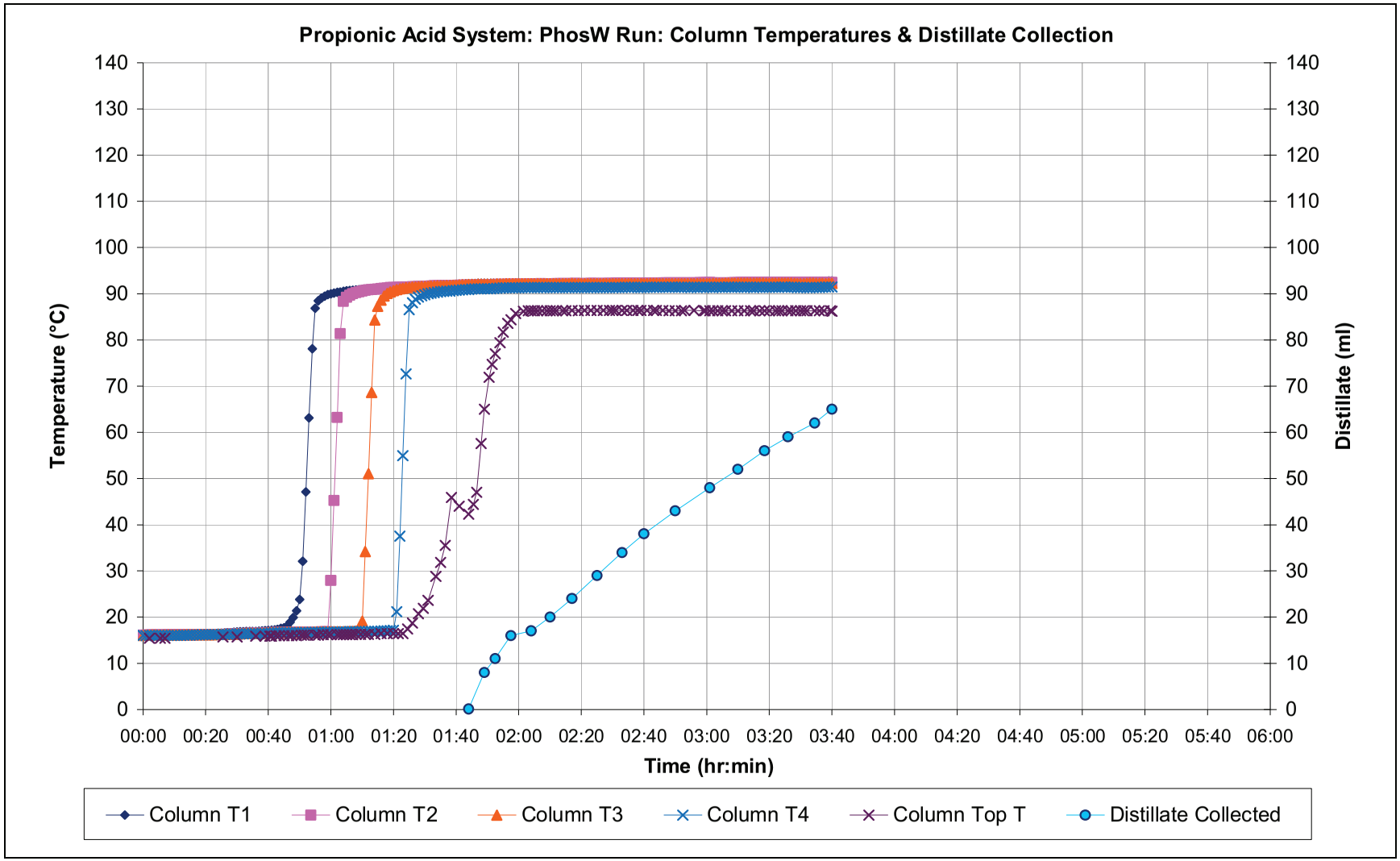

Chart K6: Propionic System RD Run PhosW Catalyst – Column Data

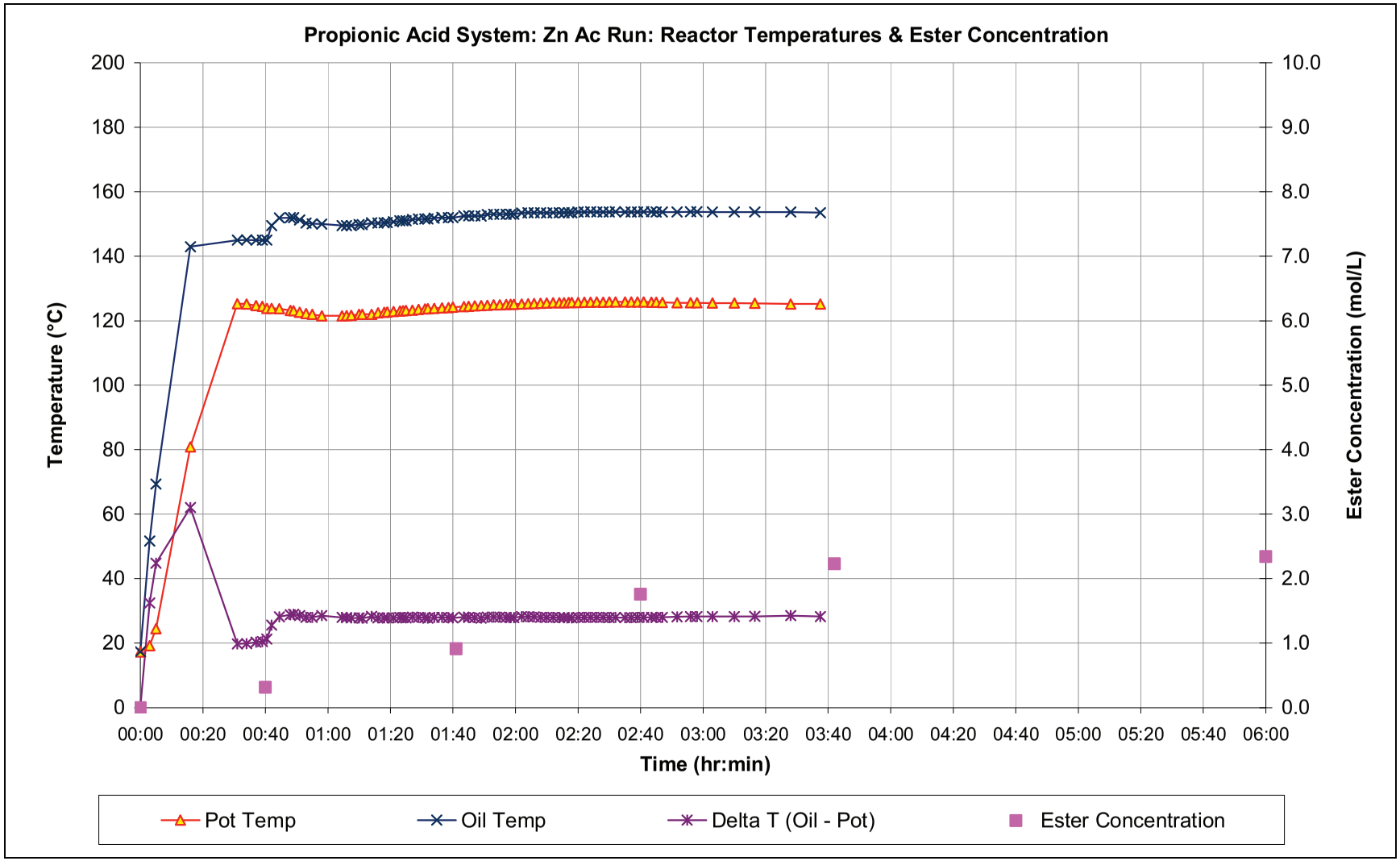

Chart K7: Propionic System RD Run Zn Ac Catalyst – Reactor Data

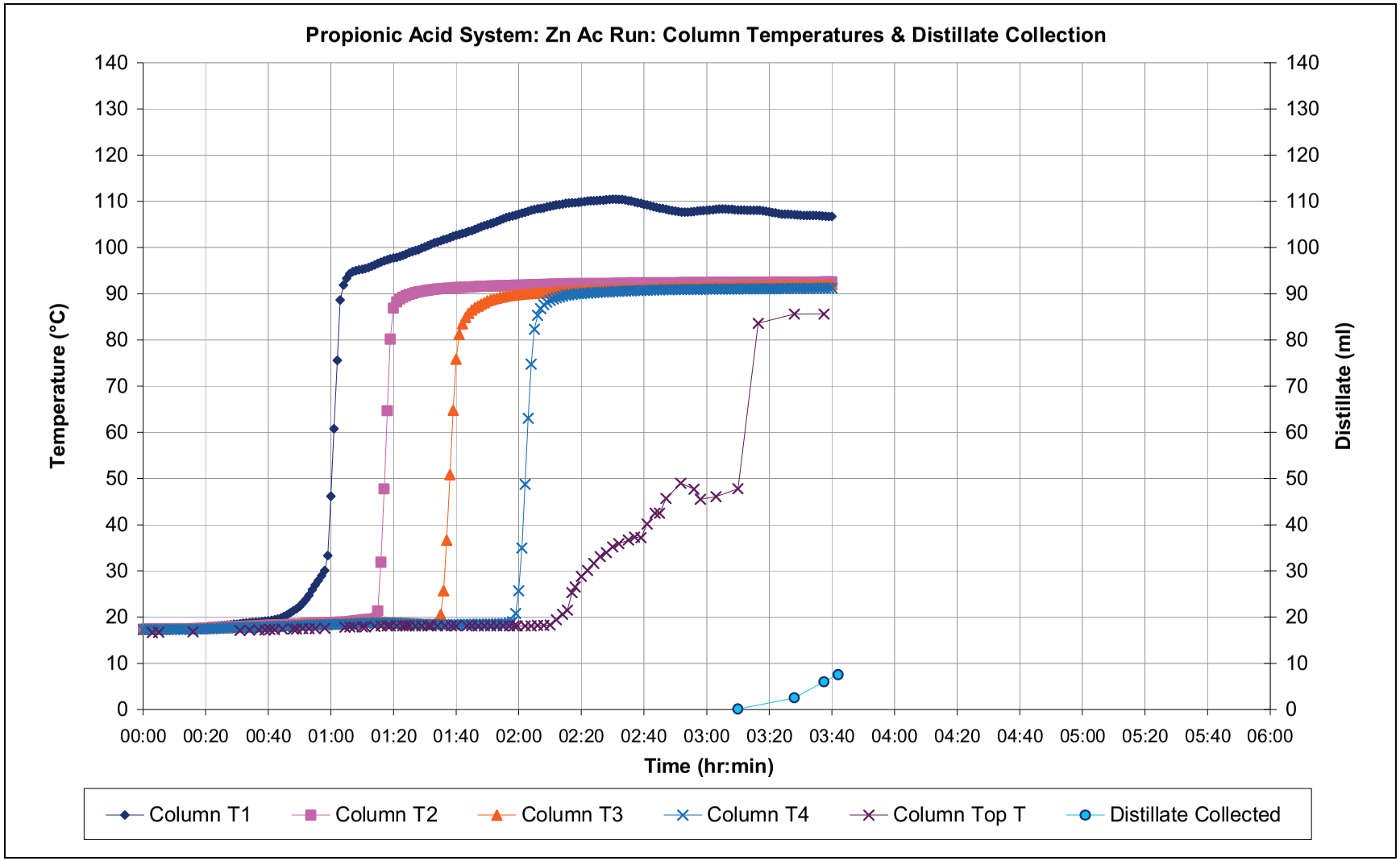

Chart K8: Propionic System RD Run Zn Ac Catalyst – Column Data

Appendix L: PT100 Probe Comparisons

Time (hh:mm:ss)	T1 (°C)	T2 (°C)	T3 (°C)	T4 (°C)
03:00:00	99.85	100.18	100.01	99.12
03:01:00	99.85	100.16	100.01	99.10
03:02:00	99.85	100.16	100.01	99.03
03:03:00	99.83	100.16	100.01	99.05
03:04:00	99.83	100.16	100.03	99.08
03:05:00	99.85	100.20	100.01	99.10
03:06:00	99.85	100.18	100.01	99.17
03:07:00	99.85	100.20	100.01	99.17
03:08:00	99.87	100.20	100.01	99.15
03:09:00	99.87	100.16	100.03	99.14
03:10:00	99.88	100.16	100.03	99.14
03:11:00	99.88	100.15	100.02	99.14
03:12:00	99.88	100.18	100.02	99.14
03:13:00	99.88	100.22	100.02	99.14
03:14:00	99.87	100.24	100.00	99.12
03:15:00	99.87	100.26	100.03	99.14
03:16:00	99.85	100.26	100.01	99.12
03:17:00	99.85	100.26	100.01	99.14
03:18:00	99.85	100.27	100.01	99.15
03:19:00	99.85	100.26	100.01	99.15
03:20:00	99.85	100.24	100.01	99.15
03:21:00	99.85	100.22	100.01	99.15
03:22:00	99.85	100.22	99.99	99.14
03:23:00	99.85	100.24	99.99	99.14
03:24:00	99.85	100.26	99.99	99.14
03:25:00	99.85	100.26	99.99	99.14
03:26:00	99.83	100.26	100.03	99.15
03:27:00	99.85	100.22	100.01	99.17
03:28:00	99.87	100.18	100.01	99.17
03:29:00	99.87	100.20	100.03	99.12
03:30:00	99.85	100.18	100.01	99.10
03:31:00	99.87	100.20	100.01	99.08
03:32:00	99.87	100.22	99.99	99.08
03:33:00	99.87	100.18	100.01	99.14
03:34:00	99.88	100.20	100.01	99.14
03:35:00	99.85	100.18	100.03	99.14
03:36:00	99.85	100.20	100.03	99.14
03:37:00	99.85	100.22	100.01	99.14
03:38:00	99.85	100.22	100.01	99.14
03:39:00	99.85	100.26	100.01	99.15
03:40:00	99.85	100.24	100.01	99.14
03:41:00	99.83	100.24	100.01	99.14
03:42:00	99.83	100.22	100.01	99.12
03:43:00	99.83	100.20	100.01	99.14
03:44:00	99.81	100.22	99.99	99.14
03:45:00	99.81	100.22	100.01	99.14
03:46:00	99.83	100.24	100.01	99.14
03:47:00	99.83	100.24	99.99	99.12
03:48:00	99.85	100.22	100.01	99.14
03:49:00	99.85	100.22	99.99	99.12
03:50:00	99.87	100.24	100.01	99.14
03:51:00	99.88	100.24	100.01	99.15
03:52:00	99.87	100.26	100.01	99.14
03:53:00	99.85	100.26	100.01	99.14
03:54:00	99.85	100.22	99.99	99.14
03:55:00	99.83	100.22	99.99	99.14
03:56:00	99.83	100.22	100.01	99.14
03:57:00	99.83	100.18	100.01	99.17
03:58:00	99.81	100.16	100.03	99.17
03:59:00	99.79	100.18	100.00	99.15
04:00:00	99.81	100.18	100.03	99.15

Table L1: Temperature Probe Data from Vapour Rate Test 3

The temperature data in Table L1 is from all four PT100 probes in the column which record data automatically (at positions T1, to T4) over an hour long period during

vapour rate test 3. This vapour rate test involved the boiling of water with the highest oil temperature tested, 145°C, so that water vapour moved up the column with a high driving force. The time interval chosen represents an extended period during which the temperatures were steady. The purpose of looking at this data is to compare the readings obtained with each PT100 when they would be expected to be the same, at 100°C.

The average temperatures over the hour-long period, for each temperature probe are shown in Table L2.

T1 (°C)	T2 (°C)	T3 (°C)	T4 (°C)
99.85	100.21	100.01	99.13

Table L2: Average Temperature Probe Data from Vapour Rate Test 3

Average of all four temperature probes over this time interval: 99.80°C

The average temperatures from each of the four temperature probes fall within +/- 0.7% of the overall average value, and are very close to the expected value of 100°C.

Appendix M: Details of the BatchCAD RD Model

Reactor/ Reboiler

1) Fluid Package Menu

- Select components
- Property package (NRTL Ideal-Estimate)
- Estimate binary coefficients
- Enter reaction stoichiometry and kinetics.

2) Phase Equilibrium Properties

- Select pressures

3) Equipment

- Reactor Heat Transfer parameters (select power input, heat loss, ambient temperature, scale resistance)
- Jacket Heat Transfer parameters (liquid type, film coefficient)
- Impeller diameter = 10cm, speed 50 to 2000 rpm. (Eurostar digital IKA)

4) Reactor Dimensions

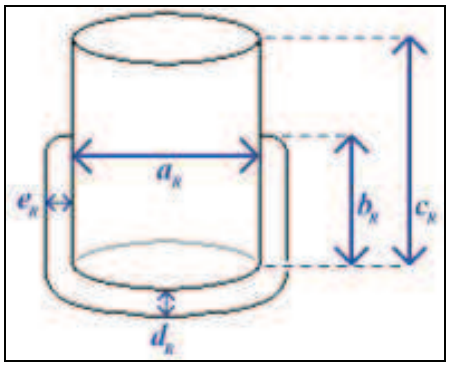

Figure M1: Sketch, not to scale.

Approximated to a flat bottomed cylinder, measured dimensions:

a_R : 14 cm

b_R : 13 cm

c_R : 30 cm

d_R : 1.5 cm

e_R : 1.5 cm

Total (max) Volume $= \pi r^2$ x height

$= \pi$ x $(14/2)^2$ x 30

= 4618 ml

= 4.618 L

The inner volume within the jacket heating area is 2L.

Heat transfer area depends upon volume:

A_{min} = Area if volume ~ 0 = Area of inner base

$= \pi r^2$

$= \pi (14/2)^2$

$= 153.9$ cm^2

A_{max} = Area inner base + area of inner cylinder when volume is at maximum 2L

$= 153.9 + (\pi$ x $\boldsymbol{b_R}$ x $\boldsymbol{a_R})$

$= 153.9 + (\pi$ x 13 x 14)

$= 725.7$ cm^2

Volume of jacket

$V_{total} = V_{cylinder} + V_{base}$

$V_{cylinder} = V_{outer} - V_{inner}$

$= [\ \pi (17/2)^2$ x 13] - [$\pi (14/2)^2$ x 13]

$= 2951 - 2001$

$= 949.5$ cm^3

$V_{base} = [\ \pi (17/2)^2$ x 1.5]

$= 340.5$ cm^2

$V_{total} = 1290$ cm^2.

Glass properties

- Thickness approx 5mm.
- Density 2225 kg/m3 (Perry & Green, 2007)
- Specific heat 0.78 kJ/kgK (Perry & Green, 2007)
- Thermal conductivity 1.1 W/mK (Perry & Green, 2007)

Recirculation fluid properties

- Capacity of Julabo heater recirculation loop 4.5L
- Dimethyl polysiloxane CAS 9016-00-6 (The Dow Chemical Company, 2003)
- Specific heat capacity Cp ~ 2 kJ/kg°C (The Dow Chemical Company, 2003)
- Density 800 kg/m3 at 60°C (The Dow Chemical Company, 2003)
- Heat transfer coefficient ~ 360 kJ/hm^2°C (The Dow Chemical Company, 2003)
- Thermal conductivity = 0.151 W/mK (Knovel, 2003)
- Heater power rating = 2kW (230V), max pressure 0.7 bar

Condenser

- Total condenser with pressure calculation ON
- Temperature cooling water 20˚C
- Pressure 101.25 kPa
- Damping factor 1.1

Distillation Column

- Inner diameter of column 5cm
- Column area = $\pi (5/2)^2 = 19.6$ cm^2
- Column packed length 1m

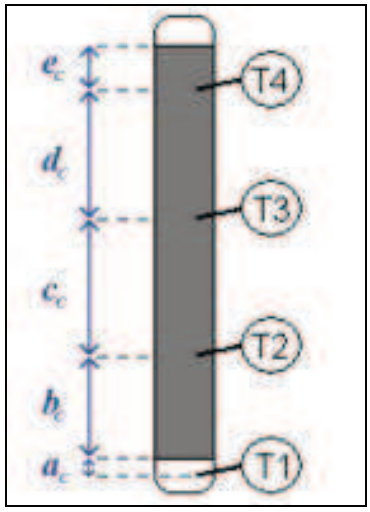

Figure M2: Sketch, not to scale.

Measured dimensions:

a_c : 3 cm

b_c : 28 cm

c_c: 30 cm

d_c : 30.5 cm

e_c : 9 cm

Thermocouple positions:

T1 = bottom of packed section: stage 1

T2 = 28.7% distance along column length from base

T3 = 59.5% distance along column length from base

T4 = 90.8% distance along column length from base

There is also a fifth thermocouple, at the top of the column near the reflux switching system. Determining the thermocouple positions as their proportional distance along the height of the column enables the selection of the relevant stage number in BatchCAD, even if number of theoretical stages is changed. Column pressure drop is negligible at atmospheric pressure.

Return stage is the top of the column, in BatchCAD entered as '-1'.
(Stages numbered from bottom to top, Reboiler / reactor = stage '0')

Appendix N: BatchCAD Simulations vs. Experimental Data for Runs with Catalyst Addition

Zinc Acetate

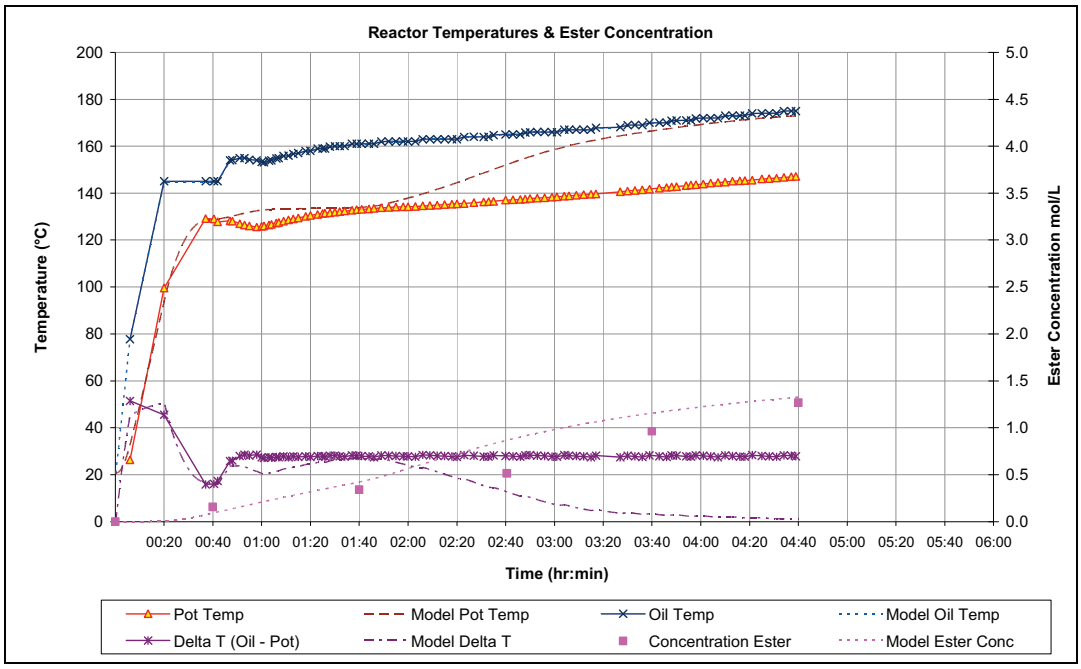

Chart N1: Real vs. BatchCAD-Simulated Reactor Profiles: RD Esterification: ZnAc

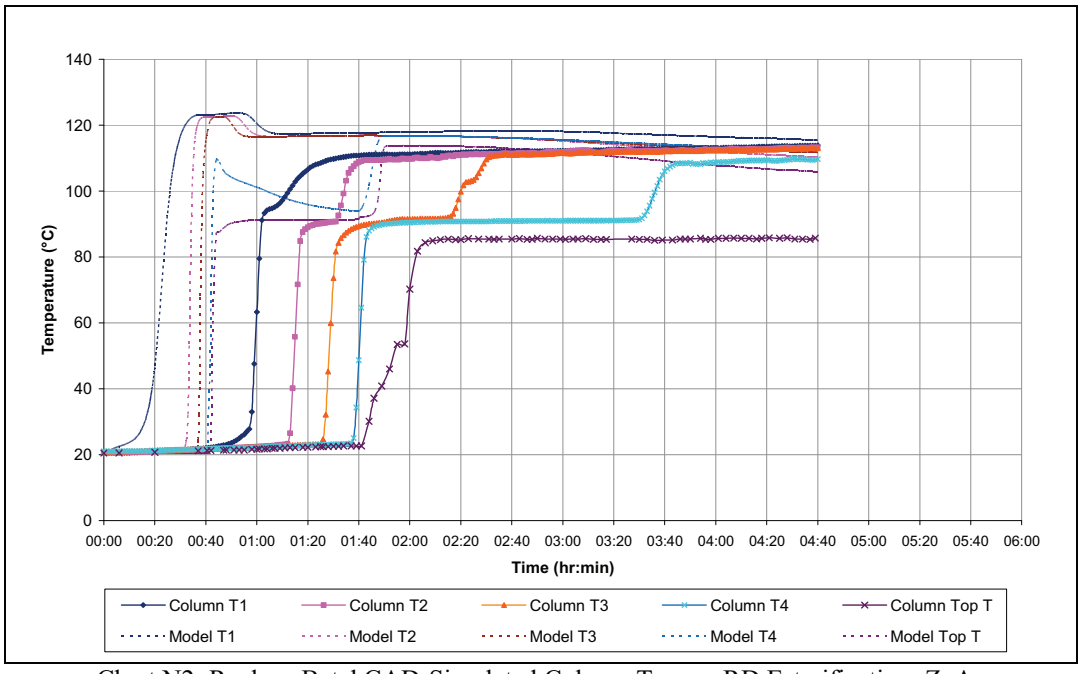

Chart N2: Real vs. BatchCAD-Simulated Column Temps: RD Esterification: ZnAc

Before zinc acetate is added, there is a good match between the real and simulated data in terms of pot temperature, jacket oil temperature and ester composition. The simulated Pre-Catalyst composition in the pot at 40.5 minutes is shown in Table N1.

Component	Nonanoic Acid	Butanol	Ester	Water
Number of Moles	$2.40x10^{-03}$	$4.19x10^{-03}$	$8.85x10^{-05}$	$4.01x10^{-05}$

Table N1: Simulated Pot Composition at 40.5 minutes for the RD Esterification with ZnAc

The BatchCAD column temperatures again start to rise far too early. The BatchCAD simulated values for T1, T2 and T3 are already rising before 40 minutes have passed.

- Approximate time real T1 reaches 40°C: 58 minutes 30 seconds
- Approximate time simulated T1 reaches 40°C: 18 minutes 55 seconds

These values are very similar to those for the run where no catalyst was used. Up to the reflux ratio switch, the runs with no catalyst and with zinc acetate are almost identical.

Catalyst Addition up to Reflux Ratio Switch

Real and Simulated Pot

The real and simulated data are very similar to that observed for the run with no catalyst. The real pot temperature falls slightly at around 40 minutes, in a similar way to that seen in the run for the run with no catalyst. The zinc acetate run was performed later in the experimental programme, so experience running the unit may have led to slight differences, for example quicker oil temperature adjustments leading to the slightly quicker attainment of the desired difference between oil and pot temperature.

Real and Simulated Column

T1 in this run starts to rise slightly later than, and does not go as high as, the real T1 with no catalyst. This could be due to the fact that the pot is briefly opened in order to add the zinc acetate, which did not occur when no catalyst was added. There appears to be no significant difference between the T2 profiles for the two runs. The BatchCAD simulated column temperature profiles are almost identical to those observed for the simulation of the run with no catalyst.

Reflux Ratio Switch (1 hour 40 minutes)

Real and Simulated Pot

As with the run with no catalyst, no immediate changes in the pot temperature or oil temperature are observed in either the real or simulated data upon the reflux ratio switch. After a slight delay, the BatchCAD simulated pot temperature deviates from the real profile, increasing gradually as it starts to approach the oil temperature.

Distillate

In the BatchCAD simulation, the collection of distillate begins as soon as the reflux ratio change is applied, while in the real experimental data the collection of distillate begins after a short delay of 15 minutes.

- Real distillate collection start: 1 hour 55 minutes
- BatchCAD starts immediately after the reflux ratio change: 1 hour 40 minutes.

The BatchCAD profile of distillate volume against time is very similar to that obtained for the run with no catalyst, slightly shifted due to the time of the reflux ratio switch.

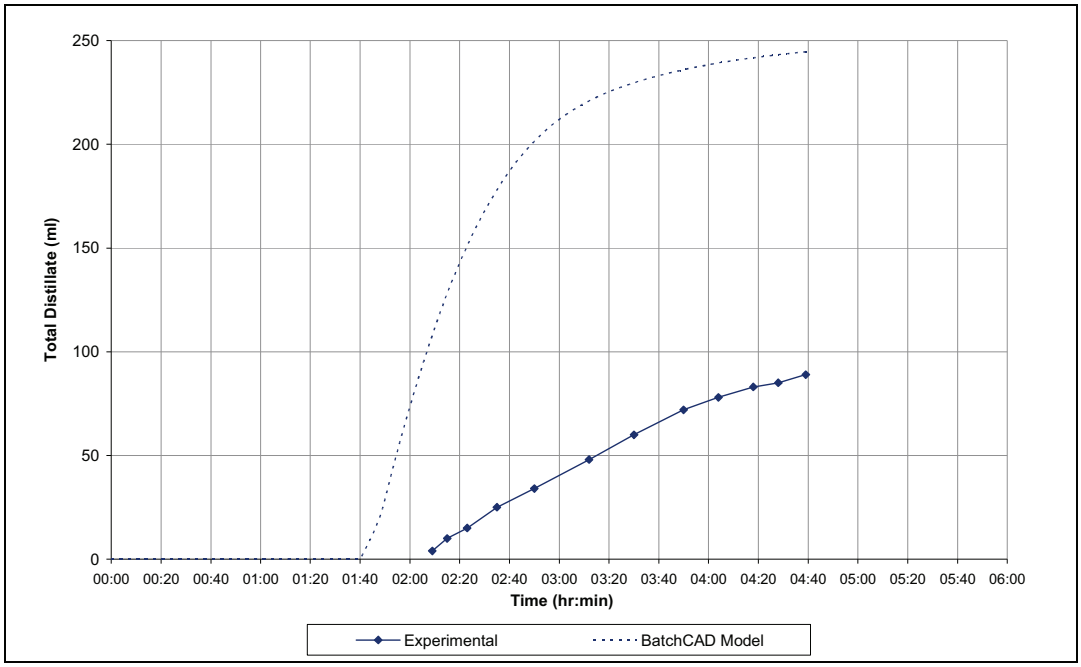

Chart N3: Real vs. BatchCAD-Simulated Distillate Collection: RD Esterification: ZnAc

Real Column

The step in the value of T3 occurs noticeably later than in the run with no catalyst. This could indicate that water is present at this position for a little longer in the run with zinc acetate. The top temperature rises slightly more quickly, with a brief step at approximately 54°C. The high, steady temperature is reached significantly quicker than with the run with no catalyst. A slightly higher vapour flow would contribute to explaining this profile.

Simulated Column

In the BatchCAD simulations, T3 and the top temperature rise to the higher level (~115°C) as soon as the reflux ration changes, which does not reflect the real data.

Summary

Results from the zinc acetate experiments and simulations show small differences to the run with no catalyst. The column temperatures in these simulations start to rise much earlier than is observed in reality and therefore there is significant mismatch.

MSA

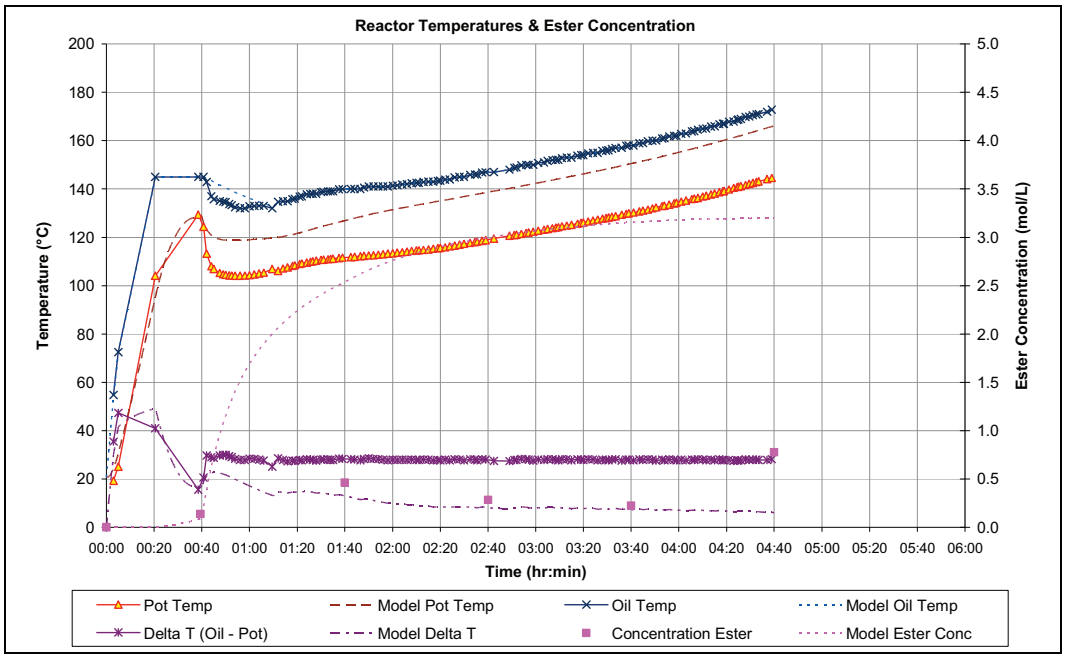

Chart N4: Real vs. BatchCAD-Simulated Reactor Profiles: RD Esterification: MSA

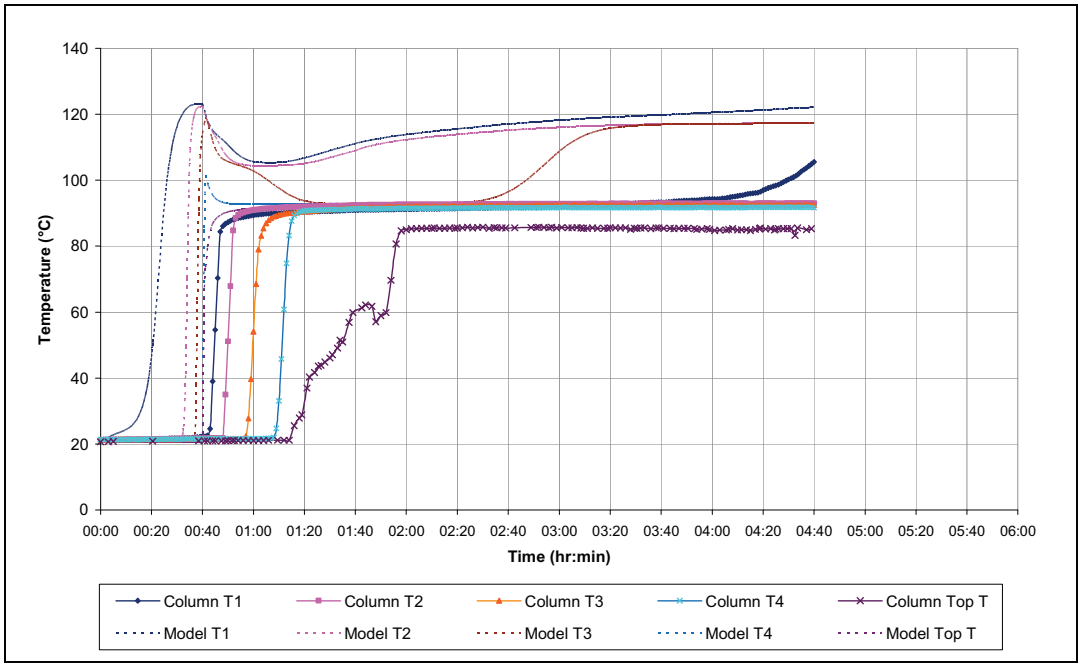

Chart N5: Real vs. BatchCAD-Simulated Column Temps: RD Esterification: MSA

Before MSA is added, there is a good match between the real and simulated data in terms of pot temperature, jacket oil temperature and ester composition.

Component	Nonanoic Acid	Butanol	Ester	Water
Number of Moles	$2.39x10^{-03}$	$4.20x10^{-03}$	$8.48x10^{-05}$	$3.99x10^{-05}$

Table N2: Simulated Pot Composition at 40 minutes for the RD Esterification with MSA

The BatchCAD column temperatures again start to rise far too early. The BatchCAD simulated values for T1, T2 and T3 are already rising before the catalyst is added.

- Approximate time real T1 reaches 40°C: 44 minutes 5 seconds
- Approximate time simulated T1 reaches 40°C: 18 minutes 50 seconds

Catalyst Addition up to Reflux Ratio Switch

Real and Simulated Pot

A sudden drop in pot temperature is observed in both the real and simulated data. The deeper and prolonged real temperature fall indicates that the real water formed does not boil off from the pot as rapidly as predicted in the BatchCAD simulations. The real oil temperature profile also falls as it is quickly adjusted to maintain the temperature difference between the oil and pot temperatures. The BatchCAD oil temperature profile fails to follow the experimental oil temperature profile, despite being programmed to follow the real temperature profile via the data manager feature of BatchCAD.

The simulations indicate a rapid production of ester as soon as the catalyst is added. The real composition does not follow this, the kinetics in the real case with MSA are not as fast as those predicted by BatchCAD. The ester composition in the real experimental data remains fairly low during the run. There could be a problem with the MSA catalyst: it may have been consumed in a reaction, or it may have been decomposed or boiled at the high temperatures used in the reactive distillation unit.

Real and Simulated Column

The real column temperatures 1 to 4 rise fairly rapidly to around 90°C after the MSA catalyst addition. The top temperature rises very hesitantly and wobbles at approximately 60°C. The simulated temperatures are considerably overestimated.

Reflux Ratio Switch (1 hour 40 minutes)

Real and Simulated Pot

There is little further increase in the ester in the pot in either the real data or in the simulation data. In the real data, the reaction has failed to progress, possibly due to

deactivation of the MSA catalyst. In the simulations, the reaction has already progressed to a high conversion. Both real and simulated rates are slow, for different reasons.

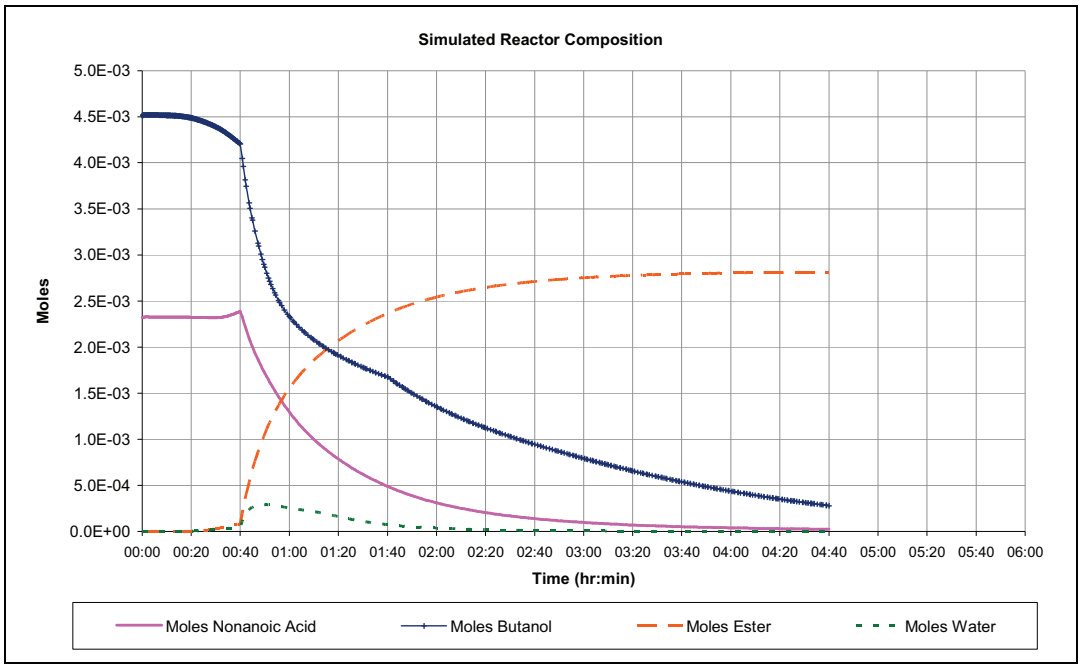

Chart N6: BatchCAD-Simulated Pot Compositions for the RD Esterification: MSA

The real pot temperature rises slowly after the initial fall upon the addition of catalyst. The slow reaction means that there is a slow rate of composition change in the pot and therefore a slow rate of change of boiling point and therefore pot temperature. The temperature in the pot is lower, so the reaction would be expected to be slower, but the rate observed here is as if there is no reaction occurring.

Real and Simulated Column

The real column temperatures remain steady at around 90°C until T1 starts to rise further very late in the run. This indicates that there is water present in the mixture in the column up until very near the end of the run. The simulated profiles for T1 and T2 are always significantly above the real profiles. From around 1 hour 20 minutes until 2 hour and 20 minutes the simulated T3, T4 and top temperature approximately match the real data but then the simulated T3 starts to increase to meet T1 and T2.

Distillate

Real distillate collection starts at 2 hours, with only a 15 to 20 minute delay after the reflux ratio switch. The real distillate is collected at a steady rate, much more slowly than predicted by the BatchCAD simulation. The BatchCAD simulated distillate collection starts immediately after the reflux ratio change at 1 hour 40 minutes.

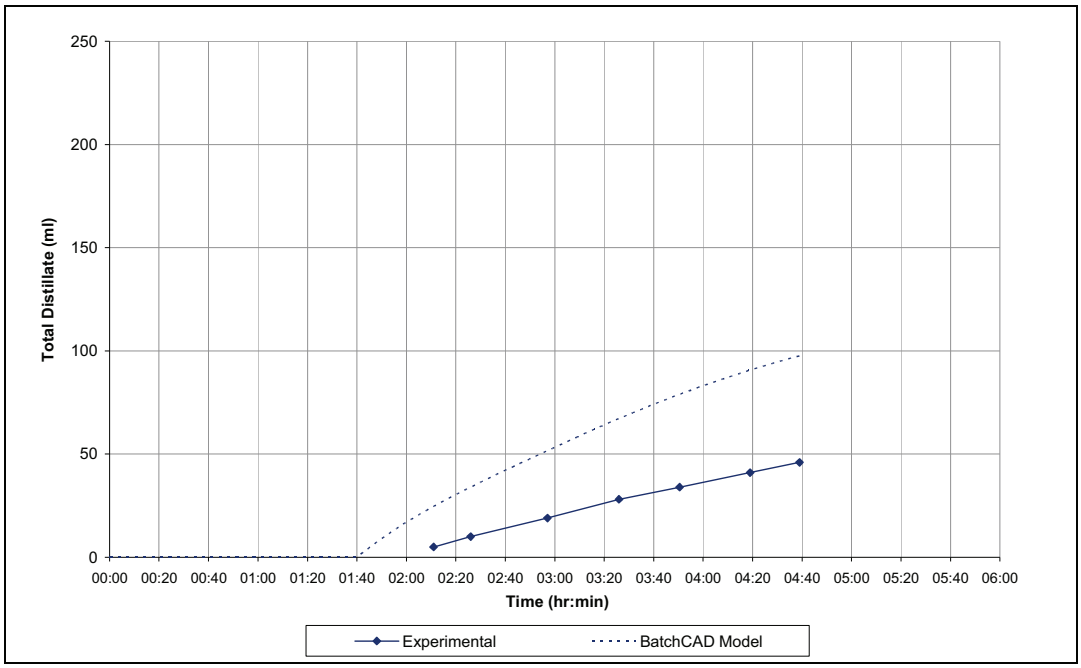

Chart N7: Real vs. BatchCAD-Simulated Distillate Collection: RD Esterification: MSA

H_2SO_4

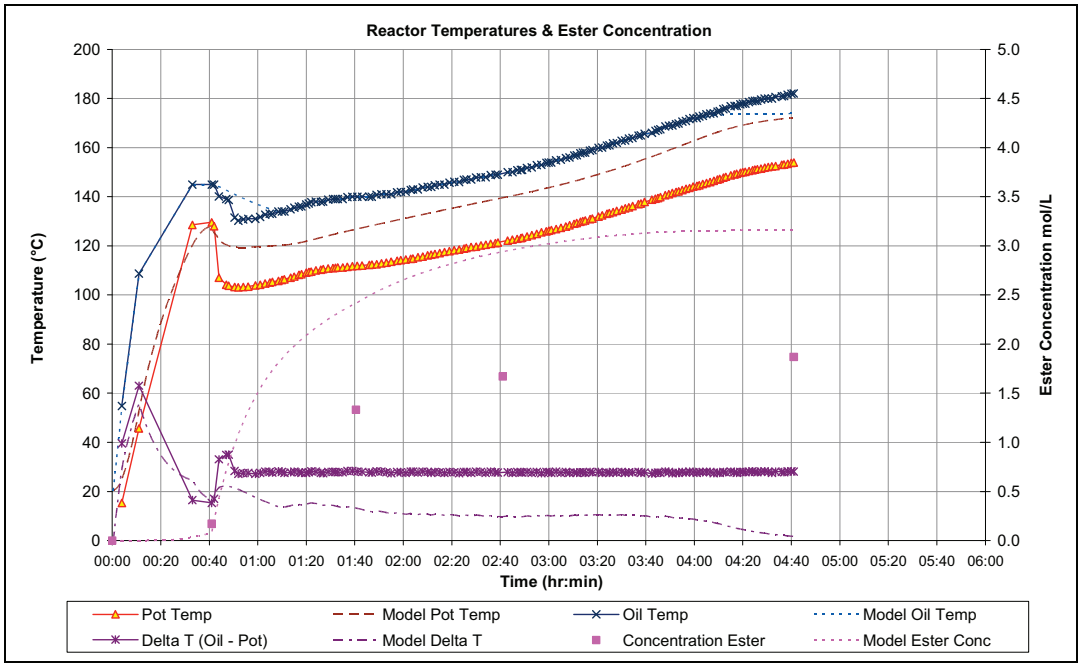

Chart N8: Real vs. BatchCAD-Simulated Reactor Profiles: RD Esterification: H_2SO_4

Before H_2SO_4 is added, there is a good match between the real and simulated data in terms of pot temperature and jacket oil temperature, and the ester composition is close.

Component	Nonanoic Acid	Butanol	Ester	Water
Number of Moles	$2.35x10^{-03}$	$4.27x10^{-03}$	$7.17x10^{-05}$	$4.10x10^{-05}$

Table N3: Simulated Pot Composition at 41 minutes for the RD Esterification with H_2SO_4

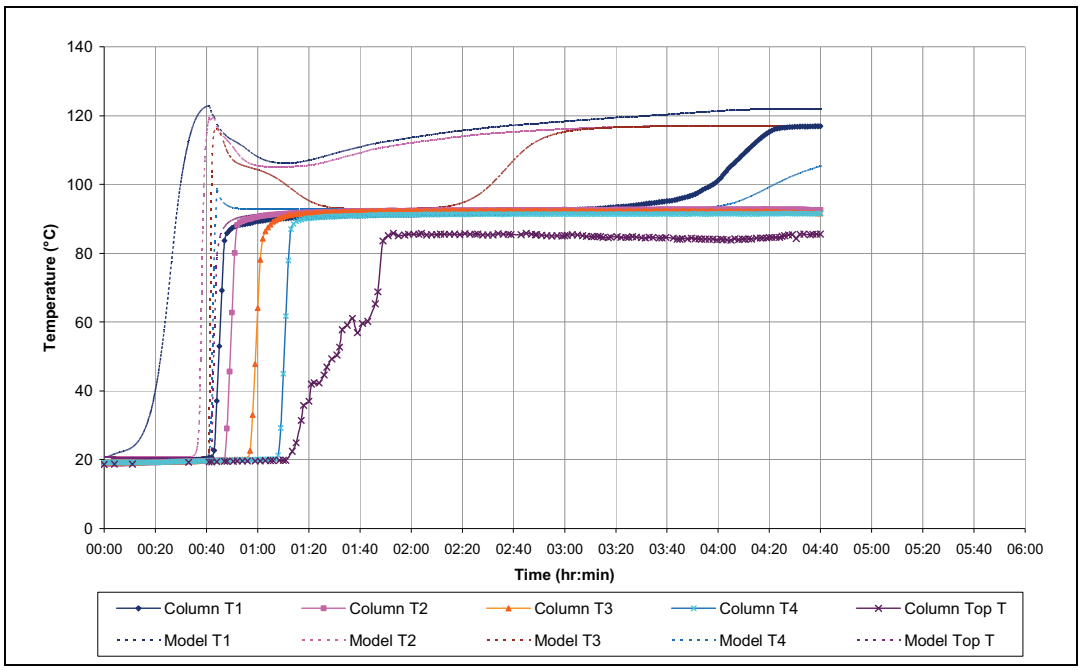

Chart N9: Real vs. BatchCAD-Simulated Column Temps: RD Esterification: H_2SO_4

The BatchCAD simulated T1 and T2 are already rising before catalyst is added.

- Approximate time real T1 reaches 40°C: 44 minutes 10 seconds
- Approximate time simulated T1 reaches 40°C: 20 minutes 0 seconds

Catalyst Addition up to Reflux Ratio Switch

Real and Simulated Pot

A sudden drop in pot temperature is again observed in both the real and simulated data due to the formation of water by reaction. The real fall in temperature is significantly more than that predicted by BatchCAD. The pot temperature prediction almost exactly matches that for the simulation of the MSA run up to the point of the reflux ratio switch. The real oil temperature profile falls as it is quickly but the BatchCAD oil temperature profile again fails to follow the experimental oil temperature profile, despite being programmed to follow the real temperature profile. The concentration of ester is predicted by BatchCAD to increase rapidly, as it was predicted for the MSA simulation.

Real and Simulated Column

Real column temperatures 1 to 4 rise rapidly after the H_2SO_4 is added. The top temperature rises slightly slower than the other column temperatures, and pauses at approximately 60°C. The column temperatures reach a steady level of around 90°C. The simulated column temperatures T1 and T2 remain significantly over estimated. T3 is also overestimated but during this phase the T3 profile falls to the near-90°C range.

Reflux Ratio Switch (1 hour 41 minutes)

Real and Simulated Pot

After the reflux ratio switch, slightly higher pot temperatures are predicted by BatchCAD than for the run with MSA. The simulated ester concentration in the pot continues to rise but the rate of increase has slowed. The rate of reaction seems to slow after 2 hours 40 minutes.

Real and Simulated Column

The real column temperatures 1 to 4 stay steady at around 90°C until very near the end of the run, when T1 starts to rise.

Distillate

- Real distillate collection start: 1 hour 39 minutes
- BatchCAD starts immediately after the reflux ratio change: 1 hour 41 minutes

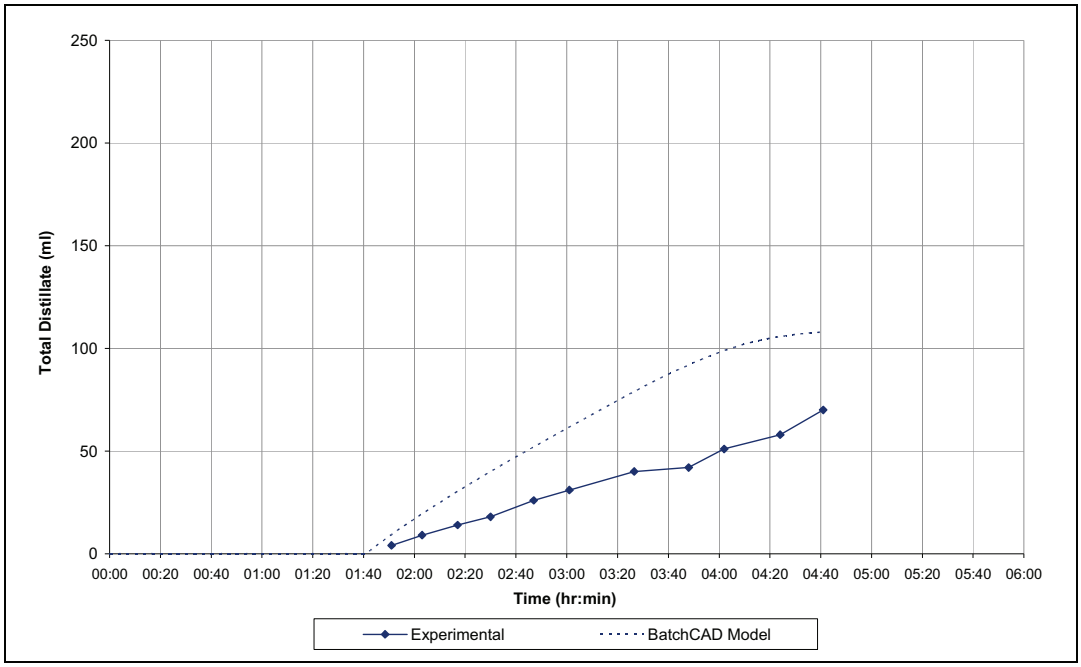

Chart N10: Real vs. BatchCAD-Simulated Distillate Collection: RD Esterification: H_2SO_4

There is a slight decrease in the real rate of distillate collection at around 3½ hours, this corresponds to the start of the increase in T1. Together, these factors indicate a change in composition in that there is less water boiling up from the pot. The reaction has significantly slowed by this time.

Summary

The H_2SO_4 appears to remain active compared to the MSA

PhosMo

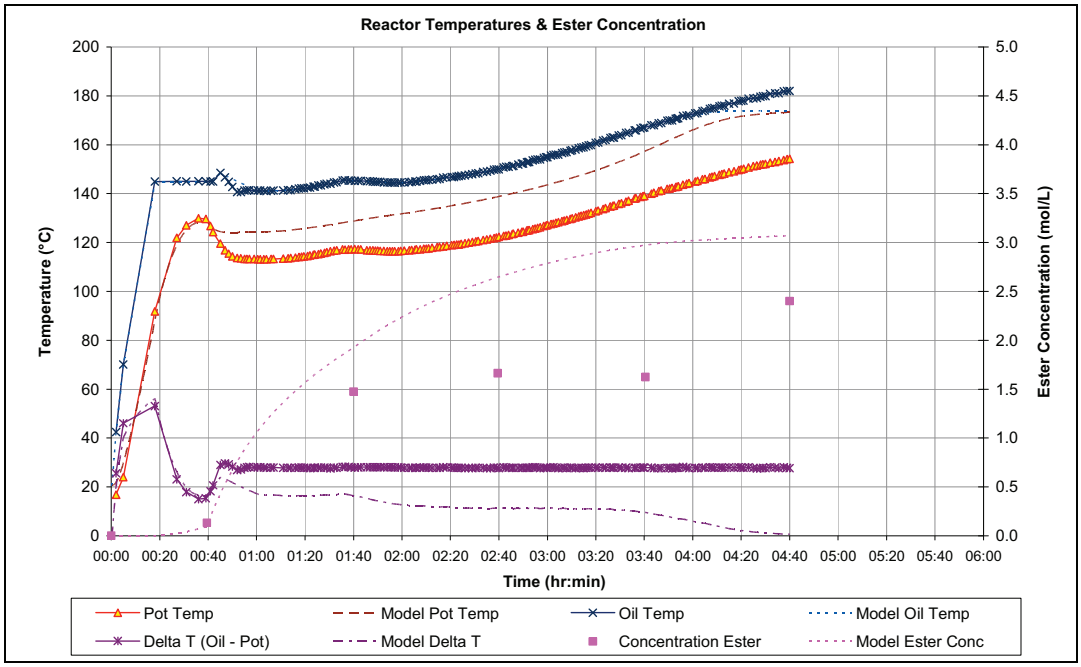

Chart N11: Real vs. BatchCAD-Simulated Reactor Profiles: RD Esterification: PhosMo

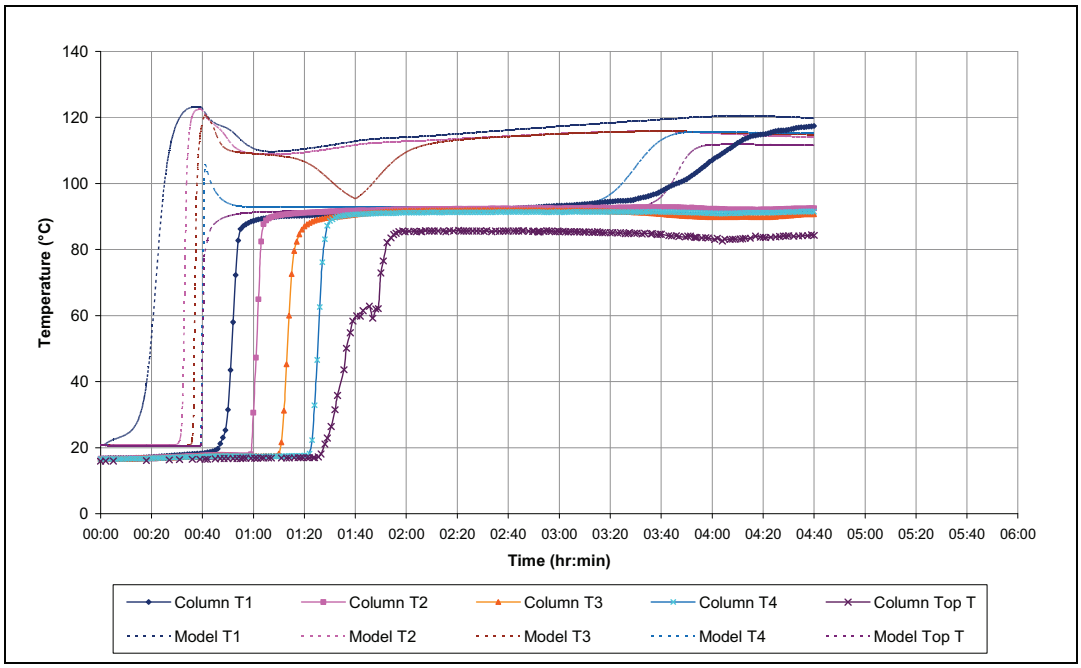

Chart N12: Real vs. BatchCAD-Simulated Column Temps: RD Esterification: PhosMo

Component	Nonanoic Acid	Butanol	Ester	Water
Number of Moles	$2.39x10^{-03}$	$4.20x10^{-03}$	$8.72x10^{-05}$	$4.00x10^{-05}$

Table N4: Simulated Pot Composition at 39.5 minutes for the RD Esterification with PhosMo

Before the catalyst is added, there is a good match between the real and simulated data in pot temperature, jacket oil temperature and ester composition. The BatchCAD simulated T1, T2 and T3 are already rising before catalyst is added. The simulated

profiles are very similar to those predicted for the MSA case, and the simulated T1 rises faster compared to the case where there was no catalyst.

- Approximate time real T1 reaches 40°C: 50 minutes 40 seconds
- Approximate time simulated T1 reaches 40°C: 18 minutes 10 seconds

Catalyst Addition up to Reflux Ratio Switch

Real and Simulated Pot

The temperature fall is less steep and of a lower magnitude compared to that seen in the runs with the strong liquid acids MSA and H_2SO_4, but more significant than the very slight fall predicted by BatchCAD for this case, indicating that the water formed does not boil off as rapidly as predicted. The simulated pot temperature does not follow the profile of the real pot temperature from this point onwards. Although the simulated oil temperature follows the experimental profile more closely than in the simulations involving the strong liquid acids, the oil temperature is still slightly overestimated by BatchCAD for a short while after catalyst addition. The concentration of ester is predicted by BatchCAD to rise fairly quickly, but slower than was predicted for the MSA and H_2SO_4 simulations. The temperature does not fall as low in this run as in those with strong liquid acids, so the reaction is able to proceed at the intermediate temperature and achieve good ester production despite the less active catalyst.

Real and Simulated Column

Real column temperatures 1 to 4 rise quite quickly after the catalyst is added, but not as rapidly as in the runs with MSA and H_2SO_4. The top temperature rises slightly slower than the other column temperatures but much more smoothly than in the data for the runs with the strong acids. The column temperatures reach a steady level of around 90°C, but BatchCAD significantly overestimates T1, T2 and T3.

Reflux Ratio Switch (1 hour 40 minutes)

Real and Simulated Pot

The mismatch between the real and simulated pot temperatures remains significant as the run continues, at 15 to 20°C after the reflux ratio switch.

Real and Simulated Column

The real column temperatures remain at around 90°C until ~3 hours 40 minutes, when T1 begins to rise and approach 120°C. This indicates that water is present in the column

until this point. This change coincides with a temporary decrease in the rate of distillate collection. At the 3 hour mark, before the change, there is more water on the top tray than butanol. The water level on this tray then starts to fall rapidly and the moles of butanol steadily increase. The new steady temperature is attained when the new steady top composition has been established, and the liquid on the tray is mostly butanol with a trace of water.

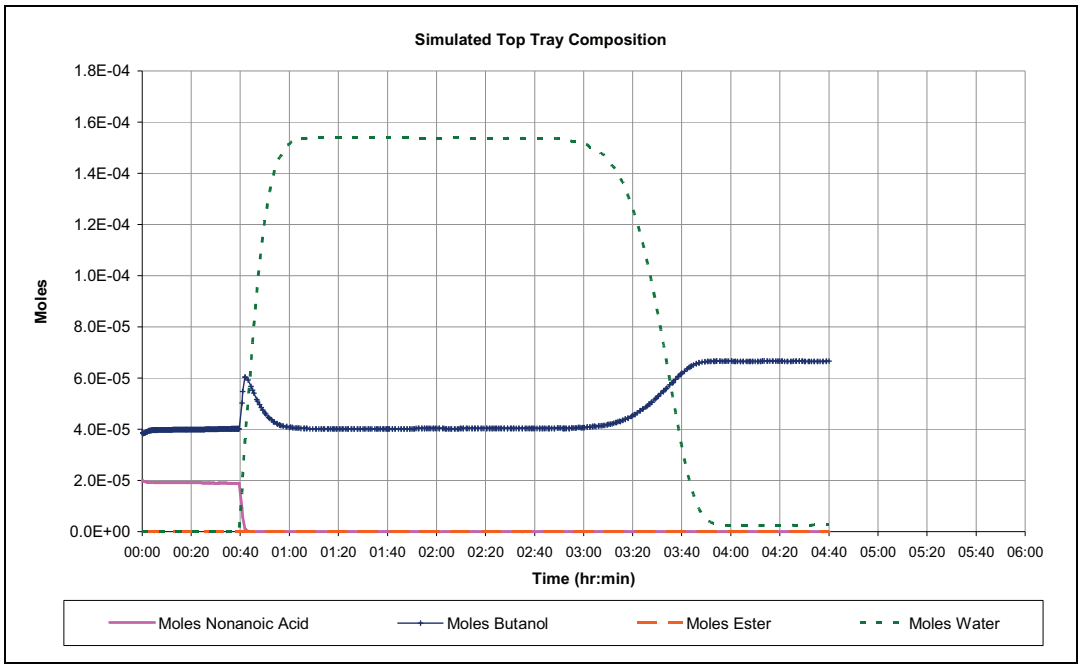

Chart N13: BatchCAD-Simulated Top Tray Composition: RD Esterification: PhosMo

Together with the real column data, it appears that when the reaction slows, less water is formed and there is less water boiling up. The composition on the trays starts to change from a water-dominated azeotropic mixture of water and butanol to a butanol dominated mixture. This can correspond to a temporary fall in the boil up rate, and an increase in the boil-up of butanol. This also explains the simulated increase in ester concentration sometimes observed towards the end of the run, despite the slowing of the reaction in the pot, and the increase in the pot temperature, as the proportion of high-boiling components in the pot increases.

Distillate

- Real distillate collection start: 1 hour 46 minutes
- BatchCAD starts immediately after the reflux ratio change: 1 hour 40 minutes

Apart from a temporary decrease in the rate of distillate collection at about 3 hours 40 minutes, the rate of distillate collection is fairly constant.

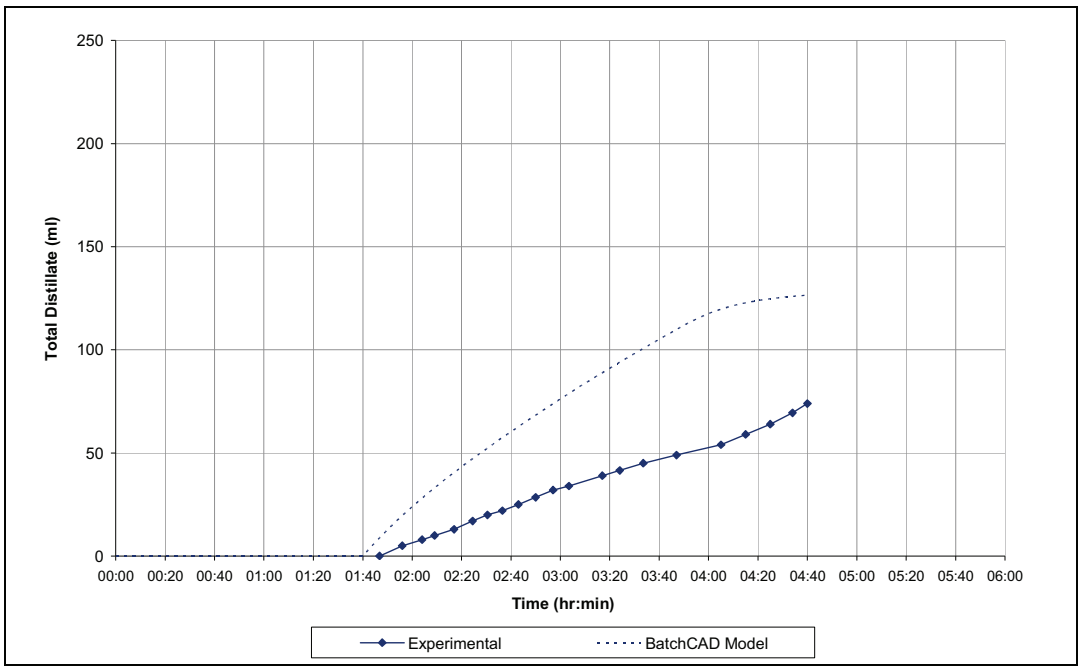

Chart N14: Real vs. BatchCAD-Simulated Distillate Collection: RD Esterification: PhosMo

Summary

With an intermediate strength catalyst, there is a less drastic temperature drop upon catalyst addition. Further evidence has been gained for the connection between tray temperature changes and composition changes.

FeSulf

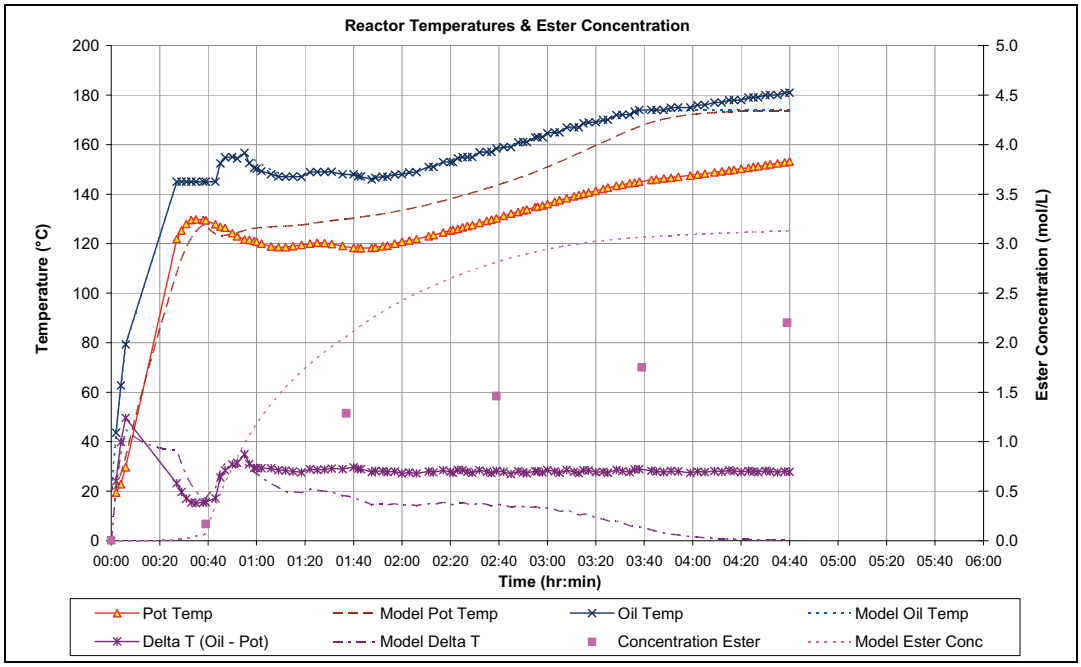

Chart N15: Real vs. BatchCAD-Simulated Reactor Profiles: RD Esterification: FeSulf

Before the catalyst is added, there is a good match between the real and simulated pot temperature and jacket oil temperature, and the ester composition is also close.

Component	Nonanoic Acid	Butanol	Ester	Water
Number of Moles	$2.34x10^{-03}$	$4.29x10^{-03}$	$6.29x10^{-05}$	$3.86x10^{-05}$

Table N5: Simulated Pot Composition at 39 minutes for the RD Esterification with FeSulf

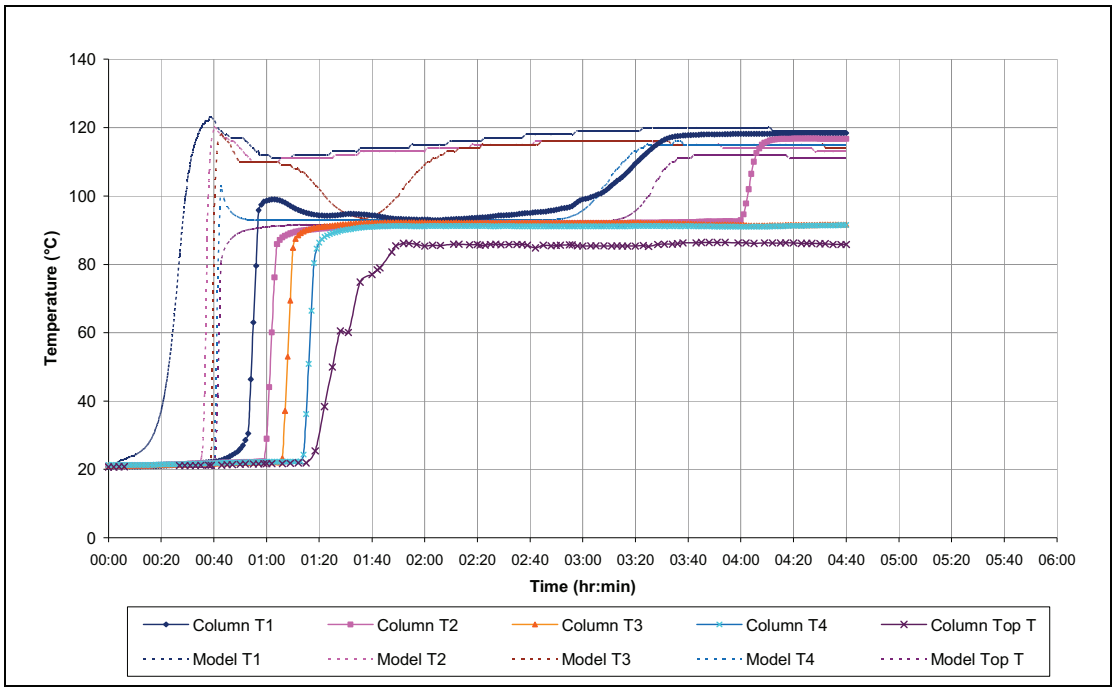

Chart N16: Real vs. BatchCAD-Simulated Column Temps: RD Esterification: FeSulf

The BatchCAD simulated values for T1, T2 and T3 are already rising before catalyst is added. The simulated profiles are very similar to those predicted for the other runs.

- Approximate time real T1 reaches 40°C: 53 minutes 35 seconds
- Approximate time simulated T1 reaches 40°C: 20 minutes 45 seconds

Catalyst Addition up to Reflux Ratio Switch

Real and Simulated Pot

After the catalyst is added there is a slow, gradual decrease in pot temperature from 129°C to just under 120°C over around 20 minutes. In the BatchCAD simulation there is a slight sudden drop to around 125°C in around 10 minutes then a gradual increase. The mismatch between the real and simulated pot temperature profiles increases over time. In the real oil temperature profile, a setting error occurred at approximately 55 minutes. The temperature was set too high for a short time, but quickly corrected. The pot temperature profile is smooth despite the sudden changes in direction in the oil temperature profile, suggesting that the error did not have a strong effect.

There are some changes in the direction of the real pot temperature profile at 1 hour 15 minutes and 1 hour 40 minutes. These were unexpected, as they had not been observed in the other runs, and the plot of the temperature difference between the oil temperature and the pot contents shows that the responding adjustments to the oil temperature were slightly inefficient. In the simulation, the BatchCAD simulated oil temperature was able to follow closely the real oil temperature profile because no sudden drops were required. The predicted ester concentration profile is very similar in this case to that predicted for the run with PhosMo.

Real and Simulated Column

In the real column temperatures there is a slight delay before the temperatures T1 to T4 rise rapidly, with very small time intervals between each subsequent temperature beginning to rise. The temperature profiles are then similar to those observed in the simulations of the runs with strong acids. The real top temperature, which usually rises very unevenly, rises quickly in this case with only a small pause at 60°C. The rate of increase can be seen to slow slightly in response to the reflux ratio switch, an effect which was not clearly seen in previous runs. The top temperature reaches approximately 85°C shortly after the reflux ratio switch. The strong increase in the top temperature could be due to a stronger vapour rate, enabled by the higher pot temperature. BatchCAD significantly overestimates T1, T2 and T3 and predicts that T4 and the top temperature increase much sooner than they do in reality.

Reflux Ratio Switch (1 hour 37 minutes)

The reflux ratio switch was made slightly earlier than in the other experimental runs, because some distillate carry-over was occurring. This also suggests that the boil up rate is stronger in this case than in the previous runs.

Simulated Pot

The simulated oil temperature is still a good match with the experimental data, but the pot temperature is significantly overestimated by BatchCAD and the simulated ester concentration is rising at a much faster rate than the real ester data indicates.

Real Pot

The pot temperature falls gradually then recovered slightly, but starts falling again just before the reflux ratio switch, at 1 hour 35 minutes. This time corresponds to the start of

the carry-over of liquid into the distillate collection, which triggers the early reflux ratio switch. A possible explanation for the second temperature fall is that at approximately 1 hour 12 minutes, the column liquid hold-up limit is reached and material is returning from the column. Once the carry-over begins to occur, some material is leaving the column so the boil up can resume, and the second temperature fall occurs.

Real and Simulated Column

After mirroring the changes in the pot temperature, the real column temperature T1 starts to increase after ~2 hours 20 minutes and T2 starts to increase close to the end of the run, after around 4 hours. This suggests that in these sections of the column, the composition has shifted, which suggests that the water boil-up rate has faltered and the reaction has slowed. The simulated column temperatures are consistently overestimated.

Distillate

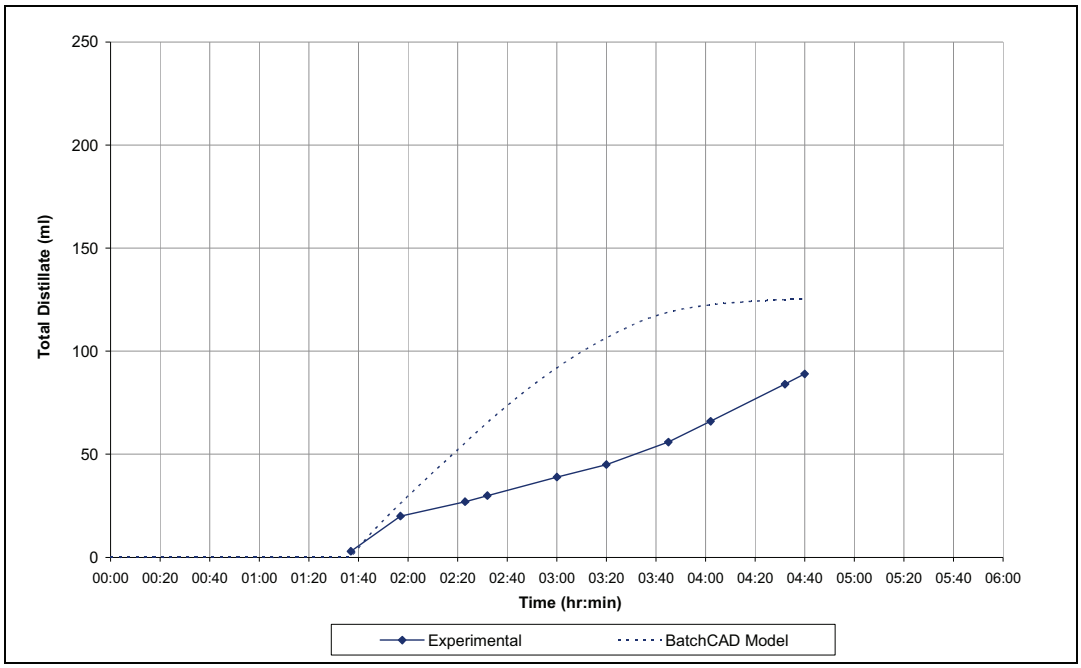

Chart N17: Real vs. BatchCAD-Simulated Distillate Collection: RD Esterification: FeSulf

The simulated distillate rate is highly overestimated. The real distillate collection begins slightly before the reflux ratio switch, due to carry-over from the column, and the early distillate collection rate is quite high. The rate then seems to steady out for a while, until a slight increase in the rate of collection at approximately 3 hours 40 minutes. This change corresponds to the period of time when the real T1 profile has begun to increase.

- Real distillate collection start: 1 hour 35 minutes
- BatchCAD starts immediately after the reflux ratio change: 1 hour 37 minutes

Summary

Out of the previous runs, the profile for the FeSulf case is most similar to that for PhosMo, but with smaller intervals between the column temperature increases and a very rapid top temperature increase. With an intermediate-activity catalyst, there is no big drop in pot temperature as with the strong acids. The pot temperature stays high as the reaction progresses, as evidenced by the long phase of water-rich distillate boil up. The reaction continues steadily, so the water is formed slowly and gradually rather than all at once, as seen with the strong acids. A possible explanation for the 'double-fall' seen in the pot temperature involves the observed carry-over from the column, taking this as an indication that the column liquid hold-up capacity has been reached.

Repeat Simulation with No Catalyst, Changed Initialisation

The purpose of this simulation was to attempt to delay the start of the simulated column temperature rises and hence reduce the simulated distillate collection and achieve more a realistic reactor composition profile. Averages were taken of the pot composition and temperature at 40 min/pre-catalyst addition point from all the simulations (Table 7.3). The initial charge was set up differently, so that the trays are filled with butanol at the start rather than with nonanoic-acid / butanol mixture. The BatchCAD simulation for the case with no catalyst is was re-run from this point.

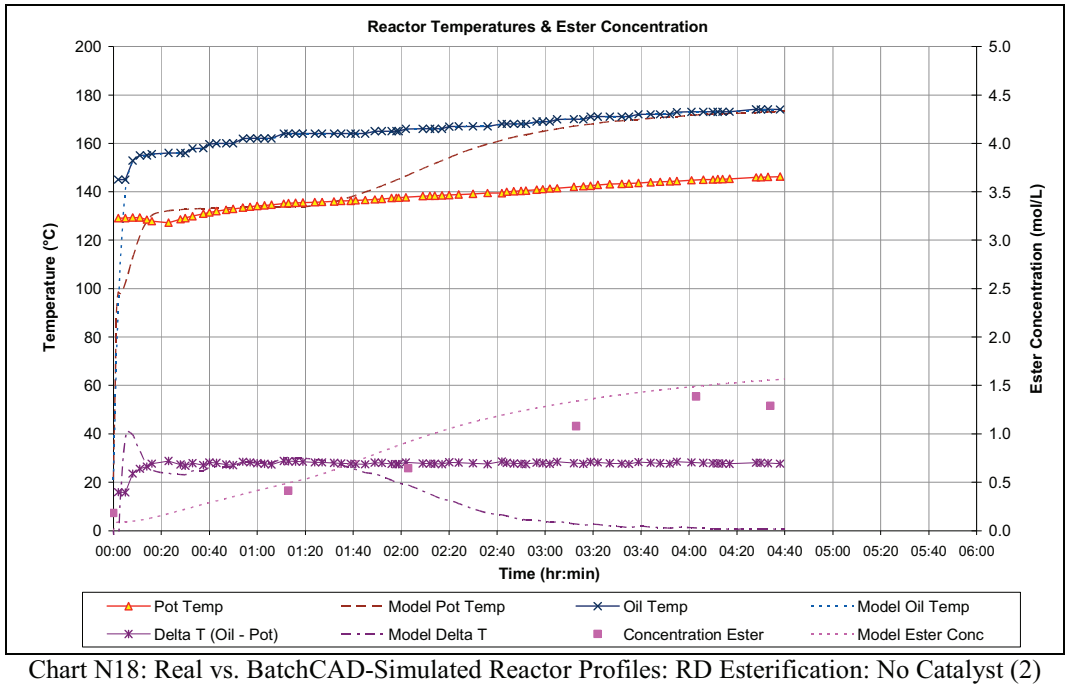

Chart N18: Real vs. BatchCAD-Simulated Reactor Profiles: RD Esterification: No Catalyst (2)

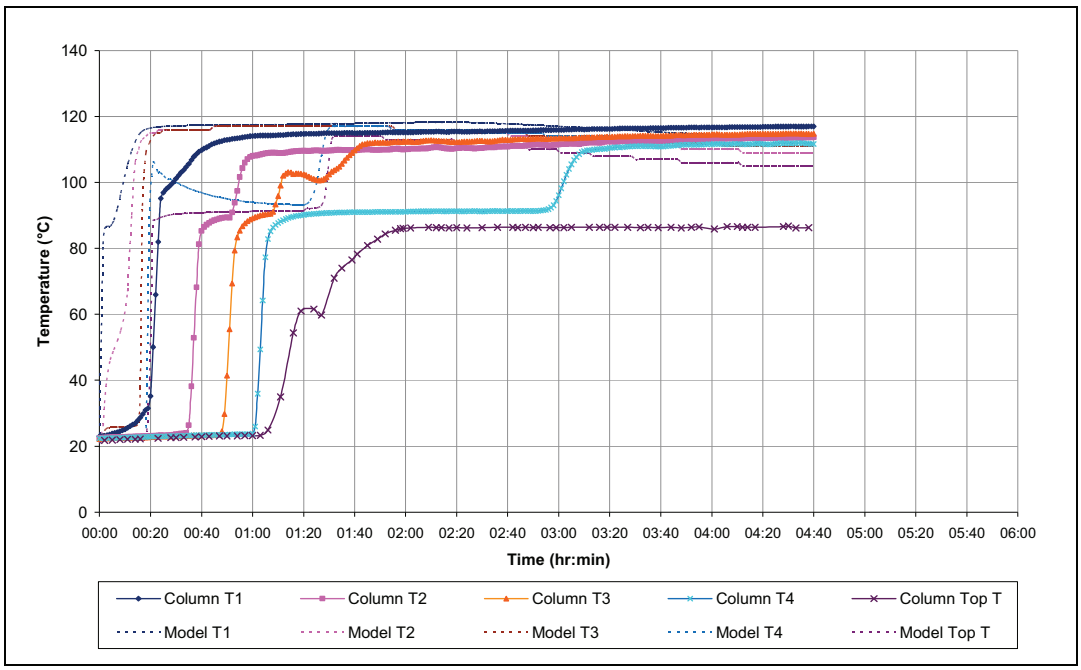

Chart N19: Real vs. BatchCAD-Simulated Column Temps: RD Esterification: No Catalyst (2)

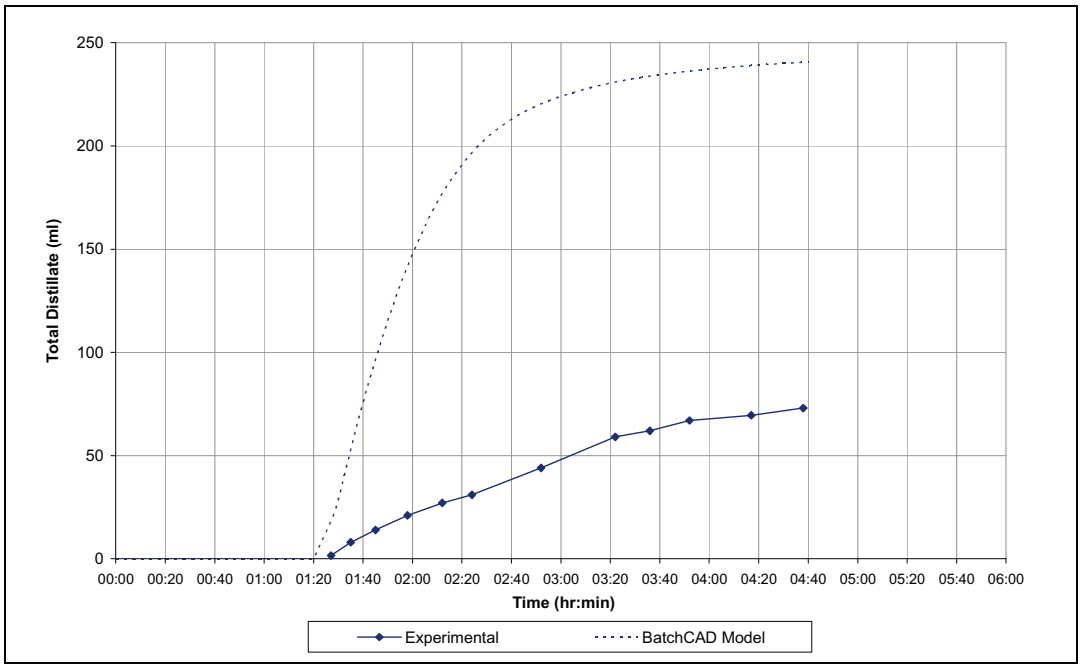

Chart N20: Real vs. BatchCAD-Simulated Distillate Collection: RD Esterification: No Catalyst (2)

It can be seen that there is very little change caused by changing the simulations in this case. The column temperatures still rise far too early compared to the experimental data and the distillate collection rate is too high, which in turn causes the large mismatch between the real and simulated pot composition.

Appendix O: Details of the Excel-Based RD Model

The starting point for the simulation is:

- Initial guess of temperature (around 130°C)
- Molar quantities of each component at the 40 minute mark.

From this, the mole fraction, mass, and mass fraction of each component are determined, along with the total mass. The vapour pressure of each component is then calculated from the 'current' temperature estimate, using equations for polynomial curves fitted to the vapour pressure vs. temperature data from Yaws (2003). These equations are shown in Table O1 where VP is vapour pressure in kPa and T is temperature in °C.

Component	**Equation for Vapour Pressure (VP) in kPa**
Nonanoic acid	$VP = 2.09 \times 10^{-15} (T^{6.93})$
Butanol	$VP = 3.84 \times 10^{-4} T^3 - 8.32 \times 10^{-2} T^2 + 7.18 T - 218.3$
Butyl nonanoate	$VP = 1.74 \times 10^{-12} (T^{5.81})$
Water	$VP = 5.57 \times 10^{-4} T^3 - 1.17 \times 10^{-1} T^2 + 10.40 T - 320.7$

Table O1: Equations relating Vapour Pressure and Temperature

The combined total pressure is found by summing the vapour pressures together weighted by mole fraction. However, if the liquid boils when the vapour pressure matches the atmospheric pressure 101kPa, the temperature of the mixture must be varied until the total vapour pressure is 101kPa, which indicates that this is the boiling point of the mixture. A 'residual' is calculated as the value calculated from the equations in Table O1 minus the atmospheric pressure, 101kPa. A macro written in Excel then uses a goal-seek type of function to adjust the value of the temperature estimate until the total vapour pressure comes to equal the atmospheric pressure of 101 kPa, and this is the boiling point of the mixture. The macro used is illustrated in Figure O1.

```
Sub Worksheet_Calculate()
    CheckGoalSeek
End Sub

Sub CheckGoalSeek()
    Static isWorking As Boolean

i = Range("A" & i + 2)

For i = 0 To 14400

'GoalSeekCell = Range("AE" & i + 2) residual, desired value = 0
'ByChangingCell = Range("D" & i + 2) temp C

    With Sheet2

        If Round(.Range("AE" & i + 2).Value, 6) <> 0 And Not isWorking Then
            isWorking = True
            .Range("D" & i + 2).Value = 130
            .Range("AE" & i + 2).GoalSeek Goal:=0, ChangingCell:=.Range("D" & i + 2)
            isWorking = False
        End If

    End With

Next

End Sub
```

Figure O1:Macro used by Excel Model to Find the Boiling Point of the Pot Mixture

The spreadsheet then uses equations from polynomial curves that have been fitted to density vs. temperature data from Yaws (2003) for each component to determine the volume at the calculated temperature. These equations (valid from 90°C to 160°C) are shown in Table O2 where ρ is liquid density in kg/m^3 and T is temperature in °C.

Component	**Equation for Density (ρ) in kg/m^3**
Nonanoic acid	$\rho = -5.137 \times 10^{-4} T^2 - 0.7546 T + 920.6$
Butanol	$\rho = -1.654 \times 10^{-3} T^2 - 0.6328 T + 819.5$
Butyl nonanoate	$\rho = -7.452 \times 10^{-4} T^2 - 0.7168 T + 868.4$
Water	$\rho = -9.179 \times 10^{-4} T^2 - 0.8239 T + 1047$

Table O2: Equations relating Density and Temperature

An estimate of overall density is then obtained from a sum of each component density multiplied by the mass fraction of that component in the mixture. The volume in the pot is calculated from the total mass (kg) divided by the overall density (kg/m3). The concentrations of the components can then be determined from the moles present of each component and the total volume in the pot. These are used by the equations representing the kinetics, which use the parameters determined from the runs at varying temperatures in the ChemSpeed (presented in Chapter 4). The rate is known so the change in composition of each component due to reaction is determined.

Isothermal rate constants:

- $k_{forward}$ = k1 = A1*EXP(-E1/(8.314*T(K)))
- $k_{reverse}$ = k2 =A2*EXP(-E2/(8.314*T(K)))

Where:

- T(K) is temperature in Kelvin
- Rates are in mol m^{-3} s^{-1}.

The equations for the rates of change of individual components are shown in Table O3.

Component	**Equation for Rate of Change**
Nonanoic acid (1)	rX(1) = -k1*cX(1)*cX(2) + k2*cX(3)*cX(4)
Butanol (2)	rX(2) = -k1*cX(1)*cX(2) + k2*cX(3)*cX(4)
Butyl nonanoate (3)	rX(3) = k1*cX(1)*cX(2) - k2*cX(3)*cX(4)
Water (4)	rX(4) = k1*cX(1)*cX(2) - k2*cX(3)*cX(4)

Table O3: Rates of change of individual components

Where:

- rX(i) = rate of change of component i
- cX(i) = concentration of component i

The total volume is known, it is possible to work out the change in composition of each component over the 1 second time interval, due to reaction. Change also occurs due to the removal of distillate, and the change in composition due to the butanol and water removal from the column is determined from the equations built on observations from the experiments.

The water removal rate is calculated from the relevant equation depending on whether a fast or slow reaction case is under consideration. The equations for the rate of water removal from the column are valid over a certain range of temperatures where collection was observed during the experiments. Below this range, no distillate is collected. If the temperature is predicted to go above the range observed in experiments, then a constant value is used, which has been selected based on a visual examination of the trend of the plot at this point.

Equations for Distillate Rate

For strong acids, heteropoly acids and ferric sulfate:

- below 114.62°C rate = 0
- above 154.92°C rate = $1.5x10^{-4}$ mol/s
- else:

  $y = (-4.339x10^{-10})x^4 + (2.406x10^{-07})x^3 – (4.959x10^{-05})x^2 +$
  $(4.504x10^{-03})x – 0.152$

For slower cases with no catalyst or zinc acetate:

- below 134°C rate = 0
- above 146.2 °C rate = $1. 5x10^{-4}$ mol/s
- else:

  $y = (8.557x10^{-07})x^3 – (3.637x10^{-04})x^2 + (5.151E-02)x – 2.430$

Where:

- y = mol/s water removed as distillate
- x = pot temperature (°C)

A ‘calculated’ amount of water removed is displayed in the spreadsheet. However, this amount of water may not actually be what is removed. Water and butanol can only be removed from the pot if there is some present. The equations are set up so that:

- If the calculated amount of butanol/water is available in the pot, then this is the value taken.
- If there is less than the calculated amount, then the simulation predicts that what is present is removed, but no more.
- If none is available, the boil up rate is zero.

The next cell along in the spreadsheet contains an ‘IF’ statement:

=IF(D2>154.2,0.00015,IF(D2>114.62,AZ2,0))

If the pot temperature is greater than 154.92°C, a fixed value is used (chosen from observation of the charts). If the pot temperature is between 154.92°C and 114.62°C then the calculated amount of water is removed. If the temperature is less than this, no water would be removed. A final condition on the water removed is whether the

distillate policy change has been applied yet. The reflux ratio is changed during the experiments from total reflux to RR=1 1hour after the catalyst is added. So if the time is less than 3600 seconds, the calculated potential water removal is overruled and the water removal is 0 mol/s.

=IF(A2<3600,0,IF(BA2>I2,I2,BA2))

To ensure mass balance, more water cannot be taken from the pot than is present. An 'IF' statement has been included in this condition so that if the calculated water to be removed is higher than the amount that is present, it can take what is present but no more. The water butanol ratio depends upon the temperature, and different equations are used depending on whether the case is fast or slow.

Fast:

=IF(D4>118,4.3,IF(D4>106,2.85,0))

Slow:

=IF(D6>136.6,4.3,IF(D6>133,2.85,0))

The amount of butanol removed is then a simple ratio of the water removal. The final cell in each row of the spreadsheet shows the total distillate removed, a sum of the water and butanol. The next row, representing the next time interval, begins with the updated molar compositions in the pot.

Appendix P: Excel Model Simulations vs. Experimental Data for Runs with Catalyst Addition

Zinc Ac

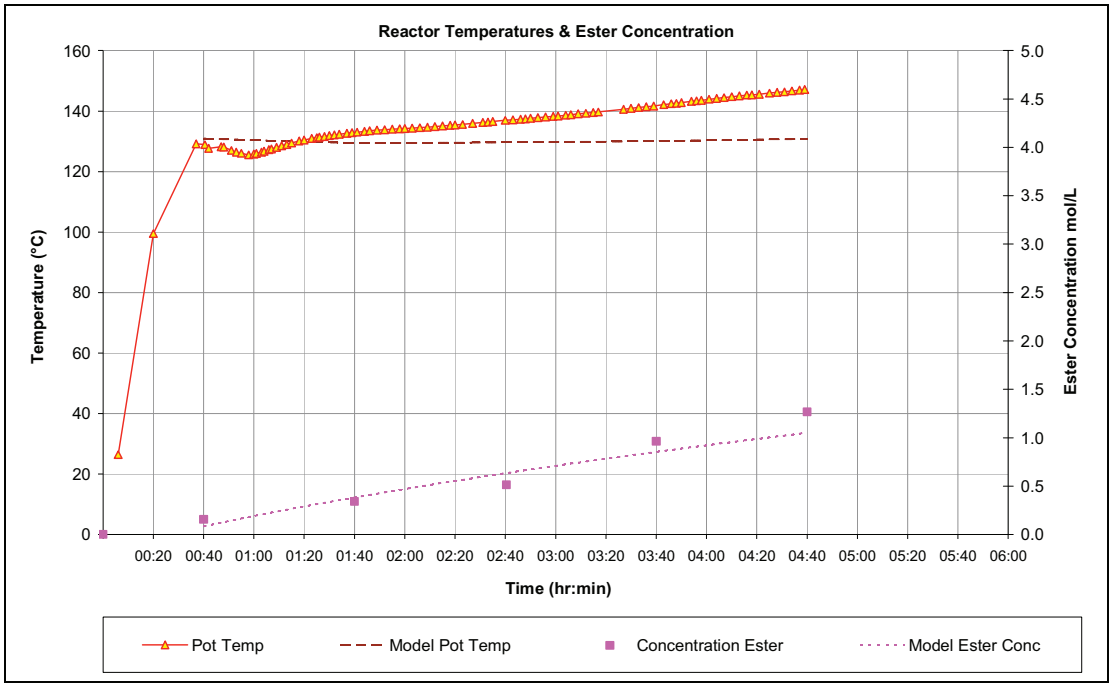

Chart P1: Real vs. Excel-Simulated Reactor Profiles: RD Esterification: ZnAc

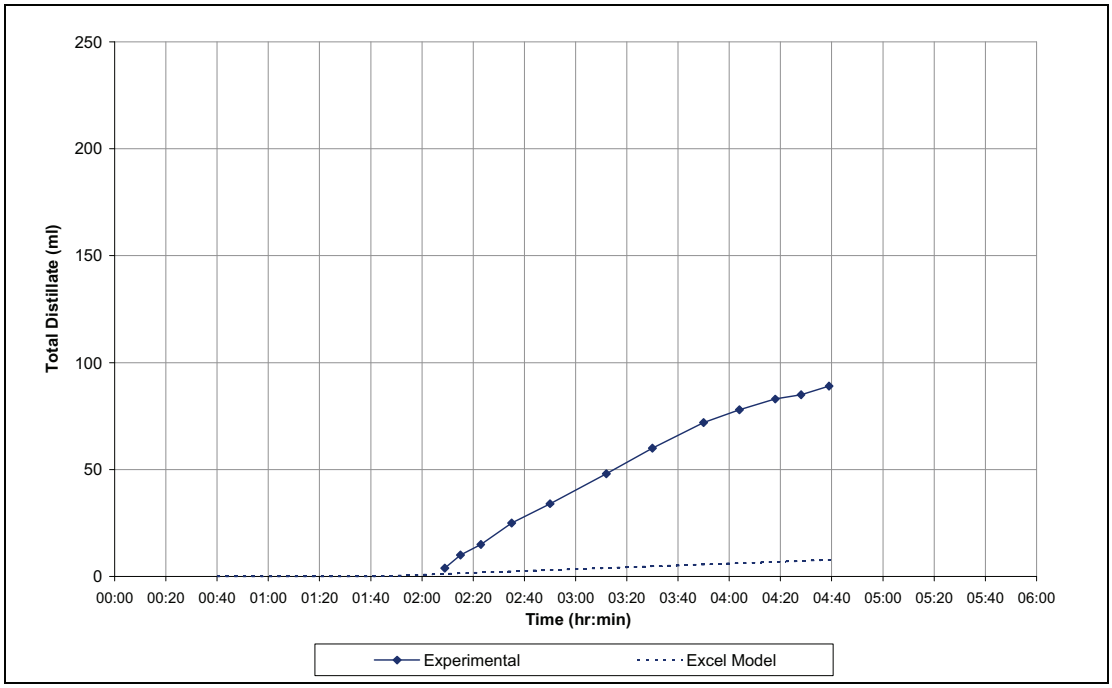

Chart P2: Real vs. Excel-Simulated Distillate Collection: RD Esterification: ZnAc

MSA

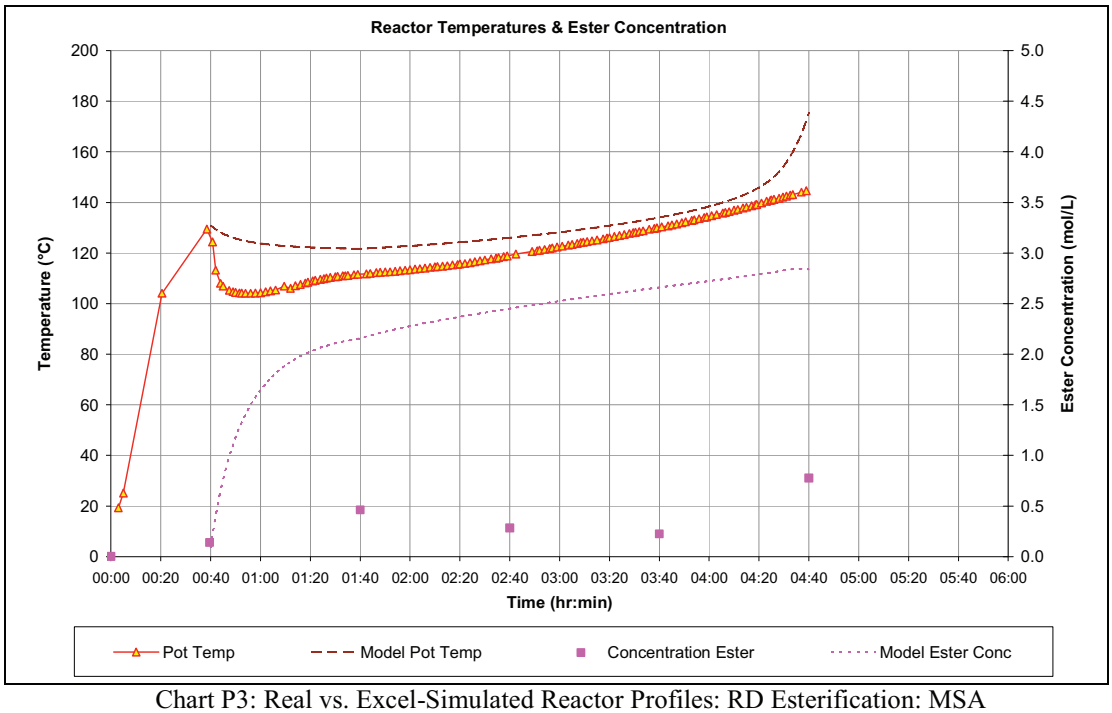

Chart P3: Real vs. Excel-Simulated Reactor Profiles: RD Esterification: MSA

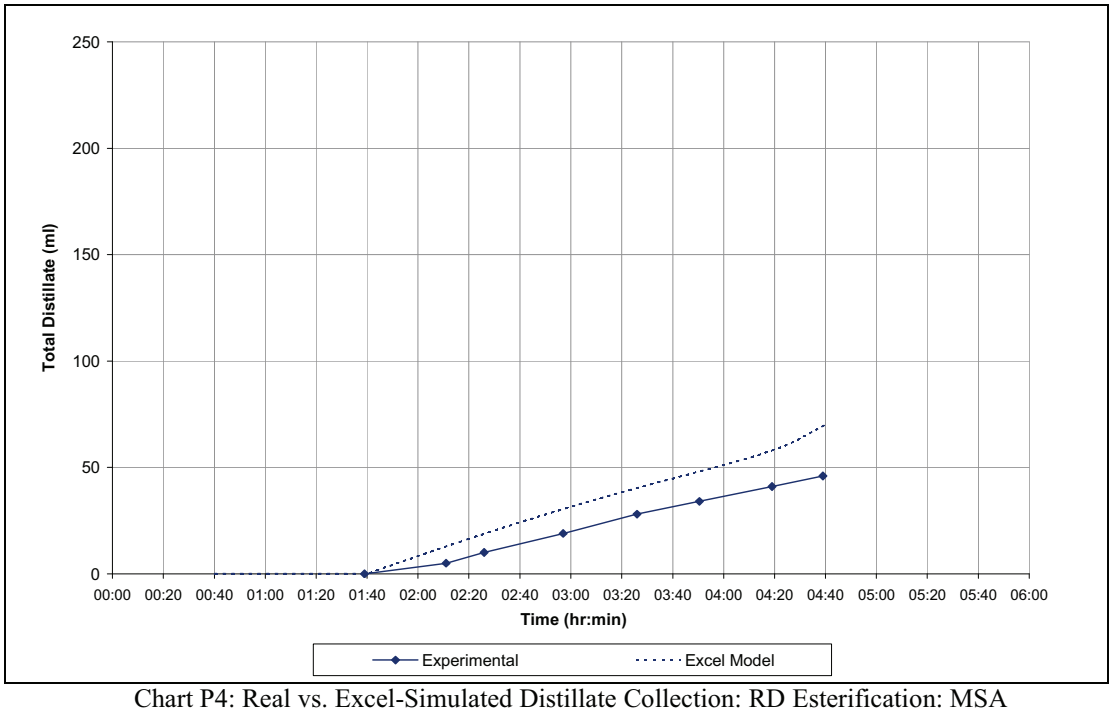

Chart P4: Real vs. Excel-Simulated Distillate Collection: RD Esterification: MSA

H2SO4

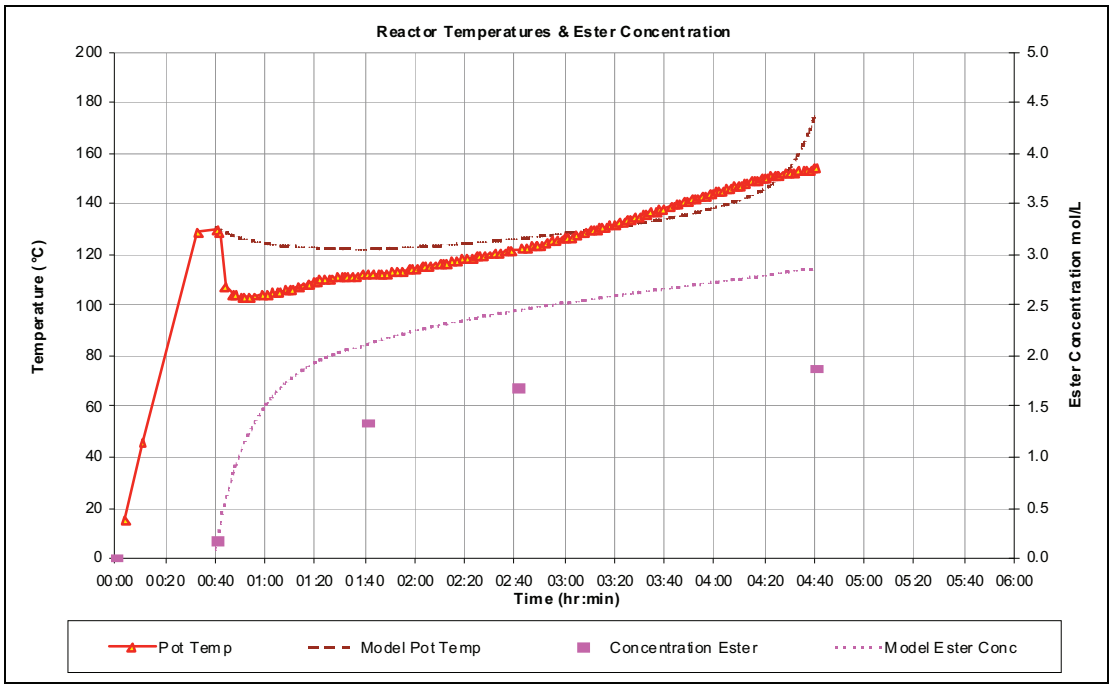

Chart P5: Real vs. Excel-Simulated Reactor Profiles: RD Esterification: H_2SO_4

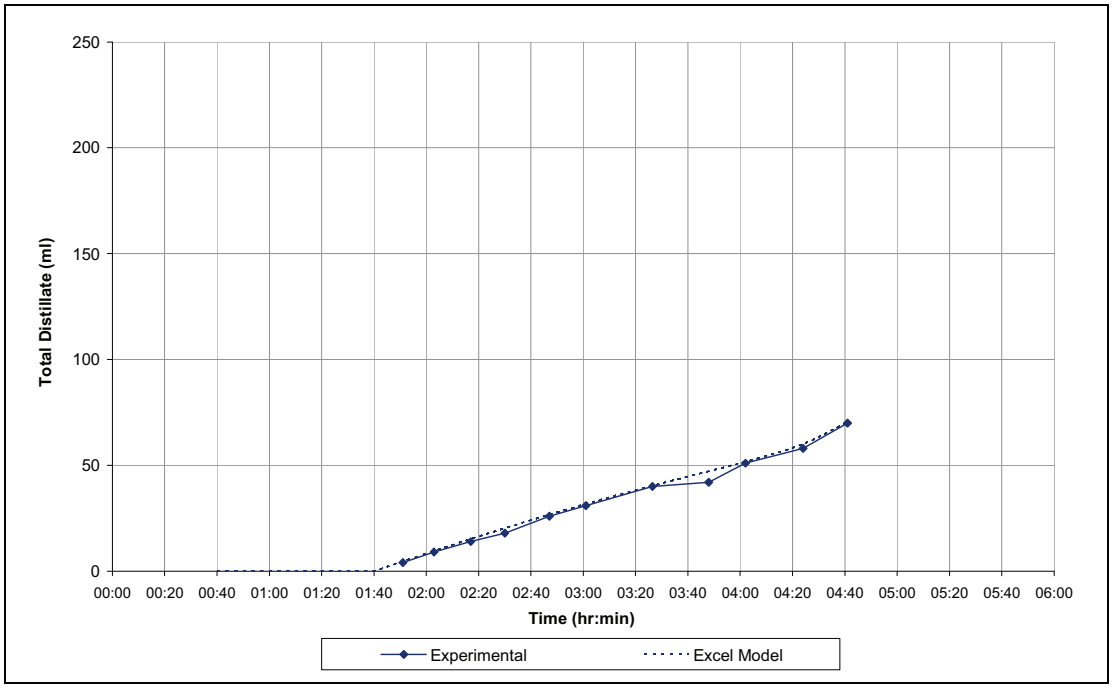

Chart P6: Real vs. Excel-Simulated Distillate Collection: RD Esterification: H_2SO_4

PhosMo

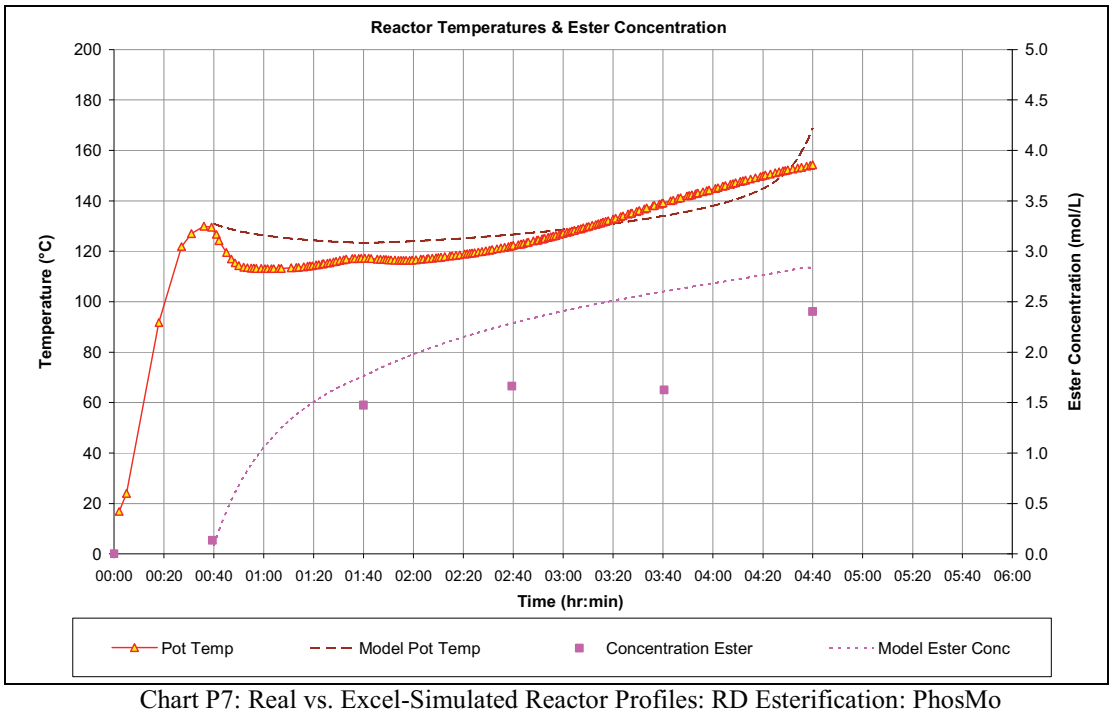

Chart P7: Real vs. Excel-Simulated Reactor Profiles: RD Esterification: PhosMo

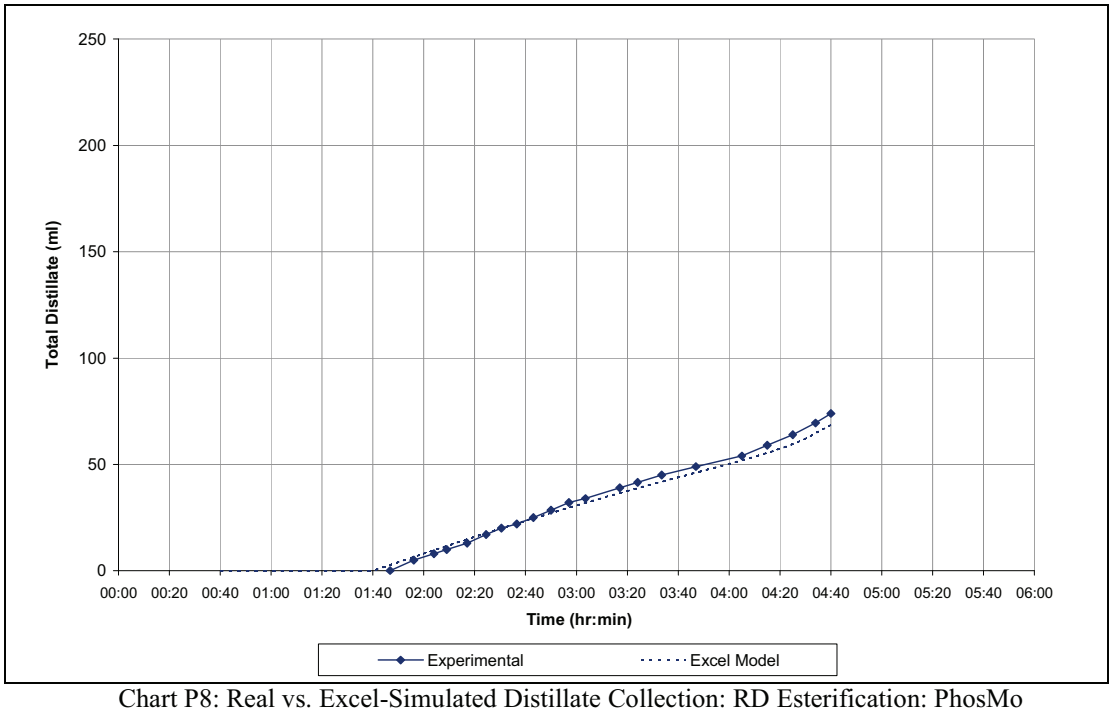

Chart P8: Real vs. Excel-Simulated Distillate Collection: RD Esterification: PhosMo

FeSulf

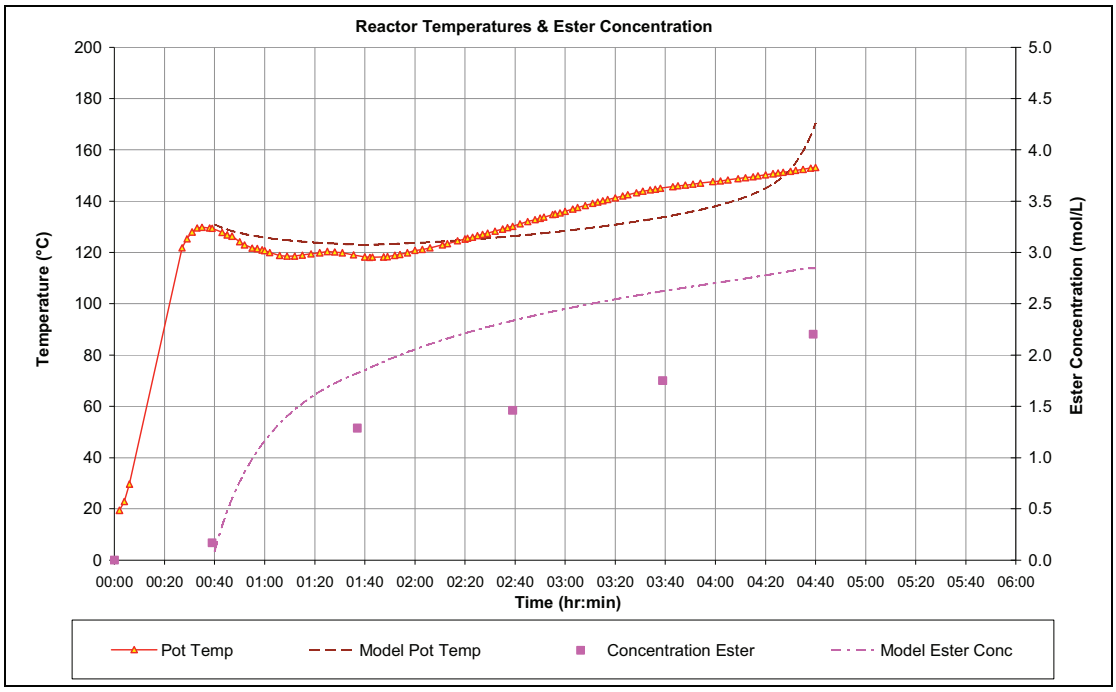

Chart P9: Real vs. Excel-Simulated Reactor Profiles: RD Esterification: FeSulf

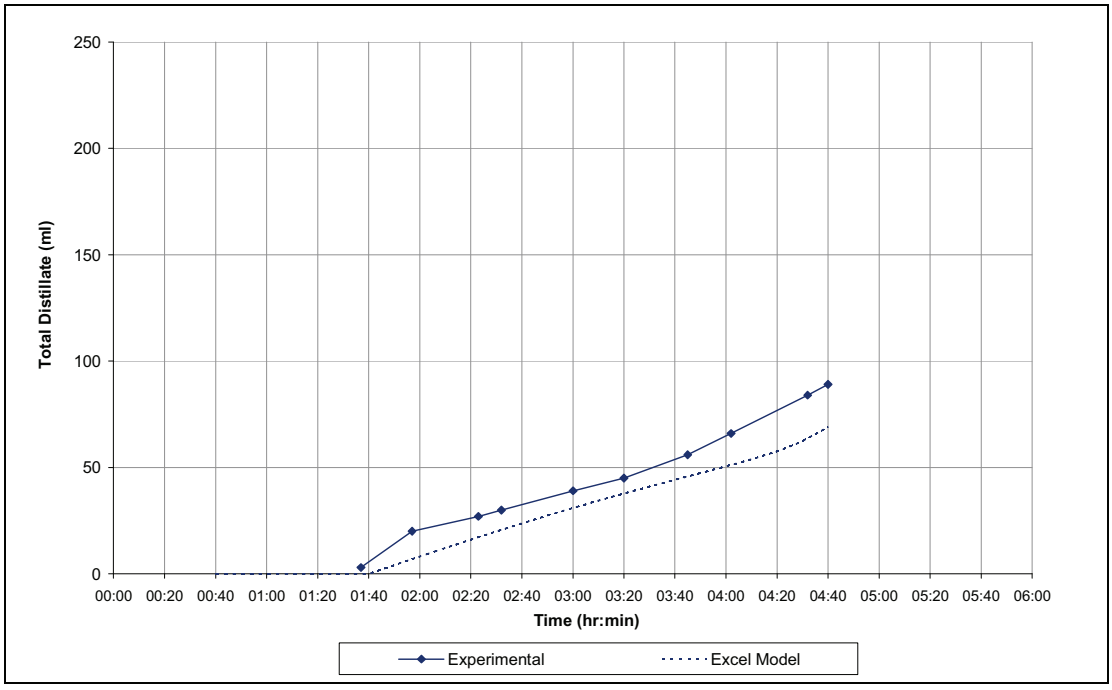

Chart P10: Real vs. Excel-Simulated Distillate Collection: RD Esterification: FeSulf

Appendix Q: List of Descriptor Variables

1. Molecular Weight [g/mol]
2. H-Bond Donor
3. H-Bond Acceptor
4. Topological Polar Surface Area
5. Heavy (Non-H) Atom Count
6. Complexity
7. Covalently-Bonded Unit Count
8. Water of hydration
9. Acetate groups
10. H-Bond Donor per Unit of MW
11. Topological Polar Surface Area per Unit of MW
12. Complexity per Unit of MW
13. Water of hydration per Unit of MW
14. Acetate groups per Unit of MW
15. MW per Covalently-Bonded Unit
16. H-Bond Donor per Covalently-Bonded Unit
17. H-Bond Acceptor per Covalently-Bonded Unit
18. Topological Polar Surface Area per Covalently-Bonded Unit
19. Heavy Atom Count per Covalently-Bonded Unit
20. Complexity per Covalently-Bonded Unit
21. MW per heavy (Non-H) atom
22. H-Bond Acceptor per heavy (Non-H) atom
23. Topological Polar Surface Area per heavy (Non-H) atom
24. Covalently-Bonded Unit Count per heavy (Non-H) atom
25. Water of hydration per heavy (Non-H) atom
26. Carbon Atom Count
27. Hydrogen Atom Count
28. Metal Atom Count
29. Phosphorus, Sulfur or Chlorine Atom Count
30. H bond acceptor (O atom) per H atom
31. Topological Polar Surface Area per H atom
32. Complexity per H atom

33. Phosphorus, Sulfur or Chlorine Atom Count per H atom
34. Carbon Percent by Mass
35. Hydrogen Percent by Mass
36. Oxygen Percent by Mass
37. Metal Percent by Mass
38. Phosphorus, Sulfur or Chlorine Percent by Mass

Appendix R: Details of Multivariate Statistical Models

R.1 Metal Acetates Only

A PCA plot shows there are no multivariate outliers, and it is observed that 3 PCs are able to explain over 87% of the variance.

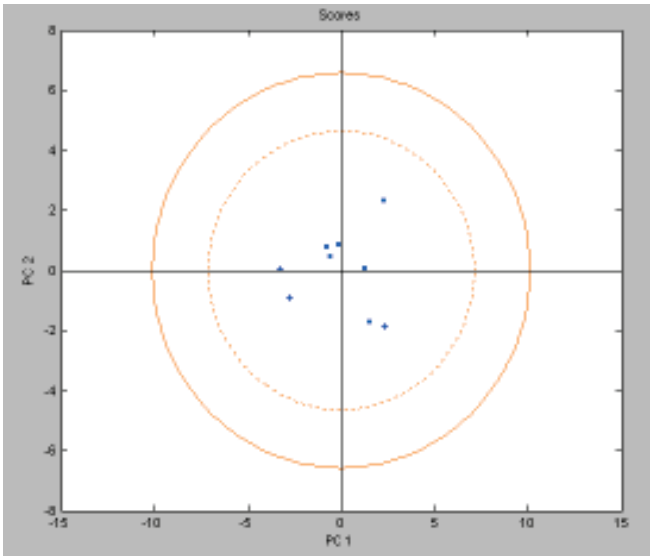

Figure R1: PCA Plot Metal Acetates Only

A cross validation performed on this data set was uninformative, but the scale on the LHS shows that the PRESS values are low for up to 4 latent variables.

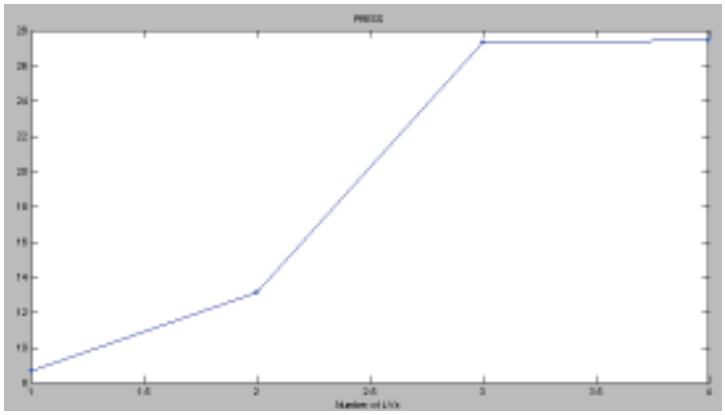

Figure R2: Cross Validation Chart Metal Acetates Only

The PLS model for this case explains 17.70% more cumulative variance than the models based on 3 runs with randomised outputs (all 4 LVs).

Latent Variable	% Cumulative Variance in Descriptors	% Cumulative Variance in Output
1	51.22	52.62
2	75.93	59.33
3	79.99	66.73
4	**92.88**	**67.40**
5	99.91	67.49
6	99.99	70.75

Table R1: Explained Variances vs. Number of Latent Variables

Randomised Run	% Cumulative Variance in Descriptors	% Cumulative Variance in Output
1	93.75	47.04
2	92.66	53.61
3	93.73	48.46
Average	**93.38**	**49.70**

Table R2: Explained Cumulative Variances for Randomised Runs

The Chart of the regression coefficients shows that the heaviest weighting is applied to LV3, followed by LV1. The 4th latent variable has a very low weighting.

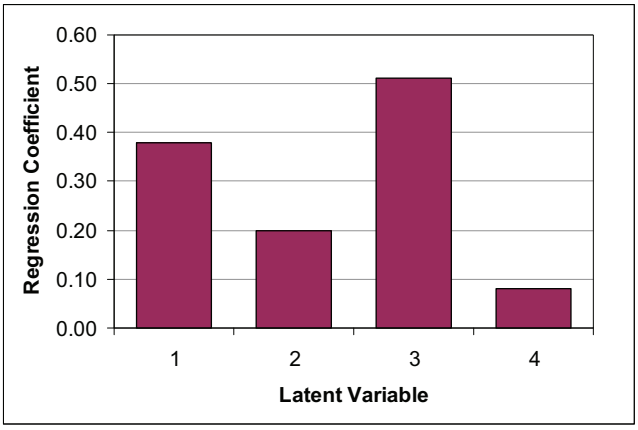

Figure R3: Regression Coefficients

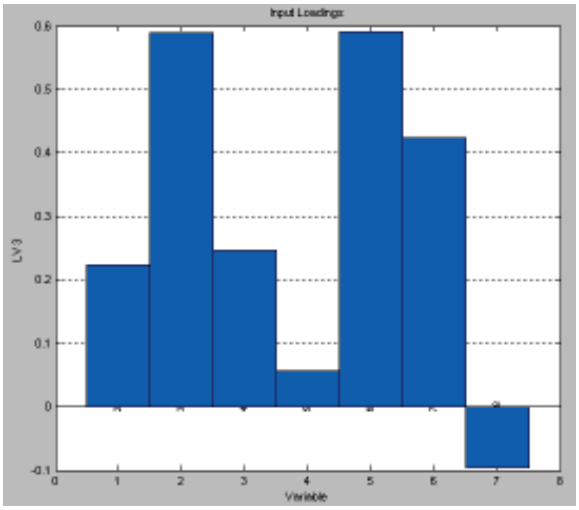

Figure R4: Input Loadings for LV3

LV3 Variables with greatest Input Loadings, greatest first:

- Topological Polar Surface Area per H atom (6)
- Water of hydration (3)
- Complexity per H atom (7)

R.2 All 12 RD Catalyst Candidates, All 9 RD Outputs

A PCA plot shows that there are no multivariate outliers in the data set. This time, catalysts 5 and 6 (the heteropoly acids) do not lie far from the rest of the cluster of catalyst data points.

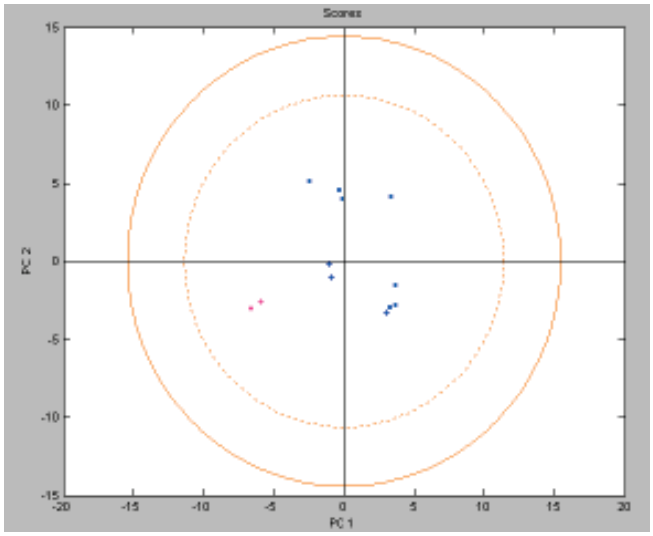

Figure R5: PCA Plot

Four PCs would be able to explain over 81% of the variance. Cross validation indicates an optimum number of latent variables to be five.

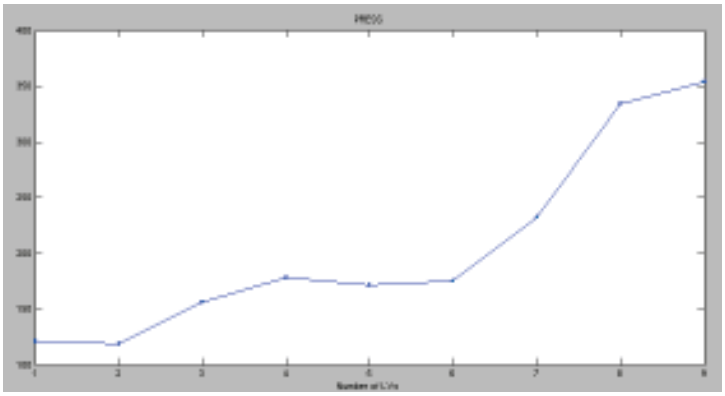

Figure R6: Cross Validation Chart

Five latent variables also give good explanation of the variances, with little benefit in going up to six. The PLS model is compared against the average of 3 runs with randomised outputs (all with 5LVs).

Latent Variable	% Cumulative Variance in Descriptors	% Cumulative Variance in Output
1	21.26	43.67
2	50.83	54.23
3	62.00	64.67
4	79.31	69.83
5	**90.46**	**73.70**
6	94.62	77.82

Table R3: Explained Variances vs. Number of Latent Variables

Randomised Run	% Cumulative Variance in Descriptors	% Cumulative Variance in Output
1	89.35	55.49
2	90.87	53.58
3	88.85	65.77
Average	**89.69**	**58.28**

Table R4: Explained Cumulative Variances for Randomised Runs

From examination of the Regression Coefficients it can be seen that LV1 is the most heavily weighted, followed by LV3.

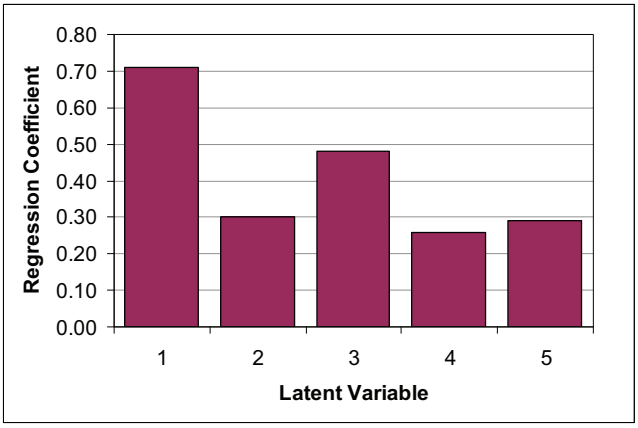

Figure R7: Regression Coefficients

Looking at the Output Loadings for LV1 reveals which outputs are dominating the PLS model. The outputs with the greatest loadings for LV1 are:

- Lowest Pot Temp (4)
- Time Col Top Temp Starts Rising (7)
- Initial Rate Pot Temp Fall (5)
- Time for Top Temp to Stabilise (8)

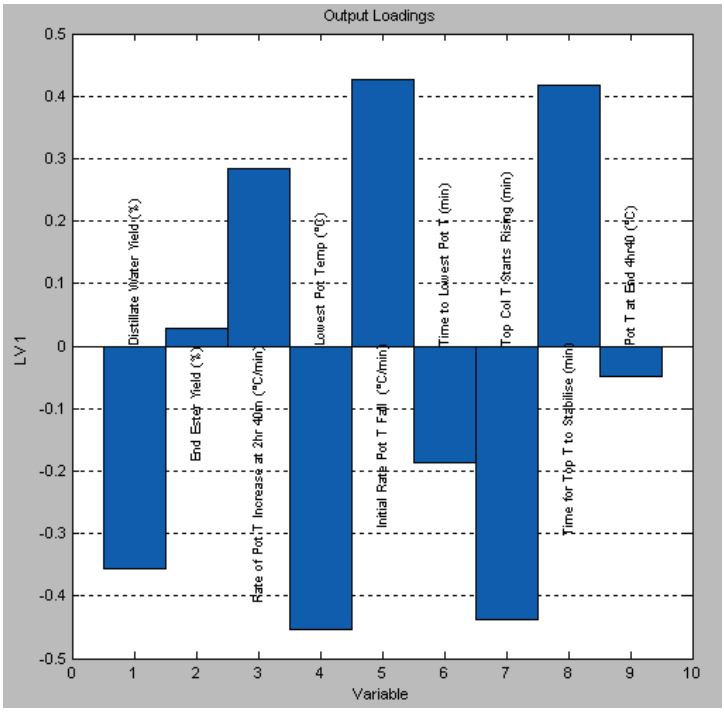

Figure R8: Output Loadings for LV1

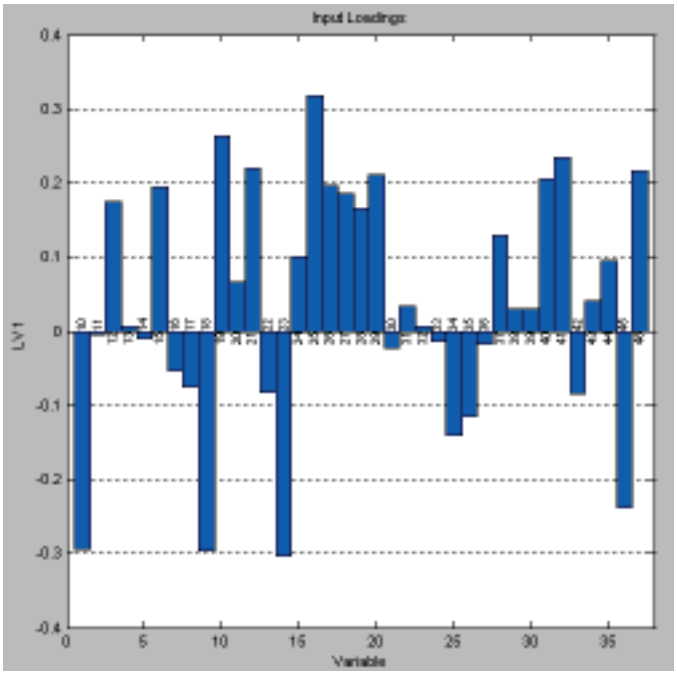

Figure R9: Input Loadings for LV1

LV1 Variables with greatest Input Loadings, greatest first:

- 25 H bond donor per covalently-bonded unit (25)
- 23 Acetate groups per unit MW (23)
- 18 Acetate groups (18)
- **10 Half Life (10)**
- 19 H bond donor per unit MW (19)

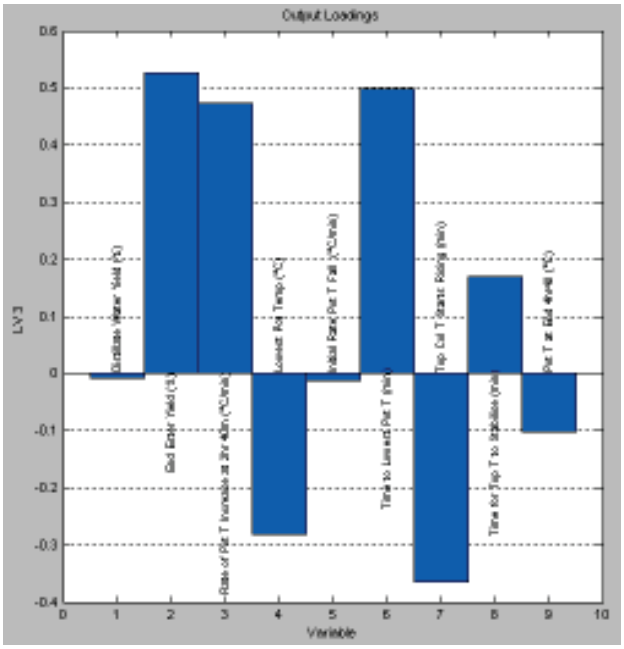

Figure R10: Output Loadings for LV3

The outputs with the greatest loadings for LV3 are:

- End Ester Yield (2)
- Time to Lowest Pot Temp (6)
- Rate of Pot Temp Increase at 2hr40min (3)
- Time Top Column Temp Starts Rising (7)

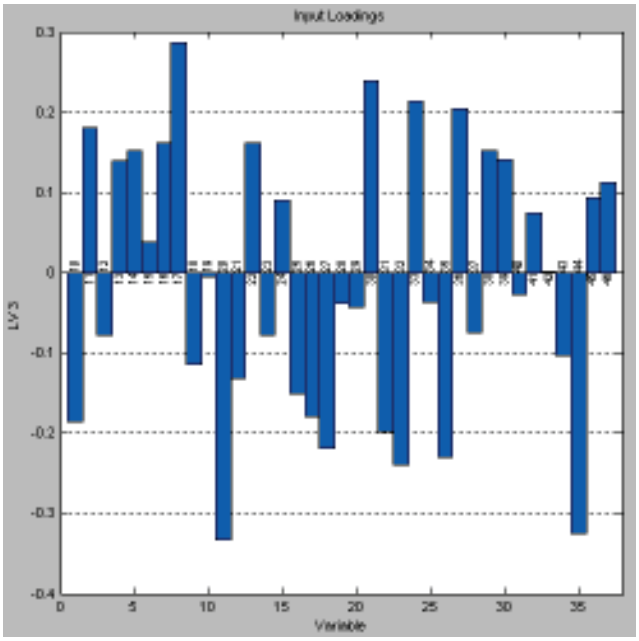

Figure R11: Input Loadings for LV3

LV3 Variables with greatest Input Loadings, greatest first:

- Topological Polar Surface Area per MW (20)
- Oxygen percent by mass (44)

- Water of hydration (17)

R.3 RD Outputs Not Correlated to Half Life

Model details: after processing with a Rank Correlation Matrix, the data set contained 36 input variables.

- Catalyst candidates: 12
- Inputs (X-block): 36 catalyst descriptors
- Output (Y-block): 5 outputs

The outputs included are:

1 Distillate Water Yield (%)

2 End Pot Ester Yield (%)

3 Time to Lowest Pot Temp (min)

4 Time for Top Temp to Stabilise (min)

5 Pot Temp at End 4hr40 (°C)

The PCA plot of the first two principal components shows that there are no multivariate outliers in this data set, but samples 5 and 6 (heteropoly acids) appear slightly separated from the rest of the catalysts. Examination of the cross validation output and the cumulative variances indicates an optimum number of latent variables to be four.

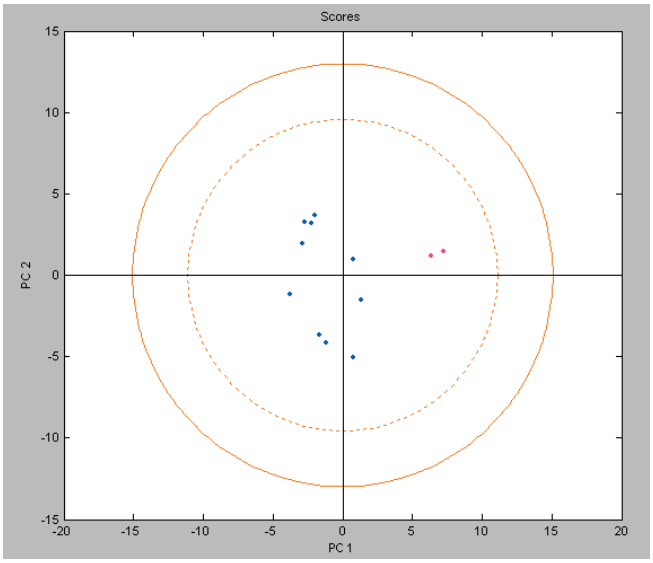

Figure R12: PCA Plot

The PLS model is compared against the average of 3 runs with randomised outputs (all with 4LVs).

Latent Variable	% Cumulative Variance in Descriptors	% Cumulative Variance in Output
1	20.30	29.55
2	49.33	41.32
3	62.65	52.08
4	**78.85**	**59.58**
5	90.44	63.00
6	93.83	69.84

Table R5: Explained Variances vs. Number of Latent Variables

Randomised Run	% Cumulative Variance in Descriptors	% Cumulative Variance in Output
1	80.15	55.08
2	85.60	49.55
3	83.73	47.26
Average	**83.16**	**50.63**

Table R6: Explained Cumulative Variances for Randomised Runs

From examination of the Regression Coefficients it can be seen that LV1 is the most heavily weighted, followed by LV3.

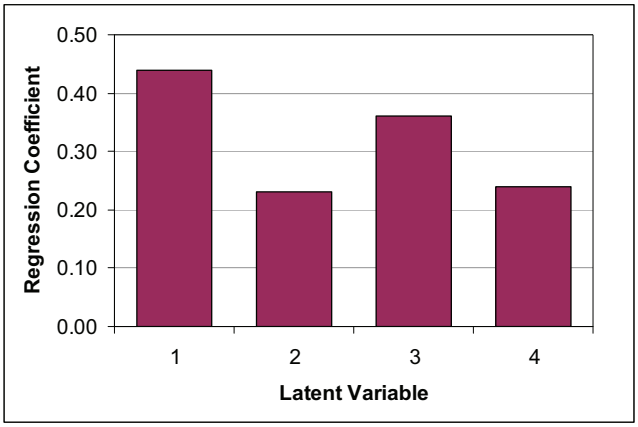

Figure R13: Regression Coefficients

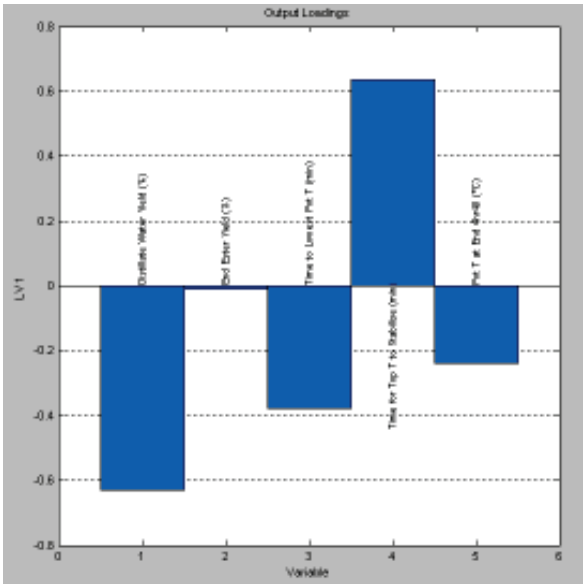

Figure R14: Output Loadings for LV1

Looking at the Output Loadings for LV1 reveals which outputs are dominating the PLS model.

- Distillate Water Yield (%) (1)
- Time for Top Temp to Stabilise (min) (4)

Of these, only 'Time for Top Temp to Stabilise' appeared in the list of more well explained outputs in the previous attempt, with all outputs included.

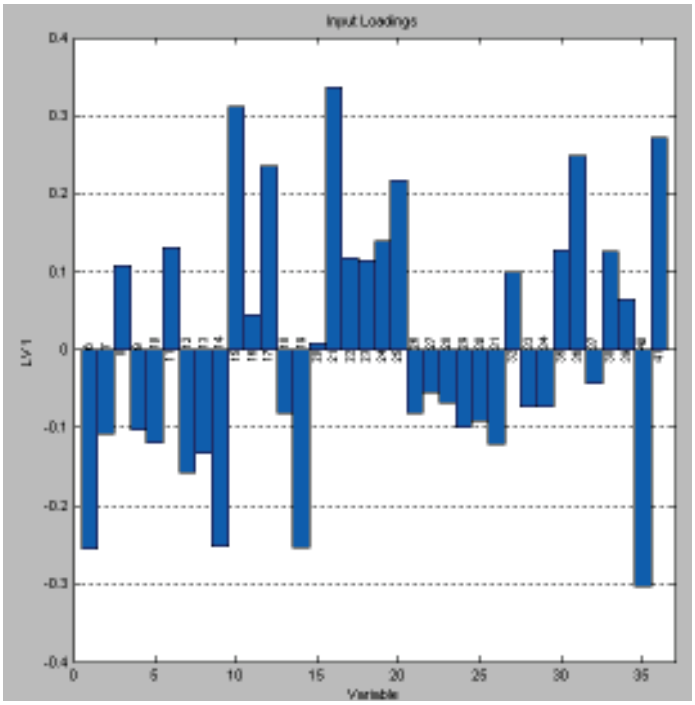

Figure R15: Input Loadings for LV1

LV1 Variables with greatest Input Loadings, greatest first:

- H-Bond Donor per Covalently-Bonded Unit (21)
- H-Bond Donor per Unit of MW (15)
- Metal Percent by Mass (40)
- Phosphorus, Sulfur or Chlorine Percent by Mass (41)

The outputs with the greatest loadings for LV3 are:

- End Ester Yield (%) (2)
- Time to Lowest Pot Temp (min) (3)

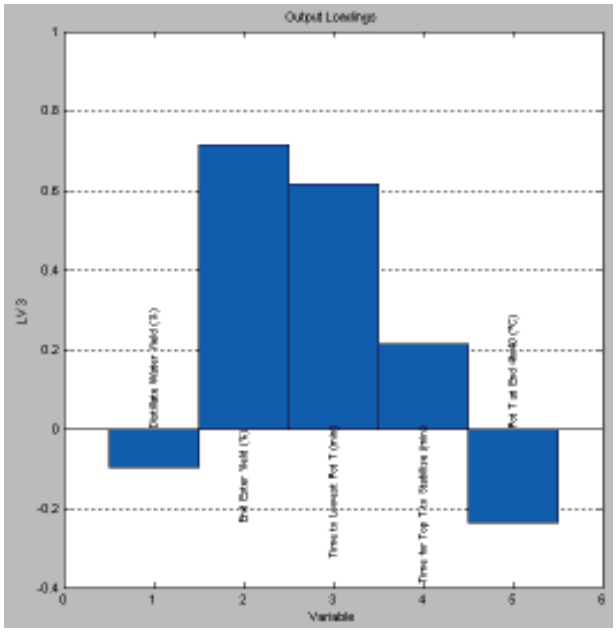

Figure R16: Output Loadings for LV3

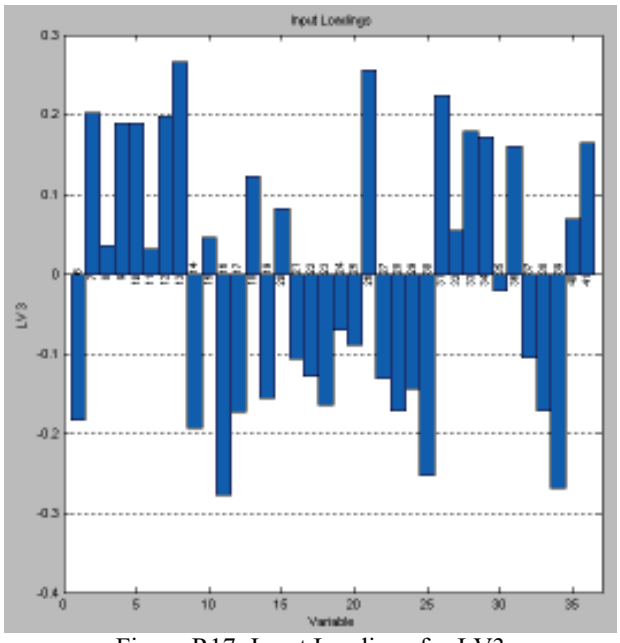

Figure R17: Input Loadings for LV3

LV3 Variables with greatest Input Loadings, greatest first:

- Topological Polar Surface Area per Unit of MW (16)
- Oxygen Percent by Mass (39)
- Water of hydration (13)
- MW per heavy (Non-H) atom (26)
- Hydrogen Atom Count (30)

R.4 Catalyst Screening – With Field Templater Variables

A PCA plot shows that the data forms a very loose cluster, but there are no multivariate outliers in the data set.

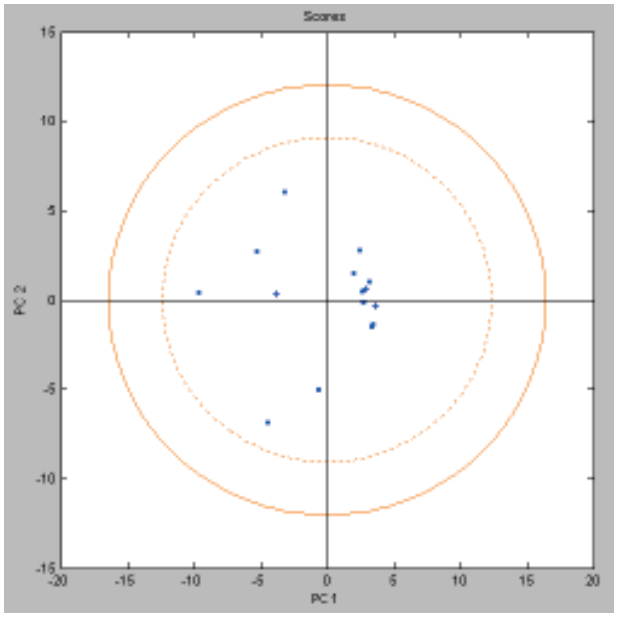

Figure R18: PCA Plot

This time, four principal components are able to explain over 85% of the variance. This is slightly better than in the previous case, but some improvement would be expected due to the removal of the high molecular weight heteropoly acids from the data set. Cross validation indicates an optimum number of latent variables to be seven.

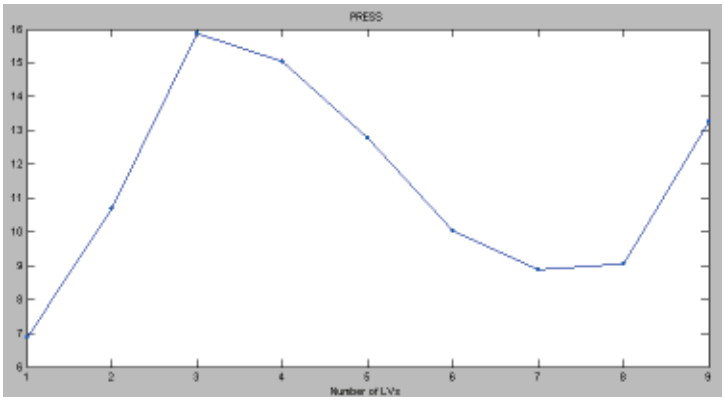

Figure R19: Cross Validation Chart

Examining the cumulative variances explained shows that there is little benefit in going over four latent variables: The PLS model is compared against the average of 3 runs with randomised outputs (all with 4LVs).

Latent Variable	% Cumulative Variance in Descriptors	% Cumulative Variance in Output
1	39.36	75.13
2	59.97	85.80
3	71.64	92.23
4	**82.79**	**95.43**
5	86.47	97.57
6	89.97	97.93

Table R7: Explained Variances vs. Number of Latent Variables

Randomised Run	% Cumulative Variance in Descriptors	% Cumulative Variance in Output
1	79.33	48.20
2	82.87	67.69
3	71.12	65.86
Average	**77.77**	**60.58**

Table R8: Explained Cumulative Variances for Randomised Runs

Catalyst half lives predicted to within +/- 5%: only 6 out of 15 predictions are this close:

- Bismuth (III) Acetate
- Lead (II) Acetate Trihydrate
- Zinc Acetate Dihydrate
- Sulfated zirconium (IV) hydroxide,
- Sodium Acetate
- Potassium Acetate

Out of these, only 3 are predicted to within 0.25hours of the experimental value: bismuth (III) acetate, sulfated zirconium (IV) hydroxide, and potassium acetate.

Looking at the Regression Coefficients for four latent variables, it is seen that LV1 is by far the most heavily weighted. The next most weighted is LV3, which has a coefficient value around half that of LV1.

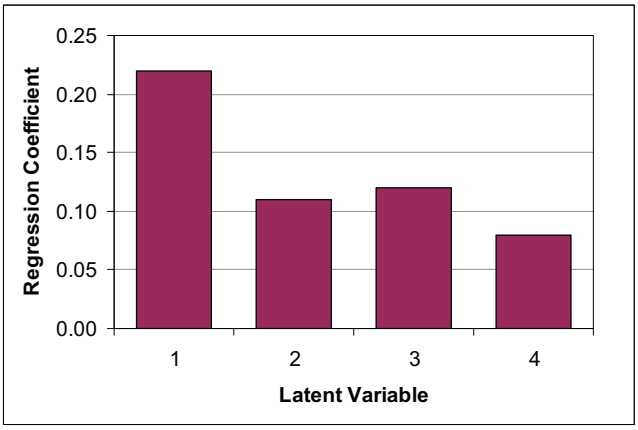

Figure R20: Regression Coefficients

Examination of the Input Loadings for LV1 reveals the key variables that the model is using to explain the variance between the half life values for the different catalysts:

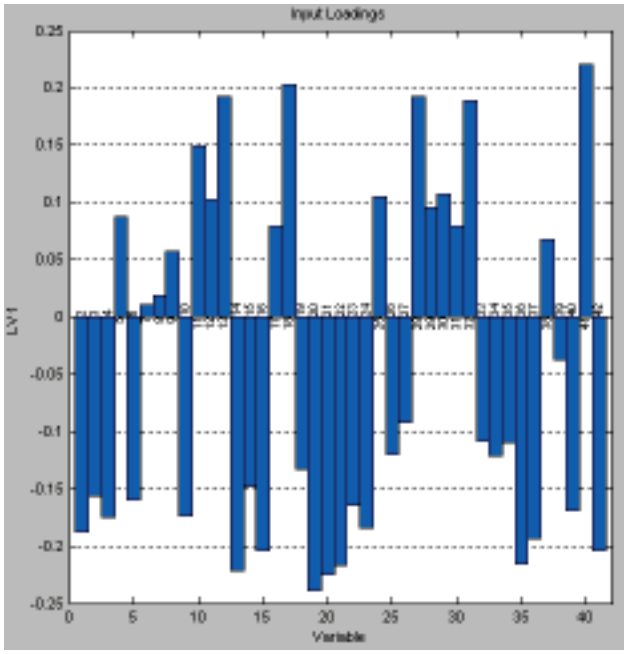

Figure R21: Input Loadings for LV1

LV1 Variables with greatest Input Loadings, greatest first:

- H Bond donor per covalently-bonded unit (20)
- H Bond acceptor per covalently-bonded unit (21)
- H Bond donor per unit MW (14)
- Metal % by mass (41)

R.5 Metal Acetates Only With FieldTemplater Variables Included

After processing with a Rank Correlation Matrix, the data set contained ten input variables.

- Catalyst candidates: 9
- Inputs (X-block): 10 (7 catalyst descriptors, 3 FieldTemplater similarity scores)
- Output (Y-block): half life

PCA shows there are no multivariate outliers and it is observed that 3 PCs are able to explain 89.5% of the variance.

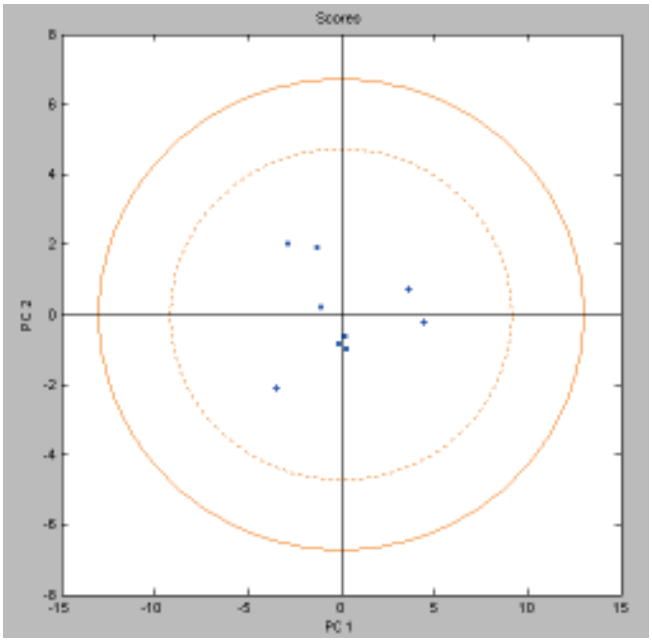

Figure R22: PCA Plot

A cross validation performed on this data set was again uninformative, but the scale on the LHS shows that the PRESS values are low for up to 5 latent variables.

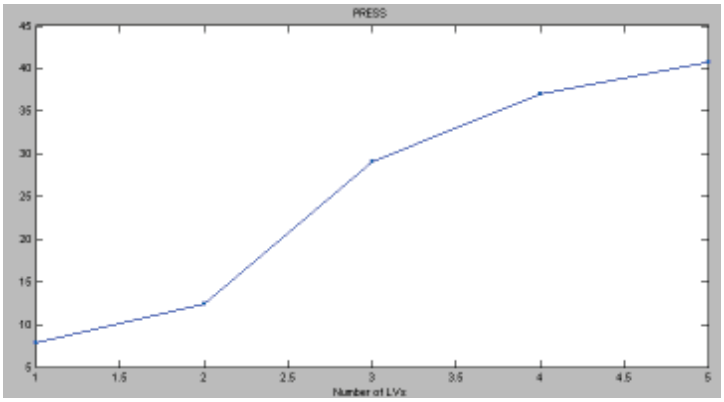

Figure R23: Cross Validation Chart

Latent Variable	% Cumulative Variance in Descriptors	% Cumulative Variance in Output
1	63.84	52.83
2	81.66	58.33
3	85.48	69.41
4	**93.31**	**73.87**
5	97.68	80.72
6	99.98	88.32

Table R9: Explained Variances vs. Number of Latent Variables

In this case there is little improvement in going over 4 latent variables. The PLS model is compared against the average of 3 runs with randomised outputs (all with 4 LVs).

Randomised Run	% Cumulative Variance in Descriptors	% Cumulative Variance in Output
1	94.47	58.58
2	96.55	63.17
3	96.77	63.02
Average	**95.93**	**61.59**

Table R10: Explained Cumulative Variances for Randomised Runs

From examination of the regression coefficients it can be seen that LV3 is the most heavily weighted, followed by LV1.

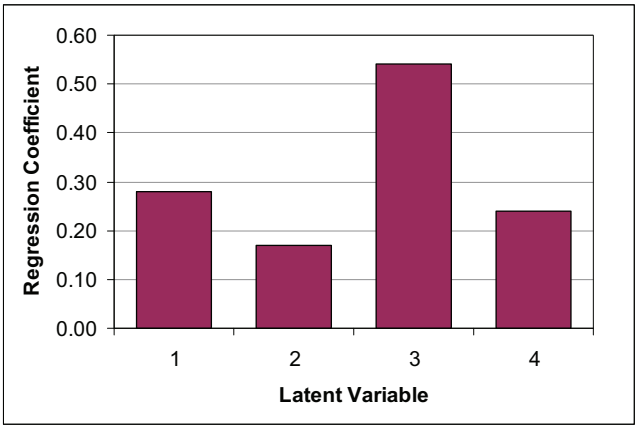

Figure R24: Regression Coefficients

Examination of the Input Loadings for LV3 reveals key variables.

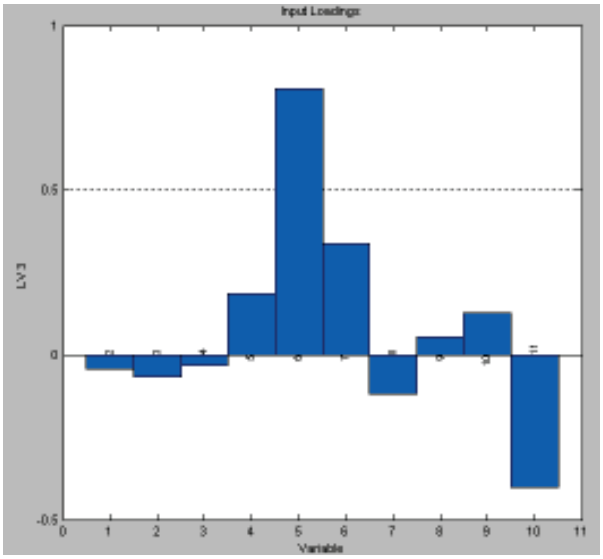

Figure R25: Input Loadings for LV3

LV3 Variables with greatest Input Loadings, greatest first:

- Water of hydration (6)
- Metal Percent by Mass % (11)
- Acetate groups (7)

Examination of the Input Loadings on LV1:

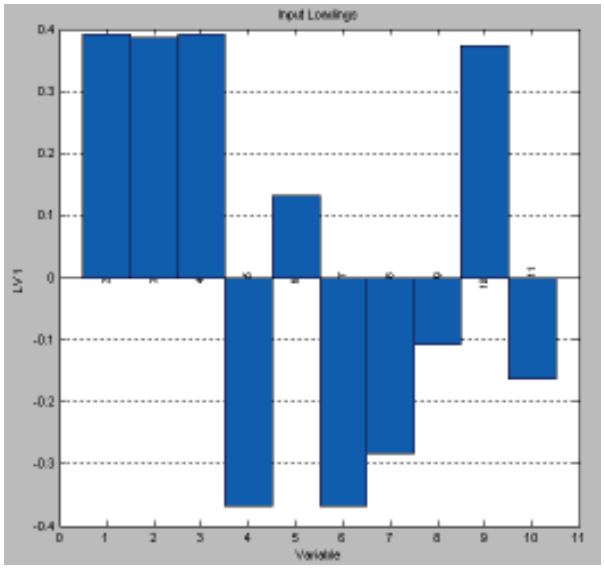

Figure R26: Input Loadings on LV1

LV1 Variables with greatest Input Loadings, greatest first:

- Similarity (2)
- Shape Similarity (4)
- Field Similarity (3)

Examination of the detail for LV1 shows that the FieldTemplater similarity variables are weighted strongly in LV1. Their inclusion could have contributed to the small improvement in the level of variance explained. However, the proportion of the variance explained by the models built on randomised outputs is also improved.

R.6 RD outputs Without FieldTemplater Similarity Variables

After processing with a Rank Correlation Matrix, the data set contained 34 input variables.

- Catalyst candidates: 9
- Inputs (X-block): 34 catalyst descriptors
- Output (Y-block): 9 outputs

The PCA plot of the first two principal components shows that there are no multivariate outliers in this data set.

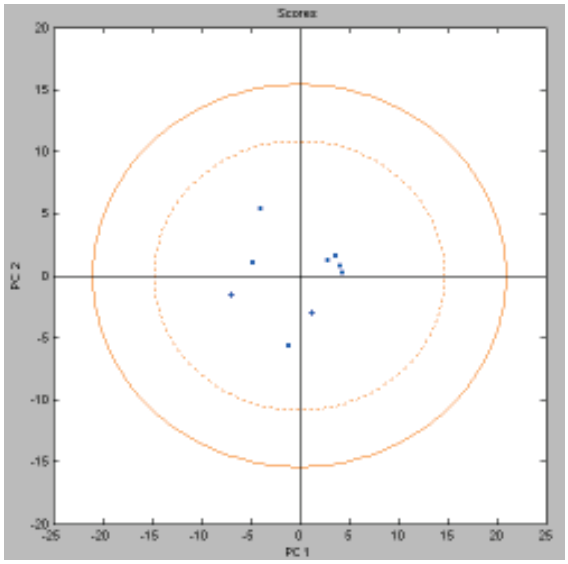

Figure R27: PCA Plot

Cross validation indicates an optimum number of latent variables to be 3.

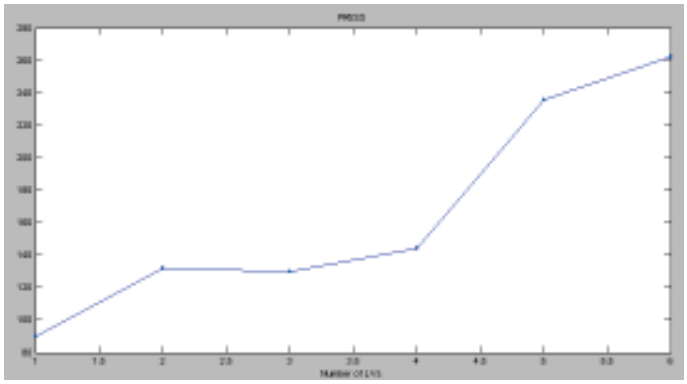
Figure R28: Cross Validation Chart

Latent Variable	% Cumulative Variance in Descriptors	% Cumulative Variance in Output
1	40.83	45.61
2	53.07	64.76
3	**79.66**	**67.01**
4	89.37	71.71
5	95.87	75.99
6	98.51	83.32

Table R11: Explained Variances vs. Number of Latent Variables

Compare these with the explained output variances from 3 runs with randomised outputs (3LVs):

Randomised Run	% Cumulative Variance in Descriptors	% Cumulative Variance in Output
1	66.74	52.39
2	79.82	53.54
3	76.34	46.87
Average	**74.30**	**50.93**

Table R12: Explained Cumulative Variances for Randomised Runs

From examination of the Regression Coefficients it can be seen that LV2 is the most heavily weighted, followed by LV1.

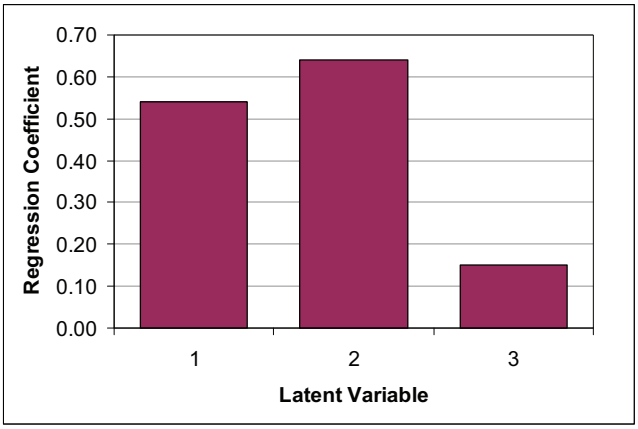

Figure R29: Regression Coefficients

The outputs with the greatest loadings for LV2 are:

3 Rate of Pot T Increase at 2hr 40m (°C/min)

6 Time to Lowest Pot T (min)

2 End Ester Yield (%)

7 Top Col T Starts Rising (min)

Examination of the Input Loadings for LV2 reveals the key variables that the model is using to explain the variance

36 Topological Polar Surface Area per H atom

35 H bond acceptor (O atom) per H atom

17 Water of hydration

38 Phosphorus, Sulfur or Chlorine Atom Count per H atom

22 Water of hydration per Unit of MW

15 Complexity

The outputs with the greatest loadings for LV1 are:

4 Lowest Pot Temp (°C)

5 Initial Rate Pot T Fall (°C/min)

8 Time for Top T to Stabilise (min)

7 Top Col T Starts Rising (min)

Examination of the Input Loadings for LV1 reveals the key variables that the model is using to explain the variance

42 Metal Percent by Mass %

25 H-Bond Donor per Covalently-Bonded Unit

37 Complexity per H atom

26 H-Bond Acceptor per Covalently-Bonded Unit

19 H-Bond Donor per Unit of MW

21 Complexity per Unit of MW

10 Half Life (hours)

R.7 RD outputs With FieldTemplater Similarity Variables

- Catalyst candidates: 9
- Inputs (X-block): 37 catalyst descriptors
- Output (Y-block): 9 outputs

The PCA plot of the first two principal components shows that there are no multivariate outliers in this data set.

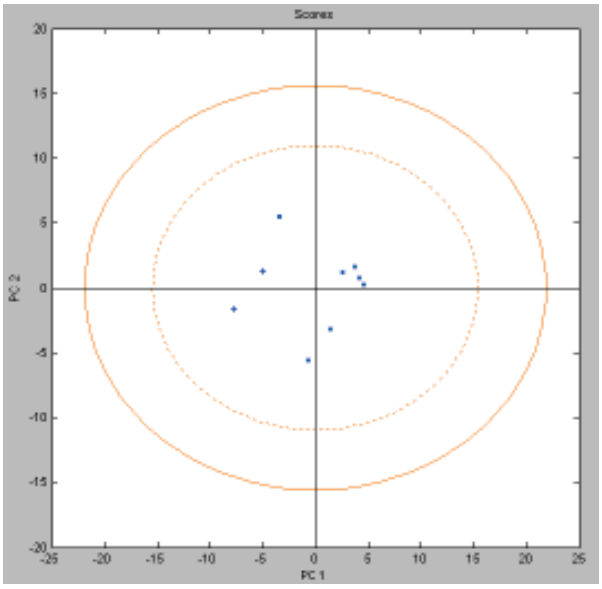

Figure R30: PCA Plot

Cross validation indicates an optimum number of latent variables to be 3.

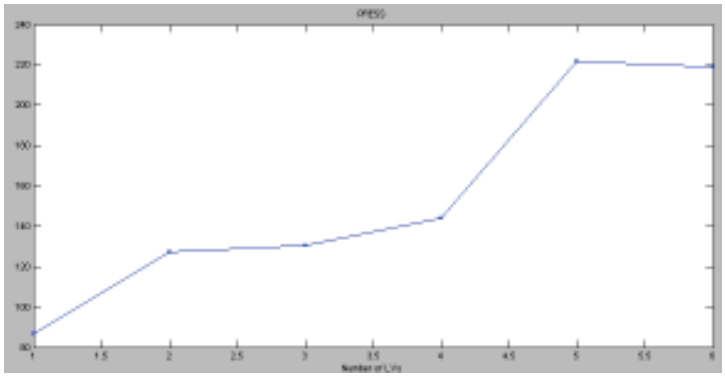

Figure R31: Cross Validation Chart

PLS model outputs are compared the explained output variances from 3 runs with randomised outputs (all with 3LVs).

Latent Variable	% Cumulative Variance in Descriptors	% Cumulative Variance in Output
1	41.86	46.35
2	53.71	65.74
3	**77.83**	**68.42**
4	89.87	72.24
5	95.18	77.26
6	98.28	83.98

Table R13: Explained Variances vs. Number of Latent Variables

Randomised Run	% Cumulative Variance in Descriptors	% Cumulative Variance in Output
1	80.38	52.63
2	76.95	45.88
3	80.64	49.07
Average	**79.32**	**49.19**

Table R14: Explained Cumulative Variances for Randomised Runs

From examination of the Regression Coefficients it can be seen that LV2 is the most heavily weighted, followed by LV1.

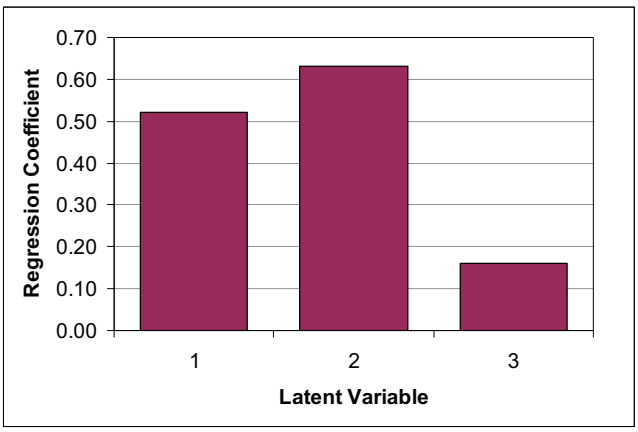

Figure R32: Regression Coefficients

The outputs with the greatest loadings for LV2 are:

3 Rate of Pot Temp Increase at 2hr 40m (°C/min)

6 Time to Lowest Pot T (min)

2 End Ester Yield (%)

7 Top Col T Starts Rising (min)

Examination of the Input Loadings for LV2 reveals the key variables that the model is using to explain the variance

39 Topological Polar Surface Area per H atom

38 H bond acceptor (O atom) per H atom

20 Water of hydration

18 Complexity

30 Heavy Atom Count per Covalently-Bonded Unit

25 Water of hydration per Unit of MW

The outputs with the greatest loadings for LV1 are:

4 Lowest Pot Temp (°C)

5 Initial Rate Pot T Fall (°C/min)

8 Time for Top T to Stabilise (min)

7 Top Col T Starts Rising (min)

Examination of the Input Loadings for LV1 reveals the key variables that the model is using to explain the variance

28 H-Bond Donor per Covalently-Bonded Unit

45 Metal Percent by Mass %

40 Complexity per H atom

22 H-Bond Donor per Unit of MW

29 H-Bond Acceptor per Covalently-Bonded Unit

24 Complexity per Unit of MW

10 Half Life (hours)

R.8 RD Simulation Outputs

R.8.1 With no Simulation Outputs Included

Latent Variable	% Cumulative Variance in Descriptors	% Cumulative Variance in Output
1	45.56	54.11
2	79.03	76.91
3	95.99	87.10
4	100.00	100.00

Table R15: Explained Variances vs. Number of Latent Variables

R.8.2 Outputs from BatchCAD Model

Latent Variable	% Cumulative Variance in Descriptors	% Cumulative Variance in Output
1	49.61	55.20
2	79.23	79.86
3	94.84	88.89
4	100.00	100.00

Table R16: Explained Variances vs. Number of Latent Variables

3LVs

Randomised Run	% Cumulative Variance in Descriptors	% Cumulative Variance in Output
1	94.79	72.99
2	94.04	76.03
3	93.13	75.76
Average	**93.99**	**74.93**

Table R17: Explained Cumulative Variances for Randomised Runs

R.8.3 Outputs from Simplified Excel Model

Latent Variable	% Cumulative Variance in Descriptors	% Cumulative Variance in Output
1	50.83	52.82
2	80.70	77.68
3	95.67	87.81
4	100.00	100.00

Table R18: Explained Variances vs. Number of Latent Variables

For 3LVs:

Randomised Run	% Cumulative Variance in Descriptors	% Cumulative Variance in Output
1	95.15	84.36
2	95.75	76.10
3	95.56	88.63
Average	**95.49**	**83.03**

Table R19: Explained Cumulative Variances for Randomised Runs